DE GRUYTER

Tharwat F. Tadros

FORMULATION SCIENCE AND TECHNOLOGY

VOLUME 1: BASIC THEORY OF INTERFACIAL PHENOMENA AND COLLOID STABILITY

Tharwat F. Tadros

Formulation Science and Technology

Also of Interest

Handbook of Colloid and Interface Science.
Volumes 1–4
Tadros, 2018
ISBN 978-3-11-054050-5

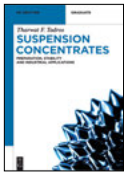

Suspension Concentrates.
Preparation, Stability and Industrial Applications
Tadros, 2017
ISBN 978-3-11-048678-0, e-ISBN 978-3-11-048687-2

Polymeric Surfactants.
Dispersion Stability and Industrial Applications
Tadros, 2017
ISBN 978-3-11-048722-0, e-ISBN 978-3-11-048728-2

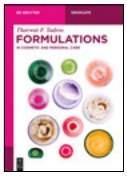

Formulations.
In Cosmetic and Personal Care
Tadros, 2016
ISBN 978-3-11-045236-5, e-ISBN 978-3-11-045238-9

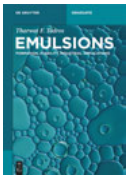

Emulsions.
Formation, Stability, Industrial Applications
Tadros, 2016
ISBN 978-3-11-045217-4, e-ISBN 978-3-11-045224-2

Tharwat F. Tadros

Formulation Science and Technology

Volume 1:
Basic Theory of Interfacial Phenomena and Colloid Stability

DE GRUYTER

Author
Prof. Tharwat F. Tadros
89 Nash Grove Lane
Workingham RG40 4HE
Berkshire, UK
tharwattadros3@gmail.com

ISBN 978-3-11-058747-0
e-ISBN (PDF) 978-3-11-058794-4
e-ISBN (EPUB) 978-3-11-058760-9

Library of Congress Control Number: 2018935454

Bibliographic information published by the Deutsche Nationalbibliothek
The Deutsche Nationalbibliothek lists this publication in the Deutsche Nationalbibliografie; detailed bibliographic data are available on the Internet at http://dnb.dnb.de.

Cover image: Nik_Merkulov / iStock / Getty Images
Typesetting: PTP-Berlin, Protago-TEX-Production GmbH, Berlin
Printing and binding: CPI books GmbH, Leck

www.degruyter.com

Preface

Several classes of formulations are encountered in the chemical industry of which disperse systems (liquid type formulations) are perhaps the most common, e.g. suspensions, emulsions (both within the colloid range, i.e. 1 nm–1 μm and outside the colloid range, i.e. > 1 μm), emulsions, suspoemulsions (mixtures of suspensions and emulsions), multiple emulsions, microemulsions, latexes, pigment formulations, ceramics, etc. In additions, many chemicals are formulated as "solids", e.g. grains, granules, tablets, etc. A third class of formulations are described as "semi-solids", e.g. gels, ointments, etc. For formulation of any chemical, it is necessary to understand the interfacial phenomena at the interface. Another important fundamental investigation is to consider the adsorption of surfactants and polymeric surfactants and their conformation at the liquid/liquid and solid/liquid interface. A very important subject that must be considered is the colloid stability of the final formulation. In most cases one starts with a colloidally stable dispersion which is then modified to reduce various phenomena such as creaming or sedimentation. Further instability problems that must be controlled are the process of Ostwald ripening, emulsions coalescence, phase inversion, sedimentation of suspensions and creaming of emulsions. Apart from the colloid stability phenomena, a very important subject that must be considered is the bulk property of the dispersion. The bulk properties of any formulation can be investigated by measuring its flow characteristics or rheology. Such measurements can be carried out both at high and low deformation conditions. It is clear that for comprehensive understanding of the various phenomena, one must consider the basic theory of interfacial phenomena and colloid stability as well as the basic principles of formulation types. These subjects are considered in Volumes 1 and 2. The industrial applications of the various formulations are described in Volumes 3 and 4.

This text (Volume 1) starts with a general introduction and classification of formulation types. This is followed by two chapters on surfactants, polymeric surfactants and their solution properties. Chapters 4–6 deal with adsorption of surfactants at the liquid/liquid and solid/liquid interfaces as well as the adsorption and conformation of polymeric surfactants at interfaces. Chapters 7 and 8 describe the electrostatic and steric stabilization of dispersions. This is followed by Chapters 9–12 on flocculation of dispersions, Ostwald ripening, emulsion coalescence and phase inversion. The sedimentation of suspensions and creaming of emulsions and their prevention are described in Chapter 13. The last chapter deals with the topic of the flow characteristics (rheology) of formulations.

This volume gives valuable information on the interfacial phenomena encountered in various formulations. It is an important text that can help the formulation scientist in establishing the main characteristics required for any formulation. This is extremely valuable for scientists in academia as well as industrial laboratories.

Tharwat Tadros May 2018

https://doi.org/10.1515/9783110587944-001

Contents

1 General introduction

1.1 General classes of formulations

Several classes of formulations are encountered in the chemical industry of which disperse systems (liquid type formulations) are perhaps the most common, e.g. suspensions (both within the colloid range, i.e. 1 nm–1 μm and outside the colloid range, i.e. > 1 μm), emulsions (also within the colloid range and outside the colloid range), suspoemulsions (mixtures of suspensions and emulsions), multiple emulsions, microemulsions, latexes, pigment formulations, ceramics, etc. In additions, many chemicals are formulated as "solids", e.g. grains, granules, tablets, etc. A third class of formulations are described as "semi-solids", e.g. gels, ointments, etc.

For formulation of any chemical, it is necessary to understand the interfacial phenomena at the interface [1, 2]. This includes analysis of the process of charge separation at the interface and formation of electrical double layers. The latter determine the electrostatic repulsion between the particles or droplets in the formulation. This repulsion must overcome the permanent van der Waals attraction that is universal in all disperse systems. Another important fundamental investigation is to consider the adsorption of surfactants at the liquid/liquid and solid/liquid interface. Surfactants, both of the ionic and nonionic types, are frequently used in the formulation of most chemicals. The adsorption and conformation of surfactant molecules at the interface determine their ability to stabilize the dispersion. Another important fundamental investigation is to consider the adsorption and conformation of polymeric surfactants that are frequently used in many disperse systems. This determines the repulsive energy between particles or droplets that counteracts the van der Waals attraction. A very important subject that must be considered is the colloid stability of the final formulation. In most cases one starts with a colloidally stable dispersion which is then modified to reduce various phenomena such as creaming or sedimentation. One should also control the flocculation of the whole dispersion. In general, the formulation is modified to produce weak and reversible flocculation that is essential in many applications. Another instability problem that must be controlled is the process of Ostwald ripening that occurs as a result of the difference in solubility between small and large particles or droplets. On storage of the formulation, the smaller particles or droplets dissolve and become deposited on the larger ones. This results in a shift of the particle or droplet size distribution to larger values. This shift can cause enhanced creaming or sedimentation and/or enhance flocculation. A special instability problem that occurs with emulsions is coalescence that results from the thinning and disruption of the liquid film between the droplets.

Apart from the above colloid stability phenomena, a very important subject that must be considered is the bulk property of the dispersion. This determines the final state of the dispersion, such as its separation and production of strong gels. The bulk

https://doi.org/10.1515/9783110587944-002

properties of any formulation can be investigated by measuring its flow characteristics or rheology. Such measurements can be carried out both at high and low deformation conditions. Such information can be used to analyse the stability/instability of the formulation as well as to predict of its long-term stability.

It is clear from the above introduction that for a comprehensive understanding of the various phenomena, one must consider the basic theory of interfacial phenomena and colloid stability as well as the basic principles of formulation types. These subjects are considered in Volumes 1 and 2. The industrial applications of the various formulations are described in Volumes 3 and 4.

In this introductory chapter, I will first consider the general classification of disperse systems and this is followed by a general description of the interfacial region that determines the physical stability/instability of the formulation. Two sections will be devoted to the formulation of solid dosage forms and semi-solid formulations.

1.2 Classification of disperse systems

A general classification of disperse systems is given in Tab. 1.1.

It should be mentioned that colloidal particles possess characteristic properties between those of true solutions (with molecules that can diffuse through membranes) and suspensions that can sometimes be easily observed by the naked eye [1]. Clearly colloidal particles are unable to diffuse through membranes and when dispersed in a liquid medium they form a heterogeneous (two-phase) system that can scatter light [1].

Tab. 1.1: Classes of colloidal dispersions.

Solid	Liquid	Suspension
Liquid	Liquid	Emulsion
Gas	Liquid	Foam
Liquid	Gas	Aerosol
Liquid	Solid	Gel
Solid	Gas	Smoke
Solid	Solid	Composite

The best definition of colloids is perhaps “systems in which a significant proportion of the molecules lie in or are associated with interfacial regions”. Simple considerations suggest that the lowest limit for colloids (whereby one can distinguish between molecules in the interfacial region and the bulk) is 1 nm. The upper limit for colloidal dispersions lies in the region of 1,000 nm (1 μm), whereby a significant proportion of the total molecules lie at the interface. Unfortunately, the exact range of colloid size is difficult to ascertain in a precise manner. For that reason Ostwald [1] described colloids as “the world of neglected dimensions”.

To visualize colloidal particles, both scanning electron microscopy (SEM) and transmission electron microscopy (TEM) are effectively used with a resolution down to 5 nm for TEM. For metallic colloids (such as gold sols), a drop of the dispersion is deposited on a TEM grid, dried and observed directly in the microscope. The images, which are the two-dimensional representation, are captured on film or digitally and the size distribution is determined from these using an image analyser. For colloids such as organic polymers, proteins and bio-colloids that can be damaged by the electron beam, a carbon or gold replica is prepared that is floated off the sample and observed in the microscope instead of the colloid. Many other techniques can be used for measuring the size of colloidal particles, of which light scattering is perhaps the most convenient to use. Both static (elastic) and dynamic (quasi-elastic) light scattering methods can be applied and these will be described in detail in Chapter 9 of Vol. 2.

It should be mentioned that colloidal particles are not always spherical and many other shapes are encountered in practice, e.g. ellipsoids, rods, discs, etc. Measurement of particle size and shape distribution is essential since these determine many of the properties of the colloidal dispersion, such as its flow characteristics (rheology), solubility rate, stability, appearance of the dispersion, processing, etc. The particles are described as monodisperse if they are of the same size, otherwise they are polydisperse. It is therefore important to determine the particle size distribution and polydispersity index.

Several examples of dispersion classes can be quoted. One of the earliest colloidal dispersions of the solid/liquid type is colloidal gold which was used in the fourth and fifth century BC by ancient Egyptians and Chinese to make ruby glass and for colouring ceramics [1]. Michel Faraday [1] prepared the first pure colloidal gold dispersion by reducing a solution of gold chloride with phosphorous. He recognized the colour of the dispersion was due to the small size of the gold particles. Nowadays such small size particles covering the size range 1–100 nm are referred to as nanoparticles. The early work of Brown on the random drifting of dispersed particles induced by thermal energy (referred to as Brownian motion) was given a theoretical treatment by Einstein [1]. Brownian motion of colloidal particles and the resultant dynamics are unique and important characteristics of colloidal systems [1].

A good example of a naturally occurring colloid of the liquid/liquid type is milk, which consists of fat droplets dispersed in an aqueous medium also containing casein micelles that are also colloidal in nature. When milk is first obtained from cows, the fat droplets may exceed 1 μm and this results in creaming of these droplets. However, when milk is homogenized (using high pressure homogenizers) the fat droplets are subdivided into submicron droplets (nanodroplets) and this prevents the process of creaming.

An example of a gas/liquid system (foam) is the beer head. When beer is poured into a glass one observes a head of foam and the air bubbles are stabilized by protein present in the beer. Several examples of liquid/gas dispersions (aerosols) can be

quoted, such as fog or mist. One of the main applications of aerosols is in pharmacy for oral and topical use. Pharmaceutical aerosols are dosage forms containing therapeutically active ingredients intended for topical administration, introduction into body cavities, or by inhalation via the respiratory tract. The aerosol product consists of two components, namely concentrate containing the active ingredient and propellant(s). The latter provides the internal pressure that forces the product out of the container when the valve is opened and delivers the product in the desired form.

Liquid/solid dispersions or gels are semi-solids consisting of a "three-dimensional" network in which the liquid is entrapped. The network can be either suspensions of small particles or large organic molecules (polymers) interpenetrated with liquid. In the first case, the inorganic particles, such as bentonite, form a three-dimensional "house of cards" structure through the gel. This is a true two-phase system. With polymers, either natural or synthetic, the molecules tend to entangle with each other due to their random motion. These systems are actually single-phase in the macro-sense; the organic molecules are dissolved in the continuous phase. However, the unique behaviour of polymers, leading to high viscosities and gel formation, makes it possible to consider the gel as a two-phase system on the microlevel; the colloidal polymer molecule and the solvent. Gels find use as delivery systems for oral administration, for topical drugs applied directly to the skin or eye as well as for long acting forms of drugs.

Examples of solid/gas dispersions are smoke and dust as well as particles produced in coal fires and diesel engines. Several examples of solid/solid dispersions can be quoted such as painted glass, pigmented plastics as well as dispersions of silica in plastic to enhance the mechanical properties of the system.

1.3 The interfacial region

In all disperse systems such as suspensions, emulsions, foams, etc., the structure of the interfacial region determines their colloidal properties [1, 2]. The larger the interfacial area, i.e. the larger the surface-to-volume ratio of the particle or droplet, the more important the role of the structure of the interfacial region. For convenience, I will list the topics of colloid and interface science under two main headings, namely disperse systems and interfacial phenomena. This subdivision does not imply any separation for the following reasons. All disperse systems involve an interface. Many interfacial phenomena are precursors for formation of disperse systems, e.g. nucleation and growth, emulsification, etc. The main objectives of the present book are to cover the following topics: The basic principles that are involved in formulation of chemicals and their stabilization.

Several interfacial phenomena may be considered when dealing with dispersions as summarized in Section 1.1 [1, 2]:

(i) Charge separation and formation of electrical double layers.
(ii) Wetting of powders and the role of surfactants.
(iii) Adsorption of surfactants and polymers at the solid/liquid and liquid/liquid interfaces and the role of the structure of the interfacial region.

The physical stability/instability of any disperse system is determined by the properties of the interfacial region. In actual fact, colloid and interface science are one individual subject. This is particularly the case with charged interfaces that form electrical double layers and those interfaces that contain adsorbed surfactants and/or polymers. With systems containing electrical double layers, repulsion between the particles or droplets takes place as a result of the overlap of double layers [1, 2]. This is particularly the case at low electrolyte concentrations and low valency of the indifferent electrolyte. This double layer repulsion overcomes the van der Waals attraction and at intermediate distances an energy barrier is produced that prevents approach of the particles. This barrier can reach several kT units (where k is the Boltzmann constant and T is the absolute temperature) which becomes much higher than the thermal motion ($\approx kT$) and this prevents particle aggregation (flocculation or coagulation). As the electrolyte concentration is increased, the range and magnitude of the repulsive energy is reduced and at a critical concentration (defined as the critical coagulation concentration, CCC) fast flocculation and irreversible aggregation occur. With adsorbed nonionic surfactants or polymers, an adsorbed layer with thickness δ is produced. When the particles or droplets approach to a surface-surface distance $h < 2\delta$, strong repulsion occurs due to the unfavourable mixing of the adsorbed chains when these are in good solvent conditions [1, 2]. This repulsion is referred to as steric interaction and at distances $< 2\delta$ a very sharp increase in repulsion energy occurs when $h < 2\delta$. This steric repulsion overcomes the van der Waals attraction at $h \approx 2\delta$. The repulsion produced by the presence of adsorbed layers of surfactants or polymers is generally more effective than the electrostatic repulsion produced by overlap of the double layers. The stability is less sensitive to addition of moderate electrolyte concentration, provided the medium remains a good solvent for the chains.

The field of colloid and interface science has no boundary since chemists, physicists, engineers, biologists and mathematicians can all be engaged in the field. For successful applications in industry, multidisciplinary teams are required. Understanding the basic principles of colloid and interface science will enable industry to develop many complex formulations in a shorter period of time. Most systems used in industry are multiphase and complex formulations. They may contain more than one disperse phase, e.g. suspension/emulsion systems (suspoemulsions).

For rational preparation of the above mentioned multiphase systems it is necessary to understand the interaction forces between the particles or droplets. The control of the long-term physical stability of these formulations requires the application of various surfactants and dispersants. It is also necessary to assess and predict the stability of these systems and this requires the application of various physical techniques.

1.4 Solid dosage forms

Many chemicals, in particular pharmaceuticals and agrochemicals, are formulated in solid dosage forms [3]. The most important solid formulations in pharmacy are tablets. They have the advantage that they are convenient and inexpensive and deliver a dosed amount of the active ingredient (AI) with great accuracy. They are generally prepared by mixing the powder with starch paste, followed by milling and drying (in a tray). The final mixture is further milled and then compressed into tablets. Although direct compression techniques are most popular, many products still have to be made by granulating techniques. The latter serve three main purposes, namely improved flow, uniform distribution of the AI and assisting the bonding together of the tablet. Once a mechanically good tablet is produced, it must be biologically available, therefore it must be able to disintegrate in contact with gastric juice. For these reasons, several ingredients are incorporated in the tablet, e.g. talc that improves the flow, a lubricant (such as magnesium stearate), an excipient such as lactose that controls the size, a disintegrant such as alginic acid and a binder such as starch paste that controls the strength of the tablet. In most cases, the tablets are coated for protective (against oxygen, moisture and light) and aesthetic purposes. Hard-shell gelatin capsules are also commonly used in the pharmaceutical industry. The empty hard-shell capsules are produced by dipping rods into gelatine melt at controlled viscosity and temperature. The capsules are then dried by exposing them to a stream of air of controlled temperature and humidity, cutting and removing them. The capsules are separated and fed into separate hoppers and the powder fill is accomplished by vacuum; the powder being pulled into a cavity of known volume and then deposited in the lower half of the capsule.

1.5 Semi-solid formulations

Several semi-solid formulations are used both in the pharmaceutical and the cosmetic industry, of which gels and ointments are probably the most commonly used. Gels are used as delivery systems for oral administration and in topical application. Gels are divided into inorganic and organic gels on the basis of the nature of the colloidal phase [4]. Bentonite magma (sodium montmorillonite) and silica are examples of inorganic gels. Organic gels typically contain polymers as the gel former. The polymer can be natural such as acacia, carrageenan and xanthan gum. Synthetic polymers include cellulose derivatives, such as carboxymethyl cellulose, hydroxyethyl cellulose and methyl hydroxypropyl cellulose. Block copolymers, namely Poloxamers (of polyethylene oxide–polypropylene oxide–polyethylene oxide, PEO–PPO–PEO) are also used as gelling agents. For gelling nonaqueous media, polyethylenes and magnesium stearate are most commonly used.

Ophthalmic ointments are commonly used for treatment of ocular disease. These ointments should be non-irritating, sterile, homogeneous (particles uniformly dispersed in the ointment vehicle), relatively non-greasy and should not cause blurred vision.

1.6 Outline of the book

This book is divided into four volumes: Volume 1 deals with the basic theory of interfacial phenomena and colloid stability. Volume 2 describes the basic principles of formulation types. Volumes 3 and 4 describe the industrial applications of the various formulation types.

Volume 1 consists of 14 chapters. Chapter 2 deals with the classification of surfactants that are commonly used in formulations, their solution properties and self-assembly structures (micelles and liquid crystalline structures) [5]. These molecules are used for the preparation and stabilization of disperse systems, e.g. suspensions, emulsions, microemulsions and foams. A simple classification of surfactants based on the nature of the hydrophilic group is commonly used. Four main classes may be distinguished, namely anionic, cationic, amphoteric and nonionic. The most common nonionic surfactants are those based on ethylene oxide, referred to as ethoxylated surfactants. Several classes can be distinguished: alcohol ethoxylates, alkyl phenol ethoxylates, fatty acid ethoxylates, monoalkaolamide ethoxylates, sorbitan ester ethoxylates, fatty amine ethoxylates and ethylene oxide-propylene oxide copolymers (sometimes referred to as polymeric surfactants). Another important class of nonionics are the multihydroxy products such as glycol esters, glycerol (and polyglycerol) esters, glucosides (and polyglucosides) and sucrose esters. Amine oxides and sulphinyl surfactants represent nonionics with a small head group.

Chapter 3 deals with polymeric surfactants used for the effective stabilization of disperse systems [6]. It starts with a section on homopolymers (that are formed from the same monomeric units). This followed by a section on "blocky" copolymers that contain segments with high affinity to the surface. The most effective polymeric surfactants are the block (A–B or A–B–A) and graft (BA_n or AB_n) copolymers with a chain B (the "anchor" chain) that has a high affinity to the surface and A chains (the stabilizing chains) that have high affinity to the solvent in which the dispersion is made. Special sections are devoted to polymeric surfactants based on polysaccharides, natural polymeric biosurfactants, silicone surfactants, polymeric surfactants for nonaqueous dispersions and polymerizable surfactants. The next section deals with the solution properties of polymeric surfactants, including the polymer conformation and structure, and the free energy of mixing of polymer with solvent with special reference to the Flory–Huggins theory. The viscosity measurements for characterizing a polymer in solution are described. This is followed by a section on the phase separation of polymer solutions. The solubility parameter concept for selecting the right solvent for a polymer is described.

Chapter 4 deals with the adsorption of surfactants at the liquid/liquid interface [2]. The adsorption amount and orientation of surfactant molecules at the liquid/liquid interface and their dependence on the nature of the surfactant are very important factors in the formation and stabilization of emulsions and microemulsions. There are generally two approaches for treating surfactant adsorption at the L/L interface. The first approach, adopted by Gibbs, treats adsorption as an equilibrium phenomenon whereby the second law of thermodynamics may be applied using surface quantities. The second approach, referred to as the equation of state approach, treats the surfactant film as a two-dimensional layer with a surface pressure π that may be related to the surface excess Γ (amount of surfactant adsorbed per unit area). Gibbs [2] derived a thermodynamic relationship between the surface or interfacial tension γ and the surface excess Γ (adsorption per unit area). In the equation of state approach one relates the surface pressure π to the surface excess Γ_2. The effectiveness of surfactant adsorption at the liquid/liquid interface is assessed from the surface excess concentration at surface saturation, Γ_m. The efficiency of surfactant adsorption at the liquid/liquid interface can be determined by measuring the surfactant concentration that produces a given amount of adsorption at the interface. Adsorption from mixtures of surfactants may show a "synergistic" interaction. In other words, the interfacial properties of the mixture are more pronounced than those of the individual components themselves. The adsorption of macromolecules at the liquid/liquid interface considers the partition of segments of a given homopolymer between the two liquid phases in a manner which reflects the two segment–solvent interaction parameters ε_{13} and ε_{23} (where 1 and 2 refer to the two liquids and 3 to the polymer segments). The last section of this chapter describes the methods that can be applied for interfacial tension measurements. These methods may be classified into two categories: those in which the properties of the meniscus are measured at equilibrium, e.g. pendent drop or sessile drop profile and Wilhelmy plate methods, and those where the measurement is made under non-equilibrium or quasi-equilibrium conditions, such as the drop volume (weight) or the du Noüy ring method. The latter methods are faster, although they suffer from the disadvantage of premature rupture and expansion of the interface, causing adsorption depletion. They are also inconvenient for measuring interfacial tension in the presence of macromolecular species where adsorption is slow. This problem is overcome by the equilibrium (static) methods. For measuring low interfacial tensions ($< 0.1\,\mathrm{mN\,m^{-1}}$) the spinning drop technique is applied.

Chapter 5 deals with the adsorption of surfactants at the solid/liquid interface [7]. Surfactants consist of a small number of units and they mostly are reversibly adsorbed, allowing one to apply thermodynamic treatments. In this case, it is possible to describe the adsorption in terms of the various interaction parameters, namely chain-surface, chain-solvent and surface-solvent. Moreover, the conformation of the surfactant molecules at the interface can be deduced from these simple interaction parameters. Four cases can be considered:

(i) adsorption of ionic surfactants on hydrophobic (nonpolar) surfaces;
(ii) adsorption of ionic surfactants on polar (charged) surfaces;
(iii) adsorption of nonionic surfactants on hydrophobic surfaces;
(iv) adsorption of nonionic surfactants on polar surfaces.

Cases (i) and (iii) are governed by hydrophobic interaction between the alkyl chain and hydrophobic surface; the charge plays a minor role. Cases (ii) and (iv) are determined by charge and/or polar interaction. At the solid/liquid interface one is interested in determining the following parameters:

(i) the amount of surfactant adsorbed Γ per unit mass or unit area of the solid adsorbent at a given temperature;
(ii) the equilibrium concentration of the surfactant C (mol dm^{-3} or mole fraction $x = C/55.51$) in the liquid phase required to produce a given value of Γ at a given temperature;
(iii) the surfactant concentration at full saturation of the adsorbent Γ_{sat};
(iv) the orientation of the adsorbed surfactant ion or molecule that can be obtained from the area occupied by the ion or molecule at full saturation;
(v) the effect of adsorption on the properties of the adsorbent (nonpolar, polar or charged).

Examples are given for adsorption isotherms for ionic surfactants on hydrophobic surfaces. This is followed by a section on the adsorption of ionic surfactants on polar surfaces that contain ionizable groups. This may show characteristic features due to additional interaction between the head group and substrate and/or possible chain–chain interaction. The adsorption of nonionic surfactants is then described. Several types of nonionic surfactants exist, depending on the nature of the polar (hydrophilic) group. The most common type is that based on a poly(oxyethylene) glycol group, i.e. $(CH_2CH_2O)_nOH$ (where n can vary from as little as 2 units to as high as 100 or more units) linked either to an alkyl (C_xH_{2x+1}) or alkyl phenyl (C_xH_{2x+1}–C_6H_4–) group. These surfactants may be abbreviated as C_xE_n or $C_x\phi E_n$ (where C refers to the number of C atoms in the alkyl chain, ϕ denotes C_6H_4 and E denotes ethylene oxide). These ethoxylated surfactants are characterized by a relatively large head group compared to the alkyl chain (when $n > 4$). However, there are nonionic surfactants with a small head group such as amine oxides ($-N \rightarrow 0$) head group, phosphate oxide ($-P \rightarrow 0$) or sulphinyl-alkanol (–SO–$(CH_2)_n$–OH). Most adsorption isotherms in the literature are based on the ethoxylated type surfactants. The adsorption isotherms of nonionic surfactants are in many cases Langmuirian, like those of most other highly surface active solutes adsorbing from dilute solutions, and adsorption is generally reversible. However, several other adsorption types are produced showing several steps in the isotherm. The steps in the isotherm may be explained in terms of the various adsorbate–adsorbate, adsorbate–adsorbent and adsorbate–solvent interactions.

Chapter 6 deals with the subject of adsorption and conformation of polymeric surfactants at the solid/liquid interface [2, 7]. The adsorption and conformation of polymeric surfactants at interfaces is key to understanding how these molecules act as stabilizers. The process of polymer adsorption is fairly complicated. In addition to the usual adsorption considerations such as polymer/surface, polymer/solvent and surface/solvent interactions, one of the principal problems to be resolved is the configuration (conformation) of the polymer at the solid/liquid interface. A model is suggested for homopolymers in which not all the segments of a macromolecule are in contact with the surface. The segments that are in direct contact with the surface are termed "trains"; those in between and extended into solution are termed "loops"; the free ends of the macromolecule also extending in solution are termed "tails". Homopolymers are not the most suitable emulsifiers or dispersants. A small variant is to use polymers that contain specific groups that have high affinity to the surface. The most convenient polymeric surfactants are those of the block and graft copolymer type. A block copolymer is a linear arrangement of blocks of variable monomer composition. The nomenclature for a diblock is poly-A-block–poly-B and for a triblock is poly-A-block–poly-B–poly-A. An example of an A–B diblock is polystyrene block-polyethylene oxide. One of the most widely used triblock polymeric surfactants are the "Pluronics", which consist of two poly-A blocks of poly(ethylene oxide) (PEO) and one block of poly(propylene oxide) (PPO). These polymeric triblocks can be applied as emulsifiers or dispersants, whereby the assumption is made that the hydrophobic PPO chain resides at the hydrophobic surface, leaving the two PEO chains dangling in aqueous solution and hence providing steric repulsion. Several other triblock copolymers have been synthesized, although these are of limited commercial availability. Typical examples are triblocks of poly(methyl methacrylate)-block poly(ethylene oxide)-block poly(methyl methacrylate). An alternative (and perhaps more efficient) polymeric surfactant is the amphipathic graft copolymer consisting of a polymeric backbone B (polystyrene or polymethyl methacrylate) and several A chains ("teeth") such as polyethylene oxide. This graft copolymer is sometimes referred to as a "comb" stabilizer. The polymer/surface interaction is described in terms of adsorption energy per segment χ^s. The polymer/solvent interaction is described in terms of the Flory–Huggins interaction parameter χ. For adsorption to occur, a minimum energy of adsorption per segment χ^s is required. When a polymer molecule adsorbs on a surface, it loses configurational entropy and this must be compensated by an adsorption energy χ^s per segment. For a full description of polymer adsorption one needs to obtain information on the following:

(i) The amount of polymer adsorbed Γ (in mg or mol) per unit area of the particles. It is essential to know the surface area of the particles in the suspension.

(ii) The fraction of segments in direct contact with the surface, i.e. the fraction of segments in trains p:

$$p = \frac{\text{number of segments in direct contact with the surface}}{\text{total number}}.$$

(iii) The distribution of segments in loops and tails, $\rho(z)$, which extend in several layers from the surface.

$\rho(z)$ is usually difficult to obtain experimentally although recently application of small angle neutron scattering could obtain such information. An alternative and useful parameter for assessing "steric stabilization" is the hydrodynamic thickness, δ_h (thickness of the adsorbed or grafted polymer layer plus any contribution from the hydration layer). Several methods can be applied to measure δ_h as described in this chapter. Two main theoretical approaches have been developed to treat the problem of polymer adsorption:

(i) The random walk approach. This is based on Flory's treatment of the polymer chain in solution; the surface was considered as a reflecting barrier.
(ii) Statistical mechanical approach. The polymer configuration was treated as being made of three types of structures: trains, loops and tails, each having a different energy state.

A useful model for treating polymer adsorption and configuration was suggested and is referred to as the step weighted random walk approach [2, 7]. In order to be able to describe all possible chain conformations, a model of a quasi-crystalline lattice with lattice layers parallel to the surface was used. The conformation probability and the free energy of mixing were calculated with the assumption of random mixing within each layer (the Brag–Williams or mean field approximation). The energy for any segment is only determined by the layer number, and each segment can be assigned a weighting or Boltzmann factor p_i which depends only on the layer number. The partition functions were derived for the mixture of free and adsorbed polymer molecules, as well as for the solvent molecules. All chain conformations were described as step weighted random walks on a quasi-crystalline lattice which extends in parallel layers from the surface. Each step in the random walk was assigned a weighting factor p_i that consists of three contributions:

(i) an adsorption energy χ^s (which exists only for the segments that are near the surface);
(ii) Configurational entropy of mixing (that exists in each layer);
(iii) Segment–solvent interaction parameter χ (the Flory–Huggins interaction parameter; note that $\chi = 0$ for an athermal solvent; $\chi = 0.5$ for a θ-solvent).

Chapter 7 deals with electrostatic stabilization of dispersions [2, 7]. The chapter starts with a section on the origin of charge on surfaces and the structure of the electrical double layer. This is followed by a section on the origin of repulsion caused by double layer overlap with particular reference to the effect of surface (or zeta) potential, electrolyte concentration and valency of ions in the bulk liquid. The next section deals with the origin of van der Waals attraction and its variation with particle or droplet separation, particle or droplet radius and the medium in which the particles

or droplets are dispersed. Combining double layer repulsion with van der Waals attraction forms the basis of the theory of colloid stability. The variation of electrostatic repulsion, van der Waals attraction and total interaction with separation distance produces energy–distance curves with an energy maximum (barrier) that prevents particle or droplet aggregation. The dependency of the energy barrier on surface potential, electrolyte concentration and valency can be used to distinguish between stable and instable dispersions. The structure of the electrical double layer is described using the diffuse double layer model and the role of specific adsorption of counterions is also considered. The origin of electrostatic interactions is described in terms of the double layer overlap that occurs when the surface-to-surface distance becomes smaller than twice the double layer thickness. One of the most important features of double layers is their strong dependency on the concentration of indifferent electrolytes. Increasing electrolyte concentration causes a reduction in the diffuse double layer potential and compression of the double layer, both of which affect the colloid stability of lyophobic colloids. In the original theory of colloid stability, the assumption was made that on the approach of surfaces the surface potentials remain constant and equal to that at infinite separation of the surfaces. There are generally two approaches for describing the van der Waals attraction G_A between macroscopic bodies such as suspension particles. The first approach considers the London–van der Waals attraction to be the sum of the forces acting between isolated molecules. This is referred to as the microscopic approach. The second approach, referred to as the macroscopic approach, is based on the correlation between electric fluctuations of two macroscopic bodies. G_A increases very sharply with h at small values. A capture distance can be defined at which all the particles become strongly attracted to each other (coagulation). At very short distances, Born repulsion appears. The combination of G_{el} and G_A, i.e. G_T, results in the well-known theory of stability of colloids. G_{el} decays exponentially with h, i.e. $G_{el} \to 0$ as h becomes large. $G_A \propto 1/h$, i.e. G_A does not decay to 0 at large h. At long distances of separation, $G_A > G_{el}$, resulting in a shallow minimum (secondary minimum). At very short distances, $G_A \gg G_{el}$, resulting in a deep primary minimum. At intermediate distances, $G_{el} > G_A$, resulting in an energy maximum, G_{max}, whose height depends on ψ_0 (or ψ_d) and the electrolyte concentration and valency. At low electrolyte concentrations ($< 10^{-2}$ mol dm^{-3} for a 1 : 1 electrolyte), G_{max} is high ($> 25kT$) and this prevents particle aggregation into the primary minimum. The higher the electrolyte concentration (and the higher the valency of the ions), the lower the energy maximum. Under some conditions (depending on electrolyte concentration and particle size), flocculation into the secondary minimum may occur. This flocculation is weak and reversible. By increasing the electrolyte concentration, G_{max} decreases until at a given concentration it vanishes and particle coagulation occurs. Using the equations for G_{el} and G_A, the critical coagulation concentration, CCC can be calculated. The theory predicts that the CCC is directly proportional to the surface potential ψ_0 and inversely proportional to the Hamaker constant A and the electrolyte valency Z. The CCC is inversely propor-

tional to Z^6 at high surface potential and inversely proportional to Z^6 at low surface potential.

Chapter 8 deals with interaction between particles or droplets containing adsorbed polymer layers and the theory of steric stabilization [2, 6]. Polymers are particularly important for the preparation of concentrated dispersions, i.e. at high volume fraction ϕ of the disperse phase. Polymers are also essential for stabilizing nonaqueous dispersions, since in this case electrostatic stabilization is not possible (due to the low dielectric constant of the medium). Examples for the stabilization of emulsions, nanoemulsions and suspensions using polymeric surfactants are given in this chapter. When two particles or droplets, each with a radius R and containing an adsorbed polymer layer with a hydrodynamic thickness δ_h, approach each other to a surface-surface separation distance h that is smaller than $2\delta_h$, the polymer layers interact with each other resulting in two main situations [6]:

(i) the polymer chains may overlap with each other;
(ii) the polymer layer may undergo some compression.

In both cases, there will be an increase in the local segment density of the polymer chains in the interaction region. Provided the dangling chains (the A chains in A–B, A–B–A block or BA_n graft copolymers) are in a good solvent, this local increase in segment density in the interaction zone will result in strong repulsion as a result of two main effects:

(i) Increasing osmotic pressure in the overlap region as a result of the unfavourable mixing of the polymer chains, when these are in good solvent conditions. This is referred to as osmotic repulsion or mixing interaction and it is described by a free energy of interaction G_{mix}.
(ii) Reduction of the configurational entropy of the chains in the interaction zone; this entropy reduction results from the decrease in the volume available for the chains when these are either overlapped or compressed. This is referred to as volume restriction interaction, entropic or elastic interaction and it is described by a free energy of interaction G_{el}.

The combination of G_{mix} and G_{el} is usually referred to as the steric interaction free energy, G_s. The sign of G_{mix} depends on the solvency of the medium for the chains. If in a good solvent, i.e. the Flory–Huggins interaction parameter χ is less than 0.5, then G_{mix} is positive and the mixing interaction leads to repulsion (see below). In contrast, if $\chi > 0.5$ (i.e. the chains are in poor solvent conditions), G_{mix} is negative and the mixing interaction becomes attractive. G_{el} is always positive and hence in some cases one can produce stable dispersions in a relatively poor solvent (enhanced steric stabilization).

Chapter 9 deals with the process of flocculation of dispersions. It starts with the mechanism of aggregation of electrostatically stabilized dispersions. The colloid stability theory predicts the process of aggregation on addition of electrolytes with different valency. Addition of electrolyte reduces the range of the repulsive component

(due to compression of the electrical double layer) and this results in a reduction of the energy maximum, G_{max}. Using the equations for the electrostatic repulsion, G_{el}, and the van der Waals attraction, G_A, the critical coagulation concentration, CCC can be calculated. The theory predicts that the CCC is directly proportional to the surface potential ψ_0 and inversely proportional to the Hamaker constant A and the electrolyte valency Z. The CCC is inversely proportional to Z^6 at high surface potential and inversely proportional to Z^2 at low surface potential. The kinetics of flocculation of dispersions is described for four cases:

(i) Diffusion limited aggregation (fast flocculation kinetics), which represents the case where no energy barrier exists and hence the process becomes diffusion controlled.
(ii) Potential limited aggregation (slow flocculation kinetics), which describes the effect of presence of an energy barrier.
(iii) Weak (reversible) flocculation that involves the secondary minimum (G_{min}) which is a few kT units.
(iv) Flocculation that occurs under shearing conditions and is referred to as orthokinetic (to distinguish it from the diffusion controlled perikinetic process).

The next section deals with the flocculation of sterically stabilized dispersions. Two main types of flocculation may be distinguished:

(i) Weak flocculation that occurs when the thickness of the adsorbed layer is small (usually < 5 nm), particularly when the particle radius and Hamaker constant are large. The minimum depth required for causing weak flocculation depends on the volume fraction of the suspension.
(ii) Incipient flocculation that occurs when the solvency of the medium is reduced to become worse than θ-solvent (i.e. $\chi > 0.5$). This reduction in solvency can be induced by temperature changes [6] or addition of a nonsolvent [6] for the stabilizing chain. When the solvency is reduced, the dispersion often exhibits a sharp transition from long-term stability to fast flocculation. This process of incipient flocculation is, for example, observed when a dispersion stabilized by poly(ethylene oxide) moieties is heated. Over a few degrees temperature rise, the turbidity of the dispersion rises sharply indicating excessive flocculation.

Flocculation can also occur by the addition of a nonsolvent, e.g. by addition of ethanol to polymethylmethacrylate dispersion stabilized by poly(hydroxystearic) acid in a hydrocarbon solvent [6]. The critical point at which flocculation is first observed is referred to as the critical flocculation temperature (CFT) or critical flocculation concentration of the added nonsolvent (CFV). Another flocculation mechanism is that produced by addition of "free" nonadsorbing polymer [6], referred to as depletion flocculation. In this case, the polymer coils cannot approach the particles to a distance Δ (that is determined by the radius of gyration of free polymer R_G), since the reduction of entropy on close approach of the polymer coils is not compensated by an adsorption

energy. The dispersion particles or droplets will be surrounded by a depletion zone with thickness Δ. Above a critical volume fraction of the free polymer, ϕ_p^+, the polymer coils are "squeezed out" from between the particles and the depletion zones begin to interact. The interstices between the particles are now free from polymer coils and hence an osmotic pressure is exerted outside the particle surface (the osmotic pressure outside is higher than in between the particles) resulting in weak flocculation [6]. Another mechanism of flocculation is bridging by polymers and polyelectrolytes. Certain long chain polymers may adsorb in such a way that different segments of the same polymer chain are adsorbed on different particles, thus binding or "bridging" the particles together, despite the electrical repulsion [6]. With polyelectrolytes of opposite charge to the particles, another possibility exists; the particle charge may be partly or completely neutralized by the adsorbed polyelectrolyte, thus reducing or eliminating the electrical repulsion and destabilizing the particles.

Chapter 10 deals with the process of Ostwald ripening in dispersions and its prevention. The driving force of Ostwald ripening is the difference in solubility between smaller and larger particles or droplets [2]. The small particles or droplets with radius r_1 will have higher solubility than the larger particle or droplet with radius r_2. The kinetics of Ostwald ripening predicts that particle or droplet growth over time will be proportional to r_c^3. It has been suggested that micelles play a role in facilitating the mass transfer between particle or emulsion droplets by acting as carriers of particle or oil molecules. The reduction of Ostwald ripening in emulsions is described in terms of two mechanisms:

(i) Addition of a small proportion of highly insoluble oil. Addition of a second disperse phase which is virtually insoluble in the continuous phase, such as squalane, can significantly reduce the Ostwald ripening rate.
(ii) Modification of the interfacial layer; it has been suggested that emulsions can be effectively stabilized against Ostwald ripening by the use of surfactants that are strongly adsorbed at the interface and which do not desorb during the Ostwald ripening process.

In this case, an increase in interfacial dilational modulus ε and a decrease in interfacial tension γ would be observed for the shrinking droplets. Eventually the difference in ε and γ between droplets would balance the difference in capillary pressure (i.e. curvature effects) leading to a quasi-equilibrium state. In this case, emulsifiers with low solubilities in the continuous phase such as proteins would be preferred. Long chain phospholipids with a very low solubility (cmc $\approx 10^{-10}$ mol dm^{-3} are also effective in reducing Ostwald ripening of some emulsions. The phospholipid would have to have a solubility in water about three orders of magnitude lower than the oil. The thermodynamic theory of crystal growth is then described. This is followed by an analysis of the molecular-kinetic theory of crystal growth. The influence of dislocations on crystal growth is described. The influence of impurities on crystal growth and habit modification is described. The effect of polymorphic changes is described

in terms of reversion of the thermodynamically less stable form to the more stable form. If this is the case, crystal growth is virtually unaffected by temperature, i.e. it is an isothermal process, which is solvent mediated. The crystal growth inhibition in suspensions in which the solid particles have substantial solubility or exist in various polymorphs, is described by considering the effects of wetting, dispersing agents as well as the presence of impurities The wetting/dispersing agent may affect the rate of dissolution by affecting the rate of transport away from the boundary layer, although their addition is not likely to affect the rate of dissolution proper (passage from the solid to the dissolved state in the immediate adjacent layer). If the wetting/dispersing agent forms micelles which can solubilize the solute, the diffusion coefficient of the solute in the micelles is greatly reduced. However, as a result of solubilization, the concentration gradient of the solute is increased to an extent depending on the extent of solubilization. The overall effect may be an increase in the crystal growth rate as a result of solubilization. In contrast, if the diffusion rate of the molecules of the wetting/dispersing agent is sufficiently rapid, their presence will lower the flux of the solute molecules compare to that in the absence of the wetting/dispersing agent. In this case, the wetting/dispersing agent will lower the rate of crystal growth. Secondly, wetting/dispersing agents are expected to influence growth when the rate is controlled by surface nucleation. Adsorption of wetting/dispersing agents on the surface of the crystal can drastically change the specific surface energy and makes it inaccessible to the solute molecules. In addition, if the wetting/dispersing agent is preferentially adsorbed at one or more of the faces of the crystal (for example by electrostatic attraction between a highly negative face of the crystal and cationic surfactant), surface nucleation is no longer possible at this particular face (or faces). Growth will then take place at the remaining faces which are either bare or incompletely covered by the wetting/dispersing agent. This will result in a change in crystal habit. Many block A–B–A and graft BA_n copolymers (with B being the "anchor" part and A the stabilizing chain) are very effective in inhibiting crystal growth. The B chain adsorbs very strongly on the surface of the crystal and sites become unavailable for deposition. This has the effect of reducing the rate of crystal growth. Apart from their influence on crystal growth, the above copolymers also provide excellent steric stabilization, providing the A chain is chosen to be strongly solvated by the molecules of the medium.

Chapter 11 deals with emulsion coalescence and its prevention. Coalescence results from the rupture of this film by considering the forces across the liquid films. Two main approaches are considered to analyse the stability of thin films in terms of the relevant interactions. The first approach introduces the concept of disjoining pressure $\pi(h)$ that is produced in the film and which balances the excess normal pressure; $\pi(h)$ may be equated to the net force (or energy) per unit area acting across the film. $\pi(h)$ is made up of three contributions due to electrostatic repulsion (π_E), steric repulsion (π_s) and van der Waals attraction (π_A). To produce a stable film $\pi_E + \pi_s > \pi_A$ and this is the driving force for prevention of coalescence which can be achieved by two mechanisms and their combination:

(i) increased repulsion, both electrostatic and steric;
(ii) dampening the fluctuation by enhancing the Gibbs elasticity.

In general, smaller droplets are less susceptible to surface fluctuations and hence coalescence is reduced. The second approach considers the interfacial tension of the film that could be related to the tangential pressure across the interface. The interfacial tension $\gamma(h)$ can be related to the variation in the tangential pressure tensor p_t across an interface. There will be a similar variation in P_t across the liquid film at some thickness h. Film rupture is a non-equilibrium effect and is associated with local thermal or mechanical fluctuations in the film thickness b. A necessary condition for rupture to occur, i.e. for a spontaneous fluctuation to occur, is that the variation of the attractive contribution of the disjoining pressure with film thickness exceeds the variation of repulsive contribution with film thickness. The concept of a critical thickness below which rupture of the film occurs is introduced. An expression for the coalescence rate of emulsion droplets is derived by assuming the rate to be proportional to the number of contact points between the droplets in an aggregate. Both flocculation and coalescence are taken into account simultaneously. The problem of coalescence is considered by incorporating an energy barrier term in order to account for the slow coalescence for emulsions stabilized by sodium oleate. Several methods can be applied for reducing coalescence:

(i) Use of mixed surfactant films that can have a synergistic effect on emulsion stability, with respect to coalescence rates. For example, the stability of Nujol/water emulsions increases markedly on addition of cetyl alcohol or cholesterol to an emulsion prepared using sodium cetyl sulphate. The enhanced stability was assumed to be associated with the formation of a densely packed interfacial layer. The maximum effect is obtained when using a water-soluble surfactant (cetyl sulphate) and an oil-soluble surfactant (cetyl alcohol), sometimes referred to as cosurfactant, in combination. Suitable combinations lead to enhanced stability compared to the individual components. These mixed surfactant films also produce a low interfacial tension, in the region of 0.1 mN m^{-1} or lower. The synergistic effect of surfactant mixtures can be accounted for by the enhanced lowering of interfacial tension of the mixture when compared with individual components. For example, addition of cetyl alcohol to an O/W emulsion stabilized by cetyl trimethyl ammonium bromide results in a lowering of the interfacial tension, and a shift of the critical micelle concentration (cmc) to lower values, probably due to the increased packing of the molecules at the O/W interface. Another effect of using surfactant mixtures is due to the enhanced Gibbs dilational elasticity, ε.

(ii) Interfacial viscosity; a high interfacial viscosity could account for the stability of liquid films. This must play a role under dynamic conditions, i.e. when two droplets approach each other. Under static conditions, the interfacial viscosity does not play a direct role. However, a high interfacial viscosity is often accompanied by a high interfacial elasticity and this may be an indirect contribution to the increased stability of

the emulsion. Another possible explanation of the enhanced stability in the presence of mixed surfactants could be connected to the hindered diffusion of the surfactant molecules in the condensed film. This would imply that the desorption of surfactant molecules is hindered on the approach of two emulsion droplets, and hence thinning of the film is prevented. The enhanced stability of emulsions formed with mixtures of surfactants is attributed to the formation of three-dimensional structures, namely, liquid crystals. These structures can form, for example, in a three-component system of surfactant, alcohol and water. The lamellar liquid crystalline phase, denoted by N (neat phase), in the phase diagram is particularly important for stabilizing the emulsion against coalescence. In this case the liquid crystals "wrap" around the droplets in several layers. And these multilayers form a barrier against coalescence.

(iii) Use of polymeric surfactants that are of the block and graft copolymer type. These polymeric surfactants are strongly adsorbed at the oil/water interface (with the "anchor" B chain) leaving the strongly hydrated A chains in bulk solution that provide effective steric stabilization.

Chapter 12 deals with the process of phase inversion and its prevention. Phase inversion is the process whereby the internal and external phases of an emulsion suddenly invert, e.g. O/W to W/O or vice versa. Catastrophic inversion is induced by increasing the volume fraction of the disperse phase. This type of inversion is not reversible; the value of the water: oil ratio at the transition when oil is added to water is not the same as that when water is added to oil. The inversion point depends on the intensity of agitation and the rate of liquid addition to the emulsion. Phase inversion can also be transitional, induced by changing factors which affect the HLB of the system, e.g. temperature and/or electrolyte concentration. The average droplet size decreases and the emulsification rate (defined as the time required to achieve a stable droplet size) increases as inversion is approached. Both trends are consistent with O/W interfacial tension reaching a minimum near the inversion point. In the early theories of phase inversion, it was postulated that inversion takes place as a result of the difficulty in packing the emulsion droplets above a certain volume fraction. An assembly of spheres of equal radii should occupy 74 % of the total volume. Thus, at phase volume $\phi > 0.74$, the emulsion droplets have to be packed more densely than is possible. This means that any attempt to increase the phase volume beyond that point should result in distortion, breaking or inversion. However, several investigations showed the invalidity of this argument, inversion being found to take place at phase volumes much greater or smaller than this critical value. Transitional inversion is caused by a change of the system HLB at constant temperature using surfactant mixtures. Several other conditions can cause transitional phase inversion, such as addition of electrolyte and/or increasing temperature, in particular for emulsions based on nonionic surfactants of the ethoxylate. In order to understand the process of phase inversion, one must consider the surfactant affinity to the oil and water phases, which is the ratio R_0 of the intermolecular attraction of oil molecules (O) and lipophilic portion of surfactant (L), C_{LO}, to that of water (W) and hydrophilic portion (H), C_{HW}. The

three cases $R_0 < 1$, $R_0 > 1$ and $R_0 = 1$ correspond to type I (O/W), type II (W/O) and type III (flat interface) phase behaviour respectively. For example, for $R_0 < 1$, increasing temperature results in reduced hydration of the hydrophilic part of the surfactant molecule and the emulsion changes from Winsor I to Winsor III to Winsor II and this causes phase inversion from O/W to W/O emulsion. This inversion occurs at a particular temperature, referred to as the phase inversion temperature (PIT). In Winsor's type I systems ($R_0 < 1$), the affinity of the surfactant for the water phase exceeds its affinity to the oil phase. Thus, the interface will be convex towards water and the nonionic surfactant–oil–water (nSOW) system can be one or two phases. A system in the two-phase system will split into an oil phase containing dissolved surfactant monomers at the cmc_o (critical micelle concentration in the oil phase) and an aqueous microemulsion-water phase containing solubilized oil in normal surfactant micelles. In Winsor's type II systems ($R_0 > 1$), the affinity of the surfactant for the oil phase exceeds its affinity to the water phase. Thus, the interface will be convex towards oil and the nonionic surfactant–oil–water (nSOW) system can be one- or two-phase. A system in the two-phase system will split into a water phase containing dissolved surfactant monomers at the cmc_w (critical micelle concentration in the water phase) and an oleic microemulsion phase containing solubilized water in inverse surfactant micelles. In Winsor's type III system ($R_0 = 1$), the surfactant's affinity for the oil and water phases is balanced. The interface will be flat and the nSOW system can have one, two or three phases depending on its composition. In the multiphase region, the system can be:

(i) two-phase, a water phase and an oleic microemulsion;
(ii) two-phase, an oil phase and an aqueous microemulsion;
(iii) three-phase, a water phase containing surfactant monomers at cmc_w, an oil phase containing surfactant monomers at cmc_o and a "surfactant phase".

The latter phase may have a bicontinuous structure, being composed of cosolubilized oil and water separated from each other by a layer of surfactant. The "surfactant phase" is sometimes called the middle phase because its intermediate density causes it to appear between the oil and water phases in a phase-separated type III n-SOW system. One way to alter the affinity in an n-SOW system is by changing the temperature which changes the surfactant's affinity to the two phases. At high temperature the nonionic surfactant becomes soluble in the oil phase whereas at low temperature it becomes more soluble in the water phase. Thus, at a constant surfactant concentration, the phase behaviour will change with temperature [9]. Thus with increasing temperature the surfactant's affinity to the oil phase increases and the system changes from Winsor I to Winsor III and finally to Winsor II, i.e. the emulsion will invert from an O/W to a W/O system at a particular temperature, referred to as the phase inversion temperature (PIT). At low temperature, over the Winsor I region, O/W emulsions can be easily formed and are quite stable. On raising the temperature the O/W emulsion stability decreases, and the macroemulsion finally resolves when the system reaches Winsor III state. Within this region, both O/W and W/O emulsions are unstable, with

the minimum stability in the balanced region. At higher temperature, over the Winsor II region, W/O emulsions become stable. This behaviour is always observed in nonionic systems if the surfactant concentration is above the cmc and the volume fractions of the components are not extreme. The macroemulsion's stability is essentially symmetrical with respect to the balanced point, just as the phase behaviour is. At positive spontaneous curvature, O/W emulsions are stable, while at negative spontaneous curvature, W/O emulsions are stable.

Chapter 13 deals with sedimentation of suspensions, creaming of emulsions and their prevention. Most suspensions undergo separation on standing as a result of the density difference between the particles and the medium, unless the particles are small enough for Brownian motion to overcome gravity. The process of creaming or sedimentation of emulsions is also the result of gravity, and occurs when the density of the droplets and the medium are not equal. When the density of the disperse phase is lower than that of the medium (as with most oil-in-water O/W emulsions), creaming occurs, whereas if the density of the disperse phase is higher than that of the medium (as with most W/O emulsions), sedimentation occurs. For a very dilute suspension or emulsion of rigid non-interacting particles or droplets, the rate of sedimentation or creaming υ_0 can be calculated by application of Stokes' law, whereby the hydrodynamic force is balanced by the gravitational force. For moderately concentrated suspensions or emulsions, $0.2 > \phi > 0.01$, sedimentation or creaming is reduced as a result of hydrodynamic interaction between the particles, which no longer sediment independently of each other. For more concentrated suspensions or emulsions ($\phi > 0.2$), the sedimentation velocity becomes a complex function of ϕ. At $\phi > 0.4$, one usually enters the hindered settling or creaming regime, in which all the particles or droplets sediment or cream at the same rate (independent of size). The sedimentation of particles or creaming of droplets in non-Newtonian fluids, such as aqueous solutions containing high molecular weight compounds (e.g. hydroxyethyl cellulose or xanthan gum), usually referred to as "thickeners", is not simple since these non-Newtonian solutions are shear thinning with viscosity decreasing as shear rate increases. These solutions show a Newtonian region at low shear rates or shear stresses, usually referred to as the residual or zero shear viscosity $\eta(0)$. The viscosity of a polymer solution increases gradually with increasing concentration and at a critical concentration, C^*, the polymer coils with a radius of gyration R_G and a hydrodynamic radius R_h (which is higher than R_G due to solvation of the polymer chains) begin to overlap and the polymer solution shows a rapid increase in viscosity. Thus, to predict sedimentation or creaming, one has to measure the viscosity at very low stresses (or shear rates). Usually one obtains good correlation between the rate of sedimentation or creaming υ and the residual viscosity $\eta(0)$. Above a certain value of $\eta(0)$, υ becomes equal to 0. Clearly, to minimize creaming or sedimentation one has to increase $\eta(0)$; an acceptable level for the high shear viscosity η_∞ must be achieved, depending on the application. In some cases, a high $\eta(0)$ may be accompanied by a high η_∞ (which may not be acceptable for the application). The stress exerted by the particles or droplets is

very small, in the region of 10^{-3}–10^{-1} Pa depending on the particle or droplet size and the density of the particles or droplets. Clearly, to predict sedimentation, one needs to measure the viscosity at these low stresses. The situation with more practical dispersions is more complex due to the interaction between the thickener and the particles or droplets. Most practical suspensions or emulsions show some weak flocculation and the "gel" produced between the particles or droplets and thickener may undergo some contraction as a result of the gravity force exerted on the whole network. A useful method to describe separation in these concentrated suspensions or emulsions is to follow the relative sediment volume V_t/V_0 or relative sediment height h_t/h_0 (where the subscripts t and 0 refer to time t and time zero respectively) with storage time. For good physical stability the values of V_t/V_0 or h_t/h_0 should be as close as possible to unity (i.e. minimum separation). This can be achieved by balancing the gravitational force exerted by the gel network with the bulk "elastic" modulus of the suspension. The latter is related to the high frequency modulus G'.

Several methods can be applied for reducing sedimentation or creaming:

(i) Balancing the density of the disperse phase and the medium. It is clear from Stokes' law that if $\Delta\rho = 0$, $\upsilon_0 = 0$. This method can be applied only when the density of the particles or droplets is not much larger or smaller than that of the medium (e.g. $\Delta\rho \approx 0.1$). By dissolving an inert substance in the continuous phase, such as sugar or glycerol, one may achieve density matching to prevent sedimentation of particles. With emulsions where the oil density is lower than that of the medium, it is possible to mix the oil with a more dense oil to achieve density matching with the continuous phase. However, apart from its limitation to particles with density not much larger than the medium and droplets with density not much smaller than the medium, the method is not very practical since density matching can only occur at one temperature. Liquids usually have large thermal expansion, whereas densities of solids vary comparatively little with temperature.

(ii) Reduction of particle or droplet size; if R is significantly reduced (to values below 0.1 μm), Brownian diffusion can overcome the gravity force and no sedimentation or creaming occurs. This is the principle of formation of nanosuspensions and nanoemulsions.

(iii) Use of high molecular weight thickeners; high molecular weight materials, such as hydroxyethyl cellulose or xanthan gum, when added above a critical concentration (at which polymer coil overlap occurs) will produce very high viscosity at low stresses or shear rates (usually in excess of several hundred Pa s) and this will prevent sedimentation of the particles or creaming of droplets. In relatively concentrated suspensions or emulsions, the situation becomes more complex, since the polymer molecules may lead to flocculation of the suspension or emulsion by bridging, depletion (see below), etc. Moreover, the polymer chains at high concentrations tend to interact with each other above a critical concentration C^* (the so-called "semi-dilute" region discussed above). Such interaction leads to viscoelasticity, where the flow behaviour shows an elastic component characterized by an elastic modulus G'

(energy elastically stored during deformation) and a viscous component G'' (loss modulus resulting from energy dissipation during flow). The elastic behaviour of such relatively concentrated polymer solutions plays a major role in reducing settling and preventing formation of dilatant clays as well as reducing creaming and formation of compact cream layers. A good example of such a viscoelastic polymer solution is that of xanthan gum, a high molecular weight polymer (molecular weight in excess of 10^6 Daltons). This polymer shows viscoelasticity at relatively low concentration (< 0.1 %) as a result of the interaction of the polymer chains, which are very long. This polymer is very effective in reducing settling of coarse suspensions at low concentrations (in the region of 0.1–0.4 % depending on the volume fraction of the suspension).

(iv) Use of associative thickeners, i.e. hydrophobically modified polymer molecules in which alkyl chains (C_{12}–C_{16}) are either randomly grafted on a hydrophilic polymer molecule such as hydroxyethyl cellulose (HEC) or simply grafted at both ends of the hydrophilic chain. An example of hydrophobically modified HEC is Natrosol plus (Hercules) which contains 3–4 C_{16} randomly grafted onto hydroxyethyl cellulose. Another example of polymer that contains two alkyl chains at both ends of the molecule is HEUR (Rohm and Haas) that is made of polyethylene oxide (PEO) that is capped at both ends with linear C_{18} hydrocarbon chains. These hydrophobically modified polymers form gels when dissolved in water. Gel formation can occur at relatively lower polymer concentrations when compared with the unmodified molecule. The most likely explanation of gel formation is due to hydrophobic bonding (association) between the alkyl chains in the molecule. This effectively causes an apparent increase in the molecular weight. These associative structures are similar to micelles, except the aggregation numbers are much smaller. The viscosity of hydrophobically modified polymers shows a rapid increase at critical concentration, which may be defined as the critical aggregation concentration (CAC). Above CAC, the polymer solution shows non-Newtonian flow (shear thinning behaviour) and its shows a high viscosity at low shear rates. With increasing polymer concentrations above CAC, the zero shear viscosity increases with increasing polymer concentration. These hydrophobically modified polymers are also viscoelastic.

(v) Controlled flocculation; the total energy–distance of separation curve for electrostatically stabilized emulsions shows a shallow minimum (secondary minimum) at relatively long distance of separation between the droplets. By addition of small amounts of electrolyte such a minimum can be made sufficiently deep for weak flocculation to occur. The same applies for sterically stabilized emulsions, which show only one minimum, whose depth can be controlled by reducing the thickness of the adsorbed layer. This can be obtained by reducing the molecular weight of the stabilizer and/or addition of a nonsolvent for the chains (e.g. electrolyte). This phenomenon of weak flocculation may be applied to reduce creaming or sedimentation, in particular for concentrated suspensions or emulsions.

(vi) Depletion flocculation; addition of free nonadsorbing polymer can produce weak flocculation above a critical volume fraction of the free polymer, ϕ_p^+, which de-

pends on its molecular weight and the volume fraction of suspension. This weak flocculation produces a "gel" structure that reduces sedimentation.

(vii) Use of "inert" fine particles; several fine particulate inorganic material produce "gels" when dispersed in aqueous media, e.g. sodium montmorillonite or silica. These particulate materials produce three-dimensional structures in the continuous phase as a result of interparticle interaction. For example, sodium montmorillonite (referred to as swellable clay) forms gels at low and intermediate electrolyte concentrations. A mechanism of montmorillonite's gel formation involving interaction of the oppositely charged double layers at the faces and edges of the clay particles has been suggested. This structure, which is usually referred to as a "card-house" structure, was considered to be the reason for the formation of the voluminous clay gel. It was also suggested that the voluminous gel is the result of the extended double layers, particularly at low electrolyte concentrations. Finely divided silica, such as Aerosil 200 (produced by Degussa), produces gel structures by simple association (by van der Waals attraction) of the particles into chains and cross chains. When incorporated into the continuous phase of a suspension, these gels prevent sedimentation.

(viii) Use of mixtures of polymers and finely divided particulate solids; by combining thickeners such as hydroxyethyl cellulose or xanthan gum with particulate solids such as sodium montmorillonite, a more robust gel structure can be produced. By using such mixtures, the concentration of the polymer can be reduced, thus overcoming the problem of dispersion on dilution (e.g. with many agrochemical suspension concentrates). This gel structure may be less temperature dependent and can be optimized by controlling the ratio of the polymer and the particles. If these combinations of, say, sodium montmorillonite and a polymer such as hydroxyethyl cellulose, polyvinyl alcohol (PVA) or xanthan gum, are balanced properly, they can provide a "three-dimensional structure", which entraps all the particles and stops settling and formation of dilatant clays. The mechanism of gelation of such combined systems depends to a large extent on the nature of the solid particles, the polymer and the conditions. If the polymer adsorbs on the particle surface (e.g. PVA on sodium montmorillonite or silica) a three-dimensional network may be formed by polymer bridging. Under conditions of incomplete coverage of the particles by the polymer, the latter becomes simultaneously adsorbed on two or more particles. In other words, the polymer chains act as "bridges" or "links" between the particles.

(ix) Use of liquid crystalline phases; surfactants produce liquid crystalline phases at high concentrations [5]. Three main types of liquid crystals can be identified: hexagonal phase (sometimes referred to as middle phase), cubic phase and lamellar (neat phase). All these structures are highly viscous and they also show an elastic response. If produced in the continuous phase of suspensions, they can eliminate sedimentation of the particles or creaming of emulsions. These liquid crystalline phases are particularly useful for applications in liquid detergents which contain high surfactant concentrations. Their presence reduces sedimentation of the coarse builder particles (phosphates and silicates).

Chapter 14 deals with the flow characteristics (rheology) of dispersions. The rheology of dispersions can be applied for evaluating the stability/instability of the dispersion without any dilution (which can cause significant changes in the structure of the system) and this requires carefully designed techniques that should cause as little disturbance to the structure as possible [8]. These measurements provide accurate information on the state of the system such as its flocculation, coalescence (with emulsions) or creaming. These measurements can also be applied for predicting the long-term physical stability of the dispersion. In this chapter, I will start with a description of the various rheological techniques that can be applied to study the state of the dispersion. This is followed by an analysis of the rheological behaviour of different dispersions. Four main types of systems will be considered, namely hard-sphere dispersions (where both repulsion and attraction are screened), electrostatically stabilized dispersions (where the rheology is mainly determined by double layer repulsion), sterically stabilized dispersions (where the rheology is determined by steric repulsion) and flocculated dispersions. In the latter case a distinction will be made between weakly and strongly flocculated systems. Four different types of rheological techniques can be applied:

(i) Steady state shear stress σ – shear rate γ measurements. In this case, the dispersion is placed in the gap between two concentric cylinders, two parallel plates or a cone and plate geometry. In the latter geometry, the cone is truncated to avoid damage to the tip of the cone and to have a sufficient gap in order to avoid grinding of the dispersion. The inner cylinder or the cone is subjected to an angular rotation Ω which allows one to calculate the shear rate $\dot{\gamma}$. The torque M on the outer cylinder or the plate is measured and this allows one to obtain the stress σ. This requires the use of a shear rate controlled instrument. Models for the analysis of flow curves are described, namely Newtonian, Bingham plastic, pseudoplastic (shear thinning) and dilatant (shear thickening) systems. The time effects during flow, namely thixotropy and negative (or anti-) thixotropy are described.

(ii) Strain relaxation after sudden application of stress, i.e. constant stress (creep) measurements. A constant stress σ is applied on the system (that may be placed in the gap between two concentric cylinders or a cone and plate geometry) and the strain (relative deformation) γ or compliance J ($= \gamma/\sigma$, Pa^{-1}) is followed as a function of time for a period of t. At $t = t$, the stress is removed and the strain γ or compliance J is followed for another period t [8].

(iii) Stress relaxation after sudden application of strain. In this case a small strain is rapidly applied within a very short period of time (that must be smaller than the relaxation time of the system) and is kept at a constant value. The shear rate remains constant within this period [8]. The stress or modulus is followed as a function of time.

(iv) Dynamic (oscillatory) measurements [8]. This is the response of the material to an oscillating stress or strain. When a sample is constrained in, say, a cone and plate or concentric cylinder assembly, an oscillating strain at a given frequency ω (rad s^{-1}) ($\omega = 2\nu\pi$, where ν is the frequency in cycles s^{-1} or Hz) can be applied to the sample.

After an initial start-up period, a stress develops in response to the applied strain, i.e. it oscillates with the same frequency. The change of the sine waves of the stress and strain with time can be analysed to distinguish between elastic, viscous and viscoelastic response. The analysis of the resulting sine waves can be used to obtain the various viscoelastic parameters.

The next section deals with rheology of dispersions; rheological measurements are useful tools for probing the microstructure of dispersions [8]. This is particularly the case if measurements are carried out at low stresses or strains. The ratio of the structural relaxation time to the experimental measurement time is given by the dimensionless Deborah number *De* which is ≈ 1 and the dispersion is viscoelastic. The rheology of dispersions depends on the balance between three main forces [8], namely Brownian diffusion, hydrodynamic interaction and interparticle forces. These forces are determined by three main parameters:

(i) the volume fraction ϕ (total volume of the particles divided by the volume of the dispersion);
(ii) the particle size and shape distribution;
(iii) the net energy of interaction G_T, i.e. the balance between repulsive and attractive forces.

The earliest theory for predicting the relationship between the relative viscosity η_r and ϕ was described by Einstein and is applicable to $\phi \leq 0.01$. When $\phi > 0.01$, hydrodynamic interaction between the particles becomes important. When the particles come close to each other the nearby stream lines and the disturbance of the fluid around one particle interact with those around a moving particle and an expression for the relative viscosity can be derived by taking into account this hydrodynamic interaction. When $\phi > 0.2$, η_r becomes a complex function of ϕ. At such high volume fractions the system mostly shows non-Newtonian flow ranging from viscous to viscoelastic to elastic response. Three responses can be considered:

(i) viscous response;
(ii) elastic response;
(iii) viscoelastic response.

These responses for any dispersion depend on the time or frequency of the applied stress or strain. Four different types of systems (with increasing complexity) can be considered [8]:

(i) Hard-sphere dispersions: where both repulsive and attractive forces are screened.
(ii) Systems with "soft" interaction that contain electrical double layers with long-range repulsion. The rheology of the dispersion is determined mainly by the double layer repulsion.
(iii) Sterically stabilized dispersions where the rheology is determined by the steric repulsion produced by adsorbed nonionic surfactant or polymer layers. The inter-

action can be "hard" or "soft" depending on the ratio of adsorbed layer thickness to particle radius (δ/R).

(iv) Flocculated systems where the net interaction is attractive. One can distinguish between weak (reversible) and strong (irreversible) flocculation depending on the magnitude of the attraction.

Volume 2 consists of nine chapters. Chapter 1 deals with formulation of solid/liquid dispersions (suspensions). There are two main processes for the preparation of suspensions [9]. The first depends on the "build-up" of particles from molecular units, i.e. the so-called "bottom-up" or condensation method, which involves two main processes, namely nucleation and growth. In this case, it is necessary first to prepare a molecular (ionic, atomic or molecular) distribution of the insoluble substances; then by changing the conditions precipitation is caused leading to the formation of nuclei that grow to the particles in question. A particular case of the condensation process is the preparation of polymer latex particles by emulsion or suspension polymerization. The second procedure for preparing suspension concentrates is usually referred to as the "top-down" or dispersion process. Dispersion is a process in which aggregates and agglomerates of powders are dispersed into "individual" units, usually followed by a wet milling process (to subdivide the particles into smaller units) and stabilization of the resulting dispersion against aggregation and sedimentation. The larger "lumps" of the insoluble substances are subdivided by mechanical or other means into smaller units. In the whole "top-down" process, it is essential to wet both the external and internal surfaces of the aggregates and agglomerates. For hydrophobic solids dispersed in aqueous media, it is essential to use a wetting agent (surfactant) that lowers the surface tension of water (under dynamic conditions) and reduces the solid/liquid interfacial tension by adsorption on the surface of the particles. After wetting, the aggregates and agglomerates are dispersed into single particles by high-speed mixing. The resulting suspension, referred to as "mill base", is then subjected to a milling process to reduce the particle size to the desired value [9].

Once a suspension is prepared, it is necessary to control its properties on storage. Three main aspects must be considered. Firstly, control of its colloid stability which requires the presence of a repulsive energy that overcomes the permanent van der Waals attraction. Three main types of stabilization may be considered:

(i) electrostatic repulsion produced by the presence of electrical double layers surrounding the particles [2];

(ii) steric repulsion produced by adsorption of nonionic surfactants or polymeric surfactants. These surfactants consist of an "anchor" chain(s) that strongly adsorbs on the particle surface and stabilizing chain(s) that remains in solution and becomes strongly solvated by the molecules of the medium [6]. One can define an adsorbed layer thickness δ which increases with increasing molar mass of the stabilizing chain(s);

(iii) electrosteric stabilization where G_{elec} and G_s are combined with G_A. In this case the G_T–h curve shows a shallow minimum at large h values, a maximum at intermediate distances and a sharp increase at distances comparable to 2δ.

Electrosteric stabilization is generally produced when using polyelectrolytes to stabilize the suspension or when using a mixture of nonionic or polymeric surfactant with an ionic one. The second property that must be controlled is the process of Ostwald ripening (crystal growth) that occurs with most suspensions of organic substances [9]. Organic substances have a finite solubility in the medium that may reach several hundred ppm (parts per million). The smaller particles with higher radius of curvature have a higher solubility when compared with the larger particles. This difference in solubility between small and large particles is the driving force for Ostwald ripening. With time, molecular diffusion occurs from the small to the large particles with the ultimate dissolution of these small particles and their molecules become deposited on the larger particles. Thus, on storage of the suspension, the particle size distribution shifts to larger particles. This will result in instability of the suspension, e.g. enhanced sedimentation. Another mechanism of Ostwald ripening is due to polymorphic changes. The particles (e.g. a drug) may contain two or more polymorphs with different solubility. The more stable polymorph has a lower solubility when compared with the metastable polymorph. With time, the more soluble polymorph gradually changes to the less soluble stable one. This Ostwald ripening problem may result in reduced bioavailability of the drug and hence it must be minimized or eliminated. Several methods can be applied to reduce Ostwald ripening in suspensions, e.g. incorporation of impurities that strongly adsorb on the particle surface, thus blocking the active sites for growth. Alternatively, one can use strongly adsorbed polymeric surfactants, which has the same effect as the added impurities. The third instability problem with suspensions is particle sedimentation [9], which occurs when the particle size is outside the colloid range and the density difference between the particles and the medium is significant. In this case the gravity force $(4/3)\pi R^3 \Delta\rho g h$ (where R is the particle radius, $\Delta\rho$ is the density difference between the particle and the medium, g is the gravity force and h is the height of the container) exceeds the Brownian motion kT (where k is the Boltzmann constant and T is the absolute temperature). With most practical suspensions with a wide particle size distribution, the larger particles sediment at a higher rate than the smaller particles. A particle concentration gradient of the particles occurs across the container. Several methods may be applied to reduce sedimentation, e.g. balancing the density of the disperse phase with that of the medium, reducing particle size (i.e. formation of nanosuspensions) and adding thickeners. The latter can be high molecular weight polymers such as xanthan gum, or addition of "inert" fine particles such as silica or clays. In all case these thickeners produce a "gel network" in the continuous phase which produces a very high viscosity at low shear rates that prevents particle sedimentation.

Chapter 2 deals with formulation of liquid/liquid dispersions (emulsions) [10]. Several breakdown processes may occur on storage depending on droplet size distribution and density differences between the droplets and the medium, magnitude of the attractive versus repulsive forces which determines flocculation, solubility of the disperse droplets and the particle size distribution which determines Ostwald ripening, stability of the liquid film between the droplets that determines coalescence, phase inversion, where the two phases exchange, e.g. an O/W emulsion inverting to W/O and vice versa. Phase inversion can be catastrophic as is the case when the oil phase in an O/W emulsion exceeds a critical value. The inversion can be transient, for example when the emulsion is subjected to a temperature increase. The thermodynamics of emulsion formation and breakdown is considered by the balance between the increase in interfacial energy $\Delta A\gamma_{12}$ (where ΔA is the increase in interfacial area when the bulk oil is subdivided into a large number of droplets and ΔS^{conf} is the increase in entropy). In most cases $\Delta A\gamma_{12} \gg T\Delta S^{\text{conf}}$, which means that the free energy of formation of the emulsion ΔG^{form} is positive, i.e. the formation of emulsions is nonspontaneous and the system is thermodynamically unstable. In the absence of any stabilization mechanism, the emulsion will break down by flocculation and coalescence. In this case there are no free energy barriers either to flocculation or coalescence. In the presence of a stabilizer (surfactant and/or polymer), an energy barrier is created between the droplets and therefore the emulsion becomes kinetically stable. The interaction forces between emulsion droplets and factors affecting their stability are described. There are three main interaction forces between emulsion droplets, namely van der Waals attraction, electrostatic (double layer) repulsion and steric repulsion. The mechanism of emulsification and the role of the emulsifier are described. An important role of the emulsifier is to prevent coalescence during emulsification. This is certainly not due to the strong repulsion between the droplets, since the pressure at which two drops are pressed together is much greater than the repulsive stresses. The counteracting stress must be due to the formation of interfacial tension gradients. The next section describes the methods of emulsification; these range from simple pipe flow (low agitation energy, L), static mixers (toothed devices such as the Ultra-Turrax and batch radial discharge mixers such as the Silverson mixers) and general stirrers (low to medium energy, L–M), colloid mills and high pressure homogenizers (high energy, H), ultrasound generators (M–H) and membrane emulsification methods. The method of preparation can be continuous (C) or batchwise (B): pipe flow – C; static mixers and general stirrers and – B, C; colloid mill and high pressure homogenizers – C; ultrasound – B, C. The next section deals with the methods that can be applied for selection of emulsifiers. Several surfactants and their mixtures are used for the preparation and stabilization of oil-in-water (O/W) and water-in-oil (W/O) emulsions. Two general methods can be applied for selecting emulsifiers, namely the hydrophilic-lipophilic balance (HLB) and the phase inversion temperature (PIT) concepts. The hydrophilic-lipophilic balance (HLB number) is a semi-empirical scale for selecting surfactants [10]. This scale is based on the rela-

tive percentage of hydrophilic to lipophilic (hydrophobic) groups in the surfactant molecule(s). For an O/W emulsion droplet, the hydrophobic chain resides in the oil phase whereas the hydrophilic head group resides in the aqueous phase. For a W/O emulsion droplet, the hydrophilic group(s) reside in the water droplet, whereas the lipophilic groups reside in the hydrocarbon phase. For an O/W emulsion the HLB range is 8–18, whereas for a W/O emulsion it is 3–6. The HLB number depends on the nature of the oil. The relative importance of the hydrophilic and lipophilic groups was first recognized when using mixtures of surfactants containing varying proportions of a low and a high HLB number. The efficiency of any combination (as judged by phase separation) was found to pass a maximum when the blend contained a particular proportion of the surfactant with the higher HLB number. The average HLB number may be calculated from additivity. Simple equations can be used for calculating the HLB number of relatively simple nonionic surfactants. These simple equations cannot be used for surfactants containing propylene oxide or butylene oxide. Nor can they be applied for ionic surfactants. A method for calculating the HLB number for surfactants from their chemical formulae has been developed, using empirically determined group numbers. A group number is assigned to various component groups. Various procedures have been developed to determine the HLB of different surfactants. A correlation between the HLB and the cloud points of 5% aqueous solution of ethoxylated surfactants has been reported. A titration procedure was developed [10] for estimating the HLB number. Gas-liquid chromatography can also be applied for determining the HLB number. The phase inversion temperature (PIT) concept was developed since many O/W emulsions stabilized with nonionic surfactants undergo a process of inversion at a critical temperature (PIT). The PIT can be determined by following the emulsion conductivity (small amount of electrolyte is added to increase the sensitivity) as a function of temperature. The conductivity of the O/W emulsion increases with increasing temperature until the PIT is reached, above which there will be a rapid reduction in conductivity (a W/O emulsion is formed). The PIT is influenced by the HLB number of the surfactant [10]; for any given oil, the PIT increases with increasing HLB number. The size of the emulsion droplets was found to depend on the temperature and HLB number of the emulsifiers. The droplets are less stable towards coalescence close to the PIT. However, by rapid cooling of the emulsion a stable system may be produced. Relatively stable O/W emulsions were obtained when the PIT of the system was 20–65 °C higher than the storage temperature. Emulsions prepared at a temperature just below the PIT followed by rapid cooling generally have smaller droplet sizes. This can be understood if one considers the change of interfacial tension with temperature. The interfacial tension decreases with increasing temperature reaching a minimum close to the PIT, after which it increases. Thus, the droplets prepared close to the PIT are smaller than those prepared at lower temperatures. These droplets are relatively unstable towards coalescence near the PIT, but by rapid cooling of the emulsion one can retain the smaller size. This procedure may be applied to prepare mini- (nano-)emulsions. At a given HLB value,

stability of the emulsion against coalescence increases markedly as the molar mass of both the hydrophilic and lipophilic components increases. The enhanced stability using high molecular weight surfactants (polymeric surfactants) can be understood from a consideration of the steric repulsion which produces more stable films. Films produced using macromolecular surfactants resist thinning and disruption, thus reducing the possibility of coalescence. The emulsions showed maximum stability when the distribution of the PEO chains was broad. The cloud point is lower but the PIT is higher than in the corresponding case for narrow size distributions. The PIT and HLB number are directly related parameters. Addition of electrolytes reduces the PIT and hence an emulsifier with a higher PIT value is required when preparing emulsions in the presence of electrolytes. Electrolytes cause dehydration of the PEO chains and in effect this reduces the cloud point of the nonionic surfactant. One needs to compensate for this effect by using a surfactant with higher HLB. The optimum PIT of the emulsifier is fixed if the storage temperature is fixed. The next section deals with emulsion instability and its prevention. Five processes of instability must be considered:

(i) Creaming/sedimentation of emulsions which is the result of gravity when the density of the droplets and the medium are not equal. When the density of the disperse phase is lower than that of the medium (as with most oil-in-water O/W emulsions), creaming occurs, whereas if the density of the disperse phase is higher than that of the medium (as with most W/O emulsions), sedimentation occurs. The rate of creaming or sedimentation υ_0 can be calculated by equating the hydrodynamic force with the gravity force. For very dilute noninteracting emulsion droplets with radius R and density difference from the medium $\Delta\rho$, the rate can be calculated using Stokes' law. For moderately concentrated emulsions ($0.2 > \phi > 0.1$), one has to take into account the hydrodynamic interaction between the droplets and the Stokes' rate is reduced to v. For more concentrated emulsions ($\phi > 0.2$), the rate of creaming or sedimentation becomes a complex function of ϕ which shows that v decreases with increasing ϕ and ultimately it approaches zero when ϕ exceeds a critical value, ϕ_p, which is the so-called "maximum packing fraction". The value of ϕ_p for monodisperse "hard spheres" ranges from 0.64 (for random packing) to 0.74 for hexagonal packing. The value of ϕ_p exceeds 0.74 for polydisperse systems. Also for emulsions which are deformable, ϕ_p can be much larger than 0.74. When ϕ approaches ϕ_p, η_r approaches ∞. In practice, most emulsions are prepared at ϕ values well below ϕ_p, usually in the range 0.2–0.5, and under these conditions creaming or sedimentation is the rule rather than the exception. Several procedures may be applied to reduce or eliminate creaming or sedimentation as discussed above.

(ii) Flocculation of emulsions in which the emulsion drops aggregate, without rupture of the stabilizing layer at the interface, if the pair interaction free energy becomes appreciably negative at a certain separation. This negative interaction is the result of van der Waals attraction G_A that is universal for all disperse systems. The flocculation of sterically stabilized emulsions occurs when the solvency of the medium

for the stabilizing chain becomes worse than a θ-solvent or the Flory–Huggins interaction parameter $\chi > 0$. The Flory–Huggins interaction parameter χ may be conveniently changed by varying the temperature, adding a nonsolvent or increasing the electrolyte concentration in the external phase. Depletion flocculation can occur on addition of "free" nonadsorbing polymer [6]. Flocculation of emulsions can be reduced by controlling the parameters that affect their stabilization. For charge stabilized emulsions, e.g. using ionic surfactants, the most important criterion is to make G_{max} as high as possible; this is achieved by three main conditions, namely high surface or zeta potential, low electrolyte concentration and low valency of ions. For sterically stabilized emulsions, four main criteria are necessary [6]:

(a) Complete coverage of the droplets by the stabilizing chains.
(b) Firm attachment (strong anchoring) of the chains to the droplets. This requires the chains to be insoluble in the medium and soluble in the oil. However, this is incompatible with stabilization requiring a chain that is soluble in the medium and strongly solvated by its molecules. These conflicting requirements are solved by the use of A–B, A–B–A block or BA_n graft copolymers (B is the "anchor" chain and A is the stabilizing chain(s)). Examples for the B chains for O/W emulsions are polystyrene, polymethylmethacrylate, polypropylene oxide and alkyl polypropylene oxide. For the A chain(s), polyethylene oxide (PEO) or polyvinyl alcohol are good examples. For W/O emulsions, PEO can form the B chain, whereas the A chain(s) could be polyhydroxy stearic acid (PHS) which is strongly solvated by most oils.
(c) Thick adsorbed layers; the adsorbed layer thickness should be in the region of 5–10 nm. This means that the molecular weight of the stabilizing chains could be in the region of 1,000–5,000.
(d) The stabilizing chain should be maintained in good solvent conditions ($\chi < 0.5$) under all conditions of temperature changes on storage.

(iii) Ostwald ripening in emulsions and its prevention. The driving force of Ostwald ripening is the difference in solubility between the smaller and larger droplets [10]. The small droplets with radius r_1 will have higher solubility than the larger droplet with radius r_2. Thus with time, molecular diffusion will occur between the smaller and larger droplets, with the ultimate disappearance of most of the small droplets. This results in a shift in the droplet size distribution to larger values on storage of the emulsion. This could lead to the formation of a dispersion droplet size > μm. This instability can cause severe problems, such as creaming or sedimentation, flocculation and even coalescence of the emulsion. Several methods can be applied to reduce Ostwald ripening: Addition of a second disperse phase which is virtually insoluble in the continuous phase, such as squalane, can significantly reduce the Ostwald ripening rate. In this case, significant partitioning between different droplets is predicted, with the component having the low solubility in the continuous phase (e.g. squalane) being expected to be concentrated in the smaller droplets. During Ostwald ripening

in a two-component disperse system, equilibrium is established when the difference in chemical potential between different sized droplets, which results from curvature effects, is balanced by the difference in chemical potential resulting from partitioning of the two components. The second method that can be applied to reduce Ostwald ripening is to modify the interfacial layer. The Ostwald ripening rate ω is directly proportional to the interfacial tension γ. Thus by reducing γ, ω is reduced. Also the rate is reduced by the use of surfactants that are strongly adsorbed at the interface and which do not desorb during the Ostwald ripening process. In this case an increase in interfacial dilational modulus ε and decreases in interfacial tension γ would be observed for the shrinking droplets. Eventually the difference in ε and γ between droplets would balance the difference in capillary pressure (i.e. curvature effects) leading to a quasi-equilibrium state. In this case, emulsifiers with low solubilities in the continuous phase such as proteins would be preferred. Long chain phospholipids with a very low solubility (cmc $\approx 10^{-10}$ mol dm^{-3} are also effective in reducing Ostwald ripening of some emulsions. The phospholipid would have to have a solubility in water about three orders of magnitude lower than the oil [10].

(iv) Emulsion coalescence and its prevention. When two emulsion droplets come in close contact in a floc or creamed layer or during Brownian diffusion, a thin liquid film or lamella forms between them [10]. Coalescence results from the rupture of this film. If the film cannot be ruptured, adhesion or engulfment may occur. Film rupture usually commences at a specified "spot" in the lamella, arising from thinning in that region. The liquid surfaces undergo some fluctuations forming surface waves. The surface waves may grow in amplitude and the apices may join as a result of the strong van der Waals attraction (the film thickness is smallest at the apex). The same applies if the film thins to a small value (critical thickness for coalescence). In order to understand the behaviour of these films, one has to consider two aspects of their physics, namely the nature of the forces acting across the film; these determine whether the film is thermodynamically stable, metastable or unstable; and the kinetic aspects associated with local (thermal or mechanical) fluctuations in film thickness. The rate of coalescence is proportional to the number of contact points between the droplets in an aggregate. Both flocculation and coalescence are taken into account simultaneously. The rate of coalescence follows a first-order kinetics. Several methods can be applied to reduce coalescence. It has long been known that mixed surfactants can have a synergistic effect on emulsion stability, with respect to coalescence rates. The enhanced stability was assumed to be associated with the formation of a densely packed interfacial layer. The maximum effect is obtained when using a water-soluble surfactant (cetyl sulphate) and an oil-soluble surfactant (cetyl alcohol), sometimes referred to as cosurfactant, in combination. Suitable combinations lead to enhanced stability as compared to the individual components. These mixed surfactant films also produce a low interfacial tension, in the region of 0.1 mN m^{-1} or lower. This reduction in interfacial tension may be due to the cooperative adsorption of the two surfactant molecules, as predicted by the Gibbs adsorption equation for multicomponent

systems. The surfactant mixture also gives a very high Gibbs elasticity. A correlation between film elasticity and coalescence rate has been observed for O/W emulsions stabilized with proteins [10]. A high interfacial viscosity could account for the stability of liquid films. This must play a role under dynamic conditions, i.e. when two droplets approach each other. Under static conditions, the interfacial viscosity does not play a direct role. However, a high interfacial viscosity is often accompanied by a high interfacial elasticity and this may be an indirect contribution to the increased stability of the emulsion. Another possible explanation of the enhanced stability in the presence of mixed surfactants could be connected to the hindered diffusion of the surfactant molecules in the condensed film. This would imply that the desorption of surfactant molecules is hindered on the approach of two emulsion droplets, and hence thinning of the film is prevented. Another effect of using surfactant mixtures is to produce liquid crystalline phase formation. These structures can form, for example, in a three-component system of surfactant, alcohol and water. The lamellar liquid crystalline phase is particularly important for stabilizing the emulsion against coalescence. In this case the liquid crystals "wrap" around the droplets in several layers. These multilayers form a barrier against coalescence. An effective method to reduce coalescence is to use polymeric surfactants. The most convenient polymeric surfactants are those of the block and graft copolymer type. A block copolymer is a linear arrangement of blocks of variable monomer composition.

(v) Phase inversion and its prevention. This is the process whereby the internal and external phase of an emulsion suddenly invert, e.g. O/W to W/O or vice versa [10]. Catastrophic inversion is induced by increasing the volume fraction of the disperse phase. This type of inversion is not reversible [10]; the value of the water: oil ratio at the transition when oil is added to water is not the same as that when water is added to oil. The inversion point depends on the intensity of agitation and the rate of liquid addition to the emulsion. Phase inversion can also be transitional induced by changing factors which affect the HLB of the system, e.g. temperature and/or electrolyte concentration. The average droplet size decreases and the emulsification rate (defined as the time required to achieve a stable droplet size) increases as inversion is approached. Both trends are consistent with O/W interfacial tension reaching a minimum near the inversion point.

Chapter 3 deals with formulation of foams that consist of gas bubbles separated by liquid layers [11]. Because of the significant density difference between the gas bubbles and the medium, the system quickly separates into two layers with the gas bubbles rising to the top, which may undergo deformation to form polyhedral structures. Pure liquids cannot foam unless a surface active material, mostly a surfactant, is present. When a gas bubble is introduced below the surface of a liquid, it burst almost immediately as a soon as the liquid has drained away. With dilute surfactant solutions, as the liquid/air interface expands and the equilibrium at the surface is disturbed, a resorting force is set up which tries to establish the equilibrium. The restoring force arises from the Gibbs–Marangoni effect. As a result of the presence of surface tension

gradients dγ (due to incomplete coverage of the film by surfactant), a dilational elasticity ε is produced (Gibbs elasticity). This surface tension gradient induces flow of surfactant molecules from the bulk to the interface and these molecules carry liquid with them (the Marangoni effect). The Gibbs–Marangoni effect prevents thinning and disruption of the liquid film between the air bubbles and this stabilizes the foam. Several surface active foaming materials may be distinguished, e.g. ionic, nonionic and zwitterionic surfactants, polymers (polymeric surfactants). Particles that accumulate at the air/solution interface can also stabilize the foam. In some cases, specifically adsorbed cations or anions from inorganic salts may also stabilize the foam bubbles. Many of the surfactants can cause foaming at extremely low concentrations (as low as 10^{-9} mol dm^{-3}). In kinetic terms, foams may be classified into two main types, namely unstable, transient foams (lifetime of seconds) and metastable or permanent foams (lifetimes of hours or days). The next section deals with foam preparation. Like most disperse systems, foams can be obtained by condensation (top-down) and dispersion (bottom-up) methods. The most commonly applied technique for generating foam is by a simple dispersion technique (mechanical shaking or whipping). This method is not satisfactory since accurate control of the amount of air incorporated is difficult to achieve. The most convenient method is to pass a flow of gas (sparging) through an orifice with well-defined radius r_o. The next section deals with foam structure. Two main types of foams may be distinguished [11]:

(i) Spherical foam ("Kugelschaum") consisting of gas bubbles separated by thick films of viscous liquid produced in freshly prepared systems. This may be considered a temporary dilute dispersion of bubbles in the liquid.
(ii) Polyhedral gas cells produced on aging; thin flat "walls" are produced with junction points of the interconnecting channels (Plateau borders). Due to the interfacial curvature, the pressure is lower and the film is thicker in the Plateau border. A capillary suction effect of the liquid occurs from the centre of the film to its periphery.

Another mechanism of foam instability is due to Ostwald ripening (disproportionation). The driving force for this process is the difference in Laplace pressure between the small and the larger foam bubbles. The smaller bubbles have higher Laplace pressure than the larger ones. The gas solubility increases with pressure and hence gas molecules will diffuse from the smaller to the larger bubbles. This process only occurs with spherical foam bubbles. This process may be opposed by the Gibbs elasticity effect. Alternatively, rigid films produced using polymers may resist Ostwald ripening as a result of the high surface viscosity. With polyhedral foam with planer liquid lamella, the pressure difference between the bubbles is not large and hence Ostwald ripening is not the mechanism for foam instability in this case. With polyhedral foam, the main driving force for foam collapse is the surface forces that act across the liquid lamella. To keep the foam stable (i.e. to prevent complete rupture of the film), this capillary suction effect must be prevented by an opposing "disjoining pressure" that acts be-

tween the parallel layers of the central flat film (see below). The generalized model for drainage involves the Plateau borders forming a "network" through which the liquid flows due to gravity. As with most disperse systems, all foams are thermodynamically unstable. For convenience, foams are classified according to the kinetics of their breakdown:

(i) Unstable (transient) foams with a lifetime of seconds. These are generally produced using "mild" surfactants, e.g. short chain alcohols, aniline, phenol, pine oil, short chain undissociated fatty acid. Most of these compounds are sparingly soluble and may produce a low degree of elasticity.
(ii) Metastable ("permanent") foams with a lifetime of hours or days. These metastable foams are capable of withstanding ordinary disturbances (thermal or Brownian fluctuations). They can collapse from abnormal disturbances (evaporation, temperature gradients, etc.).

These metastable foams are produced from surfactant solutions near or above the critical micelle concentration (cmc). Their stability is governed by the balance of surface forces. The film thickness is comparable to the range of intermolecular forces. In the absence of external disturbances, these foams may stay stable indefinitely. They are produced using proteins, long chain fatty acids or solid particles. Gravity is the main driving force for foam collapse, directly or indirectly through the Plateau border. Thinning and disruption may be opposed by surface tension gradients at the air/water interface. Alternatively, the drainage rate may be decreased by increasing the bulk viscosity of the liquid (e.g. addition of glycerol or polymers). Stability may be increased in some cases by the addition of electrolytes that produce a "gel network" in the surfactant film. Foam stability may also be enhanced by increasing the surface viscosity and/or surface elasticity. High packing of surfactant films (high cohesive forces) may also be produced using mixed surfactant films or surfactant/polymer mixtures. For investigating foam stability one must consider the role of the Plateau border under dynamic and static conditions. One should also consider foam films with intermediate lifetimes, i.e. between unstable and metastable foams. Gravity is the main driving force for film drainage. Gravity can act directly on the film or through capillary suction in the Plateau borders. As a general rule, the rate of drainage of foam films may be decreased by increasing the bulk viscosity of the liquid from which the foam is prepared. Several theories are available to describe foam stability:

(i) Surface viscosity and elasticity theory; the adsorbed surfactant film is assumed to control the mechanical-dynamical properties of the surface layers by virtue of its surface viscosity and elasticity. This concept may be true for thick films (> 100 nm) where intermolecular forces are less dominant (i.e. foam stability under dynamic conditions).
(ii) The Gibbs–Marangoni effect theory; the Gibbs coefficient of elasticity, ε, was introduced as a variable resistance to surface deformation during thinning.

(iii) Surface forces theory (disjoining pressure π); this theory operates under static (equilibrium) conditions in relatively dilute surfactant solutions ($h < 100$ nm). In the early stages of formation, foam films drain under the action of gravitation or capillary forces. Provided the films remain stable during this drainage stage, they may approach a thickness in the range of 100 nm. At this stage, surface forces come into play, i.e. the range of the surface forces now becomes comparable to the film thickness. The concept of disjoining pressure, which should remain positive to slow down further drainage and film collapse, is introduced. This is the principle of formation of thin metastable (equilibrium) films.
(iv) Stabilization by micelles (high surfactant concentrations > cmc); at high surfactant concentrations (above the cmc), micelles of ionic or nonionic surfactants can produce organized molecular structures within the liquid film. This will provide an additional contribution to the disjoining pressure.
(v) Stabilization by lamellar liquid crystalline phases; this is particularly the case with nonionic surfactants that produce a lamellar liquid crystalline structure in the film between the bubbles. These liquid crystals reduce film drainage as a result of the increase in viscosity of the film. In addition, the liquid crystals act as a reservoir of surfactant of the optimal composition to stabilize the foam.
(vi) Stabilization of foam films by mixed surfactants; a combination of surfactants gives slower drainage and improved foam stability. For example, mixtures of anionic and nonionic surfactants or anionic surfactant and long chain alcohol produce far more stable films than the single components.

The next section deals with foam inhibitors; two main types of inhibition may be distinguished, namely antifoamers that are added to prevent foam formation and deformers that are added to eliminate an existing foam. For example, alcohols such as octanol are effective as defoamers but ineffective as antifoamers. A summary of the various methods that can be applied for foam inhibition and foam breaking is given:
(i) Chemical inhibitors that lower viscosity and increase drainage.
(ii) Solubilized chemicals that cause antifoaming; solubilized antifoamers such as tributyl phosphate and methyl isobutyl carbinol when added to surfactant solutions such as sodium dodecyl sulphate and sodium oleate may reduce foam formation.
(iii) Droplets and oil lenses that cause antifoaming and defoaming; undissolved oil droplets form in the surface of the film and this can lead to film rupture. Several examples of oils may be used, namely alkyl phosphates, diols, fatty acid esters and silicone oils (polydimethyl siloxane).
(iv) Surface tension gradients (induced by antifoamers); some antifoamers act by eliminating the structure tension gradient effect in foam films by reducing the Marangoni effect.
(v) Hydrophobic particles as antifoamers; many solid particles with some degree of hydrophobicity have been shown to cause destabilization of foams, e.g. hydro-

phobic silica, PTFE particles. These particles exhibit a finite contact angle when adhering to the aqueous interface. It has been suggested that many of these hydrophobic particles can deplete the stabilizing surfactant film by rapid adsorption and can cause weak spots in the film.

(vi) Mixtures of hydrophobic particles and oils as antifoamers; the synergetic antifoaming effect of mixtures of insoluble hydrophobic particles and hydrophobic oils when dispersed in aqueous medium has been well established. These mixed antifoamers are very effective at very low concentrations (10–100 ppm). The hydrophobic particles could be hydrophobized silica and the oil is polydimethyl siloxane (PDMS).

Chapter 4 deals with formulation of gels; a gel is a "semi-solid" consisting of a "network" in which the solvent is "entrapped". It may be classified as a "liquid-in-solid" dispersion [8]. A gel shows some solid-like properties as well as liquid-like properties, i.e. it is a viscoelastic system. Depending on the gel strength, the system may behave as a viscoelastic solid or a viscoelastic liquid depending on the stress applied on the gel. For "strong" gels (such as those produced by chemical crosslinking) the system may behave as a viscoelastic solid up to high stresses and the gel could also show a significant yield value. For "weaker" gels, e.g. those produced by associative thickeners, the system may show viscoelastic liquid-like behaviour at lower applied stresses when compared with chemical gels. Several classes of gels can be identified:

(i) Gels produced as a result of repulsive interaction, e.g. expanded double layers.
(ii) Self-structured systems, in which weak flocculation is induced to produce a "gel" by the particles or droplets; this requires control of the particle size and shape, volume fraction of the dispersion and depth of the secondary minimum.
(iii) Thickeners consisting of high molecular weight polymers or finely divided particulate systems that interact in the continuous phase forming a "three-dimensional" structure.
(iv) Self-assembled structures such as associative thickeners.
(v) Crosslinked polymers (chemical gels).
(vi) Liquid crystalline structures of the hexagonal, cubic or lamellar phases. The most commonly used materials to produce a gel network are polymers, both natural and synthetic.

However, many colloidal particulate solids can form gels by some specific interactions between the particles. High concentrations of nonionic surfactants can also produce clear gels in systems containing up to 15 % mineral oil. One of the most effective techniques to characterize a gel is to investigate its rheological (viscoelastic) behaviour, in particular under conditions of low deformation [8]:

(i) Stress relaxation (after sudden application of strain) which can be applied to obtain the relaxation time of the system.

(ii) Constant stress (creep) measurements; in this case a constant stress σ is applied and the strain (deformation) γ or compliance J (= γ/σ, Pa^{-1}) is followed as a function of time. A gel that consists of a strong "three-dimensional" structure (e.g. crosslinked) behaves as viscoelastic; this behaviour may occur up to high applied stresses. A weaker gel (produced for example by high molecular weight polymers that are physically attached) behaves as a viscoelastic liquid; in this case viscoelastic solid behaviour only occurs at much lower stresses than those observed with the crosslinked gels.
(iii) Dynamic (oscillatory) measurements; a sinusoidal strain (or stress) with amplitude γ_0 and frequency ω (rad s^{-1}) is applied on the system and the resulting stress (or strain) with amplitude σ_0 is simultaneously measured allowing one to obtain the phase angle shift δ between stress and strain amplitudes. For any gel, $\delta < 90°$ and the smaller the value of δ the stronger the gel. From the amplitudes of stress and strain (σ_0 and γ_0) and the phase angle shift (δ) one can obtain the various viscoelastic parameters.

The next section in this chapter summarizes the different classes of gels:
(i) Polymer gels obtained by chain overlap; flexible polymer that produces random coils in solution can produce "gels" at a critical concentration C^*, referred to as the polymer coil "overlap" concentration.
(ii) Gels produced by associative thickeners that are hydrophobically modified polymer molecules where alkyl chains (C_{12}–C_{16}) are either randomly grafted on a hydrophilic polymer molecule such as hydroxyethyl cellulose (HEC), or simply grafted at both ends of the hydrophilic chain [4].
(iii) Crosslinked gels (chemical gels) that are produced by using crosslink agents to produce what is sometimes referred to as "microgels". These microgel particles are dispersed in the liquid and they undergo solvent swelling which may also be enhanced by some chemical modification, e.g. pH adjustment in aqueous systems.
(iv) Particulate gels; two main interactions can cause gel formation with particulate materials, namely long-range repulsions between the particles, e.g. using extended electrical double layers or steric repulsion resulting from the presence of adsorbed or grafted surfactant or polymer chains, and van der Waals attraction between the particles (flocculation) which can produce three-dimensional gel networks in the continuous phase.

All these systems produce non-Newtonian systems that show a "yield value" and high viscosity at low shear stresses or shear rates. Some specific particulate gels are given:
(i) Aqueous clay gels, e.g. sodium montmorillonite (referred to as swellable clay) forms gels at low and intermediate electrolyte concentrations.
(ii) Organo clays (Bentones) that are produced by exchanging the Na^+ ions with alkyl ammonium ions, e.g. dodecyl or cetyl trimethyl ammonium ions.

(iii) Oxide gels, e.g. silica gels that can be produced from fumed silica that are made by reaction of silicon tetrachloride with steam (Aerosil 200) or from precipitated silica. In aqueous media, the gel strength depends on the pH and electrolyte concentration.
(iv) Gels produced by mixtures of polymers and finely divided particulate solids; by combining thickeners such as hydroxyethyl cellulose or xanthan gum with particulate solids such as sodium montmorillonite, a more robust gel structure can be produced.
(v) Gels based on surfactant systems; at high surfactant concentration (> 30 % depending on the surfactant nature) they produce liquid crystalline phases of the hexagonal (H_1) and lamellar (L_α) phases which are anisotropic with high viscosities.

An alternative method for producing gels in emulsions is to use mixtures of surfactants. By proper choice of the surfactant types (e.g. their hydrophilic-lipophilic balance, HLB) one can produce lamellar liquid crystalline structures that can "wrap" around the oil droplets and extend in solution to form gel networks. These structures are referred to as oleosomes. Alternatively, the liquid crystalline structures may produce a "three-dimensional" gel network and the oil droplets become entrapped in the "holes" of the network. These structures are sometimes referred to as hydrosomes.

Chapter 5 deals with formulation of polymer colloids (latexes); polymers (latexes) are widely used in many industrial applications, e.g. in paints and coatings (film formers), as adhesives, as diagnostic markers for certain diseases, etc. In paints and coatings, latexes are used in aqueous emulsion paints that are used for home decoration. These aqueous emulsion paints are applied at room temperature and the latexes coalesce on the substrate forming a thermoplastic film. Sometimes functional polymers are used for crosslinking in the coating system. The polymer particles are typically submicron (0.1–0.5 μm). Generally speaking, there are three methods for preparing polymer dispersions, namely emulsion, dispersion and suspension polymerization. In emulsion polymerization, monomer is emulsified in a nonsolvent, commonly water, usually in the presence of a surfactant [11]. A water-soluble initiator is added, and particles of polymer form and grow in the aqueous medium as the reservoir of the monomer in the emulsified droplets is gradually used up. In dispersion polymerization (which is usually applied for preparation of nonaqueous polymer dispersions, commonly referred to as nonaqueous dispersion polymerization, NAD) monomer, initiator, stabilizer (referred as protective agent) and solvent initially form a homogeneous solution. The polymer particles precipitate when the solubility limit of the polymer is exceeded. The particles continue to grow until the monomer is consumed. In suspension polymerization the monomer is emulsified in the continuous phase using a surfactant or polymeric suspending agent. The initiator (which is oil soluble) is dissolved in the monomer droplets and the droplets are converted into insoluble particles, but no new particles are formed. A typical emulsion polymerization process

involves two stages known as the seed stage and the feed stage. In the seed stage, an aqueous charge of water, surfactant, and colloid is raised to the reaction temperature (85–90 °C) and 5–10 % of the monomer mixture is added along with a proportion of the initiator (a water-soluble persulphate). Polymeric surfactants are used to stabilize preformed latex dispersions. For this purpose polystyrene (PS) latexes are prepared using surfactant-free emulsion polymerization [11]. The stability of the latexes is determined using viscoelastic measurements. Dispersion polymerization is usually applied for the preparation of nonaqueous latex dispersions and hence it is referred to as NAD [11]. The method has also been adapted to prepare aqueous latex dispersions by using an alcohol–water mixture. Two main criteria must be considered in the process of dispersion polymerization:

(i) the insolubility of the formed polymer in the continuous phase;
(ii) the solubility of the monomer and initiator in the continuous phase.

Initially, dispersion polymerization starts as a homogeneous system but after sufficient polymerization, the insolubility of the resulting polymer in the medium forces it to precipitate. Initially polymer nuclei are produced which then grow to polymer particles. The latter are stabilized against aggregation by the block or graft copolymer that is added to the continuous phase before the process of polymerization starts. It is essential to choose the right block or graft copolymer, which should have a strong anchor chain A and good stabilizing chain B. NAD polymerization is carried in two steps:

(i) Seed stage: the diluent, portion of the monomer, portion of dispersant and initiator (azo or peroxy type) are heated to form an initial low-concentration fine dispersion.
(ii) Growth stage: the remaining monomer together with more dispersant and initiator are then fed over the course of several hours to complete the growth of the particles.

A small amount of transfer agent is usually added to control the molecular weight. Excellent control of particle size is achieved by proper choice of the designed dispersant and correct distribution of dispersant between the seed and growth stages. The process of dispersion polymerization has been applied in many cases using completely polar solvents such as alcohol or alcohol–water mixtures [11]. The results obtained showed completely different behaviour when compared with dispersion polymerization in nonpolar media.

Chapter 6 deals with formulation of microemulsions, which are better described as swollen micelles, and are a special class of nanodispersions (transparent or translucent) that actually have little in common with emulsions [12]. A convenient way to describe microemulsions is to compare them with micelles. Micelles are thermodynamically stable and may consist of spherical units with a radius that is usually less than 5 nm. Two types of micelles may be considered: normal micelles, with the hydro-

carbon tails forming the core and the polar head groups in contact with the aqueous medium, and reverse micelles (formed in nonpolar media) with a water core containing the polar head groups and the hydrocarbon tails now in contact with the oil. Normal micelles can solubilize oil in the hydrocarbon core forming O/W microemulsions, whereas reverse micelles can solubilize water forming a W/O microemulsion. The best definition of microemulsions is based on the application of thermodynamics by considering the energy and entropy terms for formation of microemulsions. The increase in surface area when forming a microemulsion is ΔA and the surface energy increase is equal to $\Delta A\gamma_{12}$. The increase in entropy is $T\Delta S^{\text{conf}}$ (a higher entropy is obtained since a large number of droplets are produced). With macroemulsions, $\Delta A\gamma_{12} \gg T\Delta S^{\text{conf}}$ and $\Delta G_{\text{m}} > 0$. The system is nonspontaneous (it requires energy for formation of the emulsion drops) and it is thermodynamically unstable. With microemulsions, $\Delta A\gamma_{12} \leq T\Delta S^{\text{conf}}$ (this is due to the ultra-low interfacial tension accompanying microemulsion formation) and $\Delta G_{\text{m}} \leq 0$. The system is produced spontaneously and it is thermodynamically stable. Several theories are described to explain the stability of microemulsions:

(i) Mixed film and solubilization theories; the film (which may consist of surfactant and cosurfactant molecules) is considered a liquid "two-dimensional" third phase in equilibrium with both oil and water. Such a monolayer could be a duplex film, i.e. giving different properties on the water side and the oil side. The initial "flat" duplex film has different tensions at the oil and water sides. This is due to the different packing of the hydrophobic and hydrophilic groups (these groups have different sizes and cross-sectional areas). The duplex film will bend, forming an O/W or W/O microemulsion.
(ii) Solubilization theories introduced by Shinoda and coworkers [6], who considered microemulsions to be swollen micelles that are directly related to the phase diagram of their components.
(iii) Thermodynamic theory; spontaneous formation of the microemulsion with decreasing free energy can only be expected if the interfacial tension is so low that the remaining free energy of the interface is over compensated for by the entropy of dispersion of the droplets in the medium.

Combining two surfactants of different nature, one predominantly water soluble (such as sodium dodecyl sulphate) and one predominantly oil soluble (such as hexanol) lowers γ to very small, or even transiently negative value. A simple model was used to calculate the free energy of formation of a model W/O microemulsion: The droplets were assumed to be of equal size. The droplets are large enough to consider the adsorbed surfactant layer to have constant composition. Several methods can be applied to characterize microemulsions:

(i) Scattering techniques (using radiation of light, X-ray or neutrons) that provide information on the size, shape and structure of microemulsions. In all these methods, measurements can be made at sufficiently low concentration to avoid complications

arising from particle–particle interactions. The results obtained are extrapolated to infinite dilution to obtain the desirable property, such as the molecular weight and radius of gyration of a polymer coil, the size and shape of micelles, etc. Unfortunately, this dilution method cannot be applied for microemulsions, which depend on a specific composition of oil, water and surfactants. Microemulsions cannot de diluted by the continuous phase since this dilution results in the breakdown of the microemulsion. Thus, when applying the scattering techniques to microemulsions, measurements have to be made at finite concentrations and the results obtained have to be analysed using theoretical treatments to take into account the droplet–droplet interactions. The droplet size can be estimated from the interfacial area, by assuming that all surfactant and cosurfactant molecules are adsorbed at the interface.

(ii) Dynamic light scattering (photon correlation spectroscopy, PCS); one measures the intensity fluctuation of light scattered by the droplets as they undergo Brownian motion.

(iii) Neutron scattering, this offers a valuable technique for determining the dimensions and structure of microemulsion droplets. The structure of the microemulsion droplet can be obtained using this method. By changing the isotopic composition of the components (e.g. using deuterated oil and H_2O-D_2O) one can match the scattering length density of the various components: By matching the scattering length density of the water core with that of the oil, one can investigate the scattering from the surfactant "shell". By matching the scattering length density of the surfactant "shell" and the oil, one can investigate the scattering from the water core.

(iv) Conductivity measurements may provide valuable information on the structural behaviour of microemulsions. In the early applications of conductivity measurements, the technique was used to determine the nature of the continuous phase. O/W microemulsions should give fairly high conductivity (that is determined by that of the continuous aqueous phase) whereas W/O microemulsions should give fairly low conductivity (that is determined by that of the continuous oil phase). Conductivity measurements were also used to study the structure of the microemulsion, which is influenced by the nature of the cosurfactant. A systematic study of the effect of cosurfactant chain length on the conductive behaviour of W/O microemulsions is described. The cosurfactant chain length was gradually increased from C_2 (ethanol) to C_7 (heptanol). With the short chain alcohols ($C < 5$), conductivity shows a rapid increase above a critical ϕ value. With longer chain alcohols, namely hexanol and heptanol, conductivity remains very low up to a high water volume fraction. With the short chain alcohols, the system shows percolation above a critical water volume fraction. Under these conditions the microemulsion is "bicontinuous". With the longer chain alcohols, the system is non-percolating and one can define definite water cores. This is sometimes referred to as a "true" microemulsion.

(v) NMR measurements which demonstrated that the organization and structure of microemulsions can be elucidated from self-diffusion measurements of all the components (using pulse gradient or spin echo NMR techniques). Within a micelle, the

molecular motion of the hydrocarbon tails (translational, reorientation and chain flexibility) is almost as rapid as in a liquid hydrocarbon. In a reverse micelle, water molecules and counterions are also highly mobile. For many surfactant-water systems, there is a distinct spatial separation between hydrophobic and hydrophilic domains. The passage of species between different regions is an improbable event and this occurs very slowly. Thus, self-diffusion, if studied over macroscopic distances, should reveal whether the process is rapid or slow depending on the geometrical properties of the inner structure. For example, a phase that is water continuous and oil discontinuous should exhibit rapid diffusion of hydrophilic components, while the hydrophobic components should diffuse slowly. An oil continuous but water discontinuous system should exhibit rapid diffusion of the hydrophobic components. One would expect that a bicontinuous structure should give rapid diffusion of all components. Using this principle, it is possible to measure the self-diffusion coefficient of all components, with particular emphasis on the role of the cosurfactant. For microemulsions consisting of water, hydrocarbon, an anionic surfactant and a short chain alcohol (C_4 and C_5), the self-diffusion coefficient of water, hydrocarbon and cosurfactant was quite high, of the order of 10^{-9} m^2 s^{-1}, i.e. two orders of magnitude higher than the value expected for a discontinuous medium (10^{-11} m^2 s^{-1}). This high diffusion coefficient was attributed to three main effects: Bicontinuous solutions, easily deformable and flexible interface and absence of any large aggregates. With microemulsions based on long chain alcohols (e.g. decanol), the self-diffusion coefficient for water was low, indicating the presence of definite (closed) water droplets surrounded by surfactant anions in the hydrocarbon medium. Thus, NMR measurements could clearly distinguish between the two types of microemulsion systems.

The formulation of microemulsions or micellar solutions, like that of conventional macroemulsions is still an art. In spite of the exact theories that explain the formation of microemulsions and their thermodynamic stability, the science of microemulsion formulation has not advanced to the point where one can predict with accuracy what happens when the various components are mixed. The very much higher ratio of emulsifier to disperse phase, which differentiates microemulsions from macroemulsions, appears at first sight to make the application of various techniques for formulation less critical. However, in the final stages of the formulation one immediately realizes that the requirements are very critical due to the greater number of parameters involved. The mechanics of forming microemulsions differ from those used in making macroemulsions. The most important difference lies in the fact that putting more work into a macroemulsion or increasing emulsifier usually improves its stability. This is not so for microemulsions. Formation of a microemulsion depends on specific interactions of the molecules of oil, water and emulsifiers. These interactions are not precisely known. If such specific interactions are not realized, no amount of work nor excess emulsifier can produce the microemulsion. If the chemistry is right, microemulsification occurs spontaneously. One should remember that for microemulsions the ratio of emulsifier to oil is much higher than that used for macroemulsions. The emul-

sifier used is at least 10 % based on the oil and in most cases it can be as high as 20–30 %. W/O systems are made by blending the oil and emulsifier with some heating if necessary. Water is the added to the oil-emulsifier blend to produce the microemulsion droplets and the resulting system should appear transparent or translucent. If the maximum amount of water that can be microemulsified is not high enough for the particular application, one should try other emulsifiers to reach the required composition. The most convenient way of producing an O/W microemulsion is to blend the oil and emulsifier and the pour the mixture into water with mild stirring. In the case of waxes, both oil-emulsifier blend and the water must be at higher temperature (above the melting point of the wax). If the melting point of the wax is above the boiling temperature of water, the process can be carried out at high pressure. Another technique to mix the ingredients is to make a crude macroemulsion of the oil and one of the emulsifiers. By using low volumes of water, a gel is formed and the system can then be titrated with the co-emulsifier until a transparent system is produced. This system may be further diluted with water to produce a transparent or translucent microemulsion. Four different emulsifier selection methods can be applied for formulation of microemulsions:

(i) the hydrophilic-lipophilic balance (HLB) system;
(ii) the phase inversion temperature (PIT) method;
(iii) the cohesive energy ratio (CER) concept;
(iv) partitioning of cosurfactant between the oil and water phases.

The first two methods are essentially the same as those used for selecting emulsifiers for macroemulsions, described above. However, with microemulsions one should try to match the chemical type of the emulsifier with that of the oil. The cosurfactant portioning plays a major role in microemulsion formation. According to the thermodynamic theory of microemulsion formation, the total interfacial tension of the mixed film of surfactant and cosurfactant must approach zero. The total interfacial tension γ_T is given by the difference between $(\gamma_{O/W})_a$, the interfacial tension of the oil in the presence of alcohol cosurfactant and the surface pressure π. $(\gamma_{O/W})_a$ seems to reach a value of 15 mN m^{-1} irrespective of the original value of $\gamma_{O/W}$. It seems that the cosurfactant which is predominantly oil soluble distributes itself between the oil and the interface and this causes a change in the composition of the oil which now is reduced to 15 mN m^{-1}. Measuring the partition of the cosurfactant between the oil and the interface is not easy. A simple procedure to select the most efficient cosurfactant is to measure the oil/water interfacial tension $\gamma_{O/W}$ as a function of cosurfactant concentration. The lower the percentage of cosurfactant required to lower $\gamma_{O/W}$ to 15 mN m^{-1}, the better the candidate.

Chapter 7 deals with controlled-release formulations which offer a number of advantages, in particular for pharmaceuticals and agrochemicals, of which the following are worth mentioning:

(i) improvement of residual activity;
(ii) reduction of application dosage;
(iii) stabilization of the core active ingredient (AI) against environmental degradation;
(iv) reduction of mammalian toxicity;
(v) reduction of phytotoxicity with agrochemicals;
(vi) reduction of fish toxicity with agrochemicals;
(vii) reduction of environmental pollution with agrochemicals.

One of the main advantages of using controlled-release formulations, in particular microcapsules, is the reduction of physical incompatibility when several drugs are used and when mixtures are used with agrochemicals in the spray tank. They also can reduce biological antagonism when mixtures are applied in the field. Several types of controlled-release systems can be identified:

(i) Microcapsules with particles in the size range 1–100 μm that consist of a distinct capsule wall (mostly a polymer) surrounding the active ingredient core.
(ii) Microparticles (size range 1–100 μm) consisting of a matrix in which the active ingredient (AI) is uniformly dissolved or dispersed.
(iii) Granules with matrix particles of 0.2–2.0 mm with the active ingredient uniformly dissolved or dispersed within the matrix.

Microencapsulation of chemicals is mainly carried out by interfacial condensation, in situ polymerization and coacervation. Interfacial condensation is perhaps the most widely used method for encapsulation in industry. The AI, which may be oil soluble, oil dispersible or an oil itself, is first emulsified in water using a convenient surfactant or polymer. A hydrophobic monomer A is placed in the oil phase (oil droplets of the emulsion) and a hydrophilic monomer B is placed in the aqueous phase. The two monomers interact at the interface between the oil and the aqueous phase forming a capsule wall around the oil droplet. Two main types of systems may be identified. For example, if the material to be encapsulated is oil soluble, oil dispersible or an oil itself, an oil-in-water (O/W) emulsion is first prepared. In this case the hydrophobic monomer is dissolved in the oil phase, which forms the dispersed phase. The role of surfactant in this process is crucial, since an oil–water emulsifier (with high hydrophilic-lipophilic balance, HLB) is required. Alternatively, a polymeric surfactant such as partially hydrolyzed polyvinyl acetate (referred to as polyvinyl alcohol, PVA) or an ethylene oxide-propylene oxide-ethylene oxide, PEO–PPO–PEO (Pluronic) block copolymer can be used. The emulsifier controls the droplet size distribution and hence the size of capsules formed. On the other hand, if the material to be encapsulated is water soluble, a water-in-oil (W/O) emulsion is prepared using a surfactant with low HLB number or an A–B–A block copolymer of polyhydroxystearic acid-polyethylene oxide-polyhydroxystearic acid (PHS–PEO–PHS). In this case the hydrophilic monomer is dissolved in the aqueous internal phase droplets. In interfacial polymerization, the monomers A and B are polyfunctional monomers capable of causing polyconden-

sation or polyaddition reaction at the interface [2]. Examples of oil-soluble monomers are polybasic acid chloride, bis-haloformate and polyisocyanates, whereas water-soluble monomers can be polyamine or polyols. Thus, a capsule wall of polyamide, polyurethane or polyurea may be formed. Some trifunctional monomers are present to allow crosslinking reactions. If water is the second reactant with polyisocyanates in the organic phase, polyurea walls are formed. The latter modification has been termed in situ interfacial polymerization. One of the most useful microencapsulation processes, commonly used with agrochemicals, involves reactions that produce formation of urea-formaldehyde (UF) resins. It should be mentioned that the role of surfactants in the encapsulation process is very important. Apart from their direct role in the preparation of microcapsule dispersions, surfactants can be used to control the release of the active ingredient (AI) from the microcapsule dispersion. There are generally two mechanisms for release of the active ingredient (AI) from a capsule:

(i) diffusion of the AI through the microcapsule wall;
(ii) destruction of the microcapsule wall by either physical means, e.g. mechanical power, or by chemical means, e.g. hydrolysis, biodegradation, thermal degradation, etc.

The release behaviour is controlled by several factors such as particle size, wall thickness, type of wall material, wall structure (porosity, degree of polymerization, crosslink density, additives, etc.), type of core material (chemical structure, physical state, presence or absence of solvents) and amount or concentration of the core material. The release behaviour is determined by interaction of these factors and optimization is essential for achieving the desirable release rate. In order to get better performance of the microcapsule for biological efficacy, time dependent or site-specific release is desirable. It is essential in this case to develop various functional microcapsules that are specific to the target. Microcapsules responsive to temperature, pH, light, and enzymes are desirable. The simplest release kinetics of microcapsules is diffusion controlled as predicted by Fick's first law. To decrease the rate of diffusion one has to use larger capsules and thicker capsule walls. There are four types of encapsulation utilizing the system of phase separation from aqueous solution:

(i) complex coacervation or phase separation resulting from two oppositely charged colloids neutralizing one another;
(ii) simple coacervation where a non-electrolyte such alcohol causes formation of a separate polymer-rich phase;
(iii) salt coacervation where a polymer separates as a result of a salting-out process;
(iv) precipitation and insolubilization of a polymer by changing the pH of the aqueous solution system.

Microencapsulation of solid particles is by far the most challenging process of encapsulation since one has to coat the particles individually without any aggregation. These particles cover the size range 0.1–5 μm with an average of 1–2 μm. Clearly, when

encapsulating these particles one has to make sure that the smallest size fraction is retained without any aggregation. This is vital for biological efficacy since the smaller particles are more effective for biological control (due to their higher solubility when compared with the larger particles).

Another method that can be applied to encapsulate solid particles is a modification of the coacervation process described above. In this method a technique of solvent evaporation is used to precipitate the polymers as intact coatings. The solid particles are suspended in a solvent solution of the polymer and emulsified into a liquid. The emulsion is then heated to evaporate the solvent causing the polymer to insolubilize as a coating around the suspended particles. Alternatively, a nonsolvent for the polymer is added to the suspension of particles in polymer solution, causing the solvent to phase separate and the polymers to insolubilze to coatings. Matrix-based microparticles are of three main types:

(i) Matrix powders where the active ingredient (AI) is dispersed throughout the matrix and the mixture is ground (if necessary) to form a powder that can be applied as wettable powder. Surface active agents are incorporated to aid wetting and dispersion of the micrparticles. The matrices used include polymers such as lignin, starch, proteins, high molecular weight natural polymers such as waxes, cyclodextrin, synthetic polymers such as urea formaldehyde resins or acrylic acid polymers. Inorganic materials such as glass, silica or diatomaceous earth can also be used. These inorganic materials can also act as carriers.
(ii) Carriers plus matrix, where the particles are based on a porous powder that is used as a carrier. Two types can be distinguished, namely co-loaded (where the AI/matrix mixture is loaded into the carrier) and postcoated (where the AI is loaded into the carrier and the matrix is then loaded separately).
(iii) Matrix emulsions, where the microparticles are made by emulsifying a hot solution of the AI plus matrix, typically in water. On cooling the emulsion droplets solidify producing an aqueous suspension of the microparticles.

Generally speaking, one component of the formulation, the "matrix", will be responsible for the controlled-release of the formulation. It is convenient to consider the controlled-release as being due to interaction among the AI, the matrix and the environment. The release of AI from conventional formulations generally follows an exponential decay, i.e. the release rate is proportional to the concentration of the AI remaining in the formulation. This decay follows first-order kinetics, which means that the initial concentration in the environment is initially very high (often resulting in an undesirable toxic effect) and decreases rapidly to a low (ineffective) level. In contrast, a controlled-release formulation generally exhibits lower initial concentrations and a longer time before the concentration decreases to an ineffective level. When using a conventional formulation, several treatments are required for biological control. During these treatments the AI concentration may reach an undesirable high concentration above the toxic limit. In contrast, a controlled-release formulation maintains

an effective concentration that is sufficient for bioefficacy without reaching the toxic limit. Thus, with a conventional treatment, a higher dose of AI is required to maintain the bioefficacy. This dose is significantly reduced when using a controlled-release formulation. The high AI concentrations reached with conventional formulations can also have adverse toxic effects on humans, birds, fish, etc. Most controlled-release systems rely on diffusion of AI through a rate controlling membrane or polymer matrix. Transport through a polymer membrane or matrix occurs by a solution-diffusion process, whereby the AI first dissolves in the polymer and then diffuses across the polymer to the external surface, where the concentration is lower. The rate of AI release from controlled-release systems can follow a variety of patterns, ranging from first-order (exponential) decay (as with conventional systems) to zero-order kinetics in which the release rate is constant over most of the lifetime of the device. In the latter case the release rate decreases proportionally to the square root of time. The most common types of controlled-release microparticles are membrane-coated reservoirs and polymeric matrices. A reservoir system consists of a core of pure or saturated AI surrounded by a rate-controlling membrane (polymer shells). The AI is released from the reservoir system by diffusion through the rate-controlling membrane at a constant rate (zero-order kinetics) and this follows Fick's law. Another important factor that affects the release rate of membrane-coated reservoir type microparticles is the polydispersity of the system. The release rate from each microparticle may be constant and hence initially the release rate may also be constant. However, with time the release rate may change as a result of polydispersity. It should also be mentioned that to maintain a constant release rate, the membrane must remain intact. In general, large microparticles and those with high loading of AI are more susceptible to rupture resulting in rapid release. Controlled-release from granules is used with many agrochemicals that are formulated as water dispersible granules (WG) which disperse quickly and completely when added to water. The main advantage of WGs is that they avoid the use of solvents, thus reducing the risk during manufacture and to farm workers during application. In addition they can be applied for slow release. Several processes can be applied to produce WGs of insoluble AI:

(i) Those in which the starting materials are essentially dry and are subsequently made wet and then re-dried.
(ii) Those in which the starting materials are wet and are granulated and dried. A typical composition of a WG is one or two AIs, dispersing agent, suspending agent, wetting agent, binder (such as lignosulphonate or a gum) and a filler (mineral filler or water-soluble salt).

Approaches to achieving controlled-release in granules fall into two main categories:

(i) the matrix (monolith) with the AI dispersed throughout the structure;
(ii) the reservoir, in which a polymeric coating entraps the AI with or without a support [9].

Particle size and uniformity are very important especially in applications where the duration of release is critical. Three types of granule dimensions can be distinguished, namely fine granules 0.3–2.5 mm in diameter, microgranules 0.1–0.6 mm and macrogranules 2–6 mm. A formulation containing a range of particle sizes from dusts to macrogranules will have an extended period of effectiveness. A controlled-release system based on a monolithic polymer granule made from extruding the AI with a release rate-modifying inert material ("porisogen") in a thermoplastic matrix can play an important role for pest management for periods (following a single treatment of a non-persistent agrochemical) of up to 2–3 years. Although the above approach based on synthetic polymers is the most successful of the controlled-release granules, natural polymers showed great success in matrix formulations for AI delivery. Examples of natural polymers are crosslinked starch, polysaccharides, crosslinked alginates and cellulose derivatives. To provide effective delay of release, alginate gels crosslinked with calcium require the incorporation of absorbents such as silica, alumina, clays or charcoal. Further control of the release rate could be achieved by combining kaolin clay with linseed oil in the granule. Other gel forming polymers include carboxymethyl cellulose stabilized with gelatin and crosslinked with cupric or aluminium ions. Coating of granules with rate-controlling polymer film can also be applied. Controlled delivery of agrochemicals has also been obtained with superabsorbent acrylamide and acrylate polymers. The biodegradability of the formulating material is an important aspect of controlled release for environmental applications. Several synthetic and natural polymers used for formulating granules are biodegradable. The delivery of bioactives from controlled-release granules can be enhanced by inclusion of biosurfactants. Several lignin-based granules have been introduced for controlled release of several AIs, in particular for oil applications. The mechanism of release from lignin matrix granules intended for use in soil and aqueous media is studied by immersing the granule in water under static, stirred or flowing conditions. Granules prepared from various lignin types always show release rates that decrease with time.

Chapter 8 deals with formulation of solid dosage systems. These are one of the most important systems used in the chemical industry, e.g. pharmaceuticals, food and speciality products. The formulation of such solid dosage forms requires the formation of the desired structure, as well as its controlled breakdown in the end use by the consumer [3]. The preparation of these systems requires an understanding of the fundamental chemistry and materials science, e.g. the biological activity in a pharmaceutical product, taste in a food, etc. The material must be produced in a form that has the correct structure and on usage and delivery one must prove that this structure is correct. It is, therefore, important to obtain information on the structure by using techniques such as electron microscopy and spectroscopy. In this chapter, I will start with a section on agglomerated products that are frequently used in instant foods (e.g. coffee), agrochemicals and detergent powders. The structure of the agglomerated product is made up by agglomeration of smaller constituent particles. In some cases, the agglomerated product is further processed by compaction to produce a tablet, as is

the case with many pharmaceutical products. The process of agglomeration is briefly described and this is followed by a section on spray drying. The next section will deal with the process of compaction which is sometimes referred to as "dry agglomeration" since in this case no liquid binders are necessary for the agglomeration process. The last section will deal with the use of solid dosage forms in the pharmaceutical industry. Three main types are used, namely tablets, hard and soft gelatine capsules and sustained-release pellets.

Chapter 9 describes the methods that can be applied for characterizing the formulation and assessing its long-term physical stability. For full characterization of the properties of formulations, three main types of investigations are needed:

(i) Fundamental investigations of the system at a molecular level. This requires investigating the structure of the solid/liquid interface, namely the structure of the electrical double layer (for charge stabilized suspensions), adsorption of surfactants, polymers and polyelectrolytes and conformation of the adsorbed layers (e.g. the adsorbed layer thickness). It is important to know how each of these parameters changes with the conditions, such as temperature, solvency of the medium for the adsorbed layers and effect of addition of electrolytes.
(ii) Investigations of the state of the suspension on standing, namely flocculation rates, flocculation points with sterically stabilized systems, spontaneity of dispersion on dilution and Ostwald ripening or crystal growth.
(iii) Investigations of emulsion coalescence. All these phenomena require accurate determination of the particle size distribution as a function of storage time.
(iv) Bulk properties of the suspension, whaich are particularly important for concentrated systems. This requires measurement of the rate of sedimentation and equilibrium sediment height.

More quantitative techniques are based on assessment of the rheological properties of the suspension (without disturbing the system, i.e. without its dilution and measurement under conditions of low deformation) and how these are affected by long-term storage. A useful parameter for describing the charge and potential distribution in charge stabilized systems is the electrokinetic or zeta potential which will be described in this chapter. Several techniques are available for obtaining information on particle and droplet size distributions in diluted systems. These measurements carried out as a function of time and temperature are essential for the assessment of flocculation, Ostwald ripening and coalescence (in case of emulsions) of the formulation. It is essential to dilute the concentrated formulation with its own dispersion medium in order not to affect the state of the dispersion during examination. The dispersion medium can be obtained by centrifugation of the formulation whereby the supernatant liquid is produced at the top (with suspensions) or bottom (with most emulsions) of the centrifuge tube. Care should be taken with dilution of the concentrated system with its supernatant liquid (i.e. with minimum shear). Electron microscopy utilizes an electron beam to illuminate the sample. The electrons behave as charged particles which

can be focused by annular electrostatic or electromagnetic fields surrounding the electron beam. Due to the very short wavelength of electrons, the resolving power of an electron microscope exceeds that of an optical microscope by ≈ 200 times. Two types are described:

(i) Transmission electron microscopy (TEM) that displays an image of the specimen on a fluorescent screen and the image can be recorded on a photographic plate or film. TEM can be used to examine particles in the range 0.001–5 μm. The sample is deposited on a Formvar (polyvinyl formal) film resting on a grid to prevent charging of the simple. The sample is usually observed as a replica by coating with an electron transparent material (such as gold or graphite).
(ii) Scanning electron microscopy (SEM) that can show particle topography by scanning a very narrowly focused beam across the particle surface. The electron beam is directed normally or obliquely at the surface. The backscattered or secondary electrons are detected in a raster pattern and displayed on a monitor screen. The image provided by secondary electrons exhibits good three-dimensional detail. The backscattered electrons, reflected from the incoming electron beam, indicate regions of high electron density.

Confocal laser scanning microscopy (CLSM) is a very useful technique for identification of formulations. It uses a variable pinhole aperture or variable width slit to illuminate only the focal plane by the apex of a cone of laser light. Out-of-focus items are dark and do not distract from the contrast of the image. As a result of extreme depth discrimination (optical sectioning) the resolution is considerably improved (up to 40 % when compared with optical microscopy). Scanning probe microscopy (SPM) can measure physical, chemical and electrical properties of the sample by scanning the particle surface with a tiny sensor of high resolution. Scanning probe microscopes do not measure a force directly; they measure the deflection of a cantilever which is equipped with a tiny stylus (the tip) functioning as the probe. The deflection of the cantilever is monitored by

(i) a tunnelling current,
(ii) laser deflection beam from the back side of the cantilever,
(iii) optical interferometry,
(iv) laser output controlled by the cantilever used as a mirror in the laser cavity, and
(v) change in capacitance.

Scanning tunnelling microscopy (STM) measures an electric current that flows through a thin insulating layer (vacuum or air) separating two conductive surfaces. The electrons are visualized to "tunnel" through the dielectric and generate a current, I, that depends exponentially on the distance, s, between the tiny tip of the sensor and the electrically conductive surface of the sample. The STM tips are usually prepared by etching a tungsten wire in an NaOH solution until the wire forms a conical tip. Pt/Ir wire has also been used. Atomic force microscopy (AFM) allows one to scan

the topography of a sample using a very small tip made of silicon nitride. The tip is attached to a cantilever that is characterized by its spring constant, resonance frequency and a quality factor. The sample rests on a piezoceramic tube which can move the sample horizontally (x, y motion) and vertically (z motion). The displacement of the cantilever is measured by the position of a laser beam reflected from the mirrored surface on the top side of the cantilever. The reflected laser beam is detected by a photodetector. AFM can be operated in either a contact or a non-contact mode. Scattering techniques are by far the most useful methods for characterizing formulations and in principle they can give quantitative information on the particle size distribution, floc size and shape. The only limitation of the methods is the need to use sufficiently dilute samples to avoid interference such as multiple scattering which makes interpretation of the results difficult. However, recently backscattering methods have been designed to allow one to measure the sample without dilution. In principle one can use any electromagnetic radiation such as light, X-ray or neutrons but in most industrial labs only light scattering is applied (using lasers). Two techniques are described for measuring the electrophoretic mobility and zeta potential, namely laser velocimetry and electroacoustic technique. Two general techniques are described for measuring the rate of flocculation of dispersions, both of which can only be applied for dilute systems. The first method is based on measuring the scattering of light by the particles or droplets. The second method for obtaining the rate constant of flocculation is by direct particle or droplet counting as a function of time. For this purpose optical microscopy or image analysis may be used, provided the particle size is within the resolution limit of the microscope. A method is described for measuring incipient flocculation which occurs with sterically stabilized dispersions when the medium for the chains becomes a θ-solvent. To obtain a measure of the rate of Ostwald ripening or crystal growth, the particle or droplet size distribution of the dispersion is followed as a function of time, using either a Coulter Counter, a Mastersizer or an optical disc centrifuge. One usually plots the cube of the average radius versus time which gives a straight line from which the rate of Ostwald ripening can be determined (the slope of the linear curve). The rate of coalescence of emulsions is determined by measuring the number of particles or droplets, or average diameter, as a function of time; the process follows first-order kinetics. Several physical measurements can be applied to assess sedimentation. The simplest method is to measure the density of the settling suspension at a known depth using a hydrometer. Unfortunately, this simple method is highly invasive due to the disturbance of the suspension by the hydrometer. A more accurate method is to use sedimentation balances in which the sediment accumulated at the base of the sedimentation column is collected and weighed. Several other techniques have been designed to monitor sedimentation of suspensions of which photosedimentation, X-ray sedimentation and laser anemometry are perhaps worth mentioning. Analysis of creaming or sedimentation rates needs a knowledge of the droplet concentration with height and time. Two methods can be applied to obtain such information, namely the use of backscattering of near infrared (NIR) and mea-

surement of ultrasound velocity as a function of height in the tube containing the suspension or emulsion.

The bulk properties of suspensions and emulsions are assessed by measuring the equilibrium sediment or cream volume (or height) and redispersion. Normally in sediment or cream volume measurements, one compares the initial volume V_0 (or height H_0) with the ultimately reached value V (or H). A colloidally stable suspension or emulsion gives a "close-packed" structure with relatively small sediment or cream volume. A weakly "flocculated" or "structured" suspension or emulsion gives a more open sediment or cream and hence a higher sediment or cream volume. Thus by comparing the relative sediment or cream volume V/V_0 or height H/H_0, one can distinguish between a stable or flocculated suspension or emulsion. Evaluation of the stability/instability of suspensions or emulsions without any dilution (which can cause significant changes in the structure of the system) requires carefully designed techniques that should cause as little disturbance to the structure as possible. The most powerful techniques that can be applied in any industrial laboratory are rheological measurements and these are described in this chapter. These measurements provide accurate information on the state of the system such as sedimentation or creaming and flocculation. These measurements are also applied for the prediction of the long-term physical stability of the suspension. The application of these methods for the assessment and prediction of the physical stability of suspensions and emulsions is described. These include assessment of sedimentation or creaming, assessment of flocculation and coalescence with emulsions. Steady state, constant stress and oscillatory techniques are applied and examples are given to illustrate their use in the assessment and prediction of the stability of the formulation.

Volume 3 considers pharmaceutical, cosmetic and personal care formulations; it consists of two parts. Part I deals with pharmaceutical formulations and it consists of seven chapters. Chapter 1 describes the pharmaceutical suspensions that are applied as oral, parenteral, topical suspensions, antacid and reconstitutable suspensions. Chapter 2 deals with parenteral emulsion systems and lipid emulsions for parenteral nutrition. This section also describes emulsion formulation and the fate of the fat emulsion after administration. The same section describes the emulsions that are used for diagnosis, perfluorochemical emulsions as artificial blood substitutes, lipid emulsions for drug delivery, emulsions as vehicles for vaccines, multiple emulsions for drug delivery, oral emulsion and topical emulsion systems. The drug release from an emulsion or semi-solid topical formulation is described. Chapter 3 deals with formulation of ophthalmic ointments and suspensions. Chapter 4 describes gels and gelling systems in pharmacy. Chapter 5 deals with aerosol dosage forms in pharmacy. Chapter 6 describes the formulation of nanodispersions in pharmacy with particular reference to the formulation of nanosuspensions, nanoemulsions, microemulsions and biodegradable nanoparticles as drug carriers. Chapter 7 describes the formulation of pharmaceutical dosage forms.

Part II deals with the formulation of cosmetics and personal care products. It consists of nine sections. Chapter 8 gives a general introduction on the various types of cosmetic formulations. Chapter 9 describes the formulation of cosmetic emulsions, control of their stability and consistency. Chapter 10 deals with the formulation of nanoemulsions and their advantages compared to the macroemulsions. Both high-energy and low-energy methods for preparing nanoemulsions are described. The origin of their stability against creaming, flocculation and coalescence is described in terms of steric stabilization. The origin of Ostwald ripening and its prevention are described. Chapter 11 deals with the formulation of multiple emulsions in cosmetics, methods of their preparation, control and assessment of their stability. Chapter 12 describes the formulation of liposomes and vesicles in cosmetic formulations, the driving force for their formation and their stabilization by using block copolymers. Chapter 13 deals with the formulation of shampoos and hair conditioners. The role of the various ingredients in the shampoo is described. Chapter 14 describes the formulation of colour cosmetics, with particular reference to the methods of their preparation and stabilization. Chapter 15 describes the formulation of sunscreens for UV protection, with particular reference to the use of titanium dioxide and the importance of size reduction. Chapter 16 deals with sensory evaluation of cosmetic products. Sensory evaluation of a personal care product such as a hand cream, lotion, foundation, shampoo or lipstick is very important for customer acceptance. One of the main challenges for the formulator is to be able to predict such acceptance before embarking on rigorous panel testing. Rheological measurements, such as steady state, constant stress (creep) and oscillatory measurements, if carefully conducted and analysed offer valuable methods for achieving this goal. This is the objective of the section.

Volume 4 describes the formulation of agrochemicals, paints and coatings, and food colloids. It is divided into three parts. Part I deals with the formulation of agrochemicals. This part is subdivided into eight sections. Chapter 1 gives a general introduction on the types of agrochemical formulations. Chapter 2 deals with formulation of emulsifiable concentrates (ECs), in which the active ingredient (AI) that may be an oil of low viscosity is mixed with appropriate emulsifiers. When the oil concentrate is added to water it emulsifies spontaneously forming an oil-in-water emulsion that should remain stable for a few hours before it is applied as a spray. Alternatively, if the AI is viscous it is mixed with an oil of low viscosity and the EC can be easily applied. If the AI is a solid, it can be dissolved in an appropriate oil, mixed with the emulsifiers and then applied in the same way as the previous systems. Chapter 3 describes the formulation of emulsion concentrates (EWs) which have several advantages when compared with ECs. Firstly, less oil (which may be phytotoxic to plants) is used. Secondly, a lower emulsifier concentration is used to formulate the EW. The only drawback of EWs is the need to apply high energy (using a high-speed mixer) and the control of their long-term physical stability. This section starts with the mechanism of emulsion formation and its thermodynamic stability. This shows that EWs are only kinetically stable and to maintain their long-term physical stability,

effective emulsifiers are needed. The second part of this section deals with the mechanism and methods of emulsification and the role of surfactants in emulsion formation. This is followed by the methods that can be applied for the selection of emulsifiers. Two main procedures can be applied, namely the hydrophilic-lipophilic balance (HLB) concept and the phase inversion temperature (PIT) concept. The last part of this section describes the factors affecting emulsion stability. Five breakdown processes are described, namely creaming or sedimentation, flocculation, Ostwald ripening, coalescence and phase inversion. The methods that can be applied to reduce or eliminate these breakdown processes are described. Chapter 4 deals with the formulation of suspension concentrates (SCs). It starts with a general introduction describing the advantages of SCs when compared with wettable powders. This is followed by the methods that can be applied for the preparation of suspension concentrates and the role of surfactants/dispersing agents. The various phenomena of wetting of powders, dispersion of aggregates and agglomerates as well as size reduction by milling (comminution) are described. This is followed by the methods that can be applied to control the physical stability of suspension concentrates. These include control of sedimentation and formation of compact sediments and their prevention, control of flocculation and Ostwald ripening. The methods that can be applied for characterizing suspension concentrates and assessing their long-term physical stability are described. Chapter 5 describes the oil-based suspension concentrates. It starts with a general introduction describing the possibility of preparing suspension concentrates in polar and nonpolar media. The stability of both types of nonaqueous suspensions is described with particular reference to the use of polymeric surfactants to stabilize the formulation. The emulsification of oil-based suspensions and the various possible mechanisms responsible for it are described. The choice of the surfactants that can be used for emulsification of the oil-based SC into water and aqueous electrolyte solutions is described. Finally, the proper choice of the antisettling system for the oil-based SC is described. This is followed by a description of the rheological characteristics of the oil-based suspensions. Chapter 6 deals with formulation of suspoemulsions, which are a mixture of suspensions and emulsions. It starts with an introduction describing the various possible interactions between the suspension particles and emulsion droplets. The various breakdown processes such as homo- and heteroflocculation, coalescence of emulsion droplets and recrystallization of the particles are described. The systems of agrochemical suspoemulsions are described, with particular reference to the effect of density difference between the particles and droplets and the effect of the volume fraction of the whole system. The methods that can be applied to reduce the instability of suspoemulsions are described. Chapter 7 describes the formulation of controlled-release systems with particular reference to the process of microencapsulation. This is followed by the methods of encapsulation by phase separation from aqueous solution and microencapsulation of solid particles. The controlled-release of agrochemicals from matrix-based microparticles and from granules is described. Chapter 8 deals with formulation of adjuvants that are incorporated with the formula-

tion to enhance biological efficacy. It starts with a general introduction describing the various types of adjuvants and the importance of formulation type. The interactions at the air/solution interface and their effect on droplet formation are described. This is followed by a description of the processes of spray impaction and adhesion, droplet sliding and spray retention, wetting and spreading as well as evaporation of spray drops and deposit formation. The process of solubilization by surfactant micelles and its effect on transport is systematically described. Finally, the interaction between surfactant, agrochemical and target species is described to illustrate the effect of adjuvant on agrochemical penetration.

Part II of Volume 4 deals with the formulation of paints and coatings. It consists of seven sections. Chapter 9 gives a general introduction, describing the various components used in paints and coatings. The disperse particles, dispersion medium and film formers are described. The deposition of particles and their adhesion to the substrate are described in terms of the long-range and short-range interaction forces. This is followed by a general description of the flow characteristics (rheology) of paints. Chapter 10 describes the formulation of film formers with particular reference to emulsion and dispersion polymerization. Chapter 11 deals with the formulation of pigment dispersions for paint applications. The various processes of wetting of powders, breaking of aggregates and agglomerates (deagglomeration) and wet milling (comminution) are described. The colloid stabilization of paint dispersions is described in terms of electrostatic double layer and steric stabilization. Chapter 12 describes the processes of enhancement of particle deposition and adhesion in paints and coatings. Chapter 13 deals with the control of the rheology of paint formulations. Chapter 14 describes the methods that can be applied to investigate the rheology of paint formulations. Chapter 15 gives examples of the flow properties of some commercial paints.

Part III of Volume 4 deals with the formulation of food colloids. It consists of six sections. Chapter 16 gives a general introduction describing the complexity of food colloids. Chapter 17 describes the interaction between food-grade agent surfactants and water and the structure of the liquid crystalline phases. Both binary and ternary phase diagrams are described. Particular reference is given to the process of monolayer formation, liquid crystalline phases and emulsion stability. Chapter 18 describes the formulation of food emulsions using proteins and protein/polysaccharides systems. The protein structure and the interfacial properties of proteins at the liquid/liquid interface are described. This is followed by the use proteins as emulsifiers. The protein-polysaccharide interactions and polysaccharide-surfactant interactions in food colloids are described. Chapter 19 deals with the subject of surfactant association structures, microemulsions and emulsions in food. Chapter 20 describes the rheology of food emulsions with particular reference to interfacial rheology and its correlation with emulsion stability. Both mixed surfactant and protein films are described. This is followed by an analysis of the bulk rheology of emulsions. Particular attention is given to the rheology of microgel dispersions and the fractal nature of the aggregated network. Chapter 22 deals with the correlation of food rheology and

mouth feel. The various rheological measurements that can be applied are briefly described. This is followed by an analysis of the break-up of Newtonian and non-Newtonian liquids. The complexity of flow in the oral cavity is described and this is followed by the rheology–texture relationship. Finally, some practical applications of food colloids are given.

References

[1] Tadros T. Handbook of colloid and interface science, Vol. 1 & 2. Berlin: De Gruyter; 2017.
[2] Tadros T. Interfacial phenomena. Vol. 1. Berlin: De Gruyter; 2015.
[3] Brockel U, Meier W, Wagner G, editors. Product design and Engineering, Vol. 1. Weinheim: Wiley-VCH; 2007.
[4] Brockel U, Meier W, Wagner G, editors. Product design and Engineering, Formulation of gels and pastes. Weinheim: Wiley-VCH; 2013.
[5] Tadros T. An introduction to surfactants. Berlin: De Gruyter; 2014.
[6] Tadros T. Polymeric surfactants. Berlin: De Gruyter; 2017.
[7] Tadros T. Dispersions of powders in liquids and stabilisation of suspensions. Weinheim: Wiley-VCH; 2012.
[8] Tadros T. Rheology of dispersions. Weinheim: Wiley-VCH; 2010.
[9] Tadros T. Suspension concentrates. Berlin: De Gruyter; 2017.
[10] Tadros T. Emulsions. Berlin: De Gruyter; 2016.
[11] Tadros T. Formulation of disperse systems. Weinheim: Wiley-VCH; 2014.
[12] Tadros T. Nanodispersions. Berlin: De Gruyter; 2016.

2 Classification of surfactants, their solution properties and self-assembly structures

2.1 Introduction

Surfactants, sometimes referred to as amphipathic or amphiphilic molecules, are used in most formulations. They are applied in solid/liquid dispersions (suspensions) as wetting and dispersing agents as well as for their stabilization against aggregation. For liquid/liquid dispersions (emulsions) surfactants are used for emulsification of oil into water or water into oil. These surfactants are also used for stabilizing the resulting oil/water (O/W) or water/oil (W/O) emulsions against flocculation and coalescence. Surfactants are also essential ingredients for the preparation of microemulsions and their stabilization. The production of stable foams also requires the presence of surfactants which accumulate at the air/water interface. Several other formulations also require the presence of surfactants, such as preparation of polymer colloids (latexes), encapsulation and preparation of solid dosage forms such as grains and granules, tablets, etc. In all these applications it is essential to use a surfactant with the right structure that produces the most effective adsorption at the interface and control of the required property. The surfactant molecules form self-assembly structures in solution that range from simple aggregates or micelles to higher order structures referred to as liquid crystalline structures. These self-assembly structures play a major role in controlling the consistency (rheology) of the resulting dispersion. Such control is very important in many applications, e.g. in hand creams and lotions, liquid detergents, etc.

In this chapter I will start with a classification of surfactants giving examples of each type. This is followed by a section on the solution properties of surfactants with special reference to the process of aggregation into micelles with different shapes. The spontaneous formation of micelles is described by considering the free energy of their formation by application of the second law of thermodynamics. By considering the enthalpy and entropy in the formation of micelles, it is possible to arrive at the driving force for micelle formation. The higher order assembly structures and formation of liquid crystalline phases are also described together with the methods that can be applied to investigate these structures.

2.2 Classification of surfactants

A simple classification of surfactants based on the nature of the hydrophilic group is commonly used. Four main classes may be distinguished, namely anionic, cationic, amphoteric and nonionic [1–3]. A useful technical reference is McCutcheon [4], which is produced annually to update the list of available surfactants. A text by van Os

https://doi.org/10.1515/9783110587944-003

et al. [5] listing the physicochemical properties of selected anionic, cationic and nonionic surfactants has been published by Elsevier. Another useful text is the Handbook of Surfactants by Porter [6]. It should be mentioned that a fifth class of surfactants, usually referred to as polymeric surfactants, has also been used for many years for the preparation of emulsions and suspensions and their stabilization.

2.2.1 Anionic surfactants

These are the most widely used class of surfactants in industrial applications [6–8]. This is due to their relatively low cost of manufacture and they are used in practically every type of detergent. For optimum detergency the hydrophobic chain is a linear alkyl group with a chain length in the region of 12–16 C atoms and the polar head group should be at the end of the chain. Linear chains are preferred since they are more effective and more degradable than the branched chains. The most commonly used hydrophilic groups are carboxylates, sulphates, sulphonates and phosphates. A general formula may be ascribed to anionic surfactants as follows:

- Carboxylates: $C_nH_{2n+1}COO^-X^+$
- Sulphates: $C_nH_{2n+1}OSO_3^-X^+$
- Sulphonates: $C_nH_{2n+1}SO_3^-X^+$
- Phosphates: $C_nH_{2n+1}OPO(OH)O^-X^+$
  with n being the range 8–16 atoms and the counterion X^+ is usually Na^+.

Several other anionic surfactants are commercially available such as sulphosuccinates, isethionates (esters of isothionic acid with the general formula $RCOOCH_2–CH_2–SO_3Na$) and taurates (derivatives of methyl taurine with the general formula $RCON(R')CH_2–CH_2–SO_3Na$), sarchosinates (with the general formula $RCON(R')COONa$) and these are sometimes used for special applications. A brief description of the above anionic classes is given below with some of their applications.

2.2.1.1 Carboxylates

These are perhaps the earliest known surfactants, since they constitute the earliest soaps, e.g. sodium or potassium stearate, $C_{17}H_{35}COONa$, sodium myristate, $C_{14}H_{29}COONa$. The alkyl group may contain unsaturated portions, e.g. sodium oleate, which contains one double bond in the C_{17} alkyl chain. Most commercial soaps will be a mixture of fatty acids obtained from tallow, coconut oil, palm oil, etc. The main attraction of these simple soaps is their low cost, their ready biodegradability and low toxicity. Their main disadvantage is their ready precipitation in water containing bivalent ions such as Ca^{2+} and Mg^{2+}. To avoid their precipitation in hard water, the carboxylates are modified by introducing some hydrophilic chains, e.g. ethoxy carboxylates with the general structure $RO(CH_2CH_2O)_nCH_2COO^-$, ester carboxyl-

ates containing hydroxyl or multiple COOH groups, sarcosinates which contain an amide group with the general structure $RCON(R')COO^-$. The addition of the ethoxylated groups results in increased water solubility and enhanced chemical stability (no hydrolysis). The modified ether carboxylates are also more compatible with electrolytes. They are also compatible with other nonionic, amphoteric and sometimes even cationic surfactants. The ester carboxylates are very soluble in water, but they suffer from the problem of hydrolysis. The sarcosinates are not very soluble in acid or neutral solutions but they are quite soluble in alkaline media. They are compatible with other anionics, nonionics and cationics. The phosphate esters have very interesting properties being intermediate between ethoxylated nonionics and sulphated derivatives. They have good compatibility with inorganic builders and they can be good emulsifiers. A specific salt of a fatty acid is lithium 12-hydroxystearic acid that forms the major constituent of greases.

2.2.1.2 Sulphates

These are the largest and most important class of synthetic surfactants, which are produced by reaction of an alcohol with sulphuric acid, i.e. they are esters of sulphuric acid. In practice sulphuric acid is seldom used and chlorosulphonic or sulphur dioxide/air mixtures are the most common methods of sulphating the alcohol. However, due to their chemical instability (hydrolysing to the alcohol, particularly in acid solutions), they have now been overtaken by the sulphonates, which are chemically stable. The properties of sulphate surfactants depend on the nature of the alkyl chain and the sulphate group. The alkali metal salts show good solubility in water, but they tend to be affected by the presence of electrolytes. The most common sulphate surfactant is sodium dodecyl sulphate (abbreviated as SDS and sometimes referred to as sodium lauryl sulphate) which is extensively used both for fundamental studies as well as in many applications in industry. At room temperature ($\approx 25\,°C$) this surfactant is quite soluble and 30 % aqueous solutions are fairly fluid (low viscosity). However, below 25 °C, the surfactant may separate out as a soft paste as the temperature falls below its Krafft point (the temperature above which the surfactant shows a rapid increase in solubility with a further increase of temperature). The latter depends on the distribution of chain lengths in the alkyl chain, the wider the distribution the lower the Krafft temperature. Thus, by controlling this distribution one may achieve a Krafft temperature of $\approx 10\,°C$. As the surfactant concentration is increased to 30–40 % (depending on the chain length distribution in the alkyl group), the viscosity of the solution increases very rapidly and may produce a gel, but then falls at about 60–70 % to give a pourable liquid, after which it increases again to a gel. The concentration at which the minimum occurs varies according to the alcohol sulphate used, and also the presence of impurities such as unsaturated alcohol. The viscosity of the aqueous solutions can be reduced by addition of short chain alcohols and glycols. The critical micelle concentration (cmc) of SDS (the concentration above which the properties of the solution show

abrupt changes) is 8×10^{-3} mol dm^{-3} (0.24 %). The alkyl sulphates give good foaming properties with an optimum at C_{12}–C_{14}. As with the carboxylates, the sulphate surfactants are also chemically modified to change their properties. The most common modification is to introduce some ethylene oxide units in the chain, usually referred to as alcohol ether sulphates. These are made by sulphation of ethoxylated alcohols. For example, sodium dodecyl 3-mole ether sulphate, which is essentially dodecyl alcohol reacted with 3 mol EO, is then sulphated and neutralized by NaOH. The presence of PEO confers improved solubility when compared with the straight alcohol sulphates. In addition, the surfactant becomes more compatible with electrolytes in aqueous solution. The ether sulphates are also more chemically stable than the alcohol sulphates. The cmc of the ether sulphates is also lower than the corresponding surfactant without the EO units. The viscosity behaviour of aqueous solutions is similar to alcohol sulphates, giving gels in the range 30–60 %. The ether sulphates show a pronounced salt effect, with a significant increase in the viscosity of a dilute solution on addition of electrolytes such as NaCl. The ether sulphates are commonly used in hand dishwashing and in shampoos in combination with amphoteric surfactants.

2.2.1.3 Sulphonates

With sulphonates, the sulphur atom is directly attached to the carbon atom of the alkyl group and this gives the molecule stability against hydrolysis, when compared with the sulphates (where the sulphur atom is indirectly linked to the carbon of the hydrophobe via an oxygen atom). The alkyl aryl sulphonates are the most common type of these surfactants (for example sodium alkyl benzene sulphonate) and these are usually prepared by reacting sulphuric acid with alkyl aryl hydrocarbons, e.g. dodecyl benzene. A special class of sulphonate surfactants are the naphthalene and alkyl naphthalene sulphonates which are commonly used as dispersants. As with the sulphates, some chemical modification is used by introducing ethylene oxide units, e.g. sodium nonyl phenol 2-mole ethoxylate ethane sulphonate $C_9H_{19}C_6H_4(OCH_2CH_2)_2SO_3^-Na^+$. The paraffin sulphonates are produced by sulphooxidation of normal linear paraffins with sulphur dioxide and oxygen and catalysed with ultraviolet or gamma radiation. The resulting alkane sulphonic acid is neutralized with NaOH. These surfactants have excellent water solubility and biodegradability. They are also compatible with many aqueous ions. The linear alkyl benzene sulphonates (LABS) are manufactured from alkyl benzene and the alkyl chain length can vary from C_8 to C_{15}. Their properties are mainly influenced by the average molecular weight and the spread of carbon number of the alkyl side chain. The cmc of sodium dodecyl benzene sulphonate is 5×10^{-3} mol dm^{-3} (0.18 %). The main disadvantage of LABS is their effect on the skin and hence they cannot be used in personal care formulations.

Another class of sulphonates is the α-olefin sulphonates which are prepared by reacting linear α-olefin with sulphur trioxide, typically yielding a mixture of

alkene sulphonates (60–70 %), 3- and 4-hydroxyalkane sulphonates (≈ 30 %) and some disulphonates and other species. The two main α-olefin fractions used as starting material are C_{12}–C_{16} and C_{16}–C_{18}. Fatty acid and ester sulphonates are produced by sulphonation of unsaturated fatty acids or esters. A good example is sulphonated oleic acid,

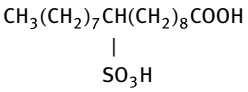

A special class of sulphonates are sulphosuccinates which are esters of sulphosuccinic acid,

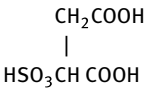

Both mono- and diesters are produced. A widely used diester in many formulations is sodium di(2-ethylhexyl)sulphosuccinate (that is sold commercially under the trade name Aerosol OT). The cmc of the diesters is very low, in the region of 0.06 % for C_6–C_8 sodium salts and they give a minimum in the surface tension of 26 mN m^{-1} for the C_8 diester. Thus these molecules are excellent wetting agents. The diesters are soluble both in water and in many organic solvents. They are particularly useful for the preparation of water-in-oil (W/O) microemulsions.

2.2.1.4 Phosphate-containing anionic surfactants

Both alkyl phosphates and alkyl ether phosphates are made by treating the fatty alcohol or alcohol ethoxylates with a phosphorylating agent, usually phosphorous pentoxide, P_4O_{10}. The reaction yields a mixture of mono- and diesters of phosphoric acid. The ratio of the two esters is determined by the ratio of the reactants and the amount of water present in the reaction mixture. The physicochemical properties of the alkyl phosphate surfactants depend on the ratio of the esters. Phosphate surfactants are used in the metal working industry due to their anticorrosive properties.

2.2.2 Cationic surfactants

The most common cationic surfactants are the quaternary ammonium compounds [9, 10] with the general formula $R'R''R'''R''''N^+X^-$, where X^- is usually a chloride ion and R represents alkyl groups. These quaternaries are made by reacting an appropriate

tertiary amine with an organic halide or organic sulphate. A common class of cationics is the alkyl trimethyl ammonium chlorides, where R contains 8–18 C atoms, e.g. dodecyl trimethyl ammonium chloride, $C_{12}H_{25}(CH_3)_3NCl$. Another widely used cationic surfactant class is that containing two long chain alkyl groups, i.e. dialkyl dimethyl ammonium chloride, with the alkyl groups having a chain length of 8–18 C atoms. These dialkyl surfactants are less soluble in water than the monoalkyl quaternary compounds, but they are commonly used in detergents as fabric softeners. A widely used cationic surfactant is alkyl dimethyl benzyl ammonium chloride (sometimes referred to as benzalkonium chloride and widely used as bactericide), having the structure,

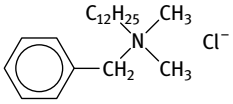

Imidazolines can also form quaternaries, the most common product being the ditallow derivative quaternized with dimethyl sulphate,

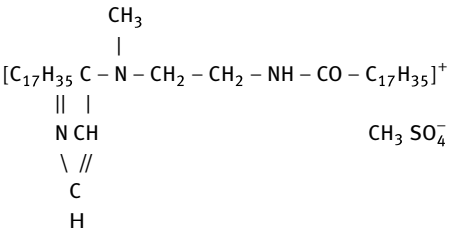

Cationic surfactants can also be modified by incorporating polyethylene oxide chains, e.g. dodecyl methyl polyethylene oxide ammonium chloride having the structure,

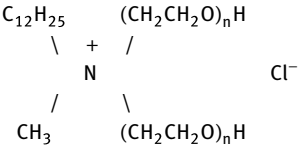

Cationic surfactants are generally water soluble when there is only one long alkyl group. When there are two or more long chain hydrophobes, the product becomes dispersible in water and soluble in organic solvents. They are generally compatible with most inorganic ions and hard water, but they are incompatible with metasilicates and highly condensed phosphates. They are also incompatible with protein-like

materials. Cationics are generally stable to pH changes, both acid and alkaline. They are incompatible with most anionic surfactants, but they are compatible with nonionics. These cationic surfactants are insoluble in hydrocarbon oils. In contrast, cationics with two or more long alkyl chains are soluble in hydrocarbon solvents, but they become only dispersible in water (sometimes forming bilayer vesicle type structures). They are generally chemically stable and can tolerate electrolytes. The cmc of cationic surfactants is close to that of anionics with the same alkyl chain length. For example, the cmc of benzalkonium chloride is 0.17 %. The prime use of cationic surfactants is their tendency to adsorb at negatively charged surfaces, e.g. anticorrosive agents for steel, flotation collectors for mineral ores, dispersants for inorganic pigments, antistatic agents for plastics and fabric softeners, hair conditioners, anticaking agent for fertilizers and as bactericides.

2.2.3 Amphoteric (zwitterionic) surfactants

These are surfactants containing both cationic and anionic groups [11]. The most common amphoterics are the N-alkyl betaines which are derivatives of trimethyl glycine $(CH_3)_3NCH_2COOH$ (that was described as betaine). An example of betaine surfactant is lauryl amido propyl dimethyl betaine $C_{12}H_{25}CON(CH^3)^2CH_2COOH$. These alkyl betaines are sometimes described as alkyl dimethyl glycinates. The main characteristic of amphoteric surfactants is their dependency on the pH of the solution in which they are dissolved. In acid pH solutions, the molecule acquires a positive charge and it behaves like a cationic, whereas in alkaline pH solutions they become negatively charged and behave like an anionic. A specific pH can be defined at which both ionic groups show equal ionization (the isoelectric point of the molecule). This can be described by the following scheme,

$$\underset{\text{acid pH} < 3}{N^+ \ldots COOH} \leftrightarrow \underset{\text{isoelectric}}{N^+ \ldots COO^-} \leftrightarrow \underset{\text{pH} > 6 \text{ alkaline}}{NH \ldots COO^-}$$

Amphoteric surfactants are sometimes referred to as zwitterionic molecules. They are soluble in water, but the solubility shows a minimum at the isoelectric point. Amphoterics show excellent compatibility with other surfactants, forming mixed micelles. They are chemically stable both in acids and alkalis. The surface activity of amphoterics varies widely and it depends on the distance between the charged groups. It shows a maximum in surface activity at the isoelectric point.

Another class of amphoterics are the N-alkyl amino propionates having the structure $R\text{-}NHCH_2CH_2COOH$. The NH group is reactive and can react with another acid molecule (e.g. acrylic) to form an amino dipropionate $R\text{-}N(CH_2CH_2COOH)_2$. Alkyl imidazoline-based product can also be produced by reacting alkyl imidazoline with a

chloro acid. However, the imidazoline ring breaks down during the formation of the amphoteric.

The change in charge with pH of amphoteric surfactants affects their properties, such as wetting, detergency, foaming, etc. At the isoelectric point (IEP), the properties of amphoterics resemble those of nonionics very closely. Below and above the IEP, the properties shift towards those of cationic and anionic surfactants respectively. Zwitterionic surfactants have excellent dermatological properties. They also exhibit low eye irritation and they are frequently used in shampoos and other personal care products (cosmetics).

2.2.4 Nonionic surfactants

The most common nonionic surfactants are those based on ethylene oxide, referred to as ethoxylated surfactants [12–14]. Several classes can be distinguished: alcohol ethoxylates, alkyl phenol ethoxylates, fatty acid ethoxylates, monoalkaolamide ethoxylates, sorbitan ester ethoxylates, fatty amine ethoxylates and ethylene oxide-propylene oxide copolymers (sometimes referred to as polymeric surfactants). Another important class of nonionics are the multihydroxy products such as glycol esters, glycerol (and polyglycerol) esters, glucosides (and polyglucosides) and sucrose esters. Amine oxides and sulphinyl surfactants represent nonionics with a small head group.

2.2.4.1 Alcohol ethoxylates

These are generally produced by ethoxylation of a fatty chain alcohol such as dodecanol. Several generic names are given to this class of surfactants such as ethoxylated fatty alcohols, alkyl polyoxyethylene glycol, monoalkyl polyethylene oxide glycol ethers, etc. A typical example is dodecyl hexaoxyethylene glycol monoether with the chemical formula $C_{12}H_{25}(OCH_2CH_2O)_6OH$ (sometimes abbreviated as $C_{12}E_6$). In practice, the starting alcohol will have a distribution of alkyl chain lengths and the resulting ethoxylate will have a distribution of ethylene oxide (EO) chain lengths. Thus the numbers listed in the literature refer to average numbers.

The cmc of nonionic surfactants is about two orders of magnitude lower than the corresponding anionics with the same alkyl chain length. At a given alkyl chain length, the cmc decreases with decreasing number of EO units. The solubility of the alcohol ethoxylates depends both on the alkyl chain length and the number of ethylene oxide units in the molecule. Molecules with an average alkyl chain length of 12 C atoms and containing more than 5 EO units are usually soluble in water at room temperature. However, as the temperature of the solution is gradually raised, the solution becomes cloudy (as a result of dehydration of the PEO chain and the change in the conformation of the PEO chain) and the temperature at which this occurs is referred to as the

cloud point (CP) of the surfactant. At a given alkyl chain length, the CP increases with increasing EO chain of the molecule. The CP changes with changing concentration of the surfactant solution and the trade literature usually quotes the CP of a 1% solution. The CP is also affected by the presence of electrolyte in the aqueous solution. Most electrolytes lower the CP of a nonionic surfactant solution. Nonionics tend to have maximum surface activity near to the cloud point. The CP of most nonionics increases markedly on addition of small quantities of anionic surfactants. The surface tension of alcohol ethoxylate solutions decreases as its concentration increases until it reaches its cmc, after which it remains constant with a further increase in its concentration. The minimum surface tension reached at and above the cmc decreases with decreasing number of EO units of the chain (at a given alkyl chain). The viscosity of a nonionic surfactant solution increases gradually as its concentration increases, but at a critical concentration (which depends on the alkyl and EO chain lengths) the viscosity shows a rapid increase and ultimately a gel-like structure appears. This results from the formation of a liquid crystalline structure of the hexagonal type. In many cases, the viscosity reaches a maximum after which it shows a decrease due to the formation of other structures (e.g. lamellar phases) (see below).

2.2.4.2 Alkyl phenol ethoxylates

These are prepared by reaction of ethylene oxide with the appropriate alkyl phenol. The most common surfactants of this type are those based on nonyl phenol. These surfactants are cheap to produce, but they suffer from the problem of biodegradability and potential toxicity (the by-product of degradation is nonyl phenol which has considerable toxicity for fish and mammals). In spite of these problems, nonyl phenol ethoxylates are still used in many industrial applications, due to their advantageous properties, such as their solubility both in aqueous and nonaqueous media, their good emulsification and dispersion properties, etc.

2.2.4.3 Fatty acid ethoxylates

These are produced by reaction of ethylene oxide with a fatty acid or a polyglycol and they have the general formula $RCOO–(CH_2CH_2O)_nH$. When a polyglycol is used, a mixture of mono- and diesters ($RCOO–(CH_2CH_2O)_n–OCOR$) is produced. These surfactants are generally soluble in water provided there are enough EO units and the alkyl chain length of the acid is not too long. The mono-esters are much more soluble in water than the diesters. With diesters, a longer EO chain is required to render the molecule soluble. The surfactants are compatible with aqueous ions, provided there is not much unreacted acid. However, these surfactants undergo hydrolysis in highly alkaline solutions.

2.2.4.4 Sorbitan esters and their ethoxylated derivatives (Spans and Tweens)

The fatty acid esters of sorbitan (generally referred to as Spans, an Atlas commercial trade name) and their ethoxylated derivatives (generally referred to as Tweens) are perhaps one of the most commonly used nonionics. They were first commercialized by Atlas in the USA, which has been purchased by ICI. The sorbitan esters are produced by reaction of sorbitol with a fatty acid at a high temperature (> 200 °C). The sorbitol dehydrates to 1,4-sorbitan and then esterification takes place. If one mole of fatty acid is reacted with one mole of sorbitol, one obtains a mono-ester (some diester is also produced as a by-product). Thus, sorbitan mono-ester has the following general formula,

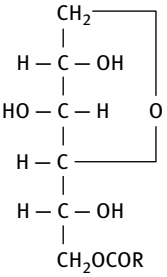

The free OH groups in the molecule can be esterified, producing di- and triesters. Several products are available depending on the nature of the alkyl group of the acid and whether the product is a mono-, di- or triester. Some examples are given below,

- Sorbitan monolaurate – Span 20
- Sorbitan monopalmitate – Span 40
- Sorbitan monostearate – Span 60
- Sorbitan mono-oleate – Span 80
- Sorbitan tristearate – Span 65
- Sorbitan trioleate – Span 85

The ethoxylated derivatives of Spans (Tweens) are produced by reaction of ethylene oxide on any hydroxyl group remaining on the sorbitan ester group. Alternatively, the sorbitol is first ethoxylated and then esterified. However, the final product has different surfactant properties to the Tweens. Some examples of Tween surfactants are given below,

- Polyoxyethylene (20) sorbitan monolaurate – Tween 20
- Polyoxyethylene (20) sorbitan monopalmitate – Tween 40
- Polyoxyethylene (20) sorbitan monostearate – Tween 60
- Polyoxyethylene (20) sorbitan mono-oleate – Tween 80
- Polyoxyethylene (20) sorbitan tristearate – Tween 65
- Polyoxyethylene (20) sorbitan tri-oleate – Tween 85

The sorbitan esters are insoluble in water, but soluble in most organic solvents (low HLB number surfactants). The ethoxylated products are generally soluble in water and they have relatively high HLB numbers. One of the main advantages of the sorbitan esters and their ethoxylated derivatives is their approval as food additives. They are also widely used in cosmetics and some pharmaceutical preparations.

2.2.4.5 Ethoxylated fats and oils

A number of natural fats and oils have been ethoxylated, e.g. lanolin (wool fat) and castor oil ethoxylates. These products are useful for applications in pharmaceutical products, e.g. as solubilizers.

2.2.4.6 Amine ethoxylates

These are prepared by addition of ethylene oxide to primary or secondary fatty amines. With primary amines both hydrogen atoms on the amine group react with ethylene oxide and therefore the resulting surfactant has the structure,

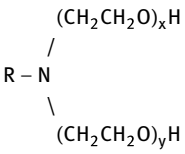

The above surfactants acquire a cationic character if the EO units are small in number and if the pH is low. However, at high EO levels and neutral pH they behave very similarly to nonionics. At low EO content, the surfactants are not soluble in water, but become soluble in an acid solution. At high pH, the amine ethoxylates are water soluble provided the alkyl chain length of the compound is not long; usually a C_{12} chain is adequate for reasonable solubility at sufficient EO content.

2.2.4.7 Amine oxides

These are prepared by oxidizing a tertiary nitrogen group with aqueous hydrogen peroxide at temperatures in the region 60–80 °C. Several examples can be quoted: N-alkyl amidopropyl-dimethyl amine oxide, N-alkyl bis(2-hydroxyethyl) amine oxide and N-alkyl dimethyl amine oxide. They have the general formula,

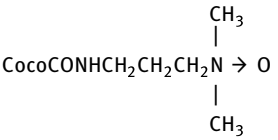

Alkyl amidopropyl-dimethyl amine oxide

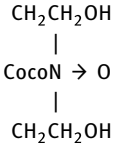

Coco bis (2-hydroxyethyl) amine oxide

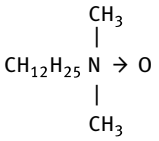

Lauryl dimethyl amine oxide

In acid solutions, the amino group is protonated and acts as a cationic surfactant. In neutral or alkaline solution the amine oxides are essentially nonionic in character. Alkyl dimethyl amine oxides are water soluble up to C_{16} alkyl chain. Above pH 9, amine oxides are compatible with most anionics. At pH 6.5 and below some anionics tend to interact and form precipitates. In combination with anionics, amine oxides can be foam boosters (e.g. in shampoos).

2.2.5 Speciality surfactants. Fluorocarbon and silicone surfactants

These surfactants can lower the surface tension of water to values below 20 mN m^{-1}. Most surfactants described above lower the surface tension of water to values above 20 mN m^{-1}, typically in the region of 25–27 mN m^{-1}. The fluorocarbon and silicone surfactants are sometimes referred to as superwetters as they cause enhanced wetting and spreading of their aqueous solution. However, they are much more expensive than conventional surfactants and they are only applied for specific applications in which the low surface tension is a desirable property. Fluorocarbon surfactants have been prepared with various structures consisting of perfluoroalkyl chains and anionic, cationic, amphoteric and polyethylene oxide polar groups. These surfactants have good thermal and chemical stability and they are excellent wetting agents for low-energy surfaces. Silicone surfactants, sometimes referred to as organosilicones, are those with polydimethylsiloxane backbone. The silicone surfactants are prepared by incorporating a water-soluble or hydrophilic group into a siloxane backbone. The latter can also be modified by incorporating a paraffinic hydrophobic chain at the end or along the polysiloxane backbone. The most common hydrophilic groups are EO/PO and the structures produced are rather complex; most manufacturers of silicone surfactants do not reveal the exact structure. The mechanism by which these

molecules lower the surface tension of water to low values is far from being well understood. The surfactants are widely applied as spreading agents on many hydrophobic surfaces. Incorporating organophilic groups into the backbone of the polydimethyl siloxane backbone can yield products that exhibit surface active properties in organic solvents.

2.2.6 Gemini surfactants

A gemini surfactant is a dimeric molecule consisting of two hydrophobic tails and two head groups linked together with a short spacer [15]. This is illustrated below for a molecule containing two cationic head groups (separated by two methylene groups) with two alkyl chains,

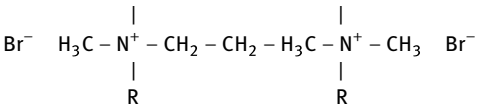

These surfactants show several interesting physicochemical properties, such as very high efficiency in lowering the surface tension and very low cmc. For example, the cmc of a conventional cationic dodecyltrimethylammonium bromide is 16 mM, whereas that of the corresponding gemini surfactant, having a two carbon linkage between the head groups, is 0.9 mM. In addition, the surface tension reached at and above the cmc is lower for gemini surfactants when compared to that of the corresponding conventional one. Gemini surfactants are also more effective in lowering the dynamic surface tension (time required for reaching the equilibrium value is shorter). These effects are due to the better packing of the gemini surfactant molecules at the air/water interface.

2.2.7 Surfactants derived from mono- and polysaccharides

Several surfactants have been synthesized starting from mono- or oligosaccharides by reaction with the multifunctional hydroxyl groups: alkyl glucosides, alkyl polyglucosides [16], sugar fatty acid esters and sucrose esters [17], etc. The technical problem is one of joining a hydrophobic group to the multihydroxyl structure. Several surfactants have been made, e.g. esterification of sucrose with fatty acids or fatty glycerides to produce sucrose esters having the following structure,

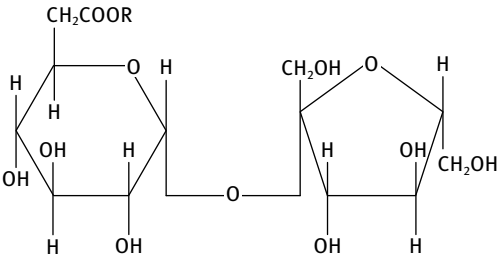

The most interesting sugar surfactants are the alkyl polyglucosides (APG) which are synthesized using a two stage transacetalization process [16]. In the first stage, the carbohydrate reacts with a short chain alcohol, e.g. butanol or propylene glycol. In the second stage, the short chain alkyl glucoside is transacetalized with a relatively long chain alcohol ($C_{12–14}$–OH) to form the required alkyl polyglucoside. This process is applied if oligo- and polyglucoses (e.g. starch, syrups with a low dextrose equivalent, DE) are used. In a simplified transacetalization process, syrups with high glucose content (DE > 96 %) or solid glucose types can react with short chain alcohols under normal pressure. The scheme for alkyl polyglucoside synthesis is shown below. Commercial alkyl polyglucosides (APG) are complex mixtures of species varying in the degree of polymerization (DP, usually in the range 1.1–3) and in the length of the alkyl chain. When the latter is shorter than C_{14} the product is water soluble. The cmc values of APGs are comparable to nonionic surfactants and they decrease with increasing alkyl chain length.

APG surfactants have good solubility in water and they have high cloud points (> 100 °C). They are stable in neutral and alkaline solutions but are unstable in strong acid solutions. APG surfactants can tolerate high electrolyte concentrations and they are compatible with most types of surfactants. They are used in personal care products for cleansing formulations as well as for skin care and hair products. They are also used in hard surface cleaners and laundry detergents. Several applications in agrochemical formulations can be mentioned such as wetting agents and penetrating agents for the active ingredient.

2.2.8 Naturally occurring surfactants

Several naturally occurring amphipathic molecules exist in the body, such as bile salts, phospholipids and cholesterol, that play an important role in various biological processes. Their interactions with other solutes, such as drug molecules, and with membranes are also very important. Bile salts are synthesized in the liver and they consist of alicyclic compounds possessing hydroxyl and carboxyl groups. As an illustration, the structure of cholic acid is given in Fig. 2.1.

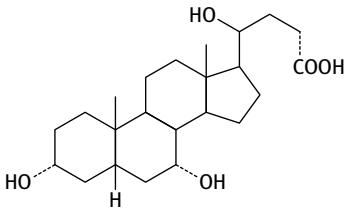

Fig. 2.1: Structure of cholic acid.

It is the positioning of the hydrophilic groups in relation to the hydrophobic steroidal nucleus that gives the bile salts their surface activity and determines their ability to aggregate. Fig. 2.2 shows the possible orientation of cholic acid at the air-water interface, the hydrophilic groups being oriented towards the aqueous phase [18, 19]. The steroid portion of the molecule is shaped like a "saucer" as the A ring is cis with respect to the B ring. Small [20] suggested that small or primary aggregates with up to 10 monomers form above the cmc by hydrophobic interactions between the nonpolar sides of the monomers. These primary aggregates form larger units by hydrogen bonding between the primary micelles. This is schematically illustrated in Fig. 2.3.

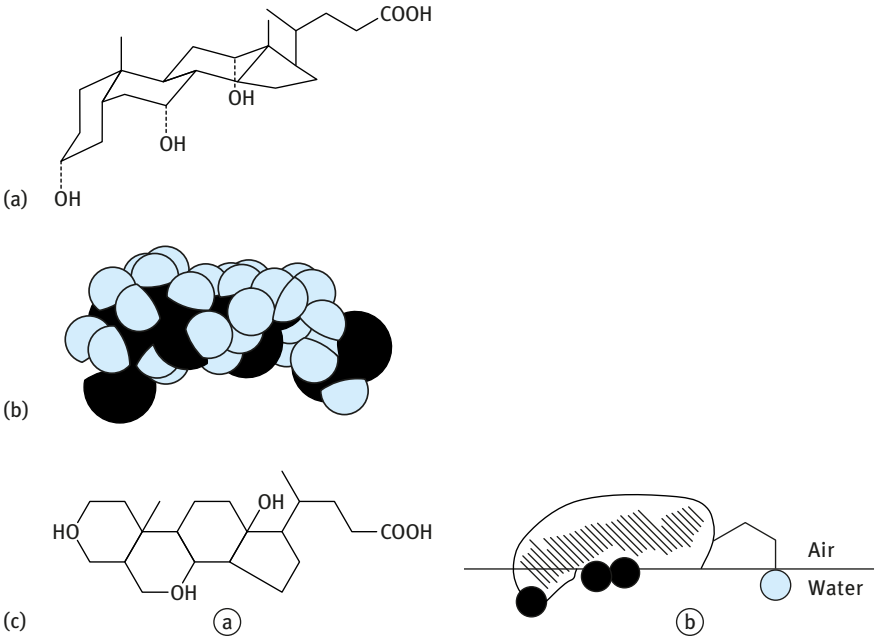

Fig. 2.2: (a) Structural formula of cholic acid showing the cis position of the A ring; (b) Courtauld space-filling model of cholic acid; (c) orientation of cholic acid molecules at the air-water interface (hydroxyl groups represented by filled circles and carboxylic acid groups by open circles).

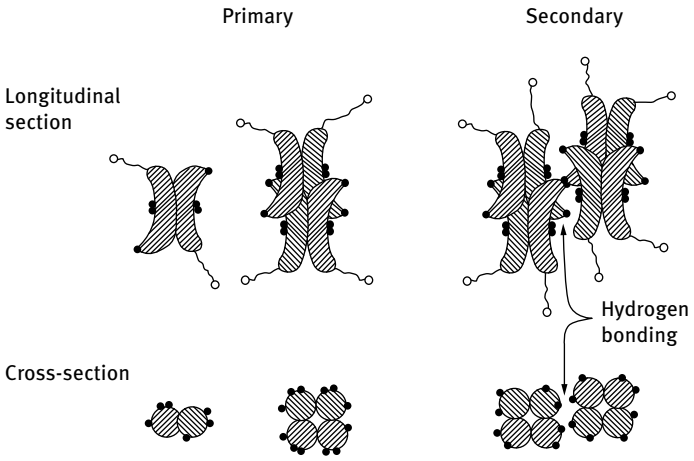

Fig. 2.3: Schematic representation of the structure of bile acid salt micelles.

Oakefull and Fisher [19, 21] stressed the role of hydrogen bonding rather than hydrophobic bonding in the association of bile salts. However, Zana [22] regarded the association as a continuous process with hydrophobic interaction as the main driving force.

The cmc of bile salts is strongly influenced by their structure; the trihydroxy cholanic acids have higher cmc than the less hydrophilic dihydroxy derivatives. As expected, the pH of solutions of these carboxylic acid salts has an influence on micelle formation. At sufficiently low pH, bile acids (which are sparingly soluble) will be precipitated from solution, initially being incorporated or solubilized in the existing micelles. The pH at which precipitation occurs, on saturation of the micellar system, is generally about one pH unit higher than the pK_a of the bile acid.

Bile salts play important roles in physiological functions and drug absorption. It is generally agreed that bile salts aid fat absorption. Mixed micelles of bile salts, fatty acids and monoglycerides can act as vehicles for fat transport. However, the role of bile salts in drug transport is not well understood. Several suggestions have been made to explain the role of bile salts in drug transport, such as facilitation of transport from liver to bile by direct effect on canicular membranes, stimulation of micelle formation inside the liver cells, binding of drug anions to micelles, etc. The enhanced absorption of medicinals on administration with deoxycholic acid may be due to a reduction in interfacial tension or micelle formation. The administration of quinine and other alkaloids in combination with bile salts has been claimed to enhance their parasiticidal action. Quinine, taken orally, is considered to be absorbed mainly from the intestine and a considerable amount of bile salts is required to maintain a colloidal dispersion of quinine. Bile salts may also influence drug absorption either by affecting membrane permeability or by altering normal gastric emptying rates. For example, sodium taurocholate increases the absorption of sulphaguanidine from the stomach, jejunum and

ileum. This is due to increasing membrane permeability induced by calcium depletion and interference with the bonding between phospholipids in the membrane.

Another important naturally occurring class of surfactants which are widely found in biological membranes are the lipids, for example phosphatidylcholine (lecithin), lysolecithin, phosphatidylethanolamine and phosphatidylinositol. The structure of these lipids is given in Fig. 2.4. These lipids are also used as emulsifiers for intravenous fat emulsions, anaesthetic emulsions as well as for the production of liposomes or vesicles for drug delivery. The lipids form coarse turbid dispersions of large aggregates (liposomes) which on ultrasonic irradiation form smaller units or vesicles. The liposomes are smectic mesophases of phospholipids organized into bilayers which assume a multilamellar or unilamellar structure. The multilamellar species are heterogeneous aggregates, most commonly prepared by dispersal of a thin film of phospholipid (alone or with cholesterol) into water. Sonication of the multilamellar units can produce the unilamellar liposomes, sometimes referred to as vesicles. The net charge of liposomes can be varied by incorporating a long chain amine, such as stearyl amine (to give a positively charged vesicle) or dicetyl phosphate (giving negatively charged species). Both lipid-soluble and water-soluble drugs can be entrapped in liposomes. The liposoluble drugs are solubilized in the hydrocarbon

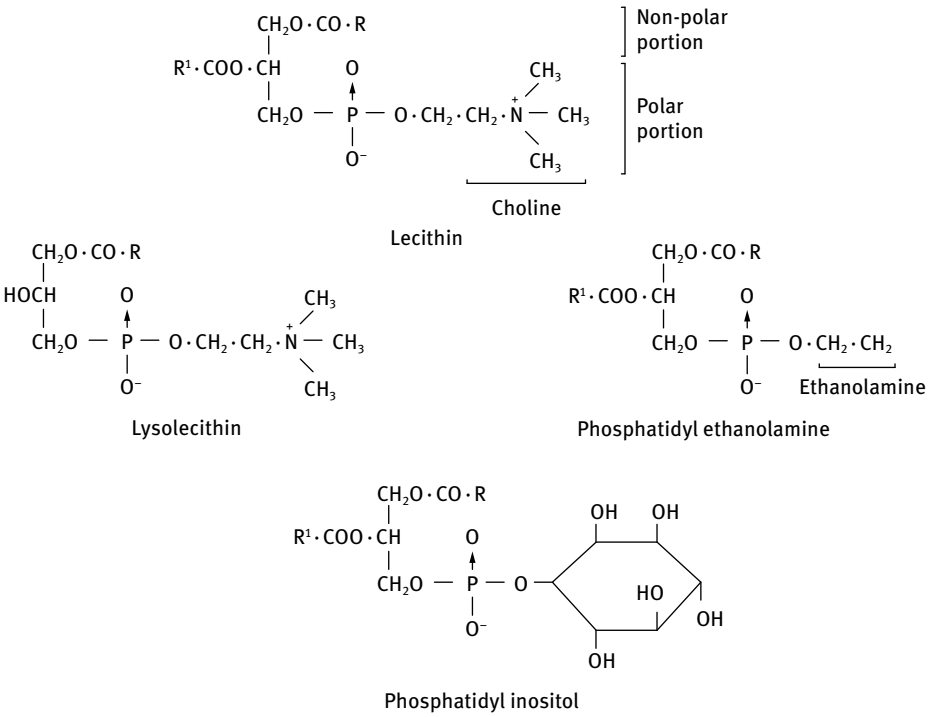

Fig. 2.4: Structure of lipids.

interiors of the lipid bilayers, whereas the water-soluble drugs are intercalated in the aqueous layers. Liposomes, like micelles, may provide a special medium for reactions to occur between the molecules intercalated in the lipid bilayers or between the molecules entrapped in the vesicle and free solute molecules.

Phospholipids play an important role in lung functions. The surface active material to be found in the alveolar lining of the lung is a mixture of phospholipids, neutral lipids and proteins. The lowering of surface tension by the lung surfactant system and the surface elasticity of the surface layers assists alveolar expansion and contraction. Deficiency of lung surfactants in newborns leads to a respiratory distress syndrome and this led to the suggestion that instillation of phospholipid surfactants could cure the problem.

2.2.9 Biosurfactants

In recent years there has been a great deal of concern regarding the use of conventional surfactants in cosmetic and personal care applications. This is due to the environmental and health concerns when using many of the currently used synthetic surfactants. These concerns can be alleviated by the use of biosurfactants that are produced from natural raw materials that possess good biodegradability, low toxicity and the desirable functional performance such as good emulsification and dispersion, high physical stability and high performance on application. The biosurfactants are produced using catalysts in the form of living microorganisms and enzymes [23–25]. Microbial biosurfactants are structurally diverse and complex and are produced in a biosynthetic root catalysed by enzymes. Several classes are available: glycolipids, e.g. rhamnolipids, sophorolipids; lipopeptides and lipoproteins, e.g. surfactin, polymyxins, gramicidins; phospholipids and fatty acids; complex combinations of biopolymers, e.g. emulsan, liposan. The enzymatic synthesis of surfactants are essentially chemical reactions in which an enzyme replaces a conventional chemical catalyst. The surfactants produced by a single enzyme are simpler in structure when compared to those produced by microorganisms. Enzymes are able to catalyse a wide range of reactions and they are unique in their specificity and selectivity. The selectivity is recognized at three levels: chemo-, regio- and enantioselectivity. Thus reactions that cannot be achieved by classical organic synthesis (that may require several steps) can be facilitated by biocatalysis. The high selectivity results in the production of fewer by-products. Development of solvent-free processes is also possible using enzymes and hence the products are safer and environmentally friendly. Biocatalysis has been used for the synthesis of surfactants with different hydrophilic groups attached to the hydrophobic chain via ester, amide or glycosidic bonds. Typical examples are the mono- and diacylglycerols. Their technical production uses a natural fat or oil (triglyceride) as the starting material. Enzymatic methods have the advantage of high selectivity. For example it is possible to make 2-monoacyl glycerols by selective

removal of the fatty acids in the 1- and 3-positions using a regiospecific lipase as a catalyst in a suitable reaction medium. Enzymes can be used to modify glycerol phospholipids by removal of one of the fatty acids to produce lysophospholipids (a good emulsifying agent). This transformation can be achieved using phospholipase A2 that removes the fatty acid in the sn^{-2} position.

Lipases have been used to synthesize a wide range of surfactant esters from fatty acids and carbohydrates. The fatty acid can be used either in the free form or as an ester. To make it possible, one needs to find a solvent that efficiently dissolves both fatty acid and carbohydrate. The carbohydrate is made more hydrophobic by converting it to an acetal, leaving one OH group for esterification. The acetal groups are removed by acid catalysis. This is illustrated in Scheme 1 in Fig. 2.5. Alternatively, the carbohydrate is made more hydrophobic by converting it to a butyl glycoside using glucosidase which is then further reacted with fatty acid using lipase as is illustrated in Scheme 2 in Fig. 2.5.

Scheme 1

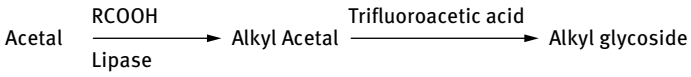

Scheme 2

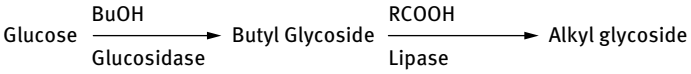

Fig. 2.5: Scheme for synthesis of an alkyl polyglucoside by a two-step enzymatic root.

Most studies of enzymatic sugar ester synthesis have focused on the esterification of monosaccharides, since the problem with poor substrate miscibility increases significantly with increasing the size of the carbohydrate. However, by careful choice of reaction conditions it has been possible to acylate several di- and trisaccharides. Solvent mixtures of 2-methyl-2-butanol and dimethylsulfoxide have been used in combination with vinyl esters (C_8–C_{18}) to successfully achieve acylation of maltose, maltotriose and leucrose. Ionic liquids are promising nonaqueous solvents for the dissolution of carbohydrates and they have been used in several studies on enzymatic sugar ester synthesis. Protease-catalysed synthesis of sugar esters has been reported. 6-O-butyl-D-glucose was prepared using subtilisin (a protease from Bacillus subtilis) as catalyst and trichloroethyl butyrate as acyl donor in anhydrous dimethyl formamide. Oligosaccharides as long as maltoheptaose were also acylated under these conditions. Bacillus protease has been used to synthesize sucrose laurate from sucrose and vinyl laurate in dimethylformamide. Lipases can accept a wide variety of nucleophiles for the deacylation of acyl enzyme synthesis. By proper choice of reaction conditions it was possible to acylate a wide range of carbohydrates. The main products are obtained by esterification of the primary hydroxyl group. In carbohydrates having more than one

primary OH group, the enzyme can selectively acylate one of them. This is the case with maltose. With fructose, mixtures are obtained. Most carbohydrate esters have been prepared using monosaccharides as substrates.

Fatty acid derivatives with an amide bond possess useful properties for surfactants, e.g. enhancing foaming properties of cleaning and personal care products, stabilizing foam and enhancing detergency. The amide bond increases the hydrophilicity of the fatty acid and therefore the surfactant becomes chemically and physically very stable under alkaline conditions. Synthesis of amides can be done by proteases, but these enzymes are very specific for certain amino acids and are more sensitive to organic solvents. Lipases have been used for synthesis of peptides, fatty amides and N-acylamino acids and the acylation of alkanolamines.

Another important class of biosurfactants are the amino-sugar derivatives. Glycamide surfactants are nonionic and biodegradable. In glycamide surfaactants the hydrophilic moiety (an amino-sugar derivative) is linked to the fatty acid by an amide bond, e.g. glucamides and lactobionamides. A conventional method for preparing sugar fatty amide surfactants includes the Schotten–Baumann reaction between an amine and a fatty acid chloride, where the chloride salt produced has to be removed. The regio- and enantioselectivity of enzymes provides a convenient method of acylation of sugars and sugar amines. Chemoselective acylation of a secondary amine, N-methyl glucamine with fatty acid is possible using lipases (from Novozym).

Alkanolamides are important fatty acid derivates for a wide range of applications, e.g. personal care and hard surface cleaning. They are characterized by their skin tolerance, good biodegradability and low toxicity. Alkanolamides are produced by condensation of fatty acids or fatty acid esters or triglyceride with alkanolamine, e.g. monoethanolamine or diethanolamine, using high temperature or a metal oxide catalyst. Alkanolamine synthesis can also be achieved using lipase. Alkanolamines are susceptible to acylation both at the amine and hydroxyl group. The main product using lipase (Novozym 435) is the amide.

Amino acid/peptide-lipid conjugates are an interesting class of surfactants with good surface activity, excellent emulsifying agents, antimicrobial activity, low toxicity and high biodegradability. They are attractive for applications in personal care products. The large variety of amino acid/peptide structures combined with fatty acids of varying structure and carbon chain length can produce surfactants with wide structural diversity and different physicochemical and biological properties. Depending on the free functional groups on the amino acids, anionic, nonionic, amphoteric and cationic surfactants can be produced. Different forms of amino acid surfactants have been synthesized using enzymes.

As mentioned before, carbohydrate ester surfactants suffer from the disadvantage of chemical instability at neutral or alkaline pH (due to the instability of the ester bond). This instability problem can be overcome by using alkyl glycosides which are based on similar building blocks. Chemical synthesis is useful for the production of mixtures of alkyl glycosides as discussed before. When pure isomers are needed, en-

zymatic synthesis offers an attractive alternative. Two main classes of enzymes can be used for coupling the carbohydrate part to a hydrophobic alcohol, namely glycosyl transferases and glycosyl hydrolases. An alternative route to alkyl glycosides is to use transglycosylation reaction with an activated carbohydrate substrate.

2.3 Aggregation of surfactants, self-assembly structures, liquid crystalline phases

2.3.1 Physical properties of surfactant solutions

The physical properties of surface active agent solutions differ from those of non-amphipathic molecule solutions (such as sugars) in one major aspect, namely the abrupt changes in their properties above a critical concentration [26]. This is illustrated in Fig. 2.6 which shows plots of several physical properties (osmotic pressure, surface tension, turbidity, solubilization, magnetic resonance, equivalent conductivity and self-diffusion) as a function of concentration for an anionic surfactant. At low concentrations, most properties are similar to those of a simple electrolyte. One notable exception is the surface tension, which decreases rapidly with increasing surfactant concentration. However, all the properties (interfacial and bulk) show an abrupt change at a particular concentration, which is consistent with the fact that at and above this concentration, surface active molecules or ions associate to form larger units. These associated units are called micelles (self-assembled structures) and the first formed aggregates are generally approximately spherical in shape. A schematic representation of a spherical micelle [27] is given in Fig. 2.7.

The concentration at which this association phenomenon occurs is known as the critical micelle concentration (cmc). Each surfactant molecules has a characteristic cmc value at a given temperature and electrolyte concentration. The most common technique for measuring the cmc is surface tension, γ, which shows a break at the cmc, after which γ remains virtually constant with any further increase in concen-

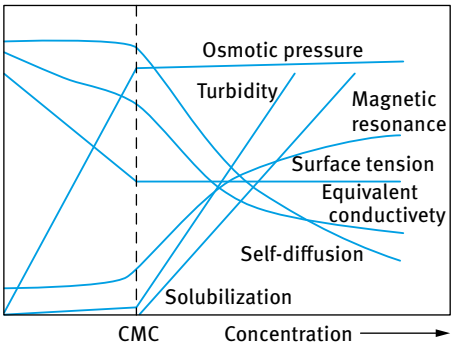

Fig. 2.6: Variation of solution properties with surfactant concentration.

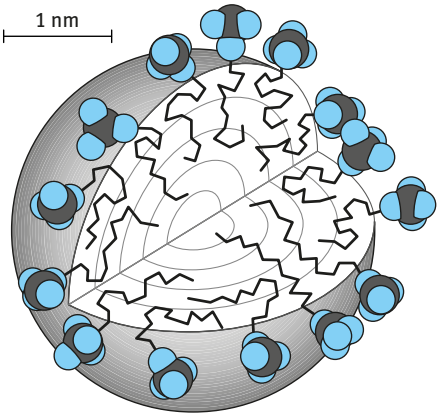

Fig. 2.7: Illustration of a spherical micelle for dodecyl sulphate [2].

tration. However, other techniques such as self-diffusion measurements, NMR and fluorescence spectroscopy can be applied. A compilation of cmc values was given in 1971 by Mukerjee and Mysels [28], which is clearly not an up-to-date text, but is an extremely valuable reference. As an illustration, the cmc values of a number of surface active agents are given in Tab. 2.1, to show some of the general trends [28]. Within any class of surface active agent, the cmc decreases with increasing chain length of the hydrophobic portion (alkyl group). As a general rule, the cmc decreases by a factor of 2 for ionics (without added salt) and by a factor of 3 for nonionics on adding one methylene group to the alkyl chain. With nonionic surfactants, increasing the length of the hydrophilic group (polyethylene oxide) causes an increase in cmc.

Tab. 2.1: Critical micelle concentration of surfactant classes.

Surface active agent	cmc (mol dm^{-3})
(A) *Anionic*	
Sodium octyl-l-sulphate	1.30×10^{-1}
Sodium decyl-l-sulphate	3.32×10^{-2}
Sodium dodecyl-l-sulphate	8.39×10^{-3}
Sodium tetradecyl-l-sulphate	2.05×10^{-3}
(B) *Cationic*	
Octyl trimethyl ammonium bromide	1.30×10^{-1}
Decetryl trimethyl ammonium bromide	6.46×10^{-2}
Dodecyl trimethyl ammonium bromide	1.56×10^{-2}
Hexactecyltrimethyl ammonium bromide	9.20×10^{-4}
(C) *Nonionic*	
Octyl hexaoxyethylene glycol monoether C_8E_6	9.80×10^{-3}
Decyl hexaoxyethylene glycol monoether $C_{10}E_6$	9.00×10^{-4}
Decyl nonaoxyethylene glycol monoether $C_{10}E_9$	1.30×10^{-3}
Dodecyl hexaoxyethylene glycol monoether $C_{12}E_6$	8.70×10^{-5}
Octylphenyl hexaoxyethylene glycol monoetherC_8E_6	2.05×10^{-4}

In general, nonionic surfactants have lower cmc values than their corresponding ionic surfactants of the same alkyl chain length. Incorporating a phenyl group into the alkyl group increases its hydrophobicity to a much smaller extent than increasing its chain length with the same number of carbon atoms. The valency of the counterion in ionic surfactants has a significant effect on the cmc. For example, increasing the valency of the counterion from 1 to 2 causes a reduction in the cmc by roughly a factor of 4.

The cmc is, to a first approximation, independent of temperature. This is illustrated in Fig. 2.8 which shows the variation of cmc of SDS with temperature. The cmc varies in a non-monotonic way by ca 10–20 % over a wide temperature range. The shallow minimum around 25 °C can be compared with a similar minimum in the solubility of hydrocarbon in water [29]. However, nonionic surfactants of the ethoxylate type show a monotonic decrease [29] in cmc with increasing temperature, as illustrated in Fig. 2.8 for $C_{10}E_5$. The effect of adding cosolutes, e.g. electrolytes and non-electrolytes, on the cmc can be very striking. For example, addition of 1 : 1 electrolyte to a solution of anionic surfactant gives a dramatic lowering of the cmc, which may amount to one order of magnitude. The effect is moderate for short chain surfactants, but is much larger for long chain ones. At high electrolyte concentrations, the reduction in cmc with an increase in the number of carbon atoms in the alkyl chain is much stronger than without added electrolyte. This rate of decrease at high electrolyte concentrations is comparable to that of nonionics. The effect of added electrolyte also depends on the valency of the added counterions. In contrast, for nonionics, addition of electrolytes causes only small variation in the cmc.

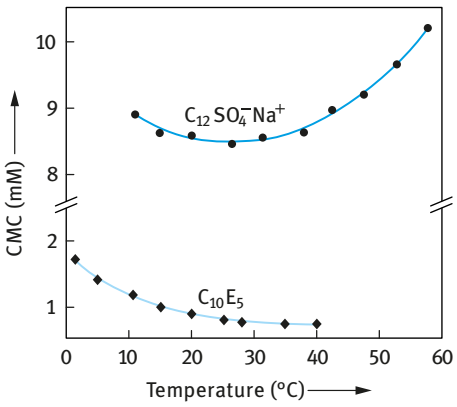

Fig. 2.8: Temperature dependency of the cmc of SDS and $C_{10}E_5$ [29].

Non-electrolytes such as alcohols can also cause a decrease in the cmc [30]. The alcohols are less polar than water and are distributed between the bulk solution and the micelles. The more preference they have for the micelles, the more they stabilize them. A longer alkyl chain leads to a less favourable location in water and more favourable location in the micelles

The presence of micelles can account for many of the unusual properties of solutions of surface active agents. For example, it can account for the near constant surface tension value, above the cmc (Fig. 2.6). It also accounts for the reduction in molar conductance of the surface active agent solution above the cmc, which is consistent with the reduction in mobility of the micelles as a result of counterion association. The presence of micelles also accounts for the rapid increase in light scattering or turbidity above the cmc The presence of micelles was originally suggested by McBain [31] who suggested that below the cmc most of the surfactant molecules are unassociated, whereas in the isotropic solutions immediately above the cmc, micelles and surfactant ions (molecules) are though to co-exist, the concentration of the latter changing very slightly as more surfactant is dissolved. However, the self-association of an amphiphile occurs in a stepwise manner with one monomer added to the aggregate at a time. For a long chain amphiphile, the association is strongly cooperative up to a certain micelle size where counteracting factors became increasingly important. Typically, the micelles have a closely spherical shape in a rather wide concentration range above the cmc. Originally, it was suggested by Adam [32] and Hartley [33] that micelles are spherical in shape and have the following properties:

(i) the association unit is spherical with a radius approximately equal to the length of the hydrocarbon chain;
(ii) the micelle contains about 50–100 monomeric units; aggregation number generally increases with increasing alkyl chain length;
(iii) with ionic surfactants, most counterions are bound to the micelle surface, thus significantly reducing the mobility from the value to be expected from a micelle with non-counterion bonding;
(iv) micellization occurs over a narrow concentration range as a result of the high association number of surfactant micelles;
(v) the interior of the surfactant micelle essentially has the properties of a liquid hydrocarbon.

This is confirmed by the high mobility of the alkyl chains and the ability of the micelles to solubilize many water-insoluble organic molecules, e.g. dyes and agrochemicals. To a first approximation, micelles can, over a wide concentration range above the cmc, be viewed as microscopic liquid hydrocarbon droplets covered with polar head groups, which interact strongly with water molecules. It appears that the radius of the micelle core constituted by the alkyl chains is close to the extended length of the alkyl chain, i.e. in the range 1.5–3.0 nm. As we will see later, the driving force for micelle formation is the elimination of the contact between the alkyl chains and water. The larger a spherical micelle, then the more efficient this is, since the volume-to-area ratio increases. It should be noted that the surfactant molecules in the micelles are not all extended. Only one molecule needs to be extended to satisfy the criterion that the radius of the micelle core is close to the extended length of the alkyl chain. The majority of surfactant molecules are in a disordered state. In other words, the interior of the

micelle is close to that of the corresponding alkane in a neat liquid oil. This explains the large solubilization capacity of the micelle towards a broad range of nonpolar and weakly polar substances. At the surface of the micelle, associated counterions (in the region of 50–80 % of the surfactant ions) are present. However, simple inorganic counterions are very loosely associated with the micelle. The counterions are very mobile (see below) and there is no specific complex formed with a definite counterion-head group distance. In other words, the counterions are associated by long-range electrostatic interactions.

A useful concept for characterizing micelle geometry is the critical packing parameter, CPP. The aggregation number N is the ratio between the micellar core volume, V_{mic}, and the volume of one chain, υ,

$$N = \frac{V_{\mathrm{mic}}}{\upsilon} = \frac{(4/3)\pi R_{\mathrm{mic}}^3}{\upsilon}, \tag{2.1}$$

where R_{mic} is the radius of the micelle.

The aggregation number, N, is also equal to the ratio of the area of a micelle, A_{mic}, to the cross sectional area, a, of one surfactant molecule,

$$N = \frac{A_{\mathrm{mic}}}{a} = \frac{4\pi R_{\mathrm{mic}}^2}{a}. \tag{2.2}$$

Combining equations (2.1) and (2.2),

$$\frac{\upsilon}{R_{\mathrm{mic}} a} = \frac{1}{3}. \tag{2.3}$$

Since R_{mic} cannot exceed the extended length of a surfactant alkyl chain, l_{max},

$$l_{\mathrm{max}} = 1.5 + 1.265 n_{\mathrm{c}}. \tag{2.4}$$

This means that for a spherical micelle,

$$\frac{\upsilon}{l_{\mathrm{max}} a} \leq \frac{1}{3}. \tag{2.5}$$

The ratio $\upsilon/(l_{\mathrm{max}} a)$ is denoted as the critical packing parameter (CPP).

Although the spherical micelle model accounts for many of the physical properties of solutions of surfactants, a number of phenomena remain unexplained if other shapes are not considered. For example, McBain [34] suggested the presence of two types of micelles, spherical and lamellar, in order to account for the drop in molar conductance of surfactant solutions. The lamellar micelles are neutral and hence they account for the reduction in conductance. Later, Harkins et al. [35] used McBain's model of lamellar micelles to interpret his X-ray results in soap solutions. Moreover, many modern techniques such as light scattering and neutron scattering indicate that in many systems the micelles are not spherical. For example, Debye and Anacker [36] proposed a cylindrical micelle to explain the light scattering results on hexadecyl

trimethyl ammonium bromide in water. Evidence for disc-shaped micelles has also been obtained under certain conditions. A schematic representation of the spherical, lamellar and rod-shaped micelles, suggested by McBain, Hartley and Debye is given in Fig. 2.9. Many ionic surfactants show dramatic temperature-dependent solubility as illustrated in Fig. 2.10. The solubility first increases gradually with rising temperature, and then, above a certain temperature, there is a sudden increase of solubility with any further increase in temperature. The cmc increases gradually with increasing temperature. At a particular temperature, the solubility becomes equal to the cmc, i.e. the solubility curve intersects the cmc and this temperature is referred to as the Krafft temperature. At this temperature an equilibrium exists between solid hydrated surfactant, micelles and monomers (i.e. the Krafft temperature is a "triple point"). Surfactants with ionic head groups and long straight alkyl chains have high Krafft temperatures. The Krafft temperature increases with increasing alkyl chain length of the surfactant molecule. It can be reduced by introducing branching in the alkyl chain. The Krafft temperature is also reduced by using alkyl chains with a wide distribution of the chain lengths. Addition of electrolytes causes an increase in the Krafft temperature.

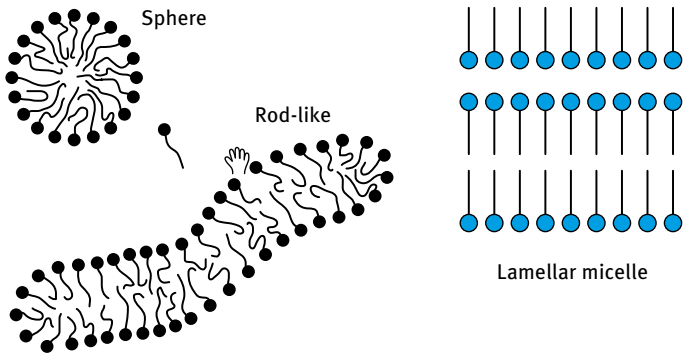

Fig. 2.9: Shapes of micelles.

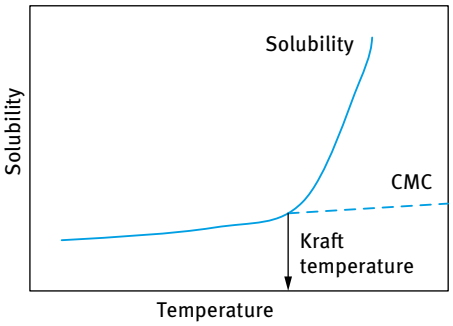

Fig. 2.10: Variation of solubility and critical micelle concentration (cmc) with temperature.

With nonionic surfactants of the ethoxylate type, increasing the temperature of a solution at a given concentration causes dehydration of the PEO chains and at a critical temperature the solution become cloudy. This is illustrated in Fig. 2.11 which shows the phase diagram of $C_{12}E_6$. Below the cloud point (CP) curve one can identify different liquid crystalline phases hexagonal – cubic – lamellar which are schematically shown in Fig. 2.12.

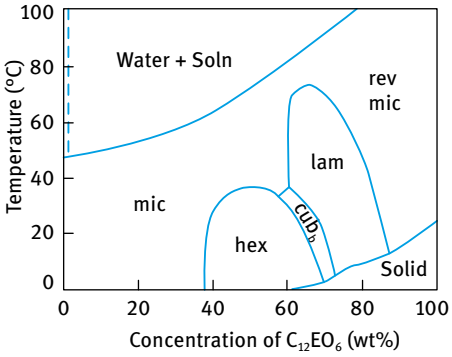

Fig. 2.11: Phase diagram of $C_{12}E_6$.

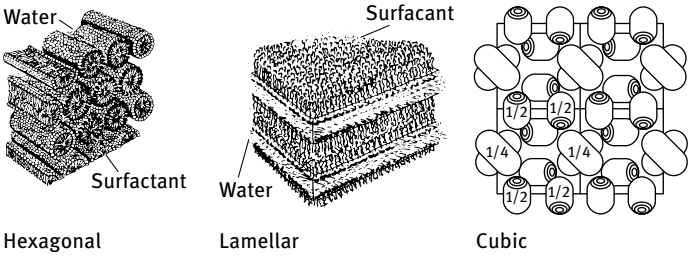

Fig. 2.12: Schematic picture of liquid crystalline phases.

2.3.2 Thermodynamics of micellization

The process of micellization is one of the most important characteristics of surfactant solution and hence it is essential to understand its mechanism (the driving force for micelle formation). This requires analysis of the dynamics of the process (i.e. the kinetic aspects) as well as the equilibrium aspects whereby the laws of thermodynamics may be applied to obtain the free energy, enthalpy and entropy of micellization.

2.3.2.1 Kinetic aspects

Micellization is a dynamic phenomenon in which n monomeric surfactant molecules associate to form a micelle S_n, i.e.,

$$nS \rightleftarrows S_n. \tag{2.6}$$

Hartley [33] envisaged a dynamic equilibrium whereby surface active agent molecules are constantly leaving the micelles whilst other molecules from solution enter the micelles. The same applies to the counterions with ionic surfactants, which can exchange between the micelle surface and bulk solution. Experimental investigations using fast kinetic methods such as stop flow, temperature and pressure jumps, and ultrasonic relaxation measurements have shown that there are two relaxation processes for micellar equilibrium [37–41] characterized by relaxation times τ_1 and τ_2. The first relaxation time, τ_1, is of the order of 10^{-7} s (10^{-8} to 10^{-3} s) and represents the lifetime of a surface active molecule in a micelle, i.e. it represents the association and dissociation rate for a single molecule entering and leaving the micelle, which may be represented by the equation,

$$S + S_{n-1} \underset{K^-}{\overset{K^+}{\rightleftarrows}} S_n, \tag{2.7}$$

where K^+ and K^- represent the association and dissociation rate respectively for a single molecule entering or leaving the micelle.

The slower relaxation time τ_2 corresponds to a relatively slow process, namely the micellization dissolution process represented by equation (2.6). The value of τ_2 is of the order of milliseconds (10^{-3}–1 s) and hence can be conveniently measured by stopped flow methods. The fast relaxation time τ_1 can be measured using various techniques depending on its range. For example, τ_1 values in the range of 10^{-8}–10^{-7} s are accessible to ultrasonic absorption methods, whereas τ_1 in the range of 10^{-5}–10^{-3} s can be measured by pressure jump methods. The value of τ_1 depends on surfactant concentration, chain length and temperature. τ_1 increases with increaing chain length of surfactants, i.e. the residence time increases with increasing chain length.

The above discussion emphasizes the dynamic nature of micelles and it is important to realize that these molecules are in continuous motion and that there is a constant interchange between micelles and solution. The dynamic nature also applies to the counterions which exchange rapidly with lifetimes in the range 10^{-9}–10^{-8} s. Furthermore, the counterions appear to be laterally mobile and not to be associated with (single) specific groups on the micelle surfaces.

2.3.2.2 Equilibrium aspects: Thermodynamics of micellization

Various approaches have been employed in tackling the problem of micelle formation. The simplest approach treats micelles as a single phase, and this is referred to as the phase separation model. In this model, micelle formation is considered as a phase separation phenomenon and the cmc is then the saturation concentration of

the amphiphile in the monomeric state whereas the micelles constitute the separated pseudophase. Above the cmc, a phase equilibrium exists with a constant activity of the surfactant in the micellar phase. The Krafft point is viewed as the temperature at which solid hydrated surfactant, micelles and a solution saturated with undissociated surfactant molecules are in equilibrium at a given pressure.

Consider an anionic surfactant, in which n surfactant anions, S^-, and n counterions M^+ associate to form a micelle, i.e.,

$$nS^- + nM^+ \rightleftarrows S_n. \tag{2.8}$$

The micelle is simply a charged aggregate of surfactant ions plus an equivalent number of counterions in the surrounding atmosphere and is treated as a separate phase. The chemical potential of the surfactant in the micellar state is assumed to be constant at any given temperature, and this may be adopted as the standard chemical potential, μ_m^0, by analogy to a pure liquid or a pure solid. Considering the equilibrium between micelles and monomer, then,

$$\mu_m^0 = \mu_1^0 + RT \ln a, \tag{2.9}$$

where μ_1 is the standard chemical potential of the surfactant monomer and a_1 is its activity, which is equal to $f_1 x_1$, where f_1 is the activity coefficient and x_1 the mole fraction. Therefore, the standard free energy of micellization per mol of monomer, ΔG_m^0, is given by,

$$\Delta G_m^0 = \mu_m^0 - \mu_1^0 = RT \ln a_1 \approx RT \ln x_1, \tag{2.10}$$

where f_1 is taken as unity (a reasonable value in very dilute solution). The cmc may be identified with x_1 so that

$$\Delta G_m^0 = RT \ln[\text{cmc}]. \tag{2.11}$$

In equation (2.10), the cmc is expressed as a mole fraction, which is equal to $C/(55.5 + C)$, where C is the concentration of surfactant in mol dm^{-3}, i.e.,

$$\Delta G_m^0 = RT \ln C - RT \ln(55.5 + C). \tag{2.12}$$

It should be stated that ΔG^0 should be calculated using the cmc expressed as a mole fraction as indicated by equation (2.12). However, most cmc quoted in the literature are given in mol dm^{-3} and, in many cases of ΔG^0 values have been quoted where the cmc was simply expressed in mol dm^{-3}. Strictly speaking, this is incorrect, since ΔG^0 should be based on x_1 rather than on C. The value of ΔG^0 when the cmc is expressed in mol dm^{-3} is substantially different from the ΔG^0 value when the cmc is expressed in mole fraction. For example, for dodecyl hexaoxyethylene glycol, the quoted cmc value is 8.7×10^{-5} mol dm^{-3} at 25 °C. Therefore,

$$\Delta G^0 = RT \ln \frac{8.7 \times 10^{-5}}{55.5 + 8.7 \times 10^{-5}} = -33.1 \text{ kJ mol}^{-1}, \tag{2.13}$$

when the mole fraction scale is used. On the other hand,

$$\Delta G^0 = RT \ln 8.7 \times 10^{-5} = -23.2 \text{ kJ mol}^{-1}, \tag{2.14}$$

when the molarity scale is used.

The phase separation model has been questioned for two main reasons. Firstly, according to this model a clear discontinuity in the physical property of a surfactant solution, such as surface tension, turbidity, etc. should be observed at the cmc. This is not always found experimentally and the cmc is not a sharp breakpoint. Secondly, if two phases actually exist at the cmc, then equating the chemical potential of the surfactant molecule in the two phases would imply that the activity of the surfactant in the aqueous phase would be constant above the cmc. If this was the case, the surface tension of a surfactant solution should remain constant above the cmc. However, careful measurements have shown that the surface tension of a surfactant solution decreases slowly above the cmc, particularly when using purified surfactants.

A convenient solution for relating ΔG_m to [cmc] was given for ionic surfactants by the following expression [42, 43],

$$\Delta G_m^0 = \{2 - (p/n)\} RT \ln[\text{cmc}], \tag{2.15}$$

where p is the number of free (unassociated) surfactant ions and n is the total number of surfactant molecules in the micelle. For many ionic surfactants, the degree of dissociation (p/n) is ≈ 0.2 so that,

$$\Delta G_m^0 = 1.8\, RT \ln[\text{cmc}]. \tag{2.16}$$

Comparison with equation (2.11) clearly shows that for similar ΔG_m, the [cmc] is about two orders of magnitude higher for ionic surfactants when compared with nonionic surfactant of the same alkyl chain length (Tab. 2.1).

In the presence of excess added electrolyte, with mole fraction x, the free energy of micellization is given by the expression,

$$\Delta G_m^0 = RT \ln[\text{cmc}] + \{1 - (p/n)\} \ln x. \tag{2.17}$$

Equation (2.17) shows that as x increases, the [cmc] decreases.

It is clear from equation (2.15) that as $p \to 0$, i.e. when most charges are associated with counterions,

$$\Delta G_m^0 = 2RT \ln[\text{cmc}], \tag{2.18}$$

whereas when $p \approx n$, i.e. the counterions are bound to micelles,

$$\Delta G_m^0 = RT \ln[\text{cmc}], \tag{2.19}$$

which is the same equation for nonionic surfactants.

2.3.2.3 Enthalpy and entropy of micellization

The enthalpy of micellization can be calculated from the variation of cmc with temperature. This follows from,

$$-\Delta H^0 = RT^2 \frac{\mathrm{d}\ln[\mathrm{cmc}]}{\mathrm{d}T}. \tag{2.20}$$

The entropy of micellization can then be calculated from the relationship between ΔG^0 and ΔH^0, i.e.,

$$\Delta G^0 = \Delta H^0 - T\Delta S^0. \tag{2.21}$$

Therefore ΔH^0 may be calculated from the surface tension–log C plots at various temperatures. Unfortunately, errors in locating the cmc (which in many cases is not a sharp point) lead to a large error in the value of ΔH^0. A more accurate and direct method of obtaining ΔH^0 is microcalorimetry. As an illustration, the thermodynamic parameters, ΔG^0, ΔH^0, and $T\Delta S^0$ for octylhexaoxyethylene glycol monoether (C_8E_6) are given in Tab. 2.2.

Tab. 2.2: Thermodynamic quantities for micellization of octylhexaoxyethylene glycol monoether.

Temp. (°C)	ΔG^0 (kJ mol^{-1})	ΔH^0 (kJ mol^{-1})		$T\Delta S^0$ (kJ mol^{-1})
		from cmc	from calorimetry	
25	−21.3 ± 2.1	8.0 ± 4.2	20.1 ± 0.8	41.8 ± 1.0
40	−23.4 ± 2.1		14.6 ± 0.8	38.0 ± 1.0

It can be seen from Tab. 2.2 that ΔG^0 is large and negative. However, ΔH^0 is positive, indicating that the process is endothermic. In addition, $T\Delta S^0$ is large and positive which implies that in the micellization process there is a net increase in entropy. This positive enthalpy and entropy points to a different driving force for micellization from that encountered in many aggregation processes.

The influence of alkyl chain length of the surfactant on the free energy, enthalpy and entropy of micellization, was demonstrated by Rosen [44] who listed these parameters as a function of alkyl chain length for sulphoxide surfactants. The results are given in Tab. 2.3 it can be seen that the standard free energy of micellization becomes increasingly negative as the chain length increases. This is to be expected since the cmc decreases with increasing alkyl chain length. However, ΔH^0 becomes less positive and $T\Delta S$ becomes more positive with increasing chain length of the surfactant. Thus, the large negative free energy of micellization is made up of a small positive enthalpy (which decreases slightly with increasing chain length of the surfactant) and a large positive entropy term $T\Delta S^0$, which becomes more positive as the chain is lengthened. As we will see in the next section, these results can be accounted for in terms of the hydrophobic effect which will be described in some detail.

Tab. 2.3: Change of thermodynamic parameters of micellization of alkyl sulphoxide with increasing chain length of the alkyl group.

Surfactant	ΔG (kJ mol^{-1})	ΔH^0 (kJ mol^{-1})	$T\Delta S^0$ (kJ mol^{-1})
$C_6H_{13}S(CH_3)O$	−12.0	10.6	22.6
$C_7H_{15}S(CH_3)O$	−15.9	9.2	25.1
$C_8H_{17}S(CH_3)O$	−18.8	7.8	26.4
$C_9H_{19}S(CH_3)O$	−22.0	7.1	29.1
$C_{10}H_{21}S(CH_3)O$	−25.5	5.4	30.9
$C_{11}H_{23}S(CH_3)O$	−28.7	3.0	31.7

2.3.2.4 Driving force for micelle formation

Until recently, the formation of micelles was regarded primarily as an interfacial energy process, analogous to the process of coalescence of oil droplets in an aqueous medium. If this was the case, micelle formation would be a highly exothermic process, as the interfacial free energy has a large enthalpy component. As mentioned above, experimental results have clearly shown that micelle formation involves only a small enthalpy change and is often endothermic. The negative free energy of micellization is the result of a large positive entropy. This led to the conclusion that micelle formation must be a predominantly entropy driven process. Two main sources of entropy have been suggested. The first is related to the so called "hydrophobic effect". This effect was first established from a consideration of the free energy enthalpy and entropy of transfer of hydrocarbon from water to a liquid hydrocarbon. Some results are listed in Tab. 2.4. This table also lists the heat capacity change ΔC_p on transfer from water to a hydrocarbon, as well as $C_p^{0,gas}$, i.e. the heat capacity in the gas phase. It can be seen from Tab. 2.4 that the principal contribution to the value of ΔG^0 is the large positive value of ΔS^0, which increases with increasing hydrocarbon chain length, whereas ΔH^0 is positive, or small and negative.

Tab. 2.4: Thermodynamic parameters for transfer of hydrocarbons from water to liquid hydrocarbon at 25 °C.

Hydrocarbon	ΔG^0 (kJ mol^{-1})	ΔH^0 (kJ mol^{-1})	ΔS^0 (kJ mol^{-1} K^{-1})	ΔC_p^0 (kJ mol^{-1} K^{-1})	$C_p^{0,gas}$ (kJ mol^{-1} K^{-1})
C_2H_6	−16.4	10.5	88.2	—	—
C_3H_8	−20.4	7.1	92.4	—	—
C_4H_{10}	−24.8	3.4	96.6	−273	−143
C_5H_{12}	−28.8	2.1	105.0	−403	−172
C_6H_{14}	−32.5	0	109.2	−441	−197
C_6H_6	−19.3	−2.1	58.8	−227	−134
$C_6H_5CH_3$	−22.7	−1.7	71.4	−265	−155
$C_6H_5C_2H_5$	−26.0	−2.0	79.8	−319	−185
$C_6H_5C_3H_8$	−29.0	−2.3	88.2	−395	—

To account for this large positive entropy of transfer, several authors [45–47] suggest that the water molecules around a hydrocarbon chain are ordered, forming "clusters" or "icebergs". On transfer of an alkane from water to a liquid hydrocarbon, these clusters are broken thus releasing water molecules which now have a higher entropy. This accounts for the large entropy of transfer of an alkane from water to a hydrocarbon medium. This effect is also reflected in the much higher heat capacity change on transfer, ΔC_p^0, when compared with the heat capacity in the gas phase, C_p^0. This effect is also operative on transfer of surfactant monomer to a micelle, during the micellization process. The surfactant monomers will also contain "structured" water around their hydrocarbon chain. On transfer of such monomers to a micelle, these water molecules are released and they have a higher entropy. The second source of entropy increase on micellization may arise from the increase in flexibility of the hydrocarbon chains on their transfer from an aqueous to a hydrocarbon medium [45]. The orientations and bendings of an organic chain are likely to be more restricted in an aqueous phase compared to an organic phase. It should be mentioned that with ionic and zwitterionic surfactants, an additional entropy contribution, associated with the ionic head groups, must be considered. Upon partial neutralization of the ionic charge by the counterions when aggregation occurs, water molecules are released. This will be associated with an entropy increase which should be added to the entropy increase resulting from the hydrophobic effect mentioned above. However, the relative contribution of the two effects is difficult to assess in a quantitative manner.

2.3.2.5 Micellization in surfactant mixtures (mixed micelles)

In most industrial applications, more than one surfactant molecule is used in the formulation. It is, therefore, necessary to predict the types of possible interactions and whether these lead to some synergistic effects. Two general cases may be considered: surfactant molecules with no net interaction (with similar head groups) and systems with net interaction [26]. The first case is that when mixing two surfactants with the same head group but with different chain lengths. In analogy with the hydrophilic-lipophilic balance (HLB) for surfactant mixtures, one can also assume that the cmc of a surfactant mixture (with no net interaction) to be an average of the two cmcs of the single components [26],

$$\mathrm{cmc} = x_1 \mathrm{cmc}_1 + x_2 \mathrm{cmc}_2, \tag{2.22}$$

where x_1 and x_2 are the mole fractions of the respective surfactants in the system. However, the mole fractions should not be those in the whole system, but those inside the micelle. This means that equation (2.22) should be modified,

$$\mathrm{cmc} = x_1^{\mathrm{m}} \mathrm{cmc}_1 + x_2^{\mathrm{m}} \mathrm{cmc}_2. \tag{2.23}$$

The superscript "m" indicates that the values are inside the micelle. If x_1 and x_2 are the solution composition, then,

$$\frac{1}{\text{cmc}} = \frac{x_1}{\text{cmc}_1} + \frac{x_2}{\text{cmc}_2}. \tag{2.24}$$

The molar composition of the mixed micelle is given by,

$$x_1^{\text{m}} = \frac{x_1 \text{cmc}_2}{x_1 \text{cmc}_2 + x_2 \text{cmc}_1}. \tag{2.25}$$

Fig. 2.13 shows the calculated cmc and the micelle composition as a function of solution composition using equations (2.24) and (2.25) for three cases where $\text{cmc}_2/\text{cmc}_1 = 1$, 0.1 and 0.01. As can be seen, the cmc and micellar composition change dramatically with solution composition when the cmcs of the two surfactants vary considerably, i.e. when the ratio of cmcs is far from 1. This fact is used when preparing microemulsions in which the addition of medium chain alcohol (like pentanol or hexanol) changes the properties considerably. If component 2 is much more surface active, i.e. $\text{cmc}_2/\text{cmc}_1 \ll 1$, and it is present in low concentrations (x_2 is of the order of 0.01), then from equation (2.25) $x_1^{\text{m}} \approx x_2^{\text{m}} \approx 0.5$, i.e. at the cmc of the systems the micelles are up to 50 % composed of component 2. This illustrates the role of contaminants in surface activity, e.g. dodecyl alcohol in sodium dodecyl sulphate (SDS).

Fig. 2.14 shows the cmc as a function of molar composition of the solution and in the micelles for a mixture of SDS and nonylphenol with 10 mol ethylene oxide ($NP-E_{10}$). If the molar composition of the micelles is used as the x-axis, the cmc is more or less the arithmetic mean of the cmcs of the two surfactants. If, on the other hand, the molar composition in the solution is used as the x-axis (which at the cmc is equal to the total molar concentration), then the cmc of the mixture shows a dramatic decrease

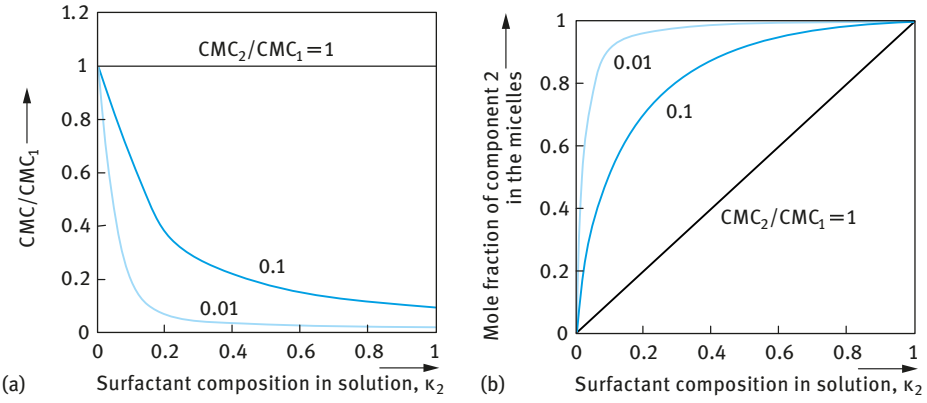

Fig. 2.13: Calculated cmc (a) and micellar composition (b) as a function of solution composition for three ratios of cmcs.

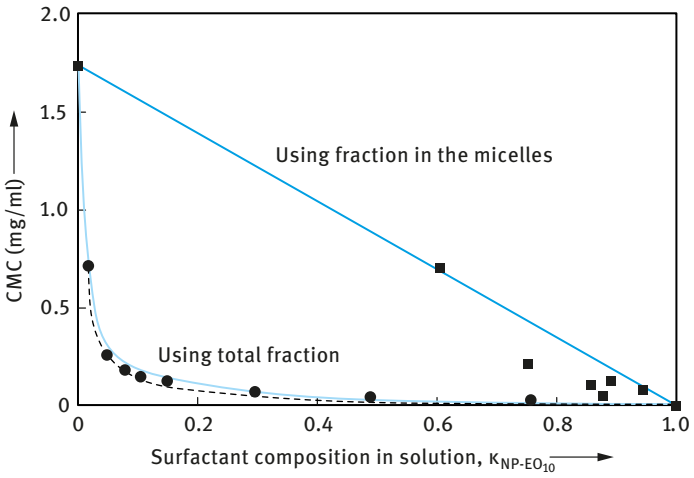

Fig. 2.14: cmc as a function of surfactant composition, x_1, or micellar surfactant composition, x_1^m for the system SDS + NP-E_{10}.

at low fractions of NP-E_{10}. This decrease is due to the preferential absorption of NP-E_{10} in the micelle. This higher absorption is due to the higher hydrophobicity of the NP-E_{10} surfactant when compared with SDS.

With many industrial formulations, surfactants of different kind are mixed together, for example anionics and nonionics. The nonionic surfactant molecules shield the repulsion between the negative head groups in the micelle and hence there will be a net interaction between the two types of molecules. Another example is the case when anionic and cationic surfactants are mixed, whereby a very strong interaction will take place between the oppositely charged surfactant molecules. To account for this interaction, equation (2.25) has to be modified by introducing activity coefficients of the surfactants, f_1^m and f_2^m in the micelle,

$$\mathrm{cmc} = x_1^m f_1^m \mathrm{cmc}_1 + x_2^m f_2^m \mathrm{cmc}_2. \tag{2.26}$$

An expression for the activity coefficients can be obtained using the regular solutions theory [26],

$$\ln f_1^m = (x_2^m)^2 \beta, \tag{2.27}$$

$$\ln f_2^m = (x_2^m)^2 \beta, \tag{2.28}$$

where β is an interaction parameter between the surfactant molecules in the micelle. A positive β value means that there is a net repulsion between the surfactant molecules in the micelle, whereas a negative β value means a net attraction.

The cmc of the surfactant mixture and the composition x_1 are given by the following equations,

$$\frac{1}{\text{cmc}} = \frac{x_1}{f_1^{\text{m}}\text{cmc}_1} + \frac{x_2}{f_2^{\text{m}}\text{cmc}_2}, \tag{2.29}$$

$$x_1^{\text{m}} = \frac{x_1 f_2^{\text{m}}\text{cmc}_2}{x_1 f_2^{\text{m}}\text{cmc}_2 + x_2 f_2^{\text{m}}\text{cmc}_1}. \tag{2.30}$$

Fig. 2.15 shows the effect of increasing the β parameter on the cmc and micellar composition for two surfactants with a cmc ratio of 0.1.

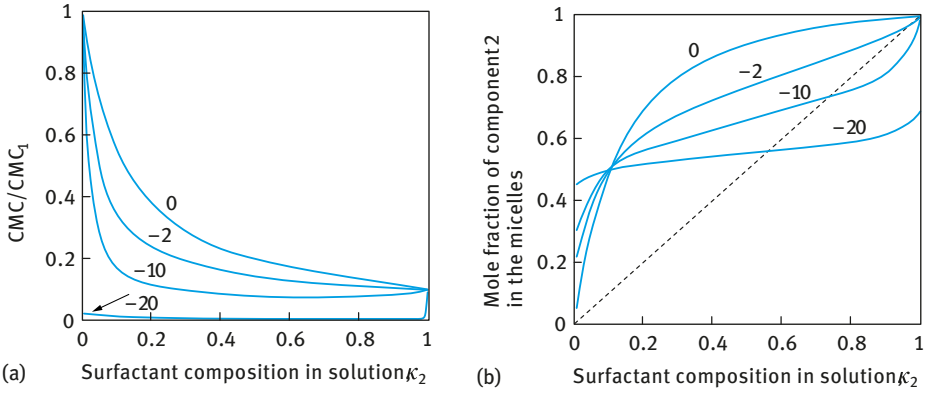

Fig. 2.15: cmc (a) and micellar composition (b) for various values of β for a system with a cmc ratio $\text{cmc}_2/\text{cmc}_1$ of 0.1.

Fig. 2.15 shows that as β becomes more negative, the cmc of the mixture decreases. β values in the region of –2 are typical for anionic/nonionic mixtures, whereas values in the region of –10 to –20 are typical of anionic/cationic mixtures. With increasing negative value of β, the mixed micelles tend towards a mixing ratio of 50 : 50, which reflects the mutual electrostatic attraction between the surfactant molecules. The predicted cmc and micellar composition depend both on the ratio of the cmcs as well as the value of β. When the cmcs of the single surfactants are similar, the predicted value of the cmc is very sensitive to small variation in β. On the other hand, when the ratio of the cmcs is large, the predicted value of the mixed cmc and the micellar composition are insensitive to variation of the β parameter. For mixtures of nonionic and ionic surfactants, the β parameter decreases with increasing electrolyte concentration. This is due to the screening of the electrostatic repulsion on the addition of electrolyte. With some surfactant mixtures, β decreases with increasing temperature, i.e. the net attraction decreases with increasing temperature.

2.4 Surfactant self-assembly

Surfactant micelles and bilayers are the building blocks of most self-assembly structures. One can divide the phase structures into two main groups [26]:

(i) those that are built of limited or discrete self-assemblies, which may be characterized roughly as spherical, prolate or cylindrical;
(ii) infinite or unlimited self-assemblies where the aggregates are connected over macroscopic distances in one, two or three dimensions.

The hexagonal phase (see below) is an example of one-dimensional continuity, the lamellar phase of two-dimensional continuity, whereas the bicontinuous cubic phase and the sponge phase (see later) are examples of three-dimensional continuity. These two types are schematically illustrated in Fig. 2.16.

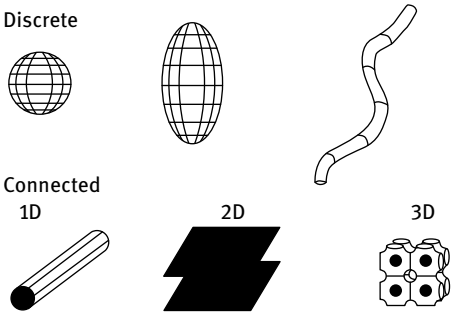

Fig. 2.16: Schematic representation of self-assembly structures.

2.4.1 Structure of liquid crystalline phases

The above mentioned unlimited self-assembly structures in 1D, 2D or 3D are referred to as liquid crystalline structures. These behave as fluids and are usually highly viscous. At the same time, X-ray studies of these phases yield a small number of relatively sharp lines which resemble those produced by crystals [26]. Since they are fluids, they are less ordered than crystals, but because of the X-ray lines and their high viscosity it is also apparent that they are more ordered than ordinary liquids. Thus, the term liquid crystalline phase is very appropriate for describing these self-assembled structures. A brief description of the various liquid crystalline structures that can be produced with surfactants is given below and Tab. 2.5 shows the most commonly used notations to describe these systems.

Tab. 2.5: Notation of the most common liquid crystalline structures.

Phase structure	Abbreviation	Notation
Micellar	mic	L_1, S
Reversed micellar	rev mic	L_2, S
Hexagonal	hex	H_1, E, M_1, middle
Reversed hexagonal	rev hex	H_2, F, M_2
Cubic (normal micellar)	cub_m	I_1, S_{1c}
Cubic (reversed micelle)	cub_m	I_2
Cubic (normal bicontinuous)	cub_b	I_1, V_1
Cubic (reversed bicontinuous)	cub_b	I_2, V_2
Lamellar	lam	L_α, D, G, neat
Gel	gel	L_β
Sponge phase (reversed)	spo	L_3 (normal), L_4

2.4.1.1 Hexagonal phase

This phase is built up of (infinitely) long cylindrical micelles arranged in a hexagonal pattern, with each micelle being surrounded by six other micelles, as schematically shown in Fig. 2.12. The radius of the circular cross section (which may be somewhat deformed) is again close to the surfactant molecule length [26].

2.4.1.2 Micellar cubic phase

This phase is built up of regular packing of small micelles, which have similar properties to small micelles in the solution phase. However, the micelles are short prolates (axial ratio 1–2) rather than spheres since this allows a better packing. The micellar cubic phase is highly viscous. A schematic representation of the micellar cubic phase [26] is shown in Fig. 2.12.

2.4.1.3 Lamellar phase

This phase is built of bilayers of surfactant molecules alternating with water layers. The thickness of the bilayers is somewhat lower than twice the surfactant molecule length. The thickness of the water layer can vary over wide ranges, depending on the nature of the surfactant. The surfactant bilayer can range from being stiff and planar to being very flexible and undulating. A schematic representation of the lamellar phase [26] is shown in Fig. 2.12.

2.4.1.4 Bicontinuous cubic phases

These phases can have a number of different structures, where the surfactant molecules form aggregates that penetrate space, forming a porous connected structure in three dimensions. They can be considered as structures formed by connecting rod-like micelles (branched micelles), or bilayer structures [26] as illustrated in Fig. 2.17.

Fig. 2.17: Bicontinuous structure with the surfactant molecules aggregated into connected films characterized by two curvatures of opposite sign [10].

2.4.1.5 Reversed structures

Except for the lamellar phase, which is symmetrical around the middle of the bilayer, the different structures have a reversed counterpart in which the polar and nonpolar parts have changed roles. For example, a hexagonal phase is built up of hexagonally packed water cylinders surrounded by the polar head groups of the surfactant molecules and a continuum of the hydrophobic parts. Similarly, reversed (micellar-type) cubic phases and reversed micelles consist of globular water cores surrounded by surfactant molecules. The radii of the water cores are typically in the range 2–10 nm.

2.5 Experimental studies of the phase behaviour of surfactants

One of the earliest (and qualitative) techniques for the identification of the different phases is the use of polarizing microscopy. This is based on the scattering of normal and polarized light which differs for isotropic (such as the cubic phase) and anisotropic (such as the hexagonal and lamellar phases) structures. Isotropic phases are clear and transparent, while anisotropic liquid crystalline phases scatter light and appear more or less cloudy. Using polarized light and viewing the samples through cross polarizers gives a black picture for isotropic phases, whereas anisotropic ones give bright images. The patterns in a polarization microscope are distinctly different for different anisotropic phases and can therefore be used to identify the phases, e.g. to distinguish between hexagonal and lamellar phases [48]. A typical optical micrograph for the hexagonal and lamellar phases (obtained using polarizing microscopy) is shown in Fig. 2.18. The hexagonal phase shows a “fan-like” appearance, whereas the lamellar phase shows “oily streaks” and “Maltese crosses”.

Another qualitative method is to measure the viscosity as a function of surfactant concentration. The cubic phase is very viscous and often quite stiff and it appears as a clear “gel”. The hexagonal phase is less viscous than the cubic phase and the lamellar phase is much less viscous than the cubic phase. However, viscosity measurements do not allow an unambiguous determination of the phases in the sample.

(a) (b)

Fig. 2.18: Texture of the hexagonal (a) and lamellar phase (b) obtained using polarizing microscopy.

Most qualitative techniques for identifying the various liquid crystalline phases are based on diffraction studies, either light, X-ray or neutron. The liquid crystalline structures have a repetitive arrangement of aggregates and observing a diffraction pattern can give evidence of long-range order and distinguish between alternative structures.

Another very useful technique to identify the different phases is NMR spectroscopy. One observes the quadrupole splittings in deuterium NMR [49]. This is illustrated in Fig. 2.19.

For isotropic phases such as micelles, cubic and sponge phases one observes a narrow singlet (Fig. 2.19 (a)). For a single isotropic phase, such as hexagonal or lamellar structures, a doublet is obtained (Fig. 2.19 (b)). The magnitude of the "split-

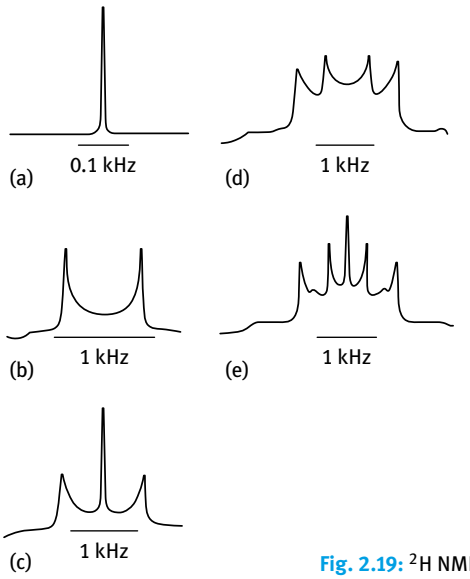

Fig. 2.19: ^{2}H NMR spectra of surfactants in heavy water (D_2O).

ting" depends on the type of liquid crystalline phase, which is twice as much for the lamellar phase when compared with the hexagonal phase. For one isotropic and one anisotropic phase, one obtains one singlet and one doublet (Fig. 2.19 (c)). For two anisotropic phases (lamellar and hexagonal), one observes two doublets (Fig. 2.14 (d)). In a three-phase region with two anisotropic phases and one isotropic phase, one observes two doublets and one singlet (Fig. 2.14 (e)).

The distinction between normal and reversed phases can be easily carried out using conductivity measurements. For normal phases, which are "water rich", the conductivity is high. In contrast, for reversed phases that are "water poor", the conductivity is much lower (by several orders of magnitude).

References

[1] Tadros T. Applied surfactants. Weinheim: Wiley-VCH; 2005.
[2] Tadros T. An introduction to surfactants. Berlin: De Gruyter; 2014.
[3] Holmberg K, Jonsson B, Kronberg B, Lindman B. Surfactants and polymers in aqueous solution. 2nd edition. John Wiley & Sons, USA; 2003.
[4] McCutcheon. Detergents and Emulsifiers. New Jersey: Allied Publishing Co. Published annually.
[5] van Os NM, Haak JR, Rupert LAM. Physico-chemical properties of selected anionic, cationic and nonionic surfactants. Amsterdam: Elsevier Publishing Co.; 1993.
[6] Porter MR. Handbook of surfactants. Blackie, USA; Chapman and Hall; 1994.
[7] Linfield WM, editor. Anionic surfactants. New York: Marcel Dekker; 1967.
[8] Lucassen-Reynders EH. Anionic surfactants – Physical chemistry of surfactant action. New York: Marcel Dekker; 1981.
[9] Jungermana E. Cationic surfactants. New York: Marcel Dekker; 1970.
[10] Rubingh N, Holland PM, editors. Cationic surfactants – Physical chemistry. New York: Marcel Dekker; 1991.
[11] Buestein BR, Hiliton CL. Amphoteric surfactants. New York: Marcel Dekker; 1982.
[12] Schick MJ, editor. Nonionic surfactants. New York: Marcel Dekker; 1966.
[13] Schick MJ, editor. Nonionic surfactants: Physical chemistry. New York: Marcel Dekker; 1987.
[14] Schonfeldt N. Surface active ethylene oxide adducts. USA: Pergamon Press; 1970.
[15] Zana RR, Alami E. Gemini surfactants. In: Holberg K, editor. Novel surfactants. New York: Marcel Dekker; 2003. Chapter 12.
[16] von Rybinsky W, Hill K. In: Holberg K, editor. Novel surfactants. New York: Marcel Dekker; 2003. Chapter 2.
[17] Drummond CJ, Fong C, Krodkiewska I, Boyd BJ, Baker IJA. In: Holberg K, editor. Novel surfactants. New York: Marcel Dekker; 2003. Chapter 3.
[18] Barry BW, Gray GMT. J Colloid Interface Sci. 1975;52:314.
[19] Oakenfull DG, Fisher LR. J Phys Chem. 1977;81:1838.
[20] Small DM. Advan Chem Ser. 1968;84:31.
[21] Oakenfull DG, Fisher LR. J Phys Chem. 1978;82:2443.
[22] Zana R. J Phys Chem. 1978;82:2440.
[23] Desai JD, Banat IM. Microbial production of surfactants and their commercial potential. Microbiol Molec Biol Rev. 1997;61:47–64.
[24] Guatam KK, Tyagi VK. Microbial surfactants; a review. J Oleo Sci. 2006;55:155–166.

[25] Straathof AJJ, Aldercreutz P, editors. Applied biocatalysis. Amsterdam: Harwood Academic; 2000.
[26] Lindman B. In: Tadros TF, editor. Surfactants. London: Academic Press; 1984.
[27] Israelachvili JN. Intermolecular and surface forces, with special applications to colloidal and biological systems. London: Academic Press; 1985. p. 251.
[28] Mukerjee P, Mysels KJ. Critical micelle concentrations of aqueous surfactant systems. Washington DC: National Bureau of Standards Publication; 1971.
[29] Elworthy PH, Florence AT, Macfarlane CB. Solubilization by surface active agents. London: Chapman and Hall; 1968.
[30] Shinoda K, Nagakawa T, Tamamushi BI, Isemura T. Colloidal surfactants, some physicochemical properties. London: Academic Press; 1963.
[31] McBain JW. Trans Faraday Soc. 1913;9:99.
[32] Adam NK. J Phys Chem. 1925;29:87.
[33] Hartley GS. Aqueous solutions of paraffin chain salts. Paris: Hermann and Cie; 1936.
[34] McBain JW. Colloid science. Boston: Heath; 1950.
[35] Harkins WD, Mattoon WD, Corrin ML. J Amer Chem Soc. 1946;68:220; J Colloid Sci. 1946;1:105.
[36] Debye P, Anaker EW. J Phys Colloid Chem. 1951;55:644.
[37] Anainsson EAG, Wall SN. J Phys Chem. 1974;78:1024; 1975;79:857.
[38] Anainsson EAG, Wall SN, Almagren M, Hoffmann H, Kielmann I, Ulbricht W, Zana R, Lang J, Tondre C. J Phys Chem. 1976;80:905.
[39] Rassing J, Sams PJ, Wyn-Jones E. J Chem Soc. Faraday II, 1974;70:1247.
[40] Jaycock MJ, Ottewill RH, Fourth Int. Congress Surface Activity. 1964;2:545.
[41] Okub T, Kitano H, Ishiwatari T, Isem N. Proc Royal Soc. 1979;A36:81.
[42] Phillips JN. Trans Faraday Soc. 1955;51:561.
[43] Kahlweit M, Teubner M. Adv Colloid Interface Sci. 1980;13:1.
[44] Rosen ML. Surfactants and interfacial phenomena. New York: Wiley-Interscience; 1978.
[45] Tanford C. The hydrophobic effect. 2nd edition. New York: Wiley; 1980.
[46] Stainsby G, Alexander AE. Trans Faraday Soc. 1950;46:587.
[47] Arnow RH, Witten L. J Phys Chem. 1960;64:1643.
[48] Rosevaar FB. J Soc Cosmet Chem. 1968;19:581.
[49] Khan A, Fontell K, Lindblom G, Lindman B. J Phys Chem. 1982;86:4266.

3 General classification of polymeric surfactants and their solution properties

3.1 Introduction

Polymeric surfactants, particularly block A–B and A–B–A or graft BA_n types (see below), are used for the stabilization of formulations consisting of disperse systems. As will be discussed in Chapter 6, the chain B (referred to as the "anchoring chain") is chosen to be highly insoluble in the medium and to have strong affinity to the surface of particles or droplets. The chain(s) A are chosen to be highly soluble in the medium and strongly solvated by its molecules. These polymeric surfactants adsorb very strongly to the surface of the particles or droplets by multipoint attachment with several small loops of the B chain. The stabilizing chain(s) that are strongly solvated by the molecules of the medium will give an adsorbed layer thickness δ greater than 5 nm with a chain(s) having a molar mass > 1,000 Daltons. These A chains provide effective steric stabilization against flocculation and/or coalescence.

In this chapter I will describe the general classification of polymeric surfactants with particular reference to block A–B and A–B–A or graft BA_n types. This is followed by sections on solution properties of polymeric surfactants. The polymer conformation and structure is then described followed by a section on the free energy of mixing of polymer with solvent, with particular reference to Flory–Huggins theory. The characterization of polymers in solution using scattering techniques and viscosity measurements is then described. Finally, the phase separation of polymer solutions is described with particular reference to the solubility parameter concept for selecting the right solvent for a polymer.

3.2 Classification of polymeric surfactants

3.2.1 Homopolymers

Perhaps the simplest type of polymeric surfactant is a homopolymer [1–4], that is formed from the same repeating units, such as poly(ethylene oxide) that is also referred to as polyethylene glycol and has the following chemical structure with the repeating units of ethylene oxide,

$$H-(O-CH_2-CH_2)_n-OH$$

Another homopolymer that is used in many pharmaceutical formulations is poly(vinyl pyrrolidone) that is formed from repeating units of vinyl pyrrolidone,

https://doi.org/10.1515/9783110587944-004

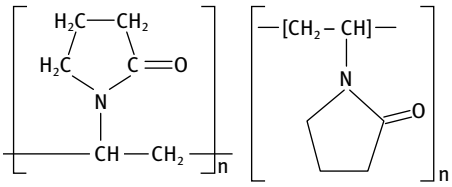

These homopolymers have little surface activity at the O/W interface, since the homopolymer segments (ethylene oxide or vinylpyrrolidone) are highly water soluble and have little affinity to the interface. However, such homopolymers may adsorb significantly at the S/L interface, e.g. on silica. Even if the adsorption energy per monomer segment to the surface is small (fraction of kT, where k is the Boltzmann constant and T is the absolute temperature), the total adsorption energy per molecule may be sufficient to overcome the unfavourable entropy loss of the molecule at the S/L interface [1–4].

3.2.2 Random copolymers

As mentioned above, homopolymers are not the most suitable emulsifiers or dispersants. A small variant is to use polymers that contain specific groups that have high affinity to the surface and are randomly attached to the polymer chain [1–4]. This is exemplified by partially hydrolysed poly(vinyl acetate) (PVAc), technically referred to as poly(vinyl alcohol) (PVA). The polymer is prepared by partial hydrolysis of PVAc, leaving some residual vinyl acetate groups. Most commercially available PVA molecules contain 4–20 mol % acetate groups. These acetate groups, which are hydrophobic, give the molecule its amphipathic character. This blocky distribution of acetate groups on the poly(vinyl alcohol) backbone provides more effective anchoring of the polymeric surfactant chain on the particles or emulsion droplets. On a hydrophobic surface, such as polystyrene or a hydrocarbon oil, the polymer adsorbs with preferential attachment of the acetate groups on the surface, leaving the more hydrophilic vinyl alcohol segments dangling in the aqueous medium. These partially hydrolysed PVA molecules also exhibit surface activity at the O/W interface as indicated by the reduction of the interfacial tension as polymer concentration increases.

3.2.3 Block and graft copolymers

The most convenient polymeric surfactants are those of the block and graft copolymer type. A block copolymer is a linear arrangement of blocks of variable monomer composition. The nomenclature for a diblock is poly-A-block–poly-B and for a triblock is poly-A-block–poly-B–poly-A. One of the most widely used triblock polymeric sur-

factants are the “Pluronics” or “Poloxamers” (BASF, Germany), which consist of two poly-A blocks of poly(ethylene oxide) (PEO) and one block of poly(propylene oxide) (PPO). Several chain lengths of PEO and PPO are available as indicated in the chemical structure below,

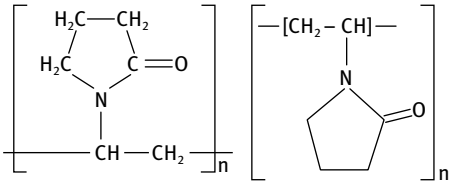

For the Pluronics, the trade name is coded with a letter L (liquid), P (paste) and F (flake) that defines its physical form at room temperature. This is followed by two or three digits; the first one or two digits multiplied by 300 indicate the approximate molar mass of PPO and the last digit multiplied by 10 indicates the percentage of PEO. For example, Pluronic L61 indicates a liquid with PPO molar mass of 1,800 and 10 % PEO. Pluronic F127 indicates a flake with PPO molar mass 3,600 and 70 % PEO. The Poloxamers (which are FDA approved) are commonly named with the letter P followed by three digits; the first two digits multiplied by 10 gives the approximate molar mas of PPO and the last digit multiplied by 10 gives the percentage of PEO. For example, Poloxamer P407 has a molar mass of PPO of 400 and 70 % PEO. Later, triblocks of PPO–PEO–PPO (inverse Pluronics) became available for some specific applications. These polymeric triblocks can be applied as emulsifiers or dispersants, whereby the assumption is made that the hydrophobic PPO chain resides at the hydrophobic surface, leaving the two PEO chains dangling in aqueous solution and hence providing steric repulsion. Although these triblock polymeric surfactants have been widely used in various applications in emulsions and suspensions, some doubt has arisen as to how effective these can be. It is generally accepted that the PPO chain is not sufficiently hydrophobic to provide a strong “anchor” to a hydrophobic surface or to an oil droplet. Indeed, the reason for the surface activity of the PEO–PPO–PEO triblock copolymers at the O/W interface may stem from a process of “rejection” anchoring of the PPO chain since it is not soluble both in oil and water [1–4].

Several other di- and triblock copolymers have been synthesized, although these are of limited commercial availability. Typical examples are diblocks of polystyrene-block-polyvinyl alcohol, triblocks of poly(methyl methacrylate)-block poly(ethylene oxide)-block poly(methyl methacrylate), diblocks of polystyrene block-polyethylene oxide and triblocks of polyethylene oxide-block polystyrene-polyethylene oxide [1–4]. An alternative (and perhaps more efficient) polymeric surfactant is the amphipathic graft copolymer consisting of a polymeric backbone B (polystyrene or polymethyl methacrylate) and several A chains (“teeth") such as polyethylene oxide. This graft

copolymer is sometimes referred to as a "comb" stabilizer. This copolymer is usually prepared by grafting a macromonomer such as methoxy polyethylene oxide methacrylate with polymethyl methacrylate. The "grafting onto" technique has also been used to synthesize polystyrene-polyethylene oxide graft copolymers.

3.2.4 Polymeric surfactants based on polysaccharides

Several surface active graft copolymers are available based on a hydrophilic backbone of polysaccharide to which several hydrophobic alkyl chains are attached. A good example is Emulsan that is produced by micro-organisms (bacteria). It consists of a backbone of hetero-polysaccharide with repeating trisaccharide carrying a negative charge. Fatty acid chains are covalently linked to the polysaccharide through ester linkages [5] as illustrated in Fig. 3.1.

Emulsan is moderately surface active, showing a small reduction of the O/W interfacial tension (for example it reduces the interfacial tension of hexane/water from 47 to around 55 mN m^{-1}). However, it has a strong tendency to adsorb at the O/W interface and can be very effective in stabilizing emulsions of specific oils in water.

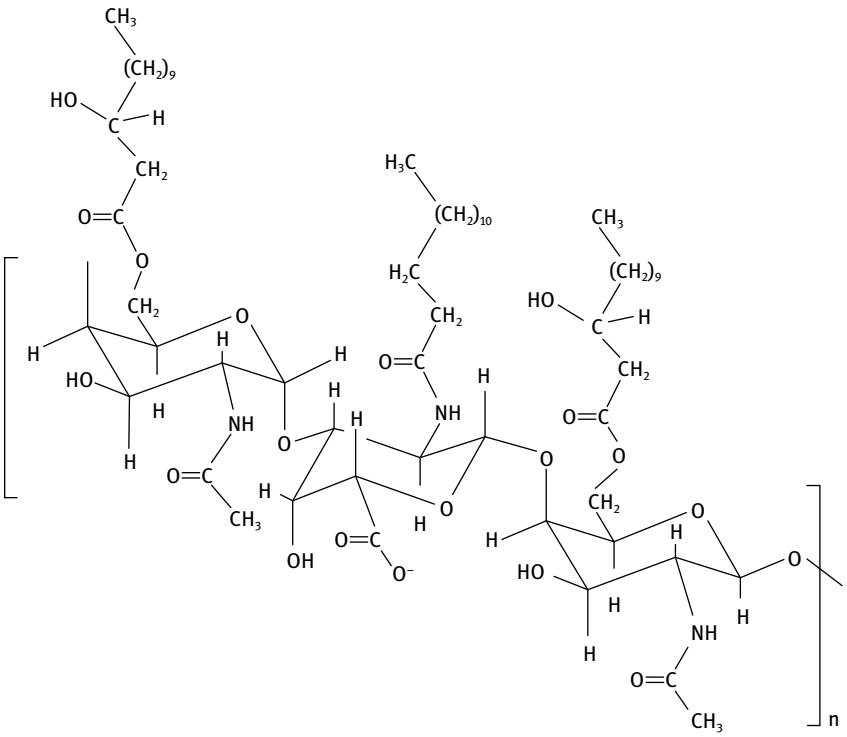

Fig. 3.1: Structure of Emulsan.

Natural polysaccharides can be chemically modified into the equivalent of lipopolysaccharides by attachment of long alkyl or alkyl acryl chains [5]. For example, cellulose can be modified with ethylene oxide and alkyl chloride. The cellulose is swollen in strong alkali and the semi-soluble material is reacted with ethylene oxide and alkyl chloride resulting in the formation of polymeric surfactant with the structure shown in Fig. 3.2. If the alkyl group is short, e.g. ethyl, the molecule is moderately surface active. If some of the ethyl groups are replaced with long chain alkyls, a polymer with higher surface activity is obtained. Such graft copolymers are commercially available and they are referred to as "associative thickeners". They are used for rheology control of many aqueous formulations, e.g. water-borne paints.

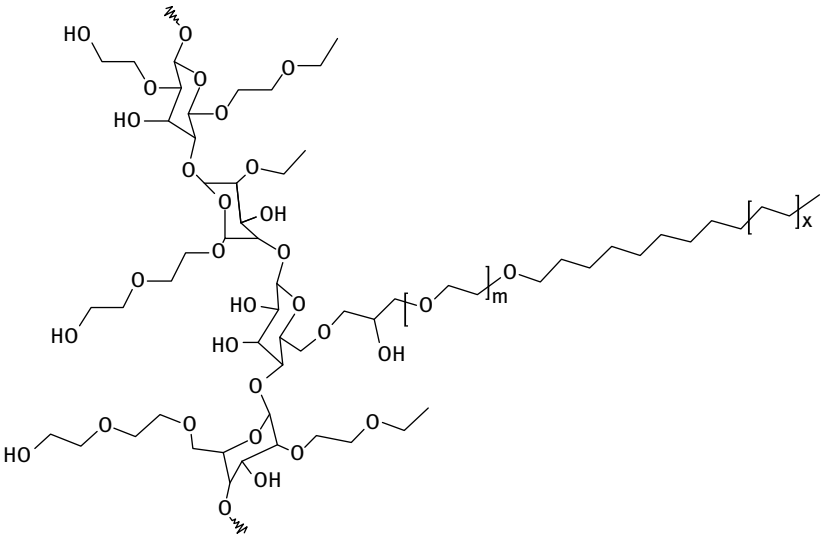

Fig. 3.2: Structure of cellulose modified with ethylene oxide and alkyl chloride.

Another example of hydrophobically modified nonionic cellulose ether (HM-EHEC) is shown in Fig. 3.3. The cellulose can be modified by a relatively random substitution of hydroxyethyl and ethyl groups to give ethyl(hydroxyethyl) cellulose (EHEC). A low fraction of hydrophobic alkyl groups is inserted to give HM-EHEC.

Another sugar-based surfactant is alkyl polyglucoside which is prepared by reacting starch or glucose with butanol using acid catalyst [6]. The resulting butyl oligoglycoside intermediate is reacted with dodecanol using acid catalyst to produce dodecyl polyglucosides as illustrated in Fig. 3.4. The reaction yields a mixture in which on average more than one glucose unit is attached to an alcohol molecule. The average number of glucose units linked to an alcohol group is described as the (average) degree of polymerization (DP). Alkyl monoglycosides are the main group of components with a content of more than 50 % followed by the diglycosides and higher oligomers up to

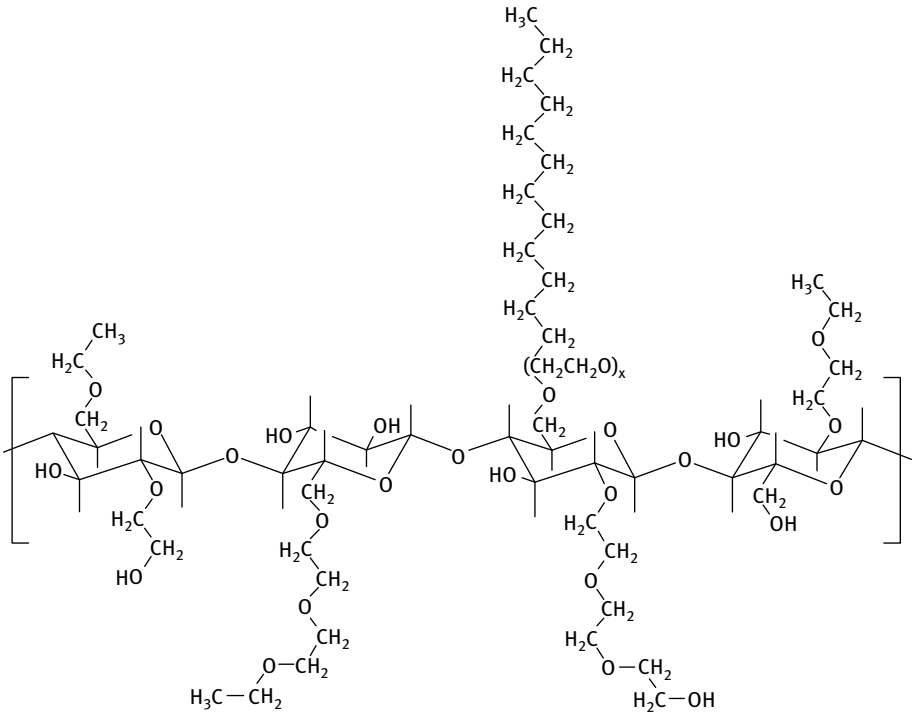

Fig. 3.3: Structure of hydrophobically modified ethylhydroxyethyl cellulose (HM-EHEC).

heptaglucosises. Due to the presence of molecules with DP > 1, the surfactant may be considered as polymeric. The alkyl polyglucosides show high surface activity at the air/water and oil/water interfaces. They also have low critical micelle concentrations comparable to those of nonionic surfactants.

More recently, graft copolymers based on polysaccharides have been developed for the stabilization of disperse systems. One of the most useful graft copolymers are those based on inulin that is obtained from chicory roots [7–9]. It is a linear polyfructose chain with a glucose end. When extracted from chicory roots, inulin has a wide range of chain lengths ranging from 2–65 fructose units. It is fractionated to obtain a molecule with narrow molecular weight distribution with a degree of polymerization >23 and this is commercially available as INUTEC® N25. This molecule is used to prepare a series of graft copolymers by random grafting of alkyl chains (using alkyl isocyanate) on the inulin backbone. The first molecule of this series is INUTEC® SP1 (Beneo-Remy, Belgium) that is obtained by random grafting of C_{12} alkyl chains. It has an average molecular weight of ≈ 5,000 Daltons and its structure is given in Fig. 3.5. The molecule is schematically illustrated in Fig. 3.6 which shows the hydrophilic polyfructose chain (backbone) and the randomly attached alkyl chains.

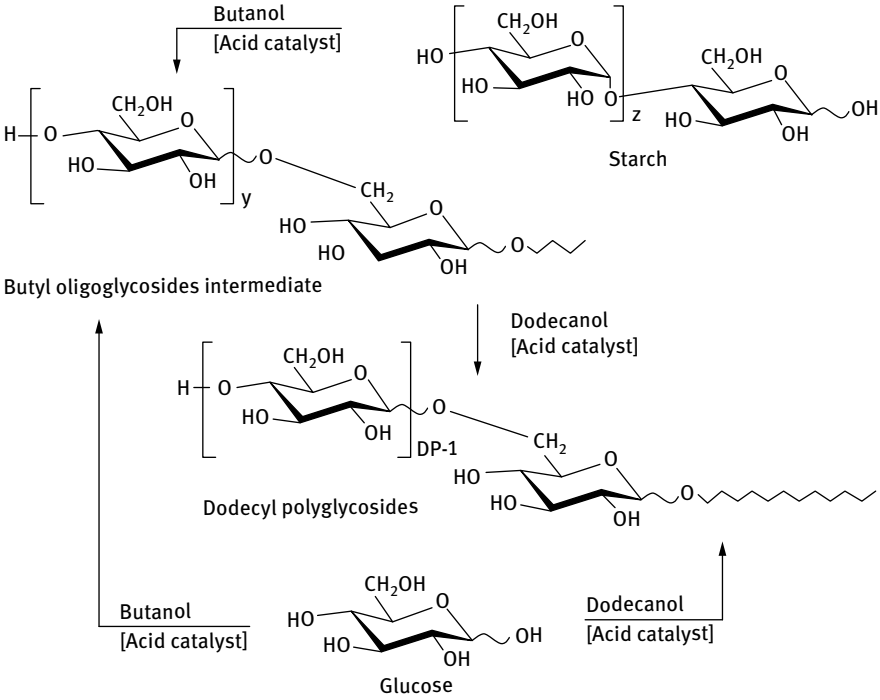

Fig. 3.4: Pathway for alkyl polyglucoside synthesis.

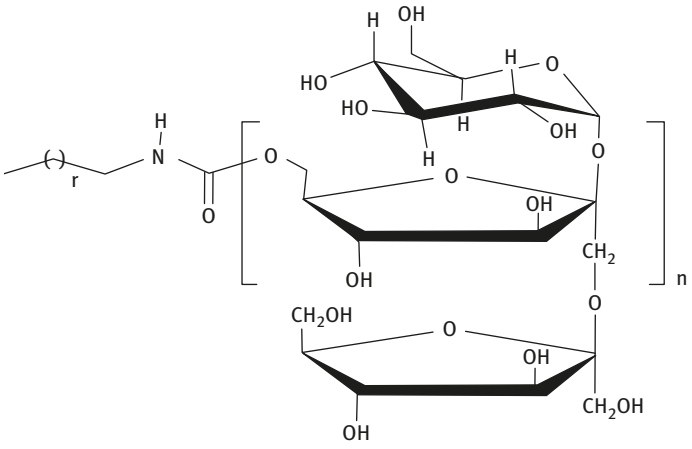

Fig. 3.5: Structure of INUTEC® SP1.

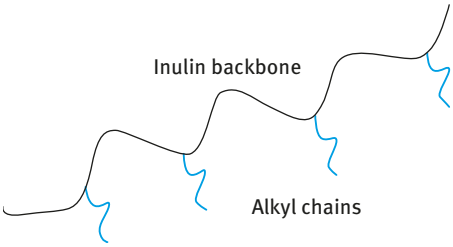

Fig. 3.6: Schematic representation of INUTEC® SP1 polymeric surfactant.

The main advantages of INUTEC® SP1 as a stabilizer for disperse systems are:

(i) Strong adsorption to the particle or droplet by multipoint attachment with several alkyl chains. This ensures lack of desorption and displacement of the molecule from the interface.
(ii) Strong hydration of the linear polyfructose chains both in water and in the presence of high electrolyte concentrations and high temperatures. This ensures effective steric stabilization [10].

3.2.5 Natural polymeric biosurfactants

Most food emulsions require the use of naturally occurring polymeric surfactants that must be approved by the Food and Drug Administration (FDA). One of the most commonly used natural polysaccharide emulsifier is gum arabic [11] which is amphiphilic. It has a nonpolar polypeptide backbone with a number of polar polysaccharide chains attached. On adsorption to oil droplet surfaces, the polypeptide chain protrudes to the oil droplet surfaces, whereas the polysaccharide chains dangle into the water. This leads to the formation of a relatively thick hydrophilic coating around the oil droplets that prevents any aggregation and coalescence of the oil droplets.

A number of other naturally occurring amphiphilic polysaccharides that are suitable for use as emulsifiers have been identified, e.g. pectin fractions isolated from beet, citrus, apple, etc. These polymeric surfactants show surface activity at the oil/water (O/W) interface and are able to stabilize the emulsion against flocculation and coalescence. Chitosan, a cationic polysaccharide, typically isolated from crustacean shells, is also capable of emulsion formation and stability.

One of the most common naturally occurring polymeric surfactants that are frequently used in food emulsions are the proteins. They are biopolymers consisting of strings of amino acid units covalently linked by peptide bonds [11]. The type, number and position of the amino acids in the polypeptide chain determine the molar mass and functional properties of food proteins. Most proteins contain a mixture of polar and nonpolar amino acids and, therefore, the amphiphilic molecules can adsorb at the O/W interface thus stabilizing the emulsion. The relative balance of polar and nonpolar groups exposed on their surfaces governs the surface activity of proteins.

If the surface hydrophobicity is too low, the driving force for protein adsorption is not strong enough to overcome the entropy loss associated with adsorption. Conversely, if the surface hydrophobicity is too high, then the proteins tend to aggregate, become water-insoluble, and lose their surface activity. Consequently, an optimum level of surface hydrophobicity is required for a protein to be a good emulsifier. Most proteins also have a mixture of anionic, nonionic and cationic amino acids along the polypeptide chains, which determines the charge of the protein molecule under different pH conditions. At a certain pH, referred to as isoelectric point (IEP), the protein molecule has a net zero charge. When the pH > IEP, the protein molecule is negatively charged, whereas when pH < IEP the protein molecule becomes positively charged. The charged chains play a major role in electrostatic stabilization.

Proteins may adopt various conformations in aqueous solution, depending on the balance of van der Waals forces, hydrophobic interactions, electrostatic interactions, hydrogen bonds, steric effects and entropy effects [11]. The balance is determined by solution and environmental conditions such as pH, ionic strength and temperature. Consequently, the conformation of a protein at an interface may change when these conditions are altered. The two mostly common conformations of surface active proteins used as emulsifiers are globular and random coil. Globular proteins have fairly compact spheroid structures where the majority of the nonpolar groups are located within the interior, and the majority of the polar groups are present at the exterior. These globular proteins have surface activity because some of the nonpolar groups remain exposed at their surfaces, which gives the driving force for adsorption at the O/W interface. Random coils have a more flexible structure, although there may still be some regions that have local order such as helical and sheet structures. The most common random coil proteins used as emulsifiers in the food industry are casein and gelatin. The structure of the protein often changes after they adsorb at the O/W interface. For example, globular proteins may unfold after they adsorb to droplet surfaces and expose groups normally located in their interiors, such as nonpolar and sulphhydryl groups. After adsorption to the oil droplet surfaces, the protein molecule may adopt a configuration where many of the hydrophilic groups protrude into the water phase, whereas most of the hydrophobic groups protrude to the oil phase. This results in high surface activity at the O/W interface and effective stabilization of the emulsion.

3.2.6 Silicone surfactants

Silicone surfactants are graft copolymers (“comb” type) with a backbone based on polydimethylsiloxane, which is highly hydrophobic and insoluble in water [5, 12]. The side chains (“teeth”) are water soluble, charged or uncharged, and the molecule becomes surface active in aqueous solution. Poly(ethylene glycol) (EO) or poly(ethylene glycol)–poly(propylene glycol) (PEO–PPO) are by far the most common constituents of the side chains. The side chain may contain a weakly polar group such as an ester

or amine or it may be an ionic group. The general structure of the silicone surfactant is shown in Fig. 3.7 with X being an ionic or nonionic polar group such as PEO or PEO–PPO. The linkage between Si and the polyether chain may be either Si–O–C or Si–C. The Si–O–C link is made by esterification of chloropolysiloxanes with hydroxyl-functional organic compounds such as PEO–PPO copolymer. This makes the molecule unstable undergoing hydrolysis in acid or alkaline conditions. However, the Si–C linkage, where a carbon of the PEO–PPO copolymer is directly linked to the Si atom, is stable. Such a linkage is usually made by a Pt-catalysed hydrosilating addition of an Si–H function in the polysiloxane to a terminal olefinic bond in the substituted polymer [5].

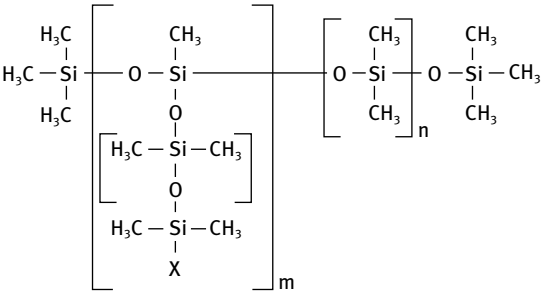

Fig. 3.7: Structure of silicone surfactants with X being an ionic or nonionic polar group such as PEO or PEO–PPO.

Silicone surfactants have unique properties when compared with hydrocarbon surfactants. They are very effective in lowering the surface tension of water to values around 20 mN m^{-1} (when compared with the value of around 30 mN m^{-1} obtained with most hydrocarbon surfactants). They also have excellent wetting on low-energy surfaces such as polytetrafluroethane (PTFE). They are also powerful antifoamers.

3.2.7 Polymeric surfactants for nonaqueous dispersions

Block and graft copolymers based on poly(12-hydroxystearic acid) are used for nonaqueous systems such as water-in-oil (W/O) emulsions and nonaqueous dispersions, e.g. paints [13]. The poly(12-hydroxystearic acid) chains (the A chains of an A–B–A block copolymer or the A side chains of a graft copolymer), which are of low molecular weight (≈ 1,000 Daltons), provide steric stabilization analogous to how PEO behaves in aqueous solution [5]. The B anchor chains are chosen to be highly insoluble in the nonaqueous medium and have some specific interaction with the surface of the droplet or particle. For water-in-oil (W/O) emulsions an A–B–A block copolymer of poly (12-hydroxystearic acid) (PHS) (the A chains) and poly (ethylene oxide) (PEO) (the B chain): PHS–PEO–PHS is commercially available (Arlacel P135). The PEO chain (that is soluble in the water droplets) forms the anchor chain, whereas the PHS chains form the stabilizing chains. PHS is highly soluble in most hydrocarbon solvents and is

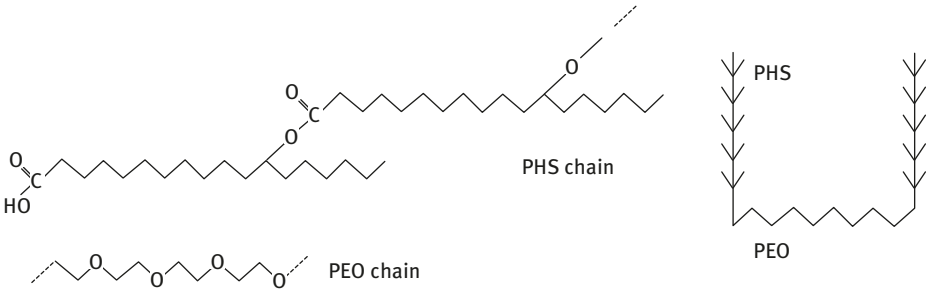

Fig. 3.8: Schematic representation of the structure of PHS–PEO–PHS block copolymer.

strongly solvated by its molecules. The structure of the PHS–PEO–PHS block copolymer is schematically shown in Fig. 3.8.

In the nonaqueous dispersion process (referred to as NAD) the monomer, normally an acrylic, is dissolved in a nonaqueous solvent, normally an aliphatic hydrocarbon and an oil-soluble initiator and a stabilizer (to protect the resulting particles from flocculation, sometimes referred to as "protective colloid") is added to the reaction mixture. The most successful stabilizers used in NAD are block and graft copolymers. These block and graft copolymers are assembled in a variety of ways to provide the molecule with an "anchor chain" and a stabilizing chain. As mentioned above, the anchor chain should be sufficiently insoluble in the medium and have a strong affinity to the polymer particles produced. In contrast, the stabilizing chain should be soluble in the medium and strongly solvated by its molecules to provide effective steric stabilization. The length of the anchor and stabilizing chains has to be carefully adjusted to ensure strong adsorption (by multipoint attachment of the anchor chain to the particle surface) and sufficiently "thick" layer of the stabilizing chain that prevents close approach of the particles to a distance where the van der Waals attraction becomes strong. Several configurations of block and graft copolymers are possible, as is illustrated in Fig. 3.9.

Typical preformed graft stabilizers based on poly(12-hydroxy stearic acid) (PHS) are simple to prepare and effective in NAD polymerization. Commercial 12-hydroxystearic acid contains 8–15 % palmitic and stearic acids which limits the molecular weight during polymerization to an average of 1,500–2,000. This oligomer may be converted to a "macromonomer" by reacting the carboxylic group with glycidyl methacrylate. The macromonomer is then copolymerized with an equal weight of methyl methacrylate (MMA) or similar monomer to give a "comb" graft copolymer with an average molecular weight of 10,000–20,000. The graft copolymer contains on average 5–10 PHS chains pendent from a polymeric anchor backbone of PMMA. This a graft copolymer can stabilize latex particles of various monomers. The major limitation of the monomer composition is that the polymer produced should be insoluble in the medium used.

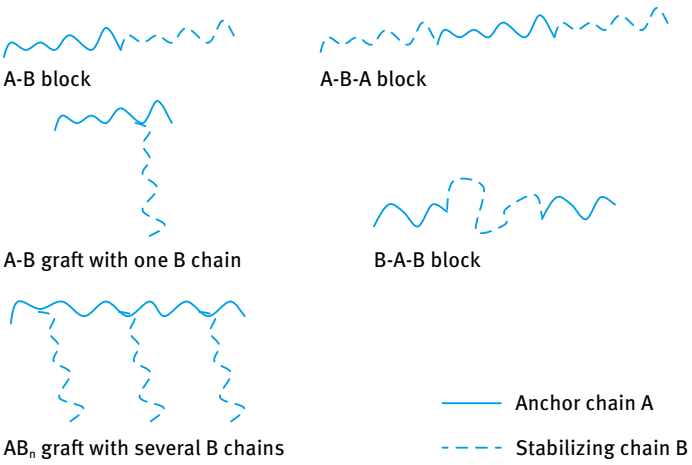

Fig. 3.9: Configurations of block and graft copolymers.

Several other examples of block and graft copolymers that are used in dispersion polymerization are given in Tab. 3.1 which also shows the continuous phase and disperse polymer that can be used with these polymers.

Tab. 3.1: Block and graft copolymers used in emulsion polymerization.

Polymeric Surfactant	Continuous phase	Disperse polymer
Polystyrene-block-poly(dimethyl siloxane)	Hexane	Polystyrene
Polystyrene-block-poly(methacrylic acid)	Ethanol	Polystyrene
Polybutadiene-graft-poly(methacrylic acid)	Ethanol	Polystyrene
Poly(2-ethylhexyl acrylate)-graft-poly(vinyl acetate)	Aliphatic hydrocarbon	Poly(methyl methacrylate)
Polystyrene-block-poly(t-butylstyrene)	Aliphatic hydrocarbon	Polystyrene

3.2.8 Polymerizable surfactants

Polymerizable surfactants are amphipathic molecules containing somewhere in their structure a polymerizable group such as styrenic, acrylic or methacrylic, vinylic, maleic, crotonic or allylic [14]. These groups may be located in different places such as at the end or head of the hydrophilic sequence, the end of the hydrophobic moiety, between the two, or finally along the surfactant structure or pendent (side) groups. They are generally referred to as surfmers [14]. One of the main applications of polymerizable surfactants is for the stabilization of vesicles. The second major use of polymerizable surfactants is their application as stabilizers in polymerization in dispersed media, both in emulsion and dispersion polymerization. The surfactant is

covalently linked to the surface of the particles, thus improving latex stability. A second kind of benefit is expected in the case of film-forming latexes. In conventional emulsion, the surfactants are not firmly attached to the particles and thus are able to migrate toward the surface of the film. This may result in defects of adhesion if the film is expected to protect the surface of a substrate. In addition, phase separation may occur during coalescence. These problems are overcome when using surfactants that are covalently linked to the surface of the latex. A third kind of benefit takes place if it is intended that the latex will release material upon flocculation. If the surfactant is covalently linked to the surface of the polymer particles, a smaller amount of it will be rejected to the water phase [13].

3.3 Solution properties of polymeric surfactants

3.3.1 Polymer conformation and structure

Long flexible macromolecules have a large number of internal degrees of freedom. A typical primary structure of such molecules is a linear chain of units connected by covalent bonds referred to as the backbone. By rotation around the bonds in the backbone the molecule changes its shape resulting in a wide spectrum of conformations. Rotation is hindered by the side groups, so that some of these conformations may be rather unfavourable. In some macromolecules such as proteins sequences of preferred orientations show up as helical or folded sections.

For flexible linear polymers, the energy barriers associated with rotation around the bonds are small with respect to the thermal motion. Such molecules have a randomly fluctuating three-dimensional tertiary structure, referred to as a random coil, as is illustrated in Fig. 3.10. The chain conformation is described as a random flight chain of N bonds of length ℓ. The fluctuating distance between the end points is r. The quantity $\langle r^2 \rangle^{1/2}$, that is referred to as the mean end-to-end distance, is a measure

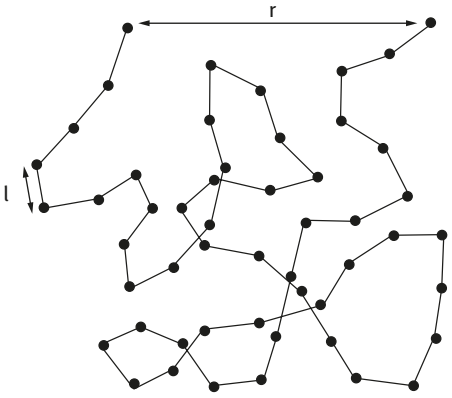

Fig. 3.10: Schematic representation of the chain conformation for a random coil.

of the size of the chain, i.e. its mean coil diameter [15],

$$\langle r^2 \rangle^{1/2} = N^{1/2} \ell. \tag{3.1}$$

Another useful parameter is the radius of gyration $\langle s^2 \rangle^{1/2}$ which is a measure of the effective size of a polymer molecule (it is the root mean-square distance of the elements of the chain from its centre of gravity).

For linear polymers,

$$\langle s^2 \rangle^{1/2} = \frac{\langle r^2 \rangle^{1/2}}{6^{1/2}}. \tag{3.2}$$

In real polymers the bonds cannot assume arbitrary directions but there are fixed angles between them. In addition, rotation about bonds is not entirely free, because the potential energy shows maxima and minima as a function of rotation angle. To account for these effects the above equations are modified by introducing a rigidity parameter p (stiffness "persistence ") which depends on the architecture of the chain,

$$\langle r^2 \rangle^{1/2} = 6^{1/2} p^{1/2} N^{1/2} \ell, \tag{3.3}$$

$$\langle s^2 \rangle^{1/2} = p^{1/2} N^{1/2} \ell. \tag{3.4}$$

$p = 1/6$ for a (hypothetically) fully flexible chain and p increases as the chain becomes less flexible, for example when the side groups are bulky. Typical p values for real chains are in the range 0.5–4.

A useful parameter, called the characteristic ratio, was introduced by Flory [15] and is defined as,

$$C_\infty = \frac{\langle r^2 \rangle}{N \ell_b^2}. \tag{3.5}$$

ℓ_b^2 stands for the sum of the squares of the lengths of the backbone bonds of one monomer unit,

$$\ell_b^2 = \sum_i a_i^2. \tag{3.6}$$

The main consequence of the above equations is that for ideal chains the dimensions (root mean-square end-to-end distance and radius of gyration) are proportional to $N^{1/2}$. This is only valid for ideal chains when the volume of the segments and solvency effects are entirely ignored. In other words, a walk may return to its origin without any hindrance. This is unrealistic for segments which occupy a volume. In good solvents where the chains swell, the excluded volume becomes important. The segments cannot overlap and there is an exclusion volume that automatically leads to coil expansion. In very good solvents, where the segments repel each other, the excluded volume is larger than the exclusion volume. In contrast, in a poor solvent the segments experience net attraction, the effective excluded volume is small and the ideal chain model gives a reasonable description.

3.3.2 Free energy of mixing of polymer with solvent – the Flory–Huggins theory

The effect of solvency for the polymer chain has been considered in the thermodynamic treatment of Flory and Huggins [16], usually referred to as the Flory–Huggins theory. This theory considers the free energy of mixing of pure polymer with pure solvent, ΔG_{mix}, in terms of two contributions, namely the enthalpy of mixing, ΔH_{mix}, and the entropy of mixing, ΔS_{mix}, i.e. using the second law of thermodynamics,

$$\Delta G_{\text{mix}} = \Delta H_{\text{mix}} - T\Delta S_{\text{mix}}. \tag{3.7}$$

Assuming that the polymer chain adopts a configuration on a lattice (provided by solvent molecules) and considering that the mixing is "random", then the entropy of mixing ΔS_{mix} is given by the following expression,

$$\Delta S_{\text{mix}} = -k[n_1 \ln \phi_1 + n_2 \ln \phi_2], \tag{3.8}$$

where k is the Boltzmann constant, n_1 is the number of solvent molecules with a volume fraction ϕ_1 and n_2 is the number of polymer molecules with a volume fraction ϕ_2.

The enthalpy of mixing, ΔH_{mix}, is given by the following expression,

$$\Delta H_{\text{mix}} = n_1 \phi_2 \chi kT, \tag{3.9}$$

where χ is a dimensionless interaction parameter and χkT expresses the difference in energy of a solvent molecule in pure solvent compared to its immersion in pure polymer. χ is usually referred to as the Flory–Huggins interaction parameter.

Combining equations (3.7)–(3.9), one obtains,

$$\Delta G_{\text{mix}} = kT[n_1 \ln \phi_1 + n_2 \ln \phi_2 + \chi n_1 \phi_2]. \tag{3.10}$$

The mixing of a pure solvent with a polymer solution creates an osmotic pressure, π, which can be expressed in terms of the polymer concentration c_2 and the volume fraction of the polymer,

$$\frac{\pi}{C_2} = RT\left[\frac{1}{M_2} + \left(\frac{\upsilon_2^2}{V_1}\right)\left(\frac{1}{2} - \chi\right)c_2 + \cdots\right], \tag{3.11}$$

where υ_2 is the partial specific volume of the polymer ($\upsilon_2 = V_2/M_2$) and V_1 is the molar volume of the solvent.

The second term in equation (3.11) is the second virial coefficient B_2, i.e.,

$$\frac{\pi}{c_2} = RT\left[\frac{1}{M_2} + B_2 + \cdots\right], \tag{3.12}$$

$$B_2 = \left(\frac{\upsilon_2^2}{V_1}\right)\left(\frac{1}{2} - \chi\right). \tag{3.13}$$

Note that $B_2 = 0$ when $\chi = 1/2$, i.e. the polymer behaves as ideal in mixing with the solvent. This condition was termed by Flory [16] as the θ-point. Under these conditions, the polymer chains in solution have no repulsion or attraction or they adopt their unperturbed dimension. Clearly, when $\chi < 1/2$, B_2 is positive and mixing is non-ideal, leading to positive deviation (repulsion); this occurs when the polymer chains are in "good" solvent conditions. In contrast, when $\chi > 1/2$, B_2 is negative and mixing is non-ideal, leading to negative deviation (attraction); this occurs when the polymer chains are in "poor" solvent conditions (precipitation of the polymer may occur under these conditions). Since the polymer solvency depends on temperature, one can also define a theta temperature θ at which $\chi = 1/2$.

The function $[(1/2) - \chi]$ can also be expressed in terms of two mixing parameters, an enthalpy parameter κ_1 and an entropy parameter ψ_1, i.e.,

$$\left(\frac{1}{2} - \chi\right) = \kappa_1 - \psi_1. \tag{3.14}$$

The θ-temperature can also be defined in terms of κ_1 and ψ_1,

$$\theta = \frac{\kappa_1 T}{\psi_1}. \tag{3.15}$$

Alternatively, one can write,

$$\left(\frac{1}{2} - \chi\right) = \psi_1\left(1 - \frac{\theta}{T}\right). \tag{3.16}$$

The θ-temperature is an important parameter which describes a polymer–solvent system. At this temperature a polymer segment will not be able to tell whether it is in contact with another segment or a solvent molecule. The polymer will have the configuration as it would have in its own liquid or it said to be in its "unperturbed dimension". In normal solvents the solvent quality increases as the temperature is raised (due to the higher thermal energy) and hence each polymer segment will have a tendency to be in contact with the solvent molecules rather in contact with the polymer's own segments. Thus, the polymer will expand its configuration. On the other hand, at temperatures below the θ-temperature, the polymer segments prefer to be in contact with other polymer segments rather than with the solvent molecules. Thus, the polymer will contract. The θ-temperature is also called the Flory temperature and the solvent or solvent mixture at this temperature is called a θ-solvent.

One can define an expansion or contraction parameter α that is given by,

$$\alpha = \frac{R_G}{R_G^0}, \tag{3.17}$$

where R_G^0 is the radius of gyration at the θ-temperature.

Although the Flory–Huggins theory is sound in principle, several experimental results cannot be accounted for. For example, it was found that the χ parameter depends on the polymer concentration in solution. Most serious is the fact that many

polymer solutions (such as PEO) show phase separation on heating, when the theory predicts that it should happen only on cooling. Another complication arises from specific interaction with the solvent, e.g. hydrogen bonding between polymer and solvent molecules (e.g. with PEO and PVA in water). Also aggregation in solution (lack of complete dissolution) may present another problem.

The derivation of the Flory–Huggins equation was carried out under the assumption that volume changes occurring upon mixing of polymer and solvent are negligible. As discussed above, the free volume concept must be considered. This predicts that near the critical point, where phase separation occurs, there are no bonds between the molecules constraining the separation of solvent molecules. They are, however, present for the segments of polymer molecules. Hence, upon heating a polymer solution, the increase in free volume for the solvent is large, and much larger than that for the polymer. This difference in free volume creates a large difference in the coefficient of expansion between the polymer and the solvent and this leads to phase separation on heating.

Prigogine et al. [17] introduced the concept of the effect of free volume dissimilarity by their theory of solutions and they questioned the association of the χ parameter with heat of mixing only. This led Flory and coworkers [16–19] to introduce some additional concepts. They pointed out that although a solution of a polymer in a chemically similar solvent would have no contact dissimilarities, it would have them due to the differences in length and size of the polymer chains. This means that the volume changes taking place during mixing, V_M, could not be neglected.

The Flory–Huggins theory only applies for ideal linear polymers. It fails to describe the properties of polymers with a structure having high monomer density, such as two- and three-dimensional branched polymers. It has been found that the theta temperature of star-branched polymers is generally lower than that of linear polymers and it also depends on the length of the arms [16–19].

Another limitation of the Flory–Huggins theory is its applicability to polymers in aqueous solutions. Firstly, water produces strong specific interaction between the polymer and water molecules, mostly by hydrogen bonds. Secondly, complete dissolution of the polymer in water is questionable due to the aggregation of the molecules. For these reasons, the Flory–Huggins theory has been found to be not applicable for polymers such as poly(ethylene oxide) (PEO) or polyvinyl alcohol (PVA) that are known to form strong hydrogen bonds between the ethylene oxide or vinyl alcohol units and water. For example, colorimetric measurements showed that at low PEO concentrations each EO unit is hydrogen bonded to two water molecules, whereas at high PEO concentrations, the number of hydrogen bonds is significantly reduced to one water molecule per two EO units.

The solution properties of copolymers are much more complicated. This is due to the fact that the two copolymer components A and B behave differently in different solvents. Only when the two components are both soluble in the same solvent, then they exhibit similar solution properties. This is the case for example for a nonpolar

copolymer in a nonpolar solvent. Dilute solutions of copolymers in solvents that are good for both components exhibit similar behaviour to homopolymer chains, resulting from interactions with solvent molecules and each other. Two possible models for copolymers have been proposed. The first one, called the segregated model, assumes that there are only a few hetero-contacts, and the two different polymer components behave like homopolymer chains. The second model, referred to as the random structure model, takes into account some overlap between different blocks creating hetero-contacts between unlike segments. Several techniques can be applied to study the possible configurations of copolymer components in solution. Most studies have been carried out for block copolymers either in good solvents or θ-solvents for the blocks. For example, light scattering, viscosity and GPC studies were carried out for polystyrene-block-polyisoprene copolymers in methyl isobutylketone as the solvent. The solvent is a near θ-solvent for these polymers. The results showed segregated conformation for the block copolymer with a limited number of hetero-contacts. Small angle neutron scattering studies for polystyrene-block–poly(methylmethacrylate) in toluene showed that the poly(methylmethacrylate) block is in a tightly coiled conformation, surrounded by a slightly expanded polystyrene shell.

In a selective solvent, in which the medium is a good solvent for one component, say A, and a poor solvent for the second component B, one part of the amphipathic block or graft separate as a distinct phase, while the other stays in solution. The insoluble portion of the amphipathic copolymer will aggregate reversibly to form micelles. It is believed that the polymeric micelles are spherical and have a narrow particle size distribution. Thus micelle formation in block and graft copolymers is analogous to small molecule surface active materials. For graft copolymers in selective solvents, the formation of "molecular micelles" has been observed. These resemble particles with an insoluble swollen core surrounded by a sheath of soluble chains. Depending on the concentration of the solution, the temperature and the nature of the solvent, multimolecular aggregates are observed. A schematic representation of monomolecular and multimolecular micelles is shown in Fig. 3.11.

The critical micelle concentration (cmc) of these block and graft copolymers is usually very low. Because of the relatively high molecular weight of block and graft copolymers (when compared with simple surfactants), the concentration of these materials has to be very low in order to precisely determine their cmc. Even at the cmc, the solution does not only contain micellar aggregates, but also single molecules over a very large range of concentrations. Similar to simple surfactants, the cmc can be determined using surface tension (γ) versus concentration measurements. From plots of γ versus log C one can obtain the cmc. γ decreases with increasing log C until the cmc is reached and then γ remains constant. Since with most block and graft copolymers the molecular weight is not sufficiently narrow, calculation of C in mol dm^{-3} is not straightforward and hence C is usually expressed in wt%.

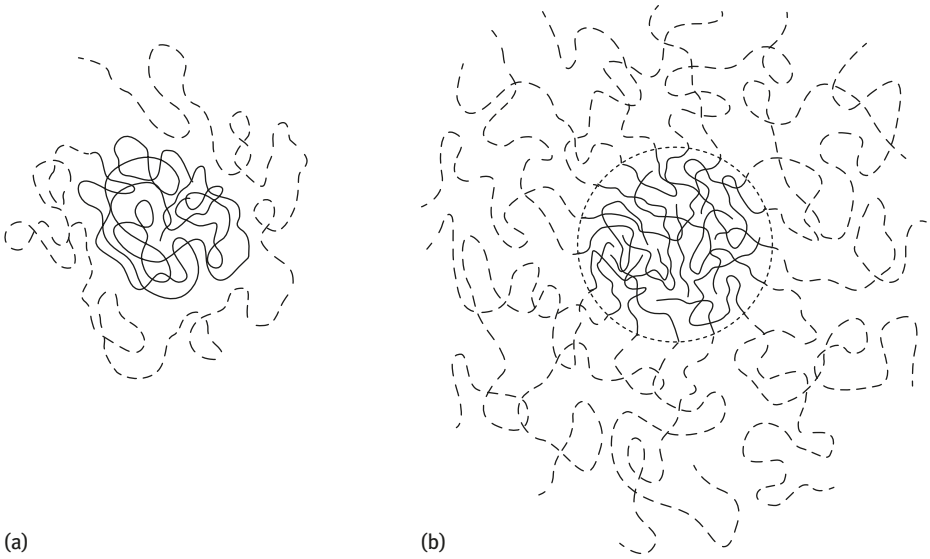

Fig. 3.11: Schematic representation of monomolecular (a) and multimolecular (b) micelles.

Several methods may be applied to obtain the micellar size and shape of block and graft copolymers, of which light scattering, small angle X-ray and neutron scattering are probably the most direct. Dynamic light scattering (photon correlation spectroscopy), described below, can also be applied to obtain the hydrodynamic radius of the micelle. This technique is relatively easy to perform when compared with static light scattering, since it does not require rigorous preparation of the samples.

3.4 Characterization of polymers in solution

3.4.1 Scattering techniques

Scattering techniques provide the most obvious methods for obtaining information on the size, shape and structure of polymers in solution. The scattering of radiation, e.g. light, neutrons, X-rays, etc. by polymer coils can be applied to obtain such information. In all these methods, measurements can be made at sufficiently low concentration to avoid complications arising from polymer-polymer interactions. The results obtained are extrapolated to infinite dilution to obtain the desired property such as the molecular weight and radius of gyration of a polymer coil, the size and shape of polymer coil. Two scattering methods will be discussed below: time-average (static) light scattering and dynamic (quasi-elastic) light scattering, referred to as photon correlation spectroscopy.

3.4.1.1 Time-average (static) light scattering

The intensity of scattered light $I(Q)$ is measured as a function of scattering vector Q,

$$Q = \left(\frac{4\pi n}{\lambda}\right)\sin\left(\frac{\theta}{2}\right), \tag{3.18}$$

where n is the refractive index of the medium, λ is the wavelength of light and θ is the angle at which the scattered light is measured.

For a fairly dilute system, $I(Q)$ is proportional to the number of polymer coils N, the square of the volume of the individual scattering units V_p and some property of the system (material constant) such as its refractive index,

$$I(Q) = [(\text{material constant})(\text{instrument constant})]NV_p^2. \tag{3.19}$$

The instrument constant depends on the geometry of the apparatus (the light path length and the scattering cell constant)

For more concentrated systems, $I(Q)$ also depends on the interference effects arising from polymer-polymer interaction,

$$I(Q) = [(\text{instrument constant})(\text{material constant})]NV_p^2P(Q)S(Q), \tag{3.20}$$

where $P(Q)$ is the polymer coil form factor which allows the scattering from a single polymer of known size and shape to be predicted as a function of Q. For a spherical polymer coil of radius R,

$$P(Q) = \left[\frac{(3\sin QR - QR\cos QR)}{(QR)^3}\right]^2. \tag{3.21}$$

$S(Q)$ is the so-called "structure factor" which takes into account the polymer-polymer interaction. $S(Q)$ is related to the radial distribution function $g(r)$, which gives the number of polymer coils in shells surrounding a central coil,

$$S(Q) = 1 - \frac{4\pi N}{Q}\int_0^\infty [g(r) - 1]r\sin QR\,\mathrm{d}r. \tag{3.22}$$

For a hard-sphere dispersion with radius R_{HS},

$$S(Q) = \frac{1}{[1 - NC(2QR_{HS})]}, \tag{3.23}$$

where C is a constant.

One usually measures $I(Q)$ at various scattering angles θ and then plots the intensity at some chosen angle (usually 90°), i_{90}, as a function of the volume fraction ϕ of the dispersion. Alternatively, the results may be expressed in terms of the Rayleigh ratio R_{90},

$$R_{90} = \left(\frac{i_{90}}{I_0}\right)r_s^2. \tag{3.24}$$

I_0 is the intensity of the incident beam and r_s is the distance from the detector.

$$R_{90} = K_0 MC\, P(90)\, S(90). \tag{3.25}$$

K_0 is an optical constant (related to the refractive index difference between the polymer and the medium). M is the molecular mass of scattering units with weight fraction C.

For small particles (as is the case with polymer coils) $P(90) \approx 1$ and,

$$M = \frac{4}{3}\pi R_c^3 N_A, \tag{3.26}$$

where N_A is the Avogadro constant.

$$C = \phi_c \rho_c, \tag{3.27}$$

where ϕ_c is the volume fraction of the polymer and ρ_c is its density.

Equation (3.25) can be written in the simple form,

$$R_{90} = K_1 \phi_c R_c^3 S(90), \tag{3.28}$$

where $K_1 = K_0(4/3)N_A\rho_c^2$.

Equation (3.28) shows that to calculate R_c from R_{90} one needs to know $S(90)$. The latter can be calculated using equations (3.22)–(3.23).

3.4.1.2 Dynamic light scattering (photon correlation spectroscopy, PCS)

In this technique one measures the intensity fluctuation of scattered light by the polymer coils as they undergo Brownian motion [1]. When a light beam passes through a polymer dispersion, an oscillating dipole movement is induced in the polymer coil, thereby radiating the light. Due to the random position of the polymer coils, the intensity of scattered light, at any instant, appears as random diffraction ("speckle" pattern). As the polymer coils undergo Brownian motion, the random configuration of the pattern will fluctuate, such that the time taken for an intensity maximum to become a minimum (the coherence time), corresponds approximately to the time required for a polymer coil to move one wavelength λ. Using a photomultiplier of active area about the diffraction maximum (i.e. one coherent area) this intensity fluctuation can be measured. The analogue output is digitized (using a digital correlator) that measures the photocount (or intensity) correlation function of scattered light.

The photocount correlation function $G^{(2)}(\tau)$ is given by,

$$g^{(2)} = B[1 + \gamma^2 g^{(1)}(\tau)]^2, \tag{3.29}$$

where τ is the correlation delay time.

The correlator compares $g^{(2)}(\tau)$ for many values of τ.

B is the background value to which $g^{(2)}(\tau)$ decays at long delay times. $g^{(1)}(\tau)$ is the normalized correlation function of the scattered electric field and γ is a constant (≈ 1).

For monodispersed non-interacting polymer coils,

$$g^{(1)}(\tau) = \exp(-\Gamma\gamma). \tag{3.30}$$

Γ is the decay rate or inverse coherence time, which is related to the translational diffusion coefficient D,

$$\Gamma = DK^2, \tag{3.31}$$

where K is the scattering vector,

$$K = \left(\frac{4\pi n}{\lambda_0}\right)\sin\left(\frac{\theta}{2}\right). \tag{3.32}$$

The polymer coil radius R can be calculated from D using the Stokes–Einstein equation,

$$D = \frac{kT}{6\pi\eta_0 R}, \tag{3.33}$$

where η_0 is the viscosity of the medium.

3.4.1.3 Viscosity measurements for characterization of a polymer in solution

A convenient way to characterize a polymer in solution at low concentrations is to measure the viscosity using capillary viscometry. The most widely used capillary viscometer is the Ostwald type shown schematically in Fig. 3.12. A variant of the Ostwald viscometer is the Cannon–Fenske type which is more convenient to use (Fig. 3.12).

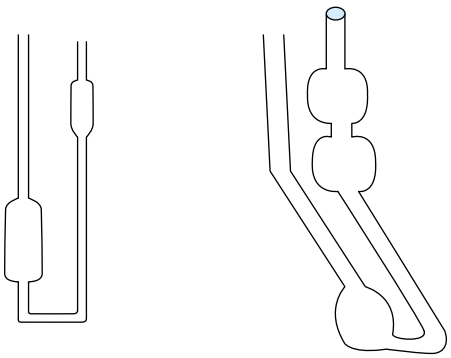

Ostwald viscometer Cannon–Fenske viscometer

Fig. 3.12: Schematic pictures of Ostwald and Cannon–Fenske viscometers.

In capillary viscometry, one measures the volumetric flow Q ($m^3\ s^{-1}$) and the viscosity η is calculated using the Poiseuille equation [20],

$$\eta = \frac{\pi R^4 p}{8QL}. \tag{3.34}$$

R is the tube radius with length L; p is the pressure drop = $h\rho g$ (where h is the liquid height with density ρ and g is the acceleration due to gravity).

One usually compares the viscosity of the liquid in question η_2 with that of a liquid with known viscosity η_1. In this way, one can measure the flow rates of the two liquids using the same viscometer with a bulb of volume V (the flow rate is simply given by V divided by the time taken for the liquid to flow between the two marks on the viscometer t_1 and t_2 for the two liquids).

Using equation (3.34) one simply obtains,

$$\frac{\eta_1}{\eta_2} = \frac{t_1\rho_1}{t_2\rho_2}. \tag{3.35}$$

t_1 and t_2 are simply measured using a stopwatch (for automatic viscometers two fibre optics are used). Accurate temperature control is necessary (±0.01 °C). The flow time t must also be measured with an accuracy of ±0.01 s.

For measuring the intrinsic viscosity $[\eta]$ of polymers, which can be used to obtain the molecular weight and solvation of the polymer chains, one measures the relative viscosity η_r as a function of polymer concentration C (in the range 0.01–0.1 %).

$$\eta_r = \frac{\eta_s}{\eta_0}, \tag{3.36}$$

where η_s is the viscosity of the polymer solution and η_0 is that of the solvent.

From η_r one can obtain the reduced viscosity η_{red}

$$\eta_{red} = (\eta_r - 1). \tag{3.37}$$

From η_{red} one can obtain the specific viscosity η_{sp}

$$\eta_{sp} = \frac{\eta_{red}}{C}. \tag{3.38}$$

A plot of η_{sp} versus C gives a straight line that can be extrapolated to $C = 0$ to obtain the intrinsic viscosity $[\eta]$. This is illustrated in Fig. 3.13.

From $[\eta]$ one can obtain the molecular weight M using the Mark–Houwink equation [20],

$$[\eta] = KM^{\alpha}, \tag{3.39}$$

where K and α are constants for a particular polymer and solvent (values for many polymer–solvent systems are tabulated in the Polymer Handbook). α is related to the solvency of the medium for the polymer chain. In a good solvent, $\alpha > 0.5$; it has values in the range 0.5–0.8. The higher the value of α, the better the solvent for the chain.

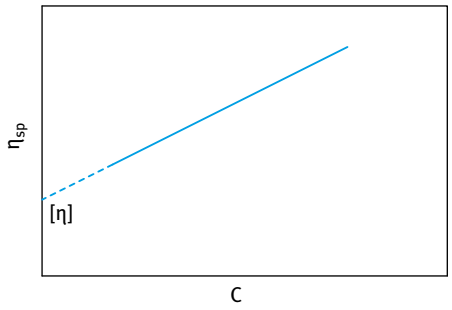

Fig. 3.13: Measurement of intrinsic viscosity of polymers.

3.5 Phase separation of polymer solutions

When dissolving two liquids, the molecules are free to move and hence the entropy for a liquid mixture is large. In contrast, when dissolving a polymer in a solvent a segment of the polymer is attached to several other segments and hence the entropy of a single segment with a free solvent molecule is much less when compared with mixing two solvents [5]. Therefore, polymer solutions have lower total entropy and hence are less stable and more prone to phase separation when compared to mixtures of ordinary liquids. This was quantified by Flory and Huggins [16] as discussed above. Flory–Huggins theory predicts that a solution with a higher molar mass is less stable towards phase when compared with a solution of the same polymer but with a lower molar mass. Hence, when a polymer phase separates in solution, the high molar mass species will separate out first, leaving the lower molar mass species in solution. This phenomenon is used for fractionation of polymer samples with respect to molar mass.

The temperature at which phase separation occurs for 1 % solution is called the cloud point, due to the increased turbidity of the polymer solution as this temperature is reached. The highest, or lowest, temperature at which a phase separation occurs is called the critical temperature and the corresponding polymer concentration is called the critical composition. The question of whether or not a polymer dissolves in a solvent is a matter of balance between the entropy and enthalpy of mixing. The entropy of mixing, which is low for polymers in solution, favours mixing. The enthalpy of mixing, which is a measure of the interaction energy between a segment and solvent molecule when compared with the interaction energy between segments and solvent molecule alone, is positive and it opposes mixing of the two components. In ordinary polymer/solvent systems, the stability with regard to phase separation will decrease with decreasing temperature. In this case, phase separation occurs when the temperature is sufficiently lowered and a concentrated polymer phase will be in equilibrium with a dilute polymer solution. Phase separation in this case can also occur by adding a nonsolvent to the polymer–solvent system.

However, some aqueous polymer solutions in which the polymer chain contains a polyoxyethylene oxide (PEO) chain, show phase separation when the temperature is increased. At very high temperatures, the two-phase region diminishes and the system is homogeneous again. This is due to the increased thermal energy that counteracts other forces at play. Thus, these polymer solutions show a low and upper critical solution temperature.

3.6 Solubility parameter concept for selecting the right solvent for a polymer

The solubility parameter is based on the assumption that "like dissolves like". A polymer is not soluble in certain liquids due to a large difference in the interaction between segments of the polymer and solvent molecules when compared to the interaction energy between segment–segment and solvent–solvent molecules. To achieve some solubility, the segment–solvent interaction energy should be as close as possible to the interaction energy between the segment–segment and solvent–solvent molecules. One method for measuring the interaction energies is to obtain the enthalpy of vaporization, ΔH_{vap}, which reflects the cohesive forces in the liquid. This concept was introduced by Hildebrand [21] who defined the cohesive energy ratio or solubility parameter δ by dividing ΔH_{vap} by the molar volume V,

$$\delta^2 = \frac{\Delta H_{\text{vap}}}{V}. \tag{3.40}$$

The units for solubility parameter are $\text{cal}^{1/2}\,\text{cm}^{-3/2}$ or $\text{J}^{1/2}\,\text{m}^{-3/2}$ (= $\text{MPa}^{1/2}$). Values of solubility parameters for various polymer–solvent systems are given in the book by Barton [22]. In order to find a suitable solvent for a polymer one should first find the solubility parameter of the polymer and then select solvents that have solubility parameters that are close to that of the polymer. For example, polystyrene has a solubility parameter of 9.1 $\text{cal}^{1/2}\,\text{cm}^{-3/2}$ and suitable solvents are cyclohexane ($\delta = 8.2$), benzene ($\delta = 9.2$) and methyl ethyl ketone ($\delta = 9.3$). In contrast, n-hexane ($\delta = 7.3$) and ethanol ($\delta = 12.7$) are nonsolvents, i.e. they do not dissolve polystyrene.

Hansen [23] subdivided δ^2 into three contributions: δ_{d}^2 (dispersion), δ_{p}^2 (polar) and δ_{h}^2 (hydrogen bonding),

$$\delta^2 = \delta_{\text{d}}^2 + \delta_{\text{p}}^2 + \delta_{\text{h}}^2. \tag{3.41}$$

Several theories and computations are available for calculating the above contributions for various polymer and solvent systems.

References

[1] Tadros T. Applied surfactants. Weinheim: Wiley-VCH; 2005.
[2] Tadros TF. In: Goddard ED, Gruber JV, editors. Principles of polymer science and technology in cosmetics and personal care. New York: Marcel Dekker; 1999.
[3] Tadros T. In: Holmberg K, editor. Novel Surfactants, New York: Marcel Dekker; 2003.
[4] Piirma I. Polymeric surfactants. Surfactant Science Series, No. 42. New York: Marcel Dekker; 1992.
[5] Holmberg K, Jonsson B, Kronberg B, Lindman B. Surfactants and polymers in aqueous solution. Chichester: John Wiley & Sons Ltd.; 2003.
[6] von Rybinski W, Hill K. Alkyl polyglucosides. In: Holmberg K, editor. Novel Surfactants. New York: Marcel Dekker; 2003.
[7] Stevens CV, Meriggi A, Peristerpoulou M, Christov PP, Booten K, Levecke B, Vandamme A, Pittevils N, Tadros TF. Biomacromolecules. 2001;2:1256.
[8] Hirst EL, McGilvary DI, Percival EG. J Chem Soc. 1950:1297.
[9] Suzuki M. In: Suzuki M, Chatterton NJ, editors. Science and technology of fructans. Boca Raton: CRC Press; 1993. p. 21.
[10] Tadros TF, Vandamme A, Levecke B, Booten K, Stevens CV. Advances Colloid Interface Sci. 2004;108–109:207.
[11] McClements DJ, Gumus CE. Advances Colloid and Interface Sci. 2016;234:3.
[12] Fleute-Schlachter I, Feldman-Krane G. Silicone surfactants. In: Holmberg K, editor. Novel Surfactants. New York: Marcel Dekker; 2003.
[13] Barrett KEJ and Thomas HR. J Polym Sci Part A1. 1969;7:2627.
[14] Guyot A. Polymerizable surfactants. In: Holmberg K, editor. Novel Surfactants. New York: Marcel Dekker; 2003.
[15] Flory PJ. Statistical mechanics of chain molecules. New York: Interscience; 1969.
[16] Flory PJ. Principles of polymer chemistry. New York: Cornell University Press; 1953.
[17] Prigogine I, Trappeniers N, Mathos V. Discussions Faraday Soc. 1953;15:93.
[18] Eichinger BE, Flory PJ. Trans Faraday Soc. 1968;64:2035,2053,2061,2066.
[19] Flory PJ, Ellenson JL, Eichinger E. Macromolecules. 1968;1:279.
[20] Tadros T. Rheology of Dispersions. Weinheim: Wiley-VCH; 2010.
[21] Hildebrand JH. Solubility of non-electrolytes. Second edition. New York: Reinhold; 1936.
[22] Barton AFM. Handbook of solubility parameters and other cohesive parameters. New York: CRC Press; 1983.
[23] Hansen CM. J Paint Technol. 1967;39:505.

4 Adsorption of surfactants at the liquid/liquid interface

4.1 Introduction

Many chemicals are formulated as emulsions which require the use of surfactants (referred to as emulsifiers) for their preparation and stabilization against flocculation and coalescence. In order to understand the role of emulsifiers in the formation of emulsions and their stabilization, it is necessary to investigate the surfactant adsorption and conformation of the molecules at the liquid/liquid interface. Before discussing the process of surfactant adsorption, it is necessary to define the interfacial region between two immiscible liquids. This will form the first section in this chapter. After describing the interface one can then consider the process of surfactant adsorption. As will be shown below, there are generally two approaches for treating surfactant adsorption at the L/L interface. The first approach, adopted by Gibbs, treats adsorption as an equilibrium phenomenon whereby the second law of thermodynamics may be applied using surface quantities. The second approach, referred to as the equation of state approach, treats the surfactant film as a two-dimensional layer with a surface pressure π that may be related the surface excess Γ (amount of surfactant adsorbed per unit area). The Gibbs approach allows one to obtain the surface excess (abbreviated as Γ_2) from the variation of surface or interfacial tension with surfactant concentration. From Γ_2 one can obtain the area occupied by the surfactant molecule at the interface. This will provide information on the orientation of the molecules at the interface and hence information on the structure of the surfactant layer at the interface is obtained. This information is essential for understanding how surfactants can be used as emulsifiers and also for the long-term stability of the emulsion. The equation of state approach allows one to relate the surface pressure π (the difference between the interfacial tension of the clean interface with that when surfactant adsorption takes place) with the surface excess Γ_2. The effectiveness of surfactant adsorption at the liquid/liquid interface is estimated from measurements of the surface excess concentration at surface saturation, Γ_m. The efficiency of surfactant adsorption at the liquid/liquid interface can be determined by measuring the surfactant concentration that produces a given amount of adsorption at the interface. A convenient measure of the efficiency of adsorption is the negative logarithm of surfactant concentration C in bulk solution required to produce a 20 mN m^{-1} reduction in the interfacial tension γ. The adsorption from mixtures of two surfactants is also described in this chapter. These mixtures of two or more different types of surfactants often show a "synergistic" interaction. In other words, the interfacial properties of the mixture are more pronounced than those of the individual components themselves. These mixtures are widely used in many industrial applications such as in emulsification and emulsion stability. The adsorption of macromolecules at the liquid/liquid interface is described for homopolymers,

https://doi.org/10.1515/9783110587944-005

where segments will partition themselves between the two liquid phases in a manner which reflects the two segment–solvent interaction parameters. The last section in this chapter describes the methods of interfacial tension measurements. These methods may be classified into two categories: those in which the properties of the meniscus are measured at equilibrium, e.g. pendent drop or sessile drop profile and Wilhelmy plate methods, and those where the measurement is made under non-equilibrium or quasi-equilibrium conditions such as the drop volume (weight) or the du Noüy ring method.

4.2 The interface (Gibbs dividing line)

When two immiscible phases α and β (oil and water) come into contact, an interfacial region develops. The interfacial region is not a layer that is one molecule thick; it is a region with thickness δ with properties different from the two bulk phases α and β. In bringing phases α and β into contact, the interfacial regions of these phases undergo some changes, resulting in a concomitant change in the internal energy [1, 2]. If we were to move a probe from the interior of α to that of β, one would at some distance from the interface start to observe deviations in composition, in density, in structure; the closer to phase β, the larger the deviations until eventually the probe arrives in the homogeneous phase β. The thickness of the transition layer will depend on the nature of the interfaces and on other factors. Gibbs [2] considered the two phases α and β to have uniform thermodynamic properties up to the interfacial region. He assumed a mathematical plane Z^σ in the interfacial region in order to define the interfacial tension γ. A schematic representation of the interfacial region and the Gibbs mathematical plane is given in Fig. 4.1.

Using the Gibbs model, it is possible to obtain a definition of the interfacial tension γ. The surface free energy $\mathrm{d}G^\sigma$ is made up of three components: an entropy term, $S^\sigma\,\mathrm{d}T$; an interfacial energy term, $A\,\mathrm{d}\gamma$; a composition term $\sum n_i\,\mathrm{d}\mu_i$ (n_i is the number of moles of component i with chemical potential μ_i).

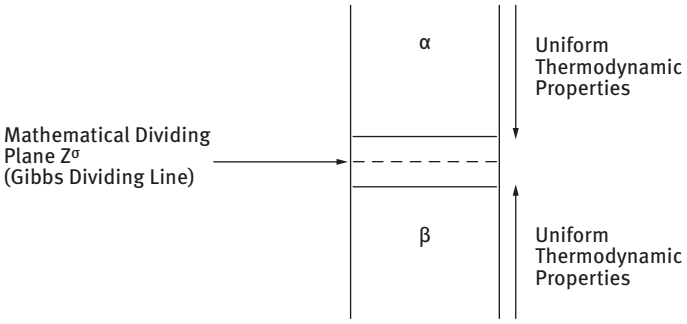

Fig. 4.1: The Gibbs dividing line.

The Gibbs–Deuhem equation is,

$$\mathrm{d}G^{\sigma} = -S^{\sigma}\,\mathrm{d}T + A\,\mathrm{d}\gamma + \sum n_i\,\mathrm{d}\mu_i. \tag{4.1}$$

At constant temperature and composition, $\mathrm{d}G^{\sigma} = A\,\mathrm{d}\gamma$,

$$\gamma = \left(\frac{\partial G^{\sigma}}{\partial A}\right)_{T,n_i} \tag{4.2}$$

For a stable interface γ is positive, i.e. if the interfacial area increases, G^{σ} increases. Note that γ is energy per unit area (mJ m^{-2}) which is dimensionally equivalent to force per unit length (mN m^{-1}), the unit usually used to define surface or interfacial tension.

For a curved interface, one should consider the effect of the radius of curvature. Fortunately, γ for a curved interface is estimated to be very close to that of a planer surface, unless the droplets are very small (< 10 nm).

Curved interfaces produce some other important physical phenomena which affect emulsion properties, e.g. the Laplace pressure Δp which is determined by the radii of curvature of the droplets,

$$\Delta p = \gamma\left(\frac{1}{r_1} + \frac{1}{r_2}\right), \tag{4.3}$$

where r_1 and r_2 are the two principal radii of curvature.

For a perfectly spherical droplet $r_1 = r_2 = r$ and

$$\Delta p = \frac{2\gamma}{r}. \tag{4.4}$$

For a hydrocarbon droplet with radius 100 nm, and $\gamma_{\mathrm{O/W}} = 50$ mN m^{-1}, $\Delta p \approx 10^6$ Pa (≈ 10 atm).

4.3 General treatment of surfactant adsorption

There are generally two approaches for treating surfactant adsorption at the L/L interface. The first approach, adopted by Gibbs, treats adsorption as an equilibrium phenomenon whereby the second law of thermodynamics may be applied using surface quantities. The second approach, referred to as the equation of state approach, treats the surfactant film as a two-dimensional layer with a surface pressure π that may be related to the surface excess Γ (amount of surfactant adsorbed per unit area). These two approaches are summarized below.

4.3.1 The Gibbs adsorption isotherm

Gibbs [2] derived a thermodynamic relationship between the surface or interfacial tension γ and the surface excess Γ (adsorption per unit area). The starting point of

this equation is the Gibbs–Deuhem equation given by equation (4.1). At equilibrium (where the rate of adsorption is equal to the rate of desorption), $dG^{\sigma} = 0$. At constant temperature, but in the presence of adsorption,

$$dG^{\sigma} = -S^{\sigma}\,dT + A\,d\gamma + \sum n_i\,d\mu_i \tag{4.5}$$

or

$$d\gamma = -\sum \frac{n_i^{\sigma}}{A}\,d\mu_i = -\sum \Gamma_i\,d\mu_i, \tag{4.6}$$

where $\Gamma_i = n_i^{\sigma}/A$ is the number of moles of component i and adsorbed per unit area.

Equation (4.6) is the general form for the Gibbs adsorption isotherm. The simplest case of this isotherm is a system of two components in which the solute (2) is the surface active component, i.e. it is adsorbed at the surface of the solvent (1). For such a case, equation (4.6) may be written as,

$$-d\gamma = \Gamma_1^{\sigma}\,d\mu_1 + \Gamma_2^{\sigma}\,d\mu_2 \tag{4.7}$$

and if the Gibbs dividing surface is used, $\Gamma_1 = 0$ and,

$$-d\gamma = \Gamma_{1,2}^{\sigma}\,d\mu_2, \tag{4.8}$$

where $\Gamma_{2,1}^{\sigma}$ is the relative adsorption of (2) with respect to (1). Since,

$$\mu_2 = \mu_2^0 + RT \ln a_2^{\mathrm{L}} \tag{4.9}$$

or

$$d\mu_2 = RT\,d\ln a_2^{\mathrm{L}}, \tag{4.10}$$

then,

$$-d\gamma = \Gamma_{2,1}^{\sigma} RT\,d\ln a_2^{\mathrm{L}} \tag{4.11}$$

or

$$\Gamma_{2,1}^{\sigma} = -\frac{1}{RT}\left(\frac{d\gamma}{d\ln a_2^{\mathrm{L}}}\right), \tag{4.12}$$

where a_2^{L} is the activity of the surfactant in bulk solution that is equal to $C_2 f_2$ or $x_2 f_2$, where C_2 is the concentration of the surfactant in mol dm^{-3} and x_2 is its mole fraction.

Equation (4.12) allows one to obtain the surface excess (abbreviated as Γ_2) from the variation of surface or interfacial tension with surfactant concentration. Note that $a_2 \approx C_2$ since in dilute solutions $f_2 \approx 1$. This approximation is valid since most surfactants have low cmc (usually less than 10^{-3} mol dm^{-3}) and adsorption is complete at or just below the cmc.

The surface excess Γ_2 can be calculated from the linear portion of the γ–log C_2 curves before the cmc. Such γ–log C curves are illustrated in Fig. 4.2 for the air/water and O/W interfaces. It can be seen that for the A/W interface γ decreases from the value for water (72 mN m^{-1} at 20 °C) reaching about 25–30 mN m^{-1} near the cmc. This

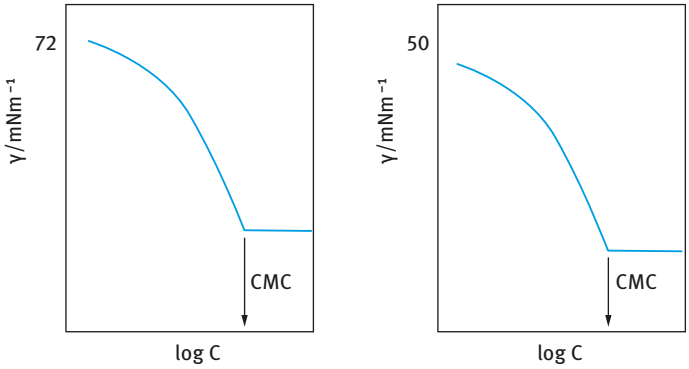

Fig. 4.2: Surface or interfacial tension–log C curves.

is clearly schematic since the actual values depend on the surfactant nature. For the O/W case, γ decreases from a value of about 50 mN m^{-1} (for a pure hydrocarbon–water interface) to ≈ 1–5 mN m^{-1} near the cmc (again depending on the nature of the surfactant).

As mentioned above, Γ_2 can be calculated from the slope of the linear position of the curves shown in Fig. 4.2 just before the cmc is reached. From Γ_2, the area per surfactant ion or molecule can be calculated since,

$$\text{area/molecule} = \frac{1}{\Gamma_2 N_{\text{av}}} \tag{4.13}$$

where N_{av} is Avogadro's constant. Determining the area per surfactant molecule is very useful since it gives information on surfactant orientation at the interface. For example, for ionic surfactants such as alkyl sulphates, the area per surfactant is determined by the area occupied by the alkyl chain and head group if these molecules lie flat at the interface. In this case the area per molecule increases with increasing alkyl chain length. For vertical orientation, the area per surfactant ion is determined by that occupied by the charged head group, which at low electrolyte concentration will be in the region of 0.40 nm^2. Such an area is larger than the geometrical area occupied by a sulphate group, as a result of the lateral repulsion between the head groups. On addition of electrolytes, this lateral repulsion is reduced and the area/surfactant ion for vertical orientation will be lower than 0.4 nm^2 (reaching in some cases 0.2 nm^2).

Another important point can be made from the γ–log C curves. At concentration just before the breakpoint, one has the condition of constant slope, which indicates that saturation adsorption has been reached.

$$\left(\frac{\gamma}{\ln a_2}\right)_{p,T} = \text{const.} \tag{4.14}$$

Just above the breakpoint,

$$\left(\frac{\gamma}{\ln a_2}\right)_{p,T} = 0, \tag{4.15}$$

indicating the constancy of γ with log C above the cmc. Integration of equation (4.15) gives,

$$\gamma = \text{const} \cdot \ln a_2 \tag{4.16}$$

Since γ is constant in this region, then a_2 must remain constant. This means that addition of surfactant molecules above the cmc must result in association to form units (micellar) with low activity.

The hydrophilic head group may be unionized, e.g. alcohols or poly(ethylene oxide) alkane or alkyl phenol compounds, weakly ionized such as carboxylic acids or strongly ionized such as sulphates, sulphonates and quaternary ammonium salts. The adsorption of these different surfactants at the air/water and oil/water interface depends on the nature of the head group. With nonionic surfactants, repulsion between the head groups is small and these surfactants are usually strongly adsorbed at the surface of water from very dilute solutions. Nonionic surfactants have much lower cmc values when compared with ionic surfactants with the same alkyl chain length. Typically, the cmc is in the region of 10^{-5}–10^{-4} mol dm^{-3}. Such nonionic surfactants form closely packed adsorbed layers at concentrations lower than their cmc values. The activity coefficient of such surfactants is close to unity and is only slightly affected by addition of moderate amounts of electrolytes (or changes in the pH of the solution). Thus, nonionic surfactant adsorption is the simplest case since the solutions can be represented by a two-component system and the adsorption can be accurately calculated using equation (4.12).

With ionic surfactants, on the other hand, the adsorption process is relatively more complicated since one has to consider the repulsion between the head groups and the effect of the presence of any indifferent electrolyte. Moreover, the Gibbs adsorption equation has to be solved taking into account the surfactant ions, the counterion and any indifferent electrolyte ions present. For a strong surfactant electrolyte such as an Na^+R^-

$$\Gamma_2 = \frac{1}{2RT} \frac{\partial \gamma}{\partial \ln a_\pm}. \tag{4.17}$$

The factor of 2 in equation (4.17) arises because both surfactant ion and counterion must be adsorbed to maintain neutrally, and dγ/d ln $a_\pm$ is twice as large as for an unionized surfactant.

If a nonadsorbed electrolyte, such as NaCl, is present in large excess, then any increase in concentration of Na^+R^- produces a negligible increase in Na^+ ion concentration and therefore dμ_{Na} becomes negligible. Moreover, dμ_{Cl} is also negligible, so that the Gibbs adsorption equation reduces to,

$$\Gamma_2 = -\frac{1}{RT}\left(\frac{\partial \gamma}{\partial \ln C_{NaR}}\right), \tag{4.18}$$

i.e. it becomes identical to that for a nonionic surfactant.

The above discussion clearly illustrates that for calculatining Γ_2 from the γ–log C curve one has to consider the nature of the surfactant and the composition of the

medium. For nonionic surfactants the Gibbs adsorption equation (4.9) can be directly used. For ionic surfactants, in the absence of electrolytes the right-hand side of the equation (4.9) should be divided by 2 to account for surfactant dissociation. This factor disappears in the presence of a high concentration of an indifferent electrolyte.

4.3.2 Equation of state approach

In this approach, one relates the surface pressure π with the surface excess Γ_2. The surface pressure is defined by the equation [3–5],

$$\pi = \gamma_0 - \gamma, \tag{4.19}$$

where γ_0 is the surface or interfacial tension before adsorption and γ that after adsorption.

For an ideal surface film, behaving as a two dimensional gas the surface pressure π is related to the surface excess Γ_2 by the equation,

$$\pi A = n_2 RT \tag{4.20}$$

or

$$\pi = (n_2/A)RT = \Gamma_2 RT. \tag{4.21}$$

Differentiating equation (4.21) at constant temperature,

$$\mathrm{d}\pi = RT\,\mathrm{d}\Gamma_2. \tag{4.22}$$

Using the Gibbs equation,

$$\mathrm{d}\pi = -\mathrm{d}\gamma = \Gamma_2 RT\,\mathrm{d}\ln a_2 \approx \Gamma_2 RT\,\mathrm{d}\ln C_2. \tag{4.23}$$

Combining equations (4.22) and (4.23)

$$\mathrm{d}\ln\Gamma_2 = \mathrm{d}\ln C_2 \tag{4.24}$$

or

$$\Gamma_2 = KC_2^{\alpha} \tag{4.25}$$

Equation (4.25) is referred to as the Henry's law isotherm which predicts a linear relationship between Γ_2 and C_2.

It is clear that equations (4.19) and (4.22) are based on an idealized model in which the lateral interaction between the molecules has not been considered. Moreover, in this model the molecules are considered to be dimensionless. This model can only be applied at very low surface coverage where the surfactant molecules are so far apart that lateral interaction may be neglected. Moreover, under these conditions the total area occupied by the surfactant molecules is relatively small compared to the total interfacial area.

At significant surface coverage, the above equations have to be modified to take into account both lateral interaction between the molecules as well as the area occupied by them. Lateral interaction may reduce π if there is attraction between the chains (e.g. with most nonionic surfactants) or it may increase π as a result of repulsion between the head groups in the case of ionic surfactants.

Various equations of state have been proposed, taking into account the above two effects, in order to fit the π–A data. The two-dimensional van der Waals equation of state is probably the most convenient for fitting these adsorption isotherms, i.e.,

$$(\pi)(A - n_2 A_2^0) = n_2 RT, \tag{4.26}$$

where A_2^0 is the excluded area or co-area of type 2 molecule in the interface and α is a parameter which allows for lateral interaction.

Equation (4.26) leads to the following theoretical adsorption isotherm, using the Gibbs equation,

$$C_2^{\alpha} = K_1\left(\frac{\theta}{1-\theta}\right)\exp\left(\frac{\theta}{1-\theta} - \frac{2\alpha\theta}{a_2^0 RT}\right), \tag{4.27}$$

where θ is the surface coverage ($\theta = \Gamma_2/\Gamma_{2,\max}$), K_1 is a constant that is related to the free energy of adsorption of surfactant molecules at the interface ($K_1 \propto \exp(-\Delta G_{\text{ads}}/kT)$) and a_2^0 is the area/molecule.

For a charged surfactant layer, equation (4.27) has to be modified to take into account the electrical contribution from the ionic head groups, i.e.,

$$C_2^{\alpha} = K_1\left(\frac{\theta}{1-\theta}\right)\exp\left(\frac{\theta}{1-\theta}\right)\exp\left(\frac{e\Psi_0}{kT}\right), \tag{4.28}$$

where Ψ_0 is the surface potential. Equation (4.28) shows how the electrical potential energy (Ψ_0/kT) of adsorbed surfactant ions affects the surface excess. Assuming that the bulk concentration remains constant, then Ψ_0 increases as θ increases. This means that $[\theta/(1-\theta)]\exp[\theta/(1-\theta)]$ increases less rapidly with C_2, i.e. adsorption is inhibited as a result of ionization.

4.3.3 The Langmuir, Szyszkowski and Frumkin equations

In addition to the Gibbs equation, three other equations have been suggested that relate the surface excess Γ_1, surface or interfacial tension, and equilibrium concentration in the liquid phase C_1. The Langmuir equation [6] relates Γ_1 to C_1 by,

$$\Gamma_1 = \frac{\Gamma_{\text{m}} C_1}{C_1 + a}, \tag{4.29}$$

where Γ_{m} is the saturation adsorption at monolayer coverage by surfactant molecules and a is a constant that is related to the free energy of adsorption ΔG_{ads}^0,

$$a = 55.3\exp\left(\frac{\Delta G_{\text{ads}}^0}{RT}\right), \tag{4.30}$$

where R is the gas constant and T is the absolute temperature.

A linear form of the Gibbs equation is,

$$\frac{1}{\Gamma_1} = \frac{1}{\Gamma_m} + \frac{a}{\Gamma_m C_1}. \tag{4.31}$$

Equation (4.31) shows that a plot of $1/\Gamma_1$ versus $1/C_1$ gives a straight line from which Γ_m and a can be calculated from the intercept and slope of the line.

The Szyszkowski [7] equation gives a relationship between the surface pressure π and bulk surfactant concentration C_1; it is a form of equation of state,

$$\gamma_0 - \gamma = \pi = 2.303RT\Gamma_m \log\left(\frac{C_1}{a} + 1\right). \tag{4.32}$$

The Frumkin equation [8] is another equation of state,

$$\gamma_0 - \gamma = \pi = -2.303RT\Gamma_m \log\left(1 - \frac{\Gamma_1}{\Gamma_m}\right). \tag{4.33}$$

4.3.4 Effectiveness of surfactant adsorption at the liquid/liquid interface

The surface excess concentration at surface saturation, Γ_m, is a useful measure of the effectiveness of the surfactant at the liquid/liquid interface [9]. This is an important factor in determining properties of the surfactant in several processes such as emulsification and emulsion stability. In most cases, a tightly packed, coherent film obtained by vertically oriented surfactant molecules is required. The area occupied by a surfactant molecule consisting of a linear alkyl chain and one hydrophilic group, either ionic or nonionic, is larger than the cross-sectional area of an aliphatic chain (which is $0.2\,nm^2$) indicating that the area occupied by a surfactant molecule is determined by the area occupied by the hydrated hydrophilic chain. For example, for a series of alkyl sulphates the area occupied by the surfactant molecule is in the region of $0.5\,nm^2$, which is the cross-sectional area of a sulphate group. As mentioned before, addition of electrolytes reduces the area occupied by the surfactant molecule due to charge screening of the sulphate group. With nonionic surfactants based on a polyethylene oxide (PEO) hydrophilic group, the amount of adsorption at saturation Γ_m decreases with increasing PEO chain length and this results in an increase in the area occupied by a singly surfactant molecule.

4.3.5 Efficiency of adsorption of surfactant at the liquid/liquid interface

The efficiency of surfactant adsorption at the liquid/liquid interface can be determined by measuring the surfactant concentration that produces a given amount of adsorption at the interface [9]. This can also be related to the free energy change involved in the adsorption. A convenient measure of the efficiency of adsorption is the negative logarithm of surfactant concentration C in bulk solution required to produce a

20 mN m^{-1} reduction in the interfacial tension γ,

$$-\log C_{(-\Delta\gamma=20)} \equiv pC_{20} \tag{4.34}$$

Observation of various γ–log C results for various surfactants at the oil/water interface shows that when γ is reduced by 20 mN m^{-1}, the surface excess concentration Γ_1 is close to its saturation value Γ_m. This is confirmed by the use of the Frumkin equation (4.33). For many surfactant systems Γ_m is in the range 1–4.4 × 10^{-6} mol m^{-2}. Solving for Γ_1 in the Frumkin equation when $\pi = \gamma_0 - \gamma = 20$ mN m^{-1}, $\Gamma_m = 1\text{–}4.4 \times 10^{-6}$ mol m^{-2}, $\Gamma_1 = 0.84\text{–}0.99\Gamma_m$ at 25 °C, indicating that when γ is reduced by 20 mN m^{-1}, the surface concentration is 84–99 % saturated.

pC_{20} can be related to the free energy change on adsorption at infinite dilution ΔG^0 by application of the Langmuir [6] and Szyszkowski [7] equations (4.29) and (4.32). As mentioned above, for $\pi = 20$ mN m^{-1}, $\Gamma_1 = 0.84\text{–}0.99\Gamma_m$. From the Langmuir equation $C_1 = 5.2\text{–}999a$. Thus,

$$\log\left[\left(\frac{C_1}{a}\right) + 1\right] \approx \log\left(\frac{C_1}{a}\right). \tag{4.35}$$

The Szyszkowski equation becomes,

$$\pi = \gamma_0 - \gamma = -2.303RT\Gamma_m \log\left(\frac{C_1}{a}\right) \tag{4.36}$$

and,

$$\log\left(\frac{1}{C_1}\right)_{\pi=20} = -\left(\log a + \frac{\gamma_0 - \gamma}{2.303RT\Gamma_m}\right). \tag{4.37}$$

Since,

$$a = 55 \exp\left(\frac{\Delta G^0}{RT}\right), \tag{4.38}$$

$$\log a = 1.74 + \frac{\Delta G^0}{2.303RT}, \tag{4.39}$$

$$\log\left(\frac{1}{C_1}\right)_{\pi=20} \equiv pC_{20} \equiv -\left(\frac{\Delta G^0}{2.303RT} + 1.74 + \frac{20}{2.303RT\,\Gamma_m}\right). \tag{4.40}$$

For a straight chain surfactant molecule consisting of m –CH_2– groups and one hydrophilic head group (h), ΔG^0 can be broken down into the standard free energy associated with the transfer of the terminal CH_3, the –CH_2– groups of the hydrocarbon chain and the hydrophilic group h from the interior of the liquid phase to the interface at $\pi = 20$ mN m^{-1}

$$\Delta G^0 = m\Delta G^0(-CH_2-) + \Delta G^0(h) + \text{const.} \tag{4.41}$$

For a homologous series of surfactants with the same hydrophilic group h, the value of Γ_m and the area per surfactant molecule does not change much with an increase in the number of C atoms and $\Delta G^0(h)$ can be considered constant. In this case, pC_{20} can be related to the free energy change per –CH_2– group by,

$$pC_{20} = \left[\frac{-\Delta G^0(-CH_2-)}{2.303RT}\right]m + \text{const.} \tag{4.42}$$

Equation (4.42) shows that pC_{20} is a linear function of the number of C atoms in the surfactant chain m. The larger the value of pC_{20}, the more efficiently the surfactant is adsorbed at the interface and the more efficiently it reduces the interfacial tension.

The efficiency of surfactant adsorption at the liquid/liquid interface as measured by pC_{20} increases with an increasing number of C atoms in the surfactant. Straight alkyl chains are generally more efficient than branched ones with the same C number. A single hydrophilic group at the end of the hydrophobic chain gives more efficient adsorption than that where the hydrophilic group is located at the centre of the chain. Nonionic and zwitterionic surfactants generally give more efficient adsorption compared to ionic ones. With ionic surfactants, increasing the ionic strength of the aqueous solution increases the efficiency of surfactant adsorption.

4.3.6 Adsorption from mixtures of two surfactants

Mixtures of two or more different types of surfactants often show a "synergistic" interaction [10, 11]. In other words, the interfacial properties of the mixture are more pronounced than those of the individual components themselves. These mixtures are widely used in many industrial applications such as in emulsification and emulsion stability. A study of the adsorption of the individual components in the mixture and the interaction between them allows one to understand the role played by each component. This also enables one to make the right selection of surfactant mixtures for specific application.

The Gibbs adsorption equation (4.8) for two surfactants in dilute solution can be written as,

$$d\gamma = RT(\Gamma_1 \, d\ln a_1 + \Gamma_2 RT \, d\ln a_2), \tag{4.43}$$

where Γ_1 and Γ_2 are the surface excess concentrations of the two surfactants at the interface and a_1 and a_2 are their respective activities in solution. Since the solutions are dilute a_1 and a_2 can be replaced by the molar concentrations C_1 and C_2.

Using equation (4.9),

$$\Gamma_1 = \frac{1}{RT}\left(-\frac{\partial\gamma}{\partial \ln C_1}\right)_{C_2} = \frac{1}{2.303RT}\left(-\frac{\partial\gamma}{\partial \log C_1}\right)_{C_2}, \tag{4.44}$$

$$\Gamma_2 = \frac{1}{RT}\left(-\frac{\partial\gamma}{\partial \ln C_2}\right)_{C_1} = \frac{1}{2.303RT}\left(-\frac{\partial\gamma}{\partial \log C2}\right)_{C_1}. \tag{4.45}$$

Therefore, the concentration of each surfactant at the interface can be calculated from the slope of the γ–log C plot of each surfactant, holding the solution concentration of the second surfactant constant.

For ideal mixing of two surfactants (with no net interaction), C_1 and C_2 are given by the expressions [12],

$$C_1 = C_1^0 f_1 X_1 \tag{4.46}$$

$$C_2 = C_2^0 f_2 X_2 \tag{4.47}$$

where f_1 and f_2 are the activity coefficients of surfactant 1 and 2 respectively, X_1 is the mole fraction of surfactant 1 at the interface, i.e. $X_1 = 1 - X_2$, C_1^0 is the molar concentration required to attain a given interfacial tension in a solution of pure surfactant 1 and C_2^0 is the molar concentration required to attain a given interfacial tension in a solution of pure surfactant 2.

For non-ideal mixing, i.e. when there is interaction between the surfactant molecules, the activity coefficient has to include the interaction parameter β^σ,

$$\ln f_1 = \beta^\sigma (1 - X_1)^2 \tag{4.48}$$

$$\ln f_2 = \beta^\sigma (X_1)^2 \tag{4.49}$$

Combining equations (4.48)–(4.49),

$$\frac{(X_1)^2 \ln\left[\frac{C_1}{C_1^0 X_1}\right]}{(1 - X_1)^2 \ln\left[\frac{C_2}{C_2^0 (1 - X_1)}\right]} = 1. \tag{4.50}$$

The interfacial tension–total surfactant concentration (C_t) curves for two pure surfactants and their mixture at a fixed value α, the mole fraction of surfactant 1 in the total surfactant in the solution phase, are used (Fig. 4.3) to determine C_1 (= αC_{12}), C_1^0, C_2 [= $(1 - \alpha)C_{12}$] and C_2^0, the molar concentration at the same surface tension. Equation (4.50) permits it to be solved iteratively for X_1 and X_2 (= $1 - X_1$). The ratio of surfactant 1 to surfactant 2 at the interface at that particular value of α is then X_1/X_2.

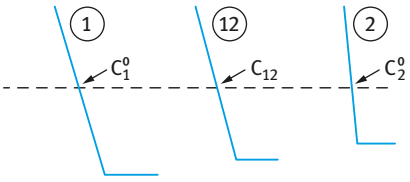

Fig. 4.3: Evaluation of X_1 and X_2. (1) Pure surfactant 1. (2) Pure surfactant 2. (12) Mixture of 1 and 2 at a fixed value of α.

4.3.7 Adsorption of Macromolecules

Most theories and experimental results on the adsorption of macromolecules have been devoted to the solid/liquid interface. At such an interface, the polymer is generally thought to adsorb in a loop-train type of conformation, with the tails at the end of the molecule [13]. Segments in trains are in contact with the solid surface, while

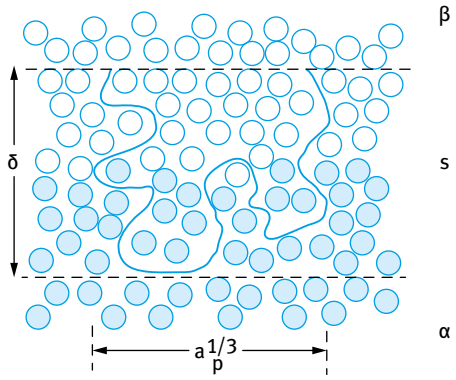

Fig. 4.4: Typical conformation of a homopolymer chain at a liquid/liquid interface (α/β).

those in loops or tails are immersed in the liquid phase. At a liquid/liquid interface, segments of a given homopolymer will partition themselves between the two liquid phases, in a manner which reflects the two segment–solvent interaction parameters ε_{13} and ε_{23} (where 1 and 2 refer to the two liquids and 3 to the polymer segments). A typical situation for an adsorbed homopolymer is illustrated in Fig. 4.4.

The time-average conformation adopted will be governed by the net energy-entropy balance for the polymer at the interface. The interfacial region with thickness δ is the region depicted by s in Fig. 4.4. There are two major distinctions to be made comparing the adsorption of macromolecules with that of small molecules. First, we have to distinguish between the adsorption of the whole molecule $\Gamma_{\mathrm{p}}^{\mathrm{s}}$ and that of segments (designated 3) Γ_{3}^{s}. Second, because the adsorption of macromolecules is irreversible [13], one cannot apply the second law of thermodynamics discussed above.

$\Gamma_{\mathrm{p}}^{\mathrm{s}}$ is related to the concentration of polymer in the two phases C_{p}^{α} and C_{p}^{β} by,

$$\Gamma_{\mathrm{p}}^{\mathrm{s}} = \frac{n_{\mathrm{p}}^{\mathrm{s}}}{\Delta A} = \frac{n_{\mathrm{p}} - (C_{\mathrm{p}}^{\alpha} V^{\alpha} + C_{\mathrm{p}}^{\beta} V^{\beta})}{\Delta A}. \tag{4.51}$$

The effective area per polymer molecule a_{p} is simply given by,

$$a_{\mathrm{p}} = \frac{1}{\Gamma_{\mathrm{p}}^{\mathrm{s}}}. \tag{4.52}$$

Determining $\Gamma_{\mathrm{p}}^{\mathrm{s}}$ as a function of C_{p}^{α} or C_{p}^{β} is one of the major considerations in any study of polymer adsorption at the liquid/liquid interface. Establishing polymer adsorption isotherms is more complex for the liquid/liquid interface than the solid/liquid interface. In the first place both the equilibrium values C_{p}^{α} and C_{p}^{β} are required and in the second place ΔA has to be known. If an emulsion is used to achieve a high value of ΔA, the latter is only determined after the emulsion has been formed in the presence of polymer. This means that one can effectively determine $\Gamma_{\mathrm{p}}^{\mathrm{s}}$ at maximum coverage concentration. Establishing the low coverage value can only be carried out using a planar liquid/liquid interface.

When using block copolymers of the A–B or A–B–A types and graft copolymers of the BA_n type (where B is the hydrophobic chain and A is the hydrophilic chain) then in an O/W emulsion the lipophilic B chain will reside in the oil phase whereas the hydrophilic A chain(s) will reside in the aqueous phase. In this case one needs to know the interaction between the B chain and the oil and the interaction between the A chain(s) and the aqueous phase. A useful method is to apply the solubility parameter concept as has been discussed in Chapter 3.

4.4 Interfacial tension measurements

These methods may be classified into two categories: those in which the properties of the meniscus are measured at equilibrium, e.g. pendent drop or sessile drop profile and Wilhelmy plate methods, and those where the measurement is made under non-equilibrium or quasi-equilibrium conditions such as the drop volume (weight) or the du Noüy ring method. The latter methods are faster, although they suffer from the disadvantage of premature rupture and expansion of the interface, causing adsorption depletion. They are also inconvenient for measuring the interfacial tension in the presence of macromolecular species, where adsorption is slow. This problem is overcome in the equilibrium (static) methods. For measuring low interfacial tensions ($< 0.1\,mN\,m^{-1}$), the spinning drop technique is applied. A brief description of each of these techniques is given below.

4.4.1 The Wilhelmy plate method

In this method [14] a thin plate made from glass (e.g. a microscope cover slide) or platinum foil is either detached from the interface (non-equilibrium condition) or its weight is measured statically using an accurate microbalance. In the detachment method, the total force F is given by the weight W of the plate and the interfacial tension force,

$$F = W + \gamma p, \tag{4.53}$$

where p is the "contact length" of the plate with the liquid, i.e. the plate perimeter. Provided the contact angle of the liquid is zero, no correction is required for equation (4.53). Thus, the Wilhelmy plate method can be applied in the same manner as the du Noüy technique that is described below.

The static technique may be applied for following the interfacial tension as a function of time (to follow the kinetics of adsorption) until equilibrium is reached. In this case, the plate (that is roughened to ensure a zero contact angle) is suspended from one arm of a microbalance and allowed to penetrate the upper liquid layer (usually the oil) into the aqueous phase to ensure wetting of the plate. The whole vessel is then lowered to bring the plate into the oil phase. At this point the microbalance is adjusted

to counteract the weight of the plate (i.e. its weight now becomes zero). The vessel is then raised until the plate touches the interface. The increase in weight ΔW is given by the following equation,

$$\Delta W = \gamma p \cos\theta, \tag{4.54}$$

where θ is the contact angle. If the plate is completely wetted by the lower liquid as it penetrates, $\theta = 0$ and γ may be calculated directly from ΔW. Care should always be taken that the plate is completely wetted by the aqueous solution. For that purpose, a roughened platinum or glass plate is used to ensure a zero contact angle. However, if the oil is denser than water, a hydrophobic plate is used so that when the plate penetrates through the upper aqueous layer and touches the interface it is completely wetted by the oil phase.

4.4.2 The pendent drop method

If a drop of oil is allowed to hang from the end of a capillary that is immersed in the aqueous phase, it will adopt an equilibrium profile shown in Fig. 4.5 that is a unique function of the tube radius, the interfacial tension, its density and the gravitational field.

The shape of the bounded menisci (those with only one solid surface supporting the liquid forming the meniscus, as is the case with the pendent drop) can be described by a single parameter β, derived by Bashforth and Adams [15],

$$\beta = \frac{\Delta\rho g b^2}{\gamma}, \tag{4.55}$$

where $\Delta\rho$ is the density difference between the two phases, g is the gravity force and b is the radius of a drop at its apex.

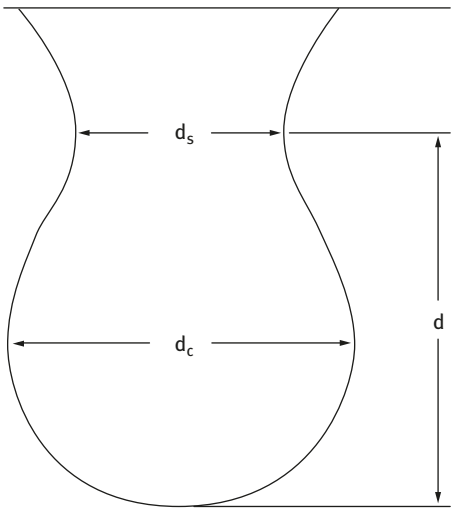

Fig. 4.5: Schematic representation of the profile of a pendent drop.

Andreas et al. [16] suggested that the most conveniently measurable shape-dependent quantity is S,

$$S = \frac{d_s}{d_e}, \tag{4.56}$$

where d_e is the equatorial diameter and d_s is the diameter measured at a distance d from the bottom of the drop. The difficulty in measuring b is overcome by combining it with β and defining a new quantity H, given by,

$$H = -\beta\left(\frac{d_e}{b}\right)^2. \tag{4.57}$$

The interfacial tension is given by the following equation,

$$\gamma = \frac{\Delta\rho g d_e^2}{H}. \tag{4.58}$$

The relationship between H and the experimental values of d_s/d_e has been obtained empirically using pendent drops of water. Accurate values of H have been obtained by Niederhauser and Bartell [17].

The pendent drop technique is used for accurate measurements of interfacial tension (±0.1 %), in particular with the development of image analysis methods for obtaining the drop shape. The technique can be applied following the kinetics of surfactant adsorption and in particular for the slow process of macromolecular adsorption.

4.4.3 Sessile drop method

This is similar to the pendent drop method except in this case a drop of the liquid with the higher density is placed on a flat plate immersed in the second liquid, as schematically shown in Fig. 4.6.

The interfacial tension γ is calculated by,

$$\gamma = \frac{\Delta\rho g b^2}{\beta}. \tag{4.59}$$

While β is difficult to determine, the Bashforth–Adam tables [15] give x_e/b as a function of β, where x_e is the equatorial radius, so that equation (4.59) may be written in the form,

$$\gamma = \Delta\rho \frac{g x_e^2}{[f(\beta)]^2} \tag{4.60}$$

with $f(\beta) = x_e/b$.

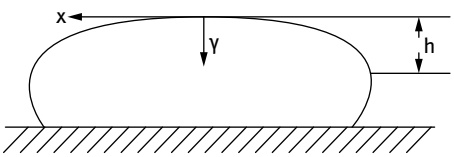

Fig. 4.6: Schematic representation of a sessile drop.

Since x_e can be determined accurately, the experimental problem reduces to the determination of β. This is achieved by comparing the drop profile to a theoretical set of profiles, for various values of β as given by the tables.

The sessile drop method has the same accuracy (±0.1 %) as the pendent drop technique and it allows one to measure the interfacial tension as a function of time (i.e. measuring the kinetics of surfactant adsorption).

4.4.4 The du Noüy ring method

Basically one measures the force required to detach a ring or loop of wire with radius R from the liquid/liquid interface [18]. As a first approximation, the detachment force is taken to be equal to the interfacial tension γ multiplied by the perimeter of the ring. The total force F in detaching the ring from the interface is the sum of its weight W and the interfacial force,

$$F = W + 4\pi R\gamma \tag{4.61}$$

Harkins and Jordan [19] introduced a correction factor f (that is a function of meniscus volume V and radius r of the wire) for a more accurate calculation of γ from F, i.e.,

$$f = \frac{\gamma}{\gamma_{\text{ideal}}} = f\left(\frac{R^3}{V}, \frac{R}{r}\right). \tag{4.62}$$

Values of the correction factor f were tabulated by Harkins and Jordan [20]. Some theoretical account of f was given by Freud and Freud [20].

When using the du Nuoy method for measuring γ one must be sure that the ring is kept horizontal during the measurement. Moreover, the ring should be free from any contaminant and this is usually achieved by using a platinum ring that is flamed before use.

4.4.5 The drop volume (weight) method

Here one determines the volume V (or weight W) of a drop of liquid (immersed in the second less dense liquid) which becomes detached from a vertically mounted capillary tip having a circular cross section of radius r. The ideal drop weight W_{ideal} is given by the expression,

$$W_{\text{ideal}} = 2\pi r\gamma. \tag{4.63}$$

In practice, a weight W is obtained which is less than W_{ideal} because a portion of the drop remains attached to the tube tip. Thus, equation (4.63) should include a correction factor ϕ, that is a function of the tube radius r and some linear dimension of the drop, i.e., $V^{1/3}$. Thus,

$$W = 2\pi r\gamma\phi\left(\frac{r}{V^{1/3}}\right). \tag{4.64}$$

Values of $(r/V^{1/3})$ have been tabulated by Harkins and Brown [21]. Lando and Oakley [22] used a quadratic equation to fit the correction function to $(r/V^{1/3})$. A better fit was provided by Wilkinson and Kidwell [23].

4.4.6 The spinning drop method

This method is particularly useful for measuring very low interfacial tensions ($< 10^{-1}$ mN m^{-1}) which are particularly important in applications such as spontaneous emulsification and the formation of microemulsions. Such low interfacial tensions may also be reached with emulsions particularly when mixed surfactant films are used. A drop of the less dense liquid A is suspended in a tube containing the second liquid B. On rotating the whole mass (Fig. 4.7) the drop of the liquid moves to the centre. With increasing speed of revolution, the drop elongates as the centrifugal force opposes the interfacial tension force that tends to maintain the spherical shape, i.e. that having minimum surface area.

An equilibrium shape is reached at any given speed of rotation. At moderate speeds of rotation, the drop approximates to a prolate ellipsoid, whereas at very high speeds of revolution, the drop approximates to an elongated cylinder. This is schematically shown in Fig. 4.7.

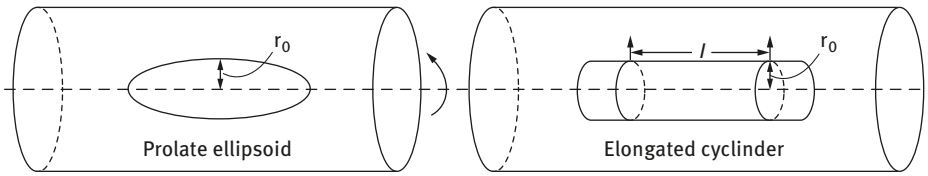

Fig. 4.7: Schematic representation of a spinning drop: (a) prolate ellipsoid; (b) elongated cylinder.

When the shape of the drop approximates a cylinder (Fig. 4.7 (b)), the interfacial tension is given by the following expression [24],

$$\gamma = \frac{\omega_2 \Delta\rho r_0^4}{4}, \tag{4.65}$$

where ω is the speed of rotation, $\Delta\rho$ is the density difference between the two liquids A and B and r_0 is the radius of the elongated cylinder. Equation (4.65) is valid when the length of the elongated cylinder is much larger than r_0.

References

[1] Guggenheim EA. Thermodynamics. 5th Edition. Amsterdam: North Holland; 1967. p. 45.
[2] Gibbs JW. Collected works. Vol. 1. New York: Longman; 1928. p. 219.
[3] Aveyard R, Briscoe BJ. Trans Faraday Soc. 1970;66:2911.
[4] Aveyard R, Briscoe BJ, Chapman J. Trans Faraday Soc. 1972;68:10.
[5] Aveyard R, Chapman J. Can J Chem. 1975;53:916.
[6] Langmuir I. J Amer Chem Soc. 1917;39:1848 .
[7] Szyszkowski B. Z Phys Chem. 1908;64:385.
[8] Frumkin A. Z Phys Chem. 1925;116:466.
[9] Rosen MJ, Kunjappu JT. Surfactants and interfacial phenomena. New Jersey: John Wiley and Sons; 2012.
[10] de Lisi R, Inglese A, Milioto S, Pellento A. Langmuir. 1997;13:192.
[11] Nakano TY, Sugihara G, Nakashima T, Yu SC. Langmuir. 2002;18:8777.
[12] Rosen MJ, Hua XY. J Colloid Interface Sci. 1982;86:164.
[13] Fleer GJ, Cohen-Stuart MA, Scheutjens JMHM, Cosgrove T, Vincent B. Polymers at interfaces. London: Chapman and Hall; 1993.
[14] Wilhelmy L. Ann Phys. 1863;119:177.
[15] Bashforth F, Adams JC. An attempt to test the theories of capillary action. Cambridge: University Press; 1883.
[16] Andreas JM, Hauser EA, Tucker WB. J Phys Chem. 1938;42:1001.
[17] Nierderhauser DO, Bartell FE. Report of progress, fundamental research on occurrence of petroleum. Publication of the American Petroleum Institute. Baltimore: Lord Baltimore Press; 1950. p. 114.
[18] Du Nouy PL. J Gen Physiol. 1919;1:521.
[19] Harkins WD, Jordan HF. J Amer Chem Soc. 1930;52:1715.
[20] Freud BB, Freud HZ. J Amer Chem Soc. 1930;52:1772.
[21] Harkins WD, Brown FE. J Amer Chem Soc. 1919;41:499.
[22] Lando JL, Oakley HT. J Colloid Interface Sci. 1967;25:526.
[23] Wilkinson MC, Kidwell RL. J Colloid Interface Sci. 1971;35:114.
[24] Vonnegut B. New Sci Intrum. 1942;13:6.

5 Surfactant adsorption at the solid/liquid interface

5.1 Introduction

Many formulations of the solid/liquid type (suspensions) are stabilized against flocculation by surfactants of the ionic or nonionic type [1, 2]. In order to understand how these surfactants act as stabilizers, it is necessary to investigate their adsorption and conformation at the solid/liquid interface. The solid particles can be hydrophobic, such as many drugs and agrochemicals, or hydrophilic, such as silica or alumina. It is also necessary to know how the surfactant adsorption is influenced by the formulation conditions, such as increase or decrease in temperature, addition of electrolytes and non-electrolytes to the formulation, etc. Surfactants consist of a small number of units and they mostly are reversibly adsorbed, allowing one to apply thermodynamic treatments. In this case, it is possible to describe the adsorption in terms of the various interaction parameters, namely chain-surface, chain-solvent and surface-solvent. Moreover, the conformation of the surfactant molecules at the interface can be deduced from these simple interactions parameters. However, in some cases these interaction parameters may involve ill-defined forces, such as hydrophobic bonding, solvation forces and chemisorption. In addition, the adsorption of ionic surfactants involves electrostatic forces particularly with polar surfaces containing ionogenic groups. For that reason, the adsorption of ionic and nonionic surfactants will be treated separately. As mentioned before, the surfaces (substrates) can be also hydrophobic or hydrophilic and these may be treated separately. Thus, four cases can be considered:

(i) adsorption of ionic surfactants on hydrophobic (nonpolar) surfaces;
(ii) adsorption of ionic surfactants on polar (charged) surfaces;
(iii) adsorption of nonionic surfactants on hydrophobic surfaces;
(iv) adsorption of nonionic surfactants on polar surfaces.

Cases (i) and (iii) are governed by hydrophobic interaction between the alkyl chain and hydrophobic surface; the charge plays a minor role. In this case the adsorption amount (mg m^{-2}) increases with increasing chain length of the alkyl chain of the surfactant (in accordance with Traube's rule). Cases (ii) and (iv) are determined by charge and/or polar interaction and these may involve specific structures that are produced at the interface.

At the solid/liquid interface one is interested in determining the following parameters:

(i) the amount of surfactant adsorbed Γ per unit mass or unit area of the solid adsorbent at a given temperature;

https://doi.org/10.1515/9783110587944-006

(ii) the equilibrium concentration of the surfactant C (mol dm^{-3} or mole fraction $x = C/55.51$) in the liquid phase required to produce a given value of Γ at a given temperature;
(iii) the surfactant concentration at full saturation of the adsorbent Γ_{sat};
(iv) the orientation of the adsorbed surfactant ion or molecule that can be obtained from the area occupied by the ion or molecule at full saturation;
(v) the effect of adsorption on the properties of the adsorbent (nonpolar, polar or charged).

The general equation for calculating the amount of surfactant adsorbed onto a solid adsorbent from a binary solution containing two components (surfactant component 1 and solvent component 2) is given by [3],

$$\frac{n_0 \Delta x_1}{m} = n_1^s x_2 - n_2^s x_1. \tag{5.1}$$

n_0 is the number of moles of solution before adsorption, $\Delta x_1 = x_{1,0} - x_1$, $x_{1,0}$ is the mole fraction of component 1 before adsorption, x_1 and x_2 are the mole fractions of components 1 and 2 at adsorption equilibrium, m is the mass of adsorbent in grams, n_1^s and n_2^s are the number of components 1 and 2 adsorbed per gram of adsorbent at adsorption equilibrium.

When the liquid phase is a dilute solution of surfactant (component 1) that is much more strongly adsorbed onto the solid substrate than the solvent (component 2), then $n_0 \Delta x_1 = \Delta n_1$ where Δn_1 is the change in number of moles of component 1 in solution, $n_2^s \approx 0$ and $x_2 \approx 1$. In this case equation (5.1) reduces to,

$$n_1^s = \frac{\Delta n_1}{m} = \frac{\Delta C_1 V}{m}, \tag{5.2}$$

where $\Delta C_1 = C_{1,0} - C_1$, $C_{1,0}$ is the molar concentration of component 1 before adsorption, C_1 is the molar concentration of component 1 after adsorption and V is the volume of the liquid phase in litres.

The surface concentration Γ_1 in mol m^{-2} can be calculated from a knowledge of surface area A (m^2 g^{-1}),

$$\Gamma_1 = \frac{\Delta C_1 V}{mA}. \tag{5.3}$$

The adsorption isotherm is represented by a plot of Γ_1 versus C_1. In most cases, the adsorption increases gradually with increasing C_1 and a plateau Γ_1^∞ is reached at full coverage corresponding to a surfactant monolayer. The area per surfactant molecule or ion at full saturation can be calculated,

$$a_1^s = \frac{10^{18}}{\Gamma_1^\infty N_{av}} \text{nm}^2, \tag{5.4}$$

where N_{av} is Avogadro's number.

5.2 Adsorption of ionic surfactants on hydrophobic surfaces

The adsorption of ionic surfactants on hydrophobic surfaces such as carbon black, polymer surfaces and ceramics (silicon carbide or silicon nitride) is governed by hydrophobic interaction between the alkyl chain of the surfactant and the hydrophobic surface. In this case, electrostatic interaction will play a relatively smaller role. However, if the surfactant head group is of the same sign of charge as that on the substrate surface, electrostatic repulsion may oppose adsorption. In contrast, if the head groups are of opposite sign to the surface, adsorption may be enhanced. Since the adsorption depends on the magnitude of the hydrophobic bonding free energy, the amount of surfactant adsorbed increases directly with increasing alkyl chain length in accordance with Traube's rule.

The adsorption of ionic surfactants on hydrophobic surfaces may be represented by the Stern–Langmuir isotherm [4]. Several assumptions have been made in deriving the Stern–Langmuir equation:

(i) Only one type of ion, the surfactant ion, is specifically adsorbed; this assumption is reasonable at low coverage.
(ii) One surfactant ion replaces one solvent molecule, i.e. the ion and solvent molecules are of the same size.
(iii) The surface is considered homogeneous.
(iv) Dipole terms and self-atmosphere potentials, as well as lateral chain–chain interactions are neglected.

Consider a substrate containing N_s sites (mol m^{-2}) on which Γ (mol m^{-2}) of surfactant ions are adsorbed. The surface coverage θ is (Γ/N_s) and the fraction of uncovered surface is $(1-\theta)$.

The rate of adsorption is proportional to the surfactant concentration expressed in mole fraction, $(C/55.5)$, and the fraction of free surface $(1-\theta)$, i.e.

$$\text{rate of adsorption} = k_{ads}\left(\frac{C}{55.5}\right)(1-\theta), \tag{5.5}$$

where k_{ads} is the rate constant for adsorption.

The rate of desorption is proportional to the fraction of surface covered θ,

$$\text{rate of desorption} = k_{des}\theta. \tag{5.6}$$

At equilibrium, the rate of adsorption is equal to the rate of desorption and the ratio of (k_{ads}/k_{des}) is the equilibrium constant K, i.e.,

$$\frac{\theta}{1-\theta} = \frac{C}{55.5}K. \tag{5.7}$$

The equilibrium constant K is related to the standard free energy of adsorption by,

$$-\Delta G^0_{ads} = RT\ln K. \tag{5.8}$$

R is the gas constant and T is the absolute temperature. Equation (5.8) can be written in the form,

$$K = \exp\left(-\frac{\Delta G^0_{\text{ads}}}{RT}\right). \tag{5.9}$$

Combining equations (5.7) and (5.9),

$$\frac{\theta}{1-\theta} = \frac{C}{55.5}\exp\left(-\frac{\Delta G^0_{\text{ads}}}{RT}\right). \tag{5.10}$$

Equation (5.10) applies only at low surface coverage ($\theta < 0.1$) where lateral interaction between the surfactant ions can be neglected.

At high surface coverage ($\theta > 0.1$) one should take the lateral interaction between the chains into account, by introducing a constant A, e.g. using the Frumkin–Fowler–Guggenheim equation [5],

$$\frac{\theta}{1-\theta}\exp(A\theta) = \frac{C}{55.5}\exp\left(-\frac{\Delta G^0_{\text{ads}}}{RT}\right). \tag{5.11}$$

The value of A can be estimated from the maximum slope $(\mathrm{d}\theta/\ln C)_{\max}$ of the isotherm which occurs at $\theta = 0.5$. Furthermore, at $\theta = 0.5$ substitution of A into equation (5.11) gives the value of ΔG^0_{ads}.

The above treatment using the FFG isotherm has two limitations. Firstly, it is assumed that A is constant and independent of surface coverage. In reality A could change in sign as well as increase in θ. At low coverages, A would reflect repulsive (electrostatic) interaction between adsorbed surfactant ions. At higher coverage, attractive chain–chain interaction becomes more important. The apparent adsorption energy becomes more favourable at high surface coverage and this could lead to the formation of "hemimicelles". Secondly, electrostatic interactions are strongly affected by the level of supporting electrolyte.

Various authors [6, 7] have used the Stern–Langmuir equation in a simple form to describe the adsorption of surfactant ions on mineral surfaces,

$$\Gamma = 2rC\exp\left(-\frac{\Delta G^0_{\text{ads}}}{RT}\right). \tag{5.12}$$

Various contributions to the adsorption free energy may be envisaged. To a first approximation, these contributions may be considered to be additive. In the first instance, ΔG_{ads} may be taken to consist of two main contributions, i.e.,

$$\Delta G_{\text{ads}} = \Delta G_{\text{elec}} + \Delta G_{\text{spec}} \tag{5.13}$$

where ΔG_{elec} accounts for any electrical interactions (coulombic as well as polar) and ΔG_{spec} is a specific adsorption term which contains all contributions to the adsorption free energy that are dependent on the "specific" (non-electrical) nature of the

system [6]. ΔG_{elec} is given by the sum of the coulombic interactions ΔG_{coul} and a dipole term, ΔG_{dip},

$$\Delta G_{elec} = \Delta G_{coul} + \Delta G_{dip}, \tag{5.14}$$

$$\Delta G_{coul} = Z_i e \psi_d, \tag{5.15}$$

where Z_i is the ion valency, e is the electronic charge and ψ_d is the Stern potential.

$$\Delta G_{dip} = \sum_j \Delta n_j \mu_j E_s \tag{5.16}$$

Δn_j is the change in the number of adsorbed dipoles j of moment μ_j and E_s is the electrical field strength across the plane of the adsorbed species (taken as the inner Helmholtz plane). Surfactant dipoles as well as water dipoles are accounted for in equation (5.16).

If one neglects ΔG_{dip} (as in the original Stern equation), the basic interpretation of ΔG_{elec} can be simplified. Three cases may be considered:

(i) When the surfactant ions are counterions to the net charge density ($\sigma_0 + \sigma_d$), then Z_i and ψ_d are of opposite sign, so $Z_i e \psi_d < 0$ and electrical interaction promotes the adsorption process. In the absence of other specifically adsorbed ions (such that σ_d is initially zero) this situation will exist at low surface coverages ($|\sigma_d| < |\sigma_0|$, where σ_d and σ_0 are of opposite sign) for cationic surfactant/negatively charged surface and anionic surfactant/positively charged surface combinations.

(ii) If ($\sigma_0 + \sigma_d$) is of the same sign as the surfactant ion, then Z_i and ψ_d are of like sign and $Z_i e \psi_d > 0$, i.e. the electrical interactions oppose adsorption. In the absence of specific adsorption, this situation will exist for anionic surfactant/negatively charged surface and cationic surfactant/positively charged surface combinations. It will also occur at high surface coverage for the combinations cited in the first example, i.e. sufficient surfactant ions, initially as counterions, adsorb until $|\sigma_d| > |\sigma_0|$ (allowed for in terms of a ΔG_{spec} contribution). In other words, the isoelectric point (IEP) is traversed and ψ_d is reversed in sign, so $Z_i e \psi_d$ becomes positive and opposes the favourable ΔG_{spec} term.

(iii) At the IEP ΔG_{elec} becomes zero and adsorption is governed by the ΔG_{spec} term.

The above predictions were confirmed by studying the adsorption of sodium dodecyl sulphonate on alumina (which has an IEP of pH = 9) as a function of pH [1]. This is illustrated in Fig. 5.1.

At low surface coverage the adsorption of the anionic surfactant on positive alumina surface (at pH < 9) is determined by ΔG_{elec}. As expected, the surfactant adsorption decreases with increasing pH since the surface becomes less positive.

Several authors subdivided ΔG_{spec} into supposedly separate independent interactions [10, 11], e.g.,

$$\Delta G_{spec} = \Delta G_{cc} + \Delta G_{cs} + \Delta G_{hs} + \cdots, \tag{5.17}$$

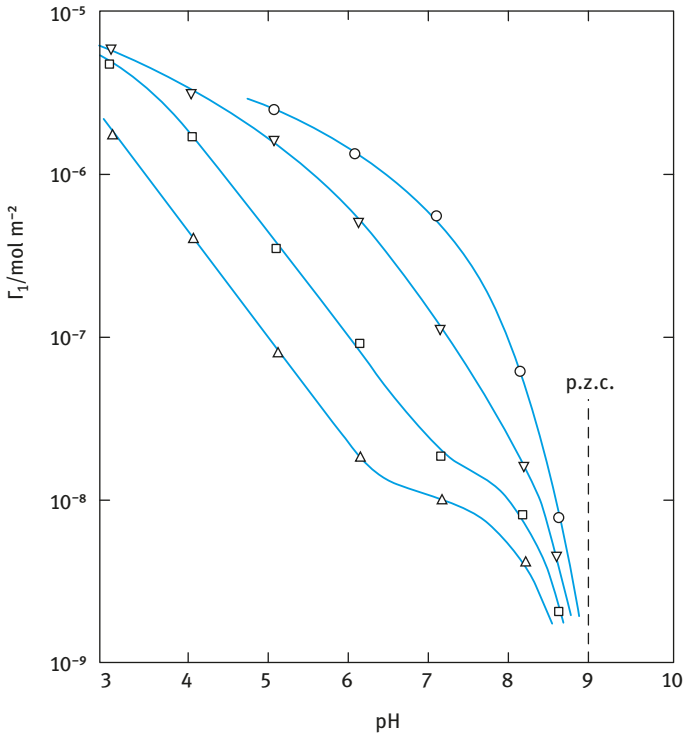

Fig. 5.1: Amount of sodium dodecyl sulphonate adsorbed on alumina as a function of pH (at 2×10^{-3} mol dm^{-3} ionic strength). Surfactant concentration in mol dm^{-3}: △, 1×10^{-5}; □, 3×10^{-5}; ▽, 1×10^{-4}; ○, 2.5×10^{-4}.

where ΔG_{cc} is a term that accounts for the cohesive chain–chain interaction between the hydrophobic moieties of the adsorbed ions, ΔG_{cs} is the term for chain/substrate interaction whereas ΔG_{hs} is a term for the head group/substrate interaction. The driving force of the hydrophobic interactions ΔG_{cc} and ΔG_{cs} is entropic in nature arising from the destruction of the short-lived structures of water molecules organized around nonpolar moieties [10]. These interactions depend on the nature of the solid surface and any associated structured water, and whether or not this structure is disrupted by the hydrophobic chains. Several other contributions to ΔG_{spec} may be envisaged e.g. ion-dipole, ion-induced dipole or dipole-induced dipole interactions.

Since there is no rigorous theory that can predict adsorption isotherms, the most suitable method to investigate adsorption of surfactants is to determine the adsorption isotherm. The measurement of surfactant adsorption is fairly straightforward. A known mass m (g) of the particles (substrate) with known specific surface area A_s ($m^2\,g^{-1}$) is equilibrated at constant temperature with surfactant solution with initial concentration C_1. The suspension is kept stirred for sufficient time to reach equilibrium. The particles are then removed from the suspension by centrifugation and the

equilibrium concentration C_2 is determined using a suitable analytical method. The amount of adsorption Γ (mol m^{-2}) is calculated using equation (5.3).

The adsorption isotherm is represented by plotting Γ versus C_2. A range of surfactant concentrations should be used to cover the whole adsorption process, i.e. from the initial low values to the plateau values. To obtain accurate results, the solid should have a high surface area (usually > 1 m^2).

5.3 Examples of adsorption isotherms for ionic surfactants on hydrophobic surfaces

Several examples may be quoted from the literature to illustrate the adsorption of surfactant ions on solid surfaces. For a model hydrophobic surface, carbon black has been chosen [9, 10]. Fig. 5.2 shows typical results for the adsorption of sodium dodecyl sulphate (SDS) on two carbon black surfaces, namely Spheron 6 (untreated) and Graphon (graphitized) which also describes the effect of surface treatment.

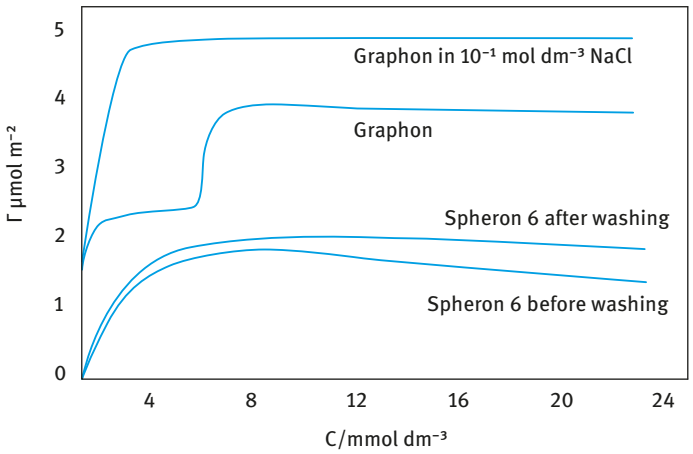

Fig. 5.2: Adsorption isotherms for sodium dodecyl sulphate on carbon substrates.

The adsorption of SDS on untreated Spheron 6 tends to show a maximum that is removed on washing. This suggests the removal of impurities from the carbon black which becomes extractable at high surfactant concentration. The plateau adsorption value is $\approx 2 \times 10^{-6}$ mol m^{-2} (≈ 2 µmol m^{-2}). This plateau value is reached at ≈ 8 mmol dm^{-3} SDS, i.e. close to the cmc of the surfactant in the bulk solution. The area per surfactant ion in this case is ≈ 0.7 nm^2. Graphitization (Graphon) removes the hydrophilic ionizable groups (e.g. –C=O or –COOH), producing a surface that is more hydrophobic. The same occurs by heating Spheron 6 to 2,700 °C. This

leads to a different adsorption isotherm (Fig. 5.2) showing a step (inflection point) at a surfactant concentration in the region of $\approx 6\,\text{mmol}\,\text{dm}^{-3}$. The first plateau value is $\approx 2.3\,\mu\text{mol}\,\text{m}^{-2}$ whereas the second plateau value (that occurs at the cmc of the surfactant) is $\approx 4\,\mu\text{mol}\,\text{m}^{-2}$. It is likely in this case that the surfactant ions adopt different orientations at the first and second plateaus. In the first plateau region, a more "flat" orientation (alkyl chains adsorbing parallel to the surface) is obtained whereas at the second plateau vertical orientation is more favourable, with the polar head groups being directed towards the solution phase. Addition of electrolyte ($10^{-1}\,\text{mol}\,\text{dm}^{-3}$ NaCl) enhances the surfactant adsorption. This increase is due to the reduction of lateral repulsion between the sulphate head groups and this enhances the adsorption. The disappearance of the inflection point in the presence of NaCl is considered to be a consequence of the much steeper rise in adsorption at low surfactant concentration.

The adsorption of ionic surfactants on hydrophobic polar surfaces resembles that for carbon black [13, 14]. For example, Saleeb and Kitchener [13, 14] found a similar limiting area for cetyltrimethyl ammonium bromide on Graphon and polystyrene ($\approx 0.4\,\text{nm}^2$). As with carbon black, the area per molecule depends on the nature and amount of added electrolyte. This can be accounted for in terms of reduction of head group repulsion and/or counterion binding.

Surfactant adsorption close to the cmc may appear Langmuirian, although this does not automatically imply a simple orientation. For example, rearrangement from horizontal to vertical orientation or electrostatic interaction and counterion binding may be masked by simple adsorption isotherms. It is essential, therefore, to combine the adsorption isotherms with other techniques such as microcalorimetry and various spectroscopic methods to obtain a full picture on surfactant adsorption.

The effect of increasing the alkyl chain length on ionic surfactant adsorption was investigated by Conner and Ottewill [15] who measured the adsorption isotherms for a series of alkyltrimethylammonium ions with C_8, C_{10}, C_{12} and C_{16} on polystyrene latex. The results are shown in Fig. 5.3. For each of these isotherms the inflection at low surfactant concentration can be accounted for by reversal of the sign of ΔG_{elec} on adsorption of the cationic ions on the negative polystyrene latex particles. Initial adsorption of the cations causes charge neutralization and at a certain surfactant concentration, the isoelectric point is reached and a further increase of surfactant concentration causes charge reversal. The inflection at the higher surfactant concentration may reflect the orientation of the alkyl chain from a horizontal orientation of saturation coverage into a vertically oriented monolayer as the surfactant concentration is increased. In this way the solid-water and surfactant chain-water interactions would be minimized at high coverage. For a hydrocarbon surface, one would expect that ΔG_{cs} per CH_2 group would be of the same order of magnitude as ΔG_{cc}, that is about $1kT$.

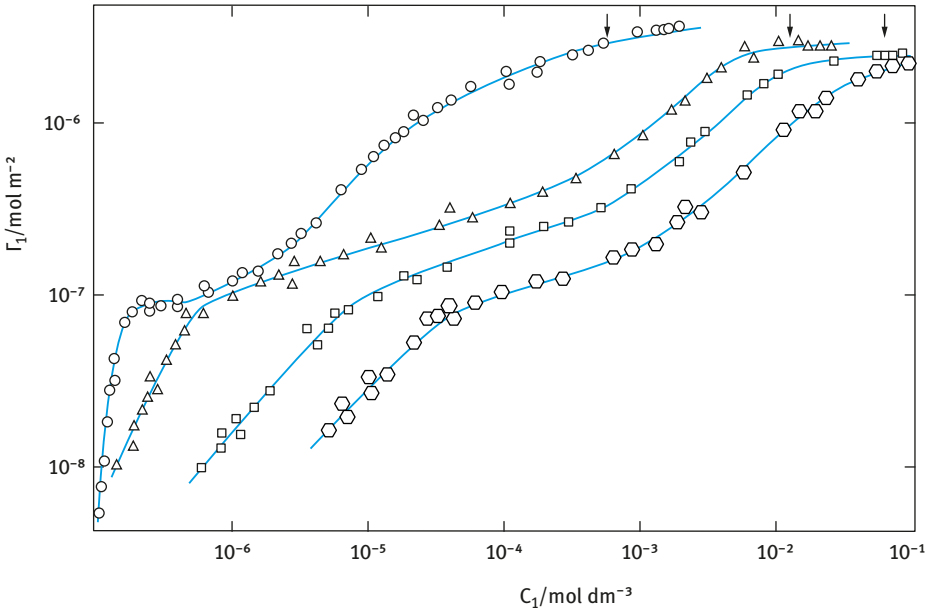

Fig. 5.3: Adsorption isotherms for alkyltrimethylammonium ions on polystyrene latex at pH = 8: ○, C_{16}; △, C_{12}; □, C_{10}.

5.4 Adsorption of ionic surfactants on polar surfaces

The adsorption of ionic surfactants on polar surfaces that contain ionizable groups may show characteristic features due to additional interaction between the head group and substrate and/or possible chain–chain interaction. This is best illustrated by the results of adsorption of sodium dodecyl sulphonate (SDSe) on alumina at pH = 7.2 obtained by Fuersetenau [16] and shown in Fig. 5.4. At the pH value, the alumina is positively charged (the isoelectric point of alumina is at pH ≈ 9) and the counterions are Cl^- from the added supporting electrolyte. In Fig. 5.4, the saturation adsorption Γ_1 is plotted versus equilibrium surfactant concentration C_1 in logarithmic scales. The figure also shows the results of zeta potential (ζ) measurements (which are a measure of the magnitude sign of charge on the surface). Both adsorption and zeta potential results show three distinct regions. The first region shows a gradual increase of adsorption with increasing concentration, with virtually no change in the value of the zeta potential. This corresponds to an ion exchange process [16]. In other words, the surfactant ions simply exchange with the counterions (Cl^-) of the supporting electrolyte in the electrical double layer. At a critical surfactant concentration, the adsorption increases dramatically with a further increase in surfactant concentration (region II). In this region, the positive zeta potential gradually decreases, reaching a zero value (charge neutralization) after which a negative value is obtained which

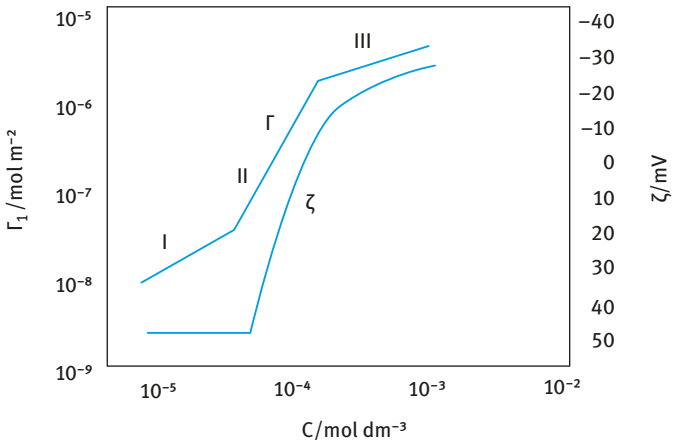

Fig. 5.4: Adsorption isotherm for sodium dodecyl sulphonate on alumina and corresponding zeta (ζ) potential.

increases rapidly with increasing surfactant concentration. The rapid increase in region II was explained in terms of "hemimicelle formation" that was originally postulated by Gaudin and Fuerestenau [17]. In other words, at a critical surfactant concentration (to be denoted the cmc of "hemimicelle formation" or better the critical aggregation concentration CAC), the hydrophobic moieties of the adsorbed surfactant chains are "squeezed out" from the aqueous solution by forming two-dimensional aggregates on the adsorbent surface. This is analogous to the process of micellization in bulk solution. However, the CAC is lower than the cmc, indicating that the substrate promotes surfactant aggregation. At a certain surfactant concentration in the hemimicellization process, the isoelectric point is exceeded and, thereafter, adsorption is hindered by the electrostatic repulsion between the hemimicelles and hence the slope of the adsorption isotherm is reduced (region III).

5.5 Adsorption of nonionic surfactants

Several types of nonionic surfactants exist, depending on the nature of the polar (hydrophilic) group. The most common type is that based on a poly(oxyethylene) glycol group, i.e. $(CH_2CH_20)_nOH$ (where n can vary from as little as 2 units to as high as 100 or more units) linked either to an alkyl (C_xH_{2x+1}) or alkyl phenyl (C_xH_{2x+1}–C_6H_4–) group. These surfactants may be abbreviated as C_xE_n or $C_x\phi E_n$ (where C refers to the number of C atoms in the alkyl chain, ϕ denotes C_6H_4 and E denotes ethylene oxide). These ethoxylated surfactants are characterized by a relatively large head group compared to the alkyl chain (when $n > 4$). However, there are nonionic surfactants with small head group such as amine oxides ($-N \rightarrow 0$) head group, phosphate oxide

($-P \rightarrow 0$) or sulphinyl-alkanol ($-SO-(CH_2)_n-OH$). Most adsorption isotherms in the literature are based on the ethoxylated type surfactants.

The adsorption isotherm of nonionic surfactants are in many cases Langmuirian, like those of most other highly surface active solutes adsorbing from dilute solutions and adsorption is generally reversible. However, several other adsorption types are produced [18] and these are illustrated in Fig. 5.5. The steps in the isotherm may be explained in terms of the various adsorbate–adsorbate, adsorbate–adsorbent and adsorbate–solvent interactions.

These orientations are schematically illustrated in Fig. 5.6. In the first stage of adsorption (denoted by I in Fig. 5.5 and 5.6), surfactant-surfactant interaction is negligible (low coverage) and adsorption occurs mainly by van der Waals interaction. On a hydrophobic surface, the interaction is dominated by the hydrophobic portion of the

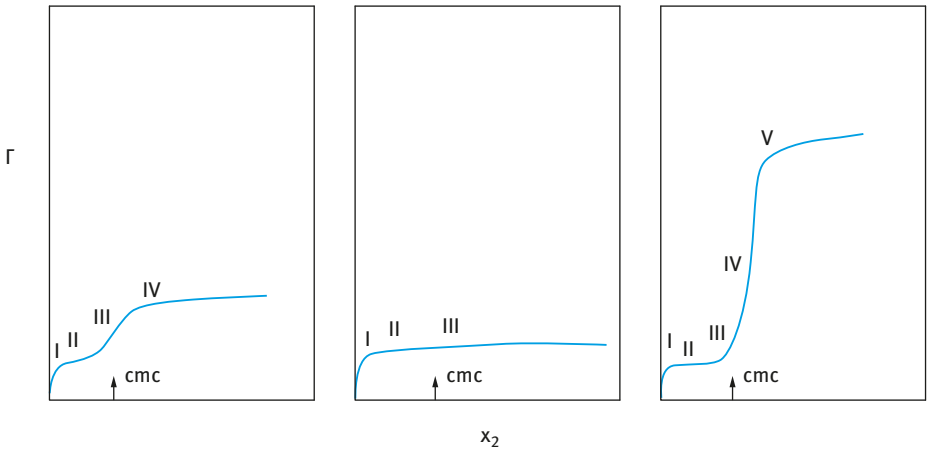

Fig. 5.5: Adsorption isotherms corresponding to the three adsorption sequences shown in Fig. 5.6.

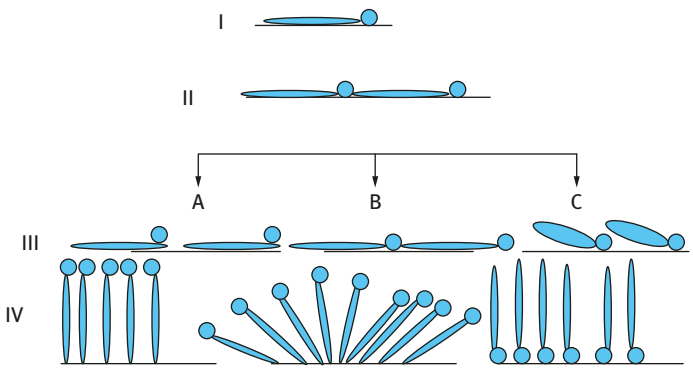

Fig. 5.6: Model for adsorption of nonionic surfactants.

surfactant molecule. This is mostly the case with pharmaceuticals and agrochemicals which have hydrophobic surfaces. Nevertheless, the polar groups of the surfactant may have some interaction with the surface, and the hydrophilic EO groups can have a slight positive adsorption even on a nonpolar adsorbent. When the interaction is due to dispersion forces, the heat of adsorption is relatively small and corresponds to the heat liberated by replacing solvent molecules with surfactant. At this stage, the molecule tends to lie flat on the surface because its hydrophobic portion is positively adsorbed, as are also most types of hydrophilic head groups, especially large PEO chains. With the molecule lying parallel to the surface, the adsorption energy will increase in almost equal increments for each additional carbon atom in its alkyl chain, and the initial slope of the isotherm will increase correspondingly, according to Traube's rule. The same also happens with each additional EO group.

The approach to monolayer saturation with the molecules lying flat (Fig. 5.6 II) is accompanied by a gradual decrease in the slope of the adsorption isotherm as shown in Fig. 5.5. Although most of the "free" solvent molecules will have been displaced from the surface by the time the monolayer is complete, the surfactant molecules themselves will probably stay hydrated at this stage. Increasing the size of the surfactant molecule, e.g. by increasing the length of the alkyl chain or the PEO chain will decrease the adsorption (expressed in mol m^{-2}). Increasing temperature should increase the adsorption because dehydration decreases the size of the adsorbate molecules. Increasing temperature reduces the solubility of the nonionic surfactant and this enhances its adsorption (higher surface activity).

The subsequent stages of adsorption are increasingly dominated by adsorbate–adsorbate interaction, although it is the adsorbate–adsorbent interaction that initially determines how the adsorption progresses when stage II is completed. The adsorbate–adsorbent interaction depends on the nature of the adsorbent and the HLB of the surfactant. When the hydrophilic group (e.g. PEO) is only weakly adsorbed it will be displaced from the surface by the alkyl chain of the surfactant molecule (Fig. 5.6 III A). This is particularly the case with nonpolar adsorbents such as C black or polystyrene when the surfactant has a short PEO chain (relatively low HLB number). However, if the interaction between the hydrophilic chain (PEO) and polar adsorbent such as silica or silicates is strong, the alkyl chain is displaced as illustrated in Fig. 5.6 III C. The intermediate situation (Fig. 5.5 III B) occurs when neither type of displacement is favoured and the adsorbate molecules remain flat on the surface.

The change in the amount of adsorption in the third stage (stage III of Fig. 5.6) is unlikely to be large, but as the concentration of the surfactant in bulk solution approaches the critical micelle concentration (cmc) there will be a tendency for the alkyl chains of the adsorbed molecules to aggregate. This will cause the molecules to be vertically oriented and there will be a large increase in adsorption (stage IV). The lateral forces due to alkyl chain interactions will compress the head group, and for a PEO chain this will result in a less coiled, more extended conformation. The longer the alkyl chain, the greater will be the cohesion force and hence the smaller the surfactant

cross-sectional area. This may explain the increase in saturation adsorption with increasing alkyl chain length and decreasing number of EO units in the PEO chain. With nonpolar adsorbents the adsorption energy per methylene group is almost the same as the micellization energy, so surface aggregation can occur quite easily even at concentrations below the cmc. However, with polar adsorbents, the head group may be strongly bound to the surface, and partial displacement of a large PEO chain from the surface, needed for close packing, may not be achieved until the surfactant concentration is above the cmc. When the adsorption layer is like that shown in Fig. 5.6 IV C, the surface becomes hydrophobic.

The interactions occurring in the adsorption layer during the fourth and subsequent stages of adsorption are similar to interactions in bulk solution where enthalpy changes caused by increased alkyl-alkyl interactions balance those due to head group interactions and the dehydration process. For this reason, the heat of adsorption remains constant, although adsorption increases with increasing temperature due to dehydration of the head group and its more compact nature.

The parallel between bulk micellization and the surface aggregation process has been emphasized by Klimenko et al. [19, 20] who suggested that above the cmc the adsorbed surfactant molecules form micellar aggregates on the surface as illustrated in Fig. 5.6 V. Both hemimicelles and full micelles can be formed on the surface. This picture was supported by Klimenko et al. [19] who found close agreement between saturation adsorption and adsorption calculated based on the assumption that the surface is covered with close-packed hemimicelles.

5.6 Theoretical treatment of surfactant adsorption

Klimenko [19, 20] developed a theoretical model for the three stages of adsorption of nonionic surfactants. In the first stage (flat orientation) a modified Langmuir adsorption equation was used,

$$c_2 K_a = \left[\frac{\Gamma_2}{\Gamma_2^* - \Gamma_2(1 - a_1/a_2')a_2'} \frac{a_1}{a_2'} \right] f_2', \tag{5.18}$$

where c_2 is the equilibrium concentration of surfactant in bulk solution, Γ_2 is the surface excess concentration at c_2, Γ_2^* is the surface excess at the cmc, K_a is a constant, a_1 and a_2' are the effective cross-sectional areas of the solvent and adsorbate molecules in the surface, and f_a' is an adsorbate surface activity coefficient. The term in the square bracket is a type of surface "concentration" which is defined as the ratio of numbers of adsorbed surfactant molecules to the number of solvent molecules in the equilibrium interfacial layer. The constant K_a allows for adsorbate–adsorbent interactions and is therefore related to the energy of adsorption at infinite dilution. The adsorbate surface activity coefficient f_a' accounts for the adsorbate–adsorbate interaction and it is assumed to have the following dependency on Γ_2 in the first stage of adsorption,

$$f_2' = \exp\left[\frac{\Gamma_2}{\Gamma_2^* - \Gamma_2} - \frac{K_2\Gamma_2}{\Gamma_2^*}\right], \tag{5.19}$$

where K_2 is an adsorbate–adsorbate interaction constant.

When all the solvent molecules have been displaced and the surface is covered with a close-packed monolayer of horizontal adsorbate molecules, the second stage begins and the EO chains are progressively displaced by alkyl chains of adsorbate molecules. This allows the surface concentration to increase by the following amount,

$$\frac{\Gamma_2 - \Gamma_2'}{\Gamma_2'(a_E'/a_1) - (\Gamma_2 - \Gamma_2')(a_2/a_1)}, \tag{5.20}$$

where Γ_2' is the surface excess at the beginning of the second stage, a_E' is the cross-sectional area of the EO chain lying flat on the surface, and a_2 is the area of the surface covered by each surfactant molecule. The adsorption isotherm for the second stage is given by [19–21],

$$c_2 K_a = \left[\frac{\Gamma_2'}{\Gamma_2^* - \Gamma_2'(1 - a_1/a_2')a_2'}\frac{a_1}{a_2'} + \frac{\Gamma_2 - \Gamma_2'}{\Gamma_2' a_E' - (\Gamma_2 - \Gamma_2')a_2}a_1\right] f_a''. \tag{5.21}$$

The activity coefficient f_a'' is assumed to include contributions from EO chain interactions and therefore to differ from f_a' in its dependency on Γ_2. The logarithm of f_a'' is arbitrarily assumed to have linear dependency on Γ_2:

$$\ln f_a'' = \ln(f_a')_{\Gamma_2'} + \left[\ln(f_a'')_{\Gamma_2^*} - \ln(f_a')_{\Gamma_2'}\right]\Gamma_2/(\Gamma_2^* - \Gamma_2'). \tag{5.22}$$

In equation (5.22) f_a' with subscript Γ_2', the maximum value of f_a' which is reached when $\Gamma_2 = \Gamma_2'$, is obtained by substituting the value of Γ_2' into equation (5.19); f_a'' with subscript Γ_2^*, the maximum value of f_a'' which is reached when $c_2 = c^*$, the cmc, and $\Gamma_2 = \Gamma_2^*$ can be obtained by substitution into equation (5.21).

In the final adsorption stage, which starts at the cmc, Klimenko [16–18] assumes that the adsorbed surfactant associates into hemimicelles on the surface. By considering the equilibrium between molecules in the bulk solution and "free" positions in these surface micelles, he derives a simple Langmuir isotherm,

$$C_2 K_a^* = \frac{\Gamma_2}{(\Gamma_2^\infty - \Gamma_2)}, \tag{5.23}$$

where Γ_2^∞ is the maximum surface excess, i.e. the surface excess when the surface is covered with close-packed hemimicelles, K_a^* is a constant that is inversely proportional to the cmc because it is assumed that the surface micelles are similar to the bulk solution micelles, and c_2 is the equilibrium concentration. Equation (5.23) does not contain an activity coefficient because it is assumed that above the cmc deviations from ideality in the surface and in bulk solution derive from a similar association effect with the result that the two activity coefficients will cancel each other out in the adsorption equation.

5.7 Examples of typical adsorption isotherms of model nonionic surfactants on hydrophobic solids

Corkill et al. [22] studied the adsorption of very pure alkyl polyoxyethylene glycol monoethers C_xE_n on Graphon (with a nitrogen BET specific surface area of 91 $m^2\ g^{-1}$). The adsorption isotherms were mostly simple Langmuirian with saturation adsorption reached near or above the cmc. The maximum adsorption increases with increasing alkyl chain length and decreasing EO chain length. From the saturation adsorption, the area per molecule at 25 °C was calculated and compared with the value obtained at the solution/air interface (which was obtained from the γ–log c curves and application of the Gibbs adsorption isotherm). The results are given in Tab. 5.1.

Tab. 5.1: Area per molecule at the Graphon/solution interface and air/solution interface at 25 °C.

Surfactant	Area/molecule (nm^2) Graphon/solution interface	Area/molecule (nm^2) Air/solution interface
E_6	1.68	—
C_6E_6	0.93	0.94
C_8E_6	0.81	0.83
$C_{10}E_6$	0.65	0.72
$C_{12}E_6$	0.55	0.61
C_8E_9	1.09	1.02
$C_{16}E_9$	—	0.47

The similarity between the areas at the two interfaces suggests that, at saturation, molecules adsorbed on the solid are vertically oriented as in Fig. 5.6 IV. Hexaoxyethylene glycol (E_6) is also positively adsorbed on Graphon, indicating some affinity to the carbon surface.

The heat of wetting of Graphon with solutions of C_8E_6 was measured as a function of surface excess and the results showed an initial linear change in heat with surface coverage corresponding to the replacement of water at the interface by the hydrated surfactant molecules until the surface is saturated with horizontal adsorbate molecules. The plateau value for the heat of immersion is reached at a molecular area of 1.32 nm^2, which is close to the cross-sectional area of C_8E_6 lying flat. The constancy of the heat of immersion at higher concentrations is attributed to the balance between decreasing enthalpy, due to elimination of the alkyl/solution interface as the molecules become vertically oriented, and increasing enthalpy associated with the dehydration of the adsorbing molecule. The adsorption thus occurs with a net increase in entropy analogous to the process of micellization.

The adsorption of nonionic surfactants based on poly(ethylene oxide) increases with increasing temperature as illustrated in Fig. 5.7 for C_8E_6 and C_8E_3. Increasing temperature gradually dehydrates the PEO head group and this makes the molecule less

hydrophilic and more compact, thus increasing the surface activity and saturation adsorption values. The importance of the surfactant/solvent interaction is apparent on the effect of temperature on the adsorption of C_8E_3. At 4.5 °C the adsorption isotherm is a simple Langmuirian, but at 25 °C and 40 °C there is a very steep rise in adsorption at high surfactant concentrations. This is characteristic of a surface condensation effect and the steep rise occurs at concentrations below those at which surfactant phase separation occurs in bulk solution. These concentrations are shown by broken lines in Fig. 5.7.

Corkill et al. [23, 24] studied the adsorption of alkylsulphinylalkanol surfactants, $C_xH_{2x+1}SO(CH_2)_nOH$ on Graphon. They found that the saturation adsorption, like that of the ethoxylated surfactants, increases with increasing alkyl chain length and decreasing head group size. A summary of the results obtained is given in Tab. 5.2. From the magnitude of the area occupied (A) by the surfactant at saturation and the observation that the carbon black dispersions were well stabilized, it was concluded that at saturation the surfactant molecule was vertically oriented. The minimum areas were slightly larger than the smallest cross-sectional area of the fully extended surfactant molecule. This difference was attributed to the head group hydration.

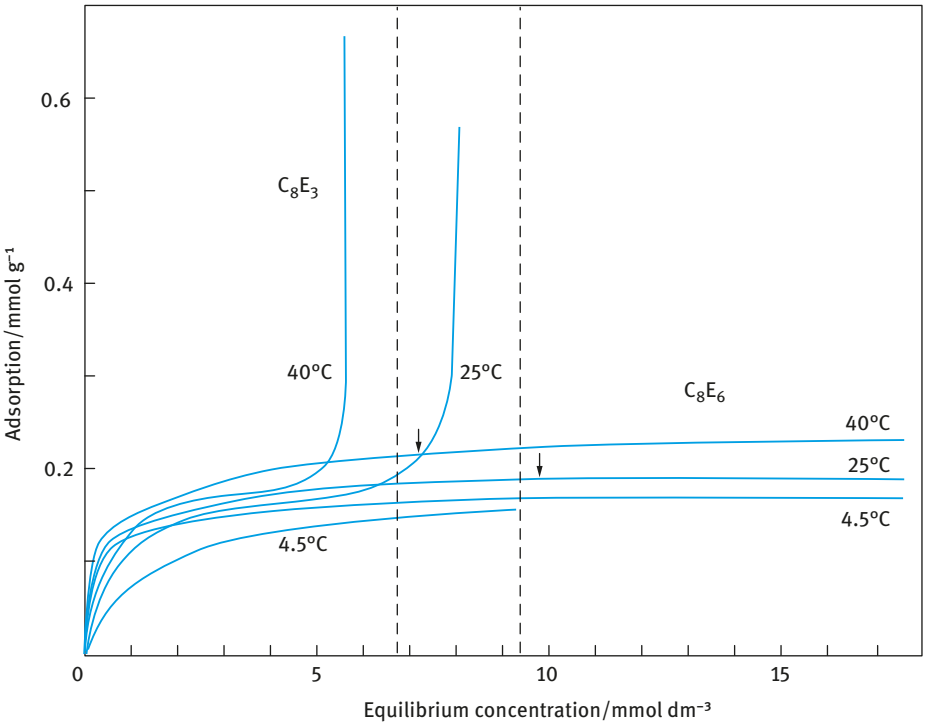

Fig. 5.7: Effect of temperature on the adsorption of C_8E_6 and C_8E_3 on Graphon.

Tab. 5.2: Adsorption results for n-alkylsulphinylalkanols on Graphon at 25 °C [24].

Adsorbate	A (nm^2)				$-\Delta H_2$ (kJ/mol)
	At isotherm inflection	From horizontal model	At saturation	From vertical model	
$C_4H_9SO(CH_2)_2OH$	—	0.58	≈ 0.83	0.25	—
$C_6H_{13}SO(CH_2)_2OH$	0.84	0.70	0.44	0.25	42
$C_8H_{17}SO(CH_2)_2OH$	1.08	0.83	0.25	0.25	59
$C_{10}H_{21}SO(CH_2)_2OH$	≈ 1.68	0.98	—	0.25	109
$C_8H_{17}SO(CH_2)_3OH$	1.31	0.90	0.32	0.25	84
$C_8H_{17}SO(CH_2)_4OH$	1.68	0.98	0.36	0.25	117

Most of the isotherms show an inflection point at the cmc as illustrated in Fig. 5.5. This is clearly illustrated in Fig. 5.8 for the adsorption of octylsulphinylethanol [24]. The heat of wetting for the alkylsulphinylalkanols changes linearly with surface coverage until adsorption reaches a value that corresponds fairly closely to the inflection point of the isotherm. Thereafter the heat of adsorption is constant except for that of decylsulphinyleethanol which continues to increase but less rapidly. This may be due to the surfactant being close to its solubility limit. The change in heat with coverage is greater for the longer alkyl chains and larger number of head group methylene groups.

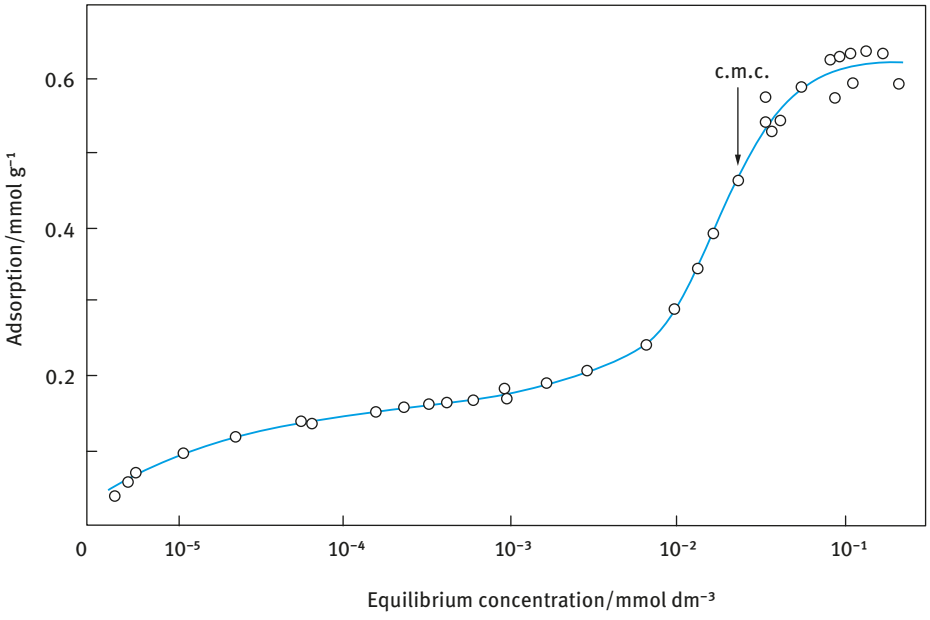

Fig. 5.8: Adsorption isotherm of octylsulphinylethanol on Graphon at 25 °C [22].

The partial molar heat of adsorption of the surfactant ΔH_2 was calculated by assuming that the surface concentration of "free" solvent became zero when the heat of wetting became constant. ΔH_2 had large negative values which increased as x and n increased (Tab. 5.2). Corkill et al. [24] concluded that the alkylsulphinylalkanol system was very similar to the ethoxylated alcohol systems.

The surfactant is initially adsorbed as a highly hydrated molecule lying parallel to the surface, and the initial enthalpy changes are associated with the displacement of the solvent molecules from the surface. When compete monolayer coverage has been achieved, adsorbate–adsorbate interactions, similar to the process of micellization in bulk solution, cause orientation changes and a large increase in adsorption occurs near the cmc. The heat of adsorption becomes constant because the negative enthalpy due to elimination of alkyl/solution interface is offset by the positive enthalpy due to de-solvation.

References

[1] Tadros T. Suspension concentrates. Berlin: De Gruyter; 2017.
[2] Tadros T. Dispersions of powders in liquids and stabilisation of suspensions. Weinheim: Wiley-VCH; 2012.
[3] Hough DB, Randall HM. In: Parfitt GD, Rochester CH, editors. Adsorption from solution at the solid/liquid interface. London: Academic Press; 1983. p. 247.
[4] Rendall HM, Smith AL, Williams LA. J Chem Soc Faraday Trans I. 1979;75:669.
[5] de Kaizer A, Lyklema J. J Colloid Interface Sci. 1980;75:171.
[6] Fuerstenau DW, Healy TW. In: Lemlich R, editor. Adsorptive bubble separation techniques. London: Academic Press; 1972. p. 91.
[7] Somasundaran P, Goddard ED. Modern Aspects Electrochem. 1979;13:207.
[8] Healy TW. J Macromol Sci Chem. 1974;118:603.
[9] Somasundaran P, Hannah HS. In: Shah DO, Schechter RS, editors. Improved oil recovery by surfactant and polymer flooding. London: Academic Press; 1979. p. 205.
[10] Clark AH, Frank F, Smani S. J Chem Soc Faraday Trans I. 1977;73:290.
[11] Greenwood FG, Parfitt GD, Picton NH, Wharton DG. Adv Chem Ser. 1968;79:135.
[12] Day RE, Greenwood FG, Parfitt GD. 4th International Congress of Surface Active Substances. 1967;18:1005.
[13] Saleeb FZ, Kitchener JA. J Chem Soc. 1965:911.
[14] Saleeb FZ, Kitchener JA. 4th International Congress of Surface Active Substances. 1967;2B:129.
[15] Conner P, Ottewill RH. J Colloid Interface Sci. 1971;37:642.
[16] Fuerestenau DW. In: Hair ML, editor. The chemistry of biosurfaces. New York: Marcel Dekker; 1971. p. 91.
[17] Gaudin AM, Fuertsenau DW. Trans AIME. 1955;202:958.
[18] Clunie JS, Ingram BT. In: Parfitt GD, Rochester CH, editors. Adsorption from solution at the solid/liquid interface. London: Academic Press; 1983. p. 105.
[19] Klimenko NA. Tryasorukova and Permilouskayan. Kolloid Zh. 1974;36:678.
[20] Klimenko NA. Kolloid Zh. 1978;40:1105.
[21] Klimenko NA. Kolloid Zh. 1979;41:781.
[22] Corkill JM, Goodman JF, Tate JR. Trans Faraday Soc. 1966;62:979.

[23] Corkill JM, Goodman JF, Tate JR. Wetting. SCI Monograph No. 2. London: Society of Chemical Industry; 1966. p. 363.
[24] Corkill JM, Goodman JF, Tate JR. Trans Faraday Soc. 1967;63:2264.

6 Adsorption and conformation of polymeric surfactants at interfaces

6.1 Introduction

Polymeric surfactants are used in the formulation of many disperse systems, of which we mention dyestuffs, paper coatings, inks, agrochemicals, pharmaceuticals, personal care products, ceramics and detergents [1–3]. One of the most important applications of polymeric surfactants is in the stabilization of oil-in-water (O/W) and water-in-oil (W/O) emulsions as well as solid/liquid dispersions [1–3]. This is particularly the case when using A–B, A–B–A block or BA_n copolymers as described in Chapter 3. In this case, the hydrophobic portion of the surfactant molecule (the B chain) should adsorb "strongly" at the O/W interface or becomes dissolved in the oil phase, leaving the hydrophilic components in the aqueous medium, whereby they become strongly solvated by the water molecules and this provides effective steric stabilization, as will be discussed in Chapter 8. Polymeric surfactants are also used for the preparation and stabilization of solid/liquid dispersions (usually referred to as suspensions). There are generally two methods for the preparation of suspensions, referred to as condensation and dispersions methods. In the first case, one starts with molecular units and builds up the particles by a process of nucleation and growth [1–3]. A typical example is the preparation of polymer latexes. In this case, the monomer (such as styrene or methylmethacrylate) is emulsified in water using an anionic or nonionic surfactant (such as sodium dodecyl sulphate or alcohol ethoxylate). An initiator such as potassium persulphate is added and when the temperature of the system is increased, initiation occurs resulting in the formation of the latex (polystyrene or polymethylmethacrylate). In the dispersion methods, preformed particles (usually powders) are dispersed in an aqueous solution containing a surfactant. The latter is essential for adequate wetting of the powder (both external and internal surfaces of the powder aggregates and agglomerates must be wetted) [2]. This is followed by dispersion of the powder using high-speed stirrers and finally the dispersion is "milled" to reduce the particle size to the appropriate range.

For stabilizing emulsions and suspensions against flocculation, coalescence and Ostwald ripening the following criteria must be satisfied:

(i) Complete coverage of the droplets or particles by the surfactant. Any bare patches may result in flocculation as a result of van der Waals attraction or bridging.
(ii) Strong adsorption (or "anchoring") of the surfactant molecule to the surface of droplet or particle.
(iii) Strong solvation (hydration) of the stabilizing chain to provide effective steric stabilization.
(iv) Reasonably thick adsorbed layer to prevent weak flocculation [1].

https://doi.org/10.1515/9783110587944-007

Most of the above criteria for stability are best served by using a polymeric surfactant. As mentioned above, molecules of the A–B, A–B–A blocks and BA_n (or AB_n) grafts are the most efficient for stabilizing emulsions and suspensions. In this case, the B chain (referred to as the "anchoring" chain) is chosen to be highly insoluble in the medium and with a high affinity to the surface in the case of suspensions, or soluble in the oil in the case of emulsions. The A chain is chosen to be highly soluble in the medium and strongly solvated by its molecules. These block and graft copolymers are ideal for preparation of concentrated emulsions and suspensions, which are needed in many industrial applications.

In this chapter, I will discuss in detail the adsorption of polymers at interfaces and their conformation. This is key to understanding how polymeric surfactants can be applied as stabilizers for disperse systems as will be discussed in Chapter 8.

6.2 Polymers at interfaces

As mentioned above understanding the adsorption and conformation of polymeric surfactants at interfaces is key to knowing how these molecules act as stabilizers. Most basic ideas on adsorption and conformation of polymers have been developed for the solid/liquid interface [4]. The first theories on polymer adsorption were developed in the 1950s and 1960s, with extensive developments in the 1970s. The process of polymer adsorption is fairly complicated. In addition to the usual adsorption considerations such as polymer/surface, polymer/solvent and surface/solvent interactions, one of the principal problems to be resolved is the configuration (conformation) of the polymer at the solid/liquid interface. This was recognized by Jenkel and Rumbach in 1951 [5] who found that the amount of polymer adsorbed per unit area of the surface would correspond to a layer more than 10 molecules thick if all the segments of the chain are attached. They suggested a model in which each polymer molecule is attached in sequences separated by bridges which extend into solution. In other words not all the segments of a macromolecule are in contact with the surface. The segments which are in direct contact with the surface are termed "trains"; those in between and extended into solution are termed "loops"; the free ends of the macromolecule also extending in solution are termed "tails". This is illustrated in Fig. 6.1 (a) for a homopolymer [1]. Examples of homopolymers that are formed from the same repeating units are poly(ethylene oxide) or poly(vinylpyrrolidone).

These homopolymers have little surface activity at the O/W interface, since the homopolymer segments (ethylene oxide or vinylpyrrolidone) are highly water soluble and have little affinity to the interface. However, such homopolymers may adsorb significantly at the S/L interface. Even if the adsorption energy per monomer segment to the surface is small (fraction of kT, where k is the Boltzmann constant and T is the absolute temperature), the total adsorption energy per molecule may be sufficient to overcome the unfavourable entropy loss of the molecule at the S/L interface. Clearly,

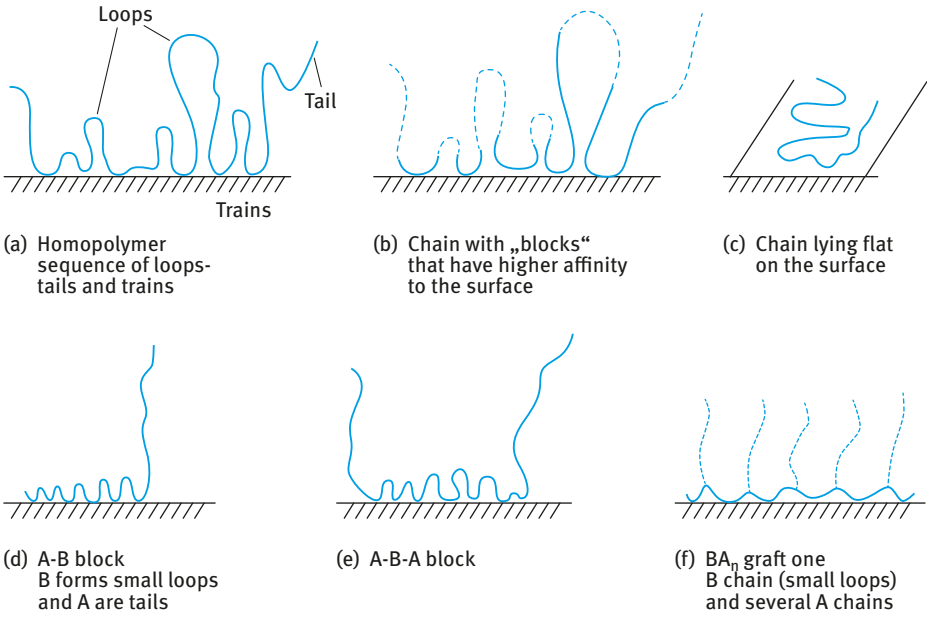

Fig. 6.1: Various conformations of macromolecules on a plane surface.

homopolymers are not the most suitable emulsifiers or dispersants. A small variant is to use polymers that contain specific groups that have high affinity to the surface. This is exemplified by partially hydrolysed poly(vinyl acetate) (PVAc), technically referred to as poly(vinyl alcohol) (PVA). The polymer is prepared by partial hydrolysis of PVAc, leaving some residual vinyl acetate groups. Most commercially available PVA molecules contain 4–12 % acetate groups. These acetate groups, which are hydrophobic, give the molecule its amphipathic character. On a hydrophobic surface such as polystyrene, the polymer adsorbs with preferential attachment of the acetate groups on the surface, leaving the more hydrophilic vinyl alcohol segments dangling in the aqueous medium. The configuration of such "blocky" copolymers is illustrated in Fig. 6.1 (b). Clearly, if the molecule is made fully from hydrophobic segments, the chain will adopt a flat configuration as is illustrated in Fig. 6.1 (c).

The most convenient polymeric surfactants are those of the block and graft copolymer type. A block copolymer is a linear arrangement of blocks of variable monomer composition. The nomenclature for a diblock is poly-A-block–poly-B and for a triblock is poly-A-block–poly-B–poly-A. An example of an A–B diblock is polystyrene block-polyethylene oxide and its conformation is represented in Fig. 6.1 (d). One of the most widely used triblock polymeric surfactants are the "Pluronics" (BASF, Germany) which consist of two poly-A blocks of poly(ethylene oxide) (PEO) and one block of poly(propylene oxide) (PPO). Several chain lengths of PEO and PPO are available. More recently, triblocks of PPO–PEO–PPO (inverse Pluronics) became available for

some specific applications. These polymeric triblocks can be applied as emulsifiers or dispersants, whereby the assumption is made that the hydrophobic PPO chain resides at the hydrophobic surface, leaving the two PEO chains dangling in aqueous solution and hence providing steric repulsion. Several other triblock copolymers have been synthesized, although these are of limited commercial availability. Typical examples are triblocks of poly(methyl methacrylate)-block poly(ethylene oxide)-block poly(methyl methacrylate). The conformation of these triblock copolymers is illustrated in Fig. 6.1 (e). An alternative (and perhaps more efficient) polymeric surfactant is the amphipathic graft copolymer consisting of a polymeric backbone B (polystyrene or polymethyl methacrylate) and several A chains ("teeth") such as polyethylene oxide. This graft copolymer is sometimes referred to as a "comb" stabilizer. Its configuration is illustrated in Fig. 6.1 (f).

The polymer/surface interaction is described in terms of adsorption energy per segment χ^s. The polymer/solvent interaction is described in terms of the Flory–Huggins interaction parameter χ. For adsorption to occur, a minimum energy of adsorption per segment χ^s is required. When a polymer molecule adsorbs on a surface, it loses configurational entropy and this must be compensated by an adsorption energy χ^s per segment. This is schematically shown in Fig. 6.2, where the adsorbed amount Γ is plotted versus χ^s The minimum value of χ^s can be very small ($< 0.1kT$) since a large number of segments per molecule are adsorbed. For a polymer with, say, 100 segments and 10 % of these are in trains, the adsorption energy per molecule now reaches $1kT$ (with $\chi^s = 0.1kT$). For 1,000 segments, the adsorption energy per molecule is now $10kT$.

As mentioned above, homopolymers are not the most suitable for stabilizing dispersions. For strong adsorption, one needs the molecule to be "insoluble" in the medium and to have strong affinity ("anchoring") to the surface. For stabilization, one needs the molecule to be highly soluble in the medium and strongly solvated by its molecules; this requires a Flory–Huggins interaction parameter less than 0.5. The above opposing effects can be resolved by introducing "short" blocks into the

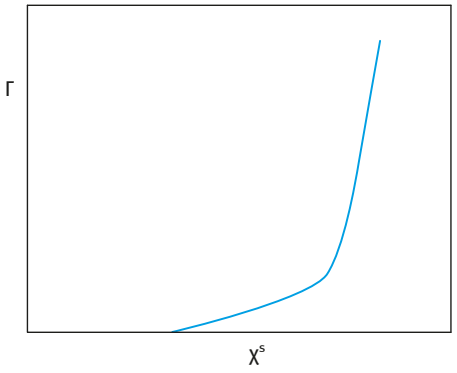

Fig. 6.2: Variation of adsorption amount Γ with adsorption energy per segment χ^s.

molecule which are insoluble in the medium and have a strong affinity to the surface, as for example partially hydrolysed polyvinyl acetate (88 % hydrolysed, i.e. with 12 % acetate groups), usually referred to as polyvinyl alcohol (PVA),

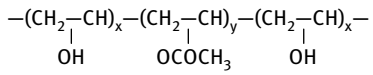

As mentioned above, these requirements are better satisfied using A–B, A–B–A and BA_n graft copolymers. B is chosen to be highly insoluble in the medium and it should have high affinity to the surface. This is essential to ensure strong "anchoring" to the surface (irreversible adsorption). A is chosen to be highly soluble in the medium and strongly solvated by its molecules. The Flory–Huggins χ parameter can be applied in this case. For a polymer in a good solvent, χ has to be lower than 0.5; the smaller the χ value the better the solvent for the polymer chains. Examples of B for hydrophobic particles in aqueous media are polystyrene, polymethylmethacrylate. Examples of A in aqueous media are polyethylene oxide, polyacrylic acid, polyvinyl pyrrolidone and polysaccharides. For nonaqueous media such as hydrocarbons, the A chain(s) could be poly(12-hydroxystearic acid).

For a full description of polymer adsorption one needs to obtain information on the following:

(i) The amount of polymer adsorbed Γ (in mg or mol) per unit area of the particles. It is essential to know the surface area of the particles in the suspension. Nitrogen adsorption on the powder surface may give such information (by application of the BET equation) provided there will be no change in area on dispersing the particles in the medium. For many practical systems, a change in surface area may occur on dispersing the powder, in which case one has to use dye adsorption to measure the surface area (some assumptions have to be made in this case).

(ii) The fraction of segments in direct contact with the surface, i.e. the fraction of segments in trains p

$$p = \frac{\text{number of segments in direct contact with the surface}}{\text{total number}}.$$

(iii) The distribution of segments in loops and tails, $\rho(z)$, which extend in several layers from the surface. $\rho(z)$ is usually difficult to obtain experimentally although recently application of small angle neutron scattering could obtain such information. An alternative and useful parameter for assessing "steric stabilization" is the hydrodynamic thickness, δ_h (thickness of the adsorbed or grafted polymer layer plus any contribution from the hydration layer). Several methods can be applied to measure δ_h as will be discussed below.

In studying polymeric surfactant adsorption, one must consider several variables such as effect of its molar mass, structure (segment distribution of the A and B blocks), effect of temperature and solvency of the medium for the stabilizing chains, effect of addition of other components in the formulation (such as electrolyte and anti-freeze), effect of the nature of the substrate (hydrophobic or hydrophilic), etc. This large number of variables requires a great deal of experimental measurements which become very time consuming. For these reasons, several theoretical treatments of polymer adsorption have been developed (see below) for prediction of some of the above mentioned variables. These theories allow one to focus on the most important variables that affect polymeric surfactant adsorption.

6.3 Theories of polymer adsorption

Two main approaches have been developed to treat the problem of polymer adsorption:

(i) Random walk approach; this is based on Flory's treatment of the polymer chain in solution; the surface was considered a reflecting barrier.
(ii) Statistical mechanical approach; the polymer configuration was treated as being made of three types of structures: trains, loops and tails, each having a different energy state.

The random walk approach is based on the random walk concept which was originally applied to the problem of diffusion and later adopted by Flory to deduce the conformations of macromolecules in solution. The earliest analysis was by Simha, Frisch and Eirich [6] who neglected excluded volume effects and treated the polymer as a random walk. Basically, the solution was represented by a three-dimensional lattice and the surface by a two-dimensional lattice. The polymer was represented by a realization of a random walk on the lattice. The probabilities of performing steps in different directions were considered to be the same except at the interface which acts as a reflecting barrier. The polymer molecules were, therefore, effectively assumed to be adsorbed with large loops protruding into the solvent and with few segments actually attached to the surface, unless the segment-surface attractive forces were very high. This theory predicts an isotherm for flexible macromolecules that is considerably different from the Langmuir-type isotherm. The number of attached segments per chain is proportional to $n^{1/2}$, where n is the total number of segments. Increasing the molecular weight results in increased adsorption, except for strong chain interaction with the surface.

This approach has been criticized by Silberberg [7] and by Di Marzio [8]. One of the major problems was the use of a reflecting barrier as the boundary condition, which meant over counting the number of distinguishable conformations. To overcome this problem, Di Marzio and McCrackin [9] used a Monte Carlo method to calculate the

average number of contacts of the chain with the surface, the end-to-end length and distribution of segments $\rho(z)$ with respect to the distance z from the surface, as a function of chain length of the polymer and the attractive energy of the surface. The same method was also used by Clayfield and Lumb [10, 11].

The statistical mechanical approach is a more realistic model for the problem of polymer adsorption since it takes into account the various interactions involved. This approach was first used by Silberberg [12] who treated separately the surface layer, which contains adsorbed units (trains), and the adjacent layer in solution (loops or tails). The units in each layer were considered to be in two different energy states and partition functions were used to describe the system. The units close to the surface are adsorbed with an internal partition function determined by the short range forces between the segments and the surface, whereas the units in loops and tails were considered to have an internal partition function equivalent to the segments in the bulk. By equating the chemical potential of macromolecules in the adsorbed state and in bulk solution, the adsorption isotherm could be determined. In this treatment, Silberberg [12] assumed a narrow distribution of loop sizes and predicted small loops for all values of the adsorption energy. Later, the loop size distribution was introduced by Hoeve et al. [13–15] and this theory predicted large loops for small adsorption free energies and small loops and more units adsorbed for larger adsorption free energies when the chains are sufficiently flexible. Most of these theories considered the case of an isolated polymer molecule at an interface, i.e. under conditions of low surface coverage, θ. These theories were extended by Silberberg [16] and Hoeve [17, 18] to take into account the lateral interaction between the molecules on the surface, i.e. high surface coverage. These theories also considered the excluded volume effect, which reduces the number of configurations available for interacting chains near the surface. Excluded volume effects are strongly dependent on the solvent as is the case for chains in solution. Some progress has been made in the analysis of the problem of multilayer adsorption [17, 18].

One feature of an adsorbed layer that is important in the theory of steric stabilization is the actual segment distribution normal to the interface. Hoeve [17, 18] was the first to calculate this quantity for an adsorbed homopolymer of loops and tails, using random flight statistics. He showed that at a distance from the interface corresponding to the thickness of the trains, there was a discontinuity in the distribution. Beyond this, the segment density falls exponentially with distance, as shown schematically in Fig. 6.3.

Similarly, Meier [19] developed an equation for the segment density distribution of a single terminally adsorbed tail. Hesselink [20, 21] has developed Meier's theory and given the segment density distribution for single tails, single loops, homopolymers and random copolymers, as illustrated in Fig. 6.4.

A useful model for treating polymer adsorption and configuration was suggested by Roe [22], Scheutjens and Fleer (SF theory) [23–26] that is referred to as the step-weighted random walk approach. In order to be able to describe all possible chain

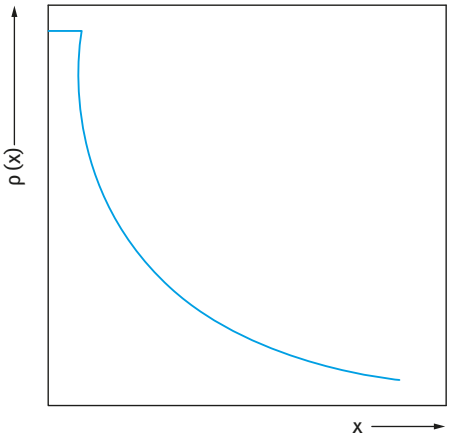

Fig. 6.3: Segment density–distance distribution.

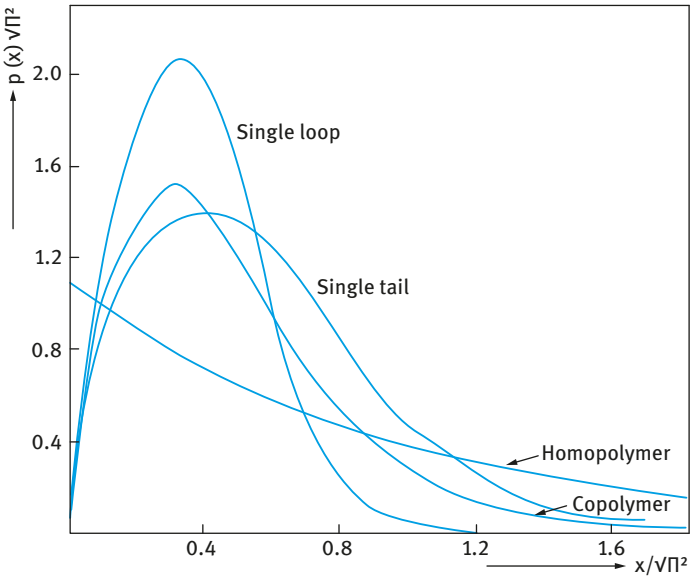

Fig. 6.4: Segment density distribution for single tails, single loops, homopolymers and random copolymers.

conformations, Scheutjens and Fleer [23–26] used a model of a quasi-crystalline lattice with lattice layers parallel to the surface. Starting from the surface the layers are numbered $I = 1, 2, 3, \ldots, M$, where M is a layer in bulk solution. All the lattice sites within one layer were considered to be energetically equivalent. The probability of finding any lattice site in layer I occupied by a segment was assumed to be equal to the volume fraction ϕ_I in this layer. The conformation probability and the free energy of mixing were calculated with the assumption of random mixing within each layer

(the Brag–Williams or mean field approximation). The energy for any segment is only determined by the layer number, and each segment can be assigned a weighting or Boltzmann factor p_i which depends only on the layer number. The partition functions were derived for the mixture of free and adsorbed polymer molecules, as well as for the solvent molecules. As mentioned before, all chain conformations were described as step-weighted random walks on a quasi-crystalline lattice which extends in parallel layers from the surface; this is schematically shown in Fig. 6.5.

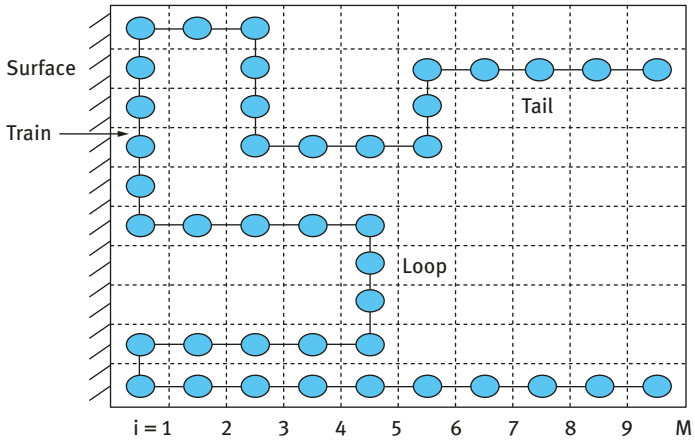

Fig. 6.5: Schematic representation of a polymer molecule adsorbing on a flat surface – quasi-crystalline lattice with segments filling layers that are parallel to the surface (random mixing of segments and solvent molecules in each layer is assumed).

The partition function is written in terms of a number of configurations. These were treated as connected sequences of segments. In each layer, random mixing between segments and solvent molecules was assumed (mean field approximation). Each step in the random walk was assigned a weighting factor p_i that consists of three contributions:

(i) an adsorption energy χ^s (which exists only for the segments that are near the surface);
(ii) configurational entropy of mixing (that exists in each layer);
(iii) segment–solvent interaction parameter χ (the Flory–Huggins interaction parameter; note that $\chi = 0$ for an athermal solvent; $\chi = 0.5$ for a θ-solvent).

The adsorption energy gives rise to a Boltzmann factor $\exp \chi_s$ in the weighting factor for the first layer, provided χ_s is interpreted as the adsorption energy difference (in units of kT) between a segment and a solvent molecule. The configurational entropy for the segment, as a part of the chain, is accounted for in the matrix procedure in which all possible chain conformations are considered. However, the configurational

entropy loss of the solvent molecule, going from a layer i with low solvent concentration to the bulk solution with a higher solvent concentration, has to be introduced in p_i. This entropy loss can be written as $\Delta s^0 = k \ln \phi_*^0/\phi_i^0$ per solvent molecule, where ϕ_i^0 and ϕ_*^0 are the solvent volume fractions in layer I and in bulk solution respectively. This change is equivalent to introducing a Boltzmann factor $\exp(-\Delta s^0/k) = \phi_i^0/\phi_*^0$ in the weighting factor p_i. The last contribution stems from the mixing energy of the exchange process. The transfer of a segment from the bulk solution to layer i is accompanied by an energy change (in units of kT) $\chi(\phi_i^0 - \phi_*^0)$, where χ is the Flory–Huggins segment solvent interaction parameter.

Fig. 6.6 shows typical adsorption isotherms plotted as surface coverage (in equivalent monolayers) versus polymer volume fraction ϕ_* in bulk solution (ϕ_* was taken to vary between 0 and 10^{-3} which is the normal experimental range).

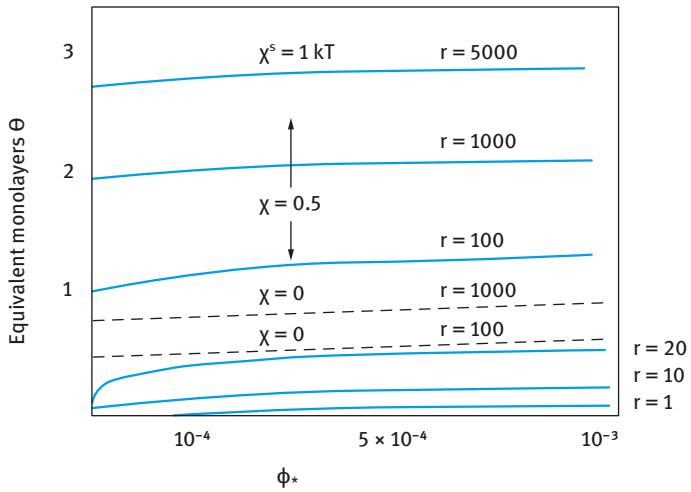

Fig. 6.6: Adsorption isotherms for oligomers and polymers in the dilute region based on the SF theory. Full curves $\chi = 0.5$; dashed curves $\chi = 0$.

The results in Fig. 6.6 show the effect of increasing the chain length r and effect of solvency (athermal solvent with $\chi = 0$ and theta solvent with $\chi = 0.5$). The adsorption energy χ^s was taken to be the same and equal to $1kT$. When $r = 1$, θ is very small and the adsorption increases linearly with increasing ϕ^* (Henry's type isotherm). On the other hand, when $r = 10$, the isotherm deviates greatly from a straight line and approaches a Langmuirian type. However, when $r \geq 20$, high affinity isotherms are obtained. This implies that the first added polymer chains are completely adsorbed, resulting in extremely low polymer concentration in solution (approaching zero). This explains the irreversibility of adsorption of polymeric surfactants with $r > 100$. The

adsorption isotherms with $r = 100$ and above are typical of those observed experimentally for most polymers that are not too polydisperse, i.e. showing a steep rise followed by a nearly horizontal plateau (which only increases few percent per decade increase of ϕ^*). In these dilute solutions, the effect of solvency is most clearly seen, with poor solvents giving the highest adsorbed amounts. In good solvents, θ is much smaller and levels off for long chains to attain an adsorption plateau which is essentially independent of molecular weight.

Some general features of the adsorption isotherms over a wide concentration range can be illustrated by using logarithmic scales for both θ and ϕ_* which highlight the behaviour in extremely dilute solutions. Such a presentation [25–27] is shown in Fig. 6.7.

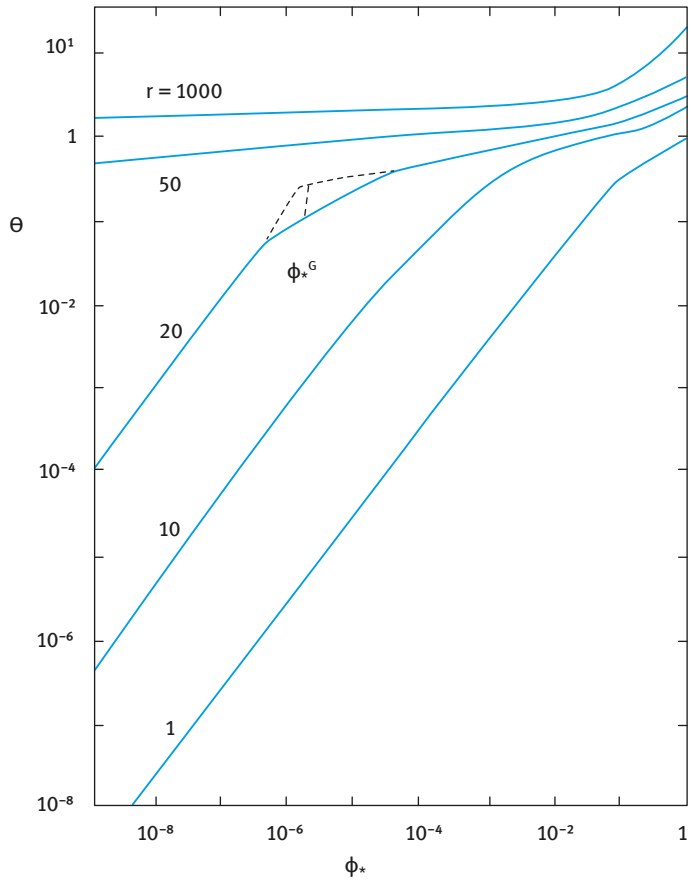

Fig. 6.7: Log-log presentation of adsorption isotherms of various r values, $\chi_S = 1; \chi = 0.5$. Hexagonal lattice.

These results show a linear Henry region followed by a pseudoplateau region. A transition concentration, ϕ_*^c, can be defined by extrapolation of the two linear parts. ϕ_*^c decreases exponentially with increasing chain length and when $r = 50$, ϕ_*^c is so small (10^{-12}) that it does not appear within the scale shown in Fig. 6.7. With $r = 1{,}000$, ϕ_*^c reaches the ridiculously low value of 10^{-235}. The region below ϕ_*^c is the Henry region where the adsorbed polymer molecules behave essentially as isolated molecules. The representation in Fig. 6.7 also answers the question of reversibility versus irreversibility for polymer adsorption. When $r > 50$, the pseudoplateau region extends down to very low concentration ($\phi_*^c = 10^{-12}$) and this explains why one cannot easily detect any desorption upon dilution. Clearly, if such extremely low concentrations can be reached, desorption of the polymer may take place. Thus, the lack of desorption (sometimes referred to as irreversible adsorption) is due to the fact that the equilibrium between adsorbed and free polymer is shifted far in favour of the surface because of the high possible number of possible attachments per chain.

Another point that emerges from the SF theory is the difference in shape between the experimental and theoretical adsorption isotherms in the low concentration region. The experimental isotherms are usually rounded, whereas those predicted from theory are flat. This is accounted for in terms of the molecular weight distribution (polydispersity) which is encountered with most practical polymers. This effect has been explained by Cohen-Stuart et al. [27]. With polydisperse polymers, the larger molecular weight fractions adsorb preferentially over the smaller ones. At low polymer concentrations, nearly all polymer fractions are adsorbed leaving a small fraction of the polymer with the lowest molecular weights in solution. As the polymer concentration is increased, the higher molecular weight fractions displace the lower ones on the surface, which are now released in solution, thus shifting the molecular weight distribution in solution to lower values. This process continues with a further increase in polymer concentration leading to fractionation whereby the higher molecular weight fractions are adsorbed at the expense of the lower fractions which are released to the bulk solution. However, in very concentrated solutions, monomers adsorb preferentially with respect to polymers and short chains with respect to larger ones. This is due to the fact that in this region, the conformational entropy term predominates over the free energy, disfavouring the adsorption of long chains.

According to the SF theory, the bound fraction p and the direct surface coverage θ_1 depend on the chain length for the same volume fraction. This is illustrated in Fig. 6.8 which shows the adsorbed amount Γ (Fig. 6.8 (a)), surface coverage θ (Fig. 6.8 (b)) and fraction of adsorbed segments $p = \theta/\Gamma$ (Fig. 6.8 (c)) as a function of volume fraction ϕ_*.

In the Henry region ($\phi_* < \phi_*^c$), p is rather high and independent of chain length for $r \geq 20$. In this region the molecules lie nearly flat on the surface, with 87 % of segments in trains. At the other end of the concentration range ($\phi_* = 1$), p is proportional to $r^{-1/2}$. At intermediate concentrations p is within these two extremes. With increasing polymer concentration, the adsorbed molecules become gradually more extended (lower p) until at very high ϕ_* values they become Gaussian at the interface. In better

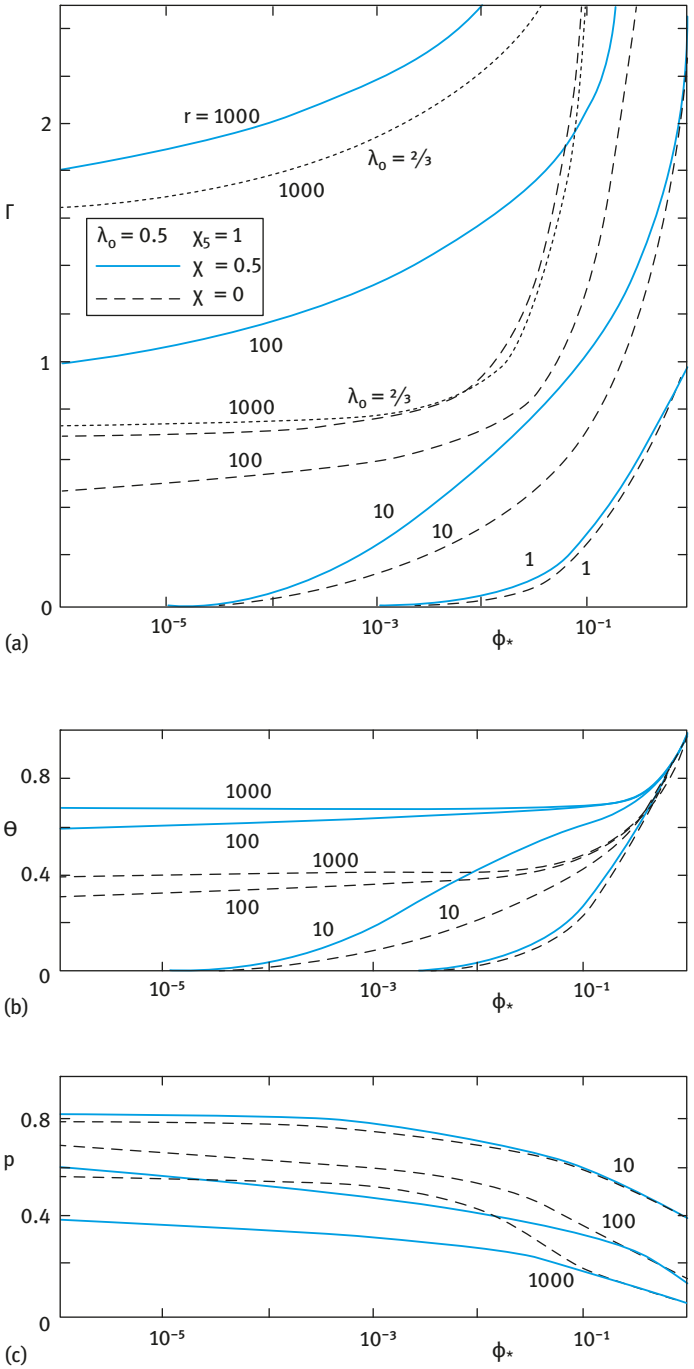

Fig. 6.8: Adsorbed amount Γ (a), surface coverage θ (b) and fraction of adsorbed segments $p = \theta/\Gamma$ (c) as a function of volume fraction ϕ_*. Full lines for a θ-solvent ($\chi = 0.5$), broken line for an athermal solvent ($\chi = 0$).

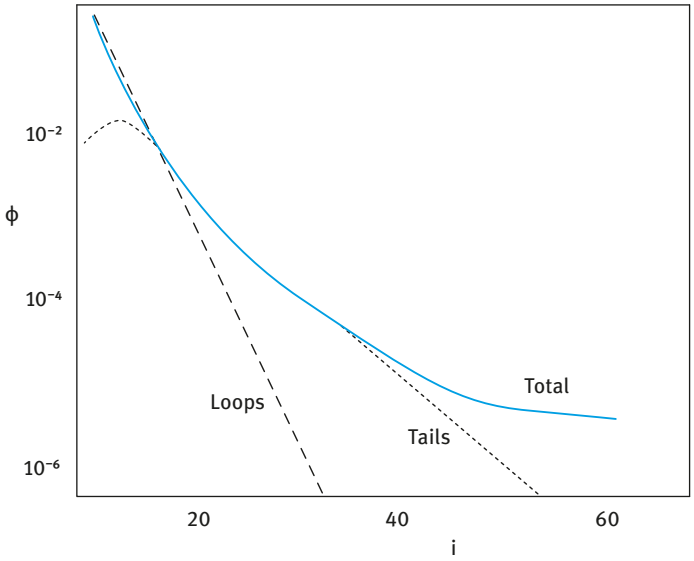

Fig. 6.9: Loop, tail and total segment profile according to the SF theory.

solvents the direct surface coverage is lower due to the stronger repulsion between the segments. This effect is more pronounced if the surface concentration differs strongly from the solution concentration. If the adsorption is small, the effect of the excluded volume effect (and therefore of χ) is rather weak; the same applies if both the concentrations in the bulk solution and near the surface are high. Both θ_1 and θ decrease with increasing solvent power (decreasing χ) but the effect is stronger for θ than for θ_1, resulting in a higher bound fraction (thus flatter chains) from better solvents at the same solution concentration.

The structure of the adsorbed layer is described in terms of the segment density distribution. As an illustration, Fig. 6.9 shows some calculations using the SF theory for loops and tails with $r = 1{,}000$, $\phi^* = 10^{-6}$ and $\chi = 0.5$. In this example, 38 % of the segments are in trains, 55.5 % in loops and 6.5 % in tails. This theory demonstrates the importance of tails, which dominate the total distribution in the outer region.

6.4 Scaling theory for polymer adsorption

De Gennes [28] introduced a simple theory for terminally attached polymer chains on a flat surface [29]. He considered the chain to be broken up into "blobs" as illustrated in Fig. 6.10.

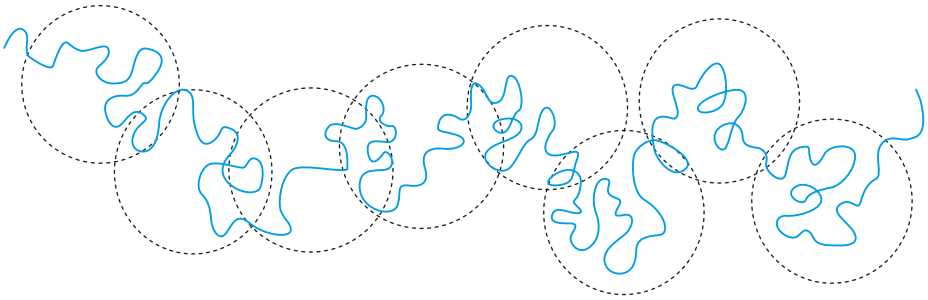

Fig. 6.10: Schematic representation of the blob model according to de Gennes [28].

Inside the blob the chain is self-avoiding but the blobs themselves can overlap and are essentially ideal. For g monomers per blob, the blob size $\xi \approx g^{\nu/2} \approx g^{2/3}$. If the blobs can overlap then $R \approx \xi^{0.5}$ and,

$$R \approx n^{0.5} g^{0.1}. \tag{6.1}$$

For an ideal chain, $g = 1$ and for a chain with full excluded volume $n = g$, which corresponds to the two extreme cases of an ideal and a swollen chain.

A schematic representation of the blob presentation of terminally attached chains is given in Fig. 6.11.

If each blob contains a self-avoiding walk of g monomers, then the blob size is given by,

$$\xi = g^{1/3}. \tag{6.2}$$

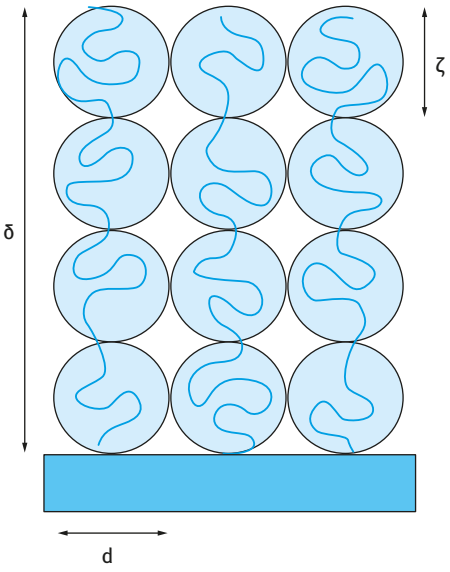

Fig. 6.11: Schematic representation of a terminally attached chain d by blobs of size ξ.

For N monomers the brush length δ is given by,

$$\delta = \left(\frac{N}{g}\right)\xi. \tag{6.3}$$

The assumption is made that the blob size is directly related to the grafted amount σ so that,

$$\sigma = \frac{1}{\xi^2}. \tag{6.4}$$

Combining equations (6.2)–(6.4),

$$\delta = N\sigma^{1/3}. \tag{6.5}$$

The above analysis predicts that the brush length is linear in chain length. This is clearly true for a rod normal to the surface but suggests that chains closely grafted together on a surface are very strongly stretched. A more sophisticated approach which confirms this result predicts that the brush volume fraction profile is parabolic [30].

6.5 Experimental techniques for studying polymeric surfactant adsorption

As mentioned above, for full characterization of polymeric surfactant adsorption one needs to determine three parameters:

(i) The adsorbed amount Γ (mg m^{-2} or mol m^{-2}) as a function of equilibrium concentration C_{eq}, i.e. the adsorption isotherm.
(ii) The fraction of segments in direct contact with the surface p (number of segments in trains relative to the total number of segments).
(iii) The segment density distribution $\rho(z)$ or the hydrodynamic adsorbed layer thickness δ_h.

It is important to obtain the adsorption parameters as a function of the important variables of the system:

(i) Solvency of the medium for the chain which can be affected by temperature, addition of salt or a nonsolvent. The Flory–Huggins interaction parameter χ could be separately measured.
(ii) The molecular weight of the adsorbed polymer.
(iii) The affinity of the polymer to the surface as measured by the value of χ^s, the segment-surface adsorption energy.
(iv) The structure of the polymer; this is particularly important for block and graft copolymers.

6.5.1 Measurement of the adsorption isotherm

This is by far the easiest to obtain. One measures the polymeric surfactant concentration before (C_{initial}, C_1) and after ($C_{\text{equilibrium}}$, C_2)

$$\Gamma = \frac{(C_1 - C_2)V}{A}, \tag{6.6}$$

where V is the total volume of the solution and A is the specific surface area ($m^2\ g^{-1}$). It is necessary in this case to separate the particles from the polymer solution after adsorption. This could be carried out by centrifugation and/or filtration. One should make sure that all particles are removed. To obtain this isotherm, one must develop a sensitive analytical technique for determining the polymeric surfactant concentration in the ppm range. It is essential to follow the adsorption as a function of time to determine the time required to reach equilibrium. For some polymer molecules such as polyvinyl alcohol, PVA, and polyethylene oxide, PEO, (or blocks containing PEO), analytical methods based on complexation with iodine/potassium iodide or iodine/boric acid potassium iodide have been established. For some polymers with specific functional groups, spectroscopic methods may be applied, e.g. UV, IR or fluorescence spectroscopy. A possible method is to measure the change in refractive index of the polymer solution before and after adsorption. This requires very sensitive refractometers. High resolution NMR has been recently applied since the polymer molecules in the adsorbed state are in a different environment than those in the bulk. The chemical shift of functional groups within the chain are different in these two environments. This has the attraction of measuring the amount of adsorption without separating the particles.

6.5.2 Measurement of the fraction of segments *p*

The fraction of segments in direct contact with the surface can be directly measured using spectroscopic techniques:

(i) IR if there is specific interaction between the segments in trains and the surface, e.g. polyethylene oxide on silica from nonaqueous solutions [31, 32].
(ii) Electron spin resonance (ESR); this requires labelling of the molecule [33].
(iii) NMR, pulse gradient or spin-echo NMR. This method is based on the fact that the segments in trains are "immobilized" and hence they have lower mobility than those in loops and tails [34].

An indirect method of determining p is to measure the heat of adsorption ΔH using microcalorimetry [35]. One should then determine the heat of adsorption of a monomer H_m (or molecule representing the monomer, e.g. ethylene glycol for PEO); p is then given by the equation,

$$p = \frac{\Delta H}{H_m n}, \tag{6.7}$$

where n is the total number of segments in the molecule.

The above indirect method is not very accurate and can only be used in a qualitative sense. It also requires very sensitive enthalpy measurements (e.g. using an LKB microcalorimeter).

6.5.3 Determination of the segment density distribution $\rho(z)$ and adsorbed layer thickness δ_h

The segment density distribution $\rho(z)$ is given by the number of segments parallel to the surface in the z-direction. Three direct methods can be applied for determining adsorbed layer thickness: ellipsometry, attenuated total reflection (ATR) and neutron scattering. Both ellipsometry and ATR [36] depend on the difference between refractive indices between the substrate, the adsorbed layer and bulk solution and they require a flat reflecting surface. Ellipsometry [36] is based on the principle that light undergoes a change in polarizability when it is reflected at a flat surface (whether covered or uncovered with a polymer layer).

The above limitations when using ellipsometry or ATR are overcome by the application technique of neutron scattering, which can be applied to both flat surfaces as well as particulate dispersions. The basic principle of neutron scattering is to measure the scattering due to the adsorbed layer, when the scattering length density of the particle is matched to that of the medium (the so-called "contrast-matching" method). Contrast matching of particles and medium can be achieved by changing the isotopic composition of the system (using deuterated particles and a mixture of D_2O and H_2O). It was used for measuring the adsorbed layer thickness of polymers, e.g. PVA or poly(ethylene oxide) (PEO) on polystyrene latex [37]. Apart from obtaining δ, one can also determine the segment density distribution $\rho(z)$.

The above technique of neutron scattering clearly gives a quantitative picture of the adsorbed polymer layer. However, its application in practice is limited, since one needs to prepare deuterated particles or polymers for the contrast matching procedure. The practical methods for the determination of the adsorbed layer thickness are mostly based on hydrodynamic methods. Several methods may be applied to determine the hydrodynamic thickness of adsorbed polymer layers of which viscosity, sedimentation coefficient (using an ultracentrifuge) and dynamic light scattering measurements are the most convenient. A less accurate method is from zeta potential measurements.

The viscosity method [38] depends on measuring the increase in the volume fraction of the particles as a result of the presence of an adsorbed layer of thickness δ_h. The volume fraction of the particles ϕ plus the contribution of the adsorbed layers is usually referred to as the effective volume fraction ϕ_{eff}. Assuming the particles be-

have as hard spheres, then the measured relative viscosity η_r is related to the effective volume fraction by the Einstein equation, i.e.,

$$\eta_r = 1 + 2.5\phi_{eff}. \tag{6.8}$$

ϕ_{eff} and ϕ are related from simple geometry by,

$$\phi_{eff} = \phi\left[1 + \left(\frac{\delta_h}{R}\right)\right]^3, \tag{6.9}$$

where R is the particle radius. Thus, from a knowledge of η_r and ϕ one can obtain δ_h using the above equations.

The sedimentation method depends on measuring the sedimentation coefficient (using an ultracentrifuge) of the particles S_0' (extrapolated to zero concentration) in the presence of the polymer layer [39]. Assuming the particles obey Stokes' law, S_0' is given by the expression,

$$S_0' = \frac{(4/3)\pi R^3(\rho - \rho_s) + (4/3)\pi[(R + \delta_h)^3 - R^3](\rho_s^{ads} - \rho_s)}{6\pi\eta(R + \delta_h)}, \tag{6.10}$$

where ρ and ρ_s are the mass density of the solid and solution phase respectively, and ρ^{ads} is the average mass density of the adsorbed layer which may be obtained from the average mass concentration of the polymer in the adsorbed layer.

In order to apply the above methods, one should use a dispersion with monodisperse particles with a radius that is not much larger than δ_h. Small model particles of polystyrene may be used.

A relatively simple sedimentation method for determining δ_h is the slow speed centrifugation applied by Garvey et al. [39]. Basically, a stable monodisperse dispersion is slowly centrifuged at low g values ($< 50g$) to form a close-packed (hexagonal or cubic) lattice in the sediment. From a knowledge of ϕ and the packing fraction (0.74 for hexagonal packing), the distance of separation between the centre of two particles R_δ may be obtained, i.e.,

$$R_\delta = R + \delta_h = \left(\frac{0.74V\rho_1R^3}{W}\right), \tag{6.11}$$

where V is the sediment volume, ρ_1 is the density of the particles and W their weight.

The most rapid technique for measuring δ_h is photon correlation spectroscopy (PCS) (sometime referred to as quasi-elastic light scattering) which allows one to obtain the diffusion coefficient of the particles with and without the adsorbed layer (D_δ and D respectively). This is obtained from the measurement of the intensity fluctuation of scattered light as the particles undergo Brownian diffusion [40]. When a light beam (e.g. monochromatic laser beam) passes through a dispersion, an oscillating dipole is induced in the particles, thus re-radiating the light. Due to the random arrangement of the particles (which are separated by a distance comparable to the wavelength of the light beam, i.e. the light is coherent with the interparticle distance), the intensity

of the scattered light will, at any instant, appear as random diffraction or a "speckle" pattern. As the particles undergo Brownian motion, the random configuration of the speckle pattern change. The intensity at any one point in the pattern will, therefore, fluctuate such that the time taken for an intensity maximum to become a minimum (i.e. the coherence time) corresponds approximately to the time required for a particle to move one wavelength. Using a photomultiplier of active area about the size of a diffraction maximum, i.e. approximately one coherence area, this intensity fluctuation can be measured. A digital correlator is used to measure the photocount or intensity correlation function of the scattered light. The photocount correlation function can be used to obtain the diffusion coefficient D of the particles. For monodisperse non-interacting particles (i.e. at sufficient dilution), the normalized correlation function $[g^{(1)}(\tau)]$ of the scattered electric field is given by the equation,

$$[g^{(1)}(\tau)] = \exp -(\Gamma\tau), \tag{6.12}$$

where τ is the correlation delay time and Γ is the decay rate or inverse coherence time. Γ is related to D by the equation,

$$\Gamma = DK^2, \tag{6.13}$$

where K is the magnitude of the scattering vector that is given by,

$$K = \left(\frac{4n}{\lambda_0}\right)\sin\left(\frac{\theta}{2}\right), \tag{6.14}$$

where n is the refractive index of the solution, λ is the wavelength of light in vacuum and θ is the scattering angle.

From D, the particle radius R is calculated using the Stokes–Einstein equation,

$$D = \frac{kT}{6\pi\eta R}, \tag{6.15}$$

where k is the Boltzmann constant and T is the absolute temperature. For a polymer coated particle, R is denoted R_δ, which is equal to $R + \delta_h$. Thus, by measuring D_δ and D, one can obtain δ_h. It should be mentioned that the accuracy of the PCS method depends on the ratio of δ_δ/R, since δ_h is determined by difference. Since the accuracy of the measurement is ±1 %, δ_h should be at least 10 % of the particle radius. This method can only be used with small particles and reasonably thick adsorbed layers.

Electrophoretic mobility, u, measurements can also be applied to measure δ_h [41]. From u, the zeta potential ζ, i.e. the potential at the slipping (shear) plane of the particles can be calculated. Adsorption of a polymer causes a shift in the shear plane from its value in the absence of a polymer layer (which is close to the Stern plane) to a value that depends on the thickness of the adsorbed layer. Thus by measuring ζ in the presence (ζ_δ) and absence (ζ) of a polymer layer, one can estimate δ_h. Assuming that the thickness of the Stern plane is Δ, then ζ_δ may be related to the ζ (which may be assumed to be equal to the Stern potential ψ_d) by the equation,

$$\tanh\left(\frac{e\psi_\delta}{4kT}\right) = \tanh\left(\frac{e\zeta}{4kT}\right)\exp[-\kappa(\delta_h - \Delta)], \tag{6.16}$$

where κ is the Debye parameter that is related to electrolyte concentration and valency.

It should be mentioned that the value of δ_h calculated using the above simple equation shows a dependency on electrolyte concentration and hence the method cannot be used in a straightforward manner. Cohen-Stuart et al. [41] showed that the measured electrophoretic thickness δ_e approaches δ_h only at low electrolyte concentrations. Thus, to obtain δ_h from electrophoretic mobility measurements, results should be obtained at various electrolyte concentrations and δ_e should be plotted versus the Debye length $(1/\kappa)$ to obtain the limiting value at high $(1/\kappa)$ (i.e. low electrolyte concentration) which now corresponds to δ_h.

6.5.4 Examples of the adsorption isotherms of nonionic polymeric surfactants

Fig. 6.12 shows the adsorption isotherms for PEO with different molecular weights on PS (at room temperature. It can be seen that the amount adsorbed in mg m^{-2} increases with increasing polymer molecular weight [42]. Fig. 6.13 shows the variation of the hydrodynamic thickness δ_h with molecular weight M. δ_h shows a linear increase with log M. δ_h increases with n, the number of segments in the chain according to,

$$\delta_h \approx n^{0.8}. \tag{6.17}$$

Fig. 6.14 shows the adsorption isotherms of PVA with various molecular weights on PS latex (at 25 °C) [43]. The polymers were obtained by fractionation of a commercial sample of PVA with an average molecular weight of 45,000. The polymer also contained 12 % vinyl acetate groups. As with PEO, the amount of adsorption increases with increasing M. The isotherms are also of the high affinity type. Γ at the plateau increases linearly with $M^{1/2}$.

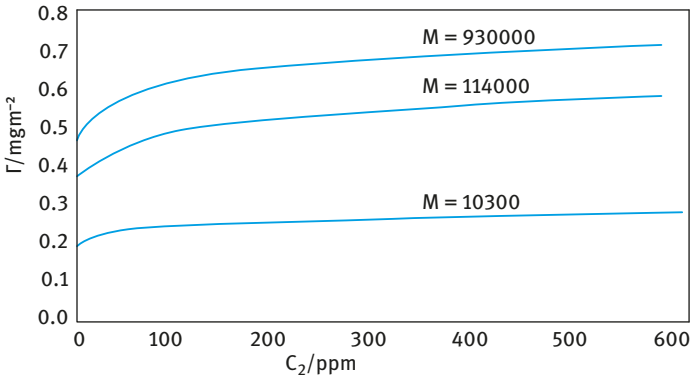

Fig. 6.12: Adsorption isotherms for PEO on PS.

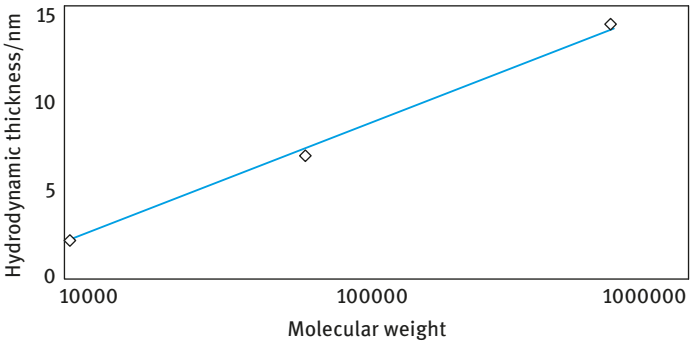

Fig. 6.13: Hydrodynamic thickness of PEO on PS as a function of the molecular weight.

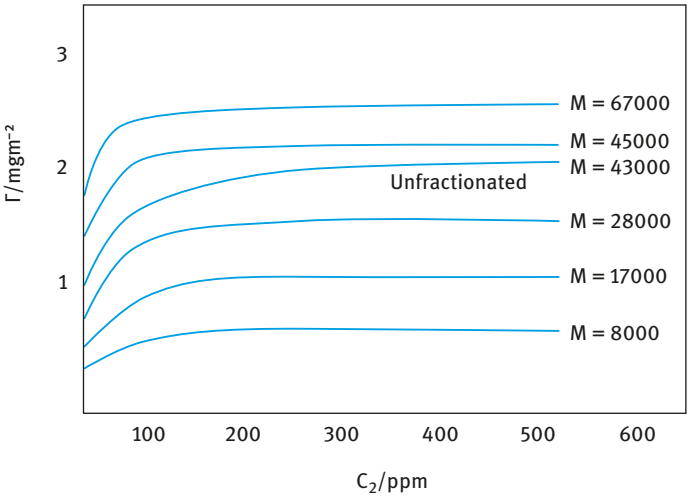

Fig. 6.14: Adsorption isotherms of PVA with different molecular weights on polystyrene latex at 25 °C.

The hydrodynamic thickness was determined using PCS and the results are given below.

M	67,000	43,000	28,000	17,000	8,000
δ_h (nm)	25.5	19.7	14.0	9.8	3.3

δ_h seems to increase linearly with increasing molecular weight.

The effect of solvency on adsorption was investigated by increasing the temperature (the PVA molecules are less soluble at higher temperature) or addition of electrolyte (KCl) [44, 45]. The results are shown in Fig. 6.15 and 6.16 for M = 65,100. As can be

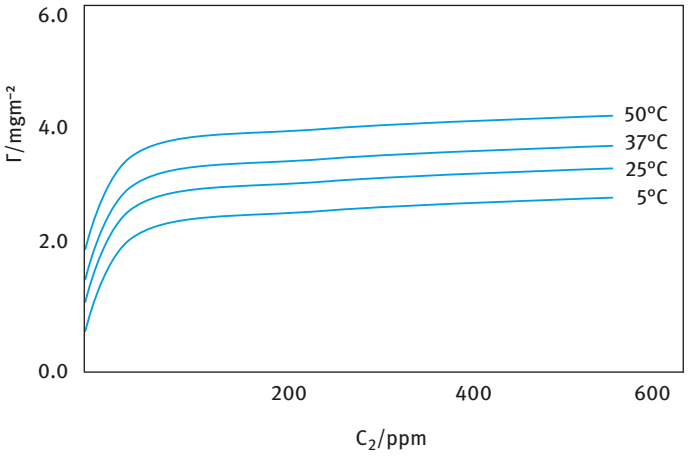

Fig. 6.15: Influence of temperature on adsorption.

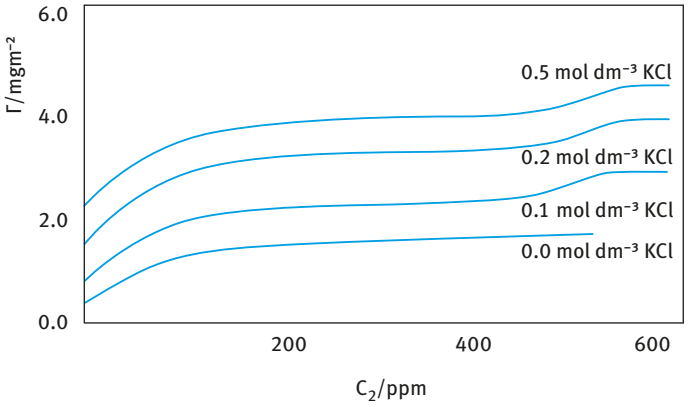

Fig. 6.16: Influence of addition of KCl on adsorption.

seen from Fig. 6.15, increasing temperature results in a reduction of solvency of the medium for the chain (due to breakdown of hydrogen bonds) and this results in an increase in the amount adsorbed. Addition of KCl (which reduces the solvency of the medium for the chain) results in an increase in adsorption (as predicted by theory).

The adsorption of block and graft copolymers is more complex since the intimate structure of the chain determines the extent of adsorption [42]. Random copolymers adsorb in an intermediate way to that of the corresponding homopolymers. Block copolymers retain the adsorption preference of the individual blocks. The hydrophilic block (e.g. PEO), the buoy, extends away from the particle surface into the bulk solution, whereas the hydrophobic anchor block (e.g. PS or PPO) provides firm attachment to the surface. Fig. 6.17 shows the theoretical prediction of diblock copolymer adsorp-

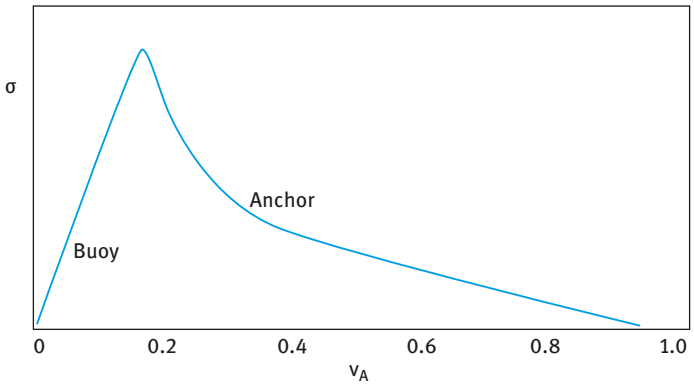

Fig. 6.17: Prediction of adsorption of diblock copolymer.

tion according to the Scheutjens and Fleer theory. The surface density σ is plotted versus the fraction of anchor segments v_A. The adsorption depends on the anchor/buoy composition.

The amount of adsorption is higher than for homopolymers and the adsorbed layer thickness is more extended and dense. For a triblock copolymer A–B–A, with two buoy chains and one anchor chain, the behaviour is similar to that of diblock copolymers. This is shown in Fig. 6.18 for PEO–PPO–PEO block (Pluronic).

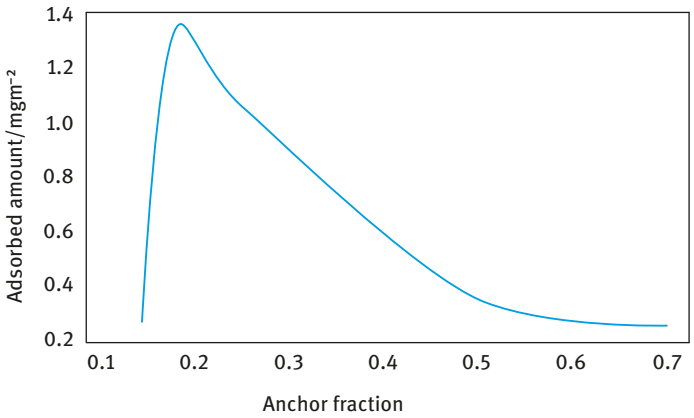

Fig. 6.18: Adsorbed amount (mg m^{-2}) versus fraction of anchor segment for an A–B–A triblock copolymer (PEO–PPO–PEO).

6.5.5 Adsorbed layer thickness results

Fig. 6.19 shows a plot of $\rho(z)$ against z for PVA (M = 37,000) adsorbed on deuterated PS latex in D_2O/H_2O.

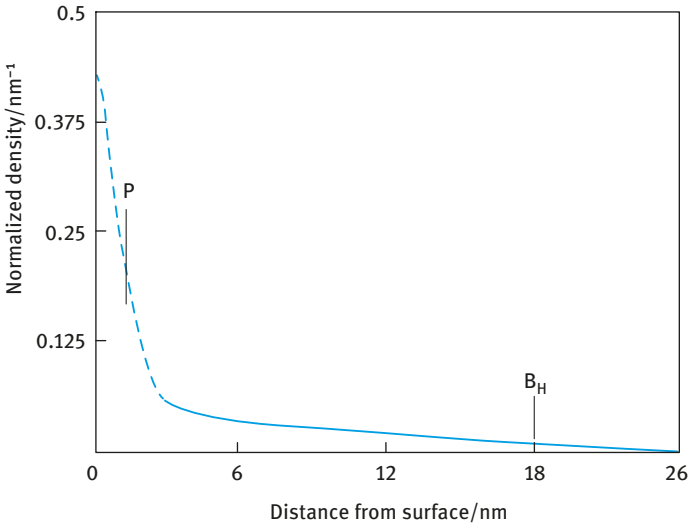

Fig. 6.19: Plot of $\rho(z)$ against z for PVA (M = 37,000) adsorbed on deuterated PS latex in D_2O/H_2O.

The results shows a monotonic decay of $\rho(z)$ with distance z from the surface and several regions may be distinguished. Close to the surface ($0 < z < 3$ nm), the decay in $\rho(z)$ is rapid and assuming a thickness of 1.3 nm for the bound layer, p was calculated to be 0.1, which is in close agreement with the results obtained using NMR measurements. In the middle region, $\rho(z)$ shows a shallow maximum followed by a slow decay which extends to 18 nm, i.e. close to the hydrodynamic layer thickness δ_h of the polymer chain (see below). δ_h is determined by the longest tails and is about 2.5 times the radius of gyration in bulk solution ($\approx$ 7.2 nm). This slow decay of $\rho(z)$ with z at long distances is in qualitative agreement with Scheutjens and Fleer's theory [23] which predicts the presence of long tails. The shallow maximum at intermediate distances suggests that the observed segment density distribution is a summation of a fast monotonic decay due to loops and trains together with the segment density for tails with a maximum density away from the surface. The latter maximum was clearly observed for a sample which had PEO grafted to a deuterated polystyrene latex [37] (where the configuration is represented by tails only).

The hydrodynamic thickness of block copolymers shows different behaviour from that of homopolymers (or random copolymers). Fig. 6.20 shows the theoretical prediction for the adsorbed layer thickness δ which is plotted as a function of ν_A.

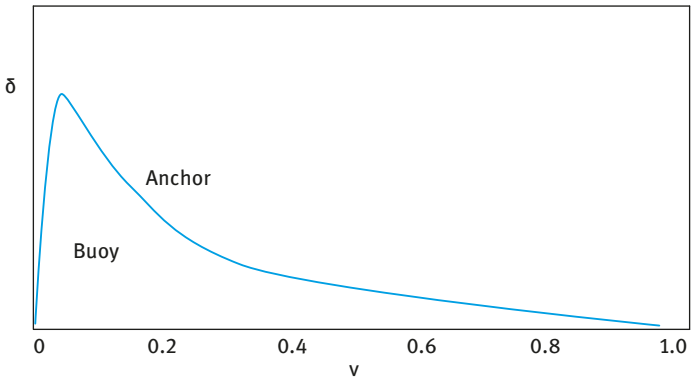

Fig. 6.20: Theoretical predictions of the adsorbed layer thickness for a diblock copolymer.

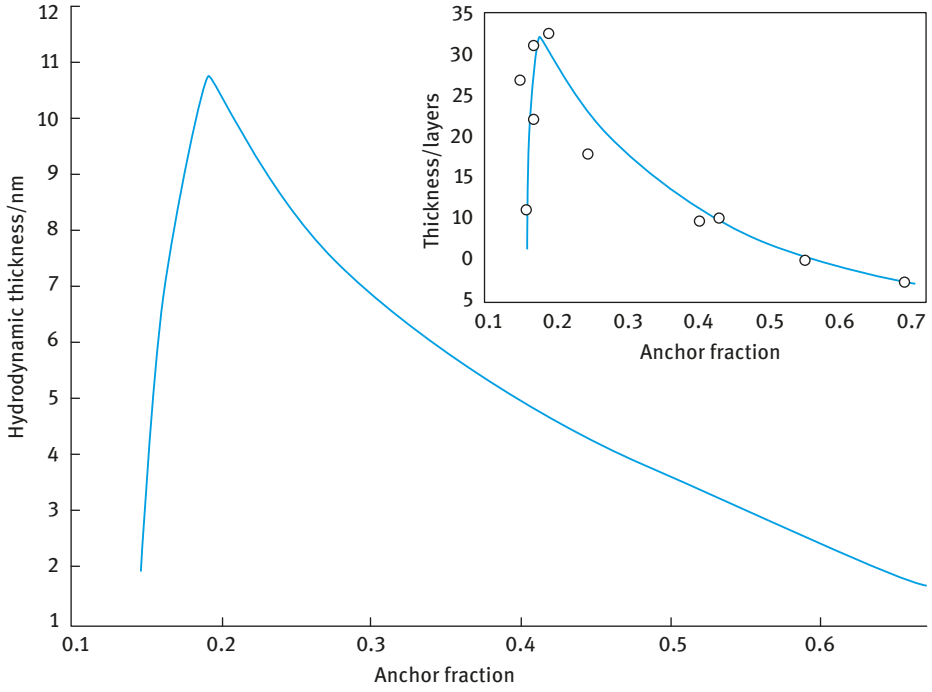

Fig. 6.21: Hydrodynamic thickness versus fraction of anchor segments v_A for PEO–PPO–PEO block copolymer onto polystyrene latex. Insert shows the mean field calculation of thickness versus anchor fraction using the SF theory.

Fig. 6.21 shows the hydrodynamic thickness versus fraction of anchor segments for an A–B–A block copolymer of (polyethylene oxide)-poly(propylene oxide)-poly(ethylene oxide) (PEO–PPO–PEO) [42] versus fraction of anchor segments. The theoretical (Scheutjens and Fleer) prediction of adsorbed amount and layer thickness versus fraction of anchor segments are shown in the inserts of Fig. 6.20. When there are two buoy blocks and a central anchor block, as in the above example, the A–B–A block shows similar behaviour to that of an A–B block. However, if there are two anchor blocks and a central buoy block, surface precipitation of the polymer molecule at the particle surface is observed and this is reflected in a continuous increase of adsorption with increasing polymer concentration as has been show for an A–B–A block of PPO–PEO–PPO [42].

6.6 Kinetics of polymer adsorption

The kinetics of polymer adsorption is a highly complex process. Several distinct processes can be distinguished, each with a characteristic timescale [42]. These processes may occur simultaneously and hence it is difficult to separate them. The first process is the mass transfer of the polymer to the surface, which may be either diffusion or convection. Having reached the surface, the polymer must then attach itself to a surface site, which depends on any local activation energy barrier. Finally, the polymer will undergo large-scale rearrangements as it changes from its solution conformation to a "tail-train-loop" conformation. Once the polymer has reached the surface, the amount of adsorption increases with time. The increase is rapid at the beginning but subsequently slows as the surface becomes saturated. The initial rate of adsorption is sensitive to the bulk polymer solution concentration and molecular weight as well as the solution viscosity. Nevertheless, all the polymer molecules arriving at the surface tend to adsorb immediately. The concentration of unadsorbed polymer around the periphery of the forming layer (the surface polymer solution) is zero and, therefore the concentration of polymer in the interfacial region is significantly greater than the bulk polymer concentration. Mass transport is found to dominate the kinetics of adsorption until 75 % of full surface coverage. At higher surface coverage, the rate of adsorption decreases since the polymer molecules arriving at the surface cannot immediately adsorb. Over time, equilibrium is set up between this interfacial concentration of polymer and the concentration of polymer in the bulk. Given that the adsorption isotherm is of the high affinity type, no significant change in adsorbed amount is expected, even over decades of polymer concentration. If the surface polymer concentration increases towards that of the bulk solution, the rate of adsorption decreases because the driving force for adsorption (the difference in concentration between the surface and bulk solutions) decreases. Adsorption processes tend to be very rapid and an equilibrated polymer layer can form within several 1,000 s. However, desorption is a much slower process and this can take several years!

References

[1] Tadros T. Polymeric surfactants. Berlin: De Gruyter; 2017.
[2] Tadros T. Suspension concentrates. Berlin: De Gruyter; 2017.
[3] Tadros T. In: Holmberg K, editor. Novel Surfactants, New York: Marcel Dekker; 2003.
[4] Tadros TF. In: Buscall R, Corner T, Stageman JF, editors. Polymer colloids. London: Applied Sciences, Elsevier; 1985. p. 105.
[5] Jenkel E, Rumbach R. Z Elekrochem. 1951;55:612.
[6] Simha R, Frisch L, Eirich FR. J Phys Chem. 1953;57:584.
[7] Silberberg A. J Phys Chem. 1962;66:1872.
[8] Di Marzio EA. J Chem Phys. 1965;42:2101.
[9] Di Marzio EA, McCrakin FL. J Chem Phys. 1965;43:539.
[10] Clayfield EJ, Lumb EC. J Colloid Interface Sci. 1966;22:269, 285.
[11] Clayfield EJ, Lumb EC. Macromolecules. 1968;1:133.
[12] Silberberg A. J Chem Phys. 1968;48:2835.
[13] Hoeve CA, Di Marzio EA, Peyser P. J Chem Phys. 1965;42:2558.
[14] Hoeve CA. J Chem Phys. 1965;44:1505; 1966;47:3007.
[15] Hoeve CA. J Polym Sci. 1970;30:361; 1971;34:1.
[16] Silberberg A. J Colloid Interface Sci. 1972;38:217.
[17] Hoeve CAJ. J Chem Phys. 1965;44:1505.
[18] Hoeve CAJ. J Chem Phys. 1966;47:3007.
[19] Meier DJ. J Phys Chem. 1965;71:1861.
[20] Hesselink FT. J Phys Chem. 1969;73:3488.
[21] Hesselink FT. J Phys Chem. 1971;75:65.
[22] Roe RJ. J Chem Phys. 1974;60:4192.
[23] Scheutjens JMHM, Fleer GJ. J Phys Chem. 1979;83:1919.
[24] Scheutjens JMHM, Fleer GJ. J Phys Chem. 1980;84:178.
[25] Scheutjens JMHM, Fleer GJ. Adv Colloid Interface Sci. 1982;16:341.
[26] Fleer GJ, Cohen-Stuart MA, Scheutjens JMHM, Cosgrove T, Vincent B. Polymers at interfaces. London: Chapman and Hall; 1993.
[27] Cohen-Stuart MA, Scheutjens JMHM, Fleer GJ. J Polym Sci Polym Phys Ed. 1980;18:559.
[28] de Gennes PG. Scaling concepts of polymer physics. Ithaca: Cornell University Press; 1979.
[29] Cosgrove T. Polymers at interfaces. Oxford: Blackwell; 2005. Chapter 7.
[30] Milner ST. Science. 1991;251:905.
[31] Killmann E, Eisenlauer E, Horn MJ. Polymer Sci. Polymer Symposium. 1977;61:413.
[32] Fontana BJ, Thomas JR. J Phys Chem. 1961;65:480.
[33] Robb ID, Smith R. Eur Polym J. 1974;10:1005.
[34] Barnett KG, Cosgrove T, Vincent B, Burgess A, Crowley TL, Kims J, Turner JD, Tadros TF. Disc Faraday Soc. 1981;22:283.
[35] Cohen-Stuart MA, Fleer GJ, Bijesterbosch B. J Colloid Interface Sci. 1982;90:321.
[36] Abeles F. In: Passaglia E, Stromberg RR, Kruger J, editors. Ellipsometry in the measurement of surfaces and thin films. Nat. Bur. Stand. Misc. Publ. 256; 1964; p. 41.
[37] Cosgrove T, Crowley TL, Ryan T. Macromolecules. 1987;20:2879.
[38] Einstein A. Investigations on the theory of the Brownian movement. New York: Dover; 1906.
[39] Garvey MJ, Tadros TF, Vincent B. J Colloid Interface Sci. 1976;55:440.
[40] Pusey PN. In: Green JHS, Dietz R, editors. Industrial polymers: Characterisation by molecular weights. London: Transcripta Books; 1973.
[41] Cohen-Stuart MA, Mulder JW. Colloids and Surfaces. 1985;15:49.

[42] Obey TM, Griffiths PC. In: Goddard ED, Gruber JV, editors. Principles of polymer science and technology in cosmetics and personal care. New York: Marcel Dekker; 1999. Chapter 2.
[43] Garvey MJ, Tadros TF, Vincent B. J Colloid Interface Sci. 1974;49:57.
[44] van den Boomgaard T, King TA, Tadros TF, Tang H, Vincent B. J Colloid Interface Sci. 1978;61:68.
[45] Tadros TF, Vincent B. J Colloid Interface Sci. 1978:72:505.

7 Electrostatic stabilization of dispersions

7.1 Introduction

Formulations of the disperse type are stabilized against flocculation and/or coalescence by using ionic surfactants. These surfactants become adsorbed on the solid particles or oil droplets thus producing a charge on the surface [1–3]. This surface charge will be compensated in bulk solution by unequal distribution of counterions (with opposite sign to the surface charge) and co-ions (with the same charge sign as the surface). As will be discussed below, the surface and counter charges form an electrical double layer and when the suspension particles or emulsion droplets approach to a separation distance where the doubly layers begin to overlap, electrostatic repulsion is produced which counteracts the van der Waals attraction resulting in colloid stability.

This chapter will start with a section on the distribution of charge and potential at the solid/liquid or liquid/liquid interface and the structure of the electrical double layer. This is followed by a section on the origin of repulsion caused by double layer overlap with particular reference on the effect of surface (or zeta) potential, electrolyte concentration and valency of ions in the bulk liquid. The next section will deal with the origin of van der Waals attraction and its variation with particle or droplet separation, particle or droplet radius and the medium in which the particles or droplets are dispersed. The combination of double layer repulsion and van der Waals attraction forms the basis of the theory of colloid stability. The variation of electrostatic repulsion, van der Waals attraction and total interaction with separation distance produces energy–distance curves with an energy maximum (barrier) that prevents particle or droplet aggregation. The dependency of the energy barrier on surface potential, electrolyte concentration and valency can be used to distinguish between stable and unstable dispersions. A definition is given for the critical coagulation concentration (CCC) and its dependency on electrolyte valency. Finally, the criteria for effective stabilization using ionic surfactants will be given.

7.2 Distribution of charge and potential at the interface and structure of the electrical double layer

As mentioned above, ionic surfactants are often added as components to disperse systems, as wetting and dispersing agents for powders to produce solid/liquid dispersions (suspensions) and as emulsifiers. In most cases the surfactant also acts as stabilizer for the final suspension or emulsion. By adsorption at the solid/liquid or liquid/liquid interface the surfactant ions produce a charge (negative for anionic surfactants and positive for cationic surfactants) on the surface of the particle. As mentioned above, this charge is compensated by unequal distribution of counterions (with

https://doi.org/10.1515/9783110587944-008

opposite charge to the surface) and co-ions (with the same charge of the surface) forming an electrical double layer. In some cases the charge on the particle is produced by adsorption of anionic or cationic polyelectrolytes. An example is polyacrylates that are used to disperse many pigments such as titania.

Two main pictures have been suggested for describing the structure of the electrical double layer:

(i) The diffuse double layer described by Gouy and Chapman [4, 5] who assumed that the charge is smeared out over a plane surface immersed in an electrolyte solution. This surface has a uniform potential ψ_0 and the compensating ions are regarded as point charges immersed in a continuous dielectric medium. The surface charge σ_0 is compensated by unequal distribution of counterions (opposite in charge to the surface) and co-ions (same sign as the surface) which extend to some distance from the surface [4, 5]. The counterion and co-ion concentration n_i near the surface can be related to the value in the bulk n_{i0} using the Boltzmann distribution principle,

$$n_i = n_{i0} \exp\left[-\frac{Z_i e \psi_x}{kT}\right], \tag{7.1}$$

where Z_i is the valency of the ion, e is the electronic charge, ψ_x is the potential at a distance x from the surface, k is the Boltzmann constant and T is the absolute temperature. Since the charge on the counterion is always opposite to that of the surface, the exponent in equation (7.1) will always be negative for the counterion concentration and positive for the co-ion concentration. Equation (7.1) shows that the concentration of counterions increases close to the surface (positively adsorbed) whereas the co-ion concentration is reduced near the surface (negative adsorption). Fig. 7.1 shows the local ion concentration profiles according to equation (7.1).

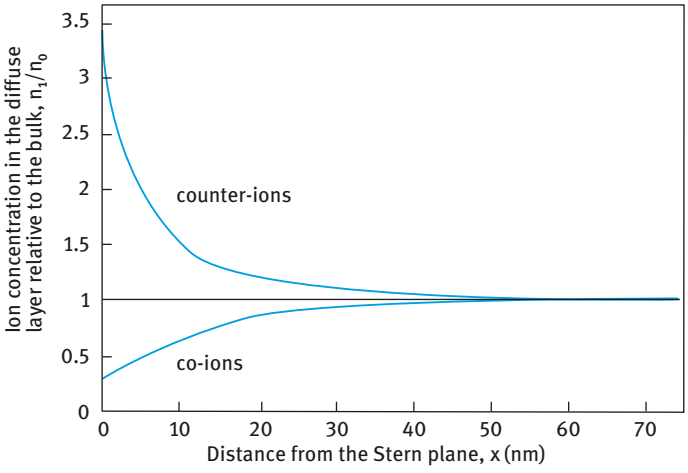

Fig. 7.1: Local ion concentration profiles: $\psi_0 = -30$ mV, in 10^{-3} mol dm^{-3} NaCl.

The number of charges per unit volume, i.e. the space charge density ρ is given by,

$$\rho = \sum_i n_i Z_i e = -2n_0 Ze \sinh\left[\frac{Ze\psi_x}{kT}\right]. \tag{7.2}$$

Note that $\sinh x = (\exp x - \exp -x)/2$.

A schematic picture of the diffuse double layer according to Gouy [4] and Chapman [5] is shown in Fig. 7.2. The potential decays exponentially with distance x.

For small potentials ($\psi(x) < 25$ mV), $Ze\psi(x)/kT < 1$ and $\sinh x \approx x$ so that equation (7.2) becomes.

$$\frac{\mathrm{d}^2\psi}{\mathrm{d}x^2} \approx \frac{2n_0(Ze)^2}{\varepsilon_0\varepsilon_r kT}\psi(x). \tag{7.3}$$

Equation (7.3) is the well-known Debye–Hückel approximation whose solution is,

$$\psi = \psi_0 \exp -(\kappa x). \tag{7.4}$$

Note that when $x = 1/\kappa$, $\psi_x = \psi_0/e$; $1/\kappa$ is referred to as the "thickness" of the double layer".

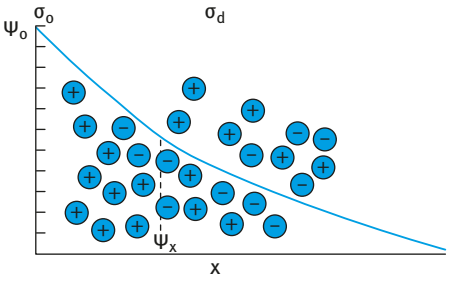

Fig. 7.2: Schematic representation of the diffuse double layer according to Gouy [4] and Chapman [5].

The double layer extension depends on electrolyte concentration and valency of the counterions,

$$n = \frac{n_0}{1 + kn_0 t}. \tag{7.5}$$

The double layer extension increases with decreasing electrolyte concentration. It also depends on the valency of the ions. An expression for $(1/\kappa)$ in terms of the electrolyte ionic strength I is,

$$\left(\frac{1}{\kappa}\right) = \left(\frac{\varepsilon_r\varepsilon_0 RT}{2{,}000F^2}\right)^{1/2} I^{-1/2} \text{ in m}^{-1} = 0.304I^{-1/2} \text{ in nm}, \tag{7.6}$$

where,

$$I = \sum c_i Z_i^2. \tag{7.7}$$

c_i is the electrolyte concentration in mol dm^{-3}.

Increasing the ionic strength causes a decrease in $(1/\kappa)$ that is referred to as compression of the double layer. The distance $(1/\kappa)$ is referred to as the thickness of the double layer. For example, for KCl in water at 25 °C, $(1/\kappa) = 96.17$ nm at $I = 10^{-5}$ mol dm^{-3} decreasing to 3.04 nm at $I = 10^{-2}$ mol dm^{-3}. Approximate values of $(1/\kappa)$ for KCl are given in Tab. 7.1.

Tab. 7.1: Approximate values of $(1/\kappa)$ for 1 : 1 electrolyte (KCl).

C (mol dm^{-3})	10^{-5}	10^{-4}	10^{-3}	10^{-2}	10^{-1}
$(1/\kappa)$ (nm)	100	33	10	3.3	1

Equations (7.6) and (7.7) show that $(1/\kappa)$ depends on the valency of the counter- and co-ions.

(ii) Stern–Grahame model of the double layer. Stern [6] recognized that the assumption in the Gouy–Chapman theory [4, 5] regarding the electrolyte ions as point charges is unsatisfactory. Furthermore, the assumption that the solvent can be treated as a structureless dielectric of constant permittivity is also unsatisfactory. He then introduced the concept of the nondiffuse part of the double layer for specifically adsorbed ions, the rest being diffuse in nature. This is schematically illustrated in Fig. 7.3.

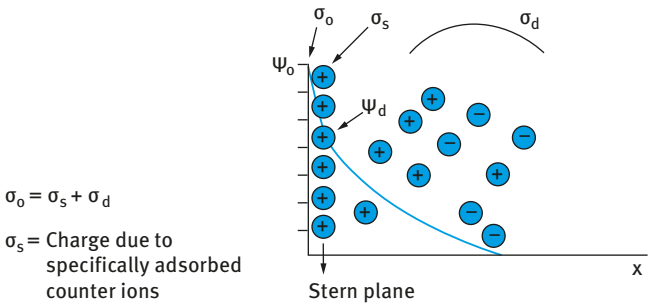

Fig. 7.3: Schematic representation of the double layer according to Stern and Grahame.

The potential drops linearly in the Stern region and then exponentially. Grahame [7] distinguished two types of ions in the Stern plane: physically adsorbed counterions (outer Helmholtz plane) and chemically adsorbed ions (that lose part of their hydration shell) (inner Helmholtz plane). The outer Helmholtz plane is considered the plane of closest approach of hydrated counterions, i.e. the Stern plane. The inner Helmholtz plane is that of specifically adsorbed counterions which may have lost part of or its complete hydration shell. The number of these specifically adsorbed ions may exceed the number of surface charges causing a reversal of the sign of the potential as illustrated in Fig. 7.4 for a positively charged surface with specifically adsorbed anions.

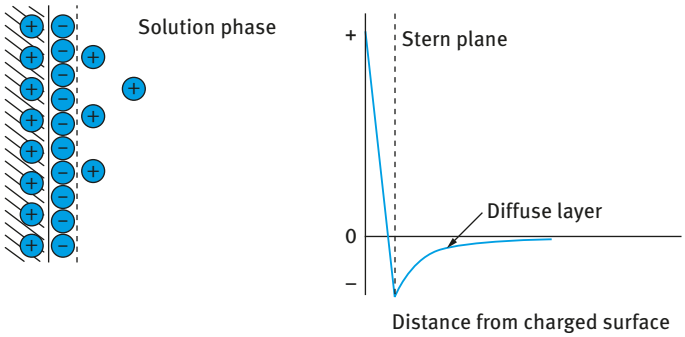

Fig. 7.4: Schematic representation of charge reversal by specifically adsorbed counterions.

For the specifically adsorbed ions the range of interaction is short, i.e. these ions must reside at the distance of closest approach, possibly within the hydration shell. For the indifferent ions, the situation is different and these ions are subjected to an attractive (for the counterions) or repulsive (for the co-ions) potential (energy = $\pm ZF\psi(x)/RT$). The space charge density due to these ions is high near the surface and decrease gradually with distance to its bulk value. Such a layer is the diffuse double layer described by Gouy–Chapman [4, 5]. Generally speaking, a double layer contains a part that is specifically adsorbed and a diffuse part. Because of the finite size of the counterions there is always a charge-free layer near the surface.

7.3 Electrical double layer repulsion

The origin of electrostatic interactions is due to the double layer overlap that occurs when the surface-to-surface distance becomes smaller than twice the double layer thickness. One of the most important features of double layers is their strong dependence on the concentration of indifferent electrolytes. As discussed above, an increase in electrolyte concentration causes a reduction in the diffuse double layer potential, ψ_{diffuse}, and compression of the double layer, i.e. reduction of the Debye length κ^{-1}. Both of these effects affect the colloid stability of lyophobic colloids as will be discussed below.

A general expression can be written to describe the electrostatic repulsion, G_{el}, in terms of the double layer property $f(\text{DL})$ determined by the relative permittivity, particle size, the double layer potential, ψ_{diffuse}, and an exponential function determined by the Debye length and separation distance h [3],

$$G_{\text{el}} = f(\text{DL})\psi^2_{\text{diffuse}} \exp(-\kappa h). \tag{7.8}$$

$(1/\kappa)$ is the Debye length that is referred to as the "thickness of the double layer" and is given by equation (7.5).

For two particles of different, but not too high, diffuse double layer potential, at large κh,

$$G_{el} = f(\mathrm{DL})\psi_1^d\psi_2^d \exp(-\kappa h). \tag{7.9}$$

In the original theory developed by Deryaguin–Landau [8], Verwey–Overbeek [9] (referred to as DLVO theory), the assumption was made that on the approach of surfaces the surface potentials remain constant and equal to that at infinite separation of the surfaces. This requires adjustment of the surface charge by surface charge regulation. In this case the isolated double layers form spontaneously by adsorption and/or desorption of potential-determining ions. This is referred to as the "constant potential" case. However, with many surfaces the charge is fixed, e.g. in clay particles, and on surface approach the surface potential has to be adjusted to keep the surface charge constant. This situation is referred to as the "constant charge" case.

For two flat plates, when the surface separation becomes less than twice the double layer extension [10], the individual double layers can no longer develop unrestrictedly, since the limited space does not allow complete potential decay (Fig. 7.5). The potential $\psi_{H/2}$ half way between the plates is no longer zero (as would be the case for isolated particles at $x \to \infty$). The potential distribution at an interparticle distance H is schematically depicted by the full line in Fig. 7.5. The Stern potential ψ_d is considered to be independent of the particle distance. The dashed curves show the potential as a function of distance x to the Helmholtz plane, had the particles been at infinite distance.

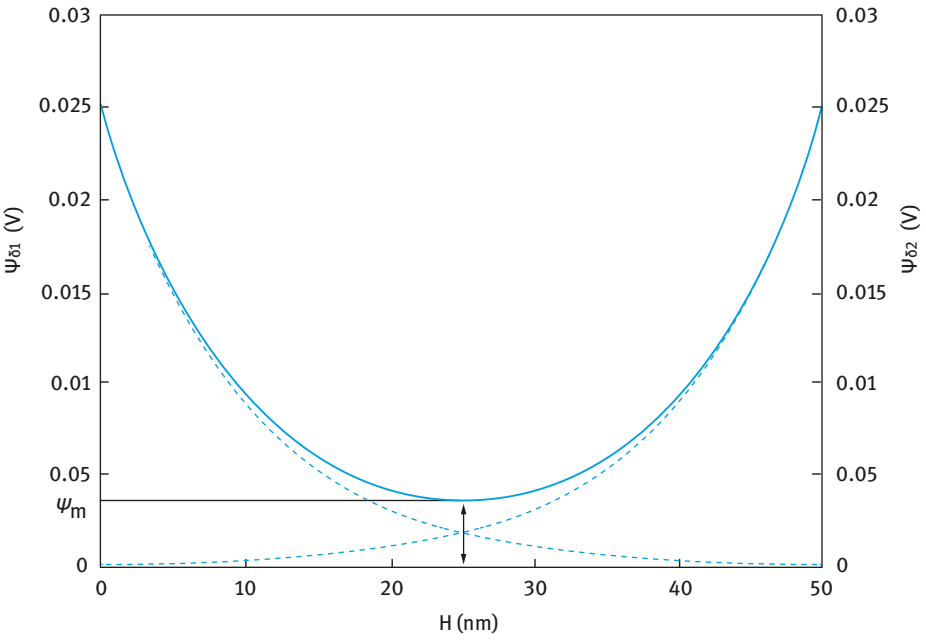

Fig. 7.5: Potential profile between two planer surfaces at 25 mV, in 10^{-3} mol dm^{-3} NaCl.

A simple model to obtain G_{el} is to calculate the ion concentration between the surfaces in order to obtain the osmotic pressure difference between the surfaces and the bulk electrolyte, i.e. the excess osmotic pressure at the mid-plane position between the surfaces separated by a distance h. At $h/2$, $d\psi_x/dx = 0$ and $\psi_x = \psi_m$.

The difference in ionic concentration at the mid-plane and the bulk electrolyte gives the osmotic pressure $\Pi(H)$,

$$\Pi(H) = kT(n_+ + n_- - 2n_0). \tag{7.10}$$

Using the Boltzmann distribution,

$$n_i = n_{i0} \exp\left[\frac{Z_i e\psi(x)}{kT}\right], \tag{7.11}$$

where Z_i is the ion valency, e is the electronic charge, k is the Boltzmann constant and T is the absolute temperature; equation (7.10) becomes,

$$\Pi(H) = 2n_0 kT\left[\cosh\left(\frac{Ze\psi_m}{kT}\right) - 1\right]. \tag{7.12}$$

For small potentials equation (7.12) reduces to,

$$\Pi(H) \approx \frac{\kappa^2 \varepsilon_r \varepsilon_0}{2}\psi_m, \tag{7.13}$$

where ε_r is the relative permittivity of the medium, ε_0 is the permittivity of free space. The mid-plane potential ψ_m is equal to twice the potential at the mid-plane,

$$\psi_m = 2\psi_{(H/2)}. \tag{7.14}$$

Equation (7.12) becomes,

$$\Pi(H) \approx \frac{\kappa^2 \varepsilon_r \varepsilon_0}{2}\left[2\psi_d \exp\left(-\frac{\kappa H}{2}\right)\right]^2 = 2\kappa^2 \varepsilon_r \varepsilon_0 \psi_d^2 \exp(-\kappa H). \tag{7.15}$$

The electrostatic repulsion is then given by,

$$G_{el} = -\int_{\infty}^{H} \Pi(H)\, dH. \tag{7.16}$$

Using the boundary conditions: $\Pi(H) \to 0$ as H$\to \infty$,

$$G_{el} = 2\kappa \varepsilon_r \varepsilon_0 \psi_d^2 \exp(-\kappa H). \tag{7.17}$$

Replacing the Stern potential ψ_d with the zeta potential ζ,

$$G_{el} \approx 2\kappa \varepsilon_r \varepsilon_0 \zeta^2 \exp(-\kappa H) \tag{7.18}$$

For higher potentials, the Debye–Hückel approximation cannot be justified, but for weak overlap, i.e. $\kappa H > 1$, the local potentials, estimated from the isolated surfaces,

can still be simply added and this results in the following expression for the double layer repulsion,

$$G_{\mathrm{el}} = \frac{64 n_0 kT}{\kappa} \tanh^2\left(\frac{Ze\psi_{\mathrm{d}}}{4kT}\right) \exp(-\kappa H). \tag{7.19}$$

Deryaguin, Landau [8], Verwey, Overbeek [9] calculated the electrostatic interaction by computing the Gibbs energy G of the system at any distance h by an isothermal reversible charging process. The change in the Gibbs energy per unit area of the interface when the distance between the plates is reduced from ∞ to h is given by,

$$G_{a,\mathrm{el}} = 2\left[\Delta G_a^{\sigma}(h) - \Delta G_a^{\sigma}(\infty)\right] = 2\left[G_a^{\sigma}(h) - G_a^{\sigma}(\infty)\right]. \tag{7.20}$$

The Δ is dropped because both terms refer to the same reference state. G_a^{σ} is related to the surface excess Γ_I (amount of adsorption in moles per unit area) and the chemical potential μ_I by the Gibbs equation,

$$G_a^{\sigma} = -\sum \mu_i \Gamma_i. \tag{7.21}$$

The most common procedure to obtain the interaction between spherical particles or droplets is to use the Deryaguin approximation [11]. The interaction energy is considered to be built up of contributions of parallel rings and to approximate the total interaction as the integral over that set of infinitesimal parallel rings. A schematic illustration of the Deryaguin approximation is shown in Fig. 7.6 [3].

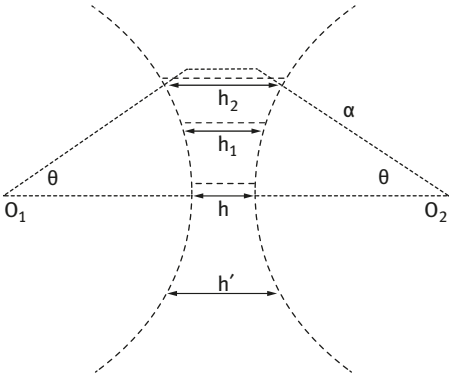

Fig. 7.6: Illustration of the Deryaguin approximation [11].

The above approximation is rigorous if there is no lateral interaction between the rings. For electrostatic interaction, this means that the field lines should run parallel to the O_1O_2 axis. This is exact for $h' = h$, but the condition becomes increasingly poorer in the direction $h' \to h_1 \to h_2$ as indicated by the dashed lines in Fig. 7.6. The Deryaguin approximation [11] is expected to work well for low κh and large κa (where a is the particle radius).

For identical spheres at $\kappa a < 5$, i.e. the diffuse layer is of similar magnitude as the particle radius,

$$G_{\mathrm{el}}^{\psi} = 2\pi\varepsilon_{\mathrm{r}}\varepsilon_0 a \psi_{\mathrm{d}}^2 \exp(-\kappa h). \tag{7.22}$$

For identical spheres at $\kappa a > 10$, i.e. the double layer is thin compared to particle radius, the result at low potential is, for the constant potential case,

$$G_{el}^{\psi} = 2\pi\varepsilon_r\varepsilon_0 a\psi_d^2 \ln[1 + \exp(-\kappa h)]. \tag{7.23}$$

h is the closest distance between the particles, i.e. $h = r - 2a$, where r is the centre-centre distance between the particles.

The constant charge expression is,

$$G_{el}^{\sigma} = -2\pi\varepsilon_r\varepsilon_0 a\psi_d^2 \ln[1 + \exp(-\kappa h)]. \tag{7.24}$$

The constant charge case, equation (7.24), should be used with caution, especially at close approach as a large overestimate can be obtained for the repulsive potential.

Increasing the electrolyte concentration results in compression of the double layer and this causes a reduction in double layer repulsion [1–3] This is illustrated in Fig. 7.7 which shows the repulsive energy versus $H/2$ for two flat plates at a Stern potential of 154 mV and three values of κ for 1 : 1 electrolyte. In general, increasing the electrolyte concentration results in decreasing electrostatic repulsion.

The effect of valency of counterions is shown in Fig. 7.8 which compares the results for $Z = 1$ with that for $Z = 3$. As expected, increasing Z results in decreasing electrostatic repulsion.

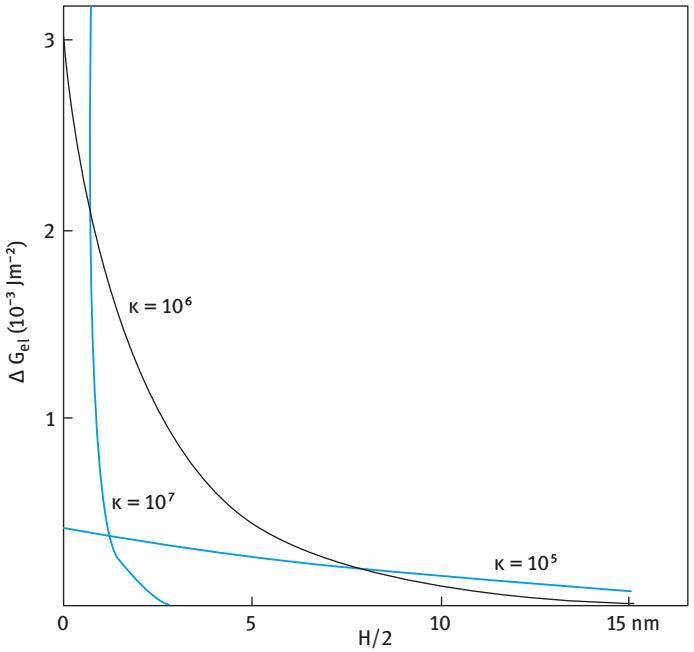

Fig. 7.7: Increase in the electrical free energy of two flat plates as a function of decreasing mutual distance for three values of the reciprocal Debye length: $\psi_d = 154$ mV; 1 : 1 electrolyte.

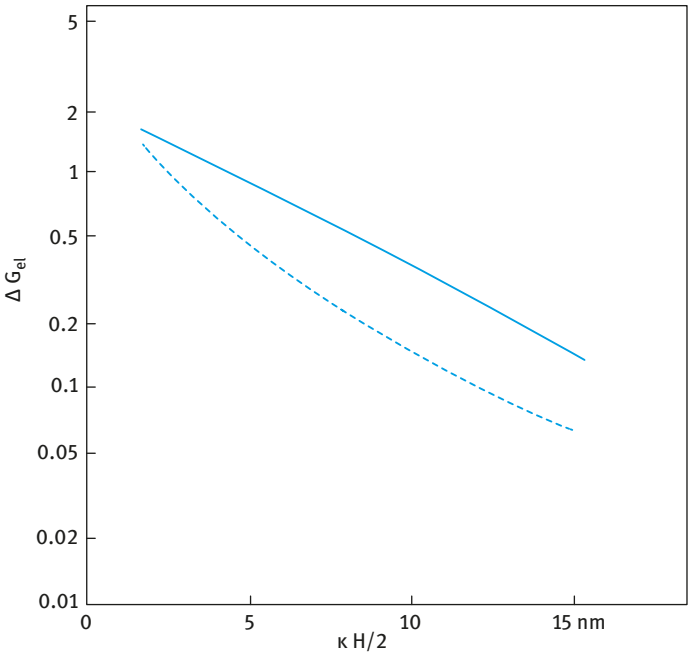

Fig. 7.8: Effect of counterion valency on the increase in free energy as a function of $\kappa H/2$ for two flat plates. Full line $y_d = 2$, $Z = 1$; dashed line $y_d = 6$, $Z = 3$. ($y_d = F\psi_d/RT$). The units on the y-axis are only relative.

The effect of increasing the Stern potential is illustrated in Fig. 7.9 which the values for three dimensionless $y_d(= F\psi_d/RT)$. An increase in the Stern potential at a given electrolyte concentrations results in an increase in electrostatic repulsion.

In all the above treatments the interaction is considered for isolated particles, where the time-average separation of the particles is much larger than the range of the diffuse layer. However, with most practical dispersions such a condition is seldom satisfied since in this case the separation of the particles become similar in magnitude to the range of the diffuse layer [10]. The background electrolyte now contains other particles with their counterions. Each charged particle is a "macro-ion" but the number is very much smaller than the number of corresponding counterions. Thus, the particle contribution can be ignored without introducing a large error. However, when the volume occupied by the particles become significant, i.e. at high volume fraction, the ionic concentration in the liquid becomes larger since the particle volume is excluded to the ions. Russel et al. [12] gave a convenient expression for κ by considering the volume fraction of the particles ϕ,

$$\kappa = \left(\frac{e^2}{\varepsilon_r \varepsilon_0 kT} \frac{2Z^2 n_0 - \frac{3\sigma_0 Z\phi}{ae}}{1-\phi} \right). \tag{7.25}$$

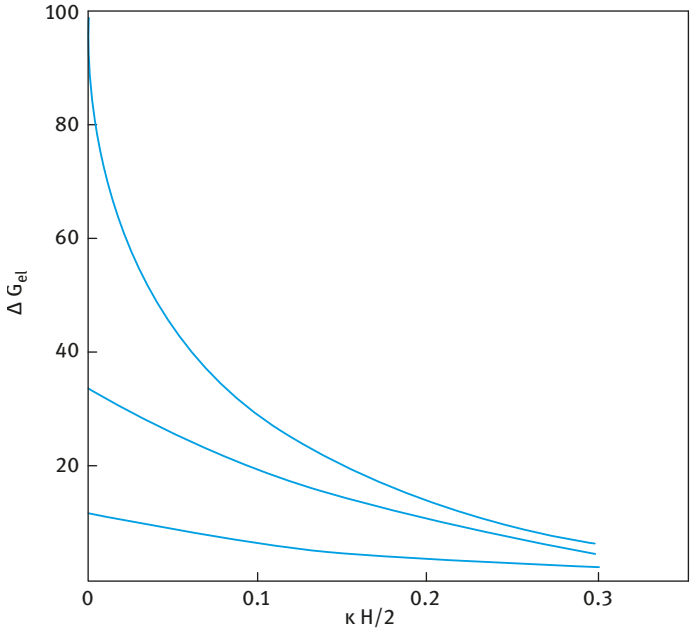

Fig. 7.9: Increase in electrical free energy of two flat plates as a function of $\kappa H/2$. From top to bottom the lines correspond to dimensionless potential y_d of 8, 6 and 4 respectively. The units on the y-axis are only relative.

The $(1 - \phi)$ term in the denominator corrects the ion concentration for the volume occupied by the particles, σ_0 is the surface charge density which can be calculated from the Stern or zeta potential. Fig. 7.10 shows the variation of Debye length with particle volume fraction in 10^{-4} mol dm^{-3} NaCl for particles of radius $a = 200$ nm and charge density σ_0 of -10 μC cm^{-2}.

It is clear from Fig. 7.10 that the Debye length decreases gradually with increasing particle volume fraction and at $\phi > 0.01$ it shows a more rapid decrease, reaching about 4 nm when $\phi \approx 0.3$. This reduction in Debye length is the consequence of the increase in ion concentration produced by the counterions of the high number concentration of the particles. This reduction in Debye length is reflected in the reduction of electrostatic repulsion illustrated in Fig. 7.11. It can be clearly seen that by increasing the particle volume fraction the electrostatic repulsion decreases due to the reduction in the Debye length (compression of the electrical double layer). This explains why in many practical dispersions prepared at high volume fraction ($\phi > 0.3$) electrostatic repulsion is insufficient for the long-term colloid stability of the dispersion.

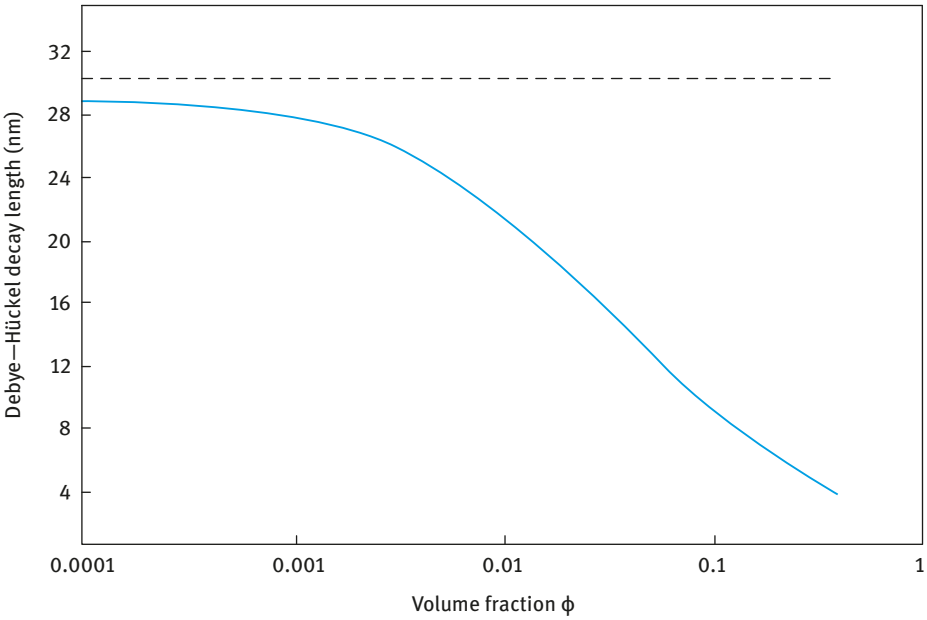

Fig. 7.10: Debye length as a function of particle volume fraction in 10^{-4} mol dm^{-3} NaCl: $a = 200$ nm; $\sigma_0 = -10$ µC cm^{-2}. The dashed line represents the limiting value for zero volume fraction.

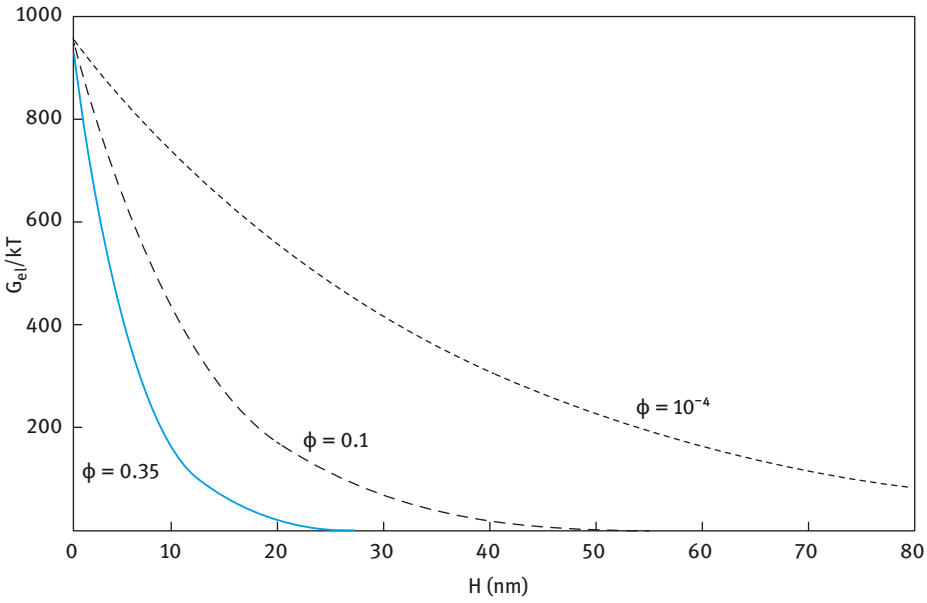

Fig. 7.11: Electrostatic repulsion for three particle volume fractions in 10^{-3} mol dm^{-3} NaCl: $a = 200$ nm; $\psi_d = -80$ mV; $\sigma_d = -10$ µC cm^{-2}.

7.4 Van der Waals attraction

The interaction between two particles or droplets can in general be considered in terms of the potential energy or the work required to separate them from a centre-to-centre distance r to some large distance apart [10]. The interaction energy includes both enthalpic and entropic contributions of all components in the system, namely particles, solvent, ions, surfactants, polymers, etc. This means that the interaction energy between any two particles should take into consideration all other components, i.e. the potential of mean force. A detailed account of both intermolecular forces and interaction between the particles was given in the text by Israelachvili [13] to which the reader should refer for more detail.

Before describing the van der Waals attraction between particles or droplets in a dispersion, one must first consider the intermolecular attraction between atoms or molecules. Three main contributions to the intermolecular interaction can be considered:

(i) Dipole–dipole interaction (Keesom–van der Waals interaction). This interaction arises from the presence of permanent dipoles [14], e.g. with HCl gas that has a strong dipole due to polarization of the covalent bond. The Keesom interaction is short range in nature being proportional to $1/r^6$. Due to marked dipole alignment, the rotational motion of the molecules is restricted and this results in a "long time" interaction that occurs at low frequency.

(ii) Dipole-induced dipole interaction (Debye–van der Waals interaction). This occurs between a polar and a nonpolar molecule [15]. The dipole on the polar molecule polarizes the electron clouds of the nonpolar molecule. The interaction free energy can be described as similar to that of the dipole–dipole interaction.

(iii) London–van der Waals interaction (dispersion interaction). The London dispersion force is the most important, since it occurs for polar and nonpolar molecules. It arises from fluctuations in the electron density distribution [16]. It is due to the movement of the electron cloud around the atomic nucleus resulting in a dipole that fluctuates. When two atoms come in close proximity, the temporary dipoles become aligned, i.e. the fluctuations become coupled and this is a preferred (or lower) energy state. The range of interaction is similar to that of Keesom and Debye, but the timescale is now that of the electronic transition, near the visible-ultraviolet part of the electromagnetic spectrum. The London–van der Waals interaction energy is given by,

$$u(r) = -\frac{\beta_{11L}}{r^6}. \tag{7.26}$$

The London dispersion constant β_{11L} for two identical atoms is proportional to the ionization energy of the outer electrons, $h\nu_1$, and the polarizability α, where h is the Planck constant and ν is the frequency of radiation in Hz (= $\omega/2\pi$, where ω is the frequency in rad s^{-1}),

$$\beta_{11L} \propto h\nu_1\alpha^2. \tag{7.27}$$

For two different atoms,

$$\beta_{12L} \propto h\frac{\nu_{11}\nu_{12}}{\nu_{11}+\nu_{12}}\alpha_1\alpha_2. \tag{7.28}$$

The London–van der Waals intermolecular interaction is mostly much larger than the Keesom–van der Waals or Debye–van der Waals contributions. Water is exceptional, since in this case the dispersion contribution is only one-quarter of the total interaction.

As described above, all three interactions are based on the attraction between dipoles and have the same distance separation. Therefore, it is possible to describe the attraction in a general way. The London constant in equations (7.27) and (7.28) depends on the ionization potential of the outer electrons which is in the region of the visible-ultraviolet part of the electromagnetic spectrum. Other electronic transitions also take place so that contributions at other frequencies can also occur. For a general approach one must consider the full range of frequencies, ranging from those of a few Hertz up to the ultraviolet region at $\approx 10^{16}$ Hz.

The above description considered the case of interaction of atoms or molecules in the absence of any intervening medium. The relative permittivity of the medium is an important factor. The relative permittivity $\varepsilon(\nu)$ as a function of frequency describes the dielectric behaviour at low frequencies and the refractive index $n(\nu)$ is a viable measure of the dielectric behaviour at the higher end of the spectrum.

There are generally two approaches for describing the van der Waals attraction between macroscopic bodies such as suspension particles. The first approach considers the London–van der Waals attraction to be the sum of the forces acting between isolated molecules. This approach, referred to as the microscopic approach, was suggested by de Boer and Hamaker [17, 18]. The second approach, developed by Lifshitz [19], is based on the correlation between electric fluctuations of two macroscopic bodies. This is referred to as the macroscopic approach.

The approach starts with the finding that the Gibbs energy of interaction can be given by the product of a material constant, $A_{ij(k)}$, and a function of geometry and distance h, $f(a, h)$ [10]. $A_{ij(k)}$, referred to as the Hamaker constant, refers to the interaction between two particles or macrobodies i and j across a medium k,

$$G_{VDW}(h) = -A_{ij(k)}f(a, h). \tag{7.29}$$

For two identical particles in an aqueous medium, $A_{ij(k)}$ becomes $A_{11(w)}$. The dimensions of the distance function, $f(a, h)$, depend on the geometry of the system. For semi-finite plates, $f(a, h) = f(h)$ is proportional to h^{-2} and $G_{VDW}(h)$ is in J m^{-2}. For two spheres, $f(a, h)$ is dimensionless and $G_{VDW}(h)$ is in J.

Consider two slabs of interacting materials as schematically represented in Fig. 7.12.

The starting point is to consider the interaction between a single molecule and a slab of material and then extend that to two slabs interacting [10]. In the microscopic approach due to Hamaker [18] the energies are assumed to be additive. In this case one

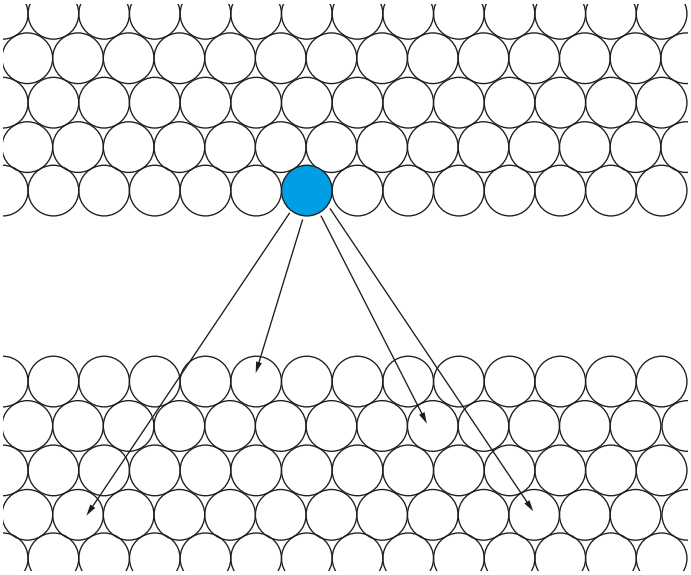

Fig. 7.12: Schematic representation of atomic dipolar interactions between two slabs of material.

can simply use equation (7.28) and add all interactions between the reference molecule in the upper slab (shown by a dark circle in Fig. 7.12) and all other molecules in the material of the lower slab. The interaction energy is given by the sum for each molecule in the lower slab. One then adds this up for all molecules in the upper slab. The interaction is then given by the sum for all molecules in the upper slab multiplied by the sum for each molecule in the lower slab.

To calculate the intermolecular distance r one can simply use the number density of molecules in the slab, $\rho_N (= N/V)$, and integrate over the volumes. This "semi-continuum" approach is the basis of the additivity assumption and it would only become a problem at very close approach. The interaction energy then follows from equation (7.29),

$$G_{\mathrm{VDW}}(h) = -\pi^2 \beta_{11\mathrm{L}} \rho_N^2 f(a, h). \tag{7.30}$$

Equation (7.30) gives a general expression for the van der Waals attraction in terms of the material constant (that is given by the electronic polarizability, the ionization potential and the square of the product of the density and molar mass) and the shape factor and separation distance between the two bodies.

For two infinitely thick slabs, the energy of unit area of one slab interacting with the whole of the other slab is given by,

$$G_{\mathrm{VDW}}(h) = -\frac{\pi \beta_{11\mathrm{L}} \rho_N^2}{12 h^2}, \tag{7.31}$$

where $G_{\mathrm{VDW}}(h)$ represents the dispersion energy of two slabs of the same material a distance h apart and it is the energy per unit area of the surface. The numerator represents the material property whereas the denominator arises from the geometry. It is common in colloid science to express the material property as a single constant, referred to as the Hamaker constant that is simply given by,

$$A_{11} = \pi^2 \beta_{11\mathrm{L}} \rho_N^2. \tag{7.32}$$

Equation (7.32) can then be written as,

$$G_{\mathrm{VDW}}(h) = -\frac{A_{11}}{12\pi h^2}. \tag{7.33}$$

If one has a slab of material 1 interacting with material 2,

$$G_{\mathrm{VDW}}(h) = -\frac{A_{12}}{12\pi h^2}. \tag{7.34}$$

And,

$$A_{12} = \pi^2 \beta_{12\mathrm{L}} \rho_{N1} \rho_{N2}. \tag{7.35}$$

If the "semi-infinite" slabs are replaced by plates with thickness t, equation (7.34) has to be modified,

$$G_{\mathrm{VDW}}(h) = -\frac{A_{11}}{12\pi}\left(\frac{1}{h^2} + \frac{1}{(h+2t)^2} - \frac{2}{(h+t)^2}\right). \tag{7.36}$$

Hamaker constants can be computed from equation (7.36) if the molecular properties of the materials under consideration are known. Alternatively, they can be derived from the macroscopic theory as will be discussed below. Direct measurement of van der Waals attraction can also be used to obtain the Hamaker constant. Their magnitude is in the order of 10^{-20}–10^{-19} J (≈ 5–$50kT$) at room temperature. As we will see later, the Hamaker constants for interaction across a medium are much lower.

For curved interfaces (as is the case of spherical particles or droplets) the expression for the van der Waals attraction is more complex. However, a useful method to derive such an expression is to use the Deryaguin approximation [11], where the curved surface is replaced by a stepped one as illustrated in Fig. 7.13. The total interaction between the macroscopic bodies is considered to be built up of contributions of parallel rings where each pair contributes an amount $G_{\mathrm{A}}(x)\,\mathrm{d}A$ where $G_{\mathrm{A}}(x)$ is given by equation (7.33). From the energy per ring, the total interaction energy is obtained by integration over y (as indicated in Fig. 7.13) after replacing $\mathrm{d}A$ by $2\pi y\,\mathrm{d}y$. As the approximation is limited to short distances, the contributions of layers with large y are negligible, so that for convenience the integration may be carried out from $y = 0$ to $y = \infty$. After relating y to x, the Deryaguin formula for two spheres of radii R_1 and R_2 becomes,

$$G_{\mathrm{A}} = -\frac{2\pi R_1 R_2}{R_1 + R_2} \int_h^\infty G_{\mathrm{A}}(x)\,\mathrm{d}x. \tag{7.37}$$

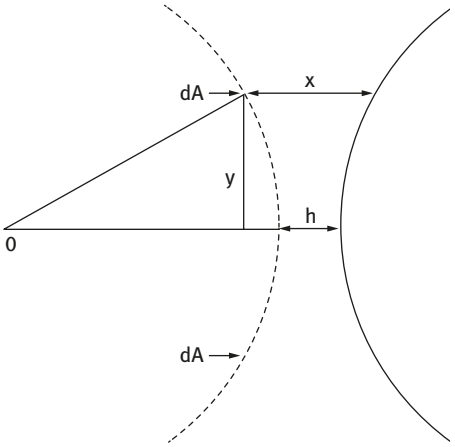

Fig. 7.13: Schematic representation of Deryaguin's approximation [11].

Substituting equation (7.33) into (7.37) and carrying out the integration gives,

$$G_{\mathrm{VDW}}(h) = -\frac{A_{12}R_1R_2}{6h(R_1+R_2)}. \tag{7.38}$$

For two spheres of equal radius,

$$G_{\mathrm{VDW}}(h) = -\frac{A_{11}R}{12h}. \tag{7.39}$$

Equations (7.38) and (7.39) apply only for the case $h < R_1, R_2$ and $h < R$ respectively. For the general case of a wide range of h, expressions can be derived both for particles with different radii and of equal radii as schematically shown in Fig. 7.14.

For two spheres with different radii R_1 and R_2,

$$G_{\mathrm{VDW}}(h) = -\frac{A_{12}}{12}\left[\frac{y}{x^2+xy+x} + \frac{y}{x^2+xy=y} = 2\ln\left\{\frac{x^2+xy+y}{x^2+xy+x+y}\right\}\right], \tag{7.40}$$

where $x = h/2R_1$ and $y = R_2/R_1$.

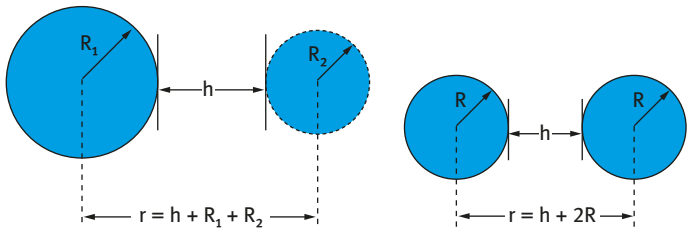

(a) Two Unequal Spheres (b) Two Equal Spheres

Fig. 7.14: Schematic representation of the interaction between spheres of different radii (a) and with the same radius (b).

For two spheres with equal radii,

$$G_{VDW}(h) = -\frac{A_{11}}{6}\left[\frac{2R^2}{r^2-4R^2} + \frac{2R^2}{r^2} + \ln\frac{r^2-4R^2}{r^2}\right]. \tag{7.41}$$

Substituting $s = r/R$,

$$G_{VDW}(h) = -\frac{A_{11}}{6}\left(\frac{2}{s^2-4} + \frac{2}{s^2} + \ln\frac{s^2-4}{s^2}\right). \tag{7.42}$$

For very short distances ($h \ll R$), equation (7.42) may be approximated by equation (7.39).

When the particles are dispersed in a liquid medium, the van der Waals attraction has to be modified to take into account the medium effect. When two particles are brought from infinite distance to h in a medium, an equivalent amount of medium has to be transported the other way round. Hamaker forces in a medium are excess forces.

Consider two identical spheres 1 at a large distance apart in a medium 2 as illustrated in Fig. 7.15 (a). In this case the attractive energy is zero. Fig. 7.15 (b) gives the same situation with arrows indicating the exchange of 1 against 2. Fig. 7.15 (c) shows the complete exchange which now shows the attraction between the two particles 1 and 1 and equivalent volumes of the medium 2 and 2.

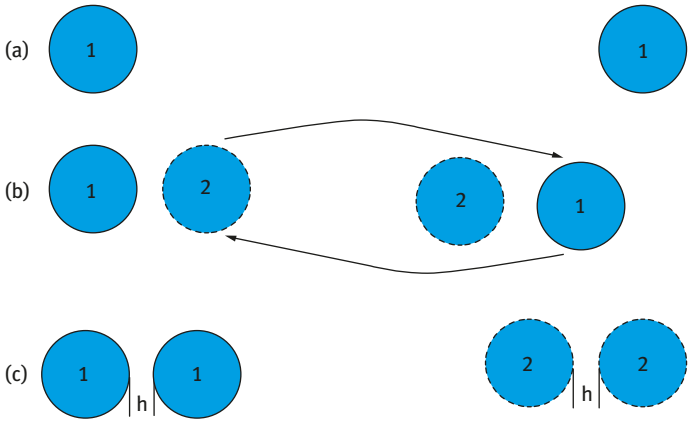

Fig. 7.15: Schematic representation of interaction of two particles or droplets in a medium.

The effective Hamaker constant for two identical particles or droplets 1 and 1 in a medium 2 is given by,

$$A_{11(2)} = A_{11} + A_{22} - 2A_{12} = (A_{11}^{1/2} - A_{22}^{1/2})^2. \tag{7.43}$$

Equation (7.43) shows that two particles of the same material attract each other unless their Hamaker constant exactly matches each other. Equation (7.39) now becomes,

$$G_{\mathrm{A}} = -\frac{AR}{12h}, \tag{7.44}$$

where $A_{11(2)}$ is the effective Hamaker constant of two identical particles with Hamaker constant A_{11} in a medium with Hamaker constant A_{22}.

In most cases the Hamaker constant of the particles is higher than that of the medium. Examples of Hamaker constants for some materials in vacuum are given in Tab. 7.2. The Hamaker constant for some liquids is given in Tab. 7.3. Tab. 7.4 gives values of the effective Hamaker constant for some particles in some liquids. Generally speaking, the effect of the liquid medium is to reduce the Hamaker constant of the particles below its value in vacuum (air).

Tab. 7.2: Hamaker constant in vacuum A_{11} for some materials.

Material	$A_{11} \times 10^{20}$ (J)
Fused quartz (SiO_2)	6.5
Al_2O_3	15.6
Silver	50.0
Copper	40.0
Poly(methylmethacrylate)	7.1
Poly(vinylchloride)	7.8

Tab. 7.3: Hamaker constant of some liquids.

Liquid	$A_{22} \times 10^{20}$ (J)
Water	3.7
Ethanol	4.2
Decane	4.8
Hexadecane	5.2
Cyclohexane	5.2

Tab. 7.4: Effective Hamaker constant $A_{11(2)}$ of some particles in water.

System	$A_{11(2)} \times 10^{20}$ (J)
Fused quartz/water	0.83
Al_2O_3/water	5.32
Copper/water	30.00
Poly(methylmethacrylate)/water	1.05
Poly(vinylchloride)/water	1.03
Poly(tetrafluoroethylene)/water	0.33

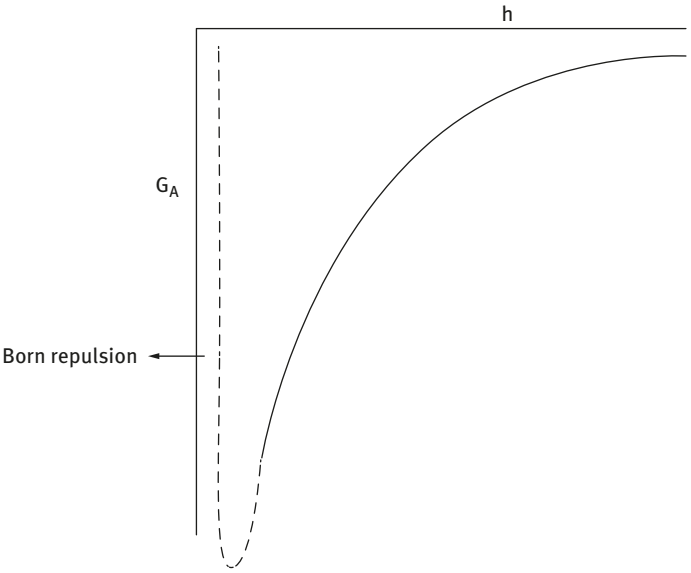

Fig. 7.16: Variation of G_A with h.

G_A decreases with increasing h as schematically shown in Fig. 7.16.

As shown in Fig. 7.16 G_A increases very sharply with h at small h values. A capture distance can be defined at which all the particles become strongly attracted to each other (coagulation). At very short distances, Born repulsion appears.

One of the problems with the microscopic approach of Hamaker [18] is the situation when one is dealing with particles in a medium such as an electrolyte solution. In this case the interaction of permanent dipoles is screened by the ionic environment and the low frequency interaction falls off more rapidly than would be the case in a vacuum. This problem can be solved by using the generalized macroscopic theory of Lifshitz [19] that is described in detail by Mahanty and Ninham [20]. It is based on the principle that the spontaneous electromagnetic fluctuations in two particles become correlated when the particles approach each other, causing a decrease in the free energy of the system. This theory treats the interacting bodies as continuous and ascribes the interactions to fluctuating electromagnetic fields arising from spontaneous electric and magnetic polarizations within the various media. One important result is that the interactions are described completely in terms of the complex dielectric constants of the media.

7.5 Total energy of interaction

7.5.1 Deryaguin–Landau–Verwey–Overbeek (DLVO) theory [8, 9]

The combination of G_{el} and G_A results in the well-known theory of stability of colloids (DLVO theory) [8, 9],

$$G_T = G_{el} + G_A. \tag{7.45}$$

A plot of G_T versus h is shown in Fig. 7.17, which represents the case at low electrolyte concentrations, i.e. strong electrostatic repulsion between the particles. G_{el} decays exponentially with h, i.e. $G_{el} \to 0$ as h becomes large. $G_A \propto 1/h$, i.e. G_A does not decay to 0 at large h.

At long distances of separation, $G_A > G_{el}$, resulting in a shallow minimum (secondary minimum). At very short distances, $G_A \gg G_{el}$, resulting in a deep primary minimum. At intermediate distances, $G_{el} > G_A$, resulting in an energy maximum, G_{max}, whose height depends on ψ_0 (or ψ_d) and the electrolyte concentration and valency.

At low electrolyte concentrations ($< 10^{-2}$ mol dm^{-3} for a 1 : 1 electrolyte), G_{max} is high ($> 25kT$) and this prevents particle aggregation into the primary minimum. The higher the electrolyte concentration (and the higher the valency of the ions), the lower the energy maximum.

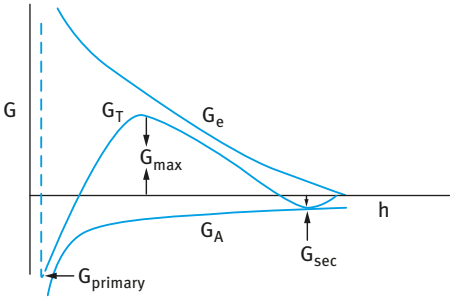

Fig. 7.17: Schematic representation of the variation of G_T with h according to the DLVO theory.

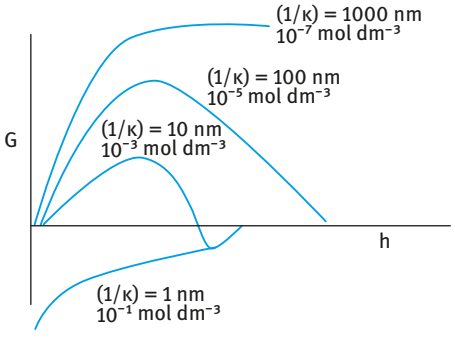

Fig. 7.18: Variation of G with h at various electrolyte concentrations.

Under some conditions (depending on electrolyte concentration and particle size), flocculation into the secondary minimum may occur. This flocculation is weak and reversible. By increasing the electrolyte concentration, G_{max} decreases until at a given concentration it vanishes and particle coagulation occurs. This is illustrated in Fig. 7.18 which shows the variation of G_T with h at various electrolyte concentrations.

Since approximate formulae are available for G_{el} and G_A, quantitative expressions for $G_T(h)$ can also be formulated. These can be used to derive expressions for the coagulation concentration, which is that concentration that causes every encounter between two colloidal particles to lead to destabilization. Verwey and Overbeek [9] introduced the following criteria for transition between stability and instability,

$$G_T(= G_{el} + G_A) = 0, \tag{7.46}$$

$$\frac{dG_T}{dh} = 0, \tag{7.47}$$

$$\frac{dG_{el}}{dh} = -\frac{dG_A}{dh}. \tag{7.48}$$

Using the equations for G_{el} and G_A, the critical coagulation concentration, CCC can be calculated. The theory predicts that the CCC is directly proportional to the surface potential ψ_0 and inversely proportional to the Hamaker constant A and the electrolyte valency Z. The CCC is inversely proportional to Z^6 at high surface potential and inversely proportional to Z^6 at low surface potential.

7.6 Criteria for stabilization of suspensions or emulsions with double layer interaction

The two main criteria for stabilization are:

(i) High surface or Stern potential (zeta potential), high surface charge. As shown in equation (7.17), the repulsive energy G_{el} is proportional to ψ_0^2. In practice, ψ_0 cannot be directly measured and, therefore, one instead uses the measurable zeta potential.

(ii) Low electrolyte concentration and low valency of counter- and co-ions. As shown in Fig. 7.18, the energy maximum increases with decreasing electrolyte concentration. The latter should be lower than 10^{-2} mol dm^{-3} for 1 : 1 electrolyte and lower than 10^{-3} mol dm^{-3} for 2 : 2 electrolyte. One should ensure that an energy maximum in excess of $25kT$ should exist in the energy–distance curve. When $G_{max} \gg kT$, the particles in the dispersion cannot overcome the energy barrier, thus preventing coagulation. In some cases, particularly with large and asymmetric particles, flocculation into the secondary minimum may occur. This flocculation is usually weak and reversible and may be advantageous for preventing the formation of hard sediments.

References

[1] Tadros T. Suspension concentrates. Berlin: De Gruyter; 2017.
[2] Tadros T. Emulsions. Berlin: De Gruyter; 2016.
[3] Tadros T. Interfacial phenomena. Berlin: De Gruyter; 2015.
[4] Gouy G. J Phys. 1910;9:457; Ann Phys. 1917;7:129.
[5] Chapman DL. Phil Mag. 1913;25:475.
[6] Stern O. Z Electrochem. 1924;30:508.
[7] Grahame DC. Chem Rev. 1947;41;441.
[8] Deryaguin BV, Landau L. Acta Physicochem USSR. 1941;14:633.
[9] Verwey EJW, Overbeek JTG. Theory of stability of lyophobic colloids. Amsterdam: Elsevier; 1948.
[10] Goodwin JW. Colloids and interfaces with surfactants and polymers. London: John Wiley and Sons; 2009.
[11] Deryaguin BV. Kolloid Z. 1934;69:155.
[12] Russel WB, Saville DA, Schowalter WR. Colloidal dispersions. Cambridge: Cambridge University Press; 1989.
[13] Israelachvili JN. Intermolecular and surface forces. London: Academic Press; 1992.
[14] Keesom WH. Proc Koninkl Nederland Wetenschap. 1915;18:636; 1920;23:939; Physik Z. 1921;22:129; 643.
[15] Debye P. Physik Z. 1920;21:178; 1921;22:302.
[16] London F. Z Physik. 1930;63:245; Trans Faraday Soc. 1937;33:8.
[17] de Boer JH. Trans Faraday Soc. 1936;32:10.
[18] Hamaker HC. Physica. 1937;4:1058.
[19] Lifshitz EM. Soviet Physics JETP. 1956;2:73.
[20] Manhanty J, Ninham BW. Dispersion forces. London: Academic Press; 1976.

8 Interaction between particles or droplets containing adsorbed polymer layers and the theory of steric stabilization

8.1 Introduction

Polymeric surfactants, particularly those of the A–B, A–B–A block and BA_n types (Chapters 3 and 6) are used for the stabilization of formulations consisting of disperse systems (suspensions and emulsions). The chain B (referred to as the "anchor chain") is chosen to be highly insoluble in the medium and have a strong affinity to the surface. The chain(s) A (referred to as the "stabilizing chain(s)") are chosen to be highly soluble in the medium and strongly solvated by its molecules, for example for hydrophobic particles or oil droplets. The B chain can be polystyrene, polymethylmethacrylate or polypropylene oxide and the A chain(s) can be poly(ethylene oxide), polyvinyl alcohol or polysaccharide. These polymeric surfactants are particularly important for the preparation of concentrated dispersions, i.e. at high volume fraction ϕ of the disperse phase,

$$\phi = \frac{\text{volume of all particles}}{\text{total volume of dispersion}}. \tag{8.1}$$

Polymers are also essential for stabilizing nonaqueous dispersions, since in this case electrostatic stabilization is not possible (due to the low dielectric constant of the medium). To understand the role of polymers in dispersion stability, it is essential to consider the adsorption and conformation of the macromolecule at the solid/liquid interface and this was discussed in detail in Chapter 6. Polymers and polyelectrolytes are also used for the destabilization of suspensions, e.g. for solid/liquid separation.

In this chapter, I will discuss the interaction between particles or droplets containing adsorbed polymeric surfactants. The latter form an adsorbed layer with thickness δ that depends on the molar mass of the stabilizing chain(s) A. As will be discussed below, when two particles or droplets approach each other to a surface-to-surface distance h, the stabilizing chains (which must be in good solvent conditions) may interpenetrate or become compressed, resulting in a high segment density of the A chain(s) in the overlap or compressed region. This forms the basis of strong repulsion between the particles or droplets that is referred to as steric stabilization. Examples for stabilization of emulsions, nanoemulsions and suspensions using polymeric surfactants are given in this chapter.

https://doi.org/10.1515/9783110587944-009

8.2 Interaction between particles or droplets containing adsorbed polymer layers

As mentioned in the introduction, when two particles or droplets each with a radius R and containing an adsorbed polymer layer with a hydrodynamic thickness δ_h, approach each other to a surface-surface separation distance h that is smaller than $2\delta_h$, the polymer layers interact with each other resulting in two main situations [1–3]:

(i) the polymer chains may overlap with each other;
(ii) the polymer layer may undergo some compression.

In both cases, there will be an increase in the local segment density of the polymer chains in the interaction region. This is schematically illustrated in Fig. 8.1. The real situation is perhaps in between the above two cases, i.e. the polymer chains may undergo some interpenetration and some compression.

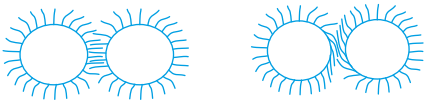

Fig. 8.1: Schematic representation of the interaction between particles or droplets containing adsorbed polymer layers.

Provided the dangling chains (the A chains in A–B, A–B–A block or BA_n graft copolymers) are in a good solvent, this local increase in segment density in the interaction zone will result in strong repulsion as a result of two main effects:

(i) An increase in the osmotic pressure in the overlap region as a result of the unfavourable mixing of the polymer chains, when these are in good solvent conditions. This is referred to as osmotic repulsion or mixing interaction and it is described by a free energy of interaction G_{mix}.
(ii) A reduction of the configurational entropy of the chains in the interaction zone; this entropy reduction results from the decrease in the volume available for the chains when these are either overlapped or compressed. This is referred to as volume restriction interaction, entropic or elastic interaction and it is described by a free energy of interaction G_{el}.

The combination of G_{mix} and G_{el} is usually referred to as the steric interaction free energy, G_s, i.e.,

$$G_s = G_{mix} + G_{el}. \tag{8.2}$$

The sign of G_{mix} depends on the solvency of the medium for the chains. If in a good solvent, i.e. the Flory–Huggins interaction parameter χ is less than 0.5, then G_{mix} is positive and the mixing interaction leads to repulsion (see below). In contrast if $\chi > 0.5$ (i.e. the chains are in a poor solvent condition), G_{mix} is negative and the mixing interaction becomes attractive. G_{el} is always positive and hence in some cases one can produce stable dispersions in a relatively poor solvent (enhanced steric stabilization).

8.2.1 Mixing interaction G_{mix}

This results from the unfavourable mixing of the polymer chains, when these are in a good solvent conditions. This is schematically shown in Fig. 8.2. Consider two spherical particles or droplets with the same radius and each containing an adsorbed polymer layer (with uniform segment density distribution) with thickness δ. Before overlap, one can define in each polymer layer a chemical potential for the solvent μ_i^{α} and a volume fraction for the polymer in the layer ϕ_2^{α}. In the overlap region (volume element dV), the chemical potential of the solvent is reduced to μ_i^{β} and the volume fraction of the polymer increases to ϕ_2^{β}.

In the overlap region, the chemical potential of the polymer chains is now higher than in the rest of the layer (with no overlap). This amounts to an increase in the osmotic pressure in the overlap region; as a result solvent will diffuse from the bulk to the overlap region, thus separating the particles and hence a strong repulsive energy arises from this effect. The above repulsive energy can be calculated by considering

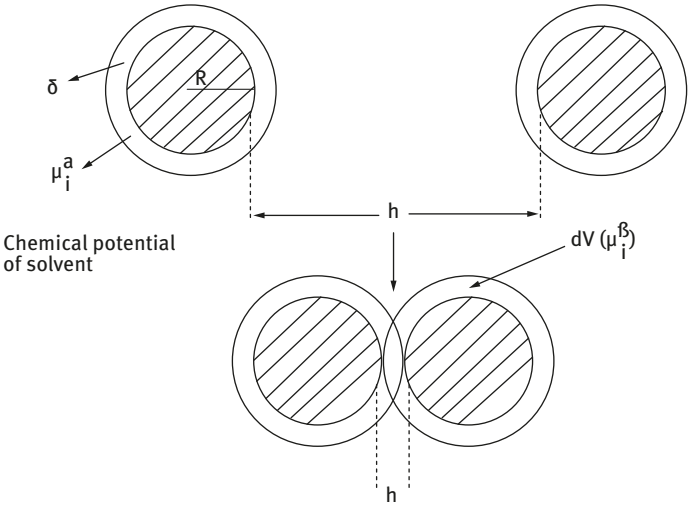

Fig. 8.2: Schematic representation of polymer layer overlap.

the free energy of mixing of two polymer solutions, as for example treated by Flory and Krigbaum [4]. The free energy of mixing is given by two terms:

(i) an entropy term that depends on the volume fraction of polymer and solvent;
(ii) an energy term that is determined by the Flory–Huggins interaction parameter χ,

$$\delta(G_{\text{mix}}) = kT(n_1 \ln \phi_1 + n_2 \ln \phi_2 + \chi n_1 \phi_2), \tag{8.3}$$

where n_1 and n_2 are the number of moles of solvent and polymer with volume fractions ϕ_1 and ϕ_2, k is the Boltzmann constant and T is the absolute temperature.

The total change in free energy of mixing for the whole interaction zone, V, is obtained by summing over all the elements in V,

$$G_{\text{mix}} = \frac{2kT\,V_2^2}{V_1}\,\nu_2\left(\frac{1}{2} - \chi\right)R_{\text{mix}}(h), \tag{8.4}$$

where V_1 and V_2 are the molar volumes of solvent and polymer respectively, ν_2 is the number of chains per unit area and $R_{\text{mix}}(h)$ is a geometric function which depends on the form of the segment density distribution of the chain normal to the surface, $\rho(z)$. k is the Boltzmann constant and T is the absolute temperature.

Using the above theory one can derive an expression for the free energy of mixing of two polymer layers (assuming a uniform segment density distribution in each layer) surrounding two spherical particles as a function of the separation distance h between the particles. The expression for G_{mix} is [5],

$$\frac{G_{\text{mix}}}{kT} = \left(\frac{2V_2^2}{V_1}\right)\nu_2^2\left(\frac{1}{2} - \chi\right)\left(\delta - \frac{h}{2}\right)^2\left(3R + 2\delta + \frac{h}{2}\right), \tag{8.5}$$

where k is the Boltzmann constant and T is the absolute temperature.

The sign of G_{mix} depends on the value of the Flory–Huggins interaction parameter χ: if $\chi < 0.5$, G_{mix} is positive and the interaction is repulsive; if $\chi > 0.5$, G_{mix} is negative and the interaction is attractive; if $\chi = 0.5$, $G_{\text{mix}} = 0$ and this defines the θ-condition.

8.2.2 Elastic interaction G_{el}

This arises from the loss in configurational entropy of the chains on the approach of a second particle or droplet. As a result of this approach, the volume available for the chains becomes restricted, resulting in loss of the number of configurations. This can be illustrated by considering a simple molecule, represented by a rod that rotates freely in a hemisphere across a surface (Fig. 8.3). When the two surfaces are separated by an infinite distance ∞, the number of configurations of the rod is $\Omega(\infty)$ which is

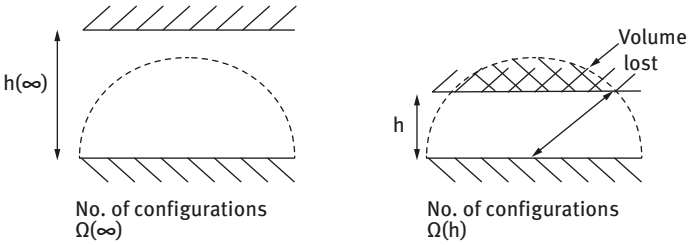

Fig. 8.3: Schematic representation of configurational entropy loss on approach of a second particle.

proportional to the volume of the hemisphere. When a second particle or droplet approaches to a distance h such that it cuts the hemisphere (losing some volume), the volume available to the chains is reduced and the number of configurations become $\Omega(h)$, which is less than $\Omega(\infty)$. For two flat plates, G_{el} is given by the following expression [6],

$$\frac{G_{el}}{kT} = -2v_2 \ln\left[\frac{\Omega(h)}{\Omega(\infty)}\right] = 2v_2 R_{el}(h), \tag{8.6}$$

where $R_{el}(h)$ is a geometric function whose form depends on the segment density distribution. It should be stressed that G_{el} is always positive and could play a major role in steric stabilization. It becomes very strong when the separation distance between the particles becomes comparable to the adsorbed layer thickness δ.

8.2.3 Total energy of interaction

The combination of G_{mix} and G_{el} with G_A gives the total energy of interaction G_T (assuming there is no contribution from any residual electrostatic interaction) [7], i.e.,

$$G_T = G_{mix} + G_{el} + G_A. \tag{8.7}$$

A schematic representation of the variation of G_{mix}, G_{el}, G_A and G_T with surface-surface separation distance h is shown in Fig. 8.4. G_{mix} increases very sharply with decreasing h when $h < 2\delta$. G_{el} increases very sharply with decreasing h when $h < \delta$. G_T versus h shows a minimum, G_{min}, at separation distances comparable to 2δ. When $h < 2\delta$, G_T shows a rapid increase with decreasing h. The depth of the minimum depends on the Hamaker constant A, the particle radius R and adsorbed layer thickness δ. G_{min} increases with increasing A and R. At a given A and R, G_{min} increases with decreasing δ (i.e. with decreasing molecular weight, M_w, of the stabilizer). This is illustrated in Fig. 8.5 which shows the energy–distance curves as a function of δ/R. The larger the value of δ/R, the smaller the value of G_{min}. In this case the system may approach thermodynamic stability as is the case with nanodispersions.

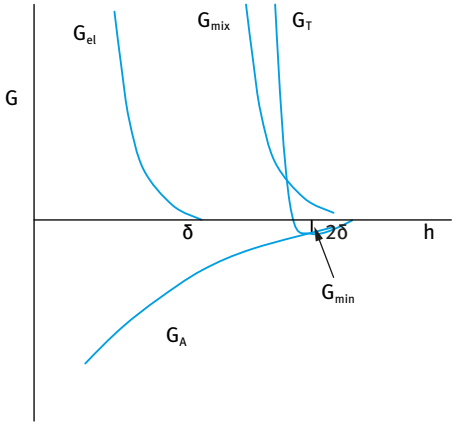

Fig. 8.4: Energy–distance curves for sterically stabilized systems.

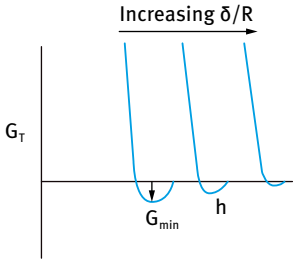

Fig. 8.5: Variation of G_{min} with δ/R.

8.2.4 Criteria for effective steric stabilization

(i) The particles or droplets should be completely covered by the polymer (the amount of polymer should correspond to the plateau value). Any bare patches may cause flocculation either by van der Waals attraction (between the bare patches) or by bridging flocculation (when a polymer molecule becomes simultaneously adsorbed on two or more particles or droplets).

(ii) The polymer should be strongly "anchored" to the particle surfaces, to prevent any displacement during particle approach. This is particularly important for concentrated suspensions and emulsions. For this purpose A–B, A–B–A block and BA_n graft copolymers are the most suitable where the chain B is chosen to be highly insoluble in the medium and to have a strong affinity to the surface. Examples of B groups for hydrophobic particles or droplets in aqueous media are polystyrene and polymethylmethacrylate.

(iii) The stabilizing chain A should be highly soluble in the medium and strongly solvated by its molecules. Examples of A chains in aqueous media are poly(ethylene oxide) and poly(vinyl alcohol).

(iv) δ should be sufficiently large (> 5 nm) to prevent weak flocculation.

8.3 Emulsions stabilized by polymeric surfactants

The most effective method for emulsion stabilization is to use polymeric surfactants that strongly adsorb at the O/W or W/O interface and produce effective steric stabilization against strong flocculation, coalescence and Ostwald ripening [1, 8].

As mentioned in Chapter 3, a graft copolymer of the AB_n type was synthesized by grafting several alkyl groups on an inulin (polyfructose) chain [9–11]. The polymeric surfactant (INUTEC® SP1) consists of a linear polyfructose chain (the stabilizing A chain) and several alkyl groups (the B chains) that provide multianchor attachment to the oil droplets. This polymeric surfactant produces enhanced steric stabilization both in water and high electrolyte concentrations as will be discussed later.

For water-in-oil (W/O) emulsions an A–B–A block copolymer of poly (12-hydroxystearic acid) (PHS) (the A chains) and poly(ethylene oxide) (PEO) (the B chain): PHS–PEO–PHS is commercially available (Arlacel P135, UNIQEMA). The PEO chain (that is soluble in the water droplets) forms the anchor chain, whereas the PHS chains form the stabilizing chains. PHS is highly soluble in most hydrocarbon solvents and is strongly solvated by its molecules. The structure of the PHS–PEO–PHS block copolymer is schematically shown in Fig. 8.6.

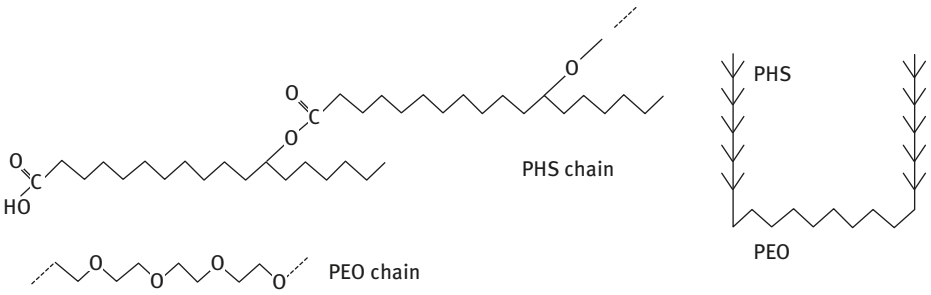

Fig. 8.6: Schematic representation of the structure of PHS–PEO–PHS block copolymer.

The conformation of the polymeric surfactant at the W/O interface is schematically shown in Fig. 8.7.

Emulsions of Isopar M/water and cyclomethicone/water were prepared using INUTEC® SP1. 50/50 (v/v) O/W emulsions were prepared and the emulsifier concentration was varied from 0.25 to 2 (w/v) % based on the oil phase. 0.5 (w/v) % emulsifier was sufficient for stabilization of these 50/50 (v/v) emulsions [12].

The emulsions were stored at room temperature and 50 °C and optical micrographs were taken at intervals of time (for a year) in order to check the stability. Emulsions prepared in water were very stable showing no change in droplet size distribution over more than a one year period and this indicated absence of coalescence. Any weak flocculation that occurred was reversible and the emulsion could

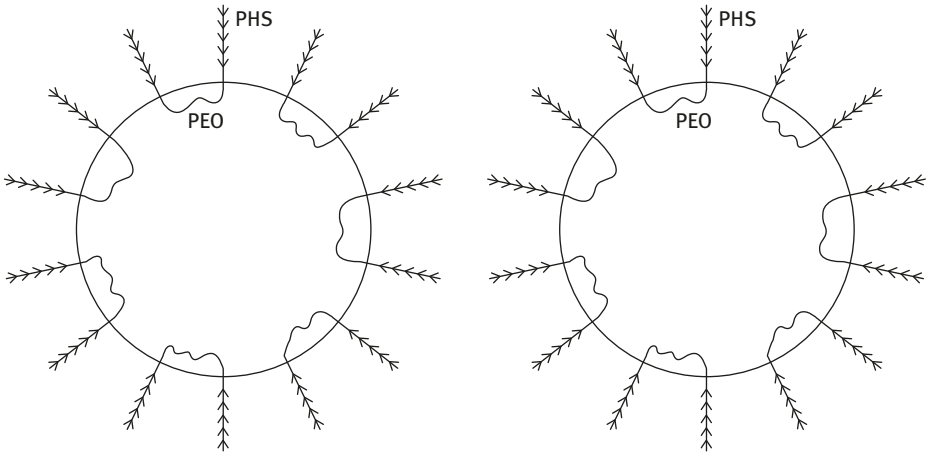

Fig. 8.7: Conformation of PHS–PEO–PHS polymeric surfactant at the W/O interface.

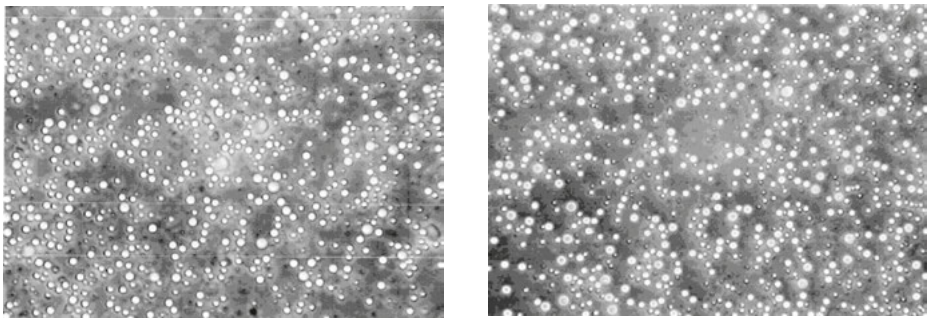

(a) (b)

Fig. 8.8: Optical micrographs of O/W emulsions stabilized with INUTEC® SP1 stored at 50 °C for 1.5 weeks (A) and 14 weeks (B).

be redispersed by gentle shaking. Fig. 8.8 shows an optical micrograph for a dilute 50/50 (v/v) emulsion that was stored for 1.5 and 14 weeks at 50 °C. No change in droplet size was observed after storage for more than one year at 50 °C, indicating absence of coalescence. The same result was obtained when using different oils. Emulsions were also stable against coalescence in the presence of high electrolyte concentrations (up to 4 mol dm^{-3} or ≈ 25 % NaCl). This stability in high electrolyte concentrations is not observed with polymeric surfactants based on polyethylene oxide.

The high stability observed using INUTEC® SP1 is related to its strong hydration both in water and in electrolyte solutions. The hydration of inulin (the backbone of HMI) could be assessed using cloud point measurements. A comparison was also made with PEO with two molecular weights, namely 4,000 and 20,000. Solutions of PEO 4,000 and 20,000 showed a systematic decrease of cloud point with increas-

ing NaCl or $MgSO_4$ concentration. In contrast, inulin showed no cloud point up to 4 mol dm^{-3} NaCl and up to 1 mol dm^{-3} $MgSO_4$. These results explain the difference between PEO and inulin. With PEO, the chains show dehydration when the NaCl concentration is increased above 2 mol dm^{-3} or 0.5 mol dm^{-3} $MgSO_4$. The inulin chains remain hydrated at much higher electrolyte concentrations. It seems that the linear polyfructose chains remain strongly hydrated at high temperature and high electrolyte concentrations.

The high emulsion stability obtained when using INUTEC® SP1 can be accounted for by the following factors:

(i) the multipoint attachment of the polymer by several alkyl chains that are grafted on the backbone;
(ii) the strong hydration of the polyfructose "loops" both in water and high electrolyte concentrations (χ remains below 0.5 under these conditions);
(iii) the high volume fraction (concentration) of the loops at the interface;
(iv) enhanced steric stabilization; this is the case with multipoint attachment which produces strong elastic interaction.

Evidence for the high stability of the liquid film between emulsion droplets when using INUTEC® SP1 was obtained by Exerowa et al. [13] using disjoining pressure measurements. This is illustrated in Fig. 8.9 which shows a plot of disjoining pressure versus separation distance between two emulsion droplets at various electrolyte concentrations. The results show that by increasing the capillary pressure a stable Newton black film (NBF) is obtained at a film thickness of ≈ 7 nm. The lack of rupture of the film at the highest pressure applied of 4.5×10^4 Pa indicates the high stability of the film in water and in high electrolyte concentrations (up to 2.0 mol dm^{-3} NaCl).

The lack of rupture of the NBF up to the highest pressure applied, namely 4.5×10^4 Pa clearly indicates the high stability of the liquid film in the presence of high NaCl concentrations (up to 2 mol dm^{-3}). This result is consistent with the high emulsion stability obtained at high electrolyte concentrations and high temperature. Emulsions of Isopar M-in-water are very stable under such conditions and this could be accounted for by the high stability of the NBF. The droplet size of 50 : 50 O/W emulsions prepared using 2% INUTEC® SP1 is in the region of 1–10 μm. This corresponds to a capillary pressure of $\approx 3 \times 10^4$ Pa for the 1 μm drops and $\approx 3 \times 10^3$ Pa for the 10 μm drops. These capillary pressures are lower than those to which the NBF have been subjected and this clearly indicates the high stability obtained against coalescence in these emulsions.

W/O emulsions (the oil being Isopar M) were prepared using PHS–PEO–PHS block copolymer at high water volume fractions (> 0.7). The emulsions have a narrow droplet size distribution with a *z*-average radius of 183 nm [14]. They also remained fluid up to high water volume fractions (> 0.6). This can be illustrated from viscosity–volume fraction curves as shown in Fig. 8.10.

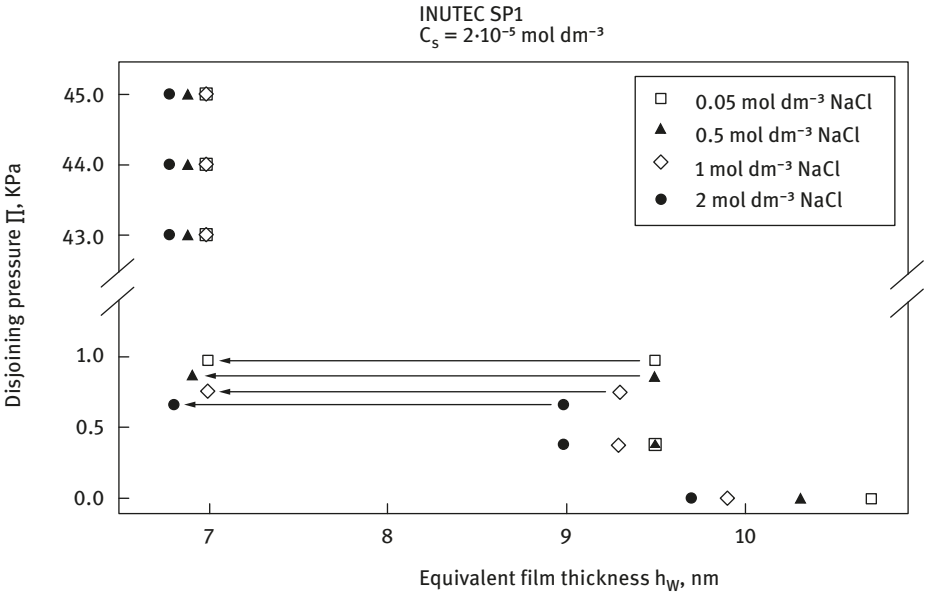

Fig. 8.9: Variation of disjoining pressure with equivalent film thickness at various NaCl concentrations.

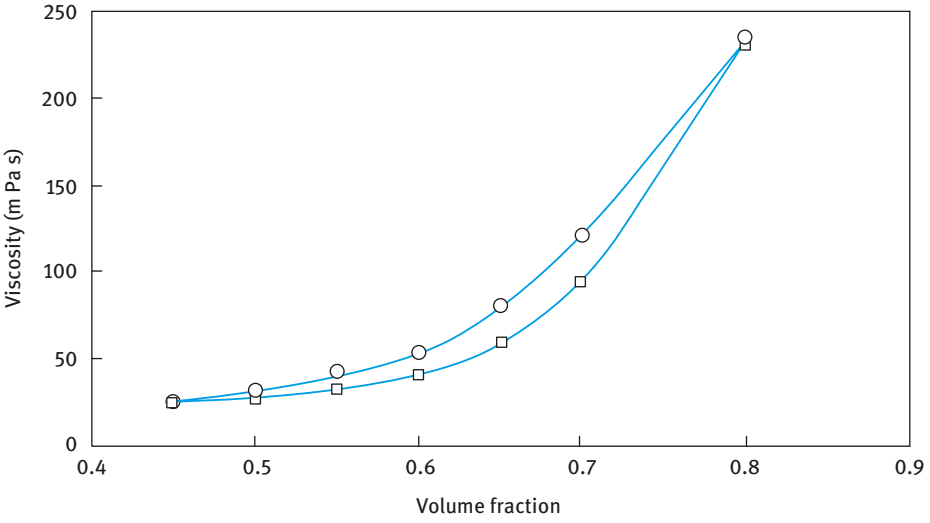

Fig. 8.10: Viscosity–volume fraction for W/O emulsion stabilized with PHS–PEO–PHS block copolymer.

The effective volume fraction ϕ_{eff} of the emulsions (the core droplets plus the adsorbed layer) can be calculated from the relative viscosity and using the Dougherty–Krieger equation [15],

$$\eta_r = \left[1 - \frac{\phi_{\text{eff}}}{\phi_p}\right]^{-[\eta]\phi_p}, \tag{8.8}$$

where η_r is the relative viscosity, ϕ_p is the maximum packing fraction (≈ 0.7) and $[\eta]$ is the intrinsic viscosity that is equal to 2.5 for hard spheres.

The calculations based on equation (8.8) are shown in Fig. 8.9 (square symbols). From the effective volume fraction ϕ_{eff} and the core volume fraction ϕ, the adsorbed layer thickness could be calculated. This was found to be in the region of 10 nm at $\phi = 0.4$ and it decreased with increasing ϕ.

The W/O emulsions prepared using the PHS–PEO–PHS block copolymer remained stable both at room temperature and at 50 °C. This is consistent with the structure of the block copolymer: the B chain (PEO) is soluble in water and it forms a very strong anchor at the W/O interface. The PHS chains (the A chains) provide effective steric stabilization since the chains are highly soluble in Isopar M and are strongly solvated by its molecules.

8.4 Suspensions stabilized using polymeric surfactants

There are generally two procedures for preparation of solid/liquid dispersions [16]:

(i) Condensation methods: Build-up of particles from molecular units, i.e. nucleation and growth. A special procedure is the preparation of latexes by emulsion or dispersion polymerization.

(ii) Dispersion methods: In this case one starts with preformed large particles or crystals which are dispersed in the liquid by using a surfactant (wetting agent) with subsequent breaking up of the large particles by milling (comminution) to achieve the desirable particle size distribution. A dispersing agent (usually a polymeric surfactant) is used for the dispersion process and subsequent stabilization of the resulting suspension.

There are generally two procedures for preparation of latexes:

(i) Emulsion polymerization: The monomers that are essentially insoluble in the aqueous medium are emulsified using a surfactant and an initiator is added while heating the system to produce the polymer particles that are stabilized electrostatically (when using ionic surfactants) or sterically (when using nonionic surfactants.

(ii) Dispersion polymerization: The monomers are dissolved in a solvent in which the resulting polymer particles are insoluble. A protective colloid (normally a block or graft copolymer) is added to prevent flocculation of the resulting polymers particles that are produced on addition of an initiator. This method is usually applied

for the production of nonaqueous latex dispersions and is sometimes referred to as nonaqueous dispersion polymerization (NAD).

Surfactants play a crucial role in the process of latex preparation since they determine the stabilizing efficiency, and the effectiveness of the surface active agent ultimately determines the number of particles and their size. The effectiveness of any surface active agent in stabilizing the particles is the dominant factor and the number of micelles formed is relatively unimportant. In the NAD process the monomer, normally an acrylic, is dissolved in a nonaqueous solvent, normally an aliphatic hydrocarbon and an oil-soluble initiator and a stabilizer (to protect the resulting particles from flocculation) are added to the reaction mixture. The most successful stabilizers used in NAD are block and graft copolymers. Preformed graft stabilizers based on poly(12-hydroxy stearic acid) (PHS) are simple to prepare and effective in NAD polymerization.

Dispersion methods are used for the preparation of suspensions of preformed particles. The role of surfactants (or polymers) in the dispersion process can be analysed in terms of the three processes involved:

(i) wetting of the powder by the liquid;
(ii) breaking up of the aggregates and agglomerates;
(iii) comminution of the resulting particles and their subsequent stabilization.

All these processes are affected by surfactants or polymers which adsorb on the powder surface thus aiding the wetting of the powder, break-up of the aggregates and agglomerates and subsequent reduction of particle size by wet milling.

8.4.1 Polymeric surfactants in emulsion polymerization

As mentioned above, the graft copolymer of hydrophobically modified inulin (INUTEC® SP1) has been used in emulsion polymerization of styrene, methyl methacrylate, butyl acrylate and several other monomers [17]. All latexes were prepared by emulsion polymerization using potassium persulphate as initiator. The *z*-average particle size was determined by photon correlation spectroscopy (PCS) and electron micrographs were also taken.

Emulsion polymerization of styrene or methylmethacrylate showed an optimum ratio of (INUTEC® SP1)/monomer of 0.0033 for PS and 0.001 for PMMA particles. The (initiator)/(monomer) ratio was kept constant at 0.00125. The monomer conversion was higher than 85 % in all cases. Latex dispersions of PS reaching 50 % and of PMMA reaching 40 % could be obtained using such low concentrations of INUTEC® SP1. Fig. 8.11 shows the variation of particle diameter with monomer concentration.

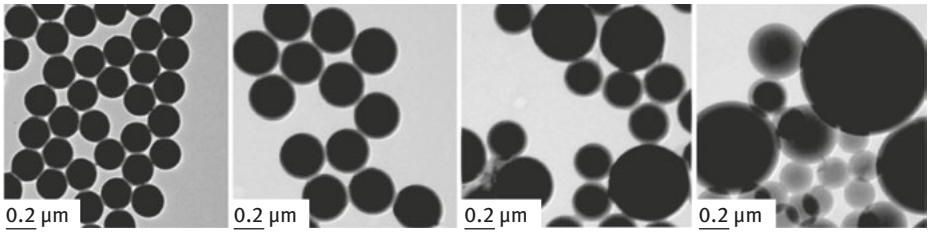

(5 wt%) (10 wt%) (30 wt%) (40 wt%)

(a) PS latexes

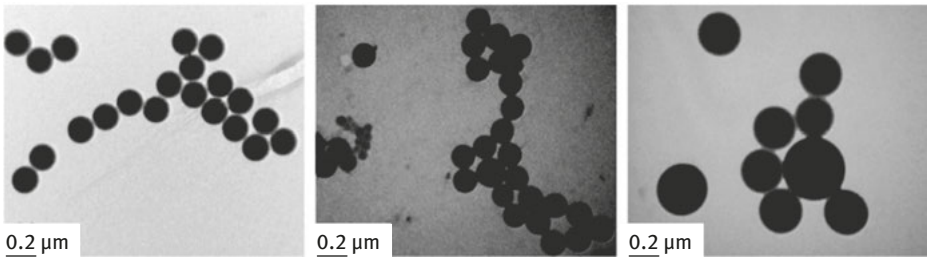

(10 wt%) (20 wt%) (30 wt%)

(b) PMMA Latexes

Fig. 8.11: Electron micrographs of the latexes.

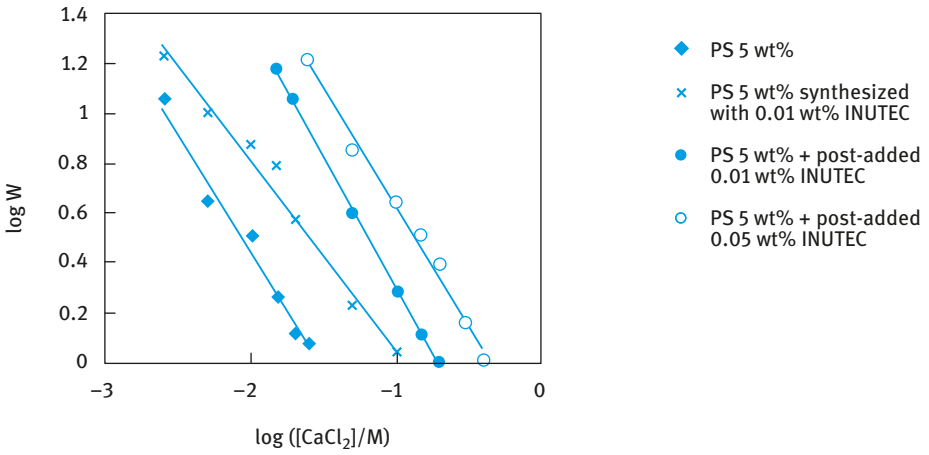

Fig. 8.12: Influence of post addition of INUTEC® SP1 on the latex's stability.

The stability of the latexes was established by determining the critical coagulation concentration (CCC) using $CaCl_2$. The CCC was low (0.0175–0.05 mol dm^{-3}) but this was higher than that for the latex prepared without surfactant. Post addition of INUTEC® SP1 resulted in a large increase in the CCC as is illustrated in Fig. 8.12 which shows log W–log C curves (where W is the stability ratio) at various additions of INUTEC® SP1.

As with the emulsions, the high stability of the latex when using INUTEC® SP1 is due to the strong adsorption of the polymeric surfactant on the latex particles and formation of strongly hydrated loops and tails of polyfructose that provide effective steric stabilization. Evidence for the strong repulsion produced when using INUTEC® SP1 was obtained from atomic force microscopy (AFM) investigations [18] in which the force between hydrophobic glass spheres and hydrophobic glass plate, both containing an adsorbed layer of INUTEC® SP1, was measured as a function of distance of separation both in water and in the presence of various Na_2SO_4 concentrations. The AFM used was capable of measuring pico-Newton surface forces at nanometre length scales. The interaction between glass spheres that were attached to the AFM cantilever and glass plates (both hydrophobized using dichlorodimethylsilane) and containing adsorbed layers of hydrophobically modified inulin (INUTEC® SP1) was measured as a function of INUTEC® SP1 concentration in water and at various Na_2SO_4 concentrations.

Measurements were initially carried out as a function of time (2, 5 and 24 hours) at 2×10^{-4} mol dm^{-3} INUTEC® SP1 [18]. After 2 and 5 hours equilibration time, the force-separation distance curve showed some residual attraction on withdrawal (Fig. 8.13). By increasing the equilibration time (24 hours), this residual attraction on withdrawal disappeared and the approach and withdrawal curves were very close, indicating full coverage of the surfaces with polymer within this time. All subsequent measurements were carried out after 24 hours to ensure complete adsorption. Measurements were carried out at five different concentrations of INUTEC® SP1: 6.6×10^{-6}, 1×10^{-5}, 6×10^{-5}, 1.6×10^{-4} and 2×10^{-4} mol dm^{-3}. At concentrations $< 1.6 \times 10^{-4}$ mol dm^{-3}, the withdrawal curve showed some residual attraction, as illustrated in Fig. 8.13 for 6×10^{-5} mol dm^{-3}. At concentrations $> 1.6 \times 10^{-4}$ mol dm^{-3}, the approach and withdrawal curves were very close to each other, as illustrated in Fig. 8.14 for 2×10^{-4} mol dm^{-3}. These results indicate full coverage of the surfaces by the polymer when the INUTEC® SP1 concentration becomes equal to or higher than 1.6×10^{-4} mol dm^{-3}. The results at full coverage give an adsorbed layer thickness of the order of 9 nm which indicate strong hydration of the loops and tails of inulin [18].

Several investigations of the stability of emulsions and suspensions stabilized using INUTEC® SP1 showed absence of flocculation in the presence of high electrolyte concentrations (up to 4 mol dm^{-3} NaCl and 1.5 mol dm^{-3} $MgSO_4$) [12]. This high stability in the presence of high electrolyte concentrations is attributed to the strong hydration of inulin (polyfructose) loops and tails. This strong hydration was confirmed by measuring the cloud point of inulin in the presence of such high elec-

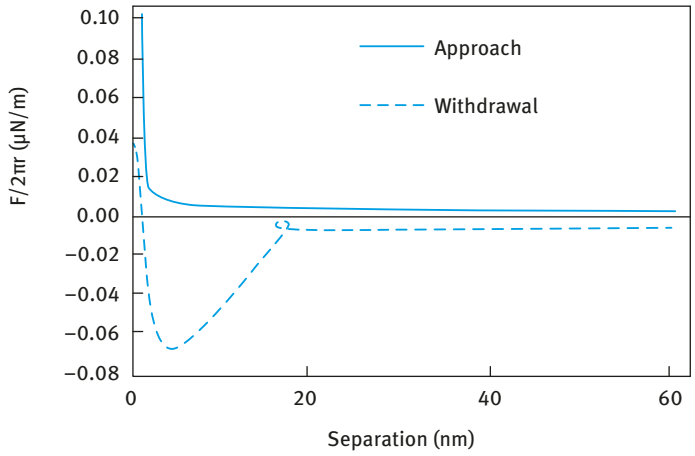

Fig. 8.13: Force–distance curves at 6×10^{-5} mol dm^{-3} INUTEC® SP1.

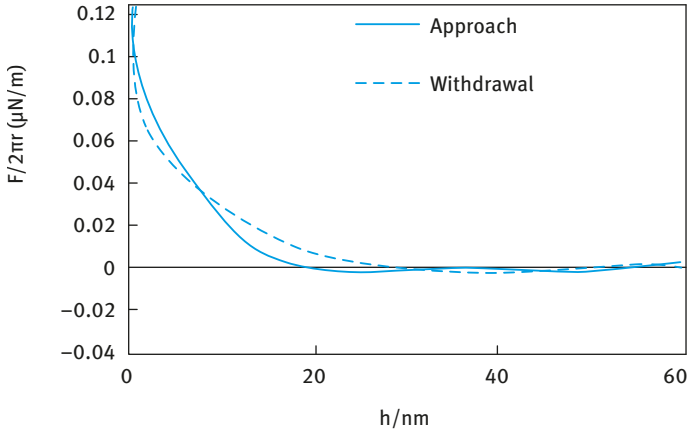

Fig. 8.14: Force–distance curves at 2×10^{-4} mol dm^{-3} INUTEC® SP1.

trolyte concentrations (the cloud point exceeded 100 °C up to 4 mol dm^{-3} NaCl and 1.0 mol dm^{-3} $MgSO_4$). Evidence of such strong repulsion was obtained from the force–distance curves in the presence of different concentrations of Na_2SO_4 as shown in Fig. 8.15.

The force–distance curves clearly show that the interaction remains repulsive up to the highest Na_2SO_4 concentration (1.5 mol dm^{-3}) studied. The adsorbed layer thickness decreases from approximately 9 nm at 0.3 mol dm^{-3} to about 3 nm at 1.5 mol dm^{-3} Na_2SO_4. This reduction in hydrodynamic thickness in the presence of high electrolyte concentrations is probably due to the change in the conformation of polyfructose loops and tails. It is highly unlikely that dehydration of the chains occurs since cloud

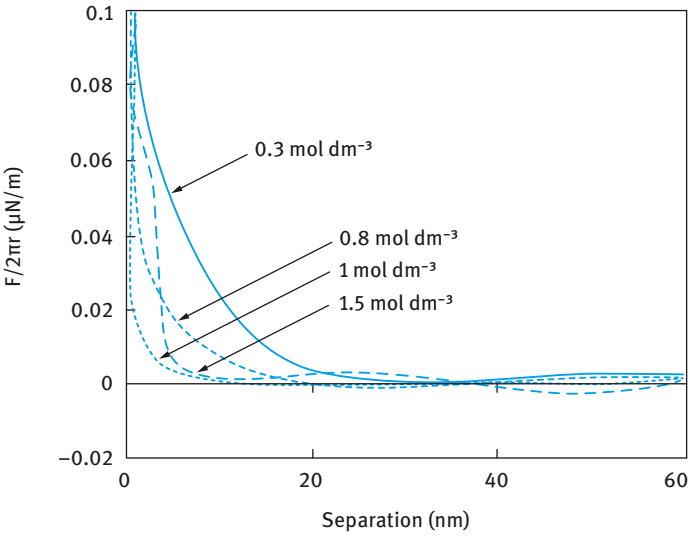

Fig. 8.15: Force–distance curves for hydrophobized glass surfaces containing adsorbed INUTEC® SP1 at various Na_2SO_4 concentrations.

point measurements have shown the absence of any cloud point up to 100 °C. Even at such low adsorbed layer thickness, strong repulsive interaction is observed indicating a high elastic repulsive term.

The interaction between INUTEC® SP1 adsorbed layers was investigated using rheological measurements. Steady state shear stress–shear rate curves were obtained at various volume fractions ϕ of polystyrene latex (PS) dispersions (in the range ϕ = 0.1–0.42) that contained adsorbed layers of INUTEC® SP1. The results showed a shear thinning behaviour with the viscosity decreasing with applied shear rate and eventually reaching a plateau value when the shear rate exceeded 100 s^{-1}. Fig. 8.16 shows the variation of the relative viscosity η_r (measured at a shear rate of 1,000 s^{-1}) as a function of the latex core volume fraction ϕ (with particle radius of 161 nm). It can be clearly seen that η_r increases gradually with increasing ϕ, but when the latter increases above 0.3 there is a rapid increase in η_r with any further increase in ϕ. This trend is typical for concentrated dispersions.

The η_r–ϕ curve was calculated on the basis of Dougherty–Krieger equation (equation (8.8)). $[\eta]$ is the intrinsic viscosity and was taken to be equal to 2.5 (for hard spheres) and ϕ_p was obtained from a plot of $1/(\eta_r)^{1/2}$ versus ϕ (straight lines were obtained) and extrapolation of the results to $1/(\eta_r)^{1/2} = 0$. This gave a value of $\phi_p = 0.51$ for PS latex dispersions containing adsorbed INUTEC® SP1 layers.

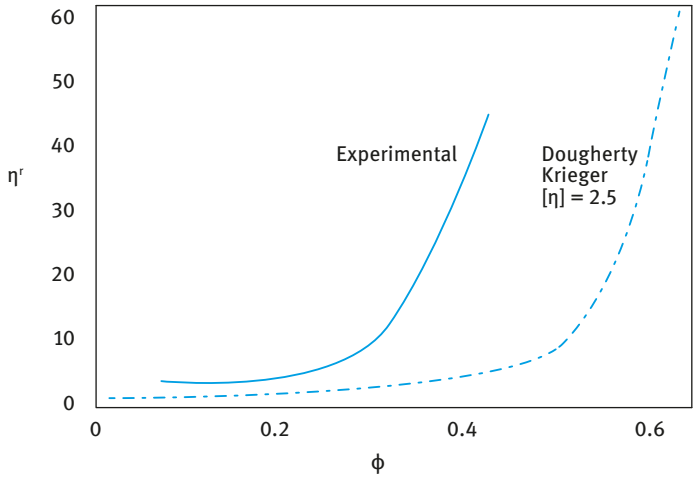

Fig. 8.16: Variation of η_r with ϕ for polystyrene latex dispersions.

It can be seen from Fig. 8.16 that the measured viscosity of the latex dispersions is significantly higher than the value calculated using the Dougherty–Krieger equation. This is due to the presence of adsorbed polymer layers on the latex particles.

From the measured η_r values one can obtain the effective volume fraction ϕ_{eff} of the latex dispersion, which can be used to obtain the adsorbed layer thickness δ,

$$\phi_{eff} = \phi\left[1 + \left(\frac{\delta}{R}\right)\right]^3. \tag{8.9}$$

This gave a value of $\delta = 9.6$ nm, which is close to the value obtained using the AFM measurements, again indicating the strong hydration of the polyfructose loops and tails.

Dynamic (oscillatory) measurements were obtained at various volume fractions ($\phi = 0.1$–0.42) of PS latex dispersions containing adsorbed layers of INUTEC® SP1. Initially, the frequency was fixed at 1 Hz (6.28 rad s^{-1}) and the storage modulus G' and the loss modulus G'' were measured as a function of applied stress (or strain) to obtain the linear viscoelastic region (where G' and G'' are independent of applied stress or strain) (see below). Measurements were then carried out as a function of frequency (0.01–10 Hz) while keeping the strain or stress in the linear region).

Fig. 8.17 shows the variation of G' and G'' with ϕ (at a stress amplitude in the linear region and frequency of 1 Hz). At $\phi < 0.2$, $G'' > G'$, whereas at $\phi > 0.2$, $G' > G''$ with $G' = G''$ at $\phi = 0.2$, corresponding to an effective volume fraction ϕ_{eff} of 0.24. This low value of ϕ_{eff} indicates very strong repulsive interaction beginning at long separation distance (long-range interaction) between the hydrated loops and tails of polyfructose chains.

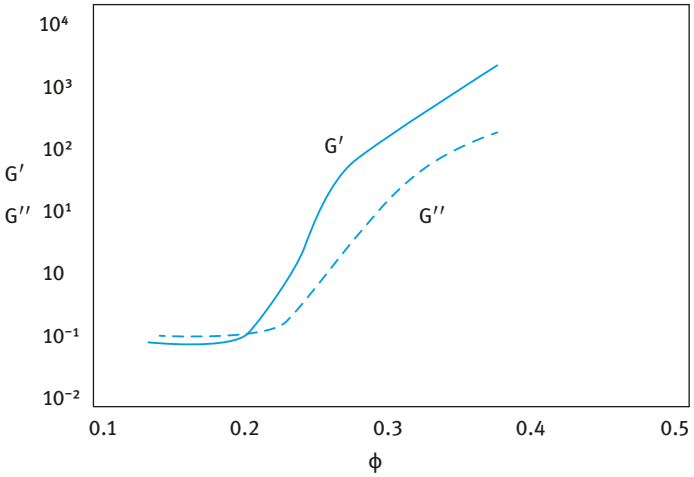

Fig. 8.17: Variation of G' and G'' (at 1 Hz) with volume fraction of PS latex with adsorbed INUTEC® SP1.

8.4.2 Dispersion polymerization

This method is usually applied for the preparation of nonaqueous latex dispersions and hence it is referred to as NAD. The method has also been adapted to prepare aqueous latex dispersions by using an alcohol–water mixture. In the NAD process the monomer, normally an acrylic, is dissolved in a nonaqueous solvent, normally an aliphatic hydrocarbon, and an oil-soluble initiator and a stabilizer (to protect the resulting particles from flocculation) are added to the reaction mixture. The most successful stabilizers used in NAD are block and graft copolymers. Preformed graft stabilizers based on poly(12-hydroxy stearic acid) (PHS) are simple to prepare and effective in NAD polymerization. Commercial 12-hydroxystearic acid contains 8–15 % palmitic and stearic acids which limits the molecular weight during polymerization to an average of 1,500–2,000. This oligomer may be converted to a "macromonomer" by reacting the carboxylic group with glycidyl methacrylate. The macromonomer is then copolymerized with an equal weight of methyl methacrylate (MMA) or similar monomer to give a "comb" graft copolymer with an average molecular weight of 10,000–20,000. The graft copolymer contains on average 5–10 PHS chains pendent from a polymeric anchor backbone of PMMA. This graft copolymer can stabilize latex particles of various monomers. The major limitation of the monomer composition is that the polymer produced should be insoluble in the medium used.

NAD polymerization is carried in two steps:

(i) Seed stage: the diluent, portion of the monomer, portion of dispersant and initiator (azo or peroxy type) are heated to form an initial low-concentration fine dispersion.

(ii) Growth stage: the remaining monomer together with more dispersant and initiator are then fed over the course of several hours to complete the growth of the particles. A small amount of transfer agent is usually added to control the molecular weight. Excellent control of particle size is achieved by proper choice of the designed dispersant and correct distribution of dispersant between the seed and growth stages. NAD acrylic polymers are applied in automotive thermosetting polymers and hydroxy monomers may be included in the monomer blend used.

8.4.3 Polymeric surfactants for stabilization of preformed latex dispersions

For this purpose, polystyrene (PS) latexes were prepared using the surfactant-free emulsion polymerization. Two latexes with *z*-average diameter of 427 and 867 (as measured using photon correlation spectroscopy, PCS) that are reasonably monodisperse were prepared [19]. Two polymeric surfactants, namely Hypermer CG-6 and Atlox 4913 were used. Both are graft ("comb") type consisting of polymethylmethacrylate/polymethacrylic acid (PMMA/PMA) backbone with methoxy-capped polyethylene oxide (PEO) side chains (M = 750 Daltons). Hypermer CG-6 is the same graft copolymer as Atlox 4913 but it contains higher proportion of methacrylic acid in the backbone. The average molecular weight of the polymer is ≈ 5,000 Daltons. Fig. 8.18 shows a typical adsorption isotherm of Atlox 4913 on the two latexes. Similar results were obtained for Hypermer CG-6 but the plateau adsorption was lower (1.2 mg m^{-2} compared with 1.5 mg m^{-2} for Atlox 4913). It is likely that the backbone of Hypermer CG-6 that contains more PMA is more polar and hence less strongly adsorbed. The amount of adsorption was independent of particle size.

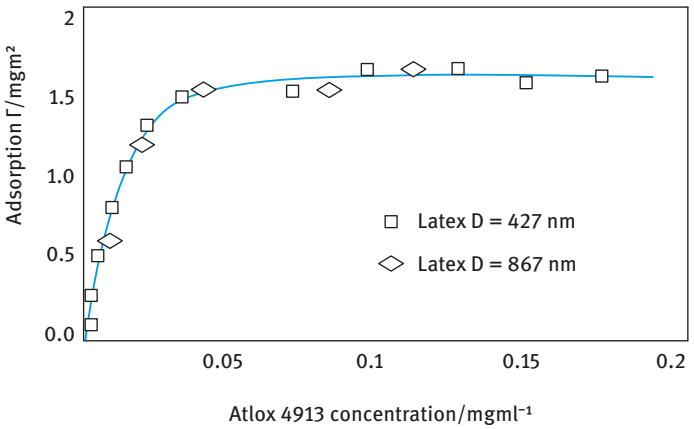

Fig. 8.18: Adsorption isotherms of Atlox 4913 on the two latexes at 25 °C.

The influence of temperature on adsorption is shown in Fig. 8.19.The amount of adsorption increases with increasing temperature. This is due to the poorer solvency of the medium for the PEO chains. The PEO chains become less hydrated at higher temperature and the reduced solubility of the polymer enhances adsorption.

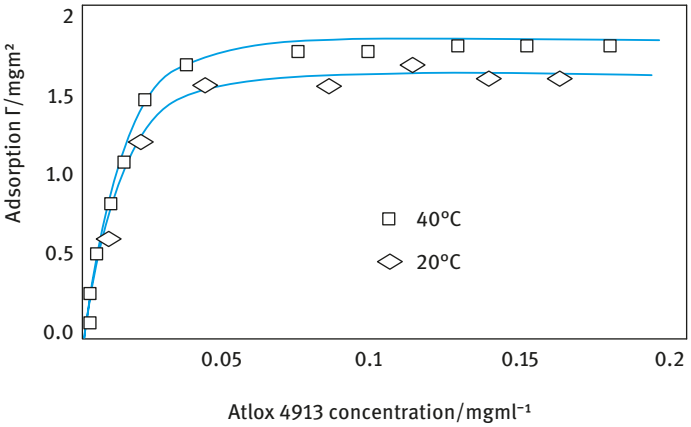

Fig. 8.19: Effect of temperature on adsorption of Atlox 4913 on PS.

The adsorbed layer thickness of the graft copolymer on the latexes was determined using rheological measurements. Steady state (shear stress σ–shear rate $\dot{\gamma}$) measurements were carried out and the results were fitted to the Bingham equation to obtain the yield value σ_β and the high shear viscosity η of the suspension,

$$\sigma = \sigma_\beta + \eta\dot{\gamma}. \tag{8.10}$$

As an illustration Fig. 8.20 shows a plot of σ_β versus volume fraction ϕ of the latex for Atlox 4913. Similar results were obtained for latexes stabilized using Hypermer CG-6.

At any given volume fraction, the smaller latex has higher σ_β when compared to the larger latex. This is due to the higher ratio of adsorbed layer thickness to particle radius, Δ/R, for the smaller latex. The effective volume fraction of the latex ϕ_{eff} is related to the core volume fraction by equation (8.9). As discussed before, ϕ_{eff} can be calculated from the relative viscosity η_r using the Dougherty–Krieger equation (equation (8.8)).

The maximum packing fraction ϕ_p can be calculated using the following empirical equation,

$$\frac{(\eta_r^{1/2} - 1)}{\phi} = \left(\frac{1}{\phi_p}\right)(\eta^{1/2} - 1) + 1.25. \tag{8.11}$$

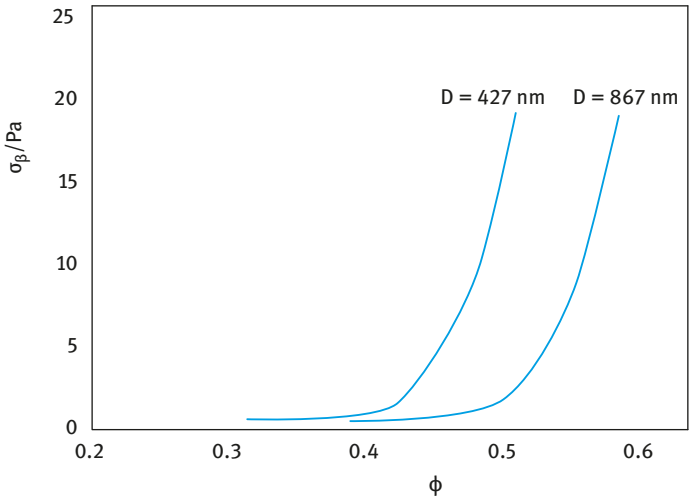

Fig. 8.20: Variation of yield stress with latex volume fraction for Atlox 4913.

The results showed a gradual decrease of adsorbed layer thickness δ with increasing volume fraction ϕ. For the latex with diameter D of 867 nm and Atlox 4913, δ decreased from 17.5 nm at $\phi = 0.36$ to 6.5 at $\phi = 0.57$. For Hypermer CG-6 with the same latex, δ decreased from 11.8 nm at $\phi = 0.49$ to 6.5 at $\phi = 0.57$. The reduction of δ with increasing ϕ may be due to overlap and/or compression of the adsorbed layers as the particles come close to each other at higher volume fraction of the latex.

The stability of the latexes was determined using viscoelastic measurements. For this purpose, dynamic (oscillatory) measurements were used to obtain the storage modulus G^*, the elastic modulus G' and the viscous modulus G'' as a function of strain amplitude γ_0 and frequency ω (rad s^{-1}). The method relies on application of a sinusoidal strain or stress and the resulting stress or strain is measured simultaneously. For a viscoelastic system, the strain and stress sine waves oscillate with the same frequency but out of phase. From the time shift Δt and ω one can obtain the phase angle shift δ.

The ratio of the maximum stress σ_0 to the maximum strain γ_0 gives the complex modulus $|G^*|$

$$|G^*| = \frac{\sigma_0}{\gamma_0}. \tag{8.12}$$

$|G^*|$ can be resolved into two components: Storage (elastic) modulus G', the real component of the complex modulus; loss (viscous) modulus G'', the imaginary component of the complex modulus. The complex modulus can be resolved into G' and G'' using vector analysis and the phase angle shift δ,

$$G' = |G^*| \cos \delta, \tag{8.13}$$

$$G'' = |G^*| \sin \delta. \tag{8.14}$$

G' is measured as a function of electrolyte concentration and/or temperature to assess the latex's stability. As an illustration Fig. 8.21 shows the variation of G' with temperature for latex stabilized with Atlox 4913 in the absence of any added electrolyte and in the presence of 0.1, 0.2 and 0.3 mol dm^{-3} Na_2SO_4. In the absence of electrolyte, G' showed no change with temperature up to 65 °C.

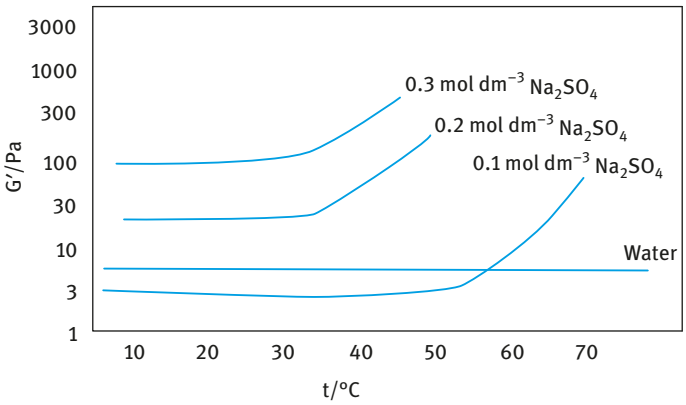

Fig. 8.21: Variation of G' with temperature in water and at various Na_2SO_4 concentrations.

In the presence of 0.1 mol dm^{-3} Na_2SO_4, G' remained constant up to 40 °C, above that temperature G' increased with any further increase of temperature. This temperature is denoted as the critical flocculation temperature (CFT). The CFT decreases with increasing electrolyte concentration reaching ≈ 30 °C in 0.2 and 0.3 mol dm^{-3} Na_2SO_4. This reduction in CFT with increaseing electrolyte concentration is due to the reduction in solvency of the PEO chains with increasing electrolyte concentrations. The latex stabilized with Hypermer CG-6 gave relatively higher CFT values when compared with that stabilized using Atlox 4913.

8.4.4 Interaction forces between adsorbed layers of PMMA/MA(PEO)$_n$ graft copolymer

The energy $E(D)$–distance curves for adsorbed layers of PMMA/MA(PEO)$_n$ (that are physically adsorbed on smooth mica sheets) are obtained using the surface force apparatus originally described by Israelachvili [20–23]. It consists of measuring the forces between mica sheets with molecularly smooth surfaces with a cross cylinder geometry. The mica sheets are partially silvered on the reverse side so that light interferometry can be used to measure the surface separation. The force between the surfaces is measured by monitoring the displacement of a leaf spring to which one of the sheets is attached. Initially, measurements are made in the presence of electrolyte solution

(10^{-2} mol dm^{-3} KNO_3) and then in the same electrolyte solution but with the mica sheets containing the adsorbed layers. In this manner one can subtract the double layer interaction from the total interaction to obtain the contribution from steric interaction.

The forces between the mica surfaces $F(D)$ bearing the copolymer layers are converted to the interaction potential energy $E(D)$ between flat surfaces using the Deryaguin approximation for cross cylinders [23],

$$E(D) = \frac{F(D)}{2\pi a}, \tag{8.15}$$

where D is the surface separation distance and a is the cylinder radius. Fig. 8.22 shows the energy–distance curve for mica sheets covered by the graft copolymer PMMA/MA$(PEO)_n$. The figure shows a monotonic and approximately exponential decrease of $E(D)$ with increasing separation distance D. The exponential decay makes it difficult to assess precisely the point at which the interaction begins. It falls below the detection limit of the instrument at ≈ 25 nm.

The energy of interaction between polymer layers can be calculated using de Gennes scaling theory [24],

$$E(D) = \frac{\beta kT}{s^3}\left[\frac{(2L)^{2.25}}{1.25(D)^{1.25}} + \frac{D^{1.75}}{1.75(2L)^{0.75}}\right] - \left[\frac{2L}{1.25} + \frac{2L}{1.75}\right], \tag{8.16}$$

where L is the stabilizer thickness on each surface (taken to be 12.5 nm, i.e. half the separation distance D at which $E(D)$ begins to increase with any further decrease of D), S is the distance between side chains k is the Boltzmann constant and T is the absolute temperature. The solid line in Fig. 8.22 shows the theoretical calculations based on equation (8.16). Agreement between theory and experiment is satisfactory.

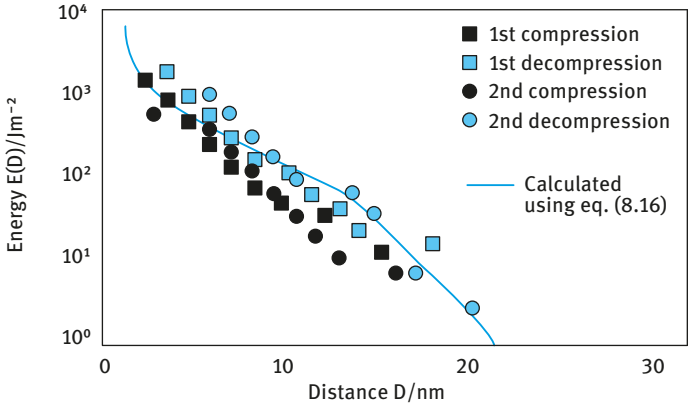

Fig. 8.22: Interaction energy $E(D)$ versus separation distance D.

The high frequency modulus of latex dispersions containing adsorbed layers of PMMA/MA(PEO)n graft copolymer was also measured. For this purpose latex dispersions were prepared using surfactant-free emulsion polymerization. The particle diameter was 330 ± 9 nm. Latex dispersions containing adsorbed PMMA/MA(PEO)$_n$ graft copolymer were prepared at various latex volume fractions.

The storage modulus G' of each dispersion was determined at low amplitudes (within the linear viscoelastic region) as a function of frequency. These measurements were obtained using dynamic (oscillatory) techniques. A plot of G' versus frequency ω (rad s^{-1}) allows one to obtain the plateau value G'_∞, i.e. the high frequency modulus which can be related to potential of mean force $V(R)$ as illustrated below.

The relationship between G_∞ and $V(R)$ is given by the following expression [24–27],

$$G'_\infty = NkT + \frac{2\pi N^2}{15}\int_0^\infty g(R)\frac{\mathrm{d}}{\mathrm{d}r}\left[R^4\left(\frac{\mathrm{d}V(R)}{\mathrm{d}R}\right)\right]\mathrm{d}R. \tag{8.17}$$

N is the number density of particles and $g(R)$ is the radius distribution function. The assumption made in the derivation of the above expression that the particle interactions involve only central pairwise additive potentials applies if the particles slip over each other without contact friction. Both short-range and long-range order have been observed in dispersions of monodisperse particles and it is likely that at least short-range order is retained where the system is under oscillatory shear with a low strain amplitude. If within the short-range domain a perfect lattice arrangement exists and $g(R)$ can be represented by a delta function centred at the nearest neighbour spacing R. Evans and Lips showed that under these conditions, equation (8.17) reduces to (8.18),

$$G'_\infty = NkT + \frac{\phi_\mathrm{m} n}{5\pi R^2}\left[4\frac{\mathrm{d}V(R)}{\mathrm{d}R} + R\frac{\mathrm{d}^2V(R)}{\mathrm{d}R^2}\right], \tag{8.18}$$

where ϕ_m is the maximum packing fraction and n is the coordination number. Equation (8.15) can be expressed in terms of interaction force F,

$$F = -\frac{\mathrm{d}V(R)}{\mathrm{d}R}. \tag{8.19}$$

The data of Fig. 8.22 are given as interaction energy between flat plates. They can be converted to the force between two spheres $E(D)$ using the Deryaguin approximation. This leads to the following expression for G'_∞,

$$G'_\infty = NkT - \frac{\phi_\mathrm{m} n a}{5R^2}\left[4E(D) + R\frac{\mathrm{d}E(D)}{\mathrm{d}D}\right]. \tag{8.20}$$

Using equation (8.16) for $E(D)$ and assuming a reasonable value for L (12.5 nm) and β (7×10^{-3}), the value giving the best fit to equation (8.20), it is possible to calculate G'_∞ as a function of the volume fraction ϕ of the latex, from the energy–distance curve. The results of these calculations are shown in Fig. 8.23 together of the measured values of G'_∞.

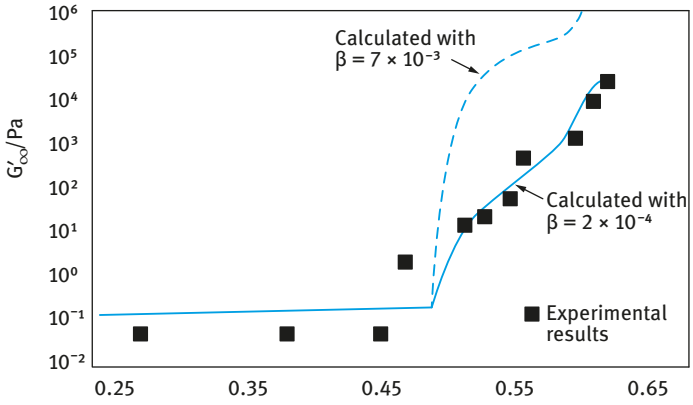

Fig. 8.23: G'_{∞} versus ϕ.

It can be seen from Fig. 8.23 that the form of G'_{∞} versus ϕ is correctly predicted. However, the calculated moduli values are about two orders of magnitude higher than the experimental values when the correct numerical prefactor β in the de Gennes expression has been used. By adjusting this numerical prefactor (solid line of Fig. 8.23) agreement between theoretical and experimental values of G'_{∞} may be obtained.

8.5 Use of polymeric surfactants for preparation and stabilization of nanoemulsions

Nanoemulsions are systems that cover the size range 20–200 nm [28–30]. They can be transparent, translucent or turbid depending on the droplet radius and refractive index difference between the droplets and the continuous phase. This can be understood from a consideration of the dependence of light scattering (turbidity) on the above two factors. For droplets with a radius that is less than (1/20) of the wavelength of light, the turbidity τ is given by the following equation,

$$\tau = KN_0V^2, \tag{8.21}$$

where K is an optical constant that is related to the difference in refractive index between the droplets n_p and the medium n_0, and N_0 is the number of droplets each with a volume V. It is clear from equation (8.21) that τ decreases with decreasing K, i.e. smaller $(n_p - n_0)$, decreasing N_0 and decreasing V. Thus to produce a transparent nanoemulsion one has to decrease the difference between the refractive index of the droplets and the medium (i.e. try to match the two refractive indices). If such matching is not possible then one has to reduce the droplet size (by high pressure homogenization) to values below 50 nm. It is also necessary to use a nanoemulsion with low oil volume fraction (in the region of 0.2).

Nanoemulsions are only kinetically stable. They have to be distinguished from microemulsions (that cover the size range 5–50 nm) which are mostly transparent and thermodynamically stable. The long-term physical stability of nanoemulsions (with no apparent flocculation or coalescence) makes them unique and they are sometimes referred to as "approaching thermodynamic stability". The inherently high colloid stability of nanoemulsions can be well understood from a consideration of their steric stabilization (when using nonionic surfactants and/or polymers) and how this is affected by the ratio of the adsorbed layer thickness to droplet radius as was discussed before.

Unless adequately prepared (to control the droplet size distribution) and stabilized against Ostwald ripening (that occurs when the oil has some finite solubility in the continuous medium), nanoemulsions may show an increase in the droplet size and an initially transparent system may become turbid on storage.

The attraction of nanoemulsions for application in personal care and cosmetics as well as in health care is due to the following advantages:

(i) The very small droplet size causes a large reduction in the gravity force and Brownian motion may be sufficient for overcoming gravity. This means that no creaming or sedimentation occurs on storage.
(ii) The small droplet size also prevents any flocculation of the droplets. Weak flocculation is prevented and this enables the system to remain dispersed with no separation.
(iii) The small droplets also prevent their coalescence, since these droplets are nondeformable and hence surface fluctuations are prevented. In addition, the significant surfactant film thickness (relative to droplet radius) prevents any thinning or disruption of the liquid film between the droplets.

The production of small droplets (submicron) requires the application of high energy. The process of emulsification is generally inefficient. Simple calculations show that the mechanical energy required for emulsification exceeds the interfacial energy by several orders of magnitude. For example, to produce a nanoemulsion at $\phi = 0.1$ with an average radius R of 200 nm, using a surfactant that gives an interfacial tension $\gamma = 10\,\mathrm{mN\,m^{-1}}$, the net increase in surface free energy is $A\gamma = 3\phi\gamma/R = 1.5 \times 10^4\,\mathrm{J\,m^{-3}}$. The mechanical energy required in a homogenizer is $1.5 \times 10^7\,\mathrm{J\,m^{-3}}$, i.e. an efficiency of 0.1 %. The rest of the energy (99.9 %) is dissipated as heat.

The intensity of the process or the effectiveness in making small droplets is often governed by the net power density ($\varepsilon(t)$).

$$p = \varepsilon(t)\,\mathrm{d}t, \tag{8.22}$$

where t is the time during which emulsification occurs.

Break-up of droplets will only occur at high ε values, which means that the energy dissipated at low ε levels is wasted. Batch processes are generally less efficient than

continuous processes. This shows why with a stirrer in a large vessel, most of the energy applied at low intensity is dissipated as heat. In a homogenizer, p is simply equal to the homogenizer pressure.

Several procedures may be applied to enhance the efficiency of emulsification when producing nanoemulsions:

(i) One should optimize the efficiency of agitation by increasing ε and decreasing dissipation time.
(ii) The nanoemulsion is preferably prepared at high volume faction of the disperse phase and diluted afterwards. However, very high ϕ values may result in coalescence during emulsification.
(iii) Add more surfactant, whereby creating a smaller γ_{eff} and possibly diminishing recoalescence.
(iv) Use a surfactant mixture that shows more reduction in γ in the individual components.
(v) If possible dissolve the surfactant in the disperse phase rather than the continuous phase; this often leads to smaller droplets.
(vi) It may be useful to emulsify in steps of increasing intensity, particularly with nanoemulsions having highly viscous disperse phase.

The high kinetic stability of nanoemulsions can be explained from a consideration of the energy–distance curves for sterically stabilized dispersions shown in Fig. 8.5. It can be seen from Fig. 8.5 that the depth of the minimum decreases with increasing δ/R. With nanoemulsions having a radius in the region of 50 nm and an adsorbed layer thickness of, say 10 nm, the value of δ/R is 0.2. This high value (when compared with the situation with macroemulsions where δ/R is at least an order of magnitude lower) results in a very shallow minimum (which could be less than kT). This situation results in very high stability with no flocculation (weak or strong). In addition, the very small size of the droplets and the dense adsorbed layers ensures lack of deformation of the interface, lack of thinning and disruption of the liquid film between the droplets and hence coalescence is also prevented.

One of the main problems with nanoemulsions is Ostwald ripening which results from the difference in solubility between small and large droplets. The difference in chemical potential of dispersed phase droplets between different sized droplets was given by Lord Kelvin [31],

$$s(r) = s(\infty)\exp\left(\frac{2\gamma V_{\text{m}}}{rRT}\right), \tag{8.23}$$

where $s(r)$ is the solubility surrounding a particle of radius r, $c(\infty)$ is the bulk phase solubility and V_{m} is the molar volume of the dispersed phase. The quantity $(2\gamma V_{\text{m}}/RT)$ is termed the characteristic length. It has an order of ≈ 1 nm or less, indicating that the difference in solubility of a 1 μm droplet is of the order of 0.1 % or less. Theoretically, Ostwald ripening should lead to condensation of all droplets into a single drop (i.e.

phase separation). This does not occur in practice since the rate of growth decreases with increasing droplet size.

For two droplets of radii r_1 and r_2 (where $r_1 < r_2$),

$$\frac{RT}{V_m} \ln\left[\frac{s(r_1)}{s(r_2)}\right] = 2\gamma\left(\frac{1}{r_1} - \frac{1}{r_2}\right). \tag{8.24}$$

Equation (8.24) shows that the greater the difference between r_1 and r_2, the higher the rate of Ostwald ripening.

Ostwald ripening can be quantitatively assessed from plots of the cube of the radius versus time t [32–34],

$$r^3 = \frac{8}{9}\left(\frac{s(\infty)\gamma V_m D}{\rho RT}\right), \tag{8.25}$$

where D is the diffusion coefficient of the disperse phase in the continuous phase and ρ is its density.

Ostwald ripening can be reduced by incorporating a second component which is insoluble in the continuous phase (e.g. squalane). In this case significant partitioning between different droplets occurs, with the component having low solubility in the continuous phase expected to be concentrated in the smaller droplets. During Ostwald ripening in two-component disperse phase system, equilibrium is established when the difference in chemical potential between different sized droplets (which results from curvature effects) is balanced by the difference in chemical potential resulting from partitioning of the two components. If the secondary component has zero solubility in the continuous phase, the size distribution will not deviate from the initial one (the growth rate is equal to zero). In the case of limited solubility of the secondary component, the distribution is the same as governed by equation (8.25), i.e. a mixture growth rate is obtained which is still lower than that of the more soluble component.

Another method for reducing Ostwald ripening depends on a modification of the interfacial film at the O/W interface. According to equation (8.25), a reduction in γ results in a reduction of Ostwald ripening. However, this alone is not sufficient since one has to reduce γ by several orders of magnitude. Walstra [35, 36] suggested that by using surfactants which are strongly adsorbed at the O/W interface (i.e. polymeric surfactants) and which do not desorb during ripening, the rate could be significantly reduced. An increase in the surface dilational modulus and a decrease in γ would be observed for the shrinking drops. The difference in γ between the droplets would balance the difference in capillary pressure (i.e. curvature effects). To achieve this effect it is useful to use A–B–A block copolymers that are soluble in the oil phase and insoluble in the continuous phase. A strongly adsorbed polymeric surfactant that has limited solubility in the aqueous phase can also be used, e.g. hydrophobically modified inulin, INUTEC® SP1. This is illustrated in Fig. 8.24 which shows plots of R^3 versus time for 20 v/v % silicone oil-in-water emulsions at two concentrations of INUTEC® SP1 (1.6 %, top curve and 2.4 %, bottom curve) [37]. The concentration of INUTEC® SP1 is much lower than that required when using nonionic surfactants.

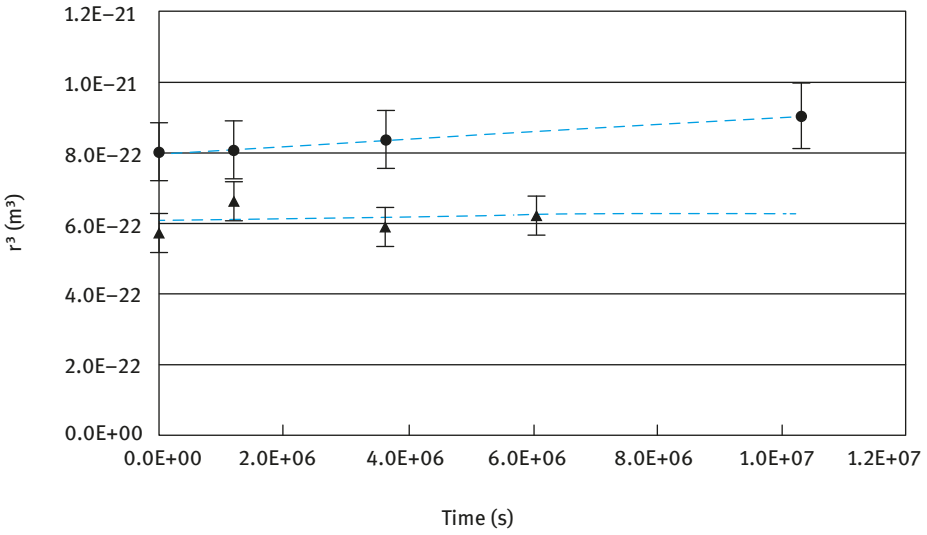

Fig. 8.24: Silicone oil-in-water nanoemulsions stabilized with INUTEC® SP1. Top curve 1.6 %; bottom curve 2.4 % INUTEC® SP1.

The rate of Ostwald ripening is 1.1×10^{-29} and 2.4×10^{-30} $m^3\,s^{-1}$ at 1.6 % and 2.4 % INUTEC® SP1 respectively. These rates are ≈ 3 orders of magnitude lower than those obtained using a nonionic surfactant. Addition of 5 % glycerol was found to decrease the rate of Ostwald ripening in some nanoemulsions.

Various nanoemulsions with hydrocarbon oils of different solubility were prepared using INUTEC® SP1. Fig. 8.25 shows plots of r^3 versus t for nanoemulsions of the hydrocarbon oils that were stored at 50 °C. It can be seen that both paraffinum liquidum with low and high viscosity give almost a zero-slope, indicating absence of Ostwald ripening in this case. This is not surprising since both oils have very low solubility and the hydrophobically modified inulin, INUTEC® SP1, strongly adsorbs at the interface giving high elasticity that reduces both Ostwald ripening and coalescence.

With the more soluble hydrocarbon oils, namely isohexadecane, there is an increase in r^3 with time, giving a rate of Ostwald ripening of 4.1×10^{-27} $m^3\,s^{-1}$. The rate for this oil is almost three orders of a magnitude lower than that obtained with a nonionic surfactant, namely laureth-4 (C_{12} alkyl chain with 4 mol ethylene oxide). This clearly shows the effectiveness of INUTEC® SP1 in reducing Ostwald ripening. This reduction can be attributed to the enhancement of the Gibbs dilational elasticity which results from the multipoint attachment of the polymeric surfactant with several alkyl groups to the oil droplets. This results in a reduction of the molecular diffusion of the oil from the smaller to the larger droplets.

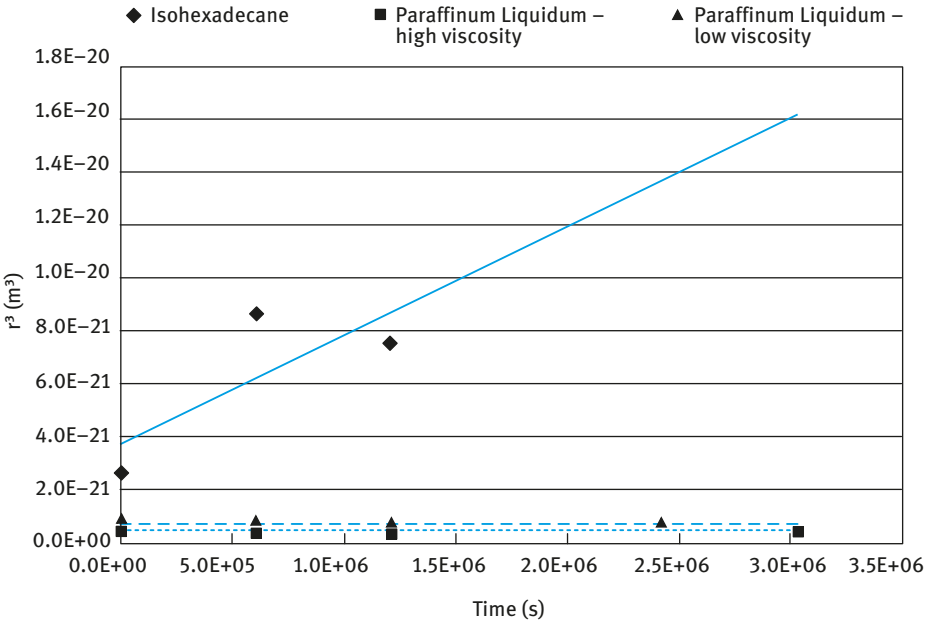

Fig. 8.25: r^3 versus t for nanoemulsions based on hydrocarbon oils.

References

[1] Tadros T. Polymeric surfactants. Berlin: De Gruyter; 2017.
[2] Tadros T. Polymeric surfactants. In: Tadros T, editor. Encyclopedia of colloid and interface science. Berlin: Springer; 2013.
[3] Napper DH. Polymeric stabilisation of colloidal dispersions. London: Academic Press; 1981.
[4] Flory PJ, Krigbaum WR. J Chem Phys. 1950;18:1086.
[5] Fischer EW. Kolloid Z. 1958;160:120.
[6] Mackor EL, van der Waals JH. J Colloid Sci. 1951;7:535.
[7] Hesselink FT, Vrij A, Overbeek JTG. J Phys Chem. 1971;75:2094.
[8] Tadros T. Emulsions. Berlin: De Gruyter; 2016.
[9] Stevens CV, Meriggi A, Peristerpoulou M, Christov PP, Booten K, Levecke B, Vandamme A, Pittevils N, Tadros TF. Biomacromolecules. 2001;2:1256.
[10] Hirst EL, McGilvary DI, Percival EG. J Chem Soc. 1950:1297.
[11] Suzuki M. In: Suzuki M, Chatterton NJ, editors. Science and technology of fructans. Boca Raton: CRC Press; 1993. p. 21.
[12] Tadros TF, Vandamme A, Levecke B, Booten K, Stevens CV. Advances Colloid Interface Sci. 2004;108–109:207.
[13] Exerowa D, Gotchev G, Kolarev T, Khristov K, Levecke B, Tadros T. Langmuir. 2007;23:1711.
[14] Tadros T. In: Tadros T, editor. Emulsion formation and stability. Weinheim: Wiley-VCH; 2013.
[15] Krieger IM, Advances Colloid and Interface Sci. 1972;3:111.
[16] Tadros T. Suspension concentrates. Berlin: De Gruyter; 2017.
[17] Nestor J, Esquena J, Solans C, Levecke B, Booten K, Tadros TF. Langmuir. 2005;21:4837.

[18] Nestor J, Esquena J, Solans C, Luckham PF, Levecke B, Tadros TF. J Colloid Interface Sci. 2007;311:430.
[19] Liang W, Bognolo G, Tadros TF. Langmuir. 1995;11:2899.
[20] Israelachvili JN, Adams GE. J Chem Soc Faraday Trans. 1978;174:975.
[21] Luckham PF. Powder Technol. 1989;58:75.
[22] De L Costello BA, Luckham PF, Tadros TF. Colloids and Surfaces. 1988/1989;34:301.
[23] De L Costello BA, Luckham PF, Tadros TF. J Colloid Interface Sci. 1992;152:237.
[24] de Gennes PG. Advances Colloid Interface Sci. 1987;27:189.
[25] White LR. J Colloid Interface Sci. 1983;95:286.
[26] Zwanzig R, Mountain RD. J Chem Phys. 1965;43:4464.
[27] Evans ID, Lips A. J Chem Soc Faraday Trans. 1990;86:3413.
[28] Nakajima H, Tomomossa S, Okabe M. First Emulsion Conference. Paris; 1993.
[29] Nakajima H. In: Solans C, H. Konieda H, editors. Industrial applications of microemulsions. New York: Marcel Dekker; 1997.
[30] Tadros TF, Izquierdo P, Esquena J, Solans C. Advances Colloid Interface Science. 2004;108–109:2004.
[31] Thompson W (Lord Kelvin). Phil Mag. 1871;42:448.
[32] Lifshitz EM, Slesov VV. Soviet Physics JETP. 1959;35:331.
[33] Wagner C. Z Electrochem. 1961;35:581.
[34] Kabalnov AS, Schukin ED. Adv Colloid Interface Sci. 1992;38:69.
[35] Walstra P. In: Becher P, editor. Encyclopedia of emulsion technology. New York: Marcel Dekker; 1983.
[36] Walstra P, Smolders PEA. In: Binks BP, editor. Modern aspects of emulsions. Cambridge: The Royal Society of Chemistry; 1998.
[37] Tadros TF, Vandekerckhove E, Vandamme A, Levecke B, Booten K. Cosmetic & Toiletries. 2005;120(2):45.

9 Flocculation of dispersions

9.1 Introduction

Most formulations of the disperse type are weakly flocculated. This is particularly the case with high volume fraction of the disperse case. In this case, weak flocculation can occur at relatively low energy of attraction. This is due to the fact that the entropy of flocculation, $T\Delta S^{\text{flocc}}$, is small and hence a small attraction energy, ΔH^{attr}, is sufficient to make the free energy of flocculation, ΔG^{flocc}, negative.

The mechanism of flocculation of electrostatically stabilized systems is different from that of sterically stabilized dispersions and, therefore, these systems will be described in separate sections. With electrostatically stabilized dispersions, fast flocculation of the system occurs when the energy barrier, $G_{\max}$, responsible for stabilization, becomes small ($< 5kT$, where k is the Boltzmann constant and T is the absolute temperature) or absent. In this case flocculation occurs by rapid diffusion of the particles or droplets forming strong aggregates (referred to as coagulation). This is characterized by a rapid flocculation rate k_0. When the energy barrier becomes large ($> 5kT$) the flocculation rate k (referred to as the slow flocculation rate) is reduced below k_0. The higher the energy barrier, the lower the rate of slow flocculation. Weak flocculation of these systems may occur when the attractive energy in the secondary minimum, $G_{\min}$, becomes significant ($> kT$). The higher the volume fraction of the dispersion, the lower the value of $G_{\min}$ required for weak flocculation to occur. Another mechanism of flocculation occurs when the system is subjected to shear. This is referred to as orthokinetic flocculation.

With sterically stabilized dispersions, strong flocculation (referred to as incipient flocculation) may occur when the solvency of the medium for the stabilizing chain becomes worse than a θ-solvent. In this case the mixing free energy term, G_{mix}, becomes negative and when combined with the van der Waals attraction results in a very deep attractive energy resulting in strong and irreversible flocculation. However, sterically stabilized dispersions show a shallow attractive energy, $G_{\min}$, at particle–particle or droplet–droplet separation distance h that is comparable to twice the adsorbed layer thickness. This attractive minimum results in weak and reversible flocculation of the dispersion. As with electrostatically stabilized dispersions, the higher the volume fraction of the disperse phase the lower the value of $G_{\min}$ required for flocculation to occur. Another mechanism of flocculation is that produced by addition of "free" (nonadsorbing) polymer in the continuous phase. In this case the free polymer coil cannot approach the particles or droplets to a distance smaller than the radius of gyration R_{G} of the free polymer chain. This results in the formation of a depletion zone (polymer-free zone) around the particles or droplets with a thickness Δ that is comparable to R_{G}. When two particles or droplets approach each other to a distance h that is smaller than 2Δ, the depletion zones overlap and the free polymer coils are "squeezed out"

https://doi.org/10.1515/9783110587944-010

from the particles or droplets. In this case the osmotic pressure outside the particle or droplets becomes higher than in between them. This osmotic pressure results in weak attraction that is referred to as depletion flocculation. Another mechanism of flocculation, referred to as bridging flocculation, results when the polymer chains become simultaneously adsorbed on two or more particles or droplets. Flocculation can also occur on addition of polyelectrolytes with opposite charge to the particle or droplet surfaces. This flocculation occurs as a result of charge neutralization and/or bridging.

9.2 Mechanism of aggregation of electrostatically stabilized dispersions

The DLVO theory [1, 2] predicts the process of aggregation on addition of electrolytes with different valency. Adding electrolyte reduces the range of the repulsive component G_{el} (due to compression of the electrical double layer) and this results in reduction of the energy maximum, G_{max}. This is illustrated in Fig. 9.1 which shows the effect of adding 1 : 1 electrolyte on the energy–distance curves.

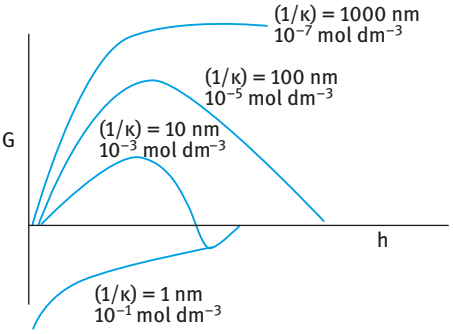

Fig. 9.1: Variation of G with h at various electrolyte concentrations.

At very low electrolyte concentration of 10^{-7} mol dm^{-3} (corresponding to a double layer thickness of 1,000 nm), the energy maximum is very high (much higher than $100kT$) and that prevents any close approach of the particles. In this case the particles remain dispersed for a very long period of time (some years). By increasing the electrolyte concentration to 10^{-5} mol dm^{-3} (corresponding to a double layer thickness of 100 nm), the energy maximum is still high ($> 100kT$) and this prevents any aggregation of the particles. On increasing the electrolyte concentration to 10^{-3} mol dm^{-3} (corresponding to a double layer thickness of 10 nm), the energy maximum is reduced but still high enough ($> 25kT$) to prevent aggregation. However, when the electrolyte concentration is increased to 10^{-1} mol dm^{-3} (corresponding to a double layer thickness of 1 nm), the energy maximum disappears and the energy–distance curve becomes attractive, arising from the van der Waals attraction, G_A, at all separation distances. In

this case, the dispersion shows rapid coagulation and the particles in the aggregates are strongly bound to each other.

Another factor that affects the electrostatic repulsion is the magnitude of the surface or zeta potential. As discussed in Chapter 7, G_{el} is proportional to the square of the surface or zeta potential. As an illustration, Fig. 9.2 shows calculations of the energy–distance curves for polystyrene latex particles of 500 nm radius at various NaCl concentrations and zeta potential [3].

It can be seen that a high energy maximum is obtained at 10^{-2} mol dm^{-3} NaCl and ζ-potential of −50 mV. When the ζ-potential is reduced to −20 mV while keeping the NaCl concentration the same, the maximum disappears. Also, at higher NaCl concentration of 4×10^{-1} mol dm^{-3} the maximum disappears even when the ζ-potential is increased to −30 mV.

Since approximate formulae are available for G_{el} and G_A, quantitative expressions for $G_T(h)$ can also be formulated. These can be used to derive expressions for the coagulation concentration, which is that concentration that causes every encounter between two colloidal particles to lead to destabilization. Verwey and Overbeek [2] introduced the following criteria for transition between stability and instability,

$$G_T(= G_{el} + G_A) = 0, \tag{9.1}$$

$$\frac{dG_T}{dh} = 0, \tag{9.2}$$

$$\frac{dG_{el}}{dh} = -\frac{dG_A}{dh}. \tag{9.3}$$

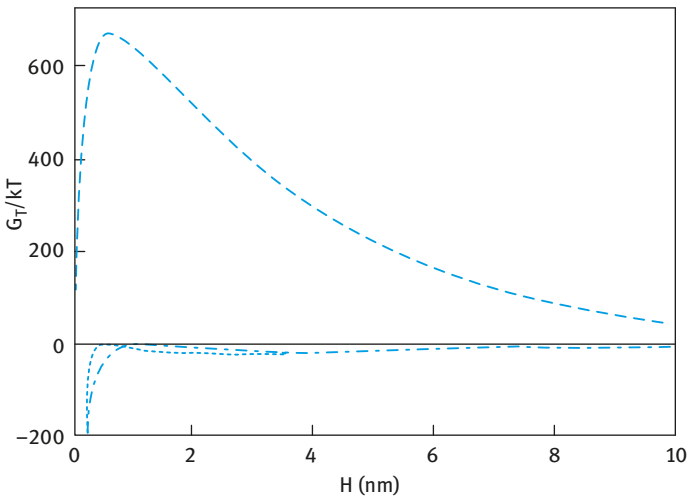

Fig. 9.2: Energy–distance curves for 500 nm radius polystyrene latex particles: (—), 10^{-2} mol dm^{-3} NaCl, ζ-potential = −50 mV; (·····), 10^{-2} mol dm^{-3} NaCl, ζ-potential = −20 mV; (···), 4×10^{-1} mol dm^{-3} NaCl, ζ-potential = −30 mV.

Using the equations for G_{el} and G_A, the critical coagulation concentration, CCC can be calculated as will be shown below. The theory predicts that the CCC is directly proportional to the surface potential ψ_0 and inversely proportional to the Hamaker constant A and the electrolyte valency Z. As will be shown below, the CCC is inversely proportional to Z^6 at high surface potential and inversely proportional to Z^2 at low surface potential.

9.3 Kinetics of flocculation of dispersions

9.3.1 Diffusion limited aggregation (fast flocculation kinetics)

Fast flocculation kinetics represents the case where no energy barrier exists and hence the process becomes diffusion controlled. This process (referred to as perikinetic flocculation) was treated by Smoluchowki [4], who modelled the system as that of diffusing spherical particles which stick on collision, but the pair potential is zero up to this contact [5, 6]. If r is the centre-to-centre distance between a reference spherical particle with radius R and an approaching particle with the same radius R (for a monodisperse dispersion), then contact occurs when $r = 2R$. As both particles are diffusing, the net diffusion coefficient is equal to $2D\ \mathrm{m^2\ s^{-1}}$ [2]. The net velocity of the incoming particle is therefore $2D/R\ \mathrm{m\ s^{-1}}$. The surface area of the "collision sphere" is $4\pi(2R)^2$. The flux resulting from Brownian diffusion J_B through the collision sphere, if there are initially no particles per unit volume, is

$$J_B = n_0 \frac{2D}{R} 4\pi(2R)^2. \tag{9.4}$$

Since the above process is occurring with each particle, the collision frequency due to Brownian diffusion is,

$$c_B = \frac{n_0 J_B}{2}. \tag{9.5}$$

The factor of 2 is introduced to prevent double counting. The diffusion coefficient is given by the Stokes–Einstein equation,

$$D = \frac{kT}{6\pi\eta R}, \tag{9.6}$$

where η_0 is the viscosity of the medium.

Combining equations (9.4)–(9.6),

$$c_B = n_0^2 \frac{8kT}{3\eta_0}. \tag{9.7}$$

As each collision results in coagulation, the initial coagulation rate is given by,

$$-\frac{\mathrm{d}n_0}{\mathrm{d}t} = n_0^2 \frac{8kT}{3\eta_0}. \tag{9.8}$$

The half-life $t_{1/2}$ for the rapid coagulation rate is determined for this second-order rate equation as,

$$t_{1/2} = \frac{3\eta_0}{4kTn_0}. \tag{9.9}$$

A simple analysis of fast flocculation kinetics is to consider the process to be represented by second-order kinetics and the process is simply diffusion controlled. The number of particles n at any time t may be related to the initial number (at $t = 0$) n_0 by the following expression,

$$n = \frac{n_0}{1 + kn_0t}, \tag{9.10}$$

where k_0 is the rate constant for fast flocculation that is related to the diffusion coefficient of the particles D, i.e.,

$$k = 8\pi DR. \tag{9.11}$$

D is given by the Stokes–Einstein equation (9.6).

Combining equations (9.6) and (9.11),

$$k = \frac{4}{3}\frac{kT}{\eta} = 5.5 \times 10^{-18}\,\mathrm{m^3\,s^{-1}} \quad \text{for water at 25 °C.} \tag{9.12}$$

Equation (9.12) shows that the rate constant for flocculation is directly proportional to the temperature and inversely proportional to the viscosity of the medium. It should also be mentioned that the viscosity of the medium decreases with increasing temperature which means that the overall effect of an increase of temperature will be an increase in the rate constant.

The half-life $t_{1/2}$ ($n = (1/2)n_0$) can be calculated at various n_0 or volume fractions ϕ as give in Tab. 9.1.

Tab. 9.1: Half-life of suspension flocculation.

R (µm)	ϕ			
	10^{-5}	10^{-2}	10^{-1}	5×10^{-1}
0.1	765 s	76 ms	7.6 ms	1.5 ms
1.0	21 h	76 s	7.6 s	1.5 s
10.0	4 month	21 h	2 h	25 min

9.3.2 Potential limited aggregation (slow flocculation kinetics)

Slow flocculation kinetics was treated by Fuchs [7] who considered the effect of the presence of an energy barrier. In this case, the pair potential slows the approach of two particles. At any distance, the fraction of particles with thermal energy in excess of the potential at that distance is given by the Boltzmann factor: $\exp(-G_T/kT)$. The

flux through successive spherical shells as the particles approach is slowed from the simple collision case and only a fraction of the particles that encounter one another approach close enough to stick. The fraction of encounters that stick is $1/W$, where W is known as the stability ratio.

$$W = \frac{k_0}{k}. \tag{9.13}$$

W can be expressed as the ratio of the two fluxes,

$$W = 2R \int_{2R}^{\infty} \exp\left(\frac{G_T}{kT}\right) \frac{dr}{r^2}. \tag{9.14}$$

Reerink and Overbeek [8] pointed out that the maximum in the pair potential, G_{max}, is the dominant factor in restricting the approach of particles and they showed a useful approximation to the integral of equation (9.14),

$$W \approx \frac{1}{2\kappa R} \exp\left(\frac{G_{max}}{kT}\right). \tag{9.15}$$

Since G_{max} is determined by the salt concentration C and valency, one can derive an expression relating W to C and Z [8],

$$\log W = -2.06 \times 10^9 \left(\frac{R\gamma^2}{Z^2}\right) \log C, \tag{9.16}$$

where γ is a function that is determined by the surface potential ψ_0,

$$\gamma = \left[\frac{\exp(Ze\psi_0/kT) - 1}{\exp(Ze\psi_0/kT) + 1}\right]. \tag{9.17}$$

Plots of log W versus log C are shown in Fig. 9.3. The condition log $W = 0$ ($W = 1$) is the onset of fast flocculation. The electrolyte concentration at this point defines the critical flocculation concentration CCC. Above the CCC, $W < 1$ (due to the contribution of van der Waals attraction which accelerates the rate above the Smoluchowski value). Below the CCC, $W > 1$ and it increases with decreasing electrolyte concentration. The above figure also shows that the CCC decreases with increasing valency. At low surface potentials, CCC $\propto 1/Z^2$. This referred to as the Schulze–Hardy rule.

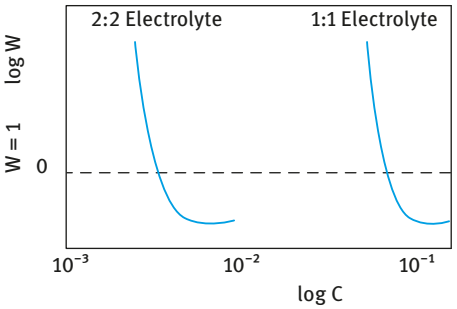

Fig. 9.3: log W–log C curves.

9.3.3 Weak (reversible) flocculation

Another mechanism of flocculation is that involving the secondary minimum (G_{min}), which is few kT units. In this case flocculation is weak and reversible and hence one must consider both the rate of flocculation (forward rate k_f) and deflocculation (backward rate k_b). In this case the rate or decrease of particle number with time is given by the expression,

$$-\frac{dn}{dt} = -k_f n^2 + k_b n. \tag{9.18}$$

The backward reaction (break-up of weak flocs) reduces the overall rate of flocculation.

9.3.4 Orthokinetic flocculation

Many formulations of the disperse type are subjected to high shear conditions during their preparation, e.g. when using high shear mixers to disperse the particles in the continuous medium. This high shear condition results in enhanced collision between the particles that may result in their aggregation. This process of flocculation that occurs under shearing conditions is referred to as orthokinetic (to distinguish it from the diffusion controlled perikinetic process). The simplest analysis is for laminar flow, since for turbulent flow with chaotic vortices (as is the case in a high-speed mixer) the particles are subjected to a wide and unpredictable range of hydrodynamic forces. For laminar flow, the particle will move at the velocity of the liquid at the plane coincident with the centre of the particle, v_p. In this case the total collision frequency due to flow, c_f, is given by the following expression,

$$c_f = \frac{16}{3} n_p^2 R^3 \left(\frac{dv}{dx}\right). \tag{9.19}$$

As the particles approach in the shear field, the hydrodynamic interactions cause the colliding pair to rotate and with the combination of the slowing approach due to liquid drainage (lubrication stress) and Brownian motion, not all collisions will lead to aggregation. Equation (9.19) must be reduced by a factor α (the collision frequency) to account for this,

$$c_f = \alpha \frac{16}{3} n_p^2 R^3 \left(\frac{dv}{dx}\right). \tag{9.20}$$

The collision frequency α is of the order 1 and a typical value would be $\alpha \approx 0.8$.

(dv/dx) is the shear rate so that equation (9.20) can be written as,

$$c_f = \alpha \frac{16}{3} n_p^2 R^3 \dot{\gamma}. \tag{9.21}$$

And the rate of orthokinetic flocculation is given by,

$$-\frac{dn}{dt} = \alpha \frac{16}{3} n_p^2 R^3 \dot{\gamma}. \tag{9.22}$$

A comparison can be made between the collision frequency or rate of orthokinetic and perikinetic flocculation by comparing equations (9.22) and (9.7),

$$\frac{c_f}{c_B} = \frac{2\alpha\eta_0 R^3\dot{\gamma}}{kT}. \tag{9.23}$$

If the particles are dispersed in water at a temperature of 25 °C, the ratio in equation (9.23) becomes,

$$\frac{c_f}{c_B} \approx 4 \times 10^{17} R^3\dot{\gamma}. \tag{9.24}$$

When a liquid is stirred in a beaker using a rod the velocity gradient r shear rate is in the range 1–10 s^{-1}, with a mechanical stirrer it is about 100 s^{-1} and at the tip of a turbine in a large reactor it can reach values as high as 1,000–10,000 s^{-1}. This means that the particle radius R must be less than 1 µm if even slow mixing can be disregarded. This shows how the effect of shear can increase the rate of aggregation.

It should be mentioned that the above analysis is for the case where there is no energy barrier, i.e. the Smoluchowski case [4]. In the presence of an energy barrier, i.e. potential limited aggregation, one must consider the contribution due to the hydrodynamic forces acting on the colliding pair [6]. Fig. 9.4 shows the forces acting on a collision doublet in simple shear [3]. The figure shows the trajectory with the points at which maximum compression and tension occurs, i.e. at an angle $\theta = 45°$ to the shear plane. The particles have the same radius R and the reference particle is at $z = 0$.

The velocity of the streamline coincident with the centre of colliding particle, υ, at the orientation giving the maximum force is,

$$\upsilon = \dot{\gamma} \cdot 2R\sin(45). \tag{9.25}$$

The radial component of the Stokes drag force on the particle is given by,

$$F_h = 6\pi\eta_0 R\upsilon_{\text{radial}} = 6\pi\eta_0 R\cos(45). \tag{9.26}$$

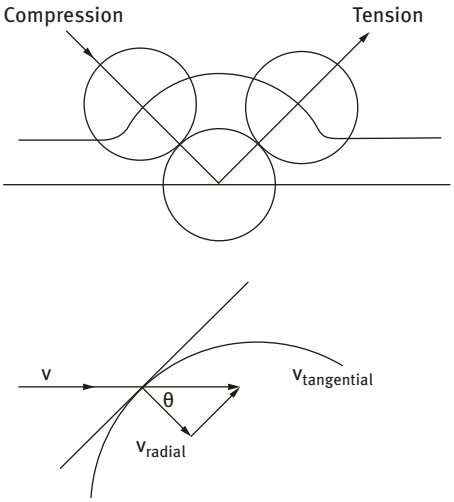

Fig. 9.4: Schematic representation of the geometry of a colliding pair of particles with maximum compression and tension at $\theta = 45°$ to the shear plane.

F_h can be written as,

$$F_h = \pm\dot{\gamma}6\pi\eta_0 \cdot 2R^2 \sin(45)\cos(45), \tag{9.27a}$$

$$F_h = \pm\dot{\gamma}6\pi\eta_0 \cdot 2R^2. \tag{9.27b}$$

where the sign ± indicates compression (+) or tension (–). The trajectory would be altered by the colloidal forces on approach, i.e. whether there is net repulsion or attraction. Equation (9.27b) can be used to indicate where the stability or instability boundaries are for a particular dispersion. This requires calculating the interparticle force at the maximum and minimum points on the force–distance curve. Some calculations were made by Goodwin [3] for polystyrene latex particles with a radius of 500 nm in the presence of 50 mM 1 : 1 electrolyte and a zeta potential of –40 mV. F_T is given by,

$$F_T = 2\pi\varepsilon_r\varepsilon_0\kappa R\psi_d \frac{\exp(-\kappa H)}{1+\exp(-\kappa H)} - \frac{A_{11}R}{12H^2}. \tag{9.28}$$

The value of κR is 368 and therefore the interparticle forces change in the region very close to the particle surface. This indicates that hydrodynamics control the trajectories until the particles are very close to each other. The force–distance curve is shown in Fig. 9.5, where ζ is assumed to be equal to ψ_d.

Fig. 9.5 shows a force maximum F_{max} of 3.96×10^{-10} N and a force minimum F_{min} of -3.8×10^{-11} N. The stability boundaries are calculated as a function of shear rate as illustrated in Fig. 9.6. This clearly shows the change in the aggregation state at different values of ζ-potential [3].

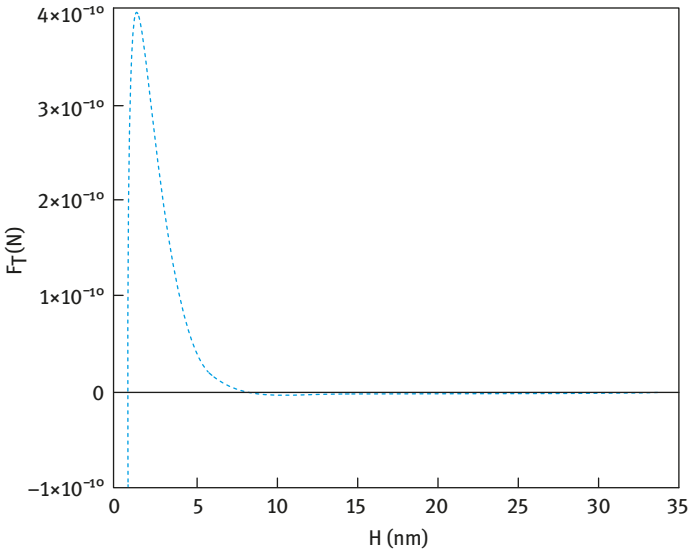

Fig. 9.5: Force–distance curve for 500 nm polystyrene particles at 50 mM 1 : 1 electrolyte and ζ-potential of –40 mV [3].

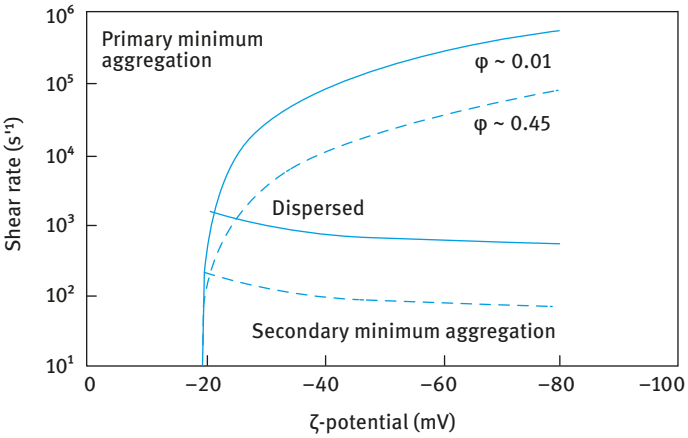

Fig. 9.6: Stability map for polystyrene latex dispersions (R = 500 nm and 1 : 1 electrolyte concentration of 50 mM) as a function of ζ-potential and shear rate.

Several features can be identified from the stability map shown in Fig. 9.6. At ζ-potentials less than −20 mV, the dispersion is coagulated at all shear rates. With a small increase in the ζ-potential above −20 mV, the dispersion shows weak flocculation (secondary minimum aggregation) at low shear rates, but at high shear rates of the order of $10^5\ s^{-1}$, the hydrodynamic forces are sufficient to cause the dispersion to form doublets which are coagulated. This shear-induced coagulation is referred to as orthokinetic flocculation as discussed above. It is interesting to note that the shear forces on this particle size, ionic strength and diffuse potential combination will only break down the doublets flocculated in the secondary minimum when the shear rates exceed $10^3\ s^{-1}$. Although such high shear rates are readily attainable in a viscometer, they would require a high stirrer speed when using a paddle stirrer. Clearly such shear rates are easily achieved in pumps and large reactors with turbine mixers. Such shear rates can also be achieved when using rotor-stator mixers (such as Ultra-Turrax and Silverson mixers). Equations (9.27a) and (9.27b) show that the shear forces increase as the square of the particle radius and so the stability boundaries drop rapidly with increasing particle size as the colloidal forces change more slowly with radius than the hydrodynamic forces. Thus particles with a radius of 3–4 μm are much more sensitive to shear-induced aggregation than particles with an order of magnitude lower radius (0.3–0.4 μm).

The effect of increasing the volume fraction of the dispersion ϕ, as is the case with most practical systems, has a big impact on the shear-induced aggregation as clearly illustrated in Fig. 9.6 which shows the stability map as ϕ is increased from 0.01 to 0.45. When dealing with concentrated dispersions one must consider the "multibody" hydrodynamic forces. Using a mean field approximation Krieger and Dougherty [9, 10], related the viscosity of the suspension η with that of the medium η_0 by the following

semi-empirical equation,

$$\eta = \eta_0 \left(1 - \frac{\phi}{\phi_p}\right)^{-[\eta]\phi_p}, \tag{9.29}$$

where ϕ_p is the maximum packing fraction that is ≈ 0.605 (for random packing) and $[\eta]$ is the intrinsic viscosity that is equal to 2.5 for hard spheres. Equation (9.29) becomes,

$$\eta = \eta_0 \left(1 - \frac{\phi}{0.605}\right)^{-1.513}. \tag{9.30}$$

The stability boundaries for $\phi = 0.45$ are shown in Fig. 9.6 (dashed line) and this clearly shows the drop resulting from the increase in the viscous forces at high volume fraction as predicted by equation (9.30). The boundaries drop in proportion to the viscous forces as expected, so it is easier to break up flocculated pairs with an applied shear field. This means that a larger fraction of the stable area that is occupied by the particles that can be considered "dispersed" occurs at lower shear rates when compared with the case of dilute dispersions. The range of stability under shear at moderate ζ-potentials is reduced with increasing the solid volume fraction.

9.3.5 Aggregate structure

When dealing with aggregated systems, the floc structure plays an important role in applications. For example, the rheological properties change dramatically so that handling can become very difficult. The mode of aggregation that occurs in the absence (diffusion-limited aggregation) of a barrier can result in the formation of an open-dendritic or fractal type of structure. In this case, the particles collide and stick as they diffuse. Computer models generate this type of open branched structure and some careful experiments have confirmed these models [6]. As these aggregates grow by accretion of "stick" particles, they grow into each other and span the available space [3]. This point is referred to as the "percolation threshold". At higher concentrations, denser structures result and these are more difficult to define by a single parameter such as the "fractal dimension". These structures are modified in practice by addition of coagulants and application of shear during mixing. The shear forces on these large and fragile structures compact them to relatively high densities [11]. In some cases, systems of monodisperse particles can be compacted by shearing the coagulating system to random packing densities $\phi \approx 0.64$. These strongly aggregated systems are "metastable" structures. The lowest energy configuration would be a very dense unit with the maximum number and/or area of contacts. However, the fractal structure of a dilute, strongly aggregated system would be very long lived in the absence of external forces since $(G_{min})_{primary} \gg kT$ and densification purely by diffusive motion would be imperceptibly slow.

The structures obtained depend on the processing and strength of the attractive interaction. The latter can be controlled by addition of materials to the surface prior

to coagulation, e.g. by adding nonionic surfactants or polymers which provide a steric barrier thus limiting the aggregation to weak flocculation [12].

9.4 Flocculation of sterically stabilized dispersions

Two main types of flocculation may be distinguished: weak and incipient flocculation.

9.4.1 Weak flocculation

This occurs when the thickness of the adsorbed layer is small (usually < 5 nm), particularly when the particle radius and Hamaker constant are large. The minimum depth required for causing weak flocculation depends on the volume fraction of the suspension. The higher the volume fraction, the lower the minimum depth required for weak flocculation. As discussed in the introduction, this can be understood if one considers the free energy of flocculation that consists of two terms, an energy term determined by the depth of the minimum (G_{min}) and an entropy term that is determined by a reduction in configurational entropy on aggregation of particles,

$$\Delta G_{flocc} = \Delta H_{flocc} - T\Delta S_{flocc}. \tag{9.31}$$

With dilute suspension, the entropy loss on flocculation is larger than with concentrated suspensions. Hence for flocculation of a dilute suspension, a higher energy minimum is required when compared with the case with concentrated suspensions.

The above flocculation is weak and reversible, i.e. on shaking the container redispersion of the suspension occurs. On standing, the dispersed particles aggregate to form a weak "gel". This process (referred to as sol ↔ gel transformation) leads to reversible time dependency of viscosity (thixotropy). On shearing the suspension, the viscosity decreases and when the shear is removed, the viscosity is recovered. This phenomenon is applied in paint formulations. On application of the paint (by a brush or roller), the gel is fluidized, allowing uniform coating of the paint. When shearing is stopped, the paint film recovers its viscosity and this avoids any dripping.

9.4.2 Incipient flocculation

This occurs when the solvency of the medium is reduced to become worse than θ-solvent (i.e. $\chi > 0.5$). This reduction in solvency can be induced by temperature changes [8, 9] or addition of a nonsolvent [8, 9] for the stabilizing chain. When the solvency is reduced, the dispersion often exhibits a sharp transition from long-term stability to fast flocculation. This process of incipient flocculation is, for example, observed when a dispersion stabilized by poly(ethylene oxide) moieties is heated.

Over a few degrees temperature rise, the turbidity of the dispersion rises sharply indicating excessive flocculation. Flocculation can also occur by the addition of a nonsolvent, e.g. by addition of ethanol to polymethylmethacrylate dispersion stabilized by poly(hydroxystearic) acid in a hydrocarbon solvent [10, 11]. The critical point at which flocculation is first observed is referred to as the critical flocculation temperature (CFT) or critical flocculation concentration of the added nonsolvent (CFV).

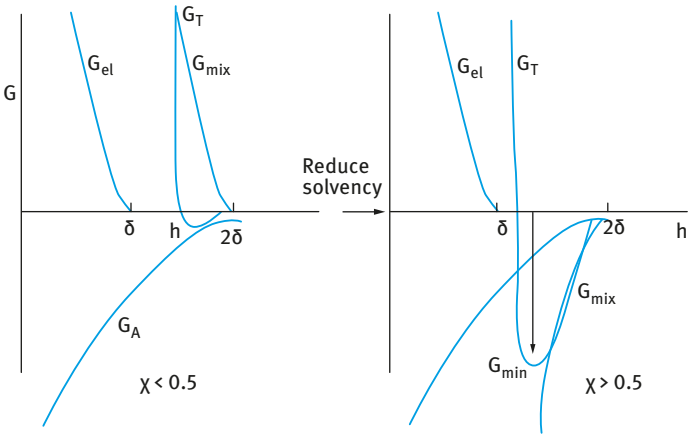

Fig. 9.7: Influence of reduction in solvency on the energy–distance curve.

An illustration of incipient flocculation is given in Fig. 9.7 where χ was increased from < 0.5 (good solvent) to > 0.5 (poor solvent). One of the characteristic features of sterically stabilized systems, which distinguish them from electrostatically stabilized dispersions, is the temperature dependency of stability. Indeed, some dispersions flocculate on heating [12, 13]; others flocculate on cooling [12, 13]. Furthermore, in some cases dispersions can be produced which do not flocculate at any accessible temperature, whilst some sterically stabilized systems have been found to flocculate both on heating and cooling. This temperature dependency led Napper [13] to describe stability in terms of the thermodynamic process that governs stabilization. Thus, the temperature dependency of the Gibbs free energy of interaction (ΔG_R) for two sterically stabilized particles or droplets is given by,

$$\frac{\partial \Delta G_R}{\partial T} = -\Delta S_R, \tag{9.32}$$

where ΔS_R is the corresponding entropy change.

In passing from the stability to the instability domain, ΔG_R must change sign, i.e. from being positive to being negative. It is convenient to split ΔG_R into its enthalpy and entropy contributions,

$$\Delta G_R = \Delta H_R - T\Delta S_R. \tag{9.33}$$

Tab. 9.2: Types of steric stabilization.

ΔH_R	ΔS_R	$\Delta H_R/T\Delta S_R$	ΔG_R	Type	Flocculation
+	+	> 1	+	Enthalpic	On heating
–	–	< 1	+	Entropic	On cooling
+	–	≥	+	Combined	Not accessible
+	–	<	+	Enthalpic = entropic	

Thus the sign of ΔG_R will depend on the signs and relative magnitudes of ΔH_R and ΔS_R as summarized in Tab. 9.2.

As a result of extensive investigations on model sterically stabilized dispersions, it has been demonstrated that a strong correlation exists between the critical flocculation point and the θ-point of the stabilizing moieties in free solution. As mentioned before, the θ-point is that at which $\chi = 0.5$, i.e. the point at which the second virial coefficient of the polymer chain is equal to zero. The absolute methods for the determination of the θ-point include light scattering and osmotic pressure measurements. Less sound methods for determining the θ-point depend on establishing the phase diagrams of polymer solutions.

Using lattices with terminally-anchored polymer chains of various kinds, it has been established that the CFT is independent of the molar mass of the chain, the size of the particle core and the nature of the disperse phase [12]. The CFT correlates strongly with the θ-temperature. Similar correlations have been found between the CFV and the θ-point [12]. However, such correlations are only obtained if the surface is fully covered by the polymer chains. Under conditions of incomplete coverage, flocculation occurs in dispersion media that are better than θ-solvents. This may be due to lateral movement of the stabilizer, desorption or even bridging flocculation (see below).

The correlation between the critical flocculation point and the θ-point implies that G_{mix} dominates the steric interaction. It has been argued that the contribution from G_{el} can be neglected until $h < \delta$, i.e. the polymer layer from one particle comes into direct contact with the second interface. With the high molar mass chains, the contribution from G_A to the total interaction is also negligible. This means that G_T is approximately equal to G_{mix} and that χ is the main parameter controlling the stability. This is clearly illustrated in Fig. 9.7 which shows a significant value of G_{min} when $\chi > 0.5$

Thus by measuring the θ-point (CFT or CFV) for the polymer chains (A) in the medium under investigation (which could be obtained from light scattering or viscosity measurements) one can establish the stability conditions for a dispersion, before its preparation. This procedure helps also in designing effective steric stabilizers such as block and graft copolymers.

9.4.3 Depletion flocculation

Depletion flocculation is produced by addition of "free" nonadsorbing polymer [15]. As mentioned in the introduction, the polymer coils cannot approach the particles to a distance Δ (that is determined by the radius of gyration of free polymer R_G), since the reduction of entropy on close approach of the polymer coils is not compensated by an adsorption energy. The suspension particles or emulsion droplets will be surrounded by a depletion zone with thickness Δ. Above a critical volume fraction of the free polymer, ϕ_p^+, the polymer coils are "squeezed out" from between the particles and the depletion zones begin to interact. The interstices between the particles are now free from polymer coils and hence an osmotic pressure is exerted outside the particle surface (the osmotic pressure outside is higher than in between the particles) resulting in weak flocculation [15]. A schematic representation of depletion flocculation is shown in Fig. 9.8.

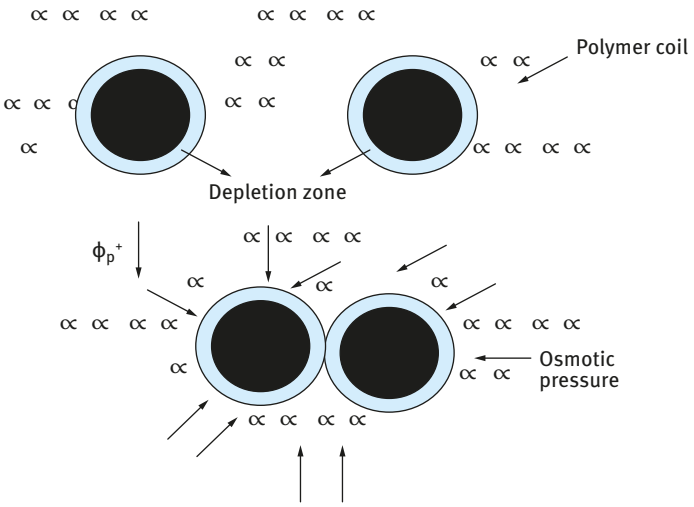

Fig. 9.8: Schematic representation of depletion flocculation.

The magnitude of the depletion attraction free energy, G_{dep}, is proportional to the osmotic pressure of the polymer solution, which in turn is determined by ϕ_p and molecular weight M. The range of depletion attraction is proportional to the thickness of the depletion zone, Δ, which is roughly equal to the radius of gyration, R_G, of the free polymer. A simple expression for G_{dep} is [15],

$$G_{dep} = \frac{2\pi R\Delta^2}{V_1}(\mu_1 - \mu_1^0)\left(1 + \frac{2\Delta}{R}\right), \tag{9.34}$$

where V_1 is the molar volume of the solvent, μ_1 is the chemical potential of the solvent in the presence of free polymer with volume fraction ϕ_p and μ_1^0 is the chemical potential of the solvent in the absence of free polymer. $(\mu_1 - \mu_1^0)$ is proportional to the osmotic pressure of the polymer solution.

9.4.4 Bridging flocculation by polymers and polyelectrolytes

Certain long chain polymers may adsorb in such a way that different segments of the same polymer chain are adsorbed on different particles or droplets, thus binding or "bridging" the particles or droplets together, despite the electrical repulsion [16, 17]. With polyelectrolytes of opposite charge to the particles, another possibility exists; the particle charge may be partly or completely neutralized by the adsorbed polyelectrolyte, thus reducing or eliminating the electrical repulsion and destabilizing the particles.

The most effective polymers that cause bridging are usually of the linear type, often of high molecular weight, which may be nonionic, anionic or cationic in character. Ionic polymers should be strictly referred to as polyelectrolytes. The most important properties are molecular weight and charge density. Several polymers that are based on natural products, e.g. starch and alginates may cause bridging, but the most commonly used polymers that cause bridging are synthetic nonionic and polyelectrolytes, e.g. polyacrylamide and copolymers of acrylamide and a suitable cationic monomer such as dimethylaminoethyl acrylate or methacrylate. Other synthetic polymers that may cause bridging are poly(vinyl alcohol), poly(ethylene oxide) (nonionic), sodium polystyrene sulphonate (anionic) and polyethyleneimine (cationic).

As mentioned above, bridging flocculation occurs because segments of a polymer chain adsorb simultaneously on different particles thus linking them together. Adsorption is an essential step and this requires favourable interaction between the polymer segments and the particles. Several types of interactions are responsible for adsorption that is irreversible in nature:

(i) Electrostatic interaction when a polyelectrolyte adsorbs on a surface bearing oppositely charged ionic groups, e.g. adsorption of a cationic polyelectrolyte on a negative oxide surface such as silica.
(ii) Hydrophobic bonding that is responsible for adsorption of nonpolar segments on a hydrophobic surface, e.g. partially hydrolysed poly(vinyl acetate) (PVA) on a hydrophobic surface such as polystyrene.
(iii) Hydrogen bonding as for example interaction of the amide group of polyacrylamide with hydroxyl groups on an oxide surface.
(iv) Ion binding as is the case of adsorption of anionic polyacrylamide on a negatively charged surface in the presence of Ca^{2+}.

Effective bridging flocculation requires that the adsorbed polymer extends far enough from the particle surface to attach to other particles and that there is sufficient free surface available for adsorption of these segments of extended chains. When excess polymer is adsorbed, the particles can be restabilized, either because of surface saturation or by steric stabilization as discussed before. This is one explanation of the fact that an "optimum dosage" of the polymer is often found; at low concentration there is insufficient polymer to provide adequate links and with larger amounts restabilization may occur. A schematic picture of bridging flocculation and restabilization by adsorbed polymer is given in Fig. 9.9.

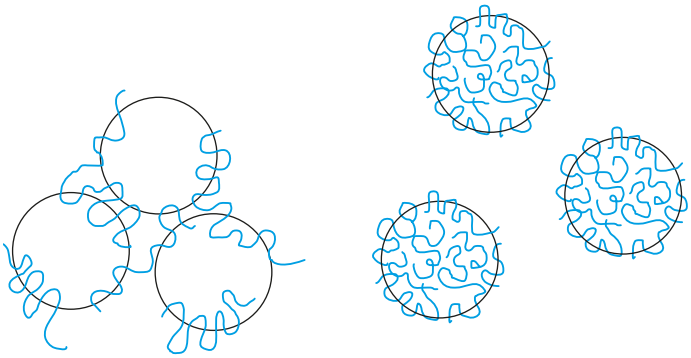

Fig. 9.9: Schematic illustration of bridging flocculation (left) and restabilization (right) by adsorbed polymer.

If the fraction of particle surface covered by polymer is θ then the fraction of uncovered surface is $(1 - \theta)$ and the successful bridging encounters between the particles should be proportional to $\theta(1 - \theta)$, which has its maximum when $\theta = 0.5$. This is the well-known condition of "half-surface coverage" that has been suggested as giving the optimum flocculation.

An important condition for bridging flocculation with charged particles is the role of electrolyte concentration. The latter determines the extension ("thickness") of the double layer which can reach values as high as 100 nm (in 10^{-5} mol dm^{-3} 1 : 1 electrolyte such as NaCl). For bridging flocculation to occur, the adsorbed polymer must extend far enough from the surface to a distance over which electrostatic repulsion occurs (> 100 nm in the above example). This means that at low electrolyte concentrations quite high molecular weight polymers are needed for bridging to occur. As the ionic strength is increased, the range of electrical repulsion is reduced and lower molecular weight polymers should be effective.

In many practical applications, it has been found that the most effective polymers that cause flocculation are polyelectrolytes with a charge opposite to that of the particles. In aqueous media most particles are negatively charged, and cationic poly-

electrolytes such as polyethyleneimine are often effective in causing flocculation. With oppositely charged polyelectrolytes it is likely that adsorption occurs to give a rather flat configuration of the adsorbed chain, due to the strong electrostatic attraction between the positive ionic groups on the polymer and the negative charged sites on the particle surface. This would probably reduce the probability of bridging contacts with other particles, especially with fairly low molecular weight polyelectrolytes with high charge density. However, the adsorption of a cationic polyelectrolyte on a negatively charged particle will reduce the surface charge of the latter, and this charge neutralization could be an important factor in destabilizing the particles. Another mechanism for destabilization has been suggested by Gregory [8] who proposed an "electrostatic-patch" model. This applies to cases where the particles have a fairly low density of immobile charges and the polyelectrolyte has a fairly high charge density. Under these conditions, it is not physically possible for each surface site to be neutralized by a charged segment on the polymer chain, even though the particle may have sufficient adsorbed polyelectrolyte to achieve overall neutrality. There are then "patches" of excess positive charge, corresponding to the adsorbed polyelectrolyte chains (probably in a rather flat configuration), surrounded by areas of negative charge, representing the original particle surface. Particles which have this "patchy" or "mosaic" type of surface charge distribution may interact in such a way that the positive and negative "patches" come into contact, giving quite strong attraction (although not as strong as in the case of bridging flocculation). A schematic illustration of this type of interaction is given in Fig. 9.10. The electrostatic patch concept (which can be regarded as another form of "bridging") can explain a number of features of flocculation of negatively charged particles with positive polyelectrolytes. These include the rather small effect of increasing the molecular weight and the effect of ionic strength on the breadth of the flocculation dosage range and the rate of flocculation at optimum dosage.

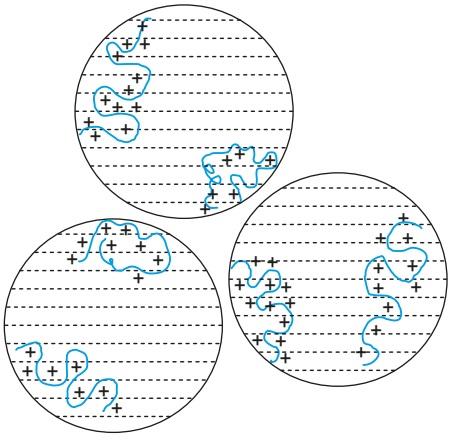

Fig. 9.10: "Electrostatic patch" model for the interaction of negatively charged particles with adsorbed cationic polyelectrolytes.

References

[1] Deryaguin BV, Landau L. Acta Physicochem USSR. 1941;14:633.
[2] Verwey EJW, Overbeek JTG. Theory of stability of lyophobic colloids. Amsterdam: Elsevier; 1948.
[3] Goodwin JW. Colloids and interfaces with surfactants and polymers. London: John Wiley and Sons; 2009.
[4] von Smoluchowski M. Physik Z. 1916;17:557, 585.
[5] Hunter RJ. Foundations of colloid science. Oxford: Oxford University Press; 1987.
[6] Russel WB, Saville DA, Schowalter WR. Colloidal dispersions. Cambridge: Cambridge University Press; 1989.
[7] Fuchs N. Z Physik. 1936;89:736.
[8] Reerink H, Overbeek JTG. Discussion Faraday Soc. 1954;18:74.
[9] Krieger IM, Dougherty TJ. Trans Soc Rheol. 1959;3:137.
[10] Krieger IM, Advances Colloid and Interface Sci. 1972;3:111.
[11] Goodwin JW, Mercer-Chalmers J. Flow induced aggregation of colloidal dispersions". In: Ottewill RH, Rennie AR, editors. Modern aspects of colloidal dispersions. Dordrecht: Kluwer; 1998. p. 61–75.
[12] Tadros T. Polymeric surfactants. Berlin: De Gruyter; 2017.
[13] Napper DH. Polymeric stabilisation of colloidal dispersions. London: Academic Press; 1983.
[14] Tadros T. Polymeric surfactants. In: Tadros T, editor. Encyclopedia of colloid and interface science. Berlin: Springer; 2013.
[15] Asakura A, Oosawa F. J Chem Phys. 1954;22:1235; J Polymer Sci. 1958;93:183.
[16] Gregory J. In: Tadros T, editor. Solid/liquid dispersions. London: Academic Press; 1987.
[17] Gregory J. Flocculation fundamentals. In: Tadros T, editor. Encyclopedia of colloid and interface science. Berlin: Springer; 2013.

10 Ostwald ripening in dispersions and its prevention

10.1 Introduction

Most formulations of the disperse type consist of particles or droplets with a mid-range of particle or droplet size distribution. Due to curvature effect, the smaller particles or droplets will have higher solubility than the larger ones. With time, diffusion of the molecules of the smaller particles or droplets to the larger ones will take place resulting in a shift of the particle or droplet size distribution to larger values. This process is referred to as Ostwald ripening and this will affect the overall physical stability of the formulation. For example, this increase in particle or droplet size will increase the rate of creaming or sedimentation. In general, the larger particles or droplets will have a higher van der Waals attraction when compared with the smaller ones and this may enhance the flocculation of the dispersion. With emulsions, the larger droplets are more deformable than the smaller ones and this may cause emulsion coalescence (Chapter 11).

In this chapter I will start with a section on the driving force of Ostwald ripening by emphasizing the effect of particle size on solubility of the particles or droplets. This is followed by a section on the theories that are used to calculate the rate of Ostwald ripening with particular reference to the effect of particle or droplet solubility. The effect of the presence of surfactant micelles in the continuous phase on the rate of Ostwald ripening will be discussed. The next section will deal with the methods that can be applied to reduce the Ostwald ripening rate for emulsions. The process of Ostwald ripening for suspensions, sometimes referred to as crystal growth, is discussed by considering the thermodynamic theory of crystal growth that considers the free energy of formation of a nucleus in terms of the surface free energy (that is positive) and the free energy of formation of a new phase (that is negative). In this way, one can define a critical nucleus size above which spontaneous formation of a nucleus occurs. The molecular-kinetic theory of crystal growth considers the energy of interaction of various particles as they are deposited on the surface of a crystal, at its corners, edges, etc., in a manner similar to a "brick laying" process. The influence of dislocations on crystal growth explains the process that can take place at extremely low supersaturation. Such defects result in the formation of steps at which crystals can grow without the need of formation of nuclei. Screw dislocations are of special importance in the growth of real crystals. The influence of impurities on crystal growth and habit modification is discussed in this section. The effect of polymorphic changes on crystal growth and habit modification is described in terms of the lower solubility of the more stable polymorph when compared with the higher solubility of the less stable one. Finally, the various methods that can be applied for crystal growth inhibition are described.

https://doi.org/10.1515/9783110587944-011

10.2 Driving force for Ostwald ripening

The driving force of Ostwald ripening is the difference in solubility between smaller and larger particles or droplets [1]. Small particles or droplets with radius r_1 will have higher solubility than a larger particle or droplet with radius r_2. This can be easily recognized from the Kelvin equation [2] which relates the solubility of a particle or droplet $S(r)$ with that of a particle or droplet with infinite radius $S(\infty)$,

$$S(r) = S(\infty)\exp\left(\frac{2\gamma V_m}{rRT}\right), \tag{10.1}$$

where γ is the solid/liquid or liquid/liquid interfacial tension, V_m is the molar volume of the disperse phase, R is the gas constant and T is the absolute temperature. The quantity $(2\gamma V_m/RT)$ has the dimension of length and is termed the characteristic length with an order of ≈ 1 nm.

A schematic representation of the enhancement the solubility $c(r)/c(0)$ with decreasing droplet size according to the Kelvin equation is shown in Fig. 10.1.

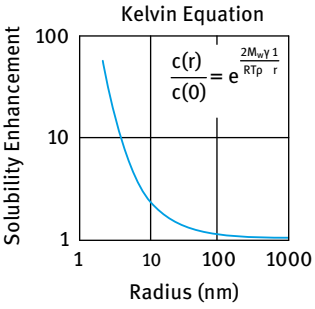

Fig. 10.1: Solubility enhancement with decreasing particle or droplet radius.

It can be seen from Fig. 10.1 that the solubility of particles or droplets increases very rapidly with decreasing radius, particularly when $r < 100$ nm. This means that a particle or droplet with a radius of, say, 4 nm will have about 10 times solubility enhancement compared, say, with a particle or droplet with 10 nm radius which has a solubility enhancement of only 2 times. Thus with time, molecular diffusion will occur between the smaller and larger particles or droplets, with the ultimate disappearance of most of the small particles or droplets. This results in a shift in the particle or droplet size distribution to larger values on storage of the dispersion. This could lead to the formation of a dispersion droplet size > μm. This instability can cause severe problems, such as creaming or sedimentation, flocculation and even coalescence of the emulsion.

For two particles or droplets with radii r_1 and r_2 $(r_1 < r_2)$,

$$\frac{RT}{V_m}\ln\left[\frac{S(r_1)}{S(r_2)}\right] = 2\gamma\left[\frac{1}{r_1} - \frac{1}{r_2}\right]. \tag{10.2}$$

Equation (10.2) is sometimes referred to as the Ostwald equation and it shows that the greater the difference between r_1 and r_2, the higher the rate of Ostwald ripening. That is why in preparation of dispersions, one aims at producing a narrow size distribution.

10.3 Kinetics of Ostwald ripening

The kinetics of Ostwald ripening is described in terms of the theory developed by Lifshitz and Slesov [3] and by Wagner [4] (referred to as LSW theory). The LSW theory assumes that:

(i) mass transport is due to molecular diffusion through the continuous phase;
(ii) the dispersed phase particles or droplets are spherical and fixed in space;
(iii) there are no interactions between neighbouring particles or droplets (the particles or droplets are separated by a distance much larger than the diameter of the droplets);
(iv) the concentration of the molecularly dissolved species is constant except adjacent to the droplet boundaries.

The rate of Ostwald ripening ω is given by,

$$\omega = \frac{\mathrm{d}}{\mathrm{d}r}\left(r_\mathrm{c}^3\right) = \left(\frac{8\gamma DS(\infty)V_\mathrm{m}}{9RT}\right)f(\phi) = \left(\frac{4DS(\infty)\alpha}{9}\right)f(\phi), \tag{10.3}$$

where r_c is the radius of a particle or droplet that is neither growing nor decreasing in size, D is the diffusion coefficient of the disperse phase in the continuous phase, $f(\phi)$ is a factor that reflects the dependency of ω on the disperse volume fraction and α is the characteristic length scale ($= 2\gamma V_\mathrm{m}/RT$).

Droplets or particles with $r > r_\mathrm{c}$ grow at the expense of smaller ones, while droplets or particles with $r < r_\mathrm{c}$ tend to disappear. The validity of the LSW theory was tested by Kabalnov et al. [5] who used 1,2 dichloroethane-in-water emulsions. The droplets were fixed to the surface of a microscope slide to prevent their coalescence. The evolution of the droplet size distribution was followed as a function of time by microscopic investigations.

LSW theory predicts that the droplet growth over time will be proportional to r_c^3. This is illustrated in Fig. 10.2 for dichloroethane-in-water emulsions.

Another consequence of LSW theory is the prediction that the size distribution function $g(u)$ for the normalized droplet or particle radius $u = r/r_\mathrm{c}$ adopts a time-independent form given by:

$$g(u) = \frac{81eu^2\exp[1/(2u/3-1)]}{32^{1/3}(u+3)^{7/3}(1.5-u)^{11/3}} \quad \text{for} \quad 0 < u \le 1.5 \tag{10.4}$$

and

$$g(u) = 0 \quad \text{for} \quad u > 1.5. \tag{10.5}$$

A characteristic feature of the size distribution is the cut-off at $u > 1.5$.

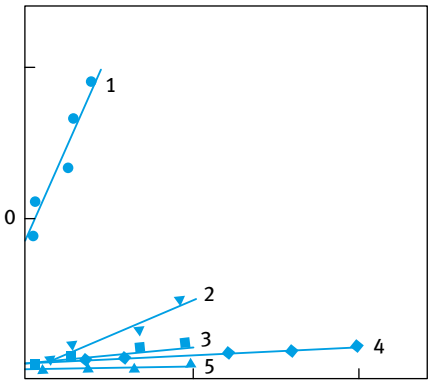

Fig. 10.2: Variation of average cube radius with time during Ostwald ripening in emulsions of: (1) 1,2 dichloroethane; (2) benzene; (3) nitrobenzene; (4) toluene; (5) p-xylene.

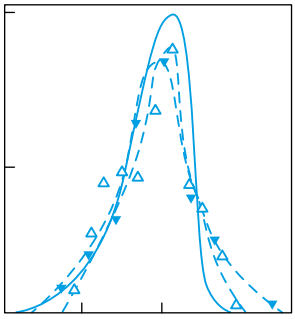

Fig. 10.3: Comparison between theoretical function $g(u)$ (full line) and experimentally determined functions obtained for 1,2 dichloroethane droplets at time 0 (open triangles) and 300 s (inverted solid triangles).

A comparison of the experimentally determined size distribution (dichloroethane-in-water emulsions) with the theoretical calculations based on the LSW theory is shown in Fig. 10.3.

The influence of the alkyl chain length of the hydrocarbon on the Ostwald ripening rate of nanoemulsions was systematically investigated by Kabalanov et al. [6]. Increasing the alkyl chain length of the hydrocarbon used for the emulsion results in a decrease in the oil solubility. According to LSW theory this reduction in solubility should result in a decrease of the Ostwald ripening rate. This was confirmed by the results of Kabalnov et al. [6] who showed that the Ostwald ripening rate decreases with increasing alkyl chain length from C_9–C_{16}. Tab. 10.1 shows the solubility of the hydrocarbon, the experimentally determined rate ω_e and the theoretical values ω_t and the ratio of ω_e/ω_t.

Although the results showed the linear dependency of the cube of the droplet radius on time in accordance with LSW theory, the experimental rates were ≈ 2–3 times higher than the theoretical values. The deviation between theory and experiment has been ascribed to the effect of Brownian motion [6]. LSW theory assumes that the droplets are fixed in space and molecular diffusion is the only mechanism of mass transfer. For droplets undergoing Brownian motion, one must take into account the contributions of molecular and convective diffusion as predicted by the Peclet

number,

$$Pe = \frac{r\upsilon}{D}, \tag{10.6}$$

where υ is the velocity of the droplets that is approximately given by,

$$\upsilon = \left(\frac{3kT}{M}\right)^{1/2}, \tag{10.7}$$

where k is the Boltzmann constant, T is the absolute temperature and M is the mass of the droplet. For $r = 100$ nm, $Pe = 8$, indicating that mass transfer will be accelerated with respect to that predicted by LSW theory.

Tab. 10.1: Influence of the alkyl chain length on the Ostwald ripening rate.

Hydrocarbon	$c(\infty)$ (ml ml^{-1})[a]	ω_e (cm^{-3} s^{-1})	ω_t (cm^{-3} s^{-1})[b]	$\omega_r = \omega_e/\omega_t$
C_9H_{20}	3.1×10^{-7}	6.8×10^{-19}	2.9×10^{-19}	2.3
$C_{10}H_{22}$	7.1×10^{-8}	2.3×10^{-19}	0.7×10^{-19}	3.3
$C_{11}H_{24}$	2.0×10^{-8}	5.6×10^{-20}	2.2×10^{-20}	2.5
$C_{12}H_{26}$	5.2×10^{-9}	1.7×10^{-20}	0.5×10^{-20}	3.4
$C_{13}H_{28}$	1.4×10^{-9}	4.1×10^{-21}	1.6×10^{-21}	2.6
$C_{14}H_{30}$	3.7×10^{-10}	1.0×10^{-21}	0.4×10^{-21}	2.5
$C_{15}H_{32}$	9.8×10^{-11}	2.3×10^{-22}	1.4×10^{-22}	1.6
$C_{16}H_{34}$	2.7×10^{-11}	8.7×10^{-23}	2.2×10^{-23}	4.0

a Molecular solubilities of hydrocarbons in water taken from: McAuliffe C. J Phys Chem. 1966:1267.
b For theoretical calculations, the diffusion coefficients were estimated according to the Hayduk–Laudie equation (Hayduk W, Laudie H. AIChE J. 1974;20:611) and the correction coefficient $f(\phi)$ assumed to be equal to 1.75 for $\phi = 0.1$ (Voorhees PW. J Stat Phys. 1985;38:231).

The LSW theory assumes that there are no interactions between the droplets and it is limited to low oil volume fractions. At higher volume fractions the rate of ripening depends on the interaction between diffusion spheres of neighbouring droplets. It is expected that emulsions with higher volume fractions of oil will have broader droplet size distribution and faster absolute growth rates than those predicted by LSW theory. However, experimental results using high surfactant concentrations (5 %) showed the rate to be independent of the volume fraction in the range $0.01 \leq \phi \leq 0.3$. It has been suggested that the emulsion droplets may have been screened from one another by surfactant micelles [7]. A strong dependence on volume fraction has been observed for fluorocarbon-in-water emulsions [8]. A three-fold increase in ω was found when ϕ was increased from 0.08 to 0.52.

It has been suggested that micelles play a role in facilitating the mass transfer between particle or emulsion droplets by acting as carriers of particle or oil molecules [9]. Three mechanisms were suggested:

(i) oil or particle molecules are transferred via direct droplet/micelle or particle/micelle collisions;

(ii) oil or solid molecules exit the oil droplet or particle and are trapped by micelles in the immediate vicinity of the droplet or particle;
(iii) oil or particle molecules exit the oil droplet or particle collectively with a large number of surfactant molecules to form a micelle.

In mechanism (i) the micellar contribution to the rate of mass transfer is directly proportional to the number of droplet/micelle or particle/micelle collisions, i.e. to the volume fraction of micelles in solution. In this case the molecular solubility of the oil or particles in the LSW equation is replaced by the micellar solubility which is much higher. Large increases in the rate of mass transfer would be expected with increasing micelle concentration. Numerous studies indicate, however, that the presence of micelles only affects mass transfer to a small extent [10]. Results were obtained for decane-in-water emulsions using sodium dodecyl sulphate (SDS) as emulsifier at concentrations above the critical micelle concentration (cmc). This is illustrated in Fig. 10.4 which shows plots of $(d_{inst}/d^0_{inst})^3$ (where d_{inst} is the diameter at time t and d^0_{inst} is the diameter at time 0) as a function of time. The results showed only a two-fold increase in ω above the cmc. This result is consistent with many other studies which showed an increase in mass transfer of only 2–5 times with increasing micelle concentration. The lack of strong dependency of mass transfer on micelle concentration for ionic surfactants may result from electrostatic repulsion between the emulsion droplets or particles and micelles, which provide a high energy barrier preventing droplet/micelle or particle/micelle collision.

In mechanism (ii), a micelle in the vicinity of an emulsion droplet or particle rapidly takes up dissolved oil or particles from the continuous phase. This "swollen" micelle diffuses to another droplet or particle, where the oil or solute is redeposited. Such a mechanism would be expected to result in an increase in mass transfer over and

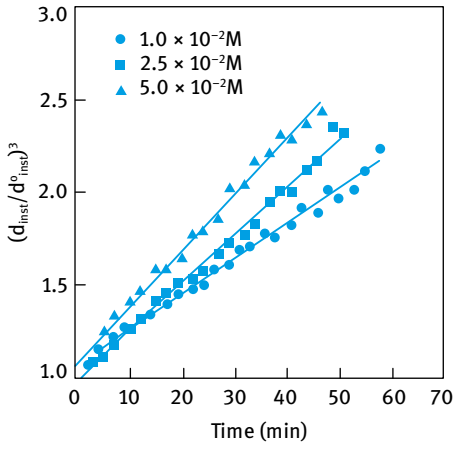

Fig. 10.4: Variation of $(d_{inst}/d^0_{inst})^3$ with time for decane-in-water emulsions for different SDS concentrations above the cmc.

above that expected from LSW theory by a factor φ given by the following equation,

$$\varphi = 1 + \frac{\phi_s \Gamma D_m}{D} = 1 + \frac{\chi^{eq} D_m}{c^{eq} D}, \tag{10.8}$$

where ϕ_s is the volume fraction of micelles in solution, $\chi^{eq} = \phi_s c_m^{eq}$ is the net oil or particle solubility in the micelle per unit volume of micellar solution reduced by the density of the solute, $\Gamma = c_m^{eq}/c^{eq} \approx 10^6$–$10^{11}$ is the partition coefficient for the oil or solute between the micelle and bulk aqueous phase at the saturation point, D_m is the micellar diffusivity ($\approx 10^{-6}$–10^{-7} cm^2 s^{-1}). For a decane-water nanoemulsion in the presence of 0.1 mol dm^{-3} SDS, equation (10.8) predicts an increase in the rate of ripening by three orders of magnitude, in sharp contrast to the experimental results.

To account for the discrepancy between theory and experiment in the presence of surfactant micelles, Kabalanov [11] considered the kinetics of micellar solubilization and he proposed that the rate of oil monomer exchange between the oil droplets and the micelles is slow, and rate-determining. Thus at low micellar concentration, only a small proportion of the micelles are able to rapidly solubilize the oil. This leads to a small, but measurable increase in the Ostwald ripening rate with micellar concentration. Taylor and Ottewill [12] proposed that micellar dynamics may also be important. According to Aniansson et al. [13], micellar growth occurs in a stepwise fashion and is characterized by two relaxation times, τ_1 and τ_2. The short relaxation time τ_1 is related to the transfer of monomers in and out of the micelles, while the long relaxation time τ_2 is the time required for break-up and reformation of the micelle. At low SDS (0.05 mol dm^{-3}) concentration $\tau_2 \approx 0.01$ s, whereas at higher SDS concentration (0.2 mol dm^{-3}) $\tau_2 \approx 6$ s. Taylor and Ottewill [12] suggested that, at low SDS concentration, τ_2 may be fast enough to have an effect on the Ostwald ripening rate, but at 5 % SDS τ_2 may be as long as 1,000 s (taking into account the effect of solubilization on τ_2) which is too long to have a significant effect on the Ostwald ripening rate.

When using nonionic surfactant micelles, larger increases in the Ostwald ripening rate might be expected due to the larger solubilization capacities of the nonionic surfactant micelles and absence of electrostatic repulsion between the nanoemulsion droplets and the uncharged micelles. This was confirmed by Weiss et al. [14] who found a large increase in the Ostwald ripening rate in tetradecane-in-water emulsions in the presence of Tween 20 micelles.

10.4 Reduction of Ostwald ripening in emulsions

10.4.1 Addition of a small proportion of highly insoluble oil

Huguchi and Misra [15] suggested that addition of a second disperse phase that is virtually insoluble in the continuous phase, such as squalane, can significantly reduce the Ostwald ripening rate. In this case, significant partitioning between different droplets

is predicted, with the component having the low solubility in the continuous phase (e.g. squalane) being expected to be concentrated in the smaller droplets. During Ostwald ripening in a two-component disperse system, equilibrium is established when the difference in chemical potential between different sized droplets, which results from curvature effects, is balanced by the difference in chemical potential resulting from partitioning of the two components. Huguchi and Misra [15] derived the following expression for the equilibrium condition, in which the excess chemical potential of the medium soluble component, $\Delta\mu_1$, is equal for all of the droplets in a polydisperse medium,

$$\frac{\Delta\mu_i}{RT} = \left(\frac{a_1}{r_{eq}}\right) + \ln(1 - X_{eq2}) = \left(\frac{a_1}{r_{eq}}\right) - X_{02}\left(\frac{r_0}{r_{eq}}\right)^3 = \text{const.}, \tag{10.9}$$

where $\Delta\mu_1 = \mu_1 - \mu_1^*$ is the excess chemical potential of the first component with respect to the state μ_1^* when the radius $r = \infty$ and $X_{02} = 0$, r_0 and r_{eq} are the radii of an arbitrary drop under initial and equilibrium conditions respectively, X_{02} and X_{eq2} are the initial and equilibrium mole fractions of the medium-insoluble component 2, a_1 is the characteristic length scale of the medium-soluble component 1.

The equilibrium determined by equation (10.9) is stable if the derivative $\partial\Delta\mu_1/\partial r_{eq}$ is greater than zero for all the droplets in a polydisperse system. Based on this analysis, Kabalanov et al. [16] derived the following criterion,

$$X_{02} > \frac{2a_1}{3d_0}, \tag{10.10}$$

where d_0 is the initial droplet diameter. If the stability criterion is met for all droplets, two patterns of growth will result, depending on the solubility characteristic of the secondary component. If the secondary component has zero solubility in the continuous phase, then the size distribution will not deviate significantly from the initial one, and the growth rate will be equal to zero. In the case of limited solubility of the secondary component, the distribution is governed by rules similar to LSW theory, i.e. the distribution function is time variant. In this case, the Ostwald ripening rate ω_{mix} will be a mixture growth rate that is approximately given by the following equation [16],

$$\omega_{mix} = \left(\frac{\phi_1}{\omega_1} + \frac{\phi_2}{\omega_2}\right)^{-1}, \tag{10.11}$$

where ϕ_1 is the volume fraction of the medium-soluble component and ϕ_2 is the volume fraction of the medium-insoluble component respectively.

If the stability criterion is not met, a bimodal size distribution is predicted to emerge from the initially monomodal one. Since the chemical potential of the soluble component is predicted to be constant for all the droplets, it is also possible to derive the following equation for the quasi-equilibrium component 1,

$$X_{02} + \frac{2a_1}{d} = \text{const.}, \tag{10.12}$$

where d is the diameter at time t.

Kabalanov et al. [17] studied the effect of addition of hexadecane to a hexane-in-water nanoemulsion. Hexadecane, which is less soluble than hexane, was studied at three levels $X_{02} = 0.001$, 0.01 and 0.1. For the higher mole fraction of hexadecane, namely 0.01 and 0.1, the emulsion had a physical appearance similar to that of an emulsion containing only hexadecane and the Ostwald ripening rate was reliably predicted by equation (10.11). However, the emulsion with $X_{02} = 0.001$ quickly separated into two layers, a sedimented layer with a droplet size of ca. 5 µm and a dispersed population of submicron droplets (i.e. a bimodal distribution). Since the stability criterion was not met for this low volume fraction of hexadecane, the observed bimodal distribution of droplets is predictable.

10.4.2 Modification of the interfacial layer for reducing Ostwald ripening

According to LSW theory, the Ostwald ripening rate ω is directly proportional to the interfacial tension γ. Thus by reducing γ, ω is reduced. This could be confirmed by measuring ω as a function of SDS concentration for decane-in-water emulsion [10] below the critical micelle concentration (cmc). Below the cmc, γ shows a linear decrease with increasing log [SDS] concentration. The results are summarized in Tab. 10.2.

Several other mechanisms have been suggested to account for the reduction in the Ostwald ripening rate by modifying the interfacial layer. For example, Walstra [18] suggested that emulsions could be effectively stabilized against Ostwald ripening by the use of surfactants that are strongly adsorbed at the interface and which do not desorb during the Ostwald ripening process. In this case, an increase in interfacial dilational modulus ε and a decrease in interfacial tension γ would be observed for the shrinking droplets. Eventually the difference in ε and γ between droplets would balance the difference in capillary pressure (i.e. curvature effects) leading to a quasi-equilibrium state. In this case, emulsifiers with low solubilities in the continuous phase such as proteins would be preferred. Long chain phospholipids with a very low solubility (cmc $\approx 10^{-10}$ mol dm^{-3}) are also effective in reducing Ostwald ripening of some emulsions. The phospholipid would have to have a solubility in water about three orders of magnitude lower than the oil [19].

Tab. 10.2: Variation of Ostwald ripening rate with SDS concentration for decane-in-water emulsions.

[SDS] Concentration (mol dm^{-3})	ω (cm^3 s^{-1})
0.0	2.50×10^{-18}
1.0×10^{-4}	4.62×10^{-19}
5.0×10^{-4}	4.17×10^{-19}
1.0×10^{-3}	3.68×10^{-19}
5.0×10^{-3}	2.13×10^{-19}

cmc of SDS = 8.0×10^{-3}

10.4.3 Influence of initial droplet size of emulsions on the Ostwald ripening rate

The influence of initial droplet size on Ostwald ripening can be realized by considering the droplet size dependency of the characteristic time, τ_{OR},

$$\tau_{OR} \approx \frac{r^3}{\alpha S(\infty) D} \approx \frac{r^3}{\omega}. \tag{10.13}$$

Values of τ_{OR} when $r = 100$ nm are given in Tab. 10.3 for a series of hydrocarbons with increasing chain length which clearly show the reduction in Ostwald ripening rate with increasing chain length (due to reduction in solubility $S(\infty)$). The dramatic dependency of τ_{OR} on increasing chain length is apparent. The characteristic time shows

Tab. 10.3: Characteristic time for Ostwald ripening in hydrocarbon-in-water nanoemulsions stabilized by 0.1 mol dm^{-3} SDS.

Hydrocarbon	ω_e (cm^3 s^{-1})	$\tau_{OR} \approx (r^3/\omega_e)$
C_9H_{20}	6.8×10^{-19}	25 min
$C_{10}H_{22}$	2.3×10^{-19}	73 min
$C_{11}H_{24}$	5.6×10^{-20}	5 h
$C_{12}H_{26}$	1.7×10^{-20}	16 h
$C_{13}H_{28}$	4.1×10^{-21}	3 d
$C_{14}H_{30}$	1.0×10^{-21}	12 d
$C_{15}H_{32}$	2.3×10^{-22}	50 d
$C_{16}H_{34}$	8.7×10^{-23}	133 d

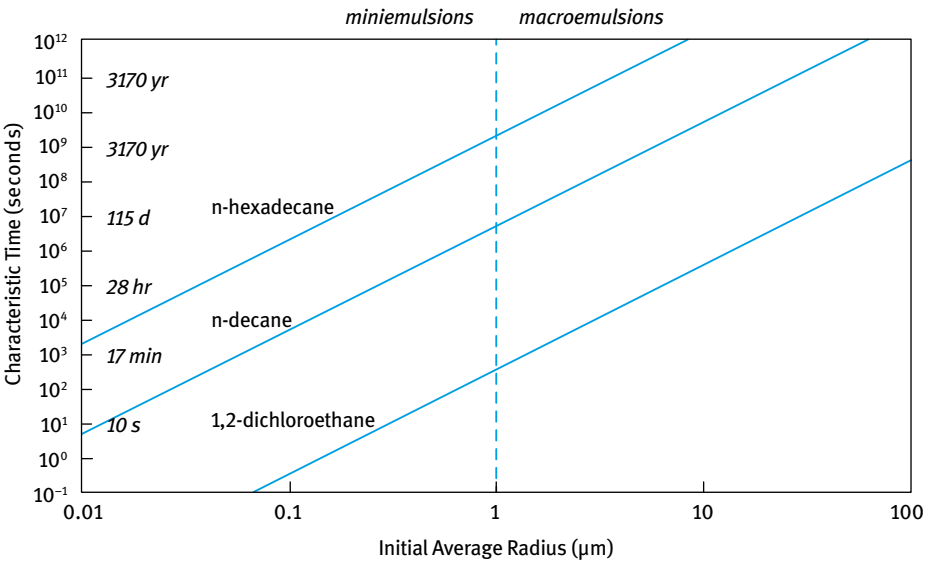

Fig. 10.5: Characteristic time for Ostwald ripening versus droplet size.

a large dependency on the initial average radius as illustrated in Fig. 10.5 for a series of emulsions. It can be seen that the Ostwald ripening rate can be extremely rapid for small droplet sizes, thereby providing a key component in determining initial droplet size. For example, it is not likely that droplets with radii less than 100 nm will be observed for decane-in-water nanoemulsions since the droplets will ripen to this size on the timescale of a few minutes. This was confirmed by Kabalanov et al. [5] who noted large differences in initial droplet size for hydrocarbon-in-water emulsions as the chain length of the hydrocarbon was decreased. For example, nonane-in-water nanoemulsions had an initial droplet size of 178 nm, decane-in-water nanoemulsions had a size of 124 nm, and undecane-in-water nanoemulsions a size of 88 nm. It is clear from Fig. 10.5 that the driving force for Ostwald ripening decreases dramatically with increasing droplet size.

10.5 Thermodynamic theory of crystal growth

This theory developed by Gibbs [25] and Volmer [26, 27] is based on the assumption of a stepwise process in which the crystal grows layer by layer. Volmer [26, 27] originally assumed that a thin adsorption layer exists at the phase boundary, whereby the atoms or molecules of the growing substance lose some of their energy as they approach the surface of the crystal without losing all their degrees of freedom. These particles are able to migrate along the surface of the crystal like molecules in a two-dimensional gas. Equilibrium between the adsorption layer and the solution is established immediately. The growth rate is determined by the capture of particles from the adsorption layer by the crystal lattice. The collision of particles in the adsorption layer results in the formation of two-dimensional nuclei, which grow to form a new crystalline layer. The time taken for a layer to form a nucleus is considerably shorter than the time necessary for the formation of a two-dimensional crystal. Thus, the formation of two-dimensional nuclei is the rate determining step.

The formation of a two-dimensional nucleus is similar to the formation of a three-dimensional nucleus. According to Gibbs [26], the free energy of formation of a spherical nucleus, ΔG, is given by the sum of two contributions: a positive surface energy term ΔG_s which increases with increasing radius of the nucleus r; and a negative contribution ΔG_v due to the appearance of a new phase, which also increases with increasing r,

$$\Delta G = \Delta G_s + \Delta G_v. \tag{10.14}$$

Thus, the sign of ΔG depends on the relative magnitudes of ΔG_s and ΔG_v, which in turn depend on the size of the two-dimensional nucleus of the new phase, l. ΔG_s for a two-dimensional nucleus is given by,

$$\Delta G_s = jl\kappa, \tag{10.15}$$

where κ is the specific linear energy and j is a shape factor.

ΔG_v is given by,

$$\Delta G_v = \frac{jl^2\kappa}{M} RT \ln \frac{S}{S_0}, \tag{10.16}$$

where (S/S_0) is the relative supersaturation.

Therefore,

$$\Delta G = 4\pi r^2 \gamma - \left(\frac{4\pi r^3 \rho}{3M}\right) RT \ln\left(\frac{S}{S_0}\right). \tag{10.17}$$

In the initial stages of nucleation, ΔG_s increases faster with increasing l when compared to ΔG_v and ΔG remains positive, reaching a maximum at a critical size l^*, after which it decreases and eventually becomes negative. This occurs since the second term in equation (10.17) rises faster with increasing l than the first term (l^2 versus l). When ΔG becomes negative, growth becomes spontaneous and the cluster grows very fast. This is illustrated in Fig. 10.6. This figure shows the critical size of the nucleus l^* above which growth becomes spontaneous. The free energy maximum ΔG^* at the critical radius represents the barrier that has to be overcome before growth becomes spontaneous. Both l^* and ΔG^* can be obtained by differentiating equation (10.17) with respect to l and equating the result to zero. This gives the following expressions,

$$r^* = \frac{2\gamma M}{\rho RT \ln(S/S_0)}, \tag{10.18}$$

$$\Delta G^* = \frac{16}{3} \frac{\pi \gamma^3 M^2}{(\rho RT)^2 [\ln(S/S_0)]^2}. \tag{10.19}$$

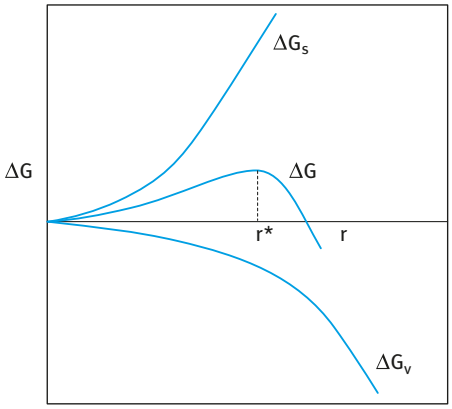

Fig. 10.6: Variation of free energy of formation of a nucleus with size l.

It is clear from equations (10.17)–(10.19) that the free energy of formation of a nucleus and the critical size l^* above which the cluster formation grows spontaneously depends on two main parameters, κ and (S/S_0), both of which are influenced by the presence of surfactants. κ is influenced in a direct way by adsorption of surfactant on the surface of the nucleus; this adsorption lowers κ and this reduces l^* and ΔG^*. In other words, spontaneous formation of clusters occurs at smaller critical radius.

In addition, surfactant adsorption stabilizes the nuclei against any flocculation. The presence of micelles in solution also affects the process of nucleation and growth directly and indirectly. The micelles can act as "nuclei" on which growth may occur. In addition, the micelles may solubilize the molecules of the material, thus affecting the relative supersaturation and this can have an effect on nucleation and growth.

The probability W of the formation of two-dimensional nuclei can be described by an Arrhenius type relationship,

$$W = K' \exp\left(-\frac{\Delta G_{\max}}{RT}\right), \tag{10.20}$$

and the linear growth rate $(\mathrm{d}l/\mathrm{d}t)$ is given by,

$$\frac{\mathrm{d}l}{\mathrm{d}t} = K'' \exp\left(-\frac{\Delta G_{\max}}{RT}\right) = K'' \exp\left(-\frac{j\kappa^2 M}{\rho R^2 T^2 \ln(S/S_0)}\right). \tag{10.21}$$

When a two-dimensional crystal grows on the face of a crystal, it evidently produces a layer of thickness r_0. The time interval t between the formation of the nuclei is inversely proportional to the formation of a two-dimensional nucleus, i.e.,

$$\frac{\mathrm{d}l}{\mathrm{d}t} = \frac{r_0}{t} = r_0 A W' = r_0 \cdot 3\kappa l^2 K'' \exp\left(-\frac{j\kappa^2 M}{\rho R^2 T^2 \ln(S/S_0)}\right), \tag{10.22}$$

where A is the surface area of a growing crystal and W is the probability of formation of a nucleus per unit surface area.

When a small crystal grows to a sufficient size, several nuclei may form on the surface. The time of formation of a monolayer then reduces to: $t_0 = (\lambda/a_{\mathrm{f}})$ where λ is the rate of growth of nuclei on the surface of a crystal and a_{f} is the average final size of two-dimensional nuclei that is given by,

$$a_{\mathrm{f}} = \left(\frac{\lambda}{W_1}\right)^{1/3} \tag{10.23}$$

and,

$$\frac{\mathrm{d}l}{\mathrm{d}t} = \frac{r_0}{t_0} = r_0 (W\lambda^2)^{1/3} = K \exp\left(-\frac{j\kappa^2 M}{3\rho R^2 T^2 \ln(S/S_0)}\right). \tag{10.24}$$

Thus, the rate of growth of small crystals depends on the degree of supersaturation and on their surface area. With large crystals $(\mathrm{d}l/\mathrm{d}t)$ depends only on the degree of supersaturation.

10.6 Molecular-kinetic theory of crystal growth

Kossel [28] developed a model for the growth of crystals in which he considered the energy of interaction of various particles as they are deposited on the surface of a crystal, at its corners, edges, etc., in a manner similar to a "brick laying" process. Various

energies will be encountered in attaching the particles to the various regions of the crystal. On the other hand, Stranskii and Kaishev [29, 30] considered the growth of crystals from a different point of view, namely the work necessary to detach the particles from the surface of the crystal to infinity. According to Stranskii and Kaishev [30], the rate of crystal growth, which is proportional to the nucleation rate, is given by,

$$\upsilon = K' a_2 \exp\left(-\frac{Wa_2^*}{RT}\right) \exp\left(-\frac{L\kappa}{2kT}\right), \tag{10.25}$$

where Wa_2^* is the work of detachment of a two-dimensional nucleus from the surface of a crystal and L is the perimeter of a two-dimensional nucleus.

10.7 The influence of dislocations on crystal growth

According to the above theories, the growth of crystals can take place only under conditions of appreciable supersaturation, mostly > 1.5 %, which ensures the necessary work of formation of two-dimensional nuclei. However, experiments on the growth of various crystals have shown that crystal growth can take place at extremely low supersaturation. The existence of a critical finite supersaturation for the growth of crystals has only been established for a few materials and then for individual faces of crystals being different from case to case; at the most it is about 1 %. However, this discrepancy is not too surprising [31] since the crystals do not have a competely perfect surface needing fresh two-dimensional nucleation in order to grow. This discrepancy may be attributed to crystal dislocations and structural defects. The latter include cracks, surface kinks and surface roughness.

According to Cabrera and Burton [32] and Frank [31], such defects result in the formation of steps at which crystals can grow without the need of formation of nuclei. Screw dislocations are of special importance in the growth of real crystals. If just one dislocation of this type emerges at the centre of the face, that crystal face can grow perpetually up a “spiral staircase”. The general importance of dislocations for crystal growth accounts for many observations, such as the individual behaviour of each crystal face, particularly on the microscopic scale.

The growth of a crystal in steps is due to three processes:

(i) exchange of particles between adsorption layer and solution;
(ii) diffusion of adsorbed particles to the steps, as well as exchange of particles between steps and adsorption layer;
(iii) diffusion of particles adsorbed by steps in the direction of kinks and exchange with these kinks.

Using these assumptions, Burton, Cabrera and Frank [31, 32] arrived at the following expression for the growth rate R of a crystal from solution,

$$R = \frac{DN_0\Omega a\beta(x_0)}{2\kappa_0\rho_c}, \tag{10.26}$$

where x_0 is the average distance between kinks in the steps, $\beta(x_0)$ is the supersaturation of the solution at distance x_0, D is the diffusion coefficient, N_0 is the equilibrium or steady state concentration of the crystallizing substance in solution, a is the distance between two equilibrium configurations on the surface of a crystal and Ω is the volume of one molecule.

The critical size of a nucleus ρ_c is given by,

$$2\rho_c = 2\gamma\frac{a}{kT}\beta(x_0), \tag{10.27}$$

where γ is a constant (Euler constant). $\beta(x_0)$ is given by,

$$\frac{\beta(x_0)}{\beta} = \left[1 + \frac{2\pi a(\delta - Y_0)}{x_0 Y_0} + \frac{2a}{x_0}\ln\left(\frac{Y_0}{x_0}\right)\right]^{-1}. \tag{10.28}$$

Y_0 is the distance between successive steps, δ is the thickness of the unsaturated layer at the surface of the crystal and β is the supersaturation elsewhere in the solution.

At low supersaturation, the third term on the right-hand side of equation (10.28) is the largest and R depends on $\beta(x_0)$ in a parabolic manner. At higher supersaturations, the second term in equation (10.28) becomes more important and $R = f(\beta)$ becomes linear. In this case equation (10.28) takes the form,

$$R_1 = \frac{DN_0\Omega\beta}{\delta}. \tag{10.29}$$

Thus, the linear growth rate should be observed at $\beta \geq 10^{-3}$.

10.8 Influence of impurities on crystal growth and habit

It has long been known that trace concentrations of certain additives can have pronounced effects on crystal growth and habit. These effects are of great importance in many fields of science and technology, but the mechanism by which these additives affect crystal growth is not clear. It is generally agreed that additives must adsorb on a crystal surface in order to affect the growth on that face.

Sufficient effects on growth behaviour with very small impurity additives are usually produced by large organic molecules on colloidal materials. One part in 10^4 or 10^5 of such materials may be sufficient to completely alter the growth. The effects of large molecules are usually nonspecific, presumably due to their adsorption on almost any point of the crystal.

Assuming growth to be governed by creation and subsequent lateral motion of steps in the crystal surface [31, 32], it is possible to derive an expression for the effect of impurities on the flow of these steps [33]. Consider the surface of a growing crystal which contains a uniform average concentration of steps n. Suppose there is a constant flux J_i of impurity molecules deposited on the crystal surface per unit time. Assuming that the impurity molecules are immobile on the surface; as the step moves along it will be stopped by a pair of molecules that are less than $2\rho_c$ apart (where ρ_c is the medium radius of curvature of the step corresponding to the supersaturation) and will squeeze itself between a pair of impurities that are more than $2\rho_c$ apart. Since the steps are curved, their average velocity v will be smaller than v_0, the velocity in the absence of impurities. A rough estimate of this reduction in velocity is given by the following approximate equation,

$$v = v_0(1 - 2\rho_c d^{1/2})^{1/2}, \tag{10.30}$$

where d is the average density of impurities just ahead of the step.

Assuming, for simplicity, that that once a step has passed beyond a certain point on the crystal the impurities adsorbed then become occluded in the crystal and do not offer a significant obstacle to the advance of the flowing step, it is clear that the density d ahead of any step will be given by,

$$d = \frac{J_i}{nv}. \tag{10.31}$$

This expression automatically makes the flux of impurities being adsorbed in the crystal equal to J_i. Substituting equation (10.31) into (10.30) and rearranging, the following equation, which may be solved for v, is obtained,

$$v^2 = v + a = 0, \tag{10.32}$$

$$v^2 = \frac{v}{v_0}; \quad \alpha^2 = \frac{4\rho_c^2 J_i}{v_0}, \tag{10.33}$$

where $v = nv$ is the flow rate of a step in the presence of impurity and $v_0 = nv_0$ is the corresponding rate in the absence of impurities.

10.9 Polymorphic changes

When the compound used for formulation of suspension concentrates exists in two polymorphs, crystal growth may take place as a result of reversion of the thermodynamically less stable form to the more stable form. If this is the case, crystal growth is virtually unaffected by temperature, i.e. it is an isothermal process, which is solvent mediated. Crystal growth involving such polymorphic changes has been carried out by various investigators [34–36]. A thermodynamic analysis based on Gibbs theory to

account for the polymorphic changes, can be made. If a crystal exists in two polymorphic forms, α and β, the Gibbs free energy is given by the expressions,

$$\Delta G^{\alpha} = \Delta G_{\mathrm{v}}^{\alpha} + \sum_{i}^{N} A_i \Delta G_{\mathrm{s}}^{\alpha}, \tag{10.34}$$

$$\Delta G^{\beta} = \Delta G_{\mathrm{v}}^{\beta} + \sum_{i}^{N} A_i \Delta G_{\mathrm{s}}^{\beta}, \tag{10.35}$$

where V is the crystal volume and A_i is the area. If $\Delta G^{\alpha} \neq \Delta G^{\beta}$, there exists a thermodynamic potential (driving force) to establish equilibrium by an appropriate change of phase or crystal habit. By this mechanism the less soluble phase grows at the expense of the more soluble phase. The different polymorphs can be characterized by X-ray diffraction.

10.10 Crystal growth inhibition

It is clear from the above discussion that crystal growth in suspension concentrates where the solid particles have substantial solubility or exist in various polymorphs is the rule rather than the exception. The task of the formulation scientist is to reduce crystal growth to an acceptable level depending on the application. This is particularly the case with pharmaceutical and agrochemical suspensions, where crystal growth leads to the shift of the particle size distribution to larger values. Apart from reducing the physical stability of the suspension, e.g. increased sedimentation, the increase in particle size of the active ingredient reduces its bioavailability (reduction of disease control). Unfortunately, crystal growth inhibition is still an "art", rather than a "science", in view of the lack of adequate fundamental understanding of the process at a molecular level.

Since suspension concentrates are prepared by using a wetting/dispersing agent (Chapter 3), it is important to discuss how these agents can affect the growth rate. In the first place, the presence of wetting/dispersing agents influences the process of diffusion of the molecules from the surface of the crystal to the bulk solution. The wetting/dispersing agent may affect the rate of dissolution by affecting the rate of transport away from the boundary layer [1], although their addition is not likely to affect the rate of dissolution proper (passage from the solid to the dissolved state in the immediate adjacent layer). If the wetting/dispersing agent forms micelles which can solubilize the solute, the diffusion coefficient of the solute in the micelles is greatly reduced. However, as a result of solubilization, the concentration gradient of the solute is increased to an extent depending on the extent of solubilization. The overall effect may be an increase in crystal growth rate as a result of solubilization. In contrast, if the diffusion rate of the wetting/dispersing agent molecules is sufficiently rapid, their presence will lower the flux of the solute molecules compared to that

in the absence of the wetting/dispersing agent. In this case, the wetting/dispersing agent will lower the rate of crystal growth.

Secondly, wetting/dispersing agents are expected to influence growth when the rate is controlled by surface nucleation [1]. Adsorption of wetting/dispersing agents on the surface of the crystal can drastically change the specific surface energy and make it inaccessible to the solute molecules. In addition, if the wetting/dispersing agent is preferentially adsorbed at one or more of the faces of the crystal (for example by electrostatic attraction between a highly negative face of the crystal and cationic surfactant), surface nucleation is no longer possible at this particular face (or faces). Growth will then take place at the remaining faces which are either bare or incompletely covered by the wetting/dispersing agent. This will result in a change in crystal habit.

The role of surfactants in modifying the crystal habit of adipic acid has been systematically studied by Michaels and collaborators [37–39]. These authors investigated the effect of various surfactants, of the anionic and cationic type on the growth of adipic acid crystals from aqueous solution. Microscopic measurements of the crystals permitted calculation of the individual growth rates of the (001), (010) and (110) faces. The growth rate is governed by the rate at which solute is supplied to the individual steps on the crystal faces and the spacing between them. In other words, the growth rate is proportional to the step velocity and the distance between steps. Surfactants may alter the growth rate by changing either of these. At constant step velocity, the spacing between steps may be altered, with a corresponding modification in the growth rate, by a variation in the rate of step generation. With constant step spacing, an alteration of step velocity will likewise modify the growth rate. Sodium dodecylbenzene sulphonate (NaDBS) retards the growth on the (010) and (110) more than the (001) face, thus favouring the formation of a prismatic or needle crystals. Cationic surfactants, such as cetyltrimethyl ammonium chloride, have the opposite effect, thus favouring growth of the micaceous faces. Michaels et al. [37–39] concluded that the anionic surfactants are physically adsorbed on the faces of adipic acid crystals, while the cationics appear to be chemisorbed. In all cases, the surfactants retarded crystal growth by adsorption on the crystal faces, thus reducing the area on which nucleation would occur. In fact with relatively large crystals, the influence of surfactants on crystal growth can be correlated satisfactorily with the Langmuir adsorption isotherm. Surfactants, in general, exhibit a far greater retarding influence on the crystal growth of very small crystals than on the growth of larger ones.

From the above discussion, it can be seen that surfactants (wetting/dispersing agents), if properly chosen, may be used for crystal growth inhibition and control of habit formation. Inhibition of crystal growth can also be achieved by polymeric surfactants and other additives. For example, Simonelli et al. [40] found that the crystal growth of the drug sulphathiazole can be inhibited by the addition of poly(vinylpyrrolidone) (PVP). The inhibition effect depends on the concentration and molecular weight of PVP. A minimum concentration (expressed as grams PVP/100 ml)

of polymer is required for inhibition, which increases with increasing molecular weight of the polymer. However, if the concentration is expressed in mol dm^{-3}, the reverse is true, i.e. the higher the molar mass of PVP the lower the number of moles required for inhibition. This led Simonelli et al. [40] to conclude that inhibition must involve kinetic effects, i.e. the rate of diffusion of PVP to the surfaces. If the rate of deposition of PVP is relatively slow compared to that of sulphathiazole molecules, it is buried by the "avalanche" of the precipitating sulphathiazole molecules. If, on the other hand, its rate is rapid, it in turn can bury the precipitating sulphathiazole molecules and sufficiently cover the crystal surface to cause inhibition of crystal growth. Clearly, a higher PVP concentration would be needed at higher supersaturation rates to cause inhibition. This is due to the increase in diffusion rate at higher supersaturation [40].

Carless et al. [41] reported that the crystal growth of cortisone acetate in aqueous suspensions can be inhibited by addition of cortisone alcohol. Crystal growth in this system is mainly inhibited by polymorphic transformation [41]. The authors assumed that cortisone alcohol is adsorbed onto the particles of the stable form and this prevents the arrival of new cortisone acetate molecules which would result in crystal growth. The authors also noticed that the particles change their shape, growing to long needles. This means that the cortisone alcohol fits into the most dense lattice plane of the cortisone acetate crystal, thus preventing preferential growth on that face.

Many block A–B–A and graft BA_n copolymers (with B being the "anchor" part and A the stabilizing chain) are very effective in inhibiting crystal growth. The B chain adsorbs very strongly on the surface of the crystal and sites become unavailable for deposition. This has the effect of reducing the rate of crystal growth. Apart from their influence on crystal growth, the above copolymers also provide excellent steric stabilization, providing the A chain is chosen to be strongly solvated by the molecules of the medium.

References

[1] Weers JG. Molecular diffusion in emulsions and emulsion mixtures. In: Binks BP, editor. modern aspects of emulsion science. Cambridge: The Royal Society of Chemistry Publication; 1998.
[2] Thompson W (Lord Kelvin). Phil Mag. 1871;42:448.
[3] Lifshitz EM, Slesov VV. Soviet Physics JETP. 1959;35:331.
[4] Wagner C. Z Electrochem. 1961;35:581.
[5] Kabalnov AS, Schukin ED. Adv Colloid Interface Sci. 1992;38:69.
[6] Kabalnov AS, Makarov KN, Pertsov AV, Shchukin ED. J Colloid Interface Sci. 1990;138:98.
[7] Taylor P. Colloids and Surfaces A. 1995;99:175.
[8] Ni Y, Pelura TJ, Sklenar TA, Kinner RA, Song D. Art Cells Blood Subs Immob Biorech. 1994;22:1307.
[9] Karaboni S, van Os NM, Esselink K, Hilbers PAJ. Langmuir. 1993;9:1175.
[10] Soma J, Papadadopoulos KD. J Colloid Interface Sci. 1996;181:225.
[11] Kabalanov AS. Langmuir. 1994;10:680.

[12] Taylor P, Ottewill RH. Colloids and Surfaces A. 1994;88:303.
[13] Anainsson EAG, Wall SN, Almagren M, Hoffmann H, Kielmann I, Ulbricht W, Zana R, Lang J, Tondre C. J Phys Chem. 1976;80:905.
[14] Weiss J, Coupland JN, Brathwaite D, McClemments DJ. Colloids and Surfaces A. 1997;121:53.
[15] Higuchi WI, Misra J. J Pharm Sci. 1962;51:459.
[16] Kabalnov AS, Pertsov AV, Shchukin ED. Colloids and Surfaces. 1987;24:19.
[17] Kabalnov AS, Pertsov AV, Aprosin YD, Shchukin ED. Kolloid Zh. 1995;47:1048.
[18] Walstra P. In: Binks BP, editor. Encyclopedia of emulsion technology, Vol. 4. New York: Marcel Dekker; 1996.
[19] Kabalnov AS, Weers JG, Arlauskas P, Tarara T. Langmuir. 1995;11:2966.
[20] Tadros TF. Advances Colloid and Interface Science. 1980;12:141.
[21] Tadros T. Applied surfactants. Weinheim: Wiley-VCH; 2005.
[22] Tadros T. Dispersion of powders in liquids and stabilisation of suspensions. Weinheim: Wiley-VCH; 2012.
[23] Tadros T. Suspensions. In: Tadros T, editor. Encyclopedia of colloid and interface science. Berlin: Springer; 2013.
[24] Tadros T. Nanodispersions. Berlin: De Gruyter; 2016.
[25] Gibbs JW. Scientific papers. London: Longman Green; 1906.
[26] Volmer M. Kinetic der Phasenbildung. Dresden: Stemkopf; 1939.
[27] Volmer M. Trans Faraday Soc. 1932;28:359.
[28] Kossel W. Nachr Ges Wiss Gottingen. 1937;123:348.
[29] Stranskii IN. Z Phys Chem. 1938;136:259.
[30] Stranskii IN, Kaishev R. Z Phys Chem. 1934;26B:100; 1934;26:317; 1934;36:393.
[31] Frank FC. Disc Faraday Soc. 1949;5:48, 67.
[32] Cabrera N, Burton W. Disc Faraday Soc. 1949;5:33, 40.
[33] Cabrera N, Vermilyea DA. Proceedings International Conference on Crystal Growth. London: John Wiley and Sons; 1958. p. 393.
[34] Pearson JT, Varney G. J Pharm Pharmac Suppl. 1969;21:60.
[35] Pearson JT, Varney G. J Pharm Pharmac Suppl. 1973;25:62.
[36] Pfeiffer PR. J Pharm Pharmac. 1971;23:75.
[37] Michaels AS, Golville A Jr. J Phys Chem. 1960;64:13.
[38] Michaels AS, Tausch FW Jr. J Phys Chem. 1961;65:1730.
[39] Michaels AS, Brian PLT, Bech WF. Chem Phys Appl Surface Active Substances. Proceedings 4th Int. Congress, 2. 1967, 1053.
[40] Simonelli PA, Mehta SC, Higuchi WI. J Pharm Sci. 1970;59:633.
[41] Carless JE, Moustafa MA, Rapson HDC. J Pharm Pharmac. 1968;20:630.

11 Emulsion coalescence and its prevention

11.1 Introduction

Many formulations consist of liquid/liquid dispersions (emulsions) which need to be stabilized against coalescence (a process where two or more droplets join each other). In order to understand the process of coalescence and its prevention, it is necessary to consider the surface forces involved in the thin liquid film between the emulsion droplets when these come into close contact. This represents the first section of this chapter. Two main approaches are considered, namely the concept of disjoining pressure which must remain positive in the film, and the interfacial tension across the liquid film. The next section considers the process of film rupture and the concept of critical film thickness below which rupture occurs. This is followed by an analysis of the rate of emulsion coalescence. The methods that can be applied for reducing coalescence are then described.

When two emulsion droplets come into close contact in a floc, a creamed layer or during Brownian diffusion, a thin liquid film or lamella forms between them [1]. This is illustrated in Fig. 11.1.

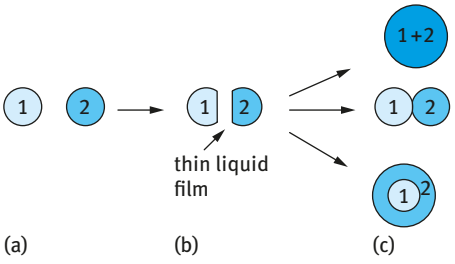

Fig. 11.1: Droplet coalescence, adhesion and engulfment.

Coalescence results from the rupture of this film as illustrated in Fig. 11.1 (c) at the top. If the film cannot be ruptured, adhesion (Fig. 11.1 (c), middle) or engulfment (Fig. 11.1 (c), bottom) may occur. Film rupture usually commences at a specified "spot" in the lamella, arising from thinning in that region. This is illustrated in Fig. 11.2 where the liquid surfaces undergo some fluctuations, forming surface waves. The surface waves may grow in amplitude and the apices may join as a result of the strong van der Waals attraction (at the apex, the film thickness is the smallest). The same applies if the film thins to a small value (critical thickness for coalescence). In order to understand the behaviour of these films, one has to consider two aspects of their physics:

https://doi.org/10.1515/9783110587944-012

(i) the nature of the forces acting across the film: these determine whether the film is thermodynamically stable, metastable or unstable;
(ii) the kinetic aspects associated with local (thermal or mechanical) fluctuations in film thickness.

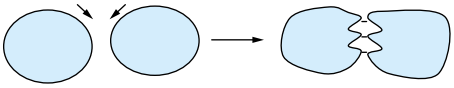

Fig. 11.2: Schematic representation of surface fluctuations.

11.2 Forces across liquid films

Fig. 11.3 shows the general features of the lamella between two droplets of phase α in a continuous phase β. The film consists of two flat parallel interfaces separated by a distance b. At the end of the film there is a border or transition region where the interfaces have a high curvature compared to the curvature of the droplets themselves.

Eventually at larger values of b (effectively beyond the range of forces operating across the film) the curvature decreases to that of the droplets themselves, i.e. becomes effectively flat, on the scale considered here, for droplets in the 1 µm region. One may define a macroscopic contact angle θ as shown in Fig. 11.3.

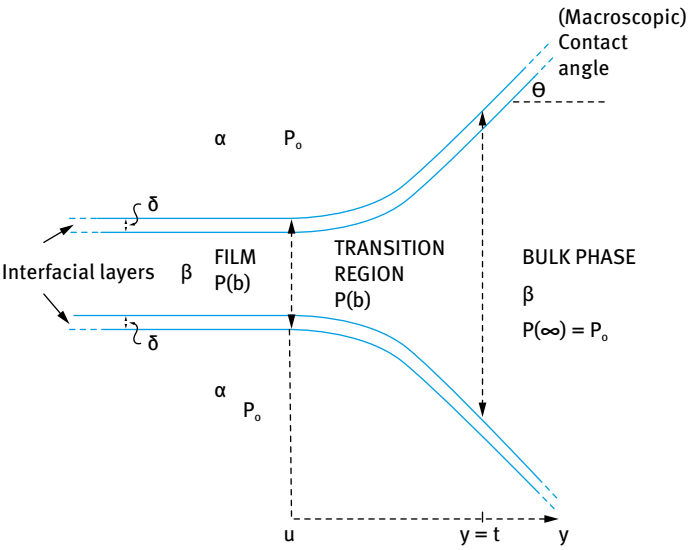

Fig. 11.3: Schematic representation of the thin film and border regions between two liquid droplets (α) in a continuous phase (β).

In considering the forces acting across the film, two regions of separation are of interest:

(i) $b > 2\delta$, where δ is the film thickness. The forces acting are long-range van der Waals forces and electrical double layer interactions as described by the DLVO (Deryaguin–Landau–Verwey–Overbeek) theory [2, 3], schematically shown in Fig. 11.4. This shows a secondary minimum, an energy maximum and a primary minimum. When the film is sitting in either the primary or secondary minimum, the net force on the film is zero (i.e. $dG/dh = 0$). These two metastable states correspond with the so-call Newton black films, respectively.

(ii) When the film is in the primary minimum and $b < 2\delta$, steric interactions come into play as discussed in Chapter 8. In this case G increases very sharply with decreasing b and for film rupture to occur these steric interactions must break down. Two main approaches were considered to analyse the stability of thin films in terms of the relevant interactions. The first approach was considered by Deryaguin [4] who introduced the concept of disjoining pressure. The second approach considered the interfacial tension of the film that could be related to the tangential pressure across the interface [5]. Both approaches are described below.

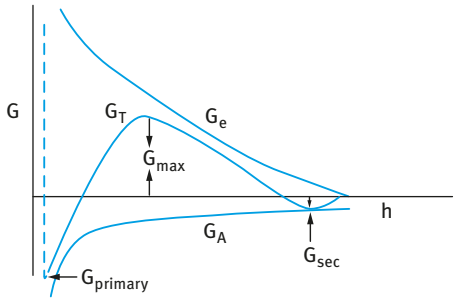

Fig. 11.4: Energy–distance curves according to the DLVO theory [2, 3].

11.2.1 Disjoining pressure approach

Deryaguin [4] suggested that a "disjoining pressure" $\pi(h)$ is produced in the film which balances the excess normal pressure,

$$\pi(b) = P(b) - P_0 \tag{11.1}$$

where $P(b)$ is the pressure of a film with thickness b and P_0 is the pressure of a sufficiently thick film such that the net interaction free energy is zero.

$\pi(b)$ may be equated to the net force (or energy) per unit area acting across the film,

$$\pi(b) = -\frac{dG_T}{db}, \tag{11.2}$$

where G_T is the total interaction energy in the film.

$\pi(b)$ is made up of three contributions due to electrostatic repulsion (π_E), steric repulsion (π_s) and van der Waals attraction (π_A),

$$\pi(b) = \pi_E + \pi_s + \pi_A. \tag{11.3}$$

To produce a stable film, $\pi_E + \pi_s > \pi_A$ and this is the driving force for the prevention of coalescence. It can be achieved by two mechanisms and their combination:

(i) increased repulsion, both electrostatic and steric;
(ii) dampening the fluctuation by enhancing the Gibbs elasticity. In general, smaller droplets are less susceptible to surface fluctuations and hence coalescence is reduced.

11.2.2 Interfacial tension of liquid films

The interfacial tension $\gamma(b)$ can be related to the variation in the tangential pressure tensor p_t across an interface. There will be a similar variation in P_t across the liquid film at some thickness b as shown schematically in Fig. 11.5.

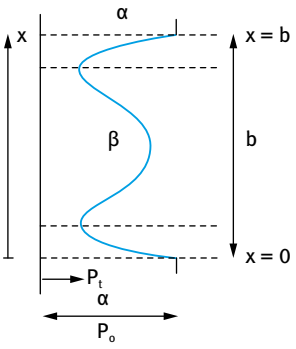

Fig. 11.5: The variation in tangential pressure P_t across a thin film.

One can define an interfacial tension for the whole film,

$$\gamma(b) = \int_0^b (P_t - P_0)\,dx. \tag{11.4}$$

By choosing some dividing plane in the middle of the film (conveniently at $x = b/2$, for a symmetrical film), one can divide $\gamma(b)$ into two contributions, one from the upper interface and one from the lower interface,

$$\gamma(b) = \gamma^{\alpha\beta}(b) + \gamma^{\beta\alpha}(b) = 2\gamma^{\alpha\beta}(b) \tag{11.5}$$

Note that $\gamma^{\alpha\beta}(b) \neq \gamma^{\alpha\beta}(\infty)$, the interfacial tension of an isolated $\alpha\beta$ interface, i.e. between the bulk liquids α or β, for an emulsion, in the region of the interface of the

droplet far away from the contact zone. $\gamma(b)$ is related to $G_i(b)$ and $\pi(b)$ through the relations,

$$\gamma(b) = \gamma(\infty) - G_i(b), \tag{11.6}$$

$$\gamma(b) = \gamma(\infty) + \int_{\infty}^{b} \pi(b)\, db. \tag{11.7}$$

Equation (11.7) is obtained by combining equations (11.6) and (11.2).

11.3 Film rupture

Film rupture is a non-equilibrium effect and is associated with local thermal or mechanical fluctuations in the film thickness b. A necessary condition for rupture to occur, i.e. for a spontaneous fluctuation to occur, is that

$$\frac{d\pi_A}{db} > \frac{d\pi_E}{db}. \tag{11.8}$$

However, this would assume that, at a given value of b, there are no changes in $\gamma(b)$ fluctuations. This is not so since a local fluctuation is necessarily accompanied by a local increase in the interfacial area, resulting in a decrease in surfactant or polymer adsorption in that region, and, therefore, a local rise in the interfacial tension. This effect (that is referred to as the Gibbs–Marangoni effect, see Chapter 2 of Vol. 2) opposes the fluctuation. Equation (11.8) has to be modified by including a term on the right-hand side to take into account the fluctuation effect in the local interfacial tension,

$$\frac{d\pi_A}{db} > \frac{d\pi_E}{db} + \frac{d\pi_\gamma}{db}. \tag{11.9}$$

As a film thins locally due to fluctuations, if the conditions of equation (11.9) are met at a critical thickness, b_{cr}, then the film becomes unstable and the fluctuation "grows" leading to rupture. Scheludko [5] introduce the concept of a critical thickness and he derived the following equation for the critical thickness,

$$b_{cr} = \left(\frac{A\pi}{32K^2\gamma_0}\right)^{1/4}, \tag{11.10}$$

where A is the net Hamaker constant of the film, K is the wave number of the fluctuation and $\gamma_0[=\gamma(\infty)]$ the interfacial tension of the isolated liquid/liquid interface. K depends on the radius of the (assumed) circular film zone.

Vrij [6] derived alternative expressions for b_{cr}. For large thicknesses, where $\pi_A \ll \pi_\gamma$,

$$b_{cr} = 0.268\left(\frac{A^2R^2}{\gamma_0\pi_\gamma f}\right). \tag{11.11}$$

For small thicknesses, where $\pi_\gamma \ll \pi_{\gamma A}$,

$$b_{cr} = 0.22\left(\frac{AR^2}{\gamma f}\right)^{1/4}, \tag{11.12}$$

where f is a factor that depends on b.

Scheludko's and Vrij's equations (11.10) and (11.12) have the same form at small thicknesses. Equation (11.12) predicts that when $\gamma \to 0$, the film should spontaneously rupture at large b values. This is certainly not observed since when $\gamma \to 0$ the emulsion becomes highly stable. Also equation (11.12) predicts that as $R \to 0$, $b_{cr} \to 0$, i.e. very small droplets should never rupture. Experiments on aqueous foam films suggest that one observes finite values for b_{cr} as $R \to 0$. Experiments on emulsion droplets showed no changes in b_{cr} with changing size of the contact area. This is because the lamella formed between two oil droplets, at non-equilibrium separations, do not have the idealized, planer interface depicted in Fig. 11.3. Rather they have a "dimple" structure as illustrated in Fig. 11.6. This "dimple" structure does not arise from fluctuations, but rather by an effect produced by the draining of the solution from the film region and associated with hydrodynamic effects. The thinnest region of the film occurs at the periphery of the contact zone, and rupture tends to occur here. With polymer-stabilized films, dimpling is far less marked due to the increased rigidity of the interface. The dimpling effect also accounts for the fact that the interfacial tension γ_0 seems to have little effect on film rupture in emulsion systems.

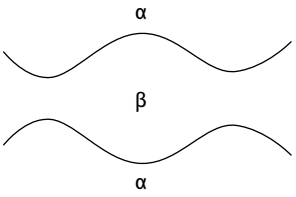

Fig. 11.6: Schematic representation of the "dimple" between two emulsion droplets.

11.4 Rate of coalescence between droplets

Van den Tempel [7] derived an expression for the coalescence rate of emulsion droplets by assuming the rate to be proportional to the number of contact points between the droplets in an aggregate. Both flocculation and coalescence are taken into account simultaneously. The average number of primary droplets n_a in an aggregate at time t is given by Smoluchowski theory (Chapter 9). The number of droplets n which have not yet combined into aggregates at time t is given by,

$$n = \frac{n_0}{(1 + kn_0t)^2}, \tag{11.13}$$

where n_0 is the initial number of droplets.

The number of aggregates n_v is given by,

$$n_v = \frac{kn_0^2 t}{(1 + kn_0 t)^2}. \tag{11.14}$$

The total number of primary droplets in all aggregates is given by,

$$n_0 - n_t = n_0\left[1 - \frac{1}{(1 + kn_0 t)^2}\right]. \tag{11.15}$$

Hence,

$$n_a = \frac{(n_0 - n_t)}{n_0} = 2 + an_0 t, \tag{11.16}$$

where a now denotes the rate of flocculation.

If m is the number of separate droplets existing in an aggregate, then $m < n_a$ as some coalescence will have occurred; m will be only slightly lower than n_a if coalescence is slow, whereas $m \to 1$ if coalescence is very rapid. The rate of coalescence is then proportional to $m - 1$, i.e. the number of contacts between droplets in an aggregate. In a small aggregate, van den Tempel [6] observed that, in sufficiently dilute emulsions, small aggregates generally contain one large droplet together with one or two small ones and are built up linearly. Thus n_v decreases in direct proportion to $m - 1$, whereas m increases at the same time by adhesion to other droplets. The rate of increase caused by flocculation is given (following equation (11.16)) by,

$$\frac{dm}{dt} = an_0 - K(m - 1), \tag{11.17}$$

where K is the rate of coalescence.

Integrating equation (11.17), for the boundary conditions $m = 2$ for $t = 0$,

$$m - 1 = \frac{an_0}{K} + \left(1 - \frac{an_0}{K}\right)\exp(-Kt). \tag{11.18}$$

The total number of droplets, whether flocculated or not, in a coagulating emulsion at time t is obtained by adding the number of unreacted primary droplets to the number of droplets in aggregates,

$$n = n_t + n_v m = \frac{n_v}{1 + kn_0 t} + \frac{kn_0^2 t}{(1 + kn_0 t)^2}\left[\frac{kn_0}{K} + \left(1 - \frac{kn_0}{K}\right)\exp(-Kt)\right]. \tag{11.19}$$

The first term on the right-hand side of equation (11.19) represents the number of droplets which would have been present if each droplet had been counted as a single droplet. The second term gives the number of droplets that arise when the composition of the aggregates is taken into account. In the limiting case $K \to \infty$, the second term on the right-hand side of equation (11.19) is equal to zero, and the equation reduces to the Smoluchowski equation (Chapter 9). On the other hand, if $K = 0$, i.e. no coalescence occurs, $n = n_0$ for all values of t. For the case $0 < K < \infty$, the effect of a change in the droplet number concentration on the rate of flocculation is given by equation (11.19).

This clearly shows that the change in droplet number concentration with time depends on the initial droplet number concentration n_0. This illustrates the difference between emulsions and suspensions. In suspensions, the rate of increase of $1/n$ with time is independent of the particle number concentration. Some calculations, using reasonable values for the rate of flocculation (denoted by a that is equivalent to k in equation (11.19)) and rate of coalescence K, are shown in Fig. 11.7 for various values of n_0.

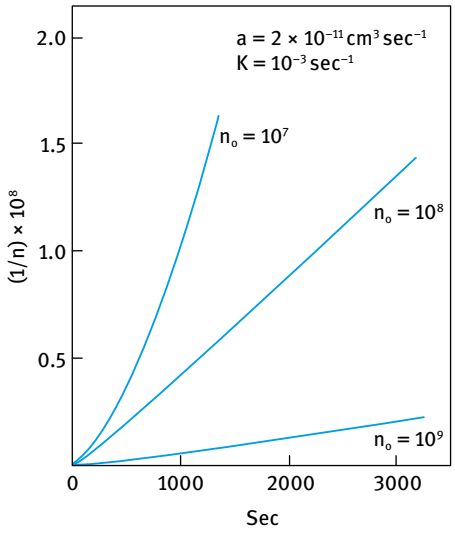

Fig. 11.7: Variation of $1/n$ with t at various n_0 values.

It is clear that the rate of increase of $1/n$ (or decrease in the droplet number concentration) with t rises more rapidly as n_0 decreases. Van den Tempel plotted $\Delta(1/n)$, i.e. the decrease in droplet number concentration after 5 minutes, versus the initial droplet number concentration n_0 for two values of K and k (or a). The results are shown in Fig. 11.8 which clearly shows the rate of flocculation, as measured by the value of $1/n$, does not change significantly with n_0, either for dilute or for concentrated emulsions. However, in the region where kn_0K is of the order of unity, the rate of flocculation decreases sharply with increasing n_0.

To simplify equation (11.19) van den Tempel made three approximations:

(i) In a flocculating concentrated emulsion $kn_0 \gg K$. In most real systems, K is generally much smaller than unity and $kn_0 \geq 1$ is sufficient to satisfy this condition. Thus kn_0 rapidly becomes larger than unity and the contribution from unreacted primary droplets may be neglected. In this case equation (11.19) reduces to,

$$n = \frac{kn_0^2 t}{(1 + kn_0 t)^2} \frac{kn_0}{K} [1 - \exp(-kt)]. \tag{11.20}$$

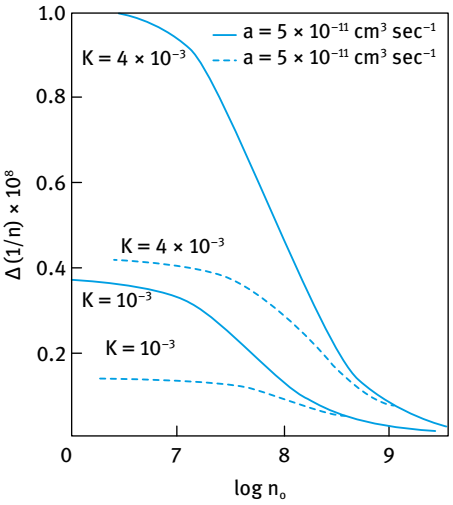

Fig. 11.8: Plot of $\Delta(1/n)$ versus log n_0 for two values of K and a (or k).

Since $kn_0t \gg 1$, then $1 + kn_0t \approx kn_0t$, so that,

$$n = \frac{n_0}{Kt}[1 - \exp(-kt)]. \tag{11.21}$$

This means that the rate of coalescence no longer depends on the rate of flocculation for concentrated emulsions. Van den Tempel calculated the change in droplet number concentration with time for concentrated ($n_0 > 10^{10}$ cm^{-3}) and dilute emulsion ($n_0 = 10^9$ cm^{-3}) and for values of $k = 5 \times 10^{-11}$ cm^3 s^{-1} and $K = 10^3$ s^{-1}; the results are shown in Fig. 11.9.

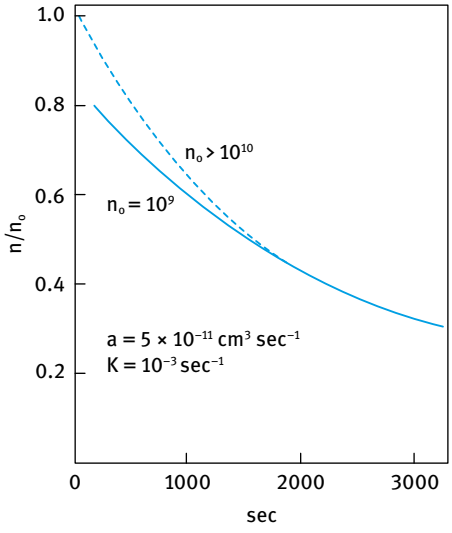

Fig. 11.9: Change in droplet number concentration with time for dilute and concentrated emulsions.

For concentrated emulsions equations (11.20)–(11.22) yield similar results, whereas for dilute emulsions, equation (11.22) gives rise to a serious deviation at values of t less than 1,000 seconds. Moreover, the droplet number concentration is found to decrease approximately exponentially with time, until Kt becomes large compared to unity. Another limitation for the application of equations (11.20)–(11.22) is the assumption made in their derivation, where the number of contact points between m droplets was taken to be $m - 1$. This is certainly not the case for concentrated emulsions, where the aggregates contain a large number of contacts. In a closely packed aggregate of spheres with the same size, each droplet touches 12 other droplets. The number of contact points will be proportional to m rather than $m - 1$. In a heterodisperse system, one droplet may even touch 12 other droplets. This can be taken into account by rewriting equation (11.17) as,

$$\frac{\mathrm{d}m}{\mathrm{d}t} = kn_0 - pKm, \tag{11.22}$$

where p has a value between 1 and 6. On integrating equation (11.22), one obtains,

$$m = \frac{kn_0}{pK} + \left(2 - \frac{kn_0}{pK}\right)\exp(-pKt) \tag{11.23}$$

which replaces equation (11.18) for concentrated emulsions.

This means that for concentrated emulsions the rate of coalescence increases with droplet concentration in a manner dependent on the droplet size distribution, the degree of packing, and on the size of aggregates.

(ii) In a very dilute emulsion, kn_0/K can be much smaller than unity if coalescence occurs very rapidly. After flocculation has proceeded for sufficient time, such that $Kt \gg 1$, the second term on the right-hand side of equation (11.19) may be neglected relative to the first term. This equation reduces to Smoluchowski's equation, i.e. the rate of flocculation is independent of any coalescence.

(iii) If the degree of coalescence is very small, the exponential term in equation (11.19) may be expanded in a power series, retaining the first two terms only when $K \ll 1$, such that the equation reduces to,

$$n = n_0\left[1 - \frac{Kt}{(1 + kn_0t)} + \frac{Kt}{(1 + kn_0t)^2}\right]. \tag{11.24}$$

Equation (11.24) predicts only a very small decrease in droplet number concentration with time, as expected.

(iv) When flocculation has proceeded for a sufficiently long time, Kt may be much greater than unity. In this case the exponential term may be neglected and then $kn_0/t \gg 1$ (in the denominator), then,

$$n = \frac{n_0}{Kt} + \frac{1}{kt}. \tag{11.25}$$

With large n_0, the first term on the right-hand side of equation (11.25) predominates, and hence, $1/kt$ can be neglected.

Davies and Rideal [8] discussed the problem of coalescence, incorporating an energy barrier term into the Smoluchowski equation, in order to account for the slow coalescence in emulsions stabilized by sodium oleate. The Smoluchowski equation may be written in terms of the mean volume V of emulsion droplets,

$$V = \frac{\phi}{n_0} + 4\pi DR\phi t, \tag{11.26}$$

where ϕ is the volume fraction of the dispersed phase, D is the diffusion coefficient of the droplets and R is the collision radius. D can be calculated using the Stokes–Einstein equation,

$$D = \frac{kT}{6\pi\eta R}. \tag{11.27}$$

k is the Boltzmann constant, T is the absolute temperature, η is the viscosity of the medium and R is the droplet radius.

Equation (11.26) predicts that the mean volume of the droplets should be doubled in about 43 seconds, whereas experiments show that in the presence of sodium oleate, this takes about 50 days. To account for this an energy barrier (ΔG_{coal}) was introduced in equation (11.26),

$$V = V_0 + 4\pi DR\phi t \exp\left(-\frac{\Delta G_{\text{coal}}}{kT}\right). \tag{11.28}$$

Substituting for D from equation (11.27) and differentiating with respect to t, the rate of coalescence for an O/W emulsion is given by,

$$\frac{\mathrm{d}V}{\mathrm{d}t} = \frac{4\phi kT}{3\eta_{\text{w}}} \exp\left(-\frac{\Delta G_{\text{coal}}}{kT}\right) = C_1 \exp\left(-\frac{\Delta G_{\text{coal}}}{kT}\right), \tag{11.29}$$

where η_{w} is the viscosity of the continuous phase (water for O/W emulsion) and C_1 is the collision factor defined by equation (11.29).

For a W/O emulsion, the corresponding relation would be,

$$\frac{\mathrm{d}V}{\mathrm{d}t} = \frac{4(1-\phi)kT}{3\eta_0} \exp\left(-\frac{\Delta G_{\text{coal}}}{kT}\right) = C_2 \exp\left(-\frac{\Delta G_{\text{coal}}}{kT}\right), \tag{11.30}$$

where η_0 is the viscosity of the oil continuous phase and C_2 is the corresponding collision factor.

Davies and Rideal considered the energy barrier in terms of the electrical potential ψ_0 at the surface of the oil droplets, arising from drops stabilized by ionic surfactants. The energy barrier preventing coalescence is proportional to ψ_0^2 according to DLVO theory [2, 3] as described above,

$$\Delta G_{\text{coal}} = B\psi_0^2, \tag{11.31}$$

where B is a constant that depends on the radius of curvature of the droplets. When two approaching droplets tend to flatten in the region of contact in a lamella, the radius of curvature to be used for emulsion droplets may be considerably different

from the actual droplet radius. However, the degree of flattening is negligible for small emulsion droplets (< 1 μm in diameter). If there is specific adsorption of counterions, the electric potential to be used in evaluating the electrical double repulsion will be less than ψ_0. In this case one has to use the Stern potential ψ_d at the plane of specifically adsorbed ions (Chapter 3), i.e.,

$$\Delta G_{coal} = B\psi_d^2. \tag{11.32}$$

11.5 Reduction of coalescence

11.5.1 Use of mixed surfactant films

It has long been known that mixed surfactants can have a synergistic effect on emulsion stability, with respect to coalescence rates. For example, Schulman and Cockbain [9] found that the stability of Nujol/water emulsions increases markedly on addition of cetyl alcohol or cholesterol to an emulsion prepared using sodium cetyl sulphate. The enhanced stability was assumed to be associated with the formation of a densely packed interfacial layer. The maximum effect is obtained when using a water-soluble surfactant (cetyl sulphate) and an oil-soluble surfactant (cetyl alcohol), sometimes referred to as cosurfactant, in combination. Suitable combinations lead to enhanced stability as compared to the individual components. These mixed surfactant films also produce a low interfacial tension, in the region of 0.1 mN m^{-1} or lower. This reduction in interfacial tension may be due to the cooperative adsorption of the two surfactant molecules, as predicted by the Gibbs adsorption equation for multicomponent systems.

For a multicomponent system i, each with an adsorption Γ_i (mol m^{-2}, referred to as the surface excess), the reduction in γ, i.e. dγ, is given by the following expression,

$$d\gamma = -\sum \Gamma_i \, d\mu_i = -\sum \Gamma_i RT \, d\ln C_i, \tag{11.33}$$

where μ_i is the chemical potential of component i, R is the gas constant, T is the absolute temperature and C_i is the concentration (mol dm^{-3}) of each surfactant component.

The reason for the lowering of γ when using two surfactant molecules can be understood by considering the Gibbs adsorption equation for multicomponent systems [9]. For two components sa (surfactant) and co (cosurfactant), equation (11.33) becomes,

$$d\gamma = -\Gamma_{sa} RT \, d\ln C_{sa} - \Gamma_{co} RT \, d\ln C_{co}. \tag{11.34}$$

Integration of equation (11.34) gives,

$$\gamma = \gamma_0 - \int_0^{C_{sa}} \Gamma_{sa} RT \, d\ln C_{sa} - \int_0^{C_{co}} \Gamma_{co} RT \, d\ln C_{co} \tag{11.35}$$

which clearly shows that γ_0 is lowered by two terms, one from the surfactant and one from the cosurfactant.

The two surfactant molecules should adsorb simultaneously and they should not interact with each other, otherwise they lower their respective activities. Thus, the surfactant and cosurfactant molecules should vary in nature, one predominantly water soluble (such as an anionic surfactant) and one predominantly oil soluble (such as a long chain alcohol).

Several mechanisms have been suggested to account for the enhanced stability produced by using mixed surfactant films and these are summarized below.

11.5.1.1 Interfacial tension and Gibbs elasticity

The synergistic effect of surfactant mixtures can be accounted for by the enhanced lowering of interfacial tension of the mixture when compared with individual components. For example, addition of cetyl alcohol to an O/W emulsion stabilized by cetyl trimethyl ammonium bromide results in lowering of the interfacial tension, and a shift of the critical micelle concentration (cmc) to lower values, probably due to the increased packing of the molecules at the O/W interface [1]. Another effect of using surfactant mixtures is due to the enhanced Gibbs dilational elasticity, ε,

$$\varepsilon = \frac{\mathrm{d}\gamma}{\mathrm{d}\ln A}, \tag{11.36}$$

where $\mathrm{d}\gamma$ is the change in interfacial tension resulting from the increase in the interfacial area $\mathrm{d}A$ on expanding the interface.

Prins and van den Tempel [9] showed that the surfactant mixture sodium laurate plus lauric acid gives a very high Gibbs elasticity (of the order of $10^3\,\mathrm{mN\,m^{-1}}$) when compared with that of sodium laurate alone. In the presence of laurate ions, lauric acid has an extremely high surface activity. At half coverage, the interface contains $1.3\,\mathrm{mol\,dm^{-3}}$ laurate ions and $4.8 \times 10^{-7}\,\mathrm{mol\,dm^{-3}}$ lauric acid. Thus, under these conditions, the minor constituent can contribute more to the Gibbs elasticity than the major constituent. Similar results were obtained by Prins et al. [10] who showed that ε increases markedly in the presence of lauryl alcohol for O/W emulsions stabilized by sodium lauryl sulphate. A correlation between film elasticity and coalescence rate has been observed for O/W emulsions stabilized with proteins [11].

11.5.1.2 Interfacial viscosity

It has long been assumed that a high interfacial viscosity could account for the stability of liquid films. This must play a role under dynamic conditions, i.e. when two droplets approach each other. Under static conditions, the interfacial viscosity does not play a direct role. However, a high interfacial viscosity is often accompanied by a high interfacial elasticity and this may be an indirect contribution to the increased

stability of the emulsion. Prins and van den Tempel [9] argued against there being any role played by the interfacial viscosity due to two main observations, namely the small changes in film stability with change in temperature (which should have a significant effect on the interfacial viscosity) and the sudden decrease of the interfacial viscosity with a slight increase in the concentration of the major component. Thus, Prins and van den Tempel [8] attributed the enhanced emulsion stability resulting from the presence of a minor component to be solely due to an increase in interfacial elasticity.

11.5.1.3 Hindrance to diffusion

Another possible explanation of the enhanced stability in the presence of mixed surfactants could be connected to the hindered diffusion of the surfactant molecules in the condensed film. This would imply that the desorption of surfactant molecules is hindered on the approach of two emulsion droplets, and hence thinning of the film is prevented.

11.5.1.4 Liquid crystalline phase formation

Friberg and coworkers [12] attributed the enhanced stability of emulsions formed with mixtures of surfactants to the formation of three-dimensional structures, namely, liquid crystals. These structures can form, for example, in a three-component system of surfactant, alcohol and water, as illustrated in Fig. 11.10. The lamellar liquid crystalline phase, denoted by N (neat phase), in the phase diagram is particularly important for stabilizing the emulsion against coalescence. In this case the liquid crystals "wrap" around the droplets in several layers as will be illustrated below. These multilayers form a barrier against coalescence as will be discussed below. Friberg et al. [12] have given an explanation in terms of the reduced attractive potential energy between two emulsion droplets, each surrounded by a layer of liquid crystalline phase. They have also considered changes in the hydrodynamic interactions in the interdroplet region; this affects the aggregation kinetics.

Friberg et al. [12] have calculated the effect on the van der Waals attraction of the presence of a liquid crystalline phase surrounding the droplets. A schematic representation of the flocculation and coalescence of droplets with and without a liquid crystalline layer is shown in Fig. 11.11.

The upper part of Fig. 11.11 (A to F) represents the flocculation process when the emulsifier is adsorbed as a monomolecular layer. The distance d between the water droplets decreases to a distance m at which the film ruptures and the droplets coalesce; m is chosen to correspond to the thickness of the hydrophilic layers in the liquid crystalline phase. This simplifies the calculations and facilitates comparison with the case in which the liquid crystalline layer is adsorbed around the droplets.

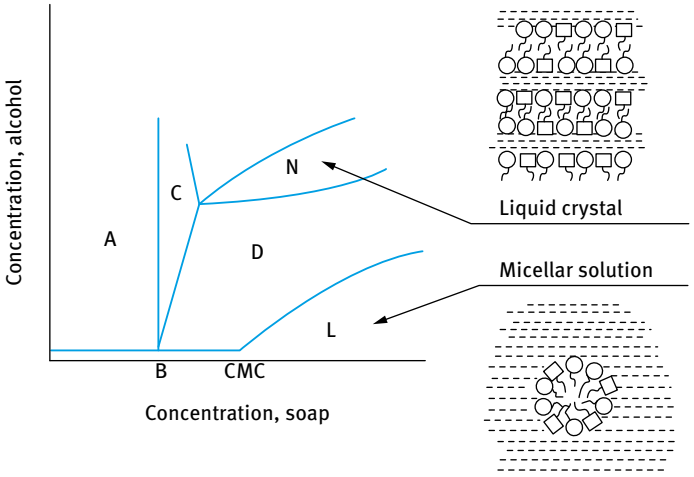

Fig. 11.10: Phase diagram of surfactant–alcohol–water system.

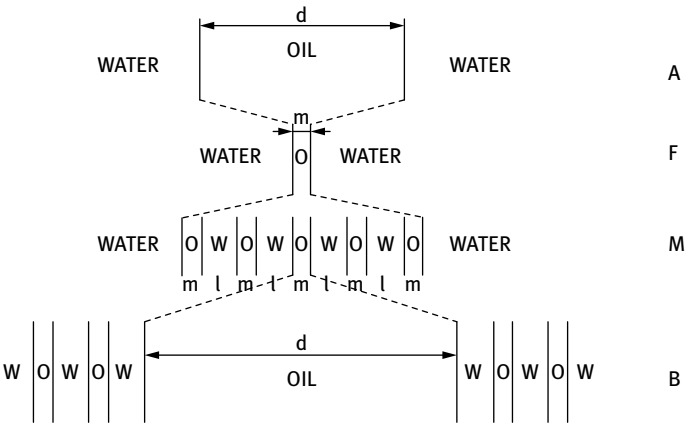

Fig. 11.11: Schematic representation of flocculation and coalescence in the presence and absence of liquid crystalline phases.

The flocculation process for the case of droplets covered with liquid crystalline layers is illustrated in the lower part of Fig. 11.11 (B to M). The oil layer between the droplets thins to thickness m. The coalescence process which follows involves the removal of successive layers between the droplets until a thickness of one layer is reached (F); the final coalescence step occurs in a similar manner to the case for a monomolecular layer of adsorbed surfactant.

For case A, the van der Waals attraction is given by the expression,

$$G_{\mathrm{A}} = -\frac{A}{12\pi d^2}, \tag{11.37}$$

where A is the effective Hamaker constant,

$$A = (A_{11}^{1/2} - A_{22}^{1/2})^2, \tag{11.38}$$

where A_{11} and A_{22} are the Hamaker constants of the two phases.

For case B, G_B can be obtained from the algebraic summation of this expression for the aqueous layer on each side of the central layer. The ratio G_B/G_A is then given by,

$$\frac{G_B}{G_A} = d^2 \left\{ \sum_{p=0}^{n} \sum_{q=0}^{n} [d + (p+q)(l+m)]^{-2} + \sum_{p=0}^{n-1} \sum_{q=0}^{n-1} [d + 2l + (p+q)(l+m)]^{-2} - \sum_{p=0}^{n} \sum_{q=0}^{n-1} [2(d+l) + (p+q)(l+m)]^{-2} \right\} \tag{11.39}$$

where l and m are the thicknesses of the water and oil layers, n is the number of water layers (which is equal to the number of oil layers), and p and q are integers.

The free energy change associated with coalescence (i.e. M → F) is calculated from the variation of the van der Waals interaction across the droplet walls. This treatment reflects the energy change associated with the layers squeezed out from the interdroplet region. The problem is circumvented by assuming that these displaced layers adhere to the enlarged droplets so that their free energy is not significantly changed in the process. In this manner, the ratio of the interaction energies in the states F and M is obtained from summation of the van der Waals interactions from the individual layers on the water parts, i.e.,

$$\frac{G_M}{G_F} = m^2 \left\{ \sum_{p=0}^{n} [(m+p)(m+l)]^{-2} - \sum_{p=0}^{n} [(p+l)(m+l)]^{-2} \right\} \tag{11.40}$$

To illustrate the relative importance of the van de Waals attraction energy, calculations were made using the above expressions, for the case of flocculation (i.e. A and B) and for the case of coalescence (i.e. F and M). The results are given in Fig. 11.12 (a) and (b), respectively.

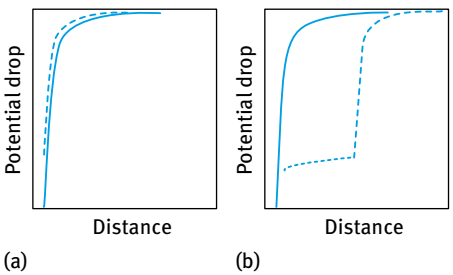

Fig. 11.12: Van der Waals potential energy–distance curves for flocculation (a) and coalescence (b) in the presence (---) and absence (—) of liquid crystalline phases.

Fig. 11.12 (a) shows that the influence of liquid crystalline layers around the droplets on the flocculation process is insignificant. In contrast, the effect on the free energy change is quite significant. For example, with nine layers on each droplet and a layer thickness of reasonable magnitude ($l = m = 5$ nm), the total van der Waals interaction is reduced to only 10 % of its original value for the coalescence process in the case of the layer structure. This is to be compared with 98 % in the case of two droplets at the same distance, but separated by the oil phase instead of the liquid crystalline phase. Even more important are the extremely small changes in attraction energy after removal of the first layers. The first layers give a drop corresponding to 1.5 % of the total van der Waals interaction energy (A to F). The last layer, before the state F is reached, corresponds to 78 % of the total van der Waals energy. It seems, therefore, that the presence of a liquid crystalline phase has a pronounced influence on the distance dependency of the van der Waals energy, leading to a drastic reduction in the force of attraction between the emulsion droplets.

11.5.1.5 Use of polymeric surfactants

The most convenient polymeric surfactants are those of the block and graft copolymer type. A block copolymer is a linear arrangement of blocks of variable monomer composition. The nomenclature for a diblock is poly-A-block–poly-B and for a triblock is poly-A-block–poly-B–poly-A. One of the most widely used triblock polymeric surfactants are the "Pluronics" (BASF, Germany) which consists of two poly-A blocks of poly(ethylene oxide) (PEO) and one block of poly(propylene oxide) (PPO). Several chain lengths of PEO and PPO are available.

The above polymeric triblocks can be applied as emulsifiers, whereby the assumption is made that the hydrophobic PPO chain resides at the hydrophobic surface, leaving the two PEO chains dangling in aqueous solution and hence providing steric repulsion, and this reduces or eliminates the coalescence of emulsions.

A-graft copolymers based on polysaccharides such as insulin, a linear polyfructose chain with a glucose end, have been developed for stabilizing emulsions [13]. This molecule is used to prepare a series of graft copolymers by random grafting of alkyl chains (using alkyl isocyanate) on the inulin backbone. The first molecule of this series is INUTEC® SP1 that is obtained by random grafting of C_{12} alkyl chains. It has an average molecular weight of ≈ 5,000 Daltons. The molecule is schematically illustrated in Fig. 11.13 which shows the hydrophilic polyfructose chain (backbone) and the randomly attached alkyl chains.

The main advantages of INUTEC® SP1 as a stabilizer for emulsions are:

(i) Strong adsorption to the droplet by multipoint attachment with several alkyl chains. This ensures the lack of desorption and displacement of the molecule from the interface.

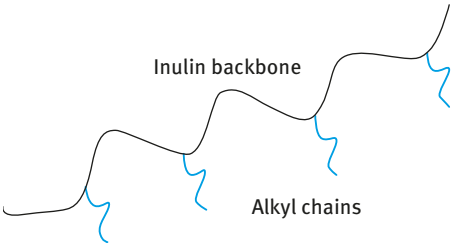

Fig. 11.13: Schematic representation of INUTEC® SP1 polymeric surfactant.

(ii) Strong hydration of the linear polyfructose chains both in water and in the presence of high electrolyte concentrations and high temperatures. This ensures effective steric stabilization.

Emulsions of Isopar M/water and cyclomethicone/water were prepared using INUTEC® SP1. 50/50 (v/v) O/W emulsions were prepared and the emulsifier concentration was varied from 0.25 to 2 (w/v) % based on the oil phase. 0.5 (w/v) % emulsifier was sufficient for the stabilization of these 50/50 (v/v) emulsions [13]. The emulsions were stored at room temperature and 50 °C and optical micrographs were taken at intervals of time (for a year) in order to check the stability. Emulsions prepared in water were very stable, showing no change in droplet size distribution over more than a one year period and this indicated absence of coalescence. Any weak flocculation that occurred was reversible and the emulsion could be redispersed by gentle shaking. Fig. 11.14 shows an optical micrograph for a dilute 50/50 (v/v) emulsion that was stored for 1.5 and 14 weeks at 50 °C. No change in droplet size was observed after storage for more than 1 year at 50 °C, indicating absence of coalescence. The same result was obtained when using different oils. Emulsions were also stable against coalescence in the presence of high electrolyte concentrations (up to 4 mol dm^{-3} or ≈ 25 % NaCl). This stability in high electrolyte concentrations is not observed with polymeric surfactants

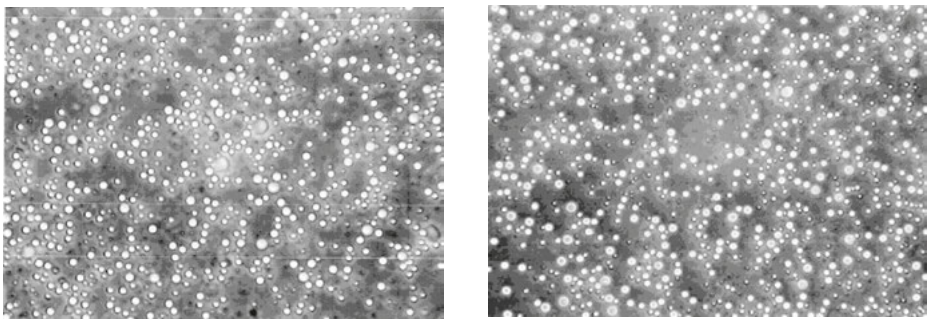

(a) (b)

Fig. 11.14: Optical micrographs of O/W emulsions stabilized with INUTEC® SP1 stored at 50 °C for 1.5 weeks (a) and 14 weeks (b).

based on polyethylene oxide. The high stability observed using INUTEC® SP1 is related to its strong hydration both in water and in electrolyte solutions. The hydration of inulin (the backbone of HMI) could be assessed using cloud point measurements. A comparison was also made with PEO with two molecular weights, namely 4,000 and 20,000.

Evidence for the high stability of the liquid film between emulsion droplets when using INUTEC® SP1 was obtained by Exerowa et al. [14] using disjoining pressure measurements. This is illustrated in Fig. 11.15 which shows a plot of disjoining pressure versus separation distance between two emulsion droplets at various electrolyte concentrations. The results show that by increasing the capillary pressure a stable Newton black film (NBF) is obtained at a film thickness of ≈ 7 nm. The lack of rupture of the film at the highest pressure applied of 4.5×10^4 Pa indicates the high stability of the film in water and in high electrolyte concentrations (up to 2.0 mol dm^{-3} NaCl).

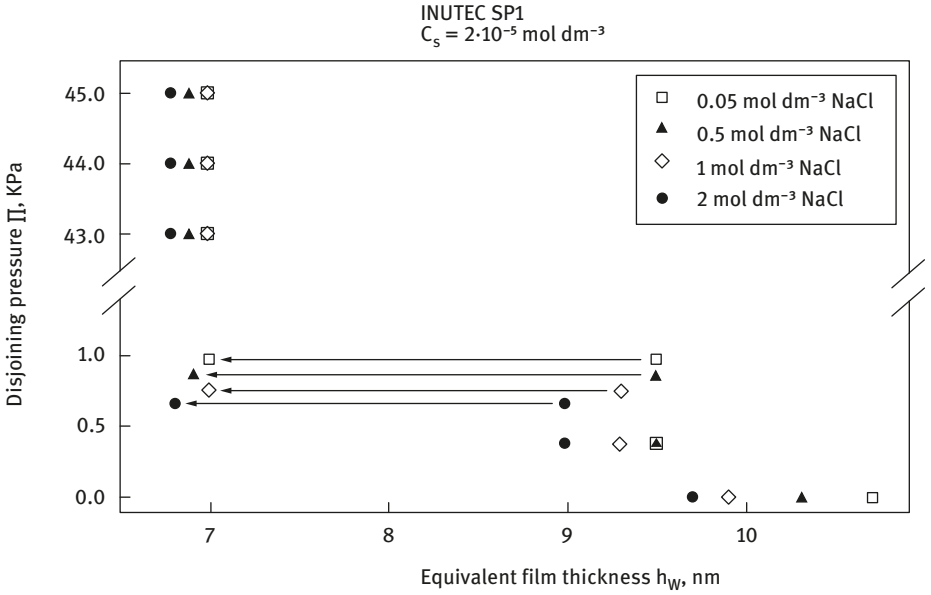

Fig. 11.15: Variation of disjoining pressure with equivalent film thickness at various NaCl concentrations.

The lack of rupture of the NBF up to the highest pressure applied, namely 4.5×10^4 Pa, clearly indicates the high stability of the liquid film in the presence of high NaCl concentrations (up to 2 mol dm^{-3}). This result is consistent with the high emulsion stability obtained at high electrolyte concentrations and high temperature. Emulsions of Isopar M-in-water are very stable under such conditions and this could be accounted for by the high stability of the NBF. The droplet size of 50 : 50 O/W emulsion using 2 %

INUTEC® SP1 is in the region of 1–10 µm. This corresponds to a capillary pressure of $\approx 3 \times 10^4$ Pa for the 1 µm drops and $\approx 3 \times 10^3$ Pa for the 10 µm drops. These capillary pressures are lower than those to which the NBF have been subjected and this clearly indicates the high stability obtained against coalescence in these emulsions.

References

[1] Tadros T. Emulsions. Berlin: De Gruyter; 2016.
[2] Deryaguin BV, Landau L. Acta Physicochem USSR. 1941;14:633.
[3] Verwey EJW, Overbeek JTG. Theory of stability of lyophobic colloids. Amsterdam: Elsevier; 1948.
[4] Deryaguin BV, Scherbaker RL. Kolloid Zh. 1961;23:33.
[5] Scheludko A. Advances Colloid Interface Sci. 1967;1:391.
[6] Vrij A. Disc Faraday Soc. 1966;42:23.
[7] van den Tempel M. REc Trav Chim. 1953;72:433, 442.
[8] Schulman JH, Cockbain EG. Transaction Faraday Soc. 1940;36:661.
[9] Prins A, van den Tempel M. Proc Int Congr Surface Activity (4th), Vol. II. London: Gordon and Breach; 1967. p. 1119.
[10] Prins A, Arcuri C, van den Tempel M. J Colloid and Interface Sci. 1967;24:811.
[11] Biswas B, Haydon DA. Proc Roy Soc. 1963;A271:296; 1963;A2:317.
[12] Friberg S, Jansson PO, Cederberg E. J Colloid Interface Sci. 1976;55:614.
[13] Tadros TF, Vandamme A, Levecke B, Booten K, Stevens CV. Advances Colloid Interface Sci. 2004;108–109:207.
[14] Exerowa D, Gotchev G, Kolarev T, Khristov K, Levecke B, Tadros T. Langmuir. 2007;23:1711.

12 Phase inversion and its prevention

12.1 Introduction

Phase inversion is the process in which the internal and external phase of an emulsion suddenly invert, e.g. O/W to W/O or vice versa [1, 2]. This process may occur with some formulations on storage, particularly when the conditions are changed, e.g. on increase of temperature. Phase inversion is of two types:

(i) Catastrophic inversion that is induced by increasing the volume fraction of the disperse phase. For example, when increasing the oil volume fraction for an oil/water emulsion, inversion to a water/oil emulsion may occur when the oil volume fraction of the oil phase is increased above a critical value, mostly above the maximum packing fraction of the oil phase. This type of inversion is not reversible [2]; the value of the water: oil ratio at the transition when oil is added to water is not the same as that when water is added to oil. The inversion point depends on the intensity of agitation and the rate of liquid addition to the emulsion.

(ii) Transitional phase inversion induced by changing factors which affect the HLB of the system, e.g. temperature and/or electrolyte concentration. The average droplet size decreases and the emulsification rate (defined as the time required to achieve a stable droplet size) increases as inversion is approached. Both trends are consistent with O/W interfacial tension reaching a minimum near the inversion point.

12.2 Catastrophic inversion

Catastrophic inversion is illustrated in Fig. 12.1 which shows the variation of viscosity and conductivity with the oil volume fraction ϕ. As can be seen, inversion occurs at a critical ϕ, which may be identified with the maximum packing fraction [1]. At ϕ_{cr}, η suddenly decreases; the inverted W/O emulsion has a much lower volume fraction. κ also decreases sharply at the inversion point since the continuous phase is now oil. Similar trends are observed if water is added to a W/O emulsion, but in this case the conductivity of the emulsion increases sharply at the inversion point. For example, if one starts with a W/O emulsion, then, on increasing the volume fraction of the water phase (the disperse phase), the viscosity of the emulsion increases gradually until a maximum value is obtained, generally ≈ 0.74. When the inversion takes place to an O/W emulsion, the volume fraction of the disperse phase (the oil) will now be ≈ 0.26; hence the dramatic decrease in viscosity.

https://doi.org/10.1515/9783110587944-013

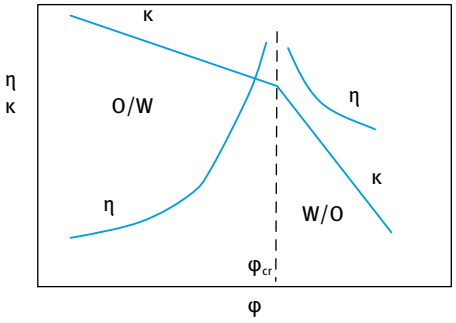

Fig. 12.1: Variation of conductivity and viscosity with volume fraction of oil.

In the early theories of phase inversion, it was postulated that the inversion takes place as a result of the difficulty in packing the emulsion droplets above a certain volume fraction. For example, according to Ostwald [3] an assembly of spheres of equal radii should occupy 74 % of the total volume. Thus, at phase volume $\phi > 0.74$, the emulsion droplets have to be packed more densely than is possible.

This means that any attempt to increase the phase volume beyond that point should result in distortion, breaking or inversion. However, several investigations showed the invalidity of this argument; inversion being found to take place at phase volumes much greater or smaller than this critical value. For example, Shinoda and Saito [4] showed that inversion of olive oil/water emulsions takes place at $\phi = 0.25$. Moreover, Sherman [5] showed that the volume fraction at which inversion takes place depends to a large extent on the nature of the emulsifier. It should be mentioned that Ostwald's theory [3] applies only to the packing of rigid, non-deformable spheres of equal size. Emulsion droplets are nether resistant to deformation, nor are they, in general, of equal size. The wide distribution of droplet size makes it possible to achieve a higher internal phase volume fraction by virtue of the fact that the smaller droplets can be fitted into the interstices between the larger ones. If one adds to this the possibility that the droplets may be deformed into polyhedra, even denser packing is possible. This is the principle of preparing high internal phase emulsions (HIPE) reaching $\phi > 0.95$.

A useful index to characterize phase inversion is to measure the emulsion inversion point (EIP). The EIP is related to the inversion of W/O emulsions to O/W emulsions at constant temperature [6]. An aqueous phase is added (incrementally) to a finite amount of oil which contains a known amount of surfactant. The mixture is agitated by a turbine blender for 15 s on each addition and the emulsion type is determined. The EIP is simply the ratio of the volume of the aqueous phase at the inversion point to the volume of the oil phase. A plot of EIP versus HLB is made and the results show that the EIP decreases with increasing HLB number until a minimum is observed. The value of the HLB at the minimum is the required HLB of the oil to produce a stable emulsion. However, the exact position of the EIP minimum can be affected by the agitation conditions.

The findings from EIP experiments include:

(i) At the EIP minimum, the inversion from W/O to O/W occurs and produces emulsions with very small drops.
(ii) The EIP increases with increasing lipophilic surfactant, whereas the EIP decreases with increasing concentration of hydrophilic surfactant.
(iii) In a series of alkanes, the higher the EIP the lower the required HLB.
(iv) Highest viscosity and lowest interfacial tension occur at the EIP.
(v) For aromatic hydrocarbons, with increasing methyl group substitutions the EIP and the required HLB decrease.
(vi) The EIP shows changes in the required HLB of an oil brought about by addition of additives, e.g. alcohols and poly(ethylene glycol).

When catastrophic inversion is brought about by addition of the aqueous phase to the oil phase (high HLB), two drop types can be present before phase inversion: Unstable water drops containing surfactant micelles, in a continuous oil phase (i.e. W_m/O) and stable oil drops within water drops, in a continuous oil phase (i.e. $O/W_m/O$). When catastrophic inversion is brought about by adding the oil phase to the water phase (low HLB), two drop types can be present before phase inversion: unstable oil drops containing surfactant micelles in a continuous aqueous phase (i.e. O_m/W); and stable water drops within oil drops in a continuous aqueous phase (i.e. $W/O_m/W$).

After catastrophic inversion has taken place the resulting emulsion consists of stable oil drops in a continuous water phase containing surfactant micelles (i.e. O/W_m) when the initial continuous phase is oil. When the initial continuous phase is aqueous, the resulting emulsion consists of stable water drops in a continuous oil phase containing surfactant micelles (i.e. W/O_m).

Ostwald [3] first modelled catastrophic inversions as being caused by the complete coalescence of the dispersed phase at the close packed condition, whereas Marzall [7] has shown that catastrophic inversion can occur over a wide range of water: oil ratios. This may be due to the formation of double emulsion drops ($O/W_m/O$) boosting the actual volume of the dispersed phase.

The dynamic factors affecting catastrophic inversion have been concerned with the movement of inversion boundaries with either changes in the system composition, or changes in the system's dynamics such as the effect of agitation conditions. For systems that do not contain stabilizing surfactant, inversion hysteresis has been shown to occur. As the viscosity of the oil phase increases, the more likely it is that the oil becomes the dispersed phase. Inversion is shifted to a higher dispersed phase fraction as the stirrer speed increases.

12.3 Transitional inversion

Transitional inversion is caused by changes in the system HLB at constant temperature using surfactant mixtures. This is illustrated in Fig. 12.2 which shows the change in the droplet Sauter diameter, d_{32} (volume/area mean diameter) and rate constant (min^{-1}) as a function of the HLB of (nonionic) surfactant mixtures [2].

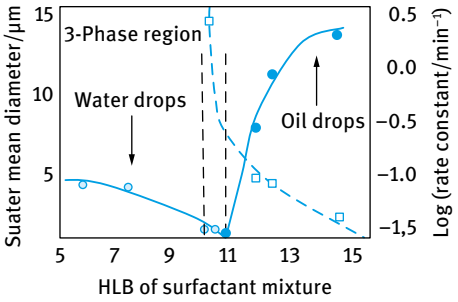

Fig. 12.2: Emulsion drop diameters (circles) and rate constant for attending steady size (squares) as a function of surfactant HLB in cyclohexane/0.067 mol dm^{-3} KCl containing nonylphenol ethoxylates at 25 °C.

It can be seen from Fig. 12.2 that the average droplet diameter decreases and the emulsification rate (defined as the time required to achieve a stable droplet size) increases as inversion is approached. The results are consistent with the oil/water interfacial tension passing through a minimum within the HLB range where the three-phase region forms. It was also noted that emulsions formed by transitional inversion are finer and they require less energy than those made by direct emulsification. Several other conditions can cause transitional phase inversion, such as addition of electrolyte and/or increase of temperature, in particular for emulsions based on nonionic surfactants of the ethoxylate.

In order to understand the process of phase inversion, one must consider the surfactant's affinity to the oil and water phases, as described by the Winsor R_0 ratio [8], which is the ratio of the intermolecular attraction of oil molecules (O) and lipophilic portion of surfactant (L), C_{LO}, to that of water (W) and hydrophilic portion (H), C_{HW},

$$R_0 = \frac{C_{LO}}{C_{HW}}. \tag{12.1}$$

Several interaction parameters may be identified at the oil and water sides of the interface. One can identify at least nine interaction parameters as schematically represented in Fig. 12.3. C_{LL}, C_{OO} and C_{LO} refer to the interaction energies between the two lipophilic parts of the surfactant molecule, the interaction energy between two oil molecules and the interaction energy between the lipophilic chain and oil respectively. C_{HH}, C_{WW} and C_{HW} refer to the interaction energies between the two hydrophilic parts of the surfactant molecule, the interaction energy between two water molecules and the interaction energy between the hydrophilic chain and water respectively. C_{LW}, C_{HO}

C_{LL}, C_{OO}, C_{LO} (at oil side)

C_{HH}, C_{WW}, C_{HW} (at water side)

C_{LW}, C_{HO}, C_{LH} (at the interface)

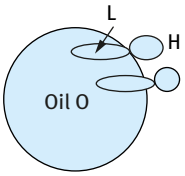

Fig. 12.3: Various interaction parameters at the oil and water phases.

and C_{LH} refer to the interaction energies at the interface between the lipophilic part of the surfactant molecule and water, the interaction energy between the hydrophilic part and oil and the interaction energy between the lipophilic and hydrophilic parts respectively.

The three cases $R_0 < 1$, $R_0 > 1$ and $R_0 = 1$ correspond to type I (O/W), type II (W/O) and type III (flat interface) phase behaviour respectively. For example, for $R_0 < 1$, increasing temperature results in reduced hydration of the hydrophilic part of the surfactant molecule and the emulsion changes from Winsor I to Winsor III to Winsor II and this causes phase inversion from O/W to W/O emulsion. This inversion occurs at a particular temperature, referred to as the phase inversion temperature (PIT) as will be discussed below.

In Winsor's type I systems ($R_0 < 1$), the affinity of the surfactant for the water phase exceeds its affinity to the oil phase. Thus, the interface will be convex towards water and the nonionic surfactant–oil–water (n-SOW) system can be one or two phases. A system in the two-phase system will split into an oil phase containing dissolved surfactant monomers at the cmc_o (critical micelle concentration in the oil phase) and an aqueous microemulsion-water phase containing solubilized oil in normal surfactant micelles.

In Winsor's type II systems ($R_0 > 1$), the affinity of the surfactant for the oil phase exceeds its affinity to the water phase. Thus, the interface will be convex towards oil and the nonionic surfactant–oil–water (n-SOW) system can be one or two phases. A system in the two-phase system will split into a water phase containing dissolved surfactant monomers at the cmc_w (critical micelle concentration in the water phase) and an oleic microemulsion phase containing solubilized water in inverse surfactant micelles.

In Winsor's type III system ($R_0 = 1$), the surfactant's affinity for the oil and water phases is balanced. The interface will be flat and the n-SOW system can have one, two or three phases depending on its composition. In the multiphase region, the system can be:

(i) two-phase, a water phase and an oleic microemulsion;
(ii) two-phase, an oil phase and an aqueous microemulsion;

(iii) three-phase, a water phase containing surfactant monomers at cmc_w, an oil phase containing surfactant monomers at cmc_o and a "surfactant phase".

The latter phase may have a bicontinuous structure, being composed of cosolubilized oil and water separated from each other by a layer of surfactant. The "surfactant phase" is sometimes called the middle phase because its intermediate density causes it to appear between the oil and water phases in a phase-separated type III n-SOW system.

12.4 The phase inversion temperature (PIT)

One way to alter the affinity in an n-SOW system is by changing the temperature, which will change the surfactant's affinity to the two phases. At high temperature the nonionic surfactant becomes soluble in the oil phase, whereas at low temperature it becomes more soluble in the water phase. Thus, at a constant surfactant concentration, the phase behaviour will change with temperature [9]. Thus with increasing temperature the surfactant's affinity to the oil phase increases and the system changes from Winsor I to Winsor III and finally to Winsor II, i.e. the emulsion will invert from an O/W to a W/O system at a particular temperature, referred to as the phase inversion temperature (PIT). A schematic representation of the change in phase behaviour in an n-SOW system is shown in Fig. 12.4.

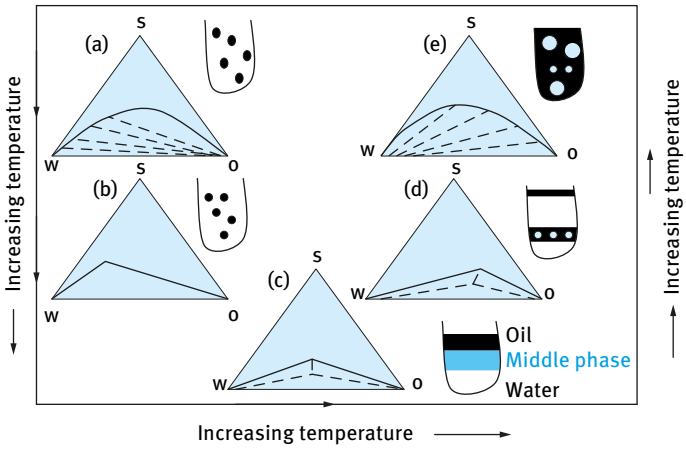

Fig. 12.4: Effect of increasing temperature on the phase behaviour of an n-SOW system. The PIT concept.

At low temperature, over the Winsor I region, O/W emulsions can be easily formed and are quite stable as shown in Fig. 12.4 (a). On raising the temperature (as shown by the arrow in Fig. 12.4) the O/W emulsion's stability decreases, and the macroemulsion finally resolves when the system reaches Winsor III state (represented in Fig. 12.4 (c)). Within this region, both O/W and W/O emulsions are unstable, with the minimum stability in the balanced region. At higher temperature, over the Winsor II region, W/O emulsions become stable as represented in Fig. 12.4 (e). This behaviour is always observed in nonionic systems if the surfactant concentration is above the cmc and the volume fractions of the components are not extreme. The macroemulsion's stability is essentially symmetrical with respect to the balanced point, just as the phase behaviour is. At positive spontaneous curvature, O/W emulsions are stable, while at negative spontaneous curvature, W/O emulsions are stable.

Fig. 12.5 represents the most clear-cut image of macroemulsion inversion as a function of temperature [9]. Equal volumes of oil and water are emulsified at various temperatures. Five hours after preparation, the macroemulsions completely cream or sediment, depending on the temperature. Below the balanced temperature, a stable O/W cream layer is formed, which does not show any visible coalescence. Similarly, above the balanced point, a stable sediment of a W/O emulsion is formed. Close to the balanced point, the narrow temperature range between 66 and 68 °C, where the three-phase equilibrium is observed, neither O/W nor W/O macroemulsions are stable.

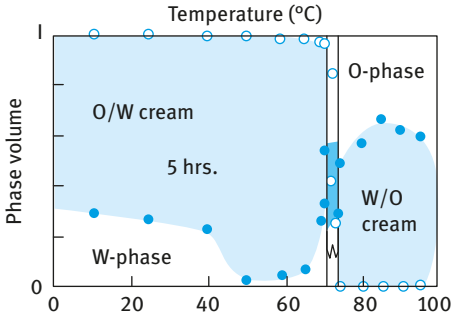

Fig. 12.5: Macroemulsion stability diagram of cyclohexane-water-polyoxyethylene (9.7) nonyl phenol ether system.

Within the Winsor III region, the stability of the macroemulsions is very temperature sensitive. Although exactly in the balanced state, the macroemulsions are very unstable and break within minutes; the system becomes stable only several tens of degrees away from the balanced point, while still being in the Winsor III region. The macroemulsion stability pattern is not completely symmetric. W/O emulsions reach maximum stability at ≈ 20 °C above the balanced point, after which the stability starts to decrease. On the other hand, there is no similar maximum stability for O/W emulsion stability at very low temperatures.

The macroemulsion phase behaviour can be "tuned" not only by changes in temperature, but also by addition of "co-solvents", cosurfactants or electrolytes [9]. For example, the balanced point of n-C_8H_{18}–$C_{10}E_5$–water system is at ≈ 45 °C, while that of the n-C_8H_{18}–$C_{10}E_5$–10 % NaCl is at ≈ 28 °C. The changes in the macroemulsion phase behaviour induced by additives lead to a similar shift in the macroemulsion stability profile. Thus, when 10 % of NaCl is added to the system, the new balanced point is now established at 28 °C and now macroemulsions prepared below 28 °C will have an O/W type. The same effect is found when the balanced location point is controlled by adding co-solvent to oil and water, changing the chain length of the oil, and adding cosurfactants.

Several empirical equations have been proposed to evaluate the location of the balanced point. For example, Salager et al. [10] proposed the following empirical equation for determining the "optimum surfactant formulation" (i.e. the balanced point) for anionic surfactant systems,

$$\ln S - K \times \mathrm{ACN} - f(A) + \sigma - a_T \Delta T = 0 \tag{12.2}$$

S is the wt% of NaCl, ACN is the alkane carbon number (a characteristic parameter of the oil phase), ΔT is the temperature deviation from a certain reference (25 °C), $f(A)$ is a function of the alcohol type and concentration, and K, σ and a_T are empirical parameters characterizing the surfactant.

A similar empirical equation was proposed for nonionic surfactants [10],

$$\alpha - \mathrm{EON} + bS - k\,\mathrm{ACN} - \phi(A) + c_T \Delta T = 0 \tag{12.3}$$

EON is the average number of ethylene oxide groups per surfactant molecule, $\phi(A)$ is another empirical function of the alcohol type and concentration, and α, c_T and k are empirical constants characterizing the surfactant. It is clear that the left-hand sides of equations (12.2) and (12.3) are proportional to the monolayer spontaneous curvature, taken with the opposite sign.

The macroemulsions invert as any of the composition parameters is continuously varied in such a way that the system passes through the optimal composition (balanced state) and the left-hand side of equations (12.2) and (12.3) changes sign. As the spontaneous curvature is varied by changing the mole fraction of one of the surfactants in the mixture, the composition of the oil phase, or the mole fraction of the alcohol, the system passes through the Winsor I–Winsor III–Winsor II sequence. This is illustrated in Fig. 12.6 where n-pentanol is added to a 50 : 50 O/W emulsion of kerosene/2 wt% NaCl using an anionic surfactant as emulsifier. It can be seen that the O/W emulsion reaches the balanced point at ≈ 5.5 % pentanol, where the emulsion stability (as measured by the lifetime of the emulsion) reaches a minimum (of several minutes) at the balanced point. Any addition of pentanol above the balanced point causes inversion of the emulsion as indicated by the rapid decrease in the conductivity of the emulsion. The lifetime of the emulsion can reach several hours or days, as one moves away from the balanced point.

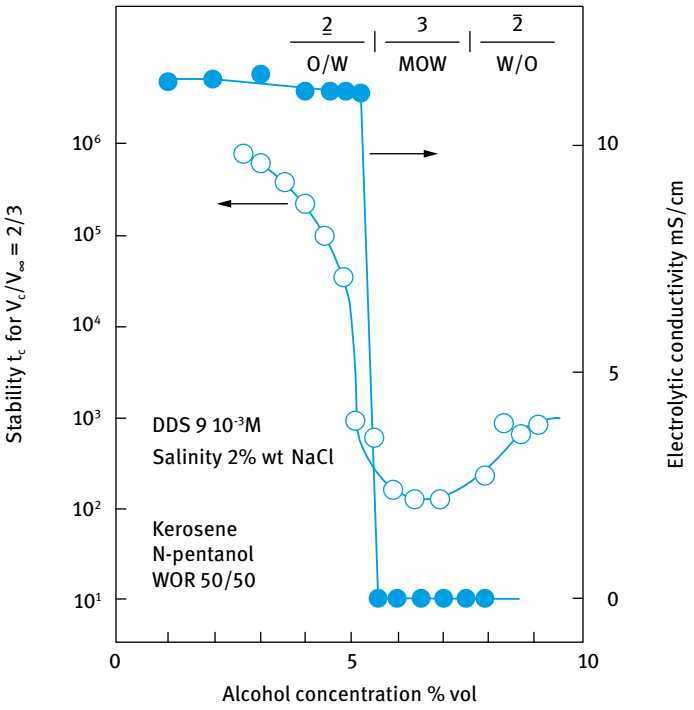

Fig. 12.6: Macroemulsion inversion caused by addition of n-pentanol.

The overall pattern of macroemulsion stability as a function of salinity or temperature is illustrated by considering an O/W emulsion of n-octane/water stabilized by a non-ionic surfactant such as $C_{12}E_5$. Fig. 12.7 shows a visual inspection of the emulsion as a function of NaCl concentration at room temperature.

At low salinities, the macroemulsion has an O/W type. As salinity increases, the system changes from very stable O/W to very stable W/O type with the inversion at the three-phase equilibrium range. O/W emulsions can be distinguished from W/O

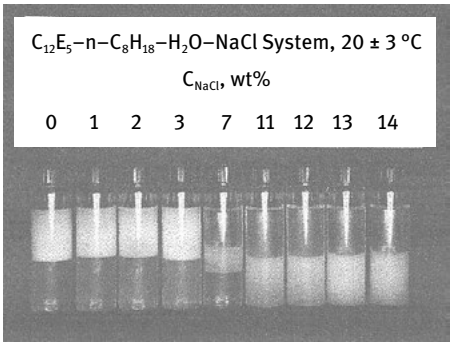

Fig. 12.7: Visual observation of the emulsion type as a function of NaCl concentration.

emulsions by the fact that the former form a cream layer at the top of the container, while the latter form a milky sediment at the bottom of the container. A schematic representation of the emulsion inversion on increasing temperature or increasing NaCl concentration (at room temperature) is shown in Fig. 12.8, which shows the variation of log lifetime ($\log \tau_{1/2}$) with increasing temperature or NaCl concentration. Both O/W and W/O emulsions are very stable far away from the balanced point. Their behaviour is not completely identical when the spontaneous curvature is controlled by temperature. Although the O/W emulsion is very stable at low temperature, the W/O emulsion's stability passes through the maximum and then decreases.

In the Winsor III region, the macroemulsion is extremely temperature- and salinity-sensitive. This is illustrated in Fig. 12.9 which shows that changes by only several tenths of a degree or several tenths of NaCl reduce the macroemulsion's stability from minutes to days.

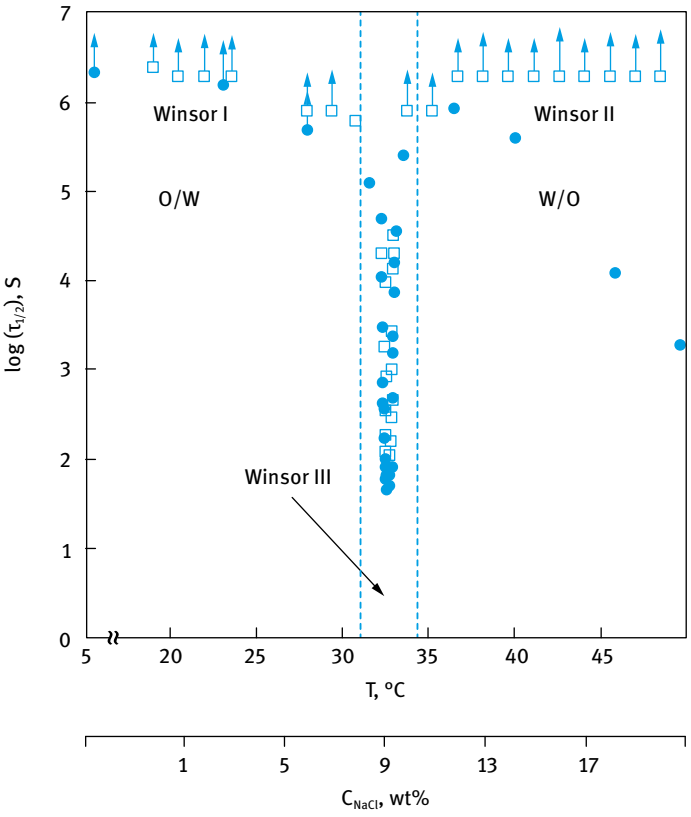

Fig. 12.8: Log macroemulsion lifetime ($\log \tau_{1/2}$) versus temperature or NaCl concentration.

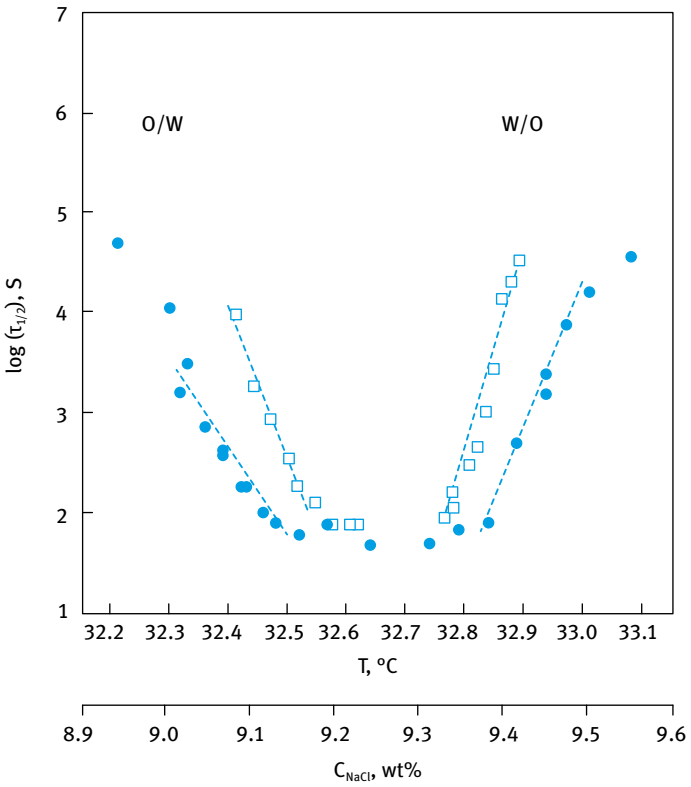

Fig. 12.9: log $\tau_{1/2}$ versus temperature (upper curve) or NaCl concentration (lower curve).

References

[1] Tadros T. Emulsions. Berlin: De Gruyter; 2016.
[2] Binks BP, editor. Modern aspects of emulsion science. Cambridge: The Royal Society of Chemistry Publication; 1998.
[3] Ostwald WO. Kolloid Z. 1910;6:103; 1910;7:64.
[4] Shinoda K, Saito H. J Colloid Interface Sci. 1969;30:258.
[5] Sherman P. J Oc Chem Inc (London). 1950;69 (Suppl. No. 2):570.
[6] Brooks BW, Richmond HN, Zefra M. Phase inversion and drop formation in agitated liquid-liquid dispersions. In: Binks BP, editor. Modern aspects of emulsion science. Cambridge: The Royal Society of Chemistry Publication; 1998.
[7] Marzall L. In: Schick MJ, editor. Nonionic surfactants: Physical chemistry. Surfactant Science Series, Vol. 23. New York: Marcel Dekker; 1967.
[8] Winsor PA. Trans Faraday Soc. 1948;44:376.
[9] Kabalnov AS. Coalescence in emulsions. In: Binks BP, editor. Modern aspects of emulsion science. Cambridge: The Royal Society of Chemistry Publication; 1998.
[10] Salager JL, Morgan J, Schechter R, Wade W, Vasques E. Soc Petrol Eng J. 1979;19:107.

13 Sedimentation of suspensions, creaming of emulsions and their prevention

13.1 Introduction

Many formulations of the disperse type (suspensions and emulsions) undergo separation on standing as a result of the density difference between the particles or droplets and the medium, unless the particles or droplets are small enough for Brownian motion to overcome gravity [1, 2]. This is illustrated in Fig. 13.1 for three cases of suspensions.

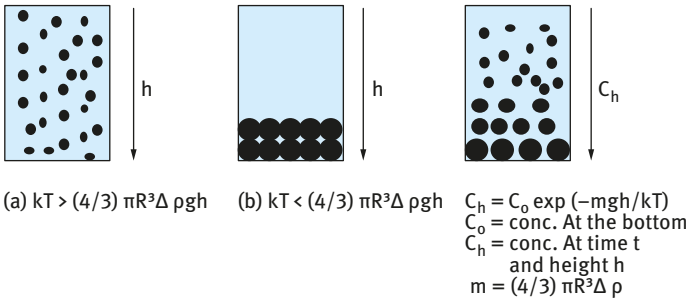

Fig. 13.1: Schematic representation of sedimentation of suspensions.

Case (a) represents the situation when the Brownian diffusion energy (which is in the region of kT, where k is the Boltzmann constant and T is the absolute temperature) is much larger than the gravitational potential energy (which is equal to $4/3\pi R^3 \Delta\rho g h$, where R is the particle radius, $\Delta\rho$ is the density difference between the particles and medium, g the acceleration due to gravity and h is the height of the container). Under these conditions, the particles become randomly distributed throughout the whole system, and no separation occurs. This situation may occur with nanosuspensions with radii less than 100 nm, particularly if $\Delta\rho$ is not large, say less than 0.1. In contrast, when $4/3\pi R^3 \Delta\rho g h \gg kT$ complete sedimentation occurs, as illustrated in Fig. 13.1 (b) with suspensions of uniform particles. In such cases, the repulsive force necessary to ensure colloid stability enables the particles to move past each other to form a compact layer [1]. As a consequence of the dense packing and small spaces between the particles, such compact sediments (which are technically referred to as "clays" or "cakes") are difficult to redisperse. In rheological terms (Chapter 14) the close packed sediment is shear thickening that is referred to as dilatancy, i.e. rapid increase in the viscosity with increasing shear rate.

https://doi.org/10.1515/9783110587944-014

The most practical situation is that represented by Fig. 13.1 (c), where a concentration gradient of the particles occurs across the container. The concentration of particles C can be related to that at the bottom of the container C_0 by the following equation,

$$C = C_0 \exp\left(-\frac{mgh}{kT}\right). \tag{13.1}$$

The process of creaming or sedimentation of emulsions is also the result of gravity, when the density of the droplets and the medium are not equal. When the density of the disperse phase is lower than that of the medium (as with most oil-in-water O/W emulsions), creaming occurs, whereas if the density of the disperse phase is higher than that of the medium (as with most W/O emulsions), sedimentation occurs. Fig. 13.2 gives a schematic picture for creaming of emulsions for three cases [2]. Case (a) represents the situation for small droplets (< 0.1 μm, i.e. nanoemulsions) in which the gravitational force is opposed by a diffusional force (i.e. associated with the translational kinetic energy of the droplets). A Boltzmann distribution is set up, where the droplet concentration C_h at height h is related to that at the top of the container C_0 by equation (13.1).

For no separation to occur, i.e. $C_h = C_0$,

$$kT \gg \frac{4}{3}\pi R^3 \Delta\rho g L. \tag{13.2}$$

Case (b) represents emulsions consisting of "monodisperse" droplets with radius >1 μm. In this case, the concentration forces are much greater than the opposing diffusional force, so that the emulsion separates into two distinct layers with the droplets forming a cream or sediment leaving the clear supernatant liquid,

$$kT \ll \frac{4}{3}\pi R^3 \Delta\rho g L. \tag{13.3}$$

Case (c) is that for a polydisperse (practical) emulsion, in which the droplets will cream or sediment at various rates. In this case, a concentration gradient builds up, as predicted by equation (13.1), with the larger droplets staying at the top of the cream layer, with some smaller droplets remaining in the bottom layer.

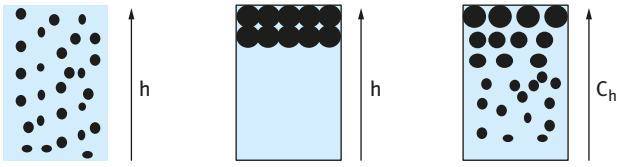

(a) $kT > (4/3)\pi R^3 \Delta\rho gh$ (b) $kT < (4/3)\pi R^3 \Delta\rho gh$ $C_h = C_o \exp(-mgh/kT)$
C_o = conc. At the bottom
C_h = conc. At time t and height h
$m = (4/3)\pi R^3 \Delta\rho$

Fig. 13.2: Representation of creaming of emulsions.

13.2 Sedimentation rate of suspensions and creaming rate of emulsions

For a very dilute suspension or emulsion of rigid non-interacting particles or droplets, the rate of sedimentation or creaming υ_0 can be calculated by applying Stokes' law, whereby the hydrodynamic force is balanced by the gravitational force,

$$\text{hydrodynamic force} = 6\pi\eta R\upsilon_0, \tag{13.4}$$

$$\text{gravity force} = (4/3)\pi R^3 \Delta\rho g, \tag{13.5}$$

$$\upsilon_0 = \frac{2}{9}\frac{R^2\Delta\rho g}{\eta}, \tag{13.6}$$

where η is the viscosity of the medium (water).

υ_0 calculated for three particle or droplet sizes (0.1, 1 and 10 μm) for a suspension or emulsion with density difference $\Delta\rho = 0.2$ is 4.4×10^{-9}, 4.4×10^{-7} and 4.4×10^{-5} m s^{-1} respectively. The time needed for complete sedimentation or creaming in a 0.1 m container is 250 days, 60 hours and 40 minutes respectively.

For moderately concentrated suspensions or emulsions, $0.2 > \phi > 0.01$, sedimentation or creaming is reduced as a result of hydrodynamic interaction between the particles, which no longer sediment independently of each other [3, 4]. The sedimentation or creaming velocity, υ, can be related to the Stokes' velocity υ_0 by the following equation,

$$\upsilon = \upsilon_0(1 - 6.55\phi). \tag{13.7}$$

This means that for a suspension or emulsion with $\phi = 0.1$, $\upsilon = 0.345\upsilon_0$, i.e. the rate is reduced by a factor of ≈ 3.

For more concentrated suspensions or emulsion ($\phi > 0.2$), the sedimentation velocity becomes a complex function of ϕ. At $\phi > 0.4$, one usually enters the hindered settling or creaming regime, where all the particles r droplets sediment or cream at the same rate (independent of size).

A schematic representation for the variation of υ with ϕ is shown in Fig. 13.3, which also shows the variation of relative viscosity with ϕ. It can be seen that v decreases exponentially with increasing ϕ and ultimately it approaches zero when ϕ approaches a critical value ϕ_p (the maximum packing fraction). The relative viscosity shows a gradual increase with increasing ϕ and when $\phi = \phi_p$, the relative viscosity approaches infinity.

The maximum packing fraction ϕ_p can be easily calculated for monodisperse rigid spheres. For hexagonal packing $\phi_p = 0.74$, whereas for random packing $\phi_p = 0.64$. The maximum packing fraction increases with polydisperse suspensions or emulsions. For example for a bimodal particle or droplet size distribution (with a ratio of $\approx 10:1$), $\phi_p > 0.8$.

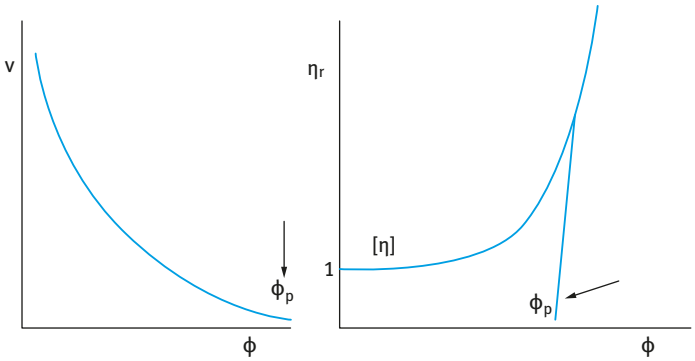

Fig. 13.3: Variation of v and η_r with ϕ.

It is possible to relate the relative sedimentation or creaming rate (v/v_0) to the relative viscosity (η/η_0),

$$\left(\frac{v}{v_0}\right) = \alpha\left(\frac{\eta_0}{\eta}\right). \tag{13.8}$$

The relative viscosity is related to the volume fraction ϕ by the Dougherty–Krieger equation [5] for hard spheres,

$$\frac{\eta}{\eta_0} = \left(1 - \frac{\phi}{\phi_p}\right)^{-[\eta]\phi_p}, \tag{13.9}$$

where $[\eta]$ is the intrinsic viscosity (= 2.5 for hard spheres).

Combining equations (13.8) and (13.9),

$$\frac{v}{v_0} = \left(1 - \frac{\phi}{\phi_p}\right)^{\alpha[\eta]\phi_p} = \left(1 - \frac{\phi}{\phi_p}\right)^{k\phi_p}. \tag{13.10}$$

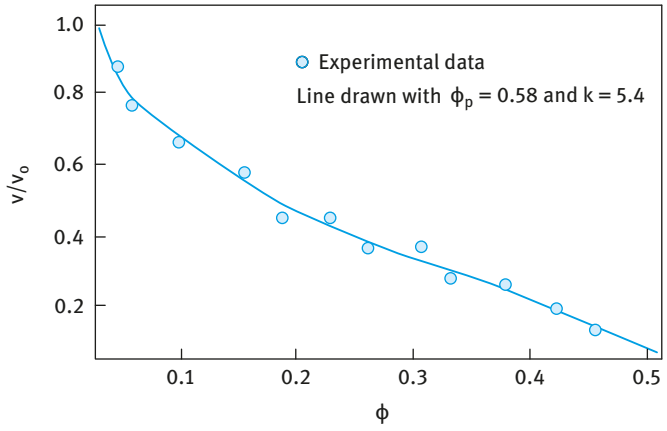

Fig. 13.4: Variation of sedimentation rate with volume fraction for polystyrene dispersions.

The above empirical relationship was tested for sedimentation of polystyrene latex suspensions with $R = 1.55\,\mu m$ in $10^{-3}\,mol\,dm^{-3}$ NaCl [6]. The results are shown in Fig. 13.4.

The circles are the experimental points, whereas the solid line is calculated using equation (13.10) with $\phi_p = 0.58$ and $k = 5.4$.

13.3 Sedimentation or creaming in non-Newtonian fluids

The sedimentation of particles or creaming of droplets in non-Newtonian fluids, such as aqueous solutions containing high molecular weight compounds (e.g. hydroxyethyl cellulose or xanthan gum), usually referred to as "thickeners", is not simple since these non-Newtonian solutions are shear thinning with the viscosity decreasing as shear rate increases. These solutions show a Newtonian region at low shear rates or shear stresses (Chapter 14), usually referred to as the residual or zero shear viscosity $\eta(0)$. This is illustrated in Fig. 13.5 which shows the variation of stress σ and viscosity η with shear rate $\dot{\gamma}$.

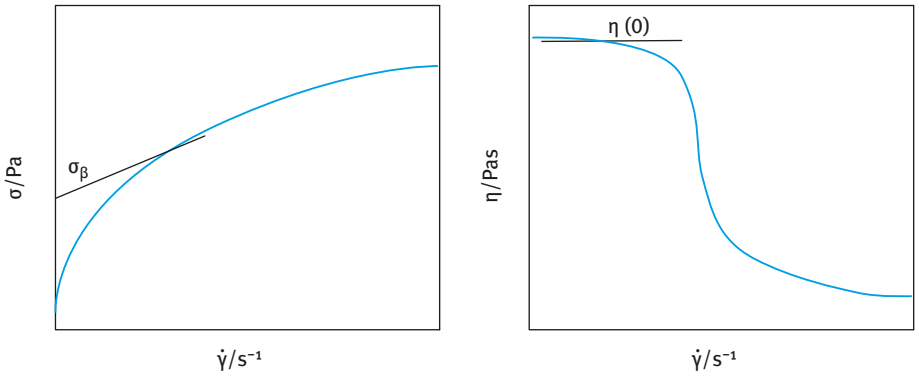

Fig. 13.5: Flow behaviour of thickeners.

The viscosity of a polymer solution increases gradually with increasing concentration and at a critical concentration, C^*, the polymer coils with a radius of gyration R_G and a hydrodynamic radius R_h (which is higher than R_G due to solvation of the polymer chains) begin to overlap and this shows a rapid increase in viscosity. This is illustrated in Fig. 13.6 which shows the variation of $\log \eta$ with $\log C$.

In the first part of the curve $\eta \propto C$, whereas in the second part (above C^*) $\eta \propto C^{3.4}$. A schematic representation of polymer coil overlap is shown in Fig. 13.7 which shows the effect of gradually increasing the polymer concentration. The polymer concentration above C^* is referred to as the semi-dilute range [7].

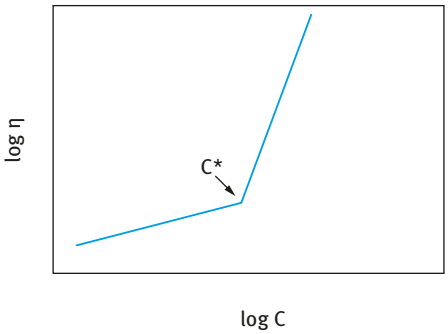

Fig. 13.6: Variation of log η with log C.

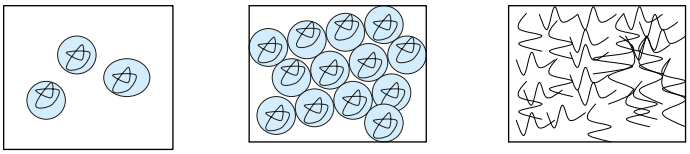

Fig. 13.7: Crossover between dilute and semi-dilute solutions.

C^* is related to R_G and the polymer molecular weight M by,

$$C^* = \frac{3M}{4\pi R_G^3 N_{av}}. \tag{13.11}$$

N_{av} is Avogadro's number. As M increases C^* becomes progressively lower. This shows that to produce physical gels at low concentrations by simple polymer coil overlap, one has to use high molecular weight polymers.

Another method to reduce the polymer concentration at which chain overlap occurs is to use polymers that form extended chains, such as xanthan gum which produces conformation in the form of a helical structure with a large axial ratio. These polymers give much higher intrinsic viscosities and they show both rotational and translational diffusion. The relaxation time for the polymer chain is much higher than a corresponding polymer with the same molecular weight but produces random coil conformation.

The above polymers interact at very low concentrations and the overlap concentration can be very low (< 0.01 %). These polysaccharides are used in many formulations to produce physical gels at very low concentrations thus reducing sedimentation.

The shear stress, σ_p, exerted by a particle (force/area) can be simply calculated [8],

$$\sigma_p = \frac{(4/3)\pi R^3 \Delta\rho g}{4\pi R^2} = \frac{\Delta\rho R g}{3}. \tag{13.12}$$

For a 10 μm radius particle with a density difference $\Delta\rho$ of 0.2 g cm^{-3}, the stress is equal to,

$$\sigma_p = \frac{0.2 \times 10^3 \times 10 \times 10^{-6} \times 9.8}{3} \approx 6 \times 10^{-3} \text{ Pa}. \quad (13.13)$$

For smaller particles smaller stresses are exerted.

Thus, to predict sedimentation or creaming, one has to measure the viscosity at very low stresses (or shear rates) (Chapter 14). These measurements can be carried out using a constant stress rheometer (Carrimed, Bohlin, Rheometrics, Haake or Physica).

Usually one obtains good correlation between the rate of sedimentation or creaming υ and the residual viscosity $\eta(0)$. Above a certain value of $\eta(0)$, υ becomes equal to 0. Clearly, to minimize creaming or sedimentation one has to increase $\eta(0)$; an acceptable level for the high shear viscosity η_∞ must be achieved, depending on the application. In some cases, a high $\eta(0)$ may be accompanied by a high η_∞ (which may not be acceptable for the application).

As discussed above, the stress exerted by the particles is very small, in the region of 10^{-3}–10^{-1} Pa depending on the particle size and the density of the particles. Clearly, to predict sedimentation one needs to measure the viscosity at this low stresses [6, 8]. This is illustrated for solutions of ethyl hydroxy ethyl cellulose (EHEC) in Fig. 13.8.

The results in Fig. 13.8 show that below a certain critical value of the shear stress the viscous behaviour is Newtonian and this critical stress value is in the region of 0.1 Pa. Above this stress the viscosity decreases with increasing shear stress, indicating the shear thinning behaviour. The plateau viscosity values at low shear stress (< 0.1 Pa) give the limiting and residual viscosity $\eta(0)$, i.e. the viscosity at near zero shear rate.

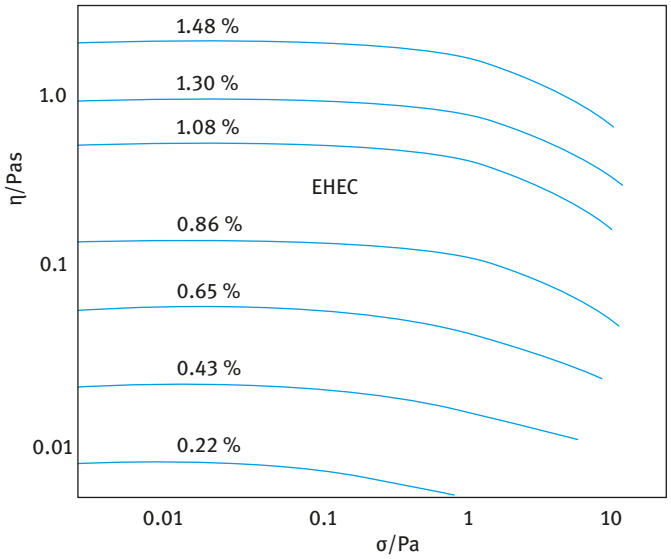

Fig. 13.8: Constant stress (creep) measurements for PS latex dispersions as a function of EHEC concentration.

The settling rate of a dispersion of polystyrene latex with radius 1.55 μm and at 5 % w/v was measured as a function of ethyl hydroxy ethyl cellulose (EHEC) concentration, using the same range as in Fig. 13.8. The settling rate, expressed as v/R^2, where R is the particle radius, is plotted versus $\eta(0)$ in Fig. 13.9 (on a log-log scale). As is clear, a linear relationship between $\log(v/R^2)$ and $\log \eta(0)$ is obtained, with a slope of –1, over three decades of viscosity, indicating that the rate of settling is proportional to $[\eta(0)] - 1$.

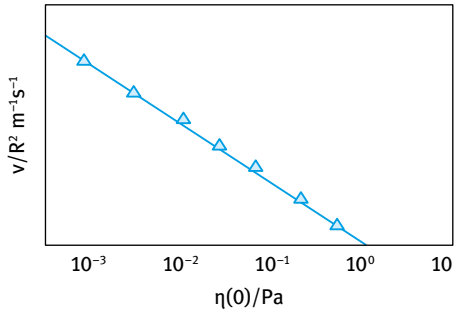

Fig. 13.9: Sedimentation rate versus residual viscosity.

The maximum shear stress developed by an isolated spherical particle as it settles through a medium of viscosity η is given by the expression [9],

$$\text{shear stress} = \frac{3v\eta}{2R}. \tag{13.14}$$

For particles or droplets at the coarse end of the colloidal range, the magnitude of this quantity will be in the range 10^{-2}–10^{-5} Pa. From the data obtained on EHEC solutions and given in Fig. 13.8, it can be seen that in this range of shear stresses the solutions behave as Newtonian fluids with zero shear viscosity $\eta(0)$. Hence isolated spheres should obey equation (13.6) with η_0 replaced by $\eta(0)$. Consequently it can be concluded that the rate of sedimentation of a particle or creaming of a droplet is determined by the zero shear rate behaviour of the medium in which it is suspended. With the present system of polystyrene latex no sedimentation occurred when $\eta(0)$ was greater than 10 Pa s.

The situation with more practical dispersions is more complex due to the interaction between the thickener and the particles or droplets. Most practical suspensions or emulsions show some weak flocculation and the "gel" produced between the particles or droplets and thickener may undergo some contraction as a result of the gravity force exerted on the whole network. A useful method to describe separation in these concentrated suspensions or emulsions is to follow the relative sediment volume V_t/V_0 or relative sediment height h_t/h_0 (where the subscripts t and 0 refers to time t and zero time respectively) with storage time. For good physical stability, the values of V_t/V_0 or h_t/h_0 should be as close as possible to unity (i.e. minimum separation). This can

be achieved by balancing the gravitational force exerted by the gel network with the bulk "elastic" modulus of the suspension. The latter is related to the high frequency modulus G' (Chapter 14 on rheology).

13.4 Prevention of sedimentation and creaming

Dilatant sediments are produced with suspensions which are colloidally stable. These dilatant sediments are difficult to redisperse and hence they must be prevented from forming on standing. With emulsions that show creaming, a dense cream layer is also produced at the top of the container which is also difficult to redisperse. Several methods may be applied to prevent sedimentation and formation of clays or cakes in a suspension and creaming of emulsions and these are summarized below.

13.4.1 Balance of the density of the disperse phase and medium

It is clear from Stokes' law that if $\Delta\rho = 0$, $v_0 = 0$. This method can be applied only when the density of the particles or droplets is not much larger or smaller than that of the medium (e.g. $\Delta\rho \approx 0.1$). By dissolving an inert substance in the continuous phase such as sugar or glycerol one may achieve density matching to prevent sedimentation of particles. With emulsions with oil density lower than the medium, it is possible to mix the oil with a more dense oil to achieve density matching with the continuous phase. However, apart from its limitation to particles with density not much larger than the medium and droplets with density not much smaller than the medium, the method is not very practical since density matching can only occur at one temperature. Liquids usually have large thermal expansion, whereas densities of solids vary comparatively little with temperature.

13.4.2 Reduction of particle or droplet size

As mentioned above, if R is significantly reduced (to values below 0.1 μm), Brownian diffusion can overcome the gravity force and no sedimentation or creaming occurs. This is the principle of formation of nanosuspensions and nanoemulsions.

13.4.3 Use of high molecular weight thickeners

As discussed above, high molecular weight materials such as hydroxyethyl cellulose or xanthan gum when added above a critical concentration (at which polymer coil overlap occurs) will produce very high viscosity at low stresses or shear rates (usually

in excess of several hundred Pa s) and this will prevent sedimentation of the particles or creaming of droplets. In relatively concentrated suspensions or emulsions, the situation becomes more complex, since the polymer molecules may lead to flocculation of the suspension or emulsion, by bridging, depletion (see below), etc. Moreover, the polymer chains at high concentrations tend to interact with each other above a critical concentration C^* (the so-called "semi-dilute" region discussed above). Such interaction leads to viscoelasticity (Chapter 14 on rheology), whereby the flow behaviour shows an elastic component characterized by an elastic modulus G' (energy elastically stored during deformation) and a viscous component G'' (loss modulus resulting from energy dissipation during flow). The elastic behaviour of such relatively concentrated polymer solutions plays a major role in reducing settling and preventing formation of dilatant clays as well as reducing creaming and formation of compact cream layers. A good example of such a viscoelastic polymer solution is that of xanthan gum, a high molecular weight polymer (molecular weight in excess of 10^6 Daltons). This polymer shows viscoelasticity at relatively low concentration (< 0.1 %) as a result of the interaction of the polymer chains, which are very long. This polymer is very effective in reducing settling of coarse suspensions at low concentrations (in the region of 0.1–0.4 % depending on the volume fraction of the suspension).

It should be mentioned that to arrive at the optimum concentration of polymer required to prevent settling and claying of a suspension concentrate or creaming of an emulsion, one needs to evaluate the rheological characteristics of the polymer solution, on the one hand, and the whole system (suspension or emulsion and polymer) on the other (Chapter 14). This will provide the formulator with the necessary information on the interaction of polymer coils with each other and with the suspended particles or droplets. Moreover, one should be careful in applying high molecular weight materials to prevent settling or creaming, depending on the system. For example, with suspensions used as coatings, such as paints, time effects in flow are very important. In this case, the polymer used for preventing settling must show reversible time dependency of viscosity (i.e. thixotropy). In other words, the polymer used has to be shear thinning on application to ensure uniform coating, but once the shearing force is removed, the viscosity has to build up quickly in order to prevent undesirable flow. On the other hand, with suspensions that need to be diluted on application, such as agrochemical suspension concentrates, it is necessary to choose a polymer that disperses readily into water, without the need for vigorous agitation. One should also consider the temperature variation of the rheology of the polymer solution. If the rheology undergoes considerable changes with temperature, the suspension may clay at high temperatures. One should also consider the ageing of the polymer, which may result from chemical or microbiological degradation. This would result in reduction of viscosity with time, and settling or claying may occur on prolonged storage.

13.4.4 Reduction of creaming/sedimentation by using associative thickeners

Associative thickeners are hydrophobically modified polymer molecules in which alkyl chains (C_{12}–C_{16}) are either randomly grafted on a hydrophilic polymer molecule such as hydroxyethyl cellulose (HEC) or simply grafted at both ends of the hydrophilic chain. An example of hydrophobically modified HEC is Natrosol plus (Hercules) which contains 3–4 C_{16} randomly grafted onto hydroxyethyl cellulose. Another example of polymer that contains two alkyl chains at both ends of the molecule is HEUR (Rohm and Haas) that is made of polyethylene oxide (PEO) that is capped at both ends with linear C_{18} hydrocarbon chain.

The above hydrophobically modified polymers form gels when dissolved in water. Gel formation can occur at relatively lower polymer concentrations when compared with the unmodified molecule. The most likely explanation of gel formation is due to hydrophobic bonding (association) between the alkyl chains in the molecule. This effectively causes an apparent increase in the molecular weight. These associative structures are similar to micelles, except the aggregation numbers are much smaller.

Fig. 13.10 shows the variation of viscosity (measured using a Brookfield at 30 rpm) as a function of the alkyl content (C_8, C_{12} and C_{16}) for hydrophobically modified HEC (i.e. HMHEC). The viscosity reaches a maximum at a given alkyl group content that decreases with increasing alkyl chain length. The viscosity maximum increases with increasing alkyl chain length.

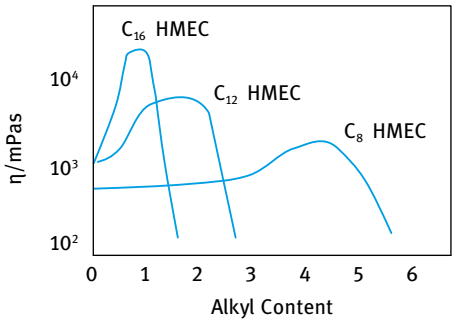

Fig. 13.10: Variation of viscosity of 1 % HMHEC versus alkyl group content of the polymer.

Associative thickeners also show interaction with surfactant micelles that are present in the formulation. The viscosity of the associative thickeners shows a maximum at a given surfactant concentration that depends on the nature of the surfactant. This is shown schematically in Fig. 13.11. The increase in viscosity is attributed to the hydrophobic interaction between the alkyl chains on the backbone of the polymer with the surfactant micelles. A schematic picture showing the interaction between HM polymers and surfactant micelles is shown in Fig. 13.12. At higher surfactant concentration, the "bridges" between the HM polymer molecules and the micelles are broken (free micelles) and η decreases.

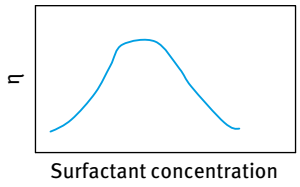

Fig. 13.11: Schematic plot of viscosity of HM polymer with surfactant concentration.

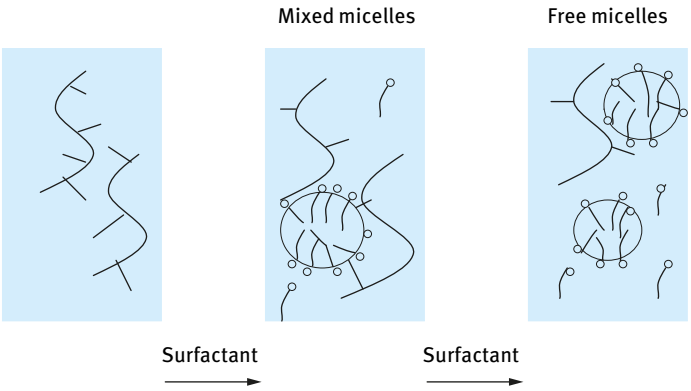

Fig. 13.12: Schematic representation of the interaction of polymers with surfactants.

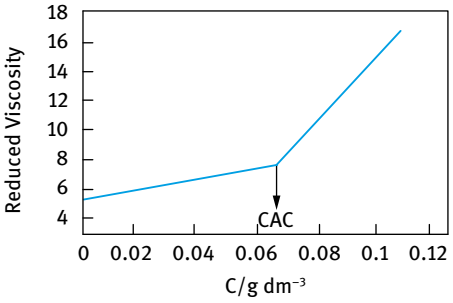

Fig. 13.13: Variation of reduced viscosity with HMHEC concentration.

The viscosity of hydrophobically modified polymers shows a rapid increase at a critical concentration, which may be defined as the critical aggregation concentration (CAC) as illustrated in Fig. 13.13 for HMHEC (WSP-D45 from Hercules). The assumption is made that the CAC is equal to the coil overlap concentration C^*.

From a knowledge of C^* and the intrinsic viscosity $[\eta]$ one can obtain the number of chains in each aggregate. For the above example $[\eta] = 4.7$ and $C^*[\eta] = 1$ giving an aggregation number of ≈ 4.

At C^* the polymer solution shows non-Newtonian flow (shear thinning behaviour) and its shows a high viscosity at low shear rates. This is illustrated in Fig. 13.14 which shows the variation of apparent viscosity with shear rate (using a constant stress

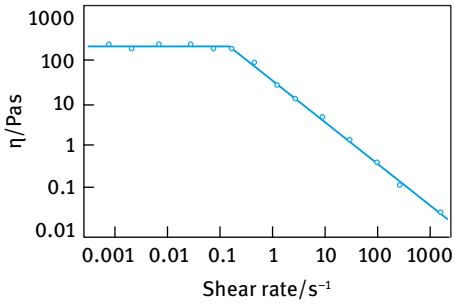

Fig. 13.14: Variation of viscosity with shear rate for HMEC WSP-47 at 0.75 g/100 cm^3.

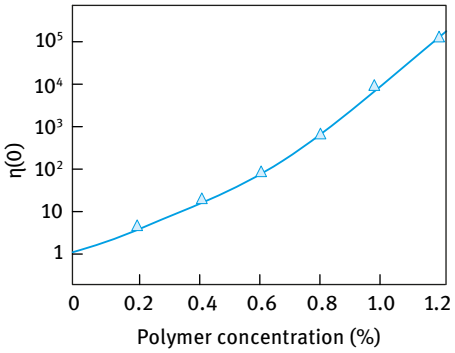

Fig. 13.15: Variation of $\eta(0)$ with polymer concentration.

rheometer). Below $\approx 0.1\,s^{-1}$, a plateau viscosity value $\eta(0)$ (referred to as residual or zero shear viscosity) is reached (≈ 200 Pa s).

With increasing polymer concentrations above C^*, the zero shear viscosity increases with increasing polymer concentration. This is illustrated in Fig. 13.15.

The above hydrophobically modified polymers are viscoelastic; this is illustrated in Fig. 13.16 for a solution 5.25 % of C_{18} end-capped PEO with $M = 35{,}000$, which shows the variation of the storage modulus G' and loss modulus G'' with frequency ω (rad s^{-1}). G' increases with increasing frequency and ultimately it reaches a plateau value at high frequency. G'' (which is higher than G' in the low frequency regime) increases with increasing frequency, reaches a maximum at a characteristic frequency ω^* (at which $G' = G''$) and then decreases to near zero value in the high frequency regime.

The above variation of G' and G'' with ω is typical for a system that shows Maxwell behaviour.

From the crossover point ω^* (at which $G' = G''$) one can obtain the relaxation time τ of the polymer in solution,

$$\tau = \frac{1}{\omega^*}. \tag{13.15}$$

For the above polymer $\tau = 8$ s.

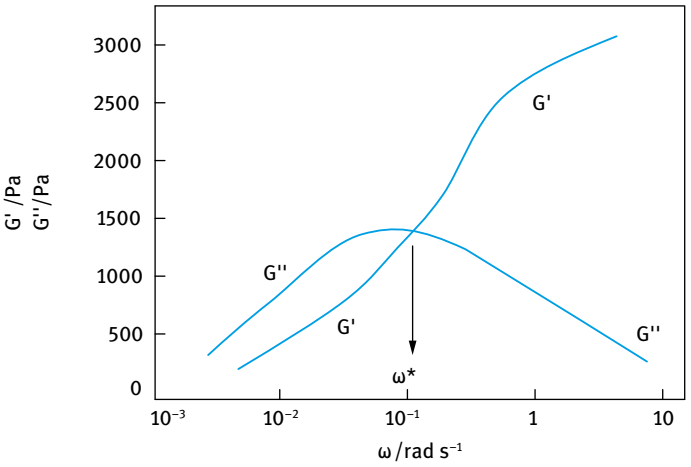

Fig. 13.16: Variation of G' and G'' with frequency for 5.24 HM PEO.

The above gels (sometimes referred to as rheology modifiers) are used for the reduction of creaming or sedimentation. These hydrophobically modified polymers can also interact with hydrophobic particles or oil droplets in the suspension or emulsion, forming several other associative structures.

13.4.5 Controlled flocculation

As discussed in Chapter 7, the total energy–distance of separation curve for electrostatically stabilized emulsions shows a shallow minimum (secondary minimum) at relatively long distance of separation between the droplets [10, 11]. By adding small amounts of electrolyte such a minimum can be made sufficiently deep for weak flocculation to occur. The same applies for sterically stabilized emulsions, which show only one minimum whose depth can be controlled by reducing the thickness of the adsorbed layer (Chapter 8). This can be achieved by reducing the molecular weight of the stabilizer and/or addition of a nonsolvent for the chains (e.g. electrolyte).

The phenomenon of weak flocculation may be applied to reduce creaming or sedimentation, in particular for concentrated suspensions or emulsions. In this case, the attractive energy required for inducing weak flocculation can be small (of the order of few kT units). This can be understood if one considers the free energy of flocculation that consists of two terms, an energy term determined by the depth of the minimum ($G_{\min}$) and an entropy term that is determined by reduction in configurational entropy on aggregation of droplets,

$$\Delta G_{\text{flocc}} = \Delta H_{\text{flocc}} - T\Delta S_{\text{flocc}}. \tag{13.16}$$

With concentrated emulsions or suspensions, the entropy loss on flocculation is small when compared with that for a dilute emulsion or suspension. Hence for flocculation of a concentrated emulsion or suspension, a small energy minimum is sufficient when compared with the case with a dilute emulsion.

As an illustration Fig. 13.17 shows energy–distance curves for a suspension stabilized by naphthalene formaldehyde sulphonated condensate (an anionic polyelectrolyte with a modest molecular weight of ≈ 1,000) at various NaCl concentrations [12].

It can be seen that at low NaCl concentration, the secondary minimum is absent and hence this suspension will show sedimentation and formation of a dilatant

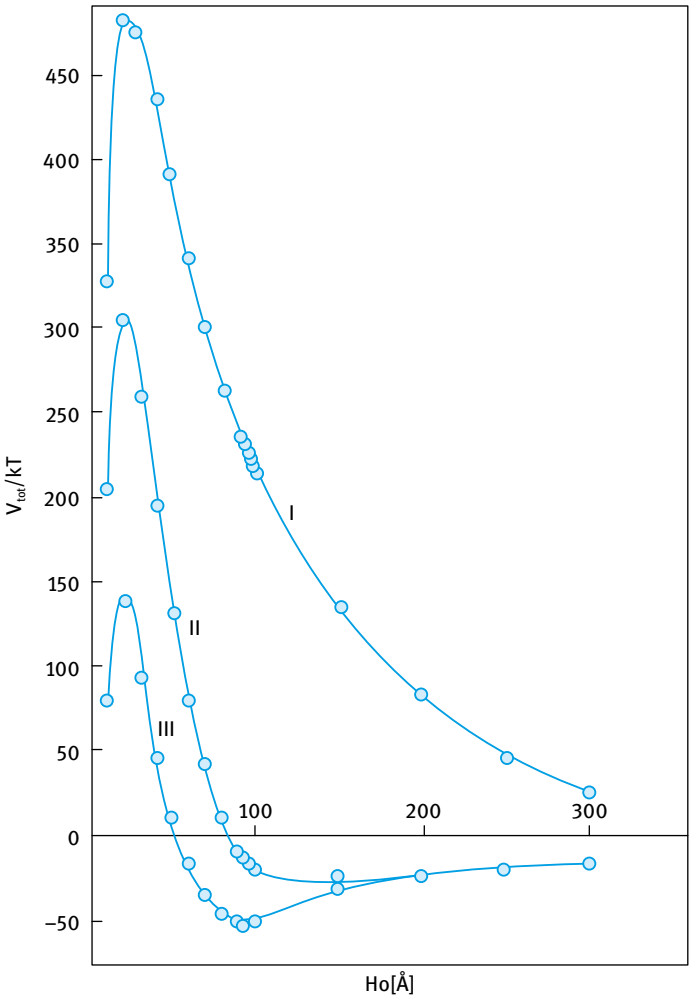

Fig. 13.17: Energy–distance curves for electrostatically stabilized suspension at various NaCl concentrations: (I) 10^{-3} mol dm^{-3}; (II) 10^{-2} mol dm^{-3}; (III) 5×10^{-2} mol dm^{-3}.

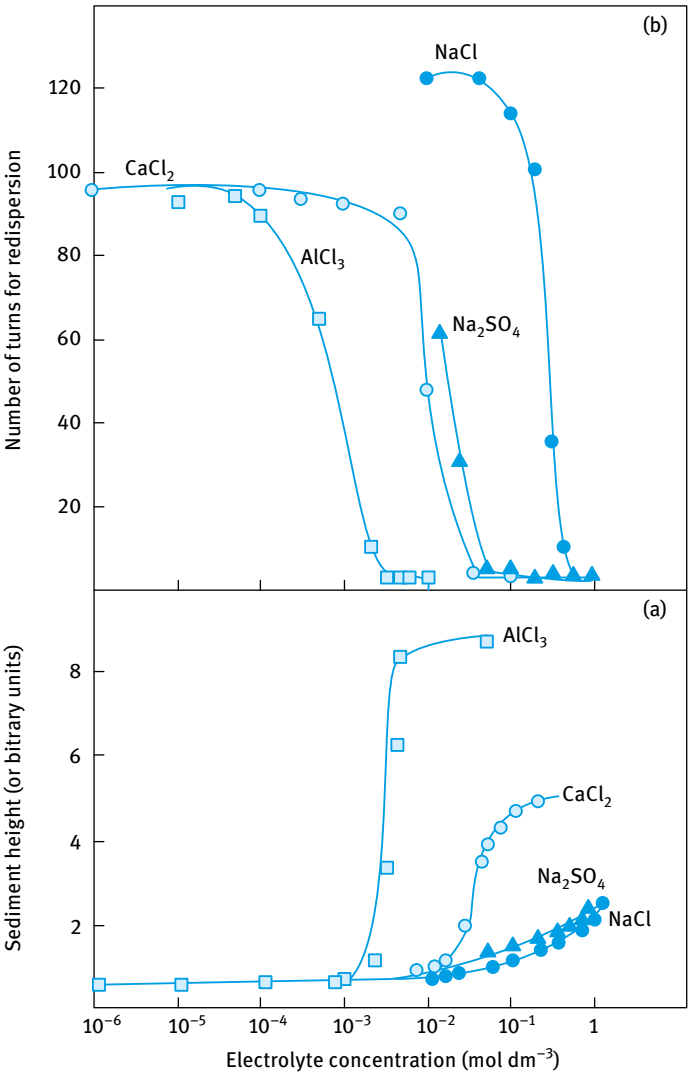

Fig. 13.18: Sediment height and redispersion as a function of electrolyte concentration.

clay. This can be illustrated by measuring the sediment height and number of turns required to redisperse the suspension as illustrated in Fig. 13.18. At 10^{-2} and 5×10^{-2} mol dm^{-3} NaCl, a secondary minimum appears in the energy–distance curve which is sufficiently deep for weak flocculation to occur. This is particularly the case with 5×10^{-2} mol dm^{-3} NaCl where the minimum depth reaches $\approx 50kT$. At such concentration the sediment height increases and the number of turns required for redispersion reaches a small value as is illustrated in Fig. 13.18.

The higher the valency of the electrolyte, the lower the concentration required to reach a sufficiently deep minimum for weak flocculation to occur. This is clearly shown in Fig. 13.18 where the sediment height and number of turns for redispersion are plotted as a function of Na_2SO_4 and $AlCl_3$ concentrations. It can be seen that for Na_2SO_4, a rapid increase in sediment height and decrease in the number of turns for redispersion occurs at $\approx 5 \times 10^{-3}$ mol dm^{-3}, whereas for $AlCl_3$ this occurs at $\approx 5 \times 10^{-4}$ mol dm^{-3}. Clearly, the electrolyte concentration (which depends on the electrolyte's valency) must be chosen carefully to induce sufficient flocculation to prevent the formation of a dilatant sediment, but this concentration should not result in irreversible coagulation (i.e. primary minimum flocculation). With polyelectrolytes, irreversible coagulation is prevented as a result of the contribution of steric interaction (which operates at moderate concentrations of electrolyte).

The application of the concept of controlled flocculation to pharmaceutical suspensions has been discussed by various authors [13–16] who demonstrated how flocculation of a sulphaguanidine suspension, by $AlCl_3$, could be used for the preparation of readily dispersible suspensions, which after prolonged storage retain satisfactory physical properties. The work was extended to other types of drug suspensions such as griseofulvin, hydrocortisone and sulfamerazine [17]. The flocculation observed was interpreted with DLVO theory. It was suggested that flocculation occurs at a minimum whose depth is restricted owing to steric stabilization by the surfactant film. It should be mentioned that when using $AlCl_3$ in controlling the flocculation, hydrolysable species are produced above pH 4 and these species play a major role in controlling the flocculation.

For systems stabilized with nonionic surfactants or macromolecules, the energy–distance curve also shows a minimum whose depth depends on particle size and shape, Hamaker constant and adsorbed layer thickness δ. Thus for a given particulate system, having a given particle size and shape and Hamaker constant, the minimum depth can be controlled by varying the adsorbed layer thickness δ. This is illustrated in Fig. 13.19, where the energy–distance curves for polystyrene latex particles containing adsorbed polyvinyl alcohol (PVA) layers of various molecular weights, i.e. various δ values are shown. These calculations were made using the theory of Hesselink et al. [18] together with the experimentally measured parameters of δ [19]. It is clear from Fig. 13.19 that with the high molecular weight PVA fractions δ is large and the energy minimum is too small for flocculation to occur. This is certainly the case with $M = 43{,}000$ ($\delta = 19.7$ nm), $M = 28{,}000$ ($\delta = 14.0$ nm) and $M = 17{,}000$ ($\delta = 9.8$ nm). However with $M = 8{,}000$ ($\delta = 3.3$ nm) an appreciable attraction prevails at a separation distance in the region of 2δ. In this case a weakly flocculated open structure could be produced for preventing formation of dilatant sediments. To illustrate this point, dispersions stabilized with PVA of various M were slowly centrifuged at 50 g, and the sediment was freeze dried and examined by electron microscopy. The results are shown in Fig. 13.20, which clearly illustrates the close-packed sediment obtained with the high molecular weight PVA fractions and the weakly flocculated open structure obtained with the fraction with low molecular weight.

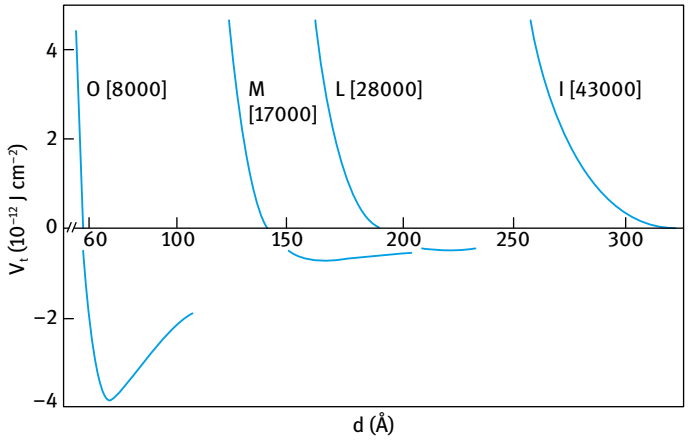

Fig. 13.19: Total energy of interaction versus separation distance for polystyrene latex with adsorbed layers of PVA of various thicknesses.

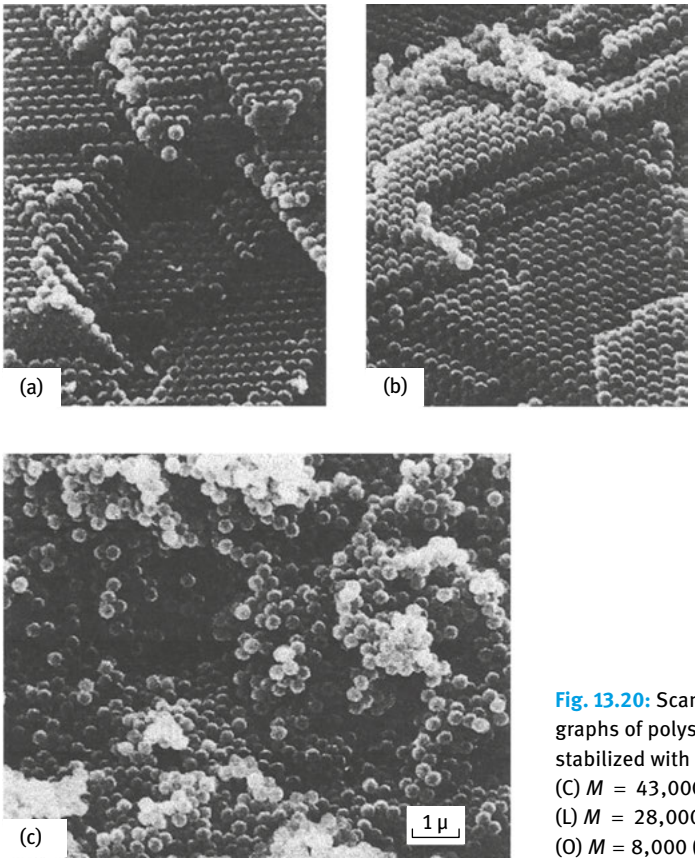

Fig. 13.20: Scanning electron micrographs of polystyrene latex sediments stabilized with PVA fractions:
(C) M = 43,000 (δ = 19.7 nm);
(L) M = 28,000 (δ = 14.0 nm);
(O) M = 8,000 (δ = 3.3 nm).

It should be mentioned that the minimum depth needed to induce flocculation depends on the volume fraction of the suspension. This can be understood, as discussed above, if one considers the balance between the interaction energy and entropy terms in the free energy of flocculation (equation (13.16)). The condition for flocculation is $\Delta G \leq 0$, and therefore the ΔG_h required for flocculation depends on the magnitude of the $T\Delta S_h$ term. The latter term decreases with increasing volume fraction ϕ, and hence the higher the ϕ value, the smaller the ΔG_h required for flocculation. This means that with more concentrated suspensions or emulsions, weak flocculation of a sterically stabilized suspension occurs at lower minimum depth.

13.4.6 Depletion flocculation

Addition of free nonadsorbing polymer can produce weak flocculation above a critical volume fraction of the free polymer, ϕ_p^+, which depends on its molecular weight and the volume fraction of suspension. This weak flocculation produces a "gel" structure that reduces sedimentation. According to Asakura and Oosawa [20, 21], when two particles approach each other within a distance of separation that is smaller than the diameter of the free polymer coil, exclusion of the polymer molecules from the interstices between the particles takes place, leading to the formation of a polymer-free zone. This is illustrated in Fig. 13.21, which shows the situation below and above ϕ_p^+. As a result of this process, an attractive energy, associated with the lower osmotic pressure in the region between the particles, is produced. Fleer et al. [22] derived the following expression for the interaction of hard spheres in the presence of nonadsorbing polymer, i.e. the decreases in free energy resulting from the transfer of solvent molecules from the depletion zone to bulk solution,

$$G_{dep} = \frac{2\pi R}{V_0}\left(\mu_1 - \mu_1^0\right)\Delta^2\left(1 + \frac{2\Delta}{3R}\right), \tag{13.17}$$

where V_0 is the molecular volume of the solvent, μ_1 is the solvent chemical potential at ϕ_p and μ_1^0 is the chemical potential of the pure solvent. Since $\mu_1 < \mu_1^0$, $(\mu_1 - \mu_1^0)$ is negative and G_{dep} is negative, resulting in flocculation.

The above phenomenon of flocculation can be applied to prevent settling and claying by forming an open structure that, under some conditions, can fill the whole volume of the suspension. Above ϕ_p^+, the suspension becomes weakly flocculated, and the extent of flocculation increases with a further increase in the concentration of free nonadsorbing polymer. This is illustrated for a suspension of an agrochemical (ethirimol, a fungicide) that is stabilized by a graft copolymer of poly(methyl methacrylate)/methacrylic acid with poly(ethylene oxide) side chains to which poly(ethylene oxide) (PEO) with M = 20,000, 35,000 or 90,000 is added for flocculation [23]. Rheological measurements showed that above ϕ_p^+ a rapid increase in the yield value is produced. This is shown in Fig. 13.22. Above ϕ_p^+ one would expect significant reduction in formation of dilatant sediments. This is illustrated in Fig. 13.23 which shows a

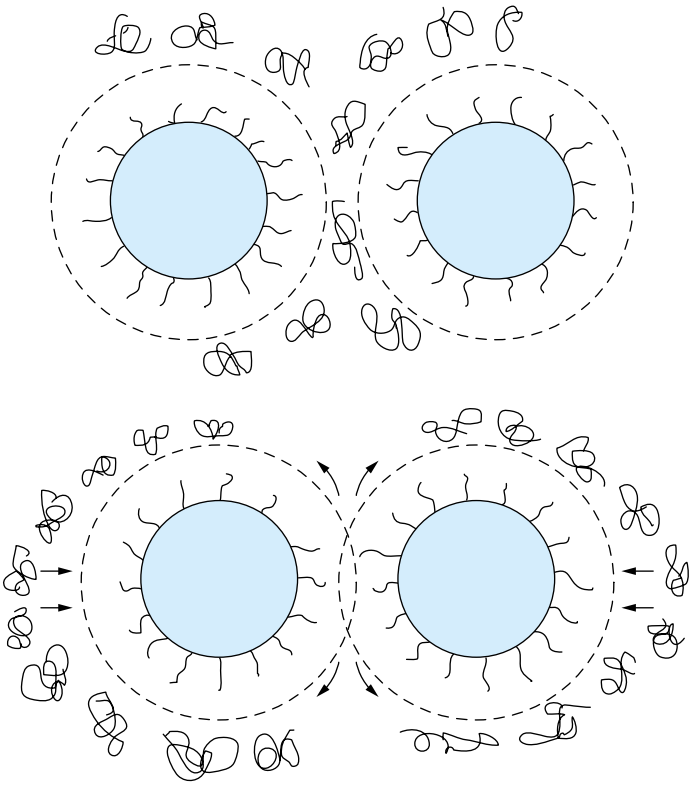

Fig. 13.21: Schematic representation of depletion flocculation.

plot of sediment height and number of revolutions for redispersion as a function of ϕ_p (for PEO 20,000). It is clear that addition of PEO results in weak flocculation and redispersion becomes easier. This redispersion is maintained up to $\phi_p = 0.04$ above which it becomes more difficult due to the increase in viscosity.

Another example for the application of depletion flocculation was obtained for the same suspension but using hydroxyethyl cellulose (HEC) with various molecular weights. The weak flocculation was studied using oscillatory measurements. Fig. 13.24 shows the variation of the complex modulus G^* with ϕ_p. Above a critical ϕ_p value (that depends on the molecular weight of HEC), G^* increases very rapidly with a further increase in ϕ_p. When ϕ_p reaches an optimum concentration, sedimentation is prevented. This is illustrated in Fig. 13.25 which shows the sediment volume in 10 cm cylinders as a function ϕ_p for various volume fractions of the suspension ϕ_s. At sufficiently high volume fraction of the suspensions ϕ_s and high volume fraction of free polymer ϕ_p a 100 % sediment volume is reached and this is effective in eliminating sedimentation and formation of dilatant sediments.

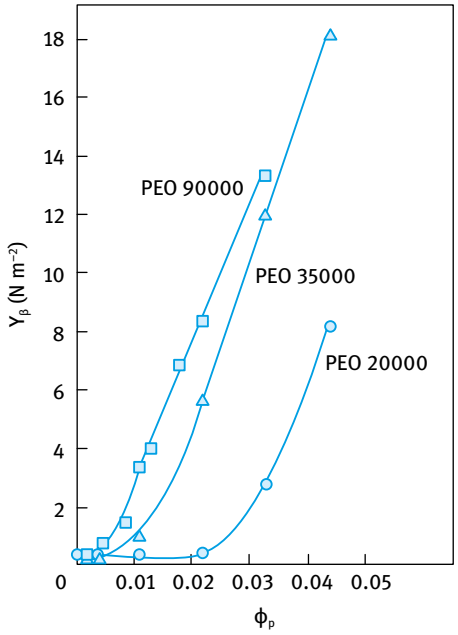

Fig. 13.22: Variation of yield value with PEO concentration.

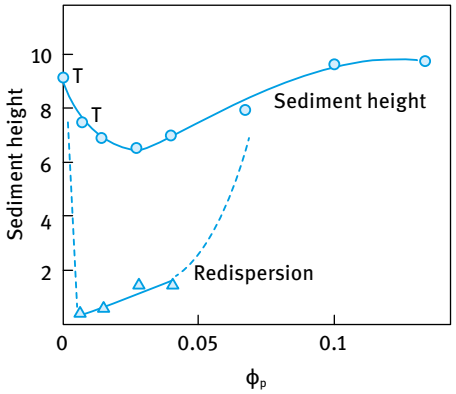

Fig. 13.23: Variation of sediment height and redispersion with ϕ_p for PEO 20,000.

The application of depletion flocculation to the reduction of creaming in emulsions was recently demonstrated by Abend et al. [24] who investigated the effect of adding xanthan gum to an O/W emulsion (the oil being Isopar V, a hydrocarbon oil) with a volume fraction $\phi = 0.5$, that was stabilized using an A–B–A block copolymer (with A being polyethylene oxide, PEO, and B being polypropylene oxide, PPO, containing 26.5 EO units and 29.7 PO units). The xanthan gum concentration was varied between 0.01 and 0.67 %. Fig. 13.26 shows the visual observation of the emulsions after 8 months of storage.

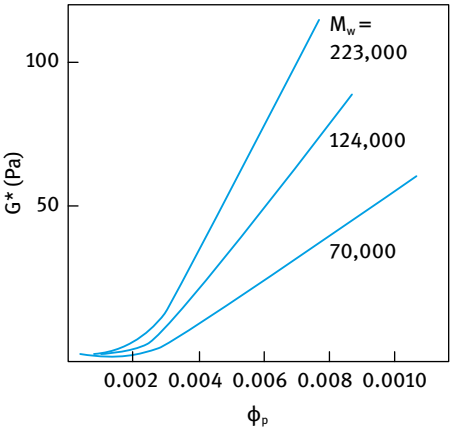

Fig. 13.24: Variation of G^* with ϕ_p for HEC with various molecular weights.

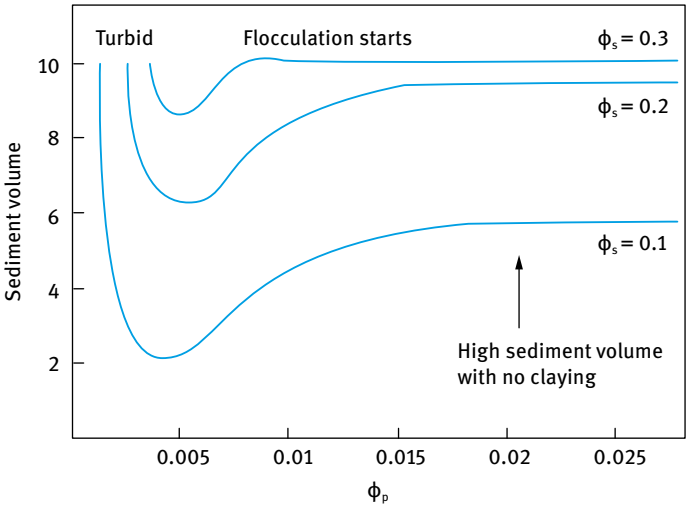

Fig. 13.25: Variation of sediment volume with ϕ_p for HEC (M = 70,000).

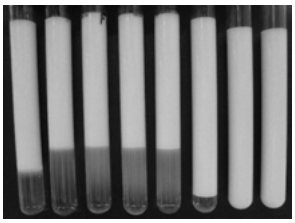

Fig. 13.26: Visual observation (after 8 months storage) of O/W emulsions (ϕ = 0.5) stabilized with an A–B–A block copolymer (PEO–PPO–PEO) at various xanthan gum concentrations; from left to right: 0.0, 0.01, 0.05, 0.1, 0.25, 0.50, 0.67 % xanthan gum.

It can be seen from Fig. 13.26 that initial addition of xanthan gum up to 0.1 % enhances the creaming of the emulsion as a result of depletion flocculation. The emulsion containing 0.25 % xanthan gum shows less creaming, but phase separation did occur. However, at 0.5 and 0.67 % xanthan gum no creaming occurred after storage for 8 months. At a concentration of 0.5 and 0.67 % xanthan gum, the arrested network formed by the droplets appears now to be strong enough to withstand the gravitational stress (creaming) and no clear water phase is visible at the bottom of the vessel even after eight months of storage.

Thus, weak flocculation can be applied to reduce creaming or sedimentation although it suffers from the following drawbacks:

(i) Temperature dependency; as the temperature increases, the hydrodynamic radius of the free polymer decreases (due to dehydration) and hence more polymer will be required to achieve the same effect at lower temperatures.
(ii) If the free polymer concentration is below a certain limit, phase separation may occur and the flocculated emulsion droplets may cream or sediment faster than in the absence of the free polymer.

13.4.7 Use of "inert" fine particles

Several fine particulate inorganic material produce "gels" when dispersed in aqueous media, e.g. sodium montmorillonite or silica. These particulate materials produce three-dimensional structures in the continuous phase as a result of interparticle interaction. For example, sodium montmorillonite (referred to as swellable clay) forms gels at low and intermediate electrolyte concentrations. This can be understood from a knowledge of the structure of the clay particles. These consist of plate-like particles consisting of an octahedral alumina sheet sandwiched between two tetrahedral silica sheets. This is shown schematically in Fig. 13.27, which also shows the change in the spacing of these sheets. In the tetrahedral sheet tetravalent Si is sometimes replaced by trivalent Al. In the octahedral sheet there may be replacement of trivalent Al by divalent Mg, Fe, Cr or Zn. The small size of these atoms allows them to take the place of small Si and Al. This replacement is usually referred to as isomorphic substitution whereby an atom of lower positive valence replaces one of higher valence, resulting in a deficit of positive charge or excess of negative charge. This excess of negative layer charge is compensated by adsorption at the layer surfaces of cations that are too big to be accommodated in the crystal. In aqueous solution, the compensation cations on the layer surfaces may be exchanged by other cations in solution, and hence may be referred to as exchangeable cations. With montmorillonite, the exchangeable cations are located on each side of the layer in the stack, i.e. they are present in the external surfaces as well as between the layers. This causes a slight increase of the local spacing from about 9.13 Å to about 9.6 Å; the difference depends on the nature of the counterion.

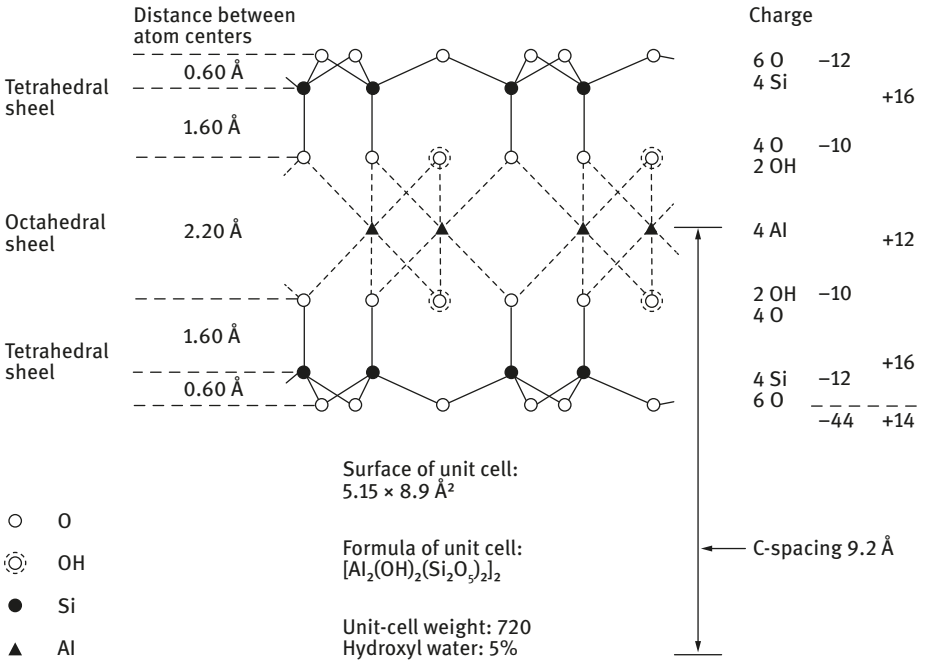

Fig. 13.27: Atom arrangement in one unit cell of 2 : 1 layer mineral.

When montmorillonite clays are placed in contact with water or water vapour the water molecules penetrate between the layers, causing interlayer swelling or (intra) crystalline swelling. This leads to a further increase in the basal spacing to 12.5–20 Å, depending on the type of clay and cation. This interlayer swelling leads, at most, to doubling of the volume of the dry clay when four layers of water are adsorbed. The much larger degree of swelling, which is the driving force for "gel" formation (at low electrolyte concentration) is due to osmotic swelling. It has been suggested that swelling of montmorillonite clays is due to the electrostatic double layers that are produced between the charge layers and cations. This is certainly the case at low electrolyte concentration where the double layer extension (thickness) is large.

As discussed above, the clay particles carry a negative charge as a result of isomorphic substitution of certain electropositive elements by elements of lower valency. The negative charge is compensated by cations, which in aqueous solution form a diffuse layer, i.e. an electric double layer is formed at the clay plate/solution interface. This double layer has a constant charge, which is determined by the type and degree of isomorphic substitution. However, the flat surfaces are not the only surfaces of the plate-like clay particles, they also expose an edge surface. The atomic structure of the edge surfaces is entirely different from that of the flat layer surfaces. At the edges, the tetrahedral silica sheets and the octahedral alumina sheets are disrupted, and the primary bonds are broken. The situation is analogous to that of the surface of silica and

alumina particles in aqueous solution. On such edges, therefore, an electric double layer is created by adsorption of potential determining ions (H^+ and OH^-) and one may, therefore identify an isoelectric point (IEP) as the point of zero charge (pzc) for these edges. With broken octahedral sheets at the edge, the surface behaves as Al-OH with an IEP in the region of pH 7–9. Thus in most cases the edges become negatively charged above pH 9 and positively charged below pH 9.

Van Olphen [25] suggested a mechanism of gel formation of montmorillonite involving interaction of the oppositely charged double layers at the faces and edges of the clay particles. This structure, which is usually referred to as a "card-house" structure, was considered to be the reason for the formation of the voluminous clay gel. However, Norrish [26] suggested that the voluminous gel is the result of the extended double layers, particularly at low electrolyte concentrations. A schematic picture of gel formation produced by double layer expansion and "card-house" structure is shown in Fig. 13.28.

Evidence for the above picture was obtained by van Olphen [10] who measured the yield value of 3.22 % montmorillonite dispersions as a function of NaCl concentration as shown in Fig. 13.29.

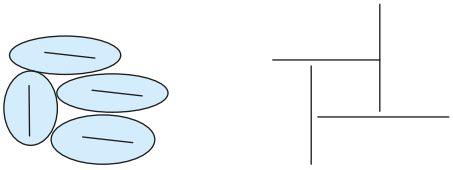

(a) Gels produced by Double layer overlap

(b) Gels produced by edge-to-face association

Fig. 13.28: Schematic representation of gel formation in aqueous clay dispersions.

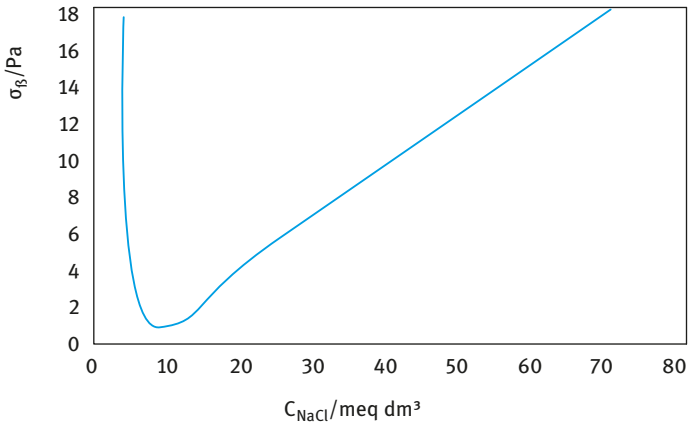

Fig. 13.29: Variation of yield value with NaCl concentration for 3.22 % sodium montmorillonite dispersions.

When $C = 0$, the double layers are extended and gel formation is due to double layer overlap (Fig. 13.28 (a)). The first addition of NaCl causes compression of the double layers and hence the yield value decreases very rapidly. At intermediate NaCl concentrations, gel formation occurs as a result of face-to-edge association (house of cards structure) (Fig. 13.28 (b)) and the yield value increases very rapidly with increasing NaCl concentration. If the NaCl concentration is increased further, face-to-face association may occur and the yield value decreases (the gel is destroyed).

Finely divided silica such as Aerosil 200 (produced by Degussa) produces gel structures by simple association (by van der Waals attraction) of the particles into chains and cross chains. When incorporated into the continuous phase of a suspension, these gels prevent sedimentation.

13.4.8 Use of mixtures of polymers and finely divided particulate solids

By combining thickeners such as hydroxyethyl cellulose or xanthan gum with particulate solids such as sodium montmorillonite, a more robust gel structure could be produced. By using such mixtures, the concentration of the polymer can be reduced, thus overcoming the problem of dispersion on dilution (e.g. with many agrochemical suspension concentrates). This gel structure may be less temperature dependent and could be optimized by controlling the ratio of the polymer and the particles. If these combinations of, say, sodium montmorillonite and a polymer such as hydroxyethyl cellulose, polyvinyl alcohol (PVA) or xanthan gum, are balanced properly, they can provide a "three-dimensional structure", which entraps all the particles and stop settling and formation of dilatant clays. The mechanism of gelation of such combined systems depends to a large extent on the nature of the solid particles, the polymer and the conditions. If the polymer adsorbs on the particle surface (e.g. PVA on sodium montmorillonite or silica) a three-dimensional network may be formed by polymer bridging. Under conditions of incomplete coverage of the particles by the polymer, the latter becomes simultaneously adsorbed on two or more particles. In other words, the polymer chains act as "bridges" or "links" between the particles.

13.4.9 Use of liquid crystalline phases

Surfactants produce liquid crystalline phases at high concentrations. Three main types of liquid crystals can be identified as illustrated in Fig. 13.30: hexagonal phase (sometimes referred to as middle phase), cubic phase and lamellar (neat) phase. All these structures are highly viscous and they also show elastic response. If produced in the continuous phase of suspensions, they can eliminate sedimentation of the particles. These liquid crystalline phases are particularly useful for application in liquid detergents which contain high surfactant concentrations. Their presence reduces sedimentation of the coarse builder particles (phosphates and silicates).

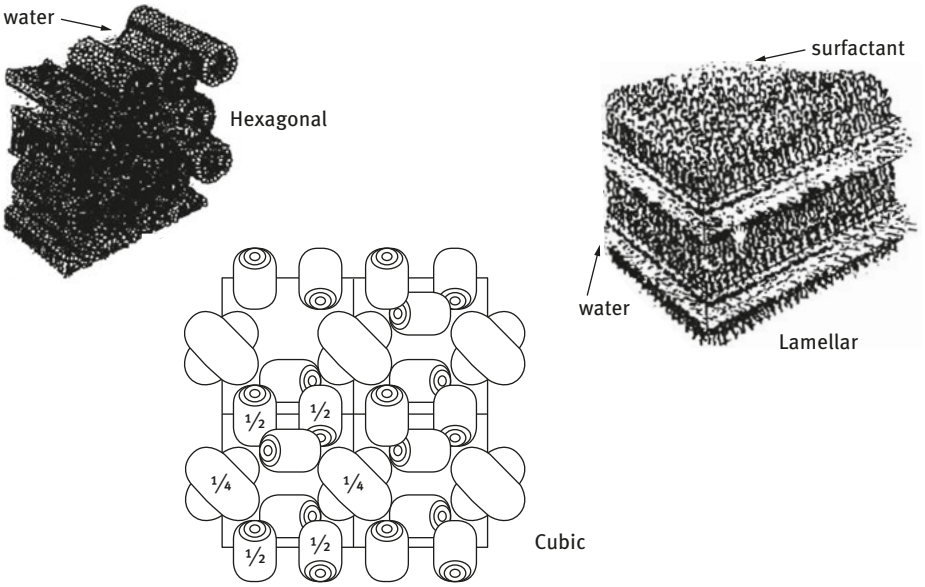

Fig. 13.30: Schematic picture of liquid crystalline phases.

References

[1] Tadros T. Suspension concentrates. Berlin: De Gruyter; 2017.
[2] Tadros T. Emulsions. Berlin: De Gruyter; 2016.
[3] Bachelor GK. J Fluid Mech. 1972;52:245.
[4] Bachelor GK. J Fluid Mech. 1976; 79:1.
[5] Krieger IM, Advances Colloid and Interface Sci. 1971;3:45.
[6] Buscall R, Goodwin JW, Ottewill RH, Tadros TF. J Colloid Interface Sci. 1982;85:78.
[7] de Gennes PG. Scaling concepts of polymer physics. Ithaca: Cornell University Press; 1979.
[8] Tadros T. Rheology of dispersions. Weinheim: Wiley-VCH; 2010.
[9] Happel J, Brenner H. Low Reynolds number hydrodynamics. London: Prentice Hall; 1965.
[10] Deryaguin BV, Landau L. Acta Physicochem USSR. 1941;14:633.
[11] Verwey EJW, Overbeek JTG. Theory of stability of lyophobic colloids. Amsterdam: Elsevier; 1948.
[12] Tadros TF. Colloids and Surfaces. 1986; 18:427.
[13] Haines BS, Martin AN. J Pharm Sci. 1961;50:228;723;756.
[14] Wilson RG, Canow BE. J Pharm Sci. 1963;50:757.
[15] Mathews BA, Rhodes CT, J Pharm Sci. 1986;57:557;569.
[16] Jones RDC, Mathews BA, Rhodes CT. J Pharm Sci. 1971:59:529.
[17] Mathews BA, Rhodes CT. J Pharm Sci. 1971;59:529.
[18] Hesselink FT, Vrij A, Overbeek JTG. J Phys Chem. 1971;75:2094.
[19] Garvey MJ, Tadros TF, Vincent B. J Colloid Interface Sci. 1976;55:440.
[20] Asakura A, Oosawa F. J Chem Phys. 1954;22:1235.
[21] Asakura A, Oosawa F. J Polymer Sci. 1958;33:183.
[22] Fleer GJ, Scheutjens JMHM, Vincent B. ACS Symposium Series. 1984:240;245.

[23] Heath D, Knott RD, Knowles DA, Tadros TF. ACS Symposium Series. 254.
[24] Abend S, Holtze C, Tadros T, Schutenberger P. Langmuir. 2012;28:7967.
[25] van Olphen H. Clay colloid chemistry. New York: Wiley; 1963.
[26] Norrish K. Discussion Faraday Soc. 1954;18:120.

14 Flow characteristics (rheology) of formulations

14.1 Introduction

Investigations on the flow characteristics, or rheology, of formulations are of considerable importance in a number of aspects. For example, the rheology of the formulation can be applied for evaluating the stability/instability of the system without any dilution (which can cause significant changes in the structure of the system) and this requires carefully designed techniques that should cause as little disturbance to the structure as possible [1–7]. These measurements provide accurate information on the state of the system such as its creaming or sedimentation, flocculation and coalescence. These measurements are also applied for predicting the long-term physical stability of the dispersion. As we will see in this chapter, the flow behaviour of most formulations is non-Newtonian, which means that their viscosity depends on the applied shear rate. In addition, some formulations show reversible time dependency of their viscosity (described as thixotropy), which finds application in many systems such as paint formulations. The rheology of any formulation has an important effect on its application. For example, a paint system is formulated in such a way that gives a high viscosity at low shear rates (to avoid its separation), but when applied by a brush or roller, the viscosity decreases significantly to allow flow and uniform coating to the surface. When the brushing or rolling is stopped, the viscosity of the system must recover in a controlled time period. If recovery is too slow, dripping of the paint may occur, whereas if the recovery is too fast the paint may show brush marks and this gives a non-smooth coating. In other applications in agrochemical formulations, the system must fluidize on shaking and it should spontaneously disperse on dilution. The rheological characteristics of most cosmetic and personal care formulations, such as hand creams and lotions, have important impact on the aesthetic characteristics of the system such as its skin feel, spreadability, etc.

In this chapter, I will start with a description of the various rheological techniques that can be applied to study the state of the formulation. This is followed by an analysis of the rheological behaviour of the different disperse systems. Four main types of systems will be considered, namely hard-sphere dispersions (where both repulsion and attraction are screened), electrostatically stabilized dispersions (where the rheology is mainly determined by double layer repulsion), sterically stabilized dispersions (where the rheology is determined by steric repulsion) and flocculated dispersions. In the latter case a distinction will be made between weakly and strongly flocculated systems. This is followed by a section on the application of rheological techniques for assessment and prediction of the long-term physical stability of the formulation.

https://doi.org/10.1515/9783110587944-015

14.2 Rheological techniques

Four different types of rheological techniques can be applied and these are summarized below.

14.2.1 Steady state shear stress σ–shear rate γ measurements

In this case, the dispersion is placed in the gap between two concentric cylinders (Fig. 14.1), two parallel plates or a cone and plate geometry (Fig. 14.2). In the latter geometry, the cone is truncated to avoid damage of the tip of the cone and to have sufficient gap in order to avoid grinding of the dispersion. The inner cylinder or the cone is subjected to an angular rotation Ω which allows one to calculate the shear rate $\dot{\gamma}$. The torque M on the outer cylinder or the plate is measured and this allows one to obtain the stress σ. This requires the use of a shear rate controlled instrument [1].

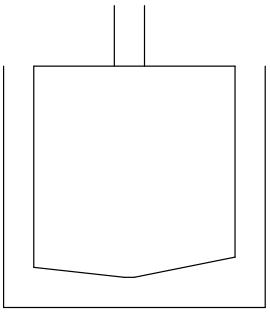

Fig. 14.1: Schematic picture of a concentric cylinder.

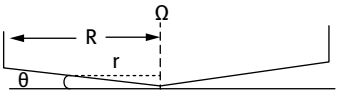

(a) Cone and plate

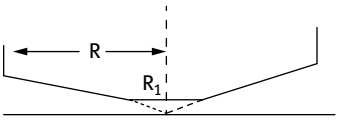

(b) Truncated cone and plate

Fig. 14.2: Schematic picture of the cone and plate.

Most dispersions, particularly those with high volume fraction and/or containing rheology modifiers, do not obey Newton's law. This can be clearly shown from plots of shear stress σ versus shear rate as illustrated in Fig. 14.3. Five different flow curves can be identified:

(a) Newtonian;
(b) Bingham plastic;
(c) pseudoplastic (shear thinning);
(d) dilatant (shear thickening);
(e) yield stress and shear thinning.

The variation of viscosity with shear rate for the above five systems is shown in Fig. 14.4. Apart from the Newtonian flow (a) all other systems show a change of viscosity with applied shear rate.

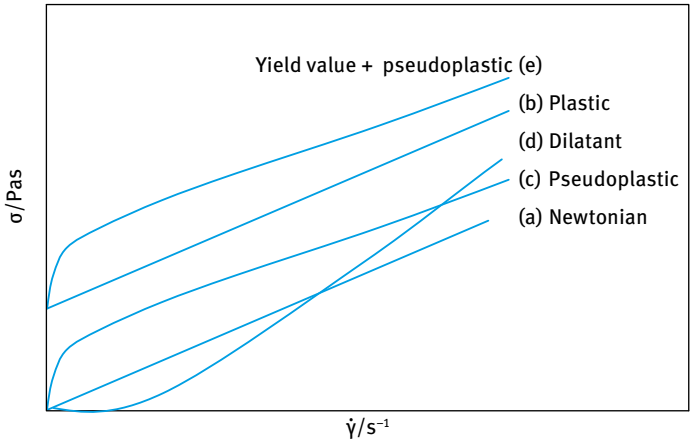

Fig. 14.3: Flow curves for various systems.

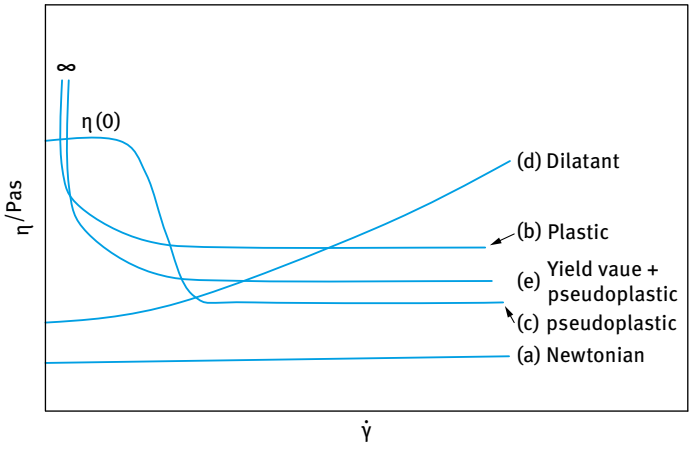

Fig. 14.4: Viscosity–shear rate relationship.

14.2.2 Rheological models for analysis of flow curves

14.2.2.1 Newtonian systems

$$\sigma = \eta\dot{\gamma}. \tag{14.1}$$

η is independent of the applied shear rate, e.g. simple liquids and very dilute dispersions.

14.2.2.2 Bingham plastic systems [8]

$$\sigma = \sigma_\beta + \eta_{\mathrm{pl}}\dot{\gamma} \tag{14.2}$$

The system shows a (dynamic) yield stress σ_β that can be obtained by extrapolation to zero shear rate. Clearly, at and below σ_β the viscosity $\eta \to \infty$. The slope of the linear curve gives the plastic viscosity η_{pl}. Some systems like clay suspensions may show a yield stress above a certain clay concentration.

The Bingham equation describes the shear stress/shear rate behaviour of many shear thinning materials at low shear rates. Unfortunately, the value of σ_β obtained depends on the shear rate ranges used for the extrapolation procedure.

14.2.2.3 Pseudoplastic (shear thinning) system

In this case the system does not show a yield value. It shows a limiting viscosity $\eta(0)$ at low shear rates (that is referred to as residual or zero shear viscosity). The flow curve can be fitted to a power law fluid model (Ostwald de Waele),

$$\sigma = k\dot{\gamma}^n, \tag{14.3}$$

where k is the consistency index and n is the shear thinning index ($n < 1$).

By fitting the experimental data to equation (14.3) one can obtain k and n. The viscosity at a given shear rate can be calculated

$$\eta = \frac{\sigma}{\dot{\gamma}} = \frac{k\dot{\gamma}^n}{\dot{\gamma}} = k\dot{\gamma}^{n-1}. \tag{14.4}$$

The power law model (equation (14.3)) fits the experimental results for many non-Newtonian systems over two or three decades of shear rate. Thus, this model is more versatile than the Bingham model, although one should be careful in applying this model outside the range of data used to define it. In addition, the power law fluid model fails at high shear rates, whereby the viscosity must ultimately reach a constant value, i.e. the value of n should approach unity.

14.2.2.4 Dilatant (shear thickening) system

In some cases the very act of deforming a material can cause rearrangement of its microstructure such that the resistance to flow increases with increasing shear rate. In other words, the viscosity increases with applied shear rate and the flow curve can be

fitted with the power law, equation (14.3), but in this case $n > 1$. The shear thickening regime extends over only about a decade of shear rate. In almost all cases of shear thickening, there is a region of shear thinning at low shear rates.

Several systems can show shear thickening such as wet sand, corn starch dispersed in milk and some polyvinyl chloride sols. Shear thickening can be illustrated when one walks on wet sand whereby some water is "squeezed out" and the sand appears dry. The deformation applied by one's foot causes rearrangement of the close-packed structure produced by the water motion. This process is accompanied by volume increase (hence the term dilatancy) as a result of "sucking in" of the water. The process amounts to a rapid increase in the viscosity.

14.2.2.5 Herschel–Bulkley general model [9]

Many systems show a dynamic yield value followed by a shear thinning behaviour. The flow curve can be analysed using the Herschel–Bulkley equation:

$$\sigma = \sigma_\beta + k\dot{\gamma}^n. \tag{14.5}$$

When $\sigma_\beta = 0$, equation (14.5) reduces to the power fluid model. When $n = 1$, equation (14.5) reduces to the Bingham model. When $\sigma_\beta = 0$ and $n = 1$, equation (14.5) becomes the Newtonian equation. The Herschel–Bulkley equation fits most flow curves with a good correlation coefficient and hence it is the most widely used model.

14.2.2.6 The Casson model [10]

This is a semi-empirical linear parameter model that has been applied to fit the flow curves of many paints and printing ink formulations,

$$\sigma^{1/2} = \sigma_C^{1/2} + \eta_C^{1/2}\dot{\gamma}^{1/2}. \tag{14.6}$$

Thus a plot of $\sigma^{1/2}$ versus $\dot{\gamma}^{1/2}$ should give a straight line from which σ_C and η_C can be calculated from the intercept and slope of the line. One should be careful in using the Casson equation since straight lines are only obtained from the results above a certain shear rate.

14.2.2.7 The Cross equation [11]

This can be used to analyse the flow curve of shear thinning systems that show a limiting viscosity $\eta(0)$ in the low shear rate regime and another limiting viscosity $\eta(\infty)$ in the high shear rate regime. These two regimes are separated by a shear thinning behaviour as schematically shown in Fig. 14.5,

$$\frac{\eta - \eta(\infty)}{\eta(0) - \eta(\infty)} = \frac{1}{1 + K\dot{\gamma}^m}, \tag{14.7}$$

where K is a constant parameter with dimension of time and m is a dimensionless constant.

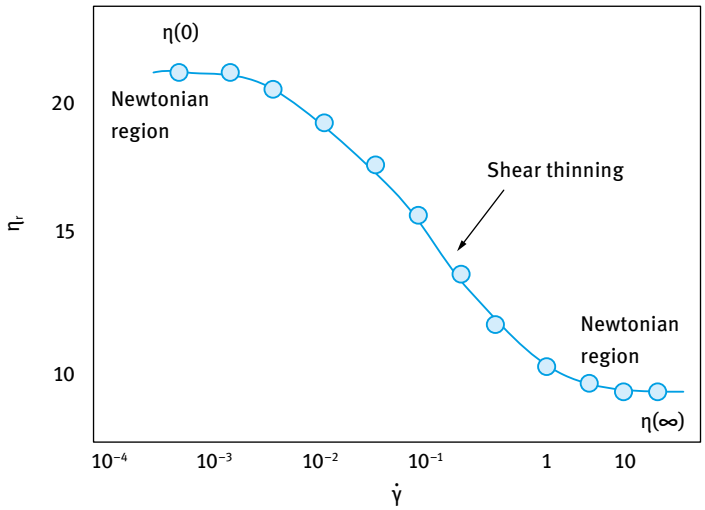

Fig. 14.5: Viscosity versus shear rate for shear thinning system.

An equivalent equation to (14.7) is,

$$\frac{\eta_0 - \eta}{\eta - \eta_\infty} = (K\dot{\gamma}^m). \tag{14.8}$$

14.2.3 Time effects during flow – thixotropy and negative (or anti-)thixotropy

When a shear rate is applied to a non-Newtonian system, the resulting stress may not be achieved simultaneously.

(i) The molecules or particles will undergo spatial rearrangement to follow the applied flow field.
(ii) The structure of the system may change: breaking of weak bonds; aligning of irregularly shaped particles; collision of particles to form aggregates.

The above changes are accompanied by a decrease or increase of viscosity with time at any given shear rate. These changes are referred to as thixotropy (if the viscosity decreases with time) or negative thixotropy or anti-thixotropy (if the viscosity increases with time).

Thixotropy refers to the reversible, time-dependent decease of viscosity. When the system is sheared for some time, the viscosity decreases but when the shear is stopped (the system is left to rest) the viscosity of the system is restored. Practical examples for systems that show thixotropy are: paint formulations (sometimes referred to as thixotropic paints); tomato ketchup; some hand creams and lotions.

Negative thixotropy or *antithixotropy*: when the system is sheared for some time, the viscosity increases but when the shear is stopped (the system is left to rest) the viscosity decreases. A practical example of the above phenomenon is corn starch suspended in milk.

Generally speaking, two methods can be applied to study thixotropy in a suspension. The first and the most commonly used procedure is the loop test whereby the shear rate is increased continuously and linearly in time from zero to some maximum value and then decreased to zero in the same way. This is illustrated in Fig. 14.6. The main problem with this procedure is the difficulty of interpreting the results. The nonlinear approach used is not ideal for developing loops because by decoupling the relaxation process from the strain one does not allow the recovery of the material. However, the loop test gives the qualitative behaviour of the suspension thixotropy.

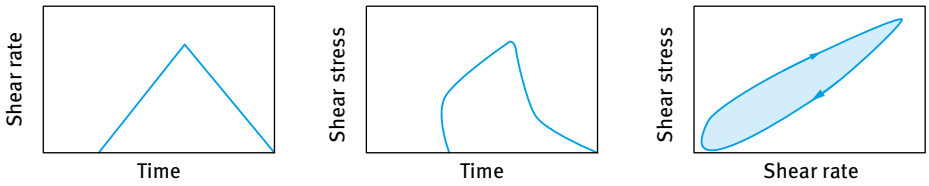

Fig. 14.6: Loop test for studying thixotropy.

An alternative method for studying thixotropy is to apply a step change test, whereby the suspension is suddenly subjected to a constant high shear rate and the stress is followed as a function of time during which the structure breaks down and an equilibrium value is reached. The stress is further followed as a function of time to evaluate the rebuilding of the structure. A schematic representation of this procedure is shown in Fig. 14.7.

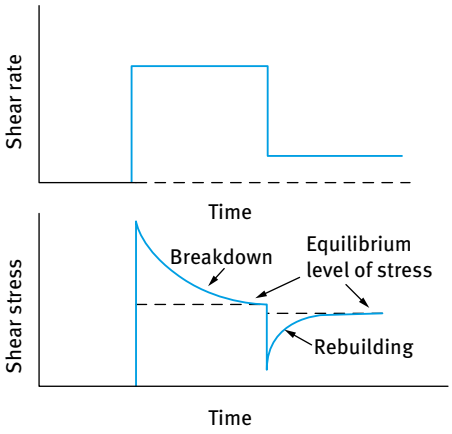

Fig. 14.7: Step change for studying thixotropy.

14.2.4 Strain relaxation after sudden application of stress – constant stress (creep) measurements

A constant stress σ is applied on the system (that may be placed in the gap between two concentric cylinders or a cone and plate geometry) and the strain (relative deformation) γ or compliance J ($= \gamma/\sigma$, Pa^{-1}) is followed as a function of time for a period of t. At $t = t$, the stress is removed and the strain γ or compliance J is followed for another period t [1].

The above procedure is referred to as "creep measurement". From the variation of J with t when the stress is applied and the change of J with t when the stress is removed (in this case J changes sign) one can distinguish between viscous, elastic and viscoelastic responses as illustrated in Fig. 14.8.

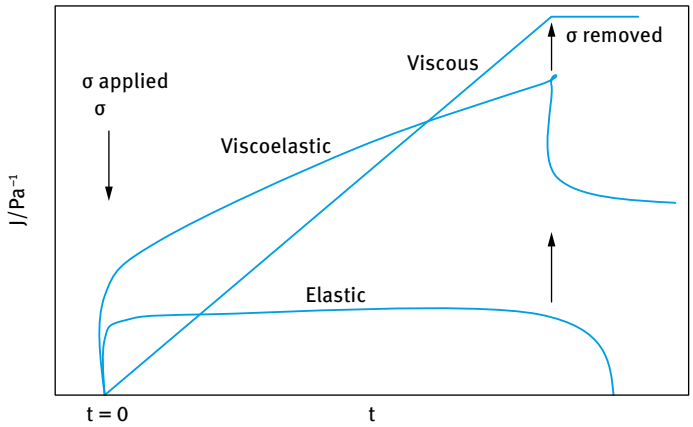

Fig. 14.8: Creep curves for viscous, elastic and viscoelastic response.

Viscous response: In this case the compliance J shows a linear increase with increasing time, reaching a certain value after time t. When the stress is removed after time t, J remains the same, i.e. in this case no creep recovery occurs.

Elastic response: In this case the compliance J shows a small increase at $t = 0$ and it remains almost constant for the whole period t. When the stress is removed, J changes sign and it reaches 0 after some time t, i.e. complete creep recovery occurs in this case.

Viscoelastic response: at $t = 0$, J shows a sudden increase and this is followed by a slower increase for the time applied. When the stress is removed, J changes sign and J shows an exponential decrease with increasing time (creep recovery) but it does not reach 0 as in the case of an elastic response.

14.2.4.1 Analysis of creep curves

Viscous fluid

The linear curve of J versus t gives a slope that is equal to the reciprocal viscosity,

$$J(t) = \frac{\gamma}{\sigma} = \frac{\dot{\gamma} t}{\sigma} = \frac{t}{\eta(0)}. \tag{14.9}$$

Elastic solid

The increase of compliance at $t = 0$ (rapid elastic response) $J(t)$ is equal to the reciprocal of the instantaneous modulus $G(0)$,

$$J(t) = \frac{1}{G(0)}. \tag{14.10}$$

Viscoelastic response

Viscoelastic liquid. Fig. 14.9 shows the case for a viscoelastic liquid where the compliance $J(t)$ is given by two components: an elastic component J_e that is given by the reciprocal of the instantaneous modulus, and a viscous component J_v that is given by $t/\eta(0)$,

$$J(t) = \frac{1}{G(0)} + \frac{t}{\eta(0)}. \tag{14.11}$$

Fig. 14.9 also shows the recovery curve which gives $\sigma_0 J_e 0$ and when this is subtracted from the total compliance gives $\sigma_0 t/\eta(0)$.

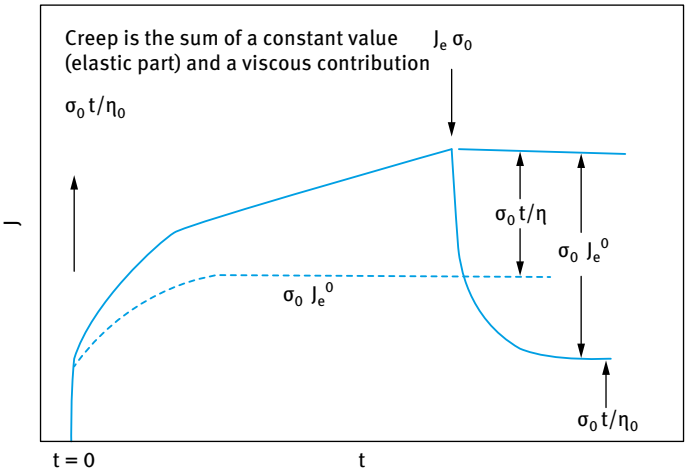

Fig. 14.9: Creep curve for a viscoelastic liquid.

The driving force for relaxation is spring and the viscosity controls the rate. The Maxwell relaxation time τ_M is given by,

$$\tau_M = \frac{\eta(0)}{G(0)}. \tag{14.12}$$

Viscoelastic solid. In this case complete recovery occurs as illustrated in Fig. 14.10 The system is characterized by a Kelvin retardation time τ_k that is also given by the ratio of $\eta(0)/G(0)$.

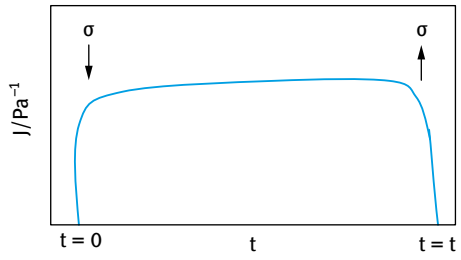

Fig. 14.10: Creep curve for a viscoelastic solid.

14.2.4.2 Creep procedure

In creep experiments one starts with a low applied stress (below the critical stress σ_{cr}, see below) at which the system behaves as a viscoelastic solid with complete recovery as illustrated in Fig. 14.10. The stress is gradually increased and several creep curves are obtained. Above σ_{cr}, the system behaves as a viscoelastic liquid showing only partial recovery as illustrated in Fig. 14.9. Fig. 14.11 shows a schematic representation of the variation of compliance J with time t at increasing σ (above σ_{cr}).

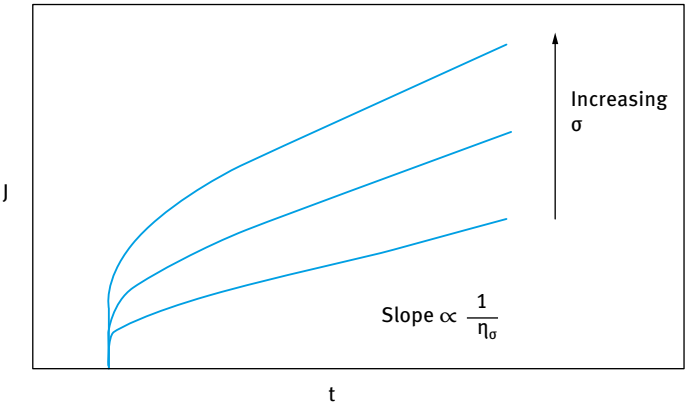

Fig. 14.11: Creep curves at increasing applied stress.

From the slopes of the lines one can obtain the viscosity η_σ at each applied stress. A plot of η_σ versus σ is shown in Fig. 14.12. This shows a limiting viscosity $\eta(0)$ below σ_{cr}, and above σ_{cr} the viscosity shows a sharp decrease with a further increase in σ. $\eta(0)$ is referred to as the residual or zero shear viscosity which is an important parameter for predicting sedimentation. σ_{cr} is the critical stress above which the structure "breaks down". It is sometimes referred to as the "true" yield stress.

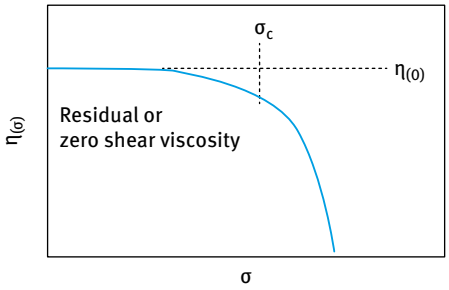

Critical stress is a useful parameter (related to yield stress) as denotes the stress at which structure „breaks down"

Fig. 14.12: Variation of viscosity with applied stress.

14.2.5 Stress relaxation after sudden application of strain

In this case a small strain is rapidly applied within a very short period of time (that must be smaller than the relaxation time of the system) and is kept at a constant value. The shear rate remains constant within this period [1]. This is illustrated in Fig. 14.13.

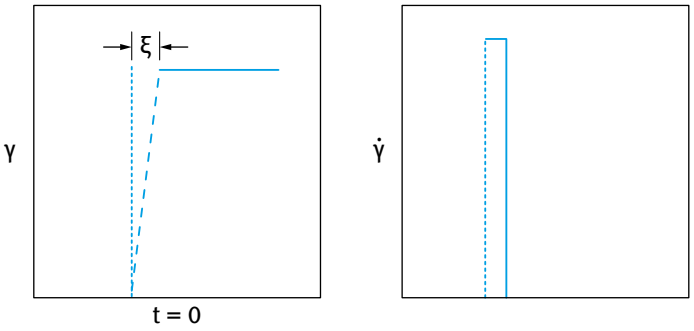

Fig. 14.13: Schematic representation of a strain experiment.

The stress will follow the strain and increases to a maximum value $\sigma(0)$. For a perfectly elastic material, $\sigma(0)$ remains constant over time t. For a viscoelastic liquid, the stress decreases exponentially with time reaching 0 at infinite time. The stress required to maintain a constant strain decreases with time due to viscous flow. This is illustrated in Fig. 14.14. For a viscoelastic solid, the stress reaches a limiting value at infinite time. The variation of stress with time is similar to a kinetic process represented by first-order equations.

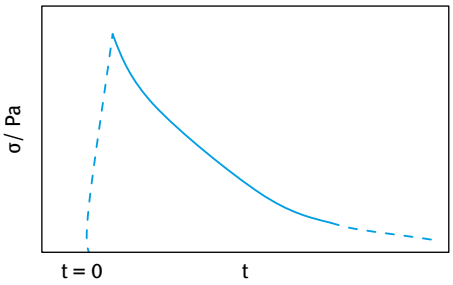

Fig. 14.14: Stress relaxation after sudden application of strain.

The stress $\sigma(t)$ is related to the initial maximum stress $\sigma(0)$ by,

$$\sigma(t) = \sigma(0)\exp\left(-\frac{t}{\tau_m}\right), \tag{14.13}$$

where τ_m is the Maxwell relaxation time that is given by the ratio of the viscosity η to the modulus G

$$\tau_m = \frac{\eta}{G}. \tag{14.14}$$

If the shear stress in equation (14.13) is divided by the applied strain γ one obtains the shear modulus $G(t)$,

$$G(t) = \frac{\sigma(t)}{\gamma} = \frac{\sigma(0)}{\gamma}\exp\left(-\frac{t}{\tau_m}\right) = G(0)\exp\left(-\frac{t}{\tau_m}\right). \tag{14.15}$$

Fig. 14.15 shows the variation of the modulus G with time for a viscoelastic liquid whereas Fig. 14.16 shows the trend for a viscoelastic solid.

For a viscoelastic solid the modulus reaches a limiting value G_e at long time (sometimes referred to as the equilibrium modulus). In this case equation (14.15) has to be modified to account for G_e,

$$G(t) = G(0)\exp\left(-\frac{t}{\tau_m}\right) + G_e. \tag{14.16}$$

Note that according to equations (14.8) and (14.10) that $t = \tau_m$ when $\sigma(t) = \sigma(0)/e$ or when $G(t) = G(0)/e$. This shows that stress relaxation can be used to obtain the relaxation time for a viscoelastic liquid.

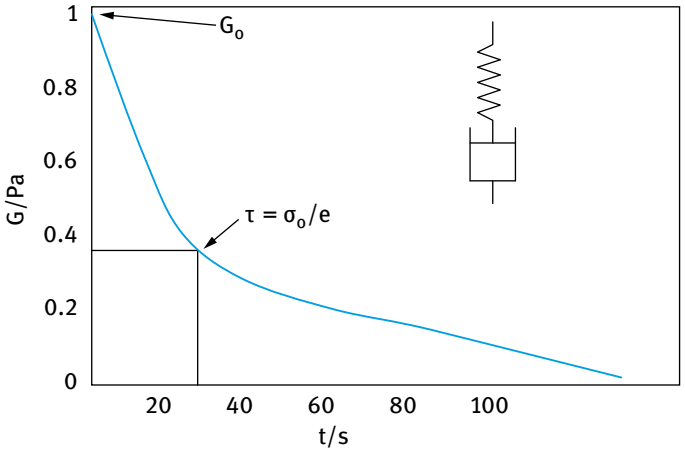

Fig. 14.15: Variation of modulus with time for a viscoelastic liquid.

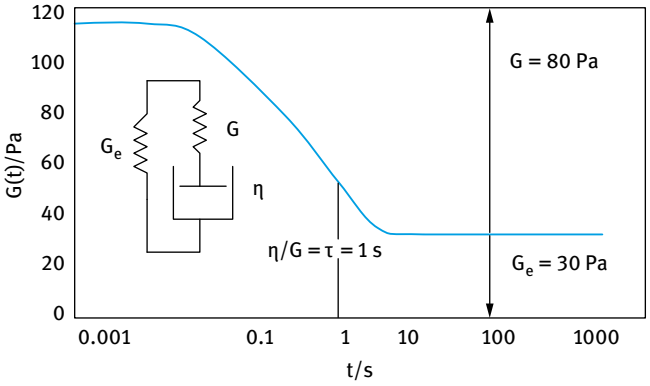

Fig. 14.16: Variation of $G(t)$ with t for a viscoelastic solid.

14.2.6 Dynamic (oscillatory) measurements [1]

This is the response of the material to an oscillating stress or strain. When a sample is constrained in, say, a cone and plate or concentric cylinder assembly, an oscillating strain at a given frequency ω (rad s^{-1}) ($\omega = 2\pi\nu$, where ν is the frequency in cycles s^{-1} or Hz) can be applied to the sample. After an initial start-up period, a stress develops in response to the applied strain, i.e. it oscillates with the same frequency. The change in the sine waves of the stress and strain with time can be analysed to distinguish between elastic, viscous and viscoelastic response. Analysis of the resulting sine waves can be used to obtain the various viscoelastic parameters as discussed below. Three cases can be considered:

Elastic response: whereby the maximum of the stress amplitude is at the same position as the maximum of the strain amplitude (no energy dissipation). In this case there no time shift between stress and strain sine waves.

Viscous response: whereby the maximum of the stress is at the point of maximum shear rate (i.e. the inflection point) where there is maximum energy dissipation. In this case the strain and stress sine waves are shifted by $\omega t = \pi/2$ (referred to as the phase angle shift δ which in this case is 90°).

Viscoelastic response: in this case the phase angle shift δ is greater than 0 but less than 90°.

14.2.6.1 Analysis of oscillatory response for a viscoelastic system

Let us consider the case of a viscoelastic system. The sine waves of strain and stress are shown in Fig. 14.17. The frequency ω is in rad s^{-1} and the time shift between strain and stress sine waves is Δt. The phase angle shift δ is given by (in dimensionless units of radians),

$$\delta = \omega \Delta t. \tag{14.17}$$

As discussed before:

- Perfectly elastic solid: $\delta = 0$
- Perfectly viscous liquid: $\delta = 90°$
- Viscoelastic system: $0 < \delta < 90°$

The ratio of the maximum stress σ_0 to the maximum strain γ_0 gives the complex modulus $|G^*|$,

$$|G^*| = \frac{\sigma_0}{\gamma_0}. \tag{14.18}$$

The complex modulus can be resolved into G' (the storage or elastic modulus) and G'' (the loss or viscous modulus) using vector analysis and the phase angle shift δ as shown below.

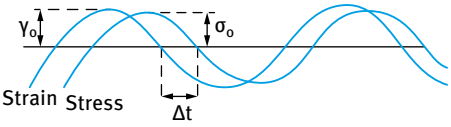

Δt = time shift for sine waves of stress and strain
Δt ω = δ, phase angle shift
ω = frequency in radian s^{-1}
ω = 2 π ν

Perfectly elasic solid	δ = 0
Perfectly viscous liquid	δ = 90°
Viscoelastic system	0 < δ < 90°

Fig. 14.17: Strain and stress sine waves for a viscoelastic system.

14.2.6.2 Vector analysis of the complex modulus

$$G' = |G^*| \cos \delta \tag{14.19}$$

$$G'' = |G^*| \sin \delta \tag{14.20}$$

$$\tan \delta = \frac{G''}{G'} \tag{14.21}$$

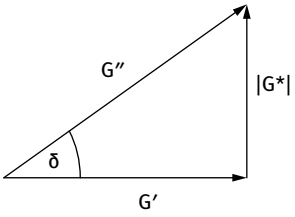

Dynamic Viscosity η':

$$\eta' = \frac{G''}{\omega}. \tag{14.22}$$

Note that $\eta \to \eta(0)$ as $\omega \to 0$.

Both G' and G'' can be expressed in terms of frequency ω and Maxwell relaxation time τ_m by,

$$G'(\omega) = G\frac{(\omega\tau_m)^2}{1 + (\omega\tau_m)^2}, \tag{14.23}$$

$$G''(\omega) = G\frac{\omega\tau_m}{1 + (\omega\tau_m)^2}, \tag{14.24}$$

where G is the plateau modulus.

In oscillatory techniques one has to carry out two types of experiments:

(i) strain sweep, in which the frequency ω is kept constant and G^*, G' and G'' are measured as a function of strain amplitude;

(ii) frequency sweep: the strain is kept constant (in the linear viscoelastic region) and G^*, G' and G'' are measured as a function of frequency.

14.2.6.3 Strain sweep

The frequency is fixed, say at 1 Hz (or 6.28 rad s^{-1}), and G^*, G' and G'' are measured as a function of strain amplitude γ_0. This is illustrated in Fig. 14.18. G^*, G' and G'' remain constant up to a critical strain γ_{cr}. This is the linear viscoelastic region where the moduli are independent of the applied strain. Above γ_{cr}, G^* and G' start to decrease whereas G'' starts to increase with a further increase in γ_0. This is the nonlinear region.

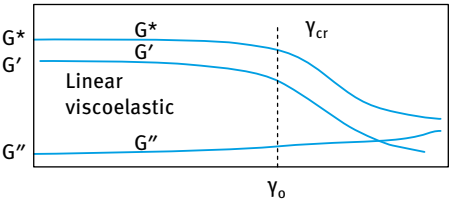

Linear viscoelastic region
G*, G′ and G″ are independent of strain amplitude
γ_{cr} is the critical strain above which systems shows non-linear response (break down of structure)

Fig. 14.18: Schematic representation of strain sweep.

γ_{cr} may be identified with the critical strain above which the structure starts to "break down". It can also be shown that above another critical strain, G'' becomes higher than G'. This is sometimes referred to as the "melting strain" at which the system becomes more viscous than elastic.

14.2.6.4 Oscillatory sweep

The strain γ_0 is fixed in the linear region (taking a midpoint, i.e. not too low a strain where the results may show some "noise" and far from γ_{cr}). G^*, G' and G'' are then measured as a function of frequency (a range of 10^{-3}–10^2 rad s^{-1} may be chosen depending on the instrument and operator patience). Fig. 14.19 shows a schematic representation of the variation of G^*, G' and G'' with frequency ω (rad s^{-1}) for a viscoelastic system that can be represented by a Maxwell model. One can identify a characteristic frequency ω^* at which $G' = G''$ (the "crossover point) which can be used to obtain the Maxwell relaxation time τ_m,

$$\tau_m = \frac{1}{\omega^*}. \tag{14.25}$$

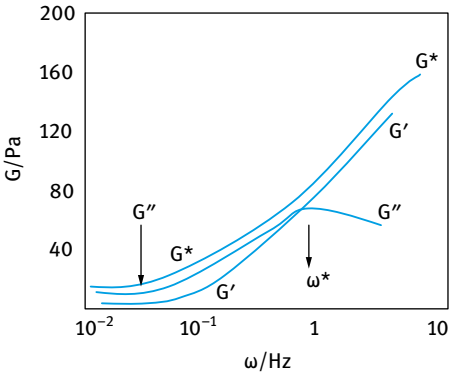

Fig. 14.19: Schematic representation of oscillatory measurements for a viscoelastic liquid.

In the low frequency regime, i.e. $\omega < \omega^*$, $G'' > G'$. This corresponds to a long time experiment (time is reciprocal of frequency) and hence the system can dissipate energy as viscous flow. In the high frequency regime, i.e. $\omega > \omega^*$, $G' > G''$. This corresponds to a short time experiment where energy dissipation is reduced. At sufficiently high frequency, $G' \gg G''$. At such a high frequency, $G'' \to 0$ and $G' \approx G^*$. The high frequency modulus $G'(\infty)$ is sometimes referred to as the "rigidity modulus" where the response is mainly elastic.

For a viscoelastic solid G' does not become zero at low frequency. G'' still shows a maximum at intermediate frequency. This is illustrated in Fig. 14.20.

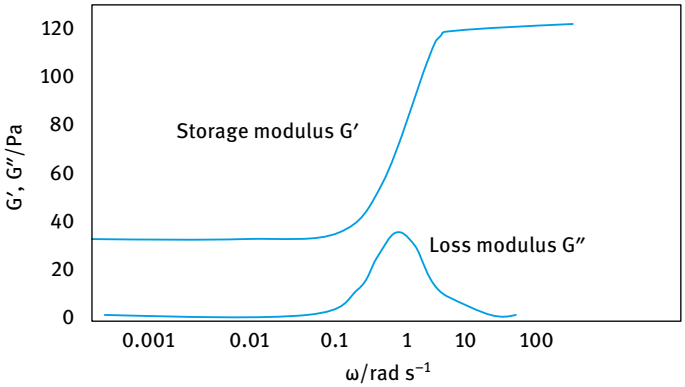

Fig. 14.20: Schematic representation for oscillatory measurements for a viscoelastic solid.

14.2.6.5 The cohesive energy density E_c

The cohesive energy density, which is an important parameter for identifying the "strength" of the structure in a dispersion, can be obtained from the change of G' with γ_0 (Fig. 14.18).

$$E_c = \int_0^{\gamma_{cr}} \sigma \, d\gamma, \tag{14.26}$$

where σ is the stress in the sample that is given by,

$$\sigma = G'\gamma, \tag{14.27}$$

$$E_c = \int_0^{\gamma_{cr}} G'\gamma_{cr} \, d\gamma = \frac{1}{2}\gamma_{cr}^2 G'. \tag{14.28}$$

Note that E_c is given in J m^{-3}.

14.3 Rheology of dispersions

Rheological measurements are useful tools for probing the microstructure of dispersions [1]. This is particularly the case if measurements are carried out at low stresses or strains as discussed above. In this case the spacial arrangement of particles is only slightly perturbed by the measurement. In other words, the convective motion due to the applied deformation is less than the Brownian diffusion. The ratio of the stress applied σ to the "thermal stress" (that is equal to $kT/6\pi a^3$, where k is the Boltzmann constant, T is the absolute temperature and a is the particle radius) is defined in terms of a dimensionless Peclet number Pe,

$$Pe = \frac{6\pi a^3 \sigma}{kT}. \tag{14.29}$$

For a colloidal particle with radius of 100 nm, σ should be less than 0.2 Pa to ensure that the microstructure is relatively undisturbed. In this case $Pe < 1$.

In order to remain in the linear viscoelastic region, the structural relaxation by diffusion must occur on a timescale comparable to the experimental time. The ratio of the structural relaxation time to the experimental measurement time is given by the dimensionless Deborah number, De, which is ≈ 1 and the dispersion appears viscoelastic.

The rheology of dispersions depends on the balance between three main forces [1], namely Brownian diffusion; hydrodynamic interaction; and interparticle forces. These forces are determined by three main parameters:

(i) the volume fraction ϕ (total volume of the particles divided by the volume of the dispersion);
(ii) the particle size and shape distribution;
(iii) the net energy of interaction G_T, i.e. the balance between repulsive and attractive forces.

The earliest theory for predicting the relationship between the relative viscosity η_r and ϕ was described by Einstein and is applicable to $\phi \leq 0.01$.

14.3.1 The Einstein equation

Einstein [12] assumed that the particles behave as hard spheres (with no net interaction). The flow field has to dilate because the liquid has to move around the flowing particles. At $\phi \leq 0.01$, the disturbance around one particle does not interact with the disturbance around another. η_r is related to ϕ by the following expression [1],

$$\eta_r = 1 + [\eta]\phi = 1 + 2.5\phi, \tag{14.30}$$

where $[\eta]$ is referred to as the intrinsic viscosity and has the value 2.5 for spherical particles.

For the above hard sphere very dilute dispersions, the flow is Newtonian, i.e. the viscosity is independent of shear rate. At higher ϕ ($0.2 > \phi > 0.1$) values one has to consider the hydrodynamic interaction suggested by Bachelor [13] that is still valid for hard spheres.

14.3.2 The Bachelor equation [13]

When $\phi > 0.01$, hydrodynamic interaction between the particles become important. When the particles come close to each other, the nearby stream lines and the disturbance of the fluid around one particle interact with that around a moving particle.

Using the above picture Bachelor [13] derived the following expression for the relative viscosity,

$$\eta_r = 1 + 2.5\phi + 6.2\phi^2 + O\phi^3. \tag{14.31}$$

The third term in equation (14.31), i.e. $6.2\,\phi^2$, is the hydrodynamic term whereas the fourth term is due to higher order interactions.

14.3.3 Rheology of concentrated dispersions

When $\phi > 0.2$, η_r becomes a complex function of ϕ. At such high volume fractions the system mostly shows non-Newtonian flow ranging from viscous to viscoelastic to elastic response. Three responses can be considered:

(i) viscous response;
(ii) elastic response;
(iii) viscoelastic response.

These responses for any dispersion depend on the time or frequency of the applied stress or strain.

Four different types of systems (with increasing complexity) can be considered as described below.

Hard-sphere dispersions: these are systems where both repulsive and attractive forces are screened.

Systems with "soft" interaction: these are systems containing electrical double layers with long-range repulsion. The rheology of the dispersion is determined mainly by the double layer repulsion.

Sterically stabilized dispersions: the rheology is determined by the steric repulsion produced by adsorbed nonionic surfactant or polymer layers. The interaction can be "hard" or "soft" depending on the ratio of adsorbed layer thickness to particle radius (δ/R).

Flocculated systems: these are systems where the net interaction is attractive. One can distinguish between weak (reversible) and strong (irreversible) flocculation depending on the magnitude of the attraction.

14.3.3.1 Rheology of hard-sphere dispersions

Hard-sphere dispersions (neutral stability) were developed by Krieger and coworkers [14, 15] using polystyrene latex suspensions. The double layer repulsion was screened by using NaCl or KCl at a concentration of 10^{-3} mol dm^{-3} or replacing water by a less polar medium such as benzyl alcohol.

The relative viscosity η_r (= η/η_0) is plotted as a function of reduced shear rate (shear rate × time for a Brownian diffusion t_r),

$$\dot{\gamma}_{red} = \dot{\gamma} t_r = \frac{6\pi\eta_0 \dot{\gamma} a^3}{kT}, \tag{14.32}$$

where a is the particle radius, η_0 is the viscosity of the medium, k is the Boltzmann constant and T is the absolute temperature.

A plot of (η/η_0) versus $(\eta_0 a^3/kT)$ is shown in Fig. 14.21 at $\phi = 0.4$ for particles with different sizes. At a constant ϕ all points fall on the same curve. The curves are shifted to higher values for larger ϕ and to lower values for smaller ϕ.

The curve in Fig. 14.21 show two limiting (Newtonian) viscosities at low and high shear rates that are separated by a shear thinning region. In the low shear rate regime, Brownian diffusion predominates over hydrodynamic interaction and the system shows a "disordered" three-dimensional structure with high relative viscosity. As the shear rate is increased these disordered structure starts to form layers coincident with the plane of shear and this results in the shear thinning region. In the high shear rate regime, the layers can "slide" freely and hence a Newtonian region (with much lower viscosity) is obtained. In this region hydrodynamic interaction predominates over Brownian diffusion.

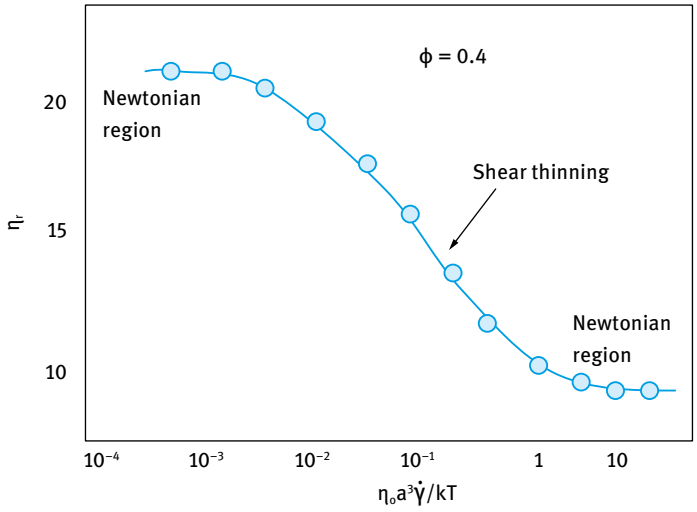

Fig. 14.21: Reduced viscosity versus reduced shear rate for hard-sphere suspensions.

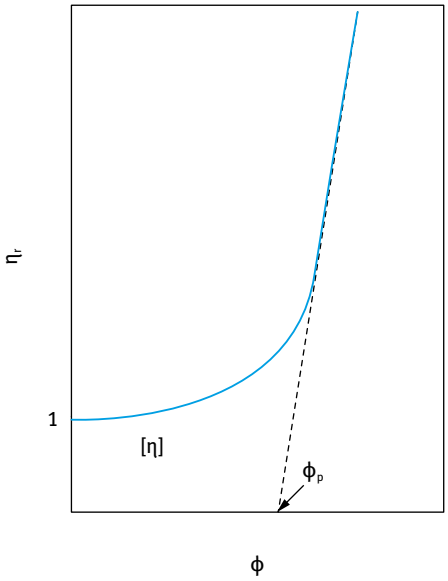

Fig. 14.22: Relative viscosity versus volume fraction for hard-sphere suspensions.

If the relative viscosity in the first or second Newtonian region is plotted versus the volume fraction one obtains the curve shown in Fig. 14.22.

The curve in Fig. 14.22 has two asymptotes:

(i) The slope of the linear portion at low ϕ values (the Einstein region) that gives the intrinsic viscosity $[\eta]$ that is equal to 2.5.

(ii) The asymptote that occurs at a critical volume fraction ϕ_p at which the viscosity shows a sharp increase with increasing ϕ. ϕ_p is referred to as the maximum packing fraction for hard spheres: For hexagonal packing of equal sized spheres, $\phi_p = 0.74$. For random packing of equal sized spheres, $\phi_p = 0.64$. For polydisperse systems, ϕ_p reaches higher values as illustrated in Fig. 14.23 for one-size, two-size, three-size and four-size suspensions.

The best analysis of the η_r–ϕ curve is due to Dougherty and Krieger [14, 15] who used a mean field approximation by calculating the increase in viscosity as small increments of the suspension are consecutively added. Each added increment corresponds to replacement of the medium by more particles.

They arrived at the following simple semi-empirical equation that could fit the viscosity data over the whole volume fraction range:

$$\eta_r = \left(1 - \frac{\phi}{\phi_p}\right)^{-[\eta]\phi_p}. \tag{14.33}$$

Equation (14.33) is referred to as the Dougherty–Krieger equation [14, 15] and is commonly used for analysis of viscosity data.

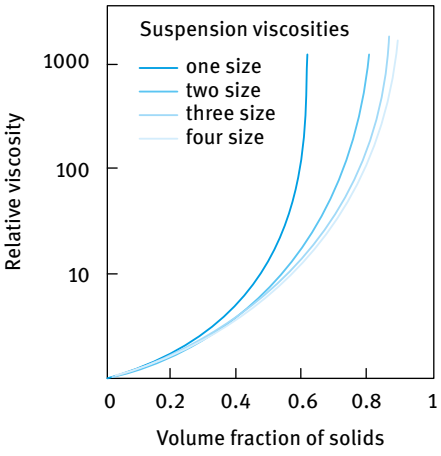

Fig. 14.23: Viscosity–volume fraction curves for polydisperse dispersions.

14.3.3.2 Rheology of systems with "soft" or electrostatic interaction

In this case the rheology is determined by the double layer repulsion, particularly with small particles and extended double layers [16]. In the low shear rate regime the viscosity is determined by Brownian diffusion and the particles approach each other to a distance of the order of $\approx 4.5\kappa^{-1}$ (where κ^{-1} is the "double layer thickness" that is determined by electrolyte concentration and valency). This means that the effective radius of the particles R_{eff} is much higher than the core radius R. For example for 100 nm particles with a zeta potential ζ of 50 mV dispersed in a medium of 10^{-5} mol dm^{-3} NaCl ($\kappa^{-1} = 100$ nm), $R_{\text{eff}} \approx 325$ nm. The effective volume fraction ϕ_{eff} is also much higher than the core volume fraction. This results in a rapid increase in the viscosity at low core volume fraction [16]. This is illustrated in Fig. 14.24 which shows the variation of η_{r} with ϕ at $5 \times 10^{-.4}$ and 10^{-3} mol dm^{-3} NaCl ($R = 85$ nm and $\zeta = 78$ mV).

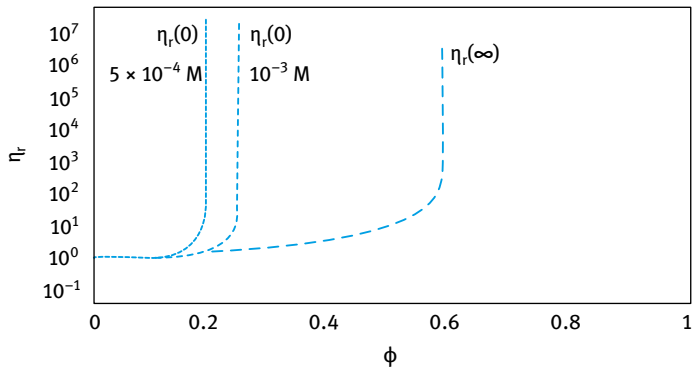

Fig. 14.24: Variation of η_{r} with ϕ for polystyrene latex dispersions at two NaCl concentrations.

The low shear viscosity $\eta_r(0)$ shows a rapid increase at $\phi \approx 0.2$ (the increase occurs at higher volume fraction at the higher electrolyte concentration). At $\phi > 0.2$, the system shows "solid-like" behaviour with $\eta_r(0)$ reaching very high values ($> 10^7$). At such high ϕ values the system shows near plastic flow.

In the high shear rate regime, the increase in η_r occurs at much higher ϕ values. This is illustrated from the plot of the high shear relative viscosity $\eta_r(\infty)$ versus ϕ. At such high shear rates hydrodynamic interaction predominates over Brownian diffusion and the system shows a low viscosity, denoted by $\eta_r(\infty)$. However, when ϕ reaches a critical value pseudoplastic flow is observed.

14.3.3.3 Rheology of sterically stabilized dispersions

These are dispersions where the particle repulsion results from the interaction between adsorbed or grafted layers of nonionic surfactants or polymers [17]. The flow is determined by the balance of viscous and steric forces. Steric interaction is repulsive as long as the Flory–Huggins interaction parameter $\chi < 1/2$. With short chains, the interaction may be represented by a hard-sphere type with $R_{eff} = R + \delta$. This is particularly the case with nonaqueous dispersions with an adsorbed layer of thickness that is smaller compared to the particle radius (any electrostatic repulsion is negligible in this case). With most sterically stabilized dispersions, the adsorbed or grafted layer has an appreciable thickness (compared to particle radius) and hence the interaction is "soft" in nature as a result of the longer range of interaction. Results for aqueous sterically stabilized dispersions were produced using polystyrene (PS) latex with grafted poly(ethylene oxide) (PEO) layers [18, 19]. As an illustration, Fig. 14.25 shows the variation of η_r with ϕ for latex dispersions with three particle radii (77.5, 306 and 502 nm). For comparison, the η_r–ϕ curve calculated using the Dougherty–Krieger equation is shown in the same figure. The η_r–ϕ curves are shifted to the left as a result

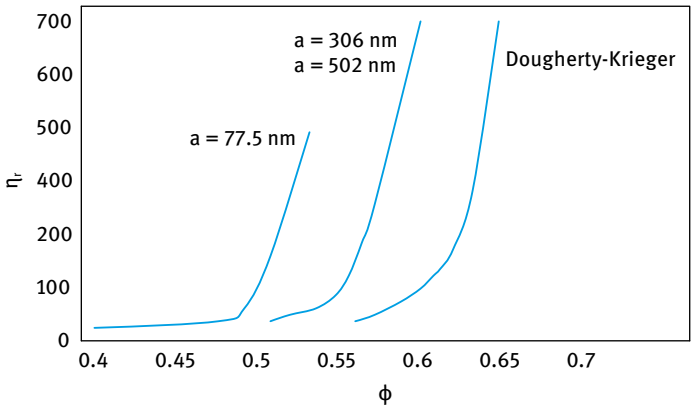

Fig. 14.25: η_r–ϕ curves for PS latex dispersions containing grafted PEO chains.

of the presence of the grafted PEO layers. The experimental relative viscosity data may be used to obtain the grafted polymer layer thickness at various volume fractions of the dispersions. Using the Dougherty–Krieger equation, one can obtain the effective volume fraction of the dispersion. From a knowledge of the core volume fraction, one can calculate the grafted layer thickness at each dispersion volume fraction.

To apply the Dougherty–Krieger equation, one needs to know the maximum packing fraction, ϕ_p. This can be obtained from a plot of $1/(\eta_r)^{1/2}$ versus ϕ and extrapolation to $1/(\eta_r)^{1/2}$, using the following empirical equation [18],

$$\frac{K}{\eta_r^{1/2}} = \phi_p - \phi. \tag{14.34}$$

The value of ϕ_p using equation (14.34) was found to be in the range 0.6–0.64. The intrinsic viscosity $[\eta]$ was assigned a value of 2.5.

Using the above calculations, the grafted PEO layer thickness δ was calculated as a function of ϕ for the three latex dispersions. For the dispersions with $R = 77.5$ nm, δ was found to be 8.1 nm at $\phi = 0.42$, decreasing to 5.0 nm when ϕ was increased to 0.543. For the dispersions with $R = 306$ nm, $\delta = 12.0$ nm at $\phi = 0.51$, decreasing to 10.1 when ϕ was increased to 0.60. For the dispersions with $R = 502$ nm, $\delta = 21.0$ nm at $\phi = 0.54$ decreasing to 14.7 as ϕ was increased to 0.61.

As mentioned above, the rheology of sterically stabilized dispersions is determined by the steric repulsion particularly for small particles with "thick" adsorbed layers. This is illustrated in Fig. 14.26 which shows the variation of G^*, G' and G'' with frequency (Hz) for polystyrene latex dispersions of 175 nm radius containing grafted poly(ethylene oxide) (PEO) with molecular weight of 2,000 (giving a hydrodynamic thickness $\delta \approx 20$ nm) [19]. The results clearly show the transition from predominantly viscous response when $\phi \leq 0.465$ to predominantly elastic response when $\phi \geq 0.5$. This behaviour reflects the steric interaction between the PEO layers. When the surface-to-surface distance between the particles h becomes $< 2\delta$ elastic interaction occurs and $G' > G''$.

The exact volume fraction at which a dispersion changes from predominantly viscous to predominantly elastic response may be obtained from plots of G^*, G' and G'' (at fixed strain in the linear viscoelastic region and fixed frequency) versus the volume fraction of the dispersion. This is illustrated in Fig. 14.27 which shows the results for the above latex dispersions. At $\phi = 0.482$, $G' = G''$ (sometimes referred to as the crossover point), which corresponds to $\phi_{eff} = 0.62$ (close to maximum random packing). At $\phi > 0.482$, G' becomes progressively larger than G'' and ultimately the value of G' approaches G^* and G'' becomes relatively much smaller than G'. At $\phi = 0.585$, $G' \approx G^* = 4.8 \times 10^3$ and at $\phi = 0.62$, $G' \approx G^* = 1.6 \times 10^5$ Pa. Such high elastic moduli values indicate that the dispersions behave as near elastic solids ("gels") as a result of interpenetration and/or compression of the grafted PEO chains.

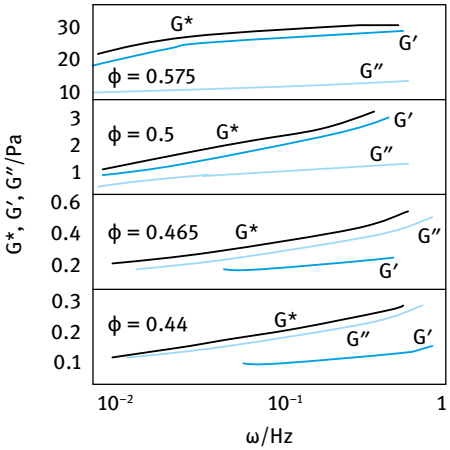

Fig. 14.26: Variation of G^*, G' and G'' with frequency for sterically stabilized dispersions.

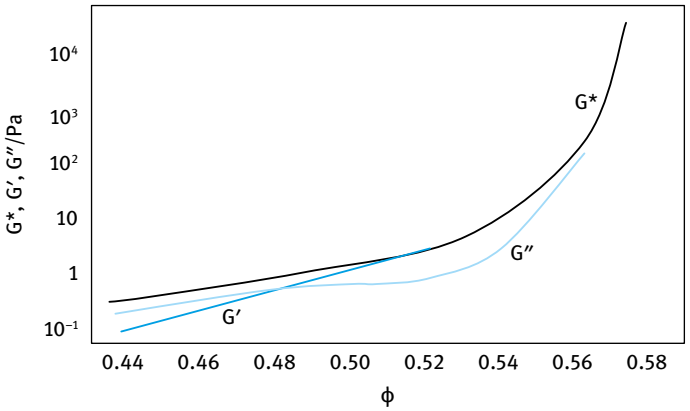

Fig. 14.27: Variation of G^*, G' and G'' (at $\omega = 1$ Hz) with ϕ for latex dispersions ($a = 175$ nm) containing grafted PEO chains.

14.3.3.4 Rheology of flocculated suspensions

The rheology of unstable systems poses problems both from the experimental and the theoretical point of view. This is due to the non-equilibrium nature of the structure, resulting from the weak Brownian motion [1]. For this reason, advances in the rheology of suspensions, where the net energy is attractive, have been slow and only of qualitative nature. On the practical side, control of the rheology of flocculated and coagulated suspensions is difficult, since the rheology depends not only on the magnitude of the attractive energies but also on how one arrives at the flocculated or coagulated structures in question. Various structures can be formed, e.g. compact flocs, weak and metastable structures, chain aggregates, etc. At high volume fraction

of the suspension, a "three-dimensional" network of the particles is formed throughout the sample. Under shear, this network is broken into smaller units of flocculated spheres which can withstand the shear forces [20, 21]. The size of the units that survive is determined by the balance of shear forces which tend to break the units down and the energy of attraction that holds the spheres together [20–22]. The appropriate dimensionless group characterizing this process (balance of viscous and van der Waals force) is $\eta_0 a^4 \dot{\gamma}/A$ (where η_0 is the viscosity of the medium, a is the particle radius, $\dot{\gamma}$ is the shear rate and A is the effective Hamaker constant). Each flocculated unit is expected to rotate in the shear field, and it is likely that these units will tend to form layers as individual spheres do. As the shear stress increases, each rotating unit will ultimately behave as an individual sphere and, therefore, a flocculated suspension will show pseudoplastic flow with the relative viscosity approaching a constant value at high shear rates. The viscosity-shear rate curve will also show a pseudo-Newtonian region at low and high shear rates (similar to the case with stable systems described above). However, the values of the low and high shear rate viscosities (η_0 and η_∞) will of course depend on the extent of flocculation and the volume fraction of the suspension. It is also clear that such systems will show an apparent yield stress (Bingham yield value, σ_β) normally obtained by extrapolation of the linear portion of the σ–$\dot{\gamma}$ curve to $\dot{\gamma} = 0$. Moreover, since the structural units of a weakly flocculated system change with change in shear rate, most flocculated suspensions show thixotropy as discussed above. Once shear is initiated, some finite time is required to break the network of agglomerated flocs into smaller units which persist under the shear forces applied. As smaller units are formed, some of the liquid entrapped in the flocs is liberated, thereby reducing the effective volume fraction, ϕ_{eff}, of the suspension. This reduction in ϕ_{eff} is accompanied by a reduction in η_{eff} and this plays a major role in generating thixotropy.

It is convenient to distinguish between two types of unstable systems depending on the magnitude of the net attractive energy:

(i) Weakly flocculated suspensions: the attraction in this case is weak (energy of few kT units) and reversible, e.g. in the secondary minimum of the DLVO curve or the shallow minimum obtained with sterically stabilized systems. A particular case of weak flocculation is that obtained on the addition of "free" (nonadsorbing) polymer referred to as depletion flocculation.

(ii) Strongly flocculated (coagulated) suspensions: the attraction in this case is strong (involving energies of several 100 kT units) and irreversible. This is the case of flocculation in the primary minimum or those flocculated by reduction of solvency of the medium (for sterically stabilized suspensions) to worse than a θ-solvent.

Study of the rheology of flocculated suspensions is difficult since the structure of the flocs is at nonequilibrium. Theories for flocculated suspensions are also qualitative and based on a number of assumptions.

Weakly flocculated dispersions

As mentioned in Chapter 9, weak flocculation may be obtained by the addition of "free" (nonadsorbing) polymer to a sterically stabilized dispersion [1]. Several rheological investigations of such systems have been carried out by Tadros and his collaborators [23–27]. This is exemplified by a latex dispersion containing grafted PEO chains of $M = 2{,}000$ to which "free" PEO is added at various concentrations. The grafted PEO chains, which were made sufficiently dense, ensure absence of adsorption of the added free polymer. Three molecular weights of PEO were used: 20,000, 35,000 and 90,000. As an illustration, Fig. 14.28–14.30 show the variation of the Bingham yield value σ_β with volume fraction of "free" polymer ϕ_p at the three PEO molecular weights studied and at various latex volume fractions ϕ_s. The latex radius R in

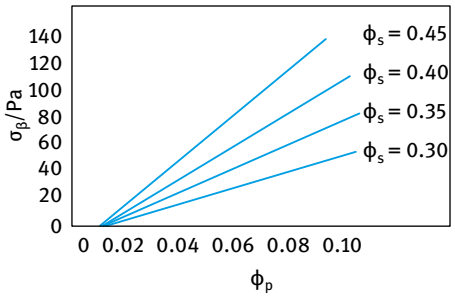

Fig. 14.28: Variation of yield value σ_β with volume fraction ϕ_p of "free polymer" (PEO; $M = 20{,}000$) at various latex volume fractions ϕ_s.

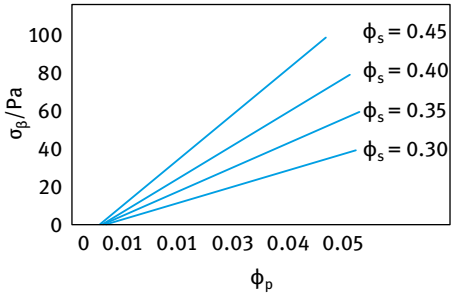

Fig. 14.29: Variation of yield value σ_β with volume fraction ϕ_p of "free polymer" (PEO; $M = 35{,}000$) at various latex volume fractions ϕ_s.

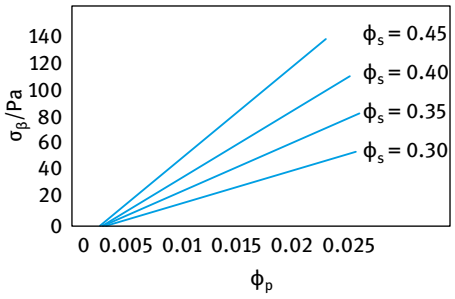

Fig. 14.30: Variation of yield value σ_β with volume fraction ϕ_p of "free polymer" (PEO; $M = 100{,}000$) at various latex volume fractions ϕ_s.

this case was 73.5 nm. The results of Fig. 14.28–14.30 show a rapid and linear increase in σ_β with increasing ϕ_p when the latter exceeds a critical value, ϕ_p^+. The latter is the critical free polymer volume fraction for depletion flocculation. ϕ_p^+ decreases with increasing molecular weight M of the free polymer, as expected. There does not seem to be any dependence of ϕ_p^+ on the volume fraction of the latex, ϕ_s.

Similar trends were obtained using larger latex particles (with radii 217.5 and 457.5 nm). However, there was a definite trend of the effect of particle size; the larger the particle size the smaller the value of ϕ_p^+. A summary of ϕ_p^+ for the various molecular weights and particle sizes is given in Tab. 14.1.

The results in Tab. 14.1 show a significant reduction in ϕ_p^+ when the molecular weight of PEO is increased from 20,000 to 35,000, whereas when M is increased from 35,000 to 100,000, the reduction in ϕ_p^+ is relatively smaller. Similarly, there is a significant reduction in ϕ_p^+ when the particle radius is increased from 73.5 to 217.5 nm, with a relatively smaller decrease on any further increase of a to 457.5 nm.

The straight line relationship between the extrapolated yield value and the volume fraction of free polymer can be described by the following scaling law [25, 26],

$$\sigma_\beta = K\phi_s^m(\phi_p - \phi_p^+), \tag{14.35}$$

where K is a constant and m is the power exponent in ϕ_s which may be related to the flocculation process. The values of m used to fit the data of σ_β versus ϕ_s are summarized in Tab. 14.2.

Tab. 14.1: Volume fraction of free polymer at which flocculation starts, ϕ_p^+.

Particle radius (nm)	M (PEO)	ϕ_p^+
73.5	20,000	0.0150
73.5	35,000	0.0060
73.5	10,000	0.0055
73.5	20,000	0.0150
217.5	20,000	0.0055
457.5	20,000	0.0050

Tab. 14.2: Power law plot for σ_β versus ϕ_s for various PEO molecular weights and latex radii.

Latex R = 73.5 nm						Latex R = 217.5 nm		Latex R = 457.5 nm	
PEO 20,000		PEO 35,000		PEO 100,000					
ϕ_p	m	ϕ_p	m	ϕ_p	m	ϕ_p	m	ϕ_p	m
0.040	3.0	0.022	2.9	0.015	2.7	0.020	3.0	0.020	2.7
0.060	2.7	0.030	3.0	0.020	2.7	0.040	2.9	0.030	2.7
0.080	2.8	0.040	2.8	0.025	2.8	0.060	2.8	0.040	2.8
0.100	2.8	0.050	2.9	—	—	0.080	2.8	0.050	2.7

It can be seen from Tab. 14.2 that m is nearly constant, being independent of particle size and free polymer concentration. An average value for m of 2.8 may be assigned for such a weakly flocculated system. This value is close to the exponent predicted for diffusion controlled aggregation (3.5 ± 0.2) predicted by Ball and Brown [28, 29] who developed a computer simulation method treating the flocs as fractals that are closely packed throughout the sample.

The near independence of ϕ_p^+ on ϕ_s can be explained on the basis of the statistical mechanical approach of Gast et al. [30] which showed such independence when the osmotic pressure of the free polymer solution is relatively low and/or the ratio of the particle diameter to the polymer coil diameter is relatively large (> 8–9). The latter situation is certainly the case with the latex suspensions with diameters of 435 and 915 nm at all PEO molecular weights. The only situation where this condition is not satisfied is with the smallest latex and the highest molecular weight.

The dependency of ϕ_p^+ on particle size can be explained from a consideration of the dependence of free energy of depletion and van der Waals attraction on particle radius as will be discussed below. Both attractions increase with increasing particle radius. Thus the larger particles would require smaller free polymer concentration at the onset of flocculation.

It is possible, in principle, to relates the extrapolated Bingham yield value, σ_β, to the energy required to separate the flocs into single units, E_{sep} [23, 24],

$$\sigma_\beta = \frac{3\phi_s n E_{sep}}{8\pi R^3}, \tag{14.36}$$

where n is the average number of contacts per particle (the coordination number). The maximum value of n is 12, which corresponds to hexagonal packing of the particles in a floc. For random packing of particles in the floc, $n = 8$. However, it is highly unlikely that such values of 12 or 8 are reached in a weakly flocculated system and a more realistic value for n is probably 4 (a relatively open structure in the floc).

In order to calculate E_{sep} from σ_β, one has to assume that all particle–particle contacts are broken by shear. This is highly likely since the high shear viscosity of the weakly flocculated latex was close to that of the latex before addition of the free polymer. Values of E_{sep} obtained using equation (14.36) with $n = 4$ are given in Tab. 14.3 at the three PEO molecular weights for the latex with the radius of 73.5 nm. It can be seen that E_{sep} at any given ϕ_p increases with increasing the volume fraction ϕ_s of the latex.

A comparison between E_{sep} and the free energy of depletion flocculation, G_{dep}, can be made using the theories of Asakura and Oosawa (AO) [31, 32] and Fleer, Vincent and Scheutjens (FVS) [33]. Asakura and Oosawa [31, 32] derived the following expression for G_{dep}, which is valid for the case where the particle radius is much larger the polymer coil radius,

$$\frac{G_{dep}}{kT} = -\frac{3}{2}\phi_2 \beta x^2; \quad 0 < x < 1, \tag{14.37}$$

where k is the Boltzmann constant, T is the absolute temperature, ϕ_2 is the volume concentration of free polymer that is given by,

$$\phi_2 = \frac{4\pi\Delta^3 N_2}{3\upsilon}. \tag{14.38}$$

Δ is the depletion layer thickness that is equal to the radius of gyration of free polymer, R_g and N_2 is the total number of polymer molecules in a volume υ of solution.

$$\beta = \frac{R}{\Delta}, \tag{14.39}$$

$$x = \frac{[\Delta - (h/2)]}{\Delta}, \tag{14.40}$$

where h is the distance of separation between the outer surfaces of the particles. Clearly, when $h = 0$, i.e. at the point where the polymer coils are "squeezed out" from the region between the particles, $x = 1$.

Fleer, Scheutjens and Vincent (FSV model) [33] developed a general approach for the interaction of hard spheres in the presence of a free polymer. This model takes into account the dependency of the range of interaction on free polymer concentration and any contribution from the non-ideal mixing of polymer solutions. This theory gives the following expression for G_{dep},

$$G_{dep} = 2\pi R\left(\frac{\mu_1 - \mu_1^0}{\upsilon_1^0}\right)\Delta^2\left(1 + \frac{2\Delta}{3R}\right), \tag{14.41}$$

where μ_1 is the chemical potential at bulk polymer concentration ϕ_p, μ_1^0 is the corresponding value in the absence of free polymer and υ_1^0 is the molecular volume of the solvent.

The difference in chemical potential $(\mu_1 - \mu_1^0)$ can be calculated from the volume fraction of free polymer ϕ_p and the polymer–solvent (Flory–Huggins) interaction parameter χ,

$$\frac{\mu_1 - \mu_1^0}{kT} = -\left[\frac{\phi_p}{n_2} + \left(\frac{1}{2} - \chi\right)\phi_p^2\right], \tag{14.42}$$

where n_2 is the number of polymer segments per chain.

A summary of the values of E_{sep}, G_{dep} calculated on the basis of the AO and FSV models is given in Tab. 14.3 at three molecular weights for PEO and for a latex with $a = 77.5$ nm.

It can be seen from Tab. 14.3 that E_{sep} at any given ϕ_p increases with increasing volume fraction ϕ_s of the latex. In contrast, the value of G_{dep} does not depend on the value of ϕ_s. The theories on depletion flocculation only show a dependency of G_{dep} on ϕ_p and a. Thus, one cannot make a direct comparison between E_{sep} and G_{dep}. The close agreement between E_{sep} and G_{dep} using Asakura and Oosawa's theory [31, 32] and assuming a value of $n = 4$ should only be considered fortuitous.

Tab. 14.3: Results of E_{sep}, G_{dep} calculated on the basis of the AO and FSV models.

ϕ_p	ϕ_s	σ_β (Ps)	$E_{sep}(kT)$	G_{dep} (kT)	
				AO model	**FSV model**
(a) M(PEO) = 20,000					
0.04	0.30	12.5	8.4	18.2	78.4
	0.35	21.0	12.1	18.2	78.4
	0.40	30.5	15.4	18.2	78.4
	0.45	40.0	18.0	18.2	78.4
(b) M(PEO) = 35,000					
0.03	0.30	17.5	11.8	15.7	78.6
	0.35	25.7	14.8	15.7	78.6
	0.40	37.3	18.9	15.7	78.6
	0.45	56.8	25.5	15.7	78.6
(c) M(PEO) = 100,000					
0.02	0.30	10.0	6.7	9.4	70.8
	0.35	15.0	8.7	9.4	70.8
	0.40	22.0	11.1	9.4	70.8
	0.45	32.5	14.6	9.4	70.8

Using equations (14.35) and (14.36), a general scaling law may be used to show the variation of E_{sep} with the various parameters of the system,

$$E_{sep} = \frac{8\pi R^3}{3\phi_s n} K_1 \phi_s^{2.8} (\phi_p - \phi_p^+) = \frac{8\pi K_1}{3n} R^3 \phi_s^{1.8} (\phi_p - \phi_p^+). \tag{14.43}$$

Equation (14.43) shows the four parameters that determine E_{sep}: the particle radius a, the volume fraction of the suspension ϕ_s, the concentration of free polymer ϕ_p and the molecular weight of the free polymer, which together with a determines ϕ_p^+.

More insight on the structure of the flocculated latex dispersions was obtained using viscoelastic measurements [26]. As an illustration, Fig. 14.31 shows the variation of the storage modulus G' with ϕ_p (M = 20,000) at various latex (a = 77.5) volume fractions ϕ_s. Similar trends were obtained for the other PEO molecular weights. All results show the same trend, namely an increase in G' with increasing ϕ_p, reaching a plateau value at high ϕ_p values. These results are different from those obtained using steady state measurements, which show a rapid and linear increase of yield value σ_β. This difference reflects the behaviour when using oscillatory (low deformation) measurements which causes little perturbation of the structure when using low amplitude and high frequency measurements. Above ϕ_p^+, flocculation occurs and G' increases in magnitude with a further increase in ϕ_p until a three-dimensional network structure is reached and G' reaches a limiting value. Any further increase in free polymer concentration may cause a change in the floc structure but this may not cause a significant increase in the number of bonds between the units formed (which determine the magnitude of G').

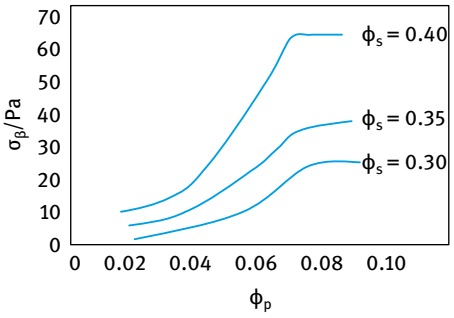

Fig. 14.31: Variation of storage modulus G with volume fraction of polymer (PEO; $M = 20{,}000$).

Strongly flocculated (coagulated) suspensions

Steady state shear stress–shear rate curves show a pseudoplastic flow curve, as illustrated in Fig. 14.32. The flow curve is characterized by three main parameters:

(i) The shear rate above which the flow curve shows linear behaviour. Above this shear rate collisions occur between the flocs and this may cause interchange between the flocculi (the smaller floc units that aggregate to form a floc). In this linear region, the ratio of the floc volume to the particle volume (ϕ_F/ϕ_p), i.e. the floc density, remains constant.

(ii) σ_β the residual stress (yield stress) that arises from the residual effect of interparticle potential.

(iii) η_{pl}: the slope of the linear portion of the flow curve that arises from purely hydrodynamic effects.

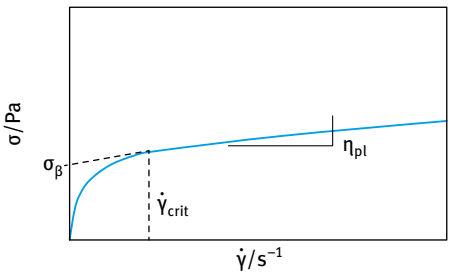

Fig. 14.32: Pseudoplastic flow curve for a flocculated suspension.

Several theories have been proposed to analyse the flow curve of Fig. 14.32 and these are summarized below.

Impulse theory: Goodeve and Gillespie [34, 35]. The interparticle interaction effects (given by σ_β) and hydrodynamic effects (given by η_{pl}) are assumed to be additive,

$$\sigma = \sigma_\beta + \eta_{pl}\dot{\gamma}. \tag{14.44}$$

To calculate σ_β, Goodeve proposed that when shearing occurs, links between particles in a flocculated structure are stretched, broken and reformed. An impulse is transferred from a fast moving layer to a slow moving layer. Non-Newtonian effects are due to effect of shear on the number of links, the lifetime of a link and any change in the size of the floc.

According to Goodeve theory the yield value is given by,

$$\sigma_\beta = \left(\frac{3\phi^2}{2\pi R^3}\right) E_A, \tag{14.45}$$

where ϕ is the volume fraction of the dispersed phase, a is the particle radius and E_A is the total binding energy.

$$E_A = n_L \varepsilon_L, \tag{14.46}$$

where n_L is the number of links with a binding energy ε_L per link.

According to equation (14.45): $\sigma_\beta \propto \phi^2 \propto (1/a^3) \propto E_A$ (the energy of attraction).

Elastic floc model: Hunter and coworkers [36, 37]. The floc is assumed to consist of an open network of "girders" as schematically shown in Fig. 14.33. The floc undergoes extension and compression during rotation in a shear flow. The bonds are stretched by a small amount Δ (that can be as small as 1% of particle radius).

To calculate σ_β, Hunter considered the energy dissipation during rupture of the flocs (assumed to consist of doublets).

The yield value σ_β is given by the expression,

$$\sigma_\beta = \alpha_0 \beta \lambda \eta \dot{\gamma} \left(\frac{R_{floc}^2}{R^3}\right) \phi_s^2 \Delta C_{FP}, \tag{14.47}$$

where α_0 is the collision frequency, β is a constant (= 27/5), λ is a correction factor (≈ 1) and C_{FP} is the floc density ($= \phi_F/\phi_s$).

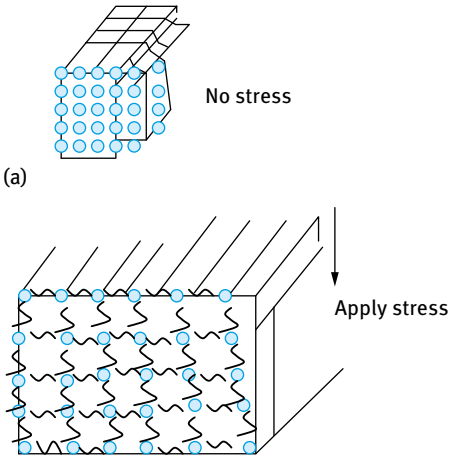

Fig. 14.33: Schematic picture of the elastic floc.

Fractal concept for flocculation. The floc structure can be treated as fractals whereby an isolated floc with radius a_F can be assumed to have uniform packing throughout that floc [38, 39].

In the above case the number of particles in a floc is given by,

$$n_f = \phi_{mf}\left(\frac{R_F}{R}\right)^3, \tag{14.48}$$

where ϕ_{mf} is the packing fraction of the floc.

If the floc does not have constant packing throughout its structure, but is dendritic in form, the packing density of the floc begins to reduce as one goes from the centre to the edge. If this reduction is with a constant power law D,

$$n_F = \left(\frac{R_F}{R}\right)^D, \tag{14.49}$$

where $0 < D \leq 3$.

D is called the packing index and it represents the packing change with distance from the centre. Two cases may be considered:

(i) *Rapid aggregation* (diffusion limited aggregation, DLA). When particles touch, they stick. Particle–particle aggregation gives $D = 2.5$; aggregate–aggregate aggregation gives $D = 1.8$. The lower the value of D, the more open the floc structure is.

(ii) *Slow aggregation* (rate limited aggregation, RLA). The particles have a lower sticking probability – some are able to rearrange and densify the floc – $D \approx 2.0$–2.2. The lower the value of D, the more open the floc structure is. Thus by determining D one can obtain information on the flocculation behaviour. If flocculation of a suspension occurs by changing the conditions (e.g. increasing temperature) one can visualize sites for nucleation of flocs occurring randomly throughout the whole volume of the suspension.

The total number of primary particles does not change and the volume fraction of the floc is given by,

$$\phi_F = \phi\left(\frac{R_F}{F}\right)^{3-D}. \tag{14.50}$$

Since the yield stress σ_β and elastic modulus G' depend on the volume fraction one can use a power law in the form,

$$\sigma_\beta = K\phi^m, \tag{14.51}$$

$$G' = K\phi^m, \tag{14.52}$$

where the exponent m reflects the fractal dimension.

Thus by plotting $\log \sigma_\beta$ or $\log G'$ versus $\log \phi$ one can obtain m from the slope which can be used to characterize the floc nature and structure, $m = 2/(3 - D)$.

14.4 Examples of strongly flocculated (coagulated) suspension

14.4.1 Coagulation of electrostatically stabilized suspensions by addition of electrolyte

As mentioned in Chapter 9, electrostatically stabilized suspensions become coagulated when the electrolyte concentration is increased above the critical coagulation concentration (CCC). This is illustrated by using a latex dispersion (prepared using surfactant-free emulsion polymerization) to which 0.2 mol dm^{-3} NaCl is added (well above the CCC, which is 0.1 mol dm^{-3} NaCl).

Fig. 14.34 shows the strain sweep results for latex dispersions at various volume fractions ϕ and in the presence of 0.2 mol dm^{-3} NaCl.

It can be seen from Fig. 14.34 that G^* and G' (which are very close to each other) remain independent of the applied strain (the linear viscoelastic region), but above a critical strain, γ_{cr}, G^* and G' show a rapid reduction with a further increase in strain (the nonlinear region). In contrast, G'' (which is much lower than G') remains constant showing an ill-defined maximum at intermediate strains. Above γ_{cr} the flocculated structure becomes broken down with applied shear.

Fig. 14.35 shows the variation of G' (measured at strains in the linear viscoelastic region) with frequency ν (in Hz) at various latex volume fractions. As mentioned above, G' is almost equal to G^* since G'' is very low.

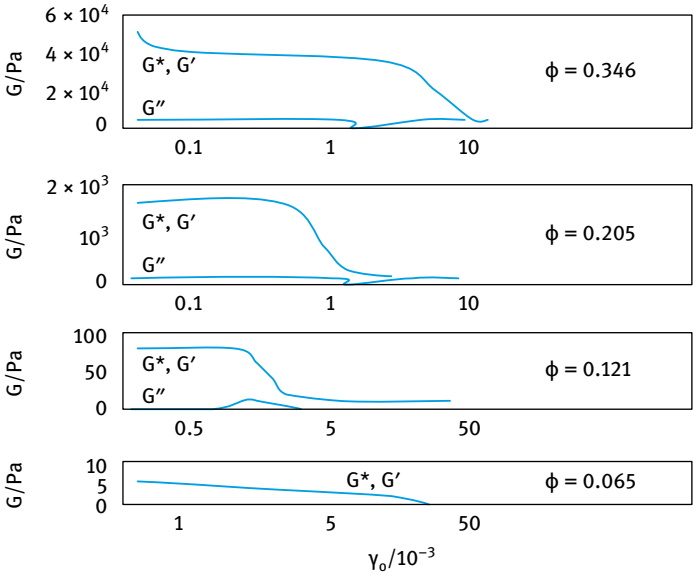

Fig. 14.34: Strain sweep results for latex dispersions at various volume fractions ϕ in the presence of 0.2 mol dm^{-3} NaCl.

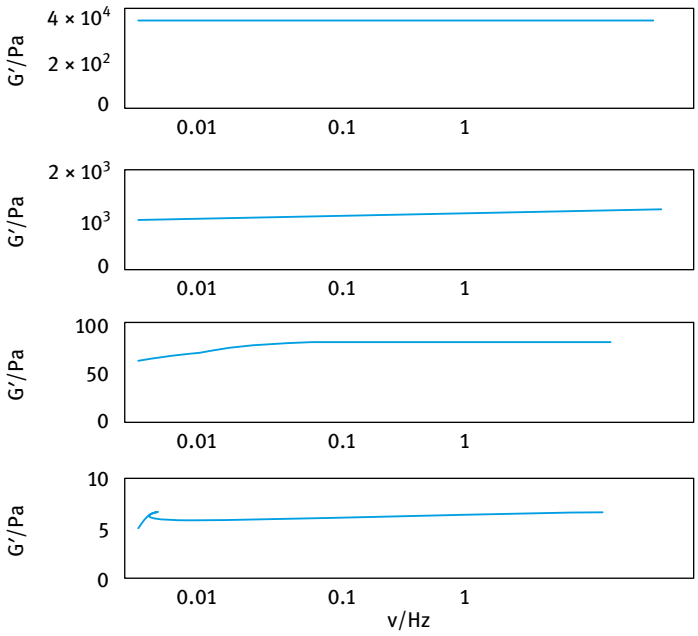

Fig. 14.35: Variation of G' with frequency at various volume fractions.

In all cases $G' \gg G''$, and it shows little dependency on frequency. This behaviour is typical of a highly elastic (coagulated) structure, whereby a "continuous gel" network structure is produced at such high volume fractions. Scaling laws can be applied for the variation of G' with the volume fraction of the latex ϕ. A log-log plot of G' versus ϕ is shown in Fig. 14.36. This plot is linear and can be represented by the following scaling equation,

$$G' = 1.98 \times 10^7 \phi^{6.0}. \tag{14.53}$$

The high power in ϕ is indicative of a relatively compact coagulated structure. This power gives a fractal dimension of 2.67 that confirms the compact structure.

It is also possible to obtain the cohesive energy of the flocculated structure E_c from a knowledge of G' (in the linear viscoelastic region) and γ_{cr}. E_c is related to the stress σ in the coagulated structure by equations (14.26)–(14.28).

A log-log plot of E_c versus ϕ is shown in Fig. 14.37 for such coagulated latex dispersions. The E_c versus ϕ curve can be represented by the following scaling relationship,

$$E_c = 1.02 \times 10^3 \phi^{9.1}. \tag{14.54}$$

The high power in ϕ is indicative of the compact structure of these coagulated suspensions.

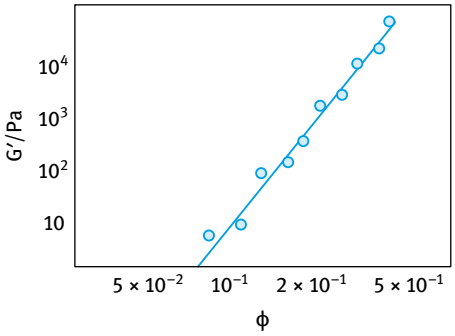

Fig. 14.36: Log-log plots of G' versus ϕ for polystyrene latex dispersions.

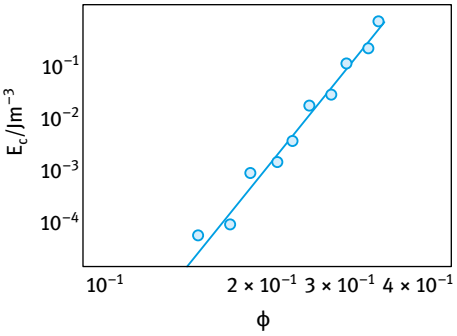

Fig. 14.37: Log-log plots of E_c versus ϕ for coagulated latex dispersions.

14.4.2 Strongly flocculated sterically stabilized systems

As mentioned in Chapter 9, sterically stabilized dispersions show strong flocculation (sometimes referred to as incipient flocculation) when the medium for the stabilizing chain becomes worse than a θ-solvent (the Flory–Huggins interaction parameter $\chi > 0.5$). Reduction of solvency for a PEO stabilizing chain can be achieved by addition of a nonsolvent for the chains or by addition of electrolyte such as Na_2SO_4. Above a critical Na_2SO_4 concentration (to be referred to as the critical flocculation concentration, CFC), the χ parameter exceeds 0.5 and this results in incipient flocculation. This process of flocculation can be investigated using rheological measurements without diluting the latex. This dilution may result in a change in the floc structure and hence investigations without dilution ensure absence of change of the floc structure, in particular when using low deformation (oscillatory) techniques [1].

Fig. 14.38 shows the variation of extrapolated yield value, σ_β, as a function of Na_2SO_4 concentration at various latex volume fractions ϕ_s at 25 °C. The latex had a z-average particle diameter of 435 nm and it contained grafted PEO with $M = 2{,}000$. It is clear that when $\phi_s < 0.52$, σ_β is virtually equal to zero up to 0.3 mol dm^{-3} Na_2SO_4 above which it shows a rapid increase in σ_β with any further increase in Na_2SO_4 concentration. When $\phi_s > 0.52$, a small yield value is obtained below 0.3 mol dm^{-3} Na_2SO_4, which may be attributed to the possible elastic interaction between the

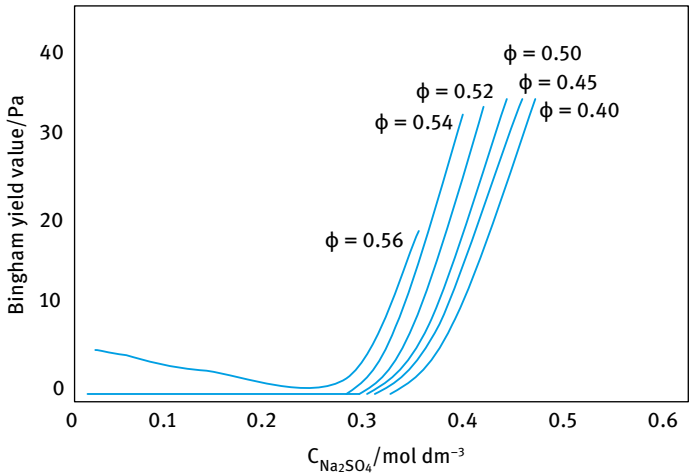

Fig. 14.38: Variation of Bingham yield value with Na_2SO_4 concentration at various volume fractions of latex.

grafted PEO chains when the particle–particle separation is less than 2δ (where δ is the grafted PEO layer thickness). Above 0.3 mol dm^{-3} Na_2SO_4, there is a rapid increase in σ_β. Thus, the CFC of all concentrated latex dispersions is around 0.3 mol dm^{-3} Na_2SO_4. It should be mentioned that at Na_2SO_4 below the CFC, σ_β shows a measurable decrease with increasing Na_2SO_4 concentration. This due to the reduction in the effective radius of the latex particles as a result of the reduction in the solvency of the medium for the chains. This accounts for a reduction in the effective volume fraction of the dispersion which is accompanied by a reduction in σ_β.

Fig. 14.39 shows the results for the variation of the storage modulus G' with Na_2SO_4 concentration. These results show the same trend as those shown in Fig. 14.38, i.e. an initial reduction in G' due to the reduction in the effective volume fraction, followed by a sharp increase above the CFC (which is 0.3 mol dm^{-3} Na_2SO_4). Log-log plots of σ_β and G' versus ϕ_s at various Na_2SO_4 concentrations are shown in Fig. 14.40 and 14.41. All the data are described by the following scaling equations,

$$\sigma_\beta = k\phi_s^m, \tag{14.55}$$

$$G' = k'\phi_s^n, \tag{14.56}$$

with $0.35 < \phi_s < 0.53$.

The values of m and n are very high at Na_2SO_4 concentration below the CFC, reaching values in the range of 30–50 and indicating the strong steric repulsion between the latex particles. When the Na_2SO_4 concentration exceeds the CFC, m and n decrease very sharply reaching a value of $m = 9.4$ and $n = 12$ when the Na_2SO_4 concentration increases to 0.4 mol dm^{-3} and a value of $m = 2.8$ and $n = 2.2$ at 0.5 mol dm^{-3} Na_2SO_4.

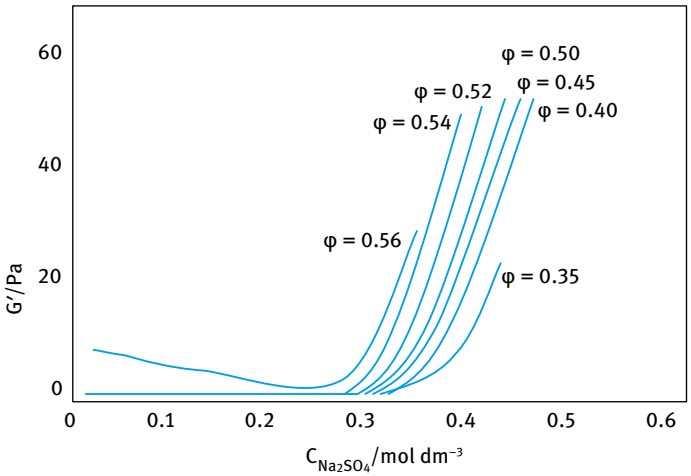

Fig. 14.39: Variation of G' with Na_2SO_4 concentration at various volume fractions of latex.

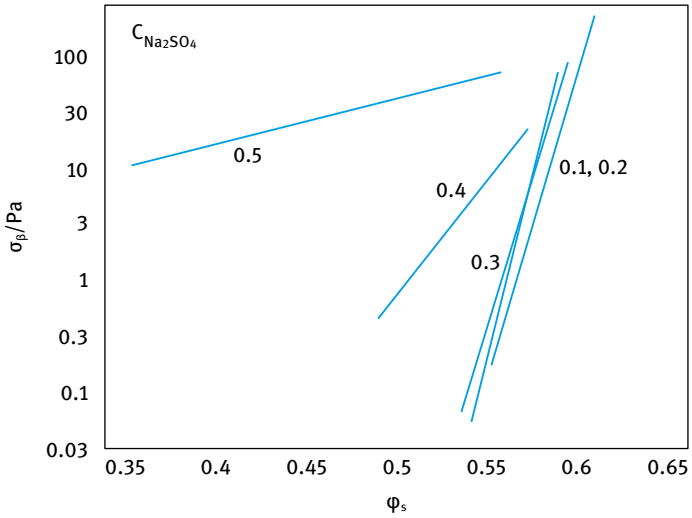

Fig. 14.40: Log-log plots of σ_β versus ϕ_s.

These slopes can be used to calculate the fractal dimensions (see above) giving a value of $D = 2.70–2.75$ at 0.4 mol dm^{-3} and $D = 1.6–1.9$ at 0.5 mol dm^{-3} Na_2SO_4.

The above results of fractal dimensions indicate a different floc structure when compared with the results obtained using electrolyte to induce coagulation. In the latter case, $D = 2.67$ indicating a compact structure similar to that obtained at 0.4 mol dm^{-3} Na_2SO_4. However, when the Na_2SO_4 concentration exceeded the CFC

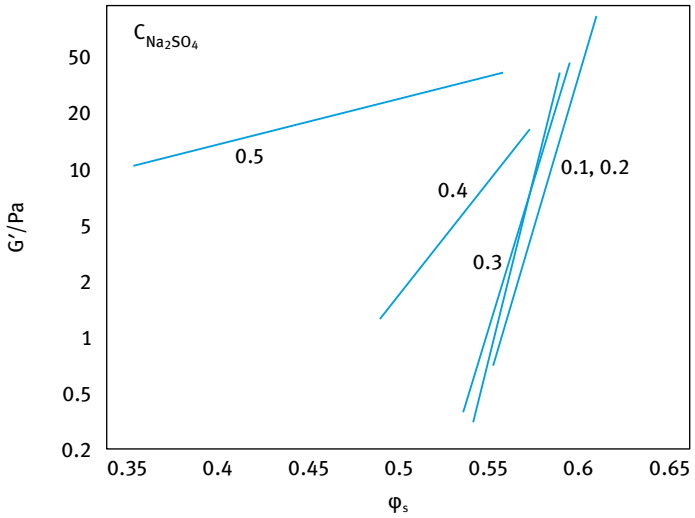

Fig. 14.41: Log-log plots of G' versus ϕ_s.

value (0.5 mol dm^{-3} Na_2SO_4) a much more open floc structure with a fractal dimension less than 2 was obtained.

Sterically stabilized dispersions with PEO chains as stabilizers also undergo flocculation on increasing the temperature. At a critical temperature (critical flocculation temperature, CFT) the Flory–Huggins interaction parameter becomes higher than 0.5 resulting in incipient flocculation. This is illustrated in Fig. 14.42 which shows the variation of the storage modulus G' and loss modulus G'' with increasing temperature for a latex dispersion with a volume fraction $\phi = 0.55$ and at an Na_2SO_4 concentration of 0.2 mol dm^{-3}. At this electrolyte concentration the latex is stable in the temperature range 10–40 °C. However, above this temperature (CFT) the latex is strongly flocculated.

The results of Fig. 14.42 show an initial systematic reduction in the moduli values with increasing temperature up to 40 °C. This is the result of a reduction in solvency of the chains with increasing temperature. The latter increase causes a breakdown in the hydrogen bonds between the PEO chains and the water molecules. This results in a reduction in the thickness of the grafted PEO chains and hence a reduction in the effective volume fraction of the dispersion. The latter causes a decrease in the moduli values. However, at 40 °C there is a rapid increase in the moduli values with any further increase of temperature. The latter indicates the onset of flocculation (the CFT). Similar results were obtained at 0.3 and 0.4 mol dm^{-3} Na_2SO_4, but in these cases the CFT was 35 and 15 °C respectively.

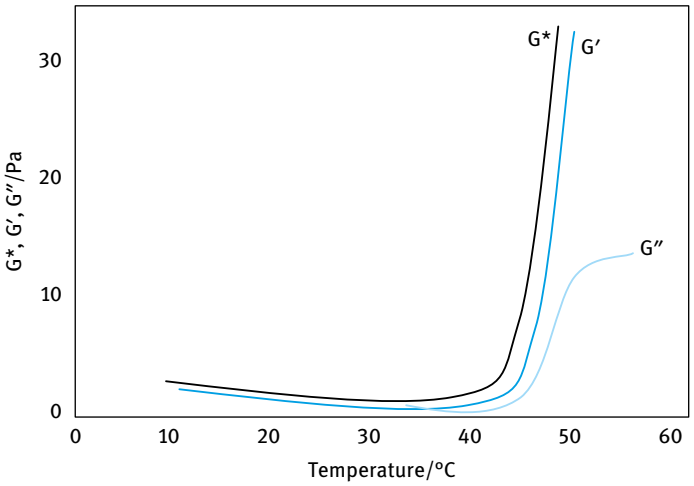

Fig. 14.42: Variation of G^*, G' and G'' with temperature with latex dispersions ($\phi_s = 0.55$) in 0.2 mol dm^{-3} Na_2SO_4.

14.4.3 Models for interpreting rheological results

14.4.3.1 Doublet floc structure model

Firth, Neville and Hunter [41] introduced a doublet floc model to deal with sterically stabilized dispersions that have undergone flocculation. They assumed that the major contribution to the excess energy dissipation in such pseudoplastic systems comes from the shear field which provides energy to separate contacting particles in a floc. The extrapolated yield value can be expressed as,

$$\sigma_\beta = \frac{3\phi_H^2}{2\pi^2(R+\delta)^2} E_{sep}, \tag{14.57}$$

where ϕ_H is the hydrodynamic volume fraction of the particles that is equal to the effective volume fraction,

$$\phi_H = \phi_s \left[1 + \frac{\delta}{R}\right]^3. \tag{14.58}$$

$(R + \delta)$ is the interaction radius of the particle and E_{sep} is the energy needed to separate a doublet, which is the sum of van der Waals and steric attractions,

$$E_{sep} = \frac{AR}{12H_0} + G_s. \tag{14.59}$$

At a particle separation of ≈ 12 nm (twice the grafted polymer layer thickness), the van der Waals attraction is very small (1.66 kT, where k is the Boltzmann constant and T is the absolute temperature) and the contribution of G_s to the attraction is significantly larger than the van der Waals attraction. Therefore, E_{sep} may be approximated to G_s.

Tab. 14.4: Results of E_{sep} calculated from σ_β for flocculated sterically stabilized latex dispersions at various latex volume fractions.

0.4 mol dm^{-3} Na_2SO_4			0.4 mol dm^{-3} Na_2SO_4		
ϕ_s	σ_β (Pa)	E_{sep} (kT)	ϕ_s	σ_β (Pa)	E_{sep} (kT)
0.43	1.3	97	0.25	3.5	804
0.45	2.4	165	0.29	5.4	910
0.51	3.3	179	0.33	7.4	961
0.54	5.3	262	0.37	11.4	1170
0.55	7.3	336	0.41	14.1	1190
0.57	9.1	397	0.44	17.0	1240
0.58	17.4	736	0.47	21.1	1380
			0.49	23.1	1390
			0.52	28.3	1510

From equation (14.57) one can estimate E_{sep} from σ_β. The results are shown in Tab. 14.4 which shows an increase in E_{sep} with increasing ϕ_s.

The values of E_{sep} given in Tab. 14.4 are unrealistically high and hence the assumptions made for calculating E_{sep} are not fully justified and hence the data of Tab. 14.4 must be only considered as qualitative.

14.4.3.2 Elastic floc model

This model [42–44] has been described above and it is based on the assumption that the structural units are small flocs of particles (called flocculi) which are characterized by the extent to which the structure is able to entrap the dispersion medium. A floc is made from an aggregate of several flocculi. The latter may range from a loose open structure (if the attractive forces between the particles are strong) to a very close-packed structure with little entrapped liquid (if the attractive forces are weak). In the system of flocculated sterically stabilized dispersions, the structure of the flocculi depends on the volume fraction of the solid and how far the system is from the critical flocculation concentration (CFC). Just above the CFC, the flocculi are probably close-packed (with relatively small floc volume), whereas far above the CFC a more open structure is found which entraps a considerable amount of liquid. Both types of flocculi persist at high shear rates, although the flocculi with weak attraction may become more compact by maximizing the number of interactions within the flocculus.

As discussed above, the Bingham yield value is given by equation (14.30) which allows one to obtain the floc radius a_{floc} provided one can calculate the floc volume ratio C_{FP} (ϕ_F/ϕ_s) and assumes a value for Δ (the distance through which bonds are stretched inside the floc by the shearing force).

At high volume fractions, ϕ_F and hence C_{FP}, can be calculated using the Krieger equation [14, 15],

$$\eta_{pl} = \eta_0 \left(1 - \frac{\phi_F}{\phi_s^m}\right)^{-[\eta]\phi_s^m}, \tag{14.60}$$

where η_0 is the viscosity of the medium, ϕ_s^m is the maximum packing fraction which may be taken as 0.74 and $[\eta]$ is the intrinsic viscosity taken as 2.5.

Assuming a value of Δ of 0.5 nm, the floc radius R_{floc} was calculated using equation (14.60). Fig. 14.43 shows the variation of R_{floc} with latex volume fraction at the two Na_2SO_4 concentrations studied. At any given electrolyte concentration, the floc radius increases with increasing latex volume fraction, as expected. This can be understood by assuming that the larger flocs are formed by fusion of two flocs and the smaller flocs by "splitting" of the larger ones. From simple statistical arguments, one can predict that a_{floc} will increase with increasing ϕ_s because in this case larger flocs are favoured over smaller ones. In addition, at any given volume fraction of latex, the floc radius increases with increasing electrolyte concentration. This is consistent with the scaling results as discussed above.

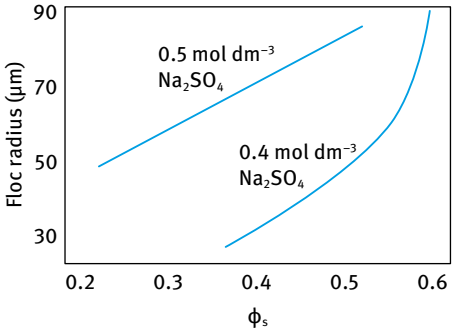

Fig. 14.43: Floc radius (a_{floc}) as a function of latex volume fraction at 0.4 and 0.5 mol dm^{-3} (above the CFC).

The above results clearly show the correlation of viscoelasticity of flocculated dispersions with their interparticle attraction. These measurements allow one to obtain the CFC and CFT of concentrated flocculated dispersions with reasonable accuracy. In addition, the results obtained can be analysed using various models to obtain some characteristics of the flocculated structure, such as the "openness" of the network, the liquid entrapped in the floc structure and the floc radius. Clearly, several assumptions have to be made, but the trends obtained are consistent with expectations from theory.

14.5 Using rheological measurements to assess and predict the long-term physical stability of formulations

14.5.1 Assessment of creaming and sedimentation

Most formulations undergo creaming or sedimentation as a result of the density difference between disperse phase particles and medium. This situation is particularly the case with most practical systems that contain particles with radii R than are large (> 1 μm) in which the Brownian diffusion is not sufficient to overcome the gravity force, i.e.,

$$kT \ll (4/3)\pi R^3 \Delta\rho g L, \tag{14.61}$$

where k is the Boltzmann constant, T is the absolute temperature, R is the particle radius, $\Delta\rho$ is the density difference between the disperse phase and the medium, g is the acceleration due to gravity and L is the height of the container.

14.5.2 Accelerated tests and their limitations

Several tests have been designed to accelerate the process of sedimentation or creaming, the most commonly used methods are based on increasing temperature or subjecting the suspension or emulsion to high g forces (using a high-speed centrifuge).

With increasing temperature, the viscosity of the system usually decreases and hence sedimentation or creaming is accelerated. The assumption is usually made that if a suspension or emulsion does not show any sedimentation, creaming or separation at 50 °C for say one month, the system will show no separation at ambient temperatures for more than one year.

The above method is only valid if the formulation viscosity η follows the Arrhenius equation that predicts a linear increase in $\ln \eta$ with $(1/T)$ where T is the absolute temperature. Most practical formulations do not follow such plot due to the possible phase changes or flocculation that may occur at high temperatures. With many surfactant systems, such phase changes may result in the formation of liquid crystalline phases that have higher viscosity at high temperatures and hence no separation results at high temperatures, although that could occur at ambient conditions.

A useful accelerated test, if carefully studied, is the application of high gravity (g) force; this has been particularly applied to emulsions. The assumption is also made here that by increasing the g force the rate of sedimentation or creaming is significantly increased and this could be applied to predict the process from measurements at short time periods.

In a centrifuge, the gravity force is given by,

$$g = \omega^2 x, \tag{14.62}$$

where x is the mean distance of the centrifuge tube from the axis of rotation and ω is the angular velocity ($\omega = 2\pi\nu$, where ν is the number of revolutions per second). Note that if the centrifuge tube is not small compared to x, then the applied centrifugal field cannot be considered to be uniform over the length of the tube.

Modern analytical ultracentrifuges allow one to follow the separation of emulsions in a quantitative manner. With typical O/W emulsions, three layers are generally observed:

(i) a clear aqueous phase;
(ii) an opaque phase consisting of distorted polyhedral oil droplets;
(iii) a clear separated oil phase, resulting from coalescence of the polyhedra.

The degree of emulsion stability may be taken as the volume of the opaque phase remaining after time t. Alternatively, one may use the volume of oil separated at infinite time as an index for stability.

A simple expression may be used to treat the data in a quantitative manner,

$$\frac{t}{V} = \frac{1}{bV_\infty} + \frac{1}{V_\infty}, \tag{14.63}$$

where V is the volume of oil separated at time t, V_∞ is the extrapolated volume at infinite time and b is a constant.

A plot of t/V versus t should give a straight line from which b and V_∞ may be calculated. These two parameters may be taken as indices for emulsion stability.

A more rigorous procedure to studying emulsion stability using the ultracentrifuge is to observe the system at various speeds of rotation. At relatively low centrifuge speeds one may observe the expected opaque cream layer. At sufficiently high centrifuge speeds, one may observe a coalesced oil layer and a cream layer which are separated by an extra layer of deformed oil droplets. This deformed layer looks like a "foam", i.e. it consists of oil droplets separated by thin aqueous films.

For certain emulsions, one may find that by increasing the centrifuge speed, the "foam"/cream layer boundary does not move. Under conditions where there is an equilibrium between the "foam"/cream layer, one may conclude that there is no barrier to be overcome in forming the foam layer from the cream layer. This implies that in the foam layer, the aqueous film separating two oil droplets thins to a "black" film under the action of van der Waals forces. The boundary between the foam layer and the coalesced layer is associated with a force (or pressure) barrier.

One may observe the minimum centrifuge speed that is necessary to produce a visible amount of coalesced oil after, say, 30 minutes of centrifugation. This centrifuge speed may be used to calculate the "critical pressure" that needs to be applied to induce coalescence.

14.5.3 Rheological techniques for predicting sedimentation or creaming

Sedimentation or creaming is prevented by addition of "thickeners" that form a "three-dimensional elastic" network in the continuous phase. If the viscosity of the elastic network at shear stresses (or shear rates) comparable to those exerted by the particles or droplets exceeds a certain value, then creaming or sedimentation is completely eliminated.

The shear stress, σ_p, exerted by a particle (force/area) can be simply calculated,

$$\sigma_p = \frac{(4/3)\pi R^3 \Delta\rho g}{4\pi R^2} = \frac{\Delta\rho R g}{3}. \tag{14.64}$$

For a 10 μm radius particle with a density difference $\Delta\rho$ of 0.2 g cm^{-3}, the stress is equal to,

$$\sigma_p = \frac{0.2 \times 10^3 \times 10 \times 10^{-6} \times 9.8}{3} \approx 6 \times 10^{-3} \text{ Pa}. \tag{14.65}$$

For smaller particles smaller stresses are exerted.

Thus, to predict creaming or sedimentation, one has to measure the viscosity at very low stresses (or shear rates). These measurements can be carried out using a constant stress rheometer (Carrimed, Bohlin, Rheometrics, Haake or Physica).

Usually one obtains a good correlation between the rate of creaming or sedimentation v and the residual viscosity $\eta(0)$. This is illustrated in Fig. 14.44. Above a certain value of $\eta(0)$, υ becomes equal to 0. Clearly, to minimize creaming or sedimentation one has to increase $\eta(0)$; an acceptable level for the high shear viscosity η_∞ must be achieved, depending on the application. In some cases, a high $\eta(0)$ may be accompanied by a high η_∞ (which may not be acceptable for the application, for example if a dispersion is required to be spread on the skin). If this is the case, the formulation chemist should look for an alternative thickener.

Another problem encountered with many formulations is that of "syneresis", i.e. the appearance of a clear liquid film at the bottom (if creaming is the case) or the top (if sedimentation is the case) of the container. "Syneresis" occurs with most "flocculated" and/or "structured" (i.e. those containing a thickener in the continuous phase) formulations. "Syneresis" may be predicted from measuring the yield value (using steady

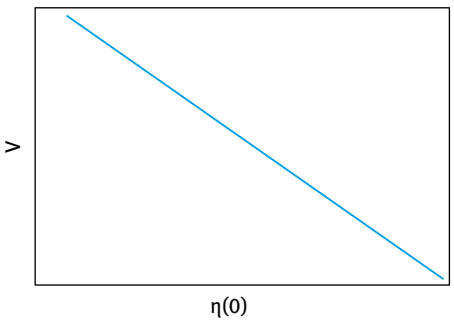

Fig. 14.44: Variation of creaming or sedimentation rate with residual viscosity.

state measurements of shear stress as a function of shear rate) as a function of time or using oscillatory techniques (whereby the storage and loss modulus are measured as a function of strain amplitude and frequency of oscillation).

The oscillatory measurements are perhaps more useful since to prevent separation the bulk modulus of the system should balance the gravity force that is given by $h\Delta\rho g$ (where h is the height of the disperse phase, $\Delta\rho$ is the density difference and g is the acceleration due to gravity).

The bulk modulus is related to the storage modulus G'. A more useful predictive test is to calculate the cohesive energy density of the structure E_c that is given by equation (4.28). The separation of a formulation decreases with increasing E_c. This is illustrated in Fig. 14.45 which schematically shows the reduction in % separation with increasing E_c. The value of E_c that is required to stop complete separation depends on the particle or droplet size distribution, the density difference between the particle or droplet and the medium as well as on the volume fraction ϕ of the dispersion.

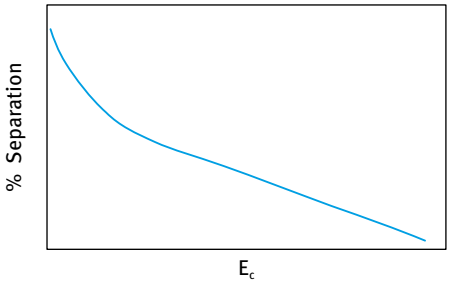

Fig. 14.45: Schematic representation of the variation of % separation with E_c.

14.5.4 Examples of correlation of sedimentation or creaming with residual (zero shear) viscosity

14.5.4.1 Model suspensions of aqueous polystyrene latex

The sedimentation rate is a complex function of the volume fraction ϕ. This was tested using polystyrene latex suspensions with radius $R = 1.55\,\mu m$ in 10^{-3} mol dm^{-3} NaCl [45].

One may be able to correlate the change in the rate of sedimentation with increasing ϕ with the viscosity of the suspension as predicted by the Dougherty–Krieger equation (14.33)

$$\frac{v}{v_0} \propto \frac{\eta_0}{\eta}, \tag{14.66}$$

$$\frac{v}{v_0} = \alpha\frac{\eta_0}{\eta}, \tag{14.67}$$

where α is a constant.

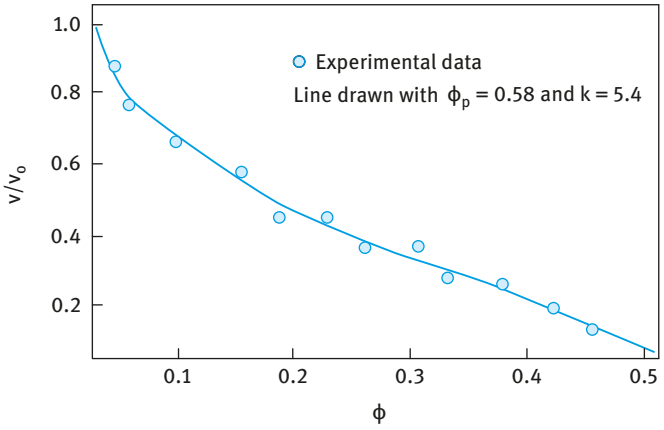

Fig. 14.46: Variation of sedimentation rate with volume fraction for polystyrene dispersions.

$$\frac{\upsilon}{\upsilon_0} = \left[1 - \left(\frac{\phi}{\phi_p}\right)\right]^{\alpha[\eta]\phi_p} = \left(1 - \frac{\phi}{\phi_p}\right)^{k\phi_p}, \tag{14.68}$$

where ϕ_p is the maximum packing fraction and $[\eta]$ is the intrinsic viscosity.

Equation (14.68) was tested for polystyrene dispersions as illustrated in Fig. 14.46.

14.5.4.2 Sedimentation and creaming in non-Newtonian liquids

To reduce sedimentation or creaming one usually adds high molecular weight material, e.g. hydroxyethyl cellulose or xanthan gum. Above a critical concentration, C^*, such polymer solutions show non-Newtonian flow in aqueous solution. This is illustrated in Fig. 14.47 which shows the variation of shear stress and viscosity with shear rate. Fig. 14.48 shows the variation of log η with log C to illustrate the onset of free coil overlap.

Before overlap $\eta \propto C$, whereas after overlap $\eta \propto C^{3.4}$. Two limiting Newtonian viscosities are identified:

(i) residual (zero shear) viscosity $\eta(0)$;
(ii) Newtonian high shear rate viscosity η_∞.

$\eta(0)$ can be several order of magnitude (10^3–10^5) higher than η_∞ and such high $\eta(0)$ can significantly reduce creaming or sedimentation. As mentioned above, thickeners reduce creaming or sedimentation by increasing the residual viscosity $\eta(0)$ which must be measured at stresses compared to those exerted by the droplets or particles (mostly less than 0.1 Pa). At such low stresses, $\eta(0)$ increases very rapidly with increasing "thickener" concentration. This rapid increase is not observed at high stresses and this illustrates the need for measurements at low stresses (using constant stress or creep measurements). As an illustration Fig. 14.49 shows the variation of η with ap-

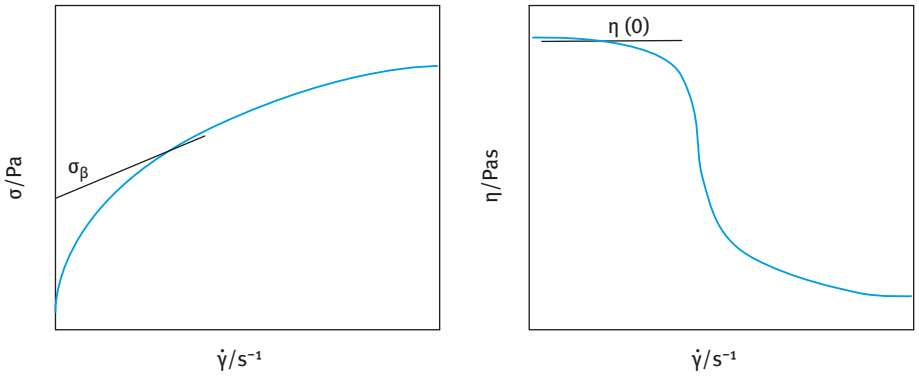

Fig. 14.47: Flow behaviour of "thickeners".

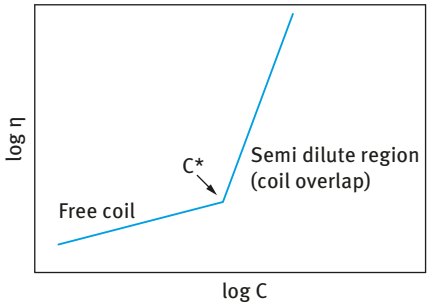

Fig. 14.48: Variation of log η with log C.

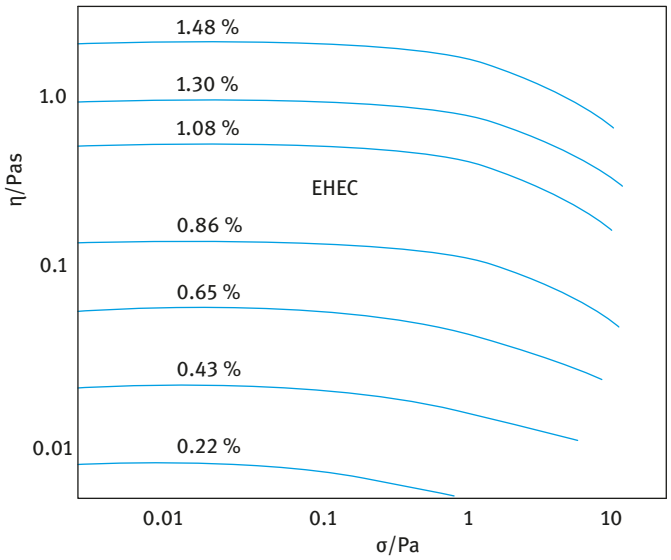

Fig. 14.49: Constant stress (creep) measurements for PS latex dispersions as a function of EHEC concentration.

plied stress σ for ethyl hydroxyethyl cellulose (EHEC), a thickener that is applied in some formulations.

It can be seen that the limiting residual viscosity increases rapidly with increasing EHEC concentration. A plot of sedimentation rate for 1.55 µm PS latex particles versus $\eta(0)$ is shown in Fig. 14.50 which shows an excellent correlation. In this case a value of $\eta(0) \geq 10$ Pa s is sufficient for reducing the rate of sedimentation to 0.

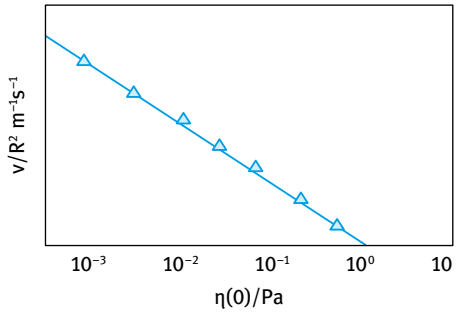

Fig. 14.50: Sedimentation rate versus $\eta(0)$.

14.5.4.3 Predicting emulsion creaming

For this purpose some model emulsions were prepared using mixtures of oils and commercial surfactants [46, 47]. The oil phase of the emulsion consisted of 10 parts Arlamol HD (Isohexadecane), 2 parts of Estol 3603 (Caprylic/capric triglyceride), 1 part of sunflower oil (Florasen 90, helanthus Annus) and 1 part of avocado oil (Persea Gratissima). Two emulsifier systems were used for the preparation of oil-in-water (O/W) emulsions. The first emulsifier was Pluronic PEF 127, an A–B–A block copolymer of polyethylene oxide, PEO (the A chains, about 100 EO units each) and propylene oxide PPO (the B chain, about 55 PO units). The second emulsifier system was Arlatone V-100, which is a nonionic emulsifier systems made of a blend of Steareth-100 (stearyl alcohol with 100 EO units), Steareth-2 (Stearyl alcohol with 2 EO units), glyceryl stearate citrate, sucrose and a mixture of two polysaccharides, namely mannan and xanthan gum. In some emulsions, xanthan gum was used as a thickener. All emulsions contained a preservative (Nipaguard BPX).

The rate of creaming and cream volume was measured using graduated cylinders. The creaming rate was assessed by comparing the cream volume V_c with that of the maximum value V_∞ obtained when the emulsion was stored at 55 °C. The time $t_{0.3}$ taken to reach a value of $V_c/V_\infty = 0.3$ (i.e. 30 % of the maximum rate) was calculated [48]. All rheological measurements were carried out using a Physica UDS 200 (universal dynamic spectrometer). A cone and plate geometry was used with a cone angle of 2°. The emulsions were also investigated using optical microscopy and image analysis.

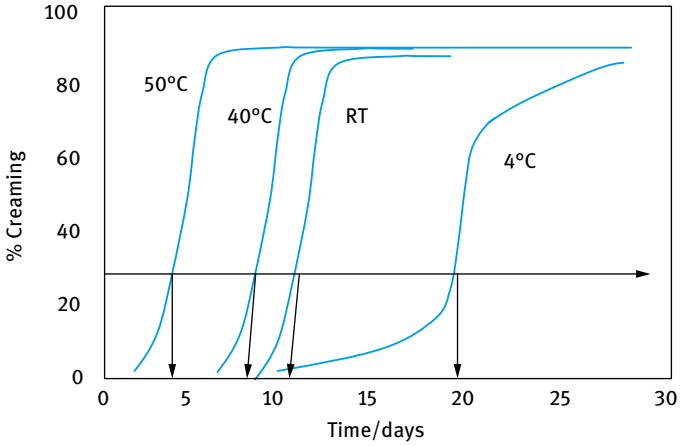

Fig. 14.51: Percentage creaming versus time at various temperatures.

Fig. 14.51 shows the results for creaming rates obtained at various temperatures, using a 20/80 O/W emulsion stabilized with Pluronic PEF 127. As is clear, $t_{0.3}$ decreases with increasing temperature.

The most useful method to predict creaming is to use constant stress (creep) measurements. From these measurements one can obtain the residual (zero shear) viscosity $\eta(0)$ as discussed above. Results were obtained for 20/80 v/v % emulsions as a function of Arlatone V-100 concentration. The results are shown in Fig. 14.52 after several periods of storage time (1 day, 1 week, 2 weeks and 1 month). $\eta(0)$ showed a large decrease after 1 day, which could be due to equilibration of the structure. The results after 1 week, two weeks and one month are close to each other. There is a significant increase in $\eta(0)$ when the Arlatone V-100 concentration increased above 0.8 %. The

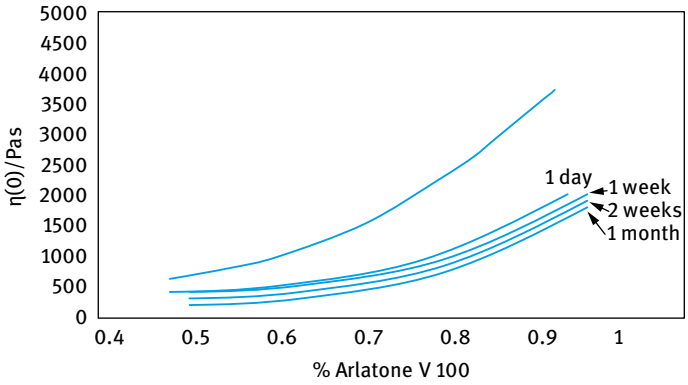

Fig. 14.52: Variation of residual viscosity with Arlatone V-100 concentration at various storage times.

creaming rate of the emulsion also showed a sharp decrease above 0.8 % Arlatone V-100 indicating the correlation between $\eta(0)$ and creaming rate.

A very useful method for predicting creaming is to measure the cohesive energy density as given by equation (4.28). As an illustration, Fig. 14.53 shows the variation of cohesive energy density E_c with Arlatone V-100 concentration. The results clearly show a rapid increase in E_c above 0.8 % Arlatone V-100. E_c seems to show a decrease in the values after storage for 2 weeks. This may be due to a small increase in droplet size (as a result of some coalescence) which results in a reduction in the cohesive energy density. This small increase in droplet size could not be detected by microscopy since the change was very small.

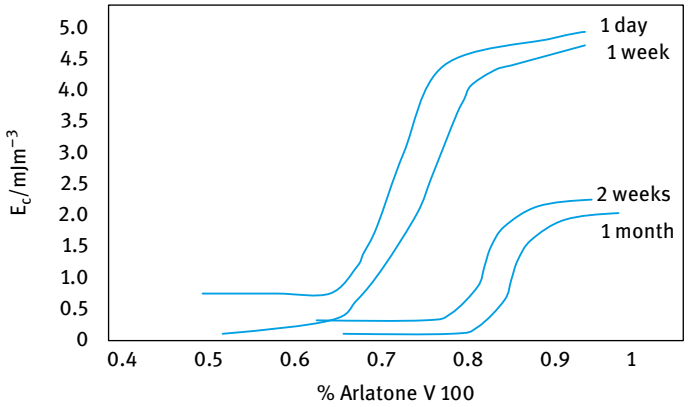

Fig. 14.53: Variation of E_c with % Arlatone V-100 in the emulsion.

14.5.5 Assessing and predicting flocculation using rheological techniques

Steady state rheological investigations may be used to investigate the state of flocculation of a formulation. Weakly flocculated dispersions usually show thixotropy and the change of thixotropy with applied time may be used as an indication of the strength of this weak flocculation. These methods are only qualitative and one cannot use the results in a quantitative manner. This is due to the possible breakdown of the structure on transferring the formulation to the rheometer and also during the uncontrolled shear experiment. Better techniques to study flocculation of a formulation are constant stress (creep) or oscillatory measurements. By careful transfer of the sample to the rheometer (with minimum) shear the structure of the flocculated system may be maintained.

A very important point that must be considered in any rheological measurement is the possibility of "slip" during the measurements. This is particularly the case with highly concentrated dispersions, where the flocculated system may form a "plug" in the gap of the platens leaving a thin liquid film at the walls of the concentric cylinder

or cone-and-plate geometry. This behaviour is caused by some "syneresis" of the formulation in the gap of the concentric cylinder or cone and plate. To reduce "slip", one should use roughened walls for the platens. A vane rheometer may also be used.

In steady state measurements, the formulation is stored at various temperatures and the yield value σ_β and plastic viscosity η_{pl} are measured at various intervals of time. Any flocculation in the formulation should be accompanied by an increase in σ_β and η_{pl}. A rapid technique to study the effect of temperature changes on the flocculation of a formulation is to carry out temperature sweep experiments, running the samples from, say 5–50 °C. The trend in the variation of σ_β and η_{pl} with temperature can quickly give an indication of the temperature range at which a formulation remains stable (during that temperature range σ_β and η_{pl} remain constant).

If Ostwald ripening and/or coalescence occur simultaneously, σ_β and η_{pl} may change in a complex manner with storage time. Ostwald ripening and/or coalescence result in a shift of the particle size distribution to higher diameters. This has the effect of reducing σ_β and η_{pl}. If flocculation occurs simultaneously (having the effect of increasing these rheological parameters), the net effect may be an increase or decrease of the rheological parameters. This trend depends on the extent of flocculation relative to Ostwald ripening and/or coalescence. Therefore, following σ_β and η_{pl} with storage time requires knowledge of Ostwald ripening and/or coalescence. Only in the absence of these latter breakdown processes can one use rheological measurements as a guide to assessing flocculation.

Constant stress (creep) measurements can also be applied to study the flocculation of a formulation. A set of creep curves are produced at various applied stresses at several storage times and temperatures. From the slope of the linear portion of the creep curve (after the system reaches a steady state), the viscosity at each applied stress, η_σ, is calculated as described before. A plot of η_σ versus σ allows one to obtain the limiting (or zero shear) viscosity $\eta(0)$ and the critical stress σ_{cr} (which may be identified with the "true" yield stress of the system). The values of $\eta(0)$ and σ_{cr} may be used to assess the flocculation of the formulation on storage. If flocculation occurs on storage (without any Ostwald ripening or coalescence), the values of $\eta(0)$ and σ_{cr} may show a gradual increase with increasing storage time. As discussed above, the trend becomes complicated if Ostwald ripening and/or coalescence occur simultaneously (both have the effect of reducing $\eta(0)$ and σ_{cr}). These measurements should be supplemented by particle size distribution measurements of the diluted dispersion (making sure that no flocs are present after dilution) to assess the extent of Ostwald ripening and/or coalescence. Another complication may arise from the nature of the flocculation. If flocculation occurs in an irregular way (producing strong and tight flocs), $\eta(0)$ may increase, while σ_{cr} may show some decrease and this complicates the analysis of the results. In spite of these complications, constant stress measurements may provide valuable information on the state of the formulation on storage.

Carrying out creep experiments and ensuring that a steady state is reached can be time consuming. One usually carries out a stress sweep experiment, in which the

stress is gradually increased (within a predetermined time period to ensure that one is not too far from reaching the steady state) and plots of η_σ versus σ are established. These experiments are carried out at various storage times (say every two weeks) and temperatures. From the change of $\eta(0)$ and σ_{cr} with storage time and temperature, one may obtain information on the degree and the rate of flocculation of the system.

One main problem in carrying out these experiments is sample preparation. When a flocculated dispersion is removed from the container, care should be taken not to cause much disturbance to that structure (minimum shear should be applied on transferring the formulation to the rheometer). It is also advisable to use separate containers for assessing flocculation; a relatively large sample is prepared and this is then transferred to a number of separate containers. Each sample is used separately at a given storage time and temperature. One should be careful in transferring the sample to the rheometer. If any separation occurs in the formulation the sample is gently mixed by placing it on a roller. It is advisable to use as minimum shear as possible when transferring the sample from the container to the rheometer (the sample is preferably transferred using a "spoon" or by simple pouring from the container). The experiment should be carried out without an initial pre-shear.

Dynamic or oscillatory measurements can also be used to investigate the flocculation of a formulation. As mentioned before, one carries out two sets of experiments:

(i) Strain sweep measurements, where the oscillation is fixed (say at 1 Hz) and the viscoelastic parameters are measured as a function of strain amplitude; G^*, G' and G'' remain virtually constant up to a critical strain value, γ_{cr}. This region is the linear viscoelastic region. Above γ_{cr}, G^* and G' starts to fall, whereas G'' starts to increase; this is the nonlinear region. The value of γ_{cr} may be identified with the minimum strain above which the "structure" of the formulation starts to break down (for example breakdown of flocs into smaller units and/or breakdown of a "structuring" agent). From γ_{cr} and G', one can obtain the cohesive energy E_c (J m^{-3}) of the flocculated structure using equation (4.28). E_c may be used in a quantitative manner as a measure of the extent and strength of the flocculated structure in a dispersion. The higher the value of E_c the more flocculated the structure is. Clearly, E_c depends on the volume fraction of the dispersion as well as the particle size distribution (which determines the number of contact points in a floc). Therefore, for quantitative comparison between various systems, one has to make sure that the volume fraction of the disperse particles is the same and the dispersions have very similar particle size distribution. E_c also depends on the strength of the flocculated structure, i.e. the energy of attraction between the droplets. This depends on whether the flocculation is in the primary or secondary minimum. Flocculation in the primary minimum is associated with a large attractive energy and this leads to higher values of E_c when compared with the values obtained for secondary minimum flocculation (weak flocculation). For a weakly flocculated dispersion, such as is the case with secondary minimum flocculation of an electrostatically stabilized system, the deeper the secondary minimum, the higher the value of E_c (at any given volume fraction and particle size distribution of the dispersion).

With a sterically stabilized dispersion, weak flocculation can also occur when the thickness of the adsorbed layer decreases. Again the value of E_c can be used as a measure of flocculation; the higher the value of E_c, the stronger the flocculation. If incipient flocculation occurs (on reducing the solvency of the medium for the change to worse than θ-condition) a much deeper minimum is observed and this is accompanied by a much larger increase in E_c. To apply this analysis, one must have an independent method for assessing the nature of the flocculation. Rheology is a bulk property that can give information on the interparticle interaction (whether repulsive or attractive) and to apply it in a quantitative manner one must know the nature of these interaction forces. However, rheology can be used in a qualitative manner to follow the change of the formulation on storage. Providing the system does not undergo any Ostwald ripening and/or coalescence, the change of the moduli with time and in particular the change of the linear viscoelastic region may be used as an indication of flocculation. Strong flocculation is usually accompanied by a rapid increase in G' and this may be accompanied by a decrease in the critical strain above which the "structure" breaks down. This may be used as an indication of formation of "irregular" and tight flocs which become sensitive to the applied strain. The floc structure will entrap a large amount of the continuous phase and this leads to an apparent increase in the volume fraction of the dispersion and hence an increase in G'.

(ii) Oscillatory sweep measurements, where the strain amplitude is kept constant in the linear viscoelastic region (one usually takes a point far from γ_{cr} but not too low, i.e. in the midpoint of the linear viscoelastic region) and measurements are carried out as a function of frequency. As mentioned before, both G^* and G' increase with increasing frequency and ultimately above a certain frequency, they reach a limiting value and show little dependency on frequency. G'' is higher than G' in the low frequency regime; it also increases with increasing frequency and at a certain characteristic frequency ω^* (that depends on the system) it becomes equal to G' (usually referred to as the crossover point), after which it reaches a maximum and then shows a reduction with any further increase in frequency. From ω^* one can calculate the relaxation time τ of the system using equation (14.25). The relaxation time may be used as a guide for the state of the dispersion. For a colloidally stable dispersion (at a given particle size distribution), τ increases with increasing volume fraction of the disperse phase, ϕ. In other words, the crossover point shifts to lower frequency with increasing ϕ. For a given dispersion, τ increases with increasing flocculation, providing the particle size distribution remains the same (i.e. no Ostwald ripening and/or coalescence).

The value of G' also increases with increasing flocculation, since aggregation of particles usually result in liquid entrapment and the effective volume fraction of the dispersion shows an apparent increase. With flocculation, the net attraction between the particles also increases and this results in an increase in G'. The latter is determined by the number of contacts between the particles and the strength of each contact (which is determined by the attractive energy).

It should be mentioned that in practice one may not obtain the full curve, due to the frequency limit of the instrument, and measurements at low frequency are also time consuming. Usually one obtains part of the frequency dependency of G' and G''. In most cases, one has a more elastic than viscous system. Most formulations used in practice are weakly flocculated and they also contain "thickeners" or "structuring" agents to reduce creaming or sedimentation and to acquire the right rheological characteristics for the application, e.g. in hand creams and lotions. The exact values of G' and G'' required depend on the system and its application. In most cases a compromise has to be made between acquiring the right rheological characteristics for the application and the optimum rheological parameters for long-term physical stability. Applying rheological measurements to achieve these conditions requires a great deal of skill and understanding of the factors that affect rheology.

14.5.6 Examples of applications of rheology to assessing and predicting flocculation

14.5.6.1 Flocculation and restabilization of clays using cationic surfactants

Hunter and Nicol [36] studied the flocculation and restabilization of kaolinite suspensions using rheology and zeta potential measurements. Fig. 14.54 shows plots of the yield value σ_β and electrophoretic mobility as a function of cetyl trimethyl ammonium bromide (CTAB) concentration at pH = 9.

σ_β increases with increasing CTAB concentration, reaching a maximum at the point where the mobility reaches zero (the isoelectric point, IEP, of the clay) and then decreasing with a further increase in CTAB concentration. This trend can be explained on the basis of flocculation and restabilization of the clay suspension. Initial addition of CTAB causes a reduction in the negative surface charge of the clay (by adsorption of

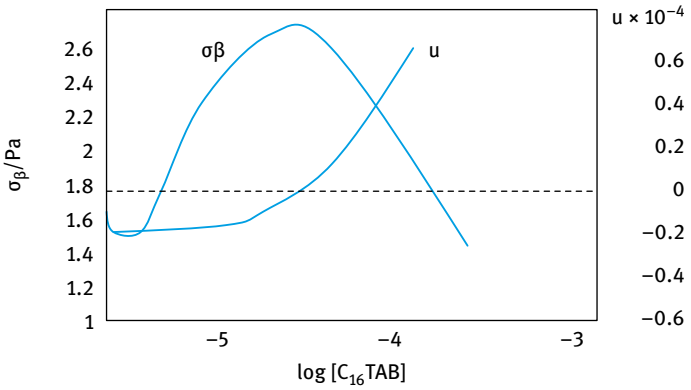

Fig. 14.54: Variation of yield value σ_β and electrophoretic mobility u with C_{16} TAB concentration.

CTA+ on the negative sites of the clay). This is accompanied by a reduction in the negative mobility of the clay. When complete neutralization of the clay particles occurs (at the IEP), maximum flocculation of the clay suspension occurs and this is accompanied by a maximum in σ_β. On a further increase in CTAB concentration, further adsorption of CTA+ occurs, resulting in charge reversal and restabilization of the clay suspension. This is accompanied by a reduction in σ_β.

14.5.6.2 Flocculation of sterically stabilized dispersions

Firth, Neville and Hunter [41] studied the flocculation of polymethylmethacrylate (PMMA) latex stabilized with poly(ethylene oxide) (PEO). Flocculation was induced by adding electrolyte and/or increasing temperature. Fig. 14.55 shows the variation of σ_β with increasing temperature at constant electrolyte concentration.

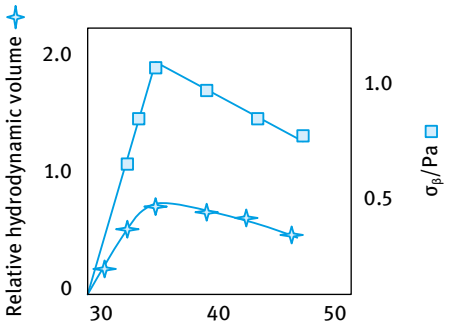

Fig. 14.55: Variation of σ_β and hydrodynamic volume with temperature.

It can be seen that σ_β increases with increasing temperature, reaching a maximum at the critical flocculation temperature (CFT) and then decreasing with a further increase in temperature. The initial increase is due to the flocculation of the latex with increasing temperature, as a result of a reduction of solvency of the PEO chains with increasing temperature. The reduction in σ_β after the CFT is due to the reduction in the hydrodynamic volume of the dispersion.

14.5.6.3 Flocculation of sterically stabilized emulsions

Emulsions were prepared using an A–B–A block copolymer of PEO–PPO–PEO (Pluronic F127). Flocculation was induced by addition of NaCl. Fig. 14.56 shows the variation of the yield value, calculated using the Herschel–Bulkley model, as a function of NaCl concentration at various storage times [47].

In the absence of NaCl, the yield value did not change with storage time over a period of 1 month, indicating absence of flocculation [47]. In the presence of NaCl, the yield value increased with increasing storage time and this increase was very sig-

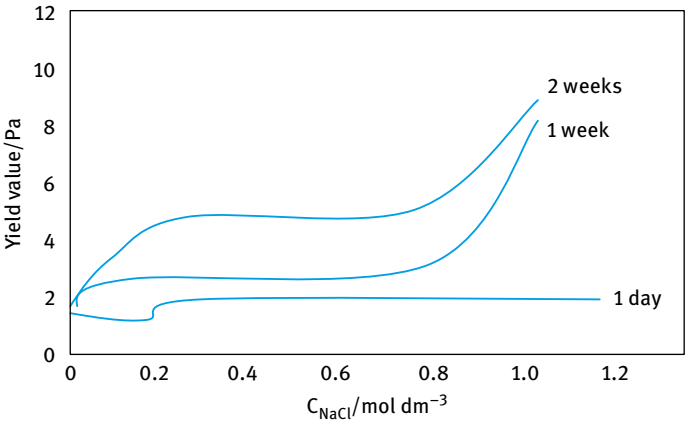

Fig. 14.56: Variation of yield value.

nificant when the NaCl concentration was increased above 0.8 mol dm^{-3} NaCl. This increase in yield value indicated flocculation of the emulsion and this was confirmed by optical microscopy. The smaller increase in yield value below 0.8 mol dm^{-3} NaCl is indicative of weak flocculation and this could be confirmed by redispersion of the emulsion by gentle shaking. Above 0.8 mol dm^{-3} NaCl, the flocculation was strong and irreversible. In this case, the solvency of the medium for the PEO chains becomes poor, resulting in incipient flocculation.

Further evidence of flocculation was also obtained from dynamic (oscillatory) measurements. Fig. 14.57 shows the variation of G' with NaCl concentration at various storage times.

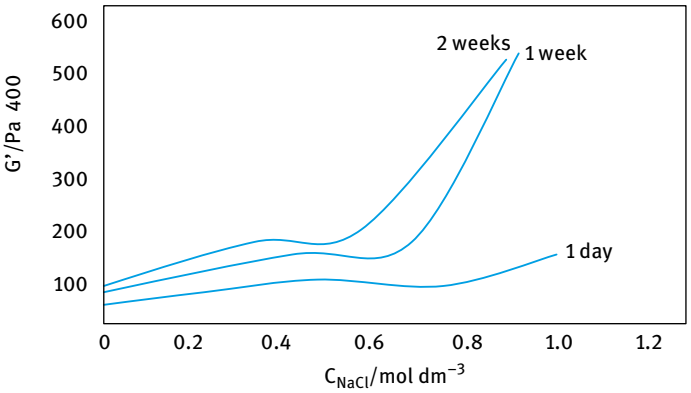

Fig. 14.57: Variation of G' with NaCl concentration.

Below 0.8 mol dm^{-3} NaCl, G' shows a modest increase in G' with storage time over a period of two weeks indicating weak flocculation. Above 0.8 mol dm^{-3} NaCl, G' shows a rapid increase in G' with increasing storage time indicating strong flocculation. This strong (incipient) flocculation is due to the reduction of solvency of PEO chains (worse than θ-solvent) resulting in strong attraction between the droplets which are difficult to redisperse.

14.5.7 Assessing and predicting emulsion coalescence using rheological techniques

As mentioned in Chapter 11, the driving force of emulsion coalescence is the thinning and disruption of the liquid film between the droplets. When two emulsion droplets come into contact, say in a cream layer or a floc, or even during Brownian collision, the liquid film between them undergoes some fluctuation in thickness; the thinnest part of the film will have the highest van der Waals attraction and this is the region where coalescence starts. Alternatively, the surfaces of the emulsion droplets may undergo fluctuation producing waves, which may grow in amplitude; the strongest van der Waals attraction is at the apices of these fluctuations and coalescence occurs by further growth of the fluctuation. One may define a critical film thickness below which coalescence occurs.

The rate of coalescence is determined by the rate at which the film thins and this usually follows a first-order kinetics,

$$N = N_0 \exp(-Kt), \tag{14.69}$$

where N is the number of droplets after time t, N_0 is the number at zero time and K is the rate constant of coalescence.

Alternatively, one can measure the average droplet diameter d as a function of time,

$$d = d_0 \exp(Kt). \tag{14.70}$$

Providing the emulsion does not undergo any flocculation, the coalescence rate can be simply measured by following the number of droplets or average diameter as a function of time. A given volume of the emulsion is carefully diluted into the Isotone solution of the Coulter Counter and the number of droplets is measured. The average diameter can be obtained using laser diffraction methods (e.g. using the Mastersizer). By following this procedure at various time periods, one can obtain the coalescence rate constant K.

Usually one plots log N or log d versus t and the slope of the line in the initial period gives the rate of coalescence K. Clearly, the higher the value of K, the higher the coalescence of the emulsion. An accelerated test may be used by subjecting the system to higher temperatures; usually the rate of coalescence increases with increasing temperature (although this is not always the case). One should be careful in the dilution

procedure, particularly if the oil is significantly soluble (say greater than 10 ppm) in the Isotone solution or in the tank of the Mastersizer. In this case, one should saturate the solution with the oil before diluting the concentrated emulsion for droplet counting or sizing.

In the absence of any flocculation, coalescence of an emulsion results in a reduction of its viscosity. At any given volume fraction of oil, an increase in droplet size results in a reduction in viscosity; this is particularly the case with concentrated emulsions. Thus by following the decrease in emulsion viscosity with time one may obtain information on its coalescence. However, one should be careful in applying simple viscosity measurements, particularly if flocculation occurs simultaneously (which results in an increase in the viscosity). It is possible in principle to predict the extent of viscosity reduction on storage, if one combines the results of droplet size analysis (or droplet number) as a function of time with the reduction in viscosity in the first few weeks.

Freshly prepared emulsions with various droplet sizes were prepared (by controlling the speed of the stirrer used for emulsification). The emulsifier concentration in these experiments should be kept constant and care should be taken that excess emulsifier is not present in the continuous phase. The viscosity of these freshly prepared emulsions is plotted versus the average droplet diameter. A master curve is produced that relates the emulsion viscosity to the average droplet size; the viscosity decreases monotonically with increasing average droplet size.

Using the Coulter Counter or Mastersizer one can determine the rate of coalescence by plotting log of the average droplet diameter versus time in the first few weeks. This allows one to predict the average droplet diameter over a longer period (say 6–12 months). The predicted average droplet diameter is used to obtain the viscosity that is reached on storage using the master curve of viscosity versus average drop size.

The above procedure is quite useful for setting the limit of viscosity that may be reached on storage as a result of coalescence. With many creams, the viscosity of the system is not allowed to drop below an acceptable limit (which is important for the application). The limit that may be reached after one year storage may be predicted from the viscosity and rate constant measurements over the first few weeks.

Emulsion coalescence can also be investigated by measuring the yield value as a function of time. Since the yield value σ_β of an emulsion depends on the number of contacts between the droplets, any coalescence should be accompanied by a reduction in the yield value. This trend is only observed if no flocculation occurs (this causes an increase in σ_β).

The above change was investigated using O/W emulsions that were stabilized with an A–B–A block copolymer of polyethylene oxide (PEO, A) and polypropylene oxide (PPO, B); Pluronic PEF 127. 60 : 40 O/W emulsions were prepared using 0.5, 1.0, 1.5, 2.0, 3, 4 and 5 % emulsifier [47]. Fig. 14.58 shows the variation of droplet size with time at various Pluronic PEF 127 concentrations. At emulsifier concentration > 2 % there is

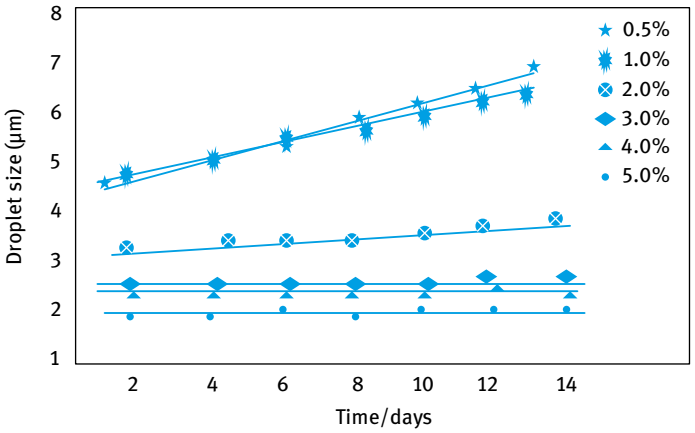

Fig. 14.58: Variation of droplet size with time at various synperonic PEF 127 concentrations.

no change of droplet size with time, indicating absence of coalescence. Below 2 % the droplet size increased with time, indicating coalescence.

Measuring the storage modulus G' as a function of time is perhaps the most sensitive method for predicting coalescence. G' is a measure of the contact points of the emulsion droplets as well as their strength. Providing no flocculation occurs (which results in an increase in G'), any reduction in G' on storage indicates coalescence. This trend was confirmed using the emulsions described above. The emulsions containing less than 3 % Pluronic PEF 127 showed a rapid reduction in G' when compared with those containing > 3 % which showed virtually no change in G' over a 2 week period. This is illustrated in Fig. 14.59.

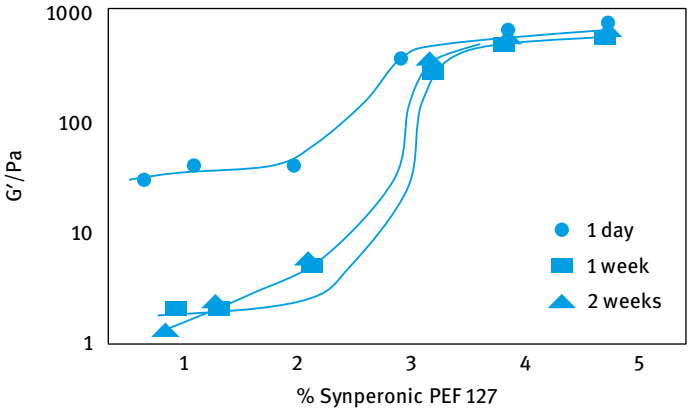

Fig. 14.59: Variation of G' with Pluronic PEF 127 concentration at various storage times.

The correlation between the emulsion elastic modulus and coalescence rate can be easily represented if one calculates the relative decrease in G' after 2 weeks,

$$\text{relative decrease of } G' = \left(\frac{G_{\text{initial}} - G_{\text{after 2 weeks}}}{G_{\text{initial}}} \right) \times 100. \tag{14.71}$$

Fig. 14.60 shows the variation in the relative decrease of G' and the relative increase in droplet size with Pluronic PEF 127 concentration. The correlation between the relative decrease in G' and the relative increase in droplet size as a result of coalescence is now very clear.

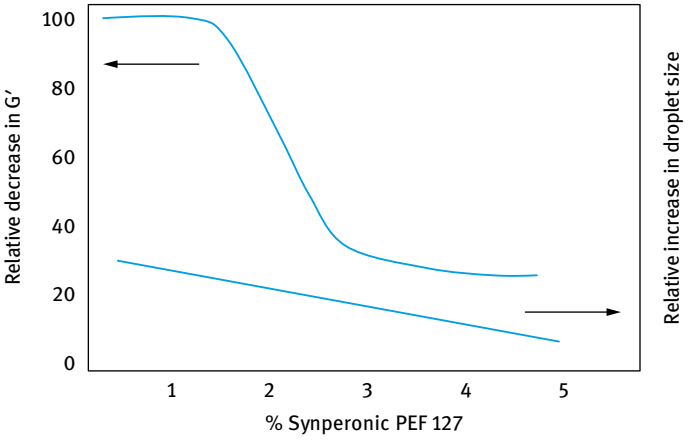

Fig. 14.60: Correlation of relative decrease in G' with relative increase in droplet size.

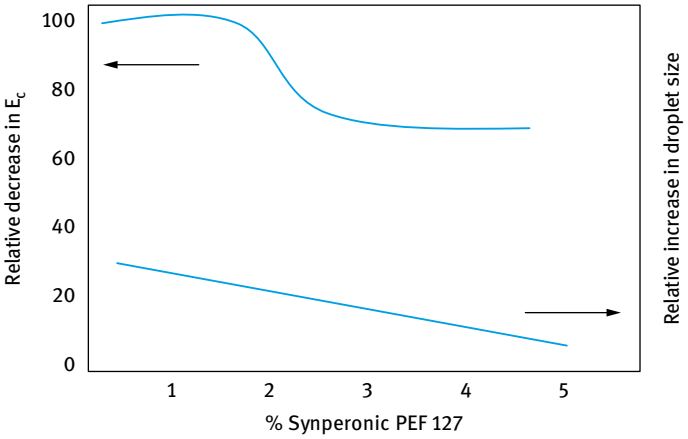

Fig. 14.61: Correlation of relative decrease in E_c with relative increase in droplet size.

The cohesive energy E_c is the most sensitive parameter for assessing coalescence. Any coalescence results in a decrease in the number of contact point and causes a reduction in E_c. Using the above mentioned emulsions, E_c was found to decrease with increasing droplet size (as a result of coalescence). At and above 3 % Pluronic PEF 127, E_c remained virtually unchanged, indicating absence of coalescence. Fig. 14.61 shows the variation of the relative decrease of E_c with the relative increase in droplet size; the correlation is clear.

References

[1] Tadros T. Rheology of Dispersions. Weinheim: Wiley-VCH; 2010.
[2] Mackosko CW. Rheology, Principles, Measurement and Applications. New York: Wiley-VCH; 1994.
[3] Goodwin JW. In: Tadros TF, editor. Surfactants. London: Academic Press; 1984.
[4] Goodwin JW, Hughes RW. Advances Colloid Interface Sci. 1992;42:303.
[5] Tadros TF. Advances Colloid and Interface Science. 1996;68:97.
[6] Goodwin JW, Hughes RW. Rheology for Chemists. Cambridge: Royal Society of Chemistry Publication; 2000.
[7] Whorlow RW. Rheological Techniques. Chichester: Ellis Horwood; 1980.
[8] Bingham EC. Fluidity and Plasticity. New York: McGraw Hill; 1922.
[9] Herschel WH, Bulkley R. Proc Amer Soc Test Materials. 1926;26:621; Kolloid Z. 1926;39:291.
[10] Casson N. In: Mill CC, editor. Rheology of Disperse Systems. New York; Pergamon Press; 1959. p. 84–104.
[11] Cross MM. J Colloid Interface Sci. 1965;20:417.
[12] Einstein A. Ann Physik. 1906;19:289; 1911;34:591.
[13] Bachelor GK. J Fluid Mech. 1977;83:97.
[14] Krieger IM, Dougherty TJ. Trans Soc Rheol. 1959;3:137.
[15] Krieger IM, Advances Colloid and Interface Sci. 1972;3:111.
[16] Goodwin JW, Hughes RW. Rheology for Chemists. Cambridge: Royal Society of Chemistry Publication; 2000.
[17] Napper DH. Polymeric stabilisation of colloidal dispersions. London: Academic Press; 1983.
[18] Liang W, Tadros TF, Luckham PF. J Colloid Interface Sci. 1992;153:131.
[19] Prestidge C, Tadros TF. J Colloid Interface Sci. 1988;124:660.
[20] Firth BA, Hunter RJ. J Colloid Interface Sci. 1976;57:248.
[21] van de Ven TGM, Hunter RJ. Rheol Acta. 1976;16:534.
[22] Hunter RJ, Frayane J. J Colloid Interface Sci. 1980;76:107.
[23] Heath D, Tadros TF. Faraday Disc Chem Soc. 1983;76:203.
[24] Prestidge C, Tadros TF. Colloids and Surfaces. 1988;31:325.
[25] Tadros TF, Zsednai A. Colloids and Surfaces. 1990;49:103.
[26] Liang W, Tadros TF, Luckham PF. J Colloid Interface Sci. 1993:155.
[27] Liang W, Tadros TF, Luckham PF. J Colloid Interface Sci. 1993;160:183.
[28] Ball R, Brown WD. Personal Communication.
[29] Buscall R, Mill PDA. J Chem Soc Faraday Trans I. 1988;84:4249.
[30] Gast AP, Hall CK, Russel WB. J Colloid Interface Sci. 1983;96:251.
[31] Asakura A, Oosawa F. J Chem Phys. 1954;22:1255.
[32] Asakura A, Oosawa F. J Polymer Sci. 1958;93:183.

[33] Fleer GJ, Scheutjens JMHM, Vincent B. ACS Symposium Series. 1984:240;245.
[34] Goodeve CV. Trans Faraday Soc. 1939;35:342.
[35] Gillespie T. J Colloid Sci. 1960;15:219.
[36] Hunter RJ, Nicol SK. J Colloid Interface Sci. 1968;28:200.
[37] Firth BA, Hunter RJ. J Colloid Interface Sci. 1976;57:248, 257, 266.
[38] Mills PDA, Goodwin JW, Grover B. Colloid Polym Sci. 1991;269:949.
[39] Goodwin JW, Hughes RW. Advances Colloid Interface Sci. 1992;42:303.
[40] Liang W, Tadros TF, Luckham PF. Langmuir. 1983;9:2077.
[41] Firth BA, Neville PC, Hunter RJ. J Colloid Interface Sci. 1974;49:214.
[42] van de Ven TGM, Hunter RJ. J Colloid Interface Sci. 1974;68:135.
[43] Hunter RJ. Advances Colloid Interface Sci. 1982;17:197.
[44] Friend JP, Hunter RJ. J Colloid Interface Sci. 1971;37:548.
[45] Buscall R, Goodwin JW, Ottewill RH, Tadros TF. J Colloid Interface Sci. 1982;85:78.
[46] Tadros TF. Colloids and Surfaces. 1994;91:39.
[47] Tadros TF. Advances Colloid and Interface Science. 2004;108–109:227.
[48] Salager JL. Pharmaceutical emulsions and suspensions. New York: Marcel Dekker; 2000.

Index